FEDERAL UNIVERSITY DUTSIN-MA
INTERNATIONAL PHYSICAL SCIENCE CONFERENCE,
FACULTY OF PHYSICAL SCIENCES
KATSINA STATE, NIGERIA

IPCS 2023
CONFERENCE PROCEEDING

Theme:

PUSHING THE PARADIGM NEW TRENDS IN PHYSICAL SCIENCE FOR SUSTAINABLE DEVELOPMENT

HELD ON 1ST - 3RD NOVEMBER 2023
Hosted By
FACULTY OF PHYSICAL SCIENCES

TABLE OF CONTENTS

A Framework for an Intelligent Recommender System (IRS) for Tourist Sites in Nigeria using Machine Learning for Sustainable Development

*Nwocha, Auzhioluka Uriah, Bakpo, F. S. and Ekle, Francis Adoba

Department of Computer Science, University of Nigeria, Nsukka.
*Corresponding author's email: **nwochaau@yahoo.com; francis.bakpo@unn.edu.ng; francisekle@gmail.com**

ABSTRACT
Unarguably, Nigeria is the most populous black nation in the world endowed with vast mineral resources such as gold, oil and gas and vast arable land for agriculture which earns her a lot of foreign exchange. Unfortunately, Nigeria is yet to fully harness and maximize the potentials inherent in the tourism sector which is the main stay of some world large economies like United Arab Emirate (Dubai), Spain, Israel and Saudi Arabia that earn billions of dollars annually from tourism. The aim of this thesis is to develop an Intelligent Recommender System for Tourist Sites in Nigeria using Machine Learning. Object Oriented Analysis and Design Methodology (OOADM), Content Based Filtering (CBF), Collaborative Filtering (CF) and K-Nearest Neighbour (KNN) Machine Learning Algorithm will be used in the analysis and design of this work.
Keywords: Tourist Sites, Content Based Filtering, Collaborative Filtering, Recommender Engine, Machine learning

INTRODUCTION

Tourism involves traveling to other locations for pleasure, business, or other reasons. The tourism industry has experienced tremendous growth in recent years, a massive leap partly attributed to the rapid development of the Internet, which has simplified the process of accessing large amounts of global data by potential tourists on points of interest, travel plans, and destinations (Hassannia et al., 2019). Tourists visit tourist sites for recreation or certain purposes and are usually faced with the task of locating tourist's sites that have been around for a long time and many new tourists' sites that are not yet known by tourists due to lack of information (Ayu et al., 2021 & Nwagba et al., 2020). Tourism is the main revenue earner for certain stable world economies like Spain, United Arab Emirate (Dubai), Israel, Saudi Arabia and so. The tourists' sites in Nigeria with great revenue earning potentials include natural attractions such as Yankari National Park, Idanre Hills, and Obudu Mountain Resort. There are also historical and cultural sites, such as the Osun-Osogbo Sacred Grove, the Ogbunike Caves, and the Benin City Walls and Moat. A myriad of man-made sites such as Port Harcourt Pleasure Park and Abuja Wonder Land also exist in the country. Although, these tourism potentials are sufficient to make Nigeria a well-known tourist destination, yet tourism remains an untapped source of revenue in several underdeveloped countries, such as Nigeria (Nwagba et al., 2020 & Olatunji et al., 2022).

To assist tourists in trip planning and help them to find the information they are looking for, recommender systems are needed (Fararni et al., 2021). Jie et al. (2015) averred that recommender systems were first applied in e-commerce to solve the information overload problem caused by Web 2.0, and they were quickly expanded to the personalization of e-government, e-business, e-learning, and e-tourism. Recommender Systems apply machine learning and data mining techniques to filter undetected information and can predict whether a user of a system would like a given resource based on his/her interests and preferences (Asabere, 2012). This can be accomplished through Internet because of its enormous resources; and it's considered as a highly effective and preferred communication platform as it can be accessed 24 hours a day from everywhere (Azahari et al., 2019). Recommender systems are so commonplace now that many of us use them without even knowing it. Because we can't possibly look through all the products or content on a website, a recommendation system plays an important role in helping us have a better user experience, while also exposing us to more inventory we might not discover otherwise (Badreesh et al., 2023). The recommender system uses explicit feedback to provide suggestions by analyzing the reaction of users (likes or dislikes) towards a specific product.

Strictly speaking, recommender systems are defined as information filtering systems that make recommendations of the most suitable services to tourists (Fararni et al., 2021). A personalized tourism recommendation system is a process that recommends important places and spots to tourists. Tourism recommendation system provides various services such as the preferences and interests of users. A tourism recommendation system analyses the visited places of users and recommends unvisited places (Nan et al., 2022). It is one of the popular machine learning algorithms and has been widely used in areas, especially ecommerce platforms (Pu et al., 2020). Tourist Recommender system has emerged as a major research interest that aims to help users to find items online by providing suggestions that closely match their interest (Singh et al., 2021).

Tourists, citizens and foreigners are limited in knowing the available tourists sites in the country. For citizens, where to visit while on vacation is still an issue, let alone foreigners who are visiting the country for the first time. Finding a suitable site that meets their standard is still a daunting task. They have to surf the web with numerous web sites and also engage in direct questioning. These are indeed time consuming, energy sapping and financially stretching because of local running. The problems encountered in the manual system leads to regrets and dissatisfactions. Recommender Systems have been used successfully in order to deal with information overload problems in a wide variety of domains ranging from e-commerce, e-tourism, to e-learning. They typically predict the ratings of unseen items by a user and recommend the top N items based on user's profile (Rawat & Dwivedi, 2019). There is a need for an intelligent system to help predict user preferences for new items. Recommender systems (RSs) emerged to deal with this problem to help users find what is genuinely relevant to their needs. RSs' main function is to predict user interest by relating the user's history, information, profile, and queries used, searched, created, and expressed (Hamada et al., 2022).

Literature Review
Some works have been done in recommender systems both within and without by scholars in the field. Ferreira et al. (2023) surveyed the application of Recommender Systems in Cybersecurity architectures. This survey discussed several studies where Recommender Systems are implemented in Cybersecurity with encouraging results. Wang et al. (2022) developed an algorithm compared with some traditional algorithms in a dataset. The algorithm deals with the similarity of user attributes and user behavior and uses content-based algorithm to deal with the relationship between scenic spots, although it faces Cold start, serendipity and scalability challenges. Fararni et al. (2021) proposed a conceptual framework for a hybrid recommender system in the tourism domain, leveraging on big data and artificial intelligence (AI) technologies. Alrasheed et al. (2021) worked on multilevel recommendation systems as well as hybrid recommendations. The work faces challenges of user feedback and adaptability, data quality and availability. Qin et al. (2019) proposed a hybrid travel recommender system considering user preferences and trip characteristics. The research faces challenges in handling sparse data and addressing the cold-start problem. Kim et al. (2019) worked on intelligent travel recommender system based on user preferences extracted from reviews. They extract user preferences from reviews for an intelligent travel recommender system. Jiang et al. (2019) considered multimodal data for context-aware travel recommendations; the work however faces challenges in data integration and processing across multiple modalities. In another research, Li et al. (2019) developed a Novel Recommendation System for Tourist Spots Based on Hierarchical Sampling Statistics and (Singular Value Decomposition++) SVD++. First a new dataset named "Smart Travel" is created for the experiments. Ten hierarchical sampling statistics (HSS) model is used to acquire the user preference for different population attributes. By and large, the Singular Value Decomposition Algorithm (SVD++) faces scalability challenge. Hassannia et al. (2019) introduced a Web-Based Recommendation System for Smart Tourism: Multi-agent Technology. Firstly, it presents an online autonomous web agency for smart tourism ecosystem, which is based on the established connection amongst all the sectors in the tourism industry. On their work, Location recommendation for location-based social networks, Yuan et al. (2013) focused on location recommendations using location-based social networks. However, it has limitations in handling scalability.

MATERIALS AND METHODS
The research design methodology used in this paper is the Object-Oriented Analysis and Design (OOAD). It is a structured approach used to design software systems by modeling real-world entities and their interactions. Designing a tourist site recommender system using OOAD involves breaking down the system into objects, classes, relationships, and interactions. In this research, Hypertext Markup Language (HTML), Cascading Style Sheet (CSS), and Javascript were proposed for developing the user interface. The Logic Tier coordinates the system by processing commands, making logical decisions and performing calculations. It also acts as a link, transmitting both processed and unprocessed data between the two neighboring layers. Python code is proposed to be used for developing the logic tier of this application. The Data Tier is accountable for information storage and retrieval to and from the database. The retrieved data is passed to the logic tier for processing and finally back to the user through the presentation tier. Both the logic and data tiers make up the server. A MYSQL database is used for designing the data tier of this application.
Developing an Intelligent Tourists' Recommender System requires a well-structured research design methodology. The recommender techniques used in designing the system are Collaborative filtering and Content-based filtering recommender techniques. A user-based approach collaborative filtering recommendation technique is used for designing the system. This was achieved using KNN supervised learning machine learning algorithm for grouping similar users together based on explicit data gotten from their personal ratings of their degree of likeness for tourist sites they have visited and explored. Pearson Correlation will be used as the statistical similarity metric function for computing the mathematical measure of similarity amongst users. While features of the tourist sites were used for

content-based recommendation technique. This research designed a switching and cascade-based hybridization approach to be used in combining the two recommender techniques used in developing the system

Source of Data
The primary source of data used for this research shall be obtained from Tourist Sites in each of the states of the six (6) geo-political zones of the country and also explicit ratings on their degree of likeness gotten from users that have visited some of these tourist sites. The target is ten (10) Tourist Sites from each geo-political zone.

Method of Data Collection
The method of data collection for this paper shall be through google form questionnaire as well as direct visit to tourist sites.

Analysis of the Existing System
The Existing system is manually driven. The system uses a manual recommendation system where recommendations are made by humans without the aid of automated algorithms. The manual operation is poses a big challenge because tourists, citizens and foreigners are limited in knowing the available tourists sites as well as their locations in the country, especially foreigners who are visiting the country for the first time. Finding a suitable site that meets their standard is still a daunting task. They have to surf the web with numerous web sites and also engage in direct questioning. These are indeed time consuming, energy sapping and financially stretching because of local running. The problems encountered in the manual system leads to regrets and dissatisfactions.

Weaknesses of the Existing System
The process has several weaknesses compared to automated intelligent systems. Some of the common weaknesses of the existing manual systems are Subjectivity and Bias**,** Limited Scalability**,** Inefficiency**,** Lack of Personalization, Limited Data Utilization, Consistency and Reliability, Difficulty in Handling Cold-Start, Scalability Issues and Limited Exploration**.** Manual tourist site recommendation systems face challenges related to subjectivity, scalability, personalization, efficiency, and adaptability. Automated intelligent systems, utilizing machine learning and data-driven approaches, aim to address many of these weaknesses.

Analysis of the Proposed System
The proposed system is an Intelligent Recommender System for tourist sites in Nigeria using machine learning; it seeks to address the problems inherent in the existing system. This is with the aim of providing an effective online intelligent recommender system that will recommend tourist sites that suits the tourist preference. In this system, forms are designed and provided using HTML technology and tourists are expected to register with their details and login credentials are provided for them in order to grant future access into the system. When logged into the system, they are provided access to the available tourist sites, where they can rate tourist sites according to their degree of likeness for the tourist sites they have visited before on a five star rating scale with 5 being the best and 1 the least. This information combined with the features of tourist sites are used for making recommendation of tourist sites to users of the system.

Design of the Proposed System
Figure 1 shows the system architecture of the proposed system framework showing the various components of the system and their linkages.
Web Users: The web users are the tourists who will be using the intelligent system directly. The users access the system via the web, called the interface.
Interface: Users' requests from the interface are routed via the host running the web server.
User Database: Inputs are gotten from both the web users and the database for the intelligent recommender system.
Content Analysis: Content analysis produces results from two sources, which are the features of the tourist site and the rating that an active user has given them.
Collaborative Filtering: Collaborative filtering systems evaluate item ratings for the current active user (user currently logged into the system) based on the ratings given by other tourists who have preferences very much correlated to the current active user.
Intelligent Recommender: Makes the appropriate recommendation in the form of a response through the web server back to the web clients of the system after preference (user's interest) generation based on the designed algorithm.

 The various components of the designed system and the flow of information from the web users (the clients) through the switching hybrid recommender to the database and back to the users displaying the recommended tourist sites after preference generation based on the designed algorithm is represented in figure 2 below:
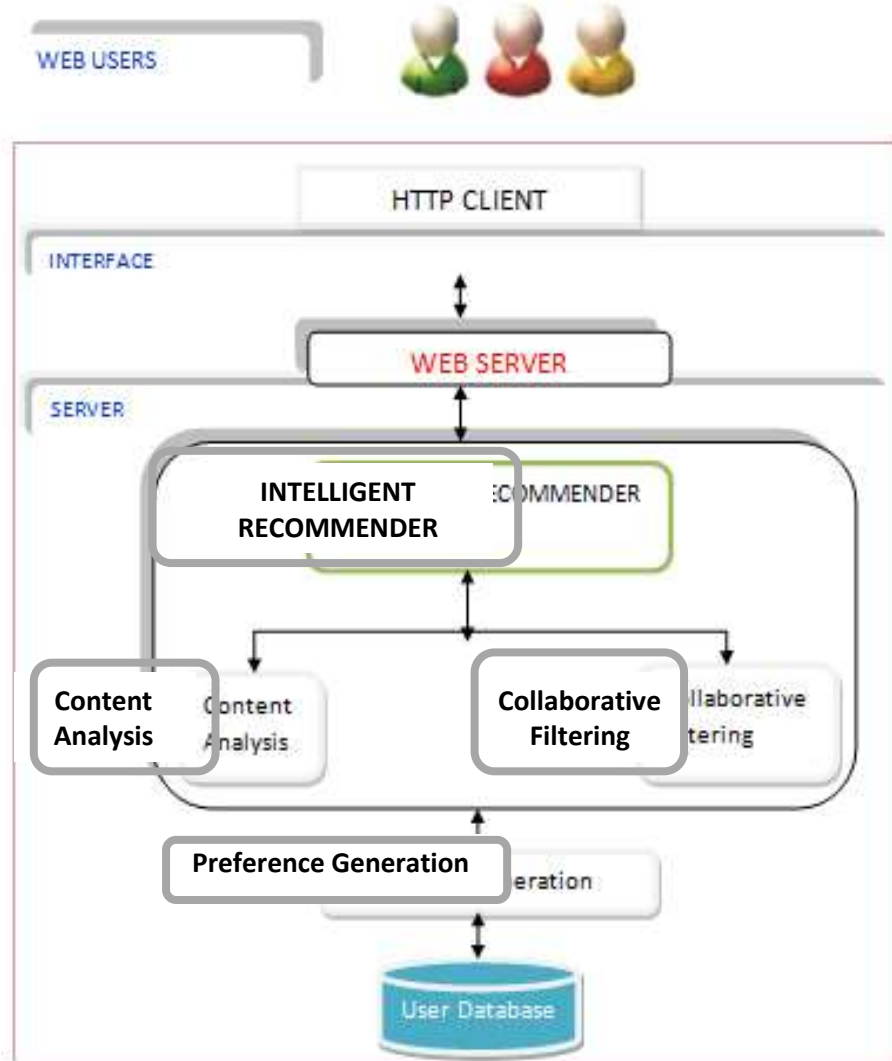
Figure 1: System Architecture of the Proposed System

Use Case Diagram
The use case diagram in figure 2 below shows activities that each of the actors performs. The users (actors) here are the administrator, the system and the tourist.
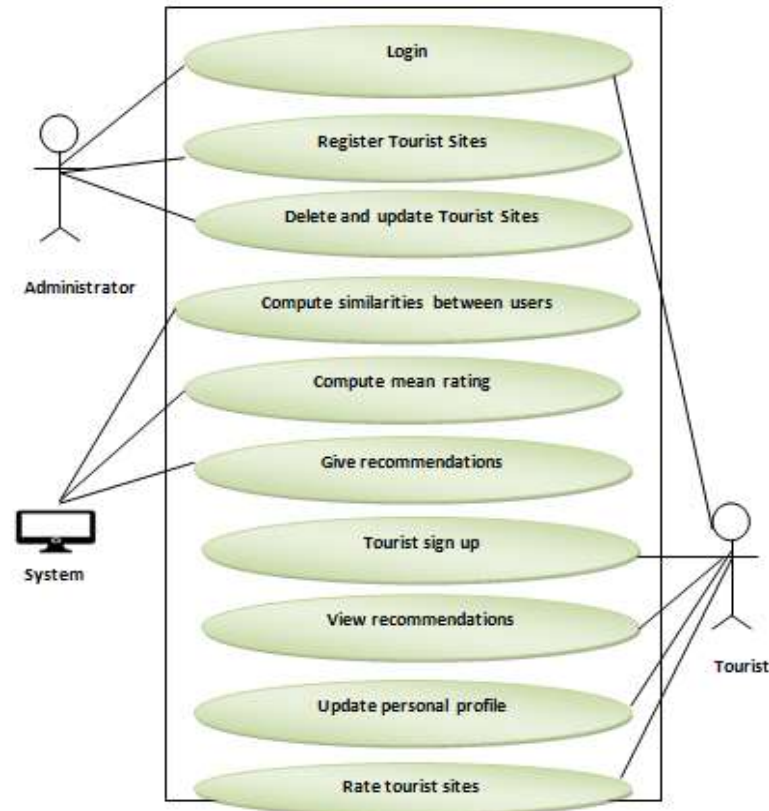
Figure 2: Use case diagram of the Proposed System

From the use case diagram in figure 3, the basic functions of the three (3) actors are outlined as follows:
The Administrator:
- The administrator is obligated to login (the process of accessing an account that has already been created) to have access into the intelligent system;
- The administrator is saddled with the task of registering available tourist sites in the country; and
- The administrator is also responsible for deleting and updating tourist sites;

*The Tourist***:**
- The tourist can Sign Up (the process of creating a new account.) in to the intelligent system;
- The tourist is obligated to login (the process of accessing an account that has already been created) to have access into the intelligent system;
- The tourist can view recommendations;
- The tourist can update his/her personal profile; and
- The tourist can rate tourist sites.

The System
- The system computes similarities between users;
- The system computes mean ratings; and
- The system gives recommendations.

Similarity Computation
Similarity computation between items or users is a critical step in memory-based collaborative filtering algorithms. For item-based *CF* algorithms, the basic idea of the similarity computation between item i and item j is first to work on the users who have rated both of these items and then to apply a similarity computation to determine the similarity, $w_{i,j}$ between the two co-rated items of the users. For a user-based *CF* algorithm, we first calculate the similarity, $w_{u,v}$, between the users u and v who have both rated the same items. There are many different methods to compute similarity or weight between users or items such as (Sarwar et al., 2001; Su & Khoshgoftaar, 2009). This paper uses correlation based similarity.

Correlation-Based Similarity

In this case, similarity $w_{u,v}$ between two users u and v, or $w_{i,j}$ between two items i and j, is measured by computing the *Pearson correlation* or other correlation-based similarities. *Pearson correlation* measures the extent to which two variables linearly relate with each other (Resnick et al., 1994). For the user based algorithm, the *Pearson correlation* between users u and v is;

$$w_{u,v} = \frac{\sum_{i\in I}(r_{u,i}-\overline{r}_u)(r_{v,i}-\overline{r}_v)}{\sqrt{\sum_{i\in I}(r_{u,i}-\overline{r}_u)^2}\sqrt{\sum_{i\in I}(r_{v,i}-\overline{r}_v)^2}}, \qquad (1)$$

where the $i \in I$ summations are over the items that both the users u and v have rated and $\overline{r}_u$ is the average rating of the co-rated items of the uth user.

Figure 3. Item-based similarity ($w_{i,j}$) calculation based on the co-rated items i and j from users   2, l and n.

For the item-based algorithm, denote the set of users $u \in U$ who rated both items i and j, then the *Pearson Correlation* will be;

$$w_{i,j} = \frac{\sum_{u\in U}(r_{u,i}-\overline{r}_i)(r_{u,j}-\overline{r}_j)}{\sqrt{\sum_{u\in U}(r_{u,i}-\overline{r}_i)^2}\sqrt{\sum_{u\in U}(r_{u,j}-\overline{r}_j)^2}}, \qquad (2)$$

Where $r_{u,i}$ is the rating of user u on item i, $\overline{r}_i$ is the average rating of the ith item by those users, see Figure 3 (Sarwar et al., 2001).

Some variations of item-based and user-based *Pearson correlations* can be found in (Mclaughlin & Herlocker, 2004). The *Pearson correlation* based *CF* algorithm is a representative *CF* algorithm, and is widely used in the *CF* research community. Other correlation-based similarities include: *constrained Pearson correlation*, a variation of *Pearson correlation* that uses midpoint instead of mean rate; *Spearman rank correlation*, similar to *Pearson correlation*, except that the ratings are ranks; and *Kendall's τ correlation*, similar to the *Spearman rank correlation*, but instead of using ranks themselves, only the relative ranks are used to calculate the correlation (Goldberg, 2001 & Herlocker, 2004). Usually the number of users in the computation of similarity is regarded as the neighborhood size of the active user, and similarity based *CF* is deemed as neighborhood based *CF*.

Proposed Algorithm for the framework

Input: User Rating Data (URD), Features of Tourist Sites.
   1.   Authenticate Users.
   2.   Set Arbitrary User = Authenticated User.
   3.   Retrieve all n users and their ratings from the database; assigned as a collection U using Associative Array.
   4.   If Neighbourhood> 0:
            For each user U_i in collection $U_i{}^n{}_{=1}$
                     Calculate the similarities between U_i and U_{i+1}, ... ,U_n using Pearson Correlation.
                     Select the 5 top most Users with the closest similarities to U_i
                     Store the similarities in an associative Array.
            Endfor;
            Break;
         ElseNeighbourhood == 0:
            For each user U_i in collection $U_i{}^n{}_{=1}$

> Find highly rated tourist sites with similar features.
> > Endfor;
> > Break;
> Endif
5. Make Predictions
6. Add predictions as User Recommendation
7. Generate Recommendation
8. Exit

Implementation Architecture
Figure 4 below shows the implementation architecture of the system. The three (3) tiers work together to provide a seamless tourist site recommendation experience.
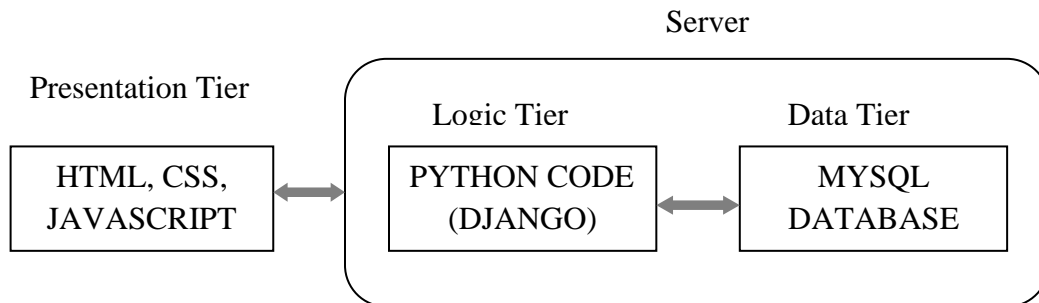
Figure 4: Implementation Architecture of the proposed system

The presentation tier handles the user interface, allowing users to interact with the system and receive recommendations. The logic tier processes user inputs and data, applying recommendation algorithms to generate personalized recommendations. The data tier manages the storage and retrieval of relevant data, supporting the logic tier's recommendation generation process. This layered architecture ensures modularity, scalability, and separation of concerns, making it easier to maintain and enhance the recommender system over time.
From Figure 4, the Presentation Tier, also known as the User Interface, is the topmost level of the application. The main function of the user's interface is to translate tasks and results into something the user can understand. In this research paper, Hypertext Markup Language (HTML), Cascading Style Sheet (CSS), and Javascript were used for developing the user interface. The Logic Tier coordinates the system by processing commands, making logical decisions and performing calculations. It also acts as a link, transmitting both processed and unprocessed data between the two neighboring layers. Python code is used for developing the logic tier of this application. The Data Tier is accountable for information storage and retrieval to and from the database. The retrieved data is passed to the logic tier for processing and finally back to the user through the presentation tier. Both the logic and data tiers make up the server. A MYSQL database is used for developing the data tier of this application
These three tiers work together to provide a seamless tourist site recommendation experience. The presentation tier handles the user interface, allowing users to interact with the system and receive recommendations. The logic tier processes user inputs and data, applying recommendation algorithms to generate personalized recommendations. The data tier manages the storage and retrieval of relevant data, supporting the logic tier's recommendation generation process. This layered architecture ensures modularity, scalability, and separation of concerns, making it easier to maintain and enhance the recommender system over time.

CONCLUSION
Tourist recommender systems are becoming more popular and important in the tourism industry as they can help tourists to discover new and personalized travel options, reduce information overload, increase customer satisfaction and loyalty, and enhance the competitiveness and profitability of tourism businesses. Recommendation system for tourist spots has very high potential value including social and economic benefits. In conclusion, Intelligent Recommender Systems for tourist sites in Nigeria have the potential to significantly impact sustainable national development by promoting diversified tourism, fostering economic growth, preserving cultural and historical heritage, encouraging environmentally responsible practices, engaging local communities, facilitating cross-cultural exchange, ensuring safety, and providing valuable data for informed decision-making. They play a vital role in aligning the tourism sector with the principles of sustainability and inclusive growth. The future work will carry out the implementation of the proposed framework.

REFERENCES

Ekle, F. A., Uzoamaka, E. D., Vaatyough, F. B., & Ezema, M. (2022). *A Switching and Cascade-Based Hybrid Recommender System for Nigerian University Bookshops*. *9*(5), 458–470.

Alrasheed, H., Alzeer, A., Alhowimel, A., Shameri, N., & Althyabi, A. (2020). A Multi-Level Tourism Destination Recommender System. *Procedia Computer Science*, *170*(2019), 333–340. https://doi.org/10.1016/j.procs.2020.03.047

Asabere, N. Y. (2012). *Towards a Perspective of Hybrid Approaches and Methodologies in Recommender Systems*. *3*(11).

Azahari, M., Yusof, M., Hani, F., Ali, M., Darus, M. Y., & Sciences, M. (2019). Classification Algorithm Against Different Types of DDoS Attacks Using Hybrid Approach. *International Journal of Innovations in Engineering and Technology (IJIET) Http://Dx.Doi.Org/10.21172/Ijiet.143.16 Classification*, *14*(3), 137–144.

Badreesh, S., Powers, J., & Pandey, P. (2023). *Recommender Systems_ In-Depth Guide & How They Work _ Built In*. file:///C:/Users/hp/Desktop/Recommender Systems_ In-Depth Guide & How They Work _ Built In.html

Fararni, K. Al, Nafis, F., Aghoutane, B., Yahyaouy, A., Riffi, J., & Sabri, A. (2021). Hybrid recommender system for tourism based on big data and AI: A conceptual framework. *Big Data Mining and Analytics*, *4*(1), 47–55. https://doi.org/10.26599/BDMA.2020.9020015

Ferreira, L., Silva, D. C., & Itzazelaia, M. U. (2023). Recommender Systems in Cybersecurity. *Knowledge and Information Systems*. https://doi.org/10.1007/s10115-023-01906-6

Hamada, M., Prasad, R., Hassan, M., Mahendran, A., & Watanobe, Y. (2022). *State-of-the-Art on Recommender Systems for E- Learning*. 10–12.

Hassannia, R., Barenji, A. V., Li, Z., & Alipour, H. (2019). *Web-Based Recommendation System for Smart Tourism : Multiagent Technology Tourism : Multiagent Technology*. *Special Issue Cultural Heritage and Smart Tourism*. https://doi.org/10.3390/su11020323

Herlocker, J. L., Konstan, J. A., Resnick, J. A., Lacovou, N., Suchak, M., Bergstrom, P., & Riedl, J. (1994). Grouplens: An open architecture for collaborative filtering of net news. *Proceedings of the ACM Conference on Computer Supported Cooperative Work*, 175– 186, New York, NY, USA.

Herlocker, J. L., Konstan, J. A., Terveen, L. G., & Riedl, J. T. (2004). Evaluating collaborative filtering recommender systems. *ACM Transactions on Information Systems*, *22*(1). 5–53.

Goldberg, K., Roeder, T., Gupta, D. and Perkins, C. (2001). Eigentaste: A constant time collaborative filtering algorithm. *Information Retrieval*, *4*(2), 133–151.

Kotkov, D., Medlar, A., & Glowacka, D. (2023). Rethinking Serendipity in Recommender Systems. *CHIIR 2023 - Proceedings of the 2023 Conference on Human Information Interaction and Retrieval*, *1*, 383–387. https://doi.org/10.1145/3576840.3578310

Li, G., Hua, J., Yuan, T., Wu, J., Jiang, Z., Zhang, H., & Li, T. (2019). *Novel Recommendation System for Tourist Spots Based on Hierarchical Sampling Statistics and SVD ++*. *2019*.

McLaughlin, M. R.J., & Herlocker, J. L. (2004). A collaborative filtering algorithm and   evaluation   metric   that accurately model the user experience. In *Proceedings of 27th Annual International ACM SIGIR Conference on Research and Development in Information Retrieval (SIGIR '04)*, 329–336, Sheffield, UK.

Melville, P., & Sindhwani, V. (2010). Encyclopaedia of Machine Learning: Recommender Systems. *Encyclopaedia of Machine Learning*, 829–838. https://link.springer.com/content/pdf/10.1007/978-1-4899-7687-

Nan, Xiang, Kayo, K., & Wang, X. (2022). *Design and Implementation of a Personalized Tourism Recommendation System Based on the Data Mining and Collaborative Filtering Algorithm*.

Nwagba, B. O., Chima, C., & Grace, A. T. (2020). *Social Insecurity and the Development of Tourism in Nigeria : the Niger Delta Social Insecurity and the Development of Tourism in Nigeria : the Niger Delta Experience , 2004 -2009. August*.

Pu, Z., Du, H., Yu, S., & Feng, D. (2020). Improved Tourism Recommendation System. *ACM International Conference Proceeding Series*, *February 2020*, 121–126. https://doi.org/10.1145/3383972.3384074

Rawat, B., & Dwivedi, S. K. (2019). State of the Art Recommendation Approaches. *Natural Language Processing*, *January*, 1621–1651. https://doi.org/10.4018/978-1-7998-0951-7.ch075

Roy, D., & Dutta, M. (2022). A systematic review and research perspective on recommender systems. *Journal of Big Data*, *9*(1). https://doi.org/10.1186/s40537-022-00592-5

Sarwar, B. M., Karypis, G., Konstan, J. A., & Riedl, j. (2001). Item based collaborative filtering recommendation algorithms. In *Proceedings of the 10th International Conference on WorldWide Web (WWW '01)*, 285–295.

Singh, P. K., Choudhury, P., Dey, A. K., & Pramanik, P. K. D. (2021). Recommender systems: an overview, research trends, and future directions. *International Journal of Business and Systems Research*, *15*(1), 14. https://doi.org/10.1504/ijbsr.2021.10033303

Su, X., & Khoshgoftaar, T. M. (2009). *A Survey of Collaborative Filtering Techniques*. *2009*(Section 3). https://doi.org/10.1155/2009/421425

Wang, X., Wang, D., Kunpeng, L., Le, W., Yanjie, F., & Xing, X. (2022). *Multi-level Recommendation Reasoning over Knowledge Graphs with Multi-level Recommendation Reasoning over Knowledge Graphs with Reinforcement Learning. April 2023*. https://doi.org/10.1145/3485447.3512083

Preparation and Characterization of Chitosan/CuO Nanocomposites

Aliyu, A. O., *Sumaila C. A., Usman, A. O. and Abdullahi, A. S.

Department of Pure and Industrial Chemistry, Prince Abubakar Audu University, P.M.B 1008, Anyigba Kogi State, Nigeria
*Corresponding author's email: muminislam2012@gmail.com

ABSTRACT
This study describes a method based on the incorporation of copper nanoparticles into chitosan polymer matrix for the creation of a novel nanocomposite. In this study, a simple preparation of chitosan is reported. The preparation consists of three steps: (1) deproteinisation of the crab shells using NaOH, (2) demineralisation of the deproteinised crab shells using HCl to produce chitin (3) the produced chitin was subjected to deacetylation using NaOH to obtain chitosan. Moreover, the copper oxide nanoparticles were synthesized using a modified sol-gel while the chitosan/CuO nanocomposite was prepared using a wet impregnation method. Furthermore, the prepared chitosan, synthesised CuO nanoparticles, and their nanocomposites were characterized by UV–visible spectroscopy and X-ray diffraction. UV–visible spectroscopy showed an electronic excitonic transition at 245 nm clearly revealing the formation of CuO-NPs. X-ray diffractogram obtained showed the phase structures of the chitosan at diffraction peaks at 2θ of $12.56°$ and $19.92°$ corresponding to planes (020) and (110) typical of semi-crystalline chitosan while that of CuO nanoparticles showed at diffraction peaks of 2θ values of 32.72, 35.9, 38.97, 48.74, 53.62, 58.34, 61.70, 66.20, 68.11, 72.54, and 75.44o correspond to the (110), (101), (002), (211), (112), (310), (202), (113), (220), (311), and (222) planes of CuO, respectively. Notably, this study showed that a novel chitosan/CuO nanocomposite could be prepared via a simple method.
Keywords: Sol-gel, CuO nanoparticles, Chitosan, Nanocomposite, Impregnation

INTRODUCTION
Nanocomposite forms of natural polymers such as chitosan seem to be useful materials due to their availability, environmentally friendly characteristics, and biodegradable, bio-compatible, and non-toxic properties (Matei *et al*., 2022). This polymer can be readily obtained from ocean life such as crabs, prawns, oysters, and shrimp which are common in the coastline areas such as Niger, Lagos, Ondo, Delta, Bayelsa, Rivers, Akwa Ibom, and Cross Rivers in Nigeria (Okogwu *et al*., 2021). It was reported by Santos *et al*. (2020) that millions of metric tonnes of chitin are produced annually all over the globe as processing wastes from shellfish, krill, clams, oysters, squid, and fungi without a proper disposal system which then results in environmental pollution. This low-value waste produced in large quantities can be treated and converted into useful biomaterials. This would be beneficial to the environment at large and also save the cost of purchasing highly expensive materials.

Chitosan is a polysaccharide composed of glucosamine and N-acetyl glucosamine linked with a β-1-4- glycosidic linkage. Chitosan is a semi-crystalline biopolymer that is biocompatible and can be degraded, the degradation products are non-toxic (Aranaz *et al*., 2021). The presence of numerous active sites in chitosan and its crystallinity plays an important role in its water treatment and antimicrobial efficiencies, but its swelling, agglomeration, and low thermal stability limit its applications. To overcome these limitations, chitosan needs to be stabilized with nanoparticles like copper oxide nanoparticles to form nanocomposites (Herdiana *et al*., 2021).

Copper oxide nanoparticles have high thermal conduction potential and exhibit good antimicrobial activity at a low concentration. Thus, the incorporation of copper nanoparticles in the chitosan polymer matrix will help to prevent possible agglomeration of chitosan and, at the same time reduce its swelling index owing to high dispersion and large surface area of the nanoparticles (Mikušová and Mikuš, 2021). Hence, in this study, chitosan–copper oxide nanocomposite was synthesised using the sol-gel method characterised by X-ray Diffraction Analysis (XRD) for its basic crystalline properties.

MATERIALS AND METHODS
Materials
All the chemicals used in this study were of analytical grade with high percentage purity.

Methods
Extraction of chitosan from crab shells
The extraction of chitosan from the ground crab shells was achieved via three main stages (deproteinisation, demineralisation, and deacetylation).

Deproteinisation of the crab shells
Exactly 5.00 g of the ground crab shells and 50 cm^3 of 1.0 M NaOH were weighed in a 250 cm^3 beaker. The mixture was heated at 100ºC for 45 minutes. After heating, the mixture was allowed to cool and settle; excess NaOH was removed by decantation, followed by washing with deionized water to neutral pH. Filtration was carried out using Whatmann filter paper No. 4, and the residue was oven-dried at 80ºC for 45 minutes.

Demineralisation of the deproteinised crab shells
Exactly 3.0g of the deproteinized crab shells were weighed in a 250 cm^3 beaker, containing 20 cm^3 of 1.0 M HCl. The mixture was heated for 60 minutes and allowed to cool and settle. The excess HCl was removed by decantation, followed by washing with deionized water to neutral pH. This was subsequently followed by filtration using Whatman filter paper No. 4, and the residue obtained was oven-dried at 80ºC for 45 minutes.

Deacetylation of chitin
Exactly 1.00 g of the chitosan and 50 cm^3 of 1.0 M CH$_3$COOH were measured in a 250 cm^3 beaker. The mixture was heated at 80ºC for 45 minutes and allowed to cool and settle. The mixture was decanted, followed by washing with deionized water to neutral pH. Thereafter, filtration was done using Whatmann filter paper No. 4, and the residues were oven dried at 80ºC for 45 minutes.

Synthesis of copper oxide nanoparticles via sol-gel method
The copper oxide nanoparticles were synthesized using a modified sol-gel method. A known mass (5g) of copper sulphate powder was measured into a 250 cm^3 beaker, and about 100.0 cm^3 of de-ionized water was added. The solution was stirred using a magnetic stirrer for 30 minutes at 150 rpm. 0.5 M NaOH was added dropwise to the solution to obtain the desired pH of 12. The mixture was stirred for 5 minutes, and a precipitate was obtained and later filtered with Whatman No. 1 filter paper. The precipitate obtained was washed with deionized water and ethanol to eliminate traces of the unreacted precursors. The final product was oven-dried at 105ºC for 45 minutes and finally calcined in the furnace at 450ºC to obtain CuO nanoparticles.

Synthesis of chitosan/CuO nanocomposites
The chitosan/CuO nanocomposite was prepared using a wet impregnation method. Firstly, 5.0 mg of as-prepared chitosan was measured into a 250 cm^3 beaker containing 50.0 cm^3 of de-ionized water, followed by stirring for 1 h at 150 rpm. Secondly, 5.0 mg of the as-synthesized CuO nanoparticles were mixed with the solution, and the mixture was homogeneously shaken for 2 hours using a mechanical shaker. The resulting mixture was dried in an oven at 80ºCuntil completely dry.

Characterization of chitosan, copper nanoparticles, and their nanocomposites
The copper nanoparticles were characterized by determining their absorption bands by UV-visible spectrophotometry while the phases of the synthesized copper nanoparticles and chitosan-copper nanocomposites were identified using Bruker AXS D8 Advance X-ray diffractometer with Cu Kα radiation at diffraction angles from 10º to 90º. The phase identifications were made by comparison with available d-spacing information and peaks from the Joint Committee on Powder Diffraction Standard (JCPDS).

RESULTS AND DISCUSSION
U-v spectrum of the synthesised copper nanoparticles
The copper nanoparticles were efficiently synthesised using a modified sol-gel method with visual observation of colour change from blue to green. The UV–vis absorption spectrum of copper oxide nanoparticles is given in Figure 1. It shows a peak at 245 nm which is attributed to the formation of copper oxide nanoparticles and in close agreement with the absorbance peak at 248 nm earlier reported by Junejo *et al* (2023) in their synthesis of copper oxide nanoparticles using his *Grewia asiatica* L. extract.
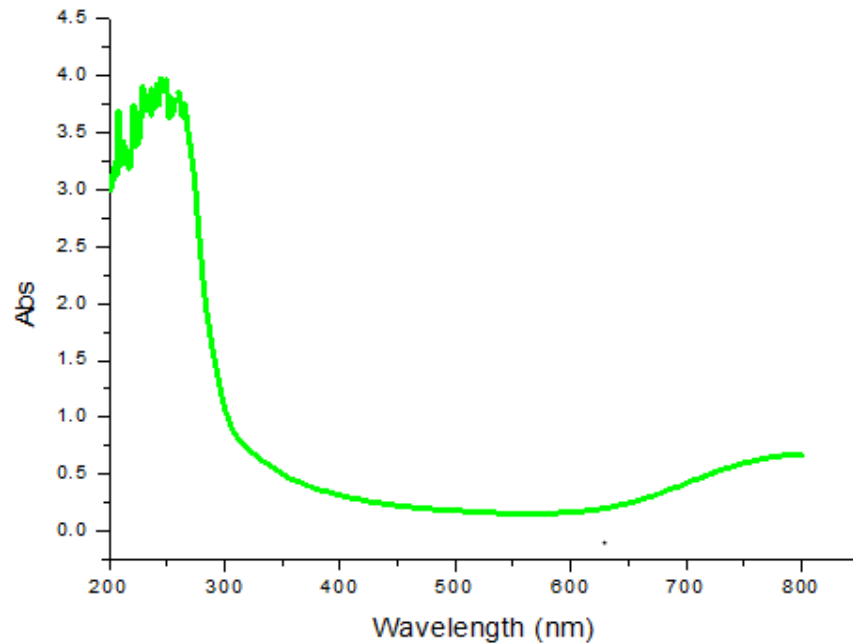
Figure 1: UV–Vis spectrum of copper nanoparticles

X-Ray diffraction (XRD) analysis of chitosan, CuO nanoparticles, and chitosan/CuO nanocomposites

The phase structures of the chitosan, CuO nanoparticles, and chitosan/CuO nanocomposites were investigated using XRD, and their diffractogram are presented in Figure 2. From Figure 2(a), the XRD pattern of the chitosan displayed two main diffraction peaks at 2θ of 12.56°, and 19.92° corresponding to planes (020) and (110) typical of semi-crystalline chitosan. These two peaks could be related to crystals in the chitosan structure and attributable to a high degree of crystallinity of the prepared chitosan. This was supported by Huang *et al* (2020) as the two characteristic crystalline peaks of chitosan at 9-10° and 19-20° were lower than their reported crystallinity. The crystallinity index (CI) of the chitosan was calculated using Equation (1).

$$\text{Crystalline Index (CI)} = \frac{(I_{110} - I_{020})}{I_{020}} \times 100 \qquad\qquad (1)$$

The crystalline index of chitosan was calculated from the diffraction pattern, and the value was 64.35 %. Pădurețu *et al* (2019) reported that the peaks at 10.5° and 19.9° for the extracted chitosan were identified. The calculated crystallinity index for the chitosan sample was 42.0 %. The results compared with this study indicated that the deacetylation could be responsible for the crystalline peaks shifting to a slightly higher 2θ angle. The processing conditions, such as temperature, duration of the processing, solvent selection, and drying methods of chitosan, could also affect the crystallization process and crystallite growth. The crystallinity development within the polymer may be attributed to chitosan structural regularity, polarity, the presence of strong hydrogen bonds, and the capacity to pack its chains. However, the presence of other peaks in the diffractogram of chitosan could be attributed to processing steps or other minerals present as components of the crab shells due to the fact that crab shells consist of layers of micronutrients.

Figure 2(b) depicts the XRD pattern of CuO nanoparticles. The diffraction peaks of 2θ values of 32.72°, 35.9°, 38.97°, 48.74°, 53.62°, 58.34°, 61.70°, 66.20°, 68.11°, 72.54°, and 75.44° correspond to the (110), (101), (002), (211), (112), (310), (202), (-113), (220), (-311), and (222) planes of CuO, respectively. These peaks indicated the formation of phase purity of Cu nanoparticles with a monoclinic crystal structure. The estimated crystallite size of the synthesized CuO nanoparticles was 40.18 nm using Debye-Scherer's equation (2). The average crystallite size was observed at approximately 37.08 nm for CuO nanoparticles, as Siddiqui *et al* (2021) reported. The disparity in the crystallite sizes could be due to reaction parameters such as temperature, time, precursor concentration, and pH, which influence the formation and growth of nanoparticles.

$$D = \frac{k\lambda}{\beta \cos\theta} \qquad\qquad (2)$$

Where D is the crystallite size, k is the Scherrer constant which is equal to 0.89, λ is the wavelength of the X-ray which is equal to 0.154 nm, and β is the full width at half maximum (FWHM) of the observed peak, and θ is the Bragg angle.

Figure 2(c) presents the XRD pattern of chitosan/copper oxide nanocomposites with two characteristic peaks of chitosan at 12.56° and 19.92° as reported in early. On the other hand, the diffractogram showed the existence of the same characteristic peaks of both chitosan and CuO nanoparticles, but broader than those of individual components, indicating evidence of interaction of CuO molecules with the chitosan. A similar result was established by Aljuhani *et al.* (2021), who synthesized chitosan/CuO nanocomposites via a simple solution casting method. The crystallite size was calculated by applying the Debye Scherrer formula on the XRD pattern and was found to be 28.11 nm. The degree of crystallinity (56.40 %) varied within the nanocomposites compared to the bared chitosan. The presence of crystalline CuO nanoparticles influences the crystallinity of the overall nanocomposite structure. The decrease in the intensities of the diffraction peaks of the chitosan on loading CuO nanoparticles in the polymer matrix could be due to the reduction of intramolecular and intermolecular hydrogen bonds of the chitosan, thus hindering the crystalline growth of the polymer. It can be further explained by interstitial sites that occupied substitute sites in the CuO lattice by minerals in chitosan, changing the crystal structure of the material.
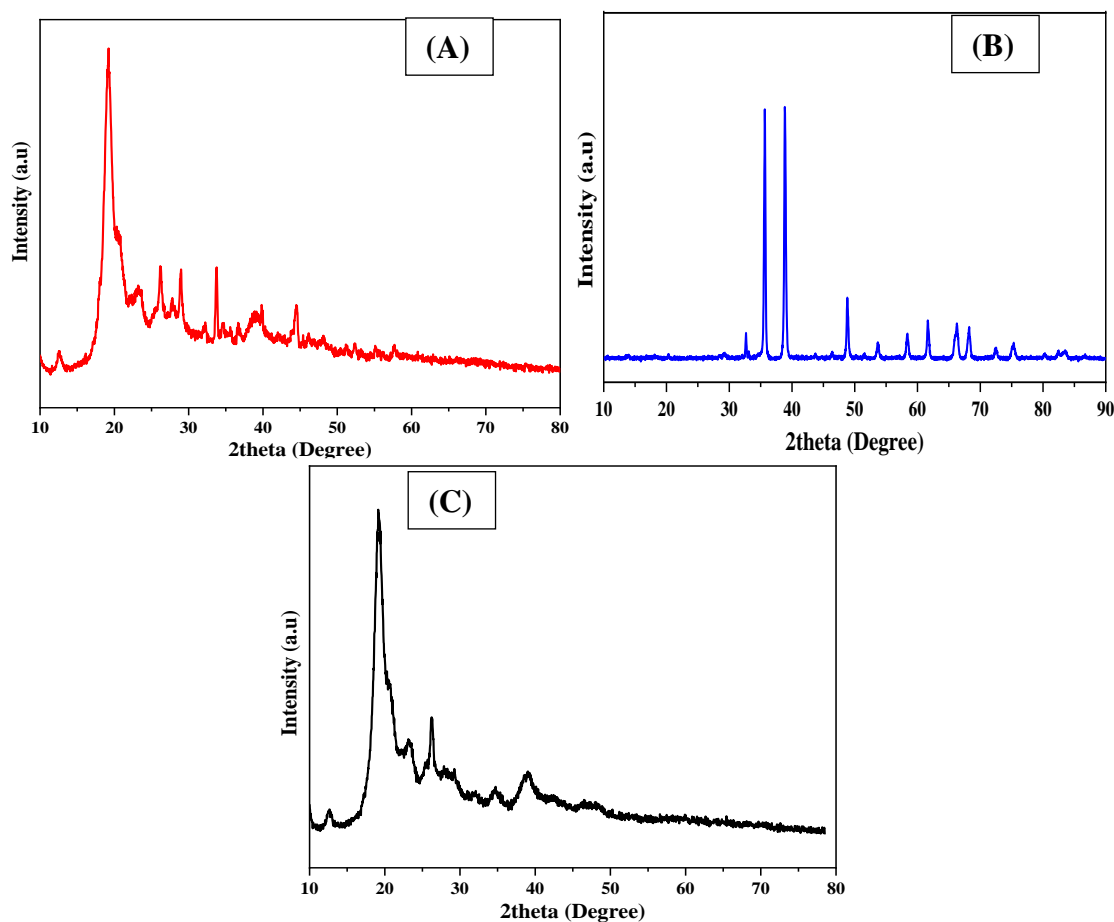
Figure 2: The XRD Patterns of the (a) Chitosan, (b) CuO nanoparticles and (c) Chitosan/CuONanocomposites

CONCLUSION

It is vital to prepare a more thermally stable and innovative chitosan-metal oxide nanocomposite to add to the list of biomaterials. In this work, chitosan copper oxide nanocomposite was prepared through impregnation of chitosan polymer matrix with copper oxide nanoparticles using a simple wet impregnation method. The UV spectrum confirmed the formation of copper nanoparticles while the XRD pattern of chitosan/copper oxide nanocomposites showed the existence of broader characteristic peaks of both chitosan and CuO nanoparticles indicating an interaction of CuO molecules with the chitosan.

REFERENCES

Aljuhani, A., Riyadh, S. M., & Khalil, K. D. (2021). Chitosan/CuO nanocomposite films mediated regioselective synthesis of 1, 3, 4-trisubstituted pyrazoles under microwave irradiation. *Journal of Saudi Chemical Society*, 25(8), 101276.

Aranaz, I., Alcántara, A. R., Civera, M. C., Arias, C., Elorza, B., Heras Caballero, A., & Acosta, N. (2021). Chitosan: An Overview of Its Properties and Applications. *Polymers*, 13 (19), 3256. https://doi.org/10.3390/polym13193256.

Herdiana, Y., Wathoni, N., Shamsuddin, S., & Muchtaridi, M. (2021). Drug release study of the chitosan-based nanoparticles. *Heliyon*, *8*(1), doi.org/10.1016/j.heliyon.2021.e08674.

Huang, L., Bi, S., Pang, J., Sun, M., Feng, C., & Chen, X. (2020). Preparation and characterization of chitosan from crab shell (Portunustrituberculatus) by NaOH/urea solution freeze-thaw pretreatment procedure. *International journal of biological macromolecules*, 147, 931-936.

Junejo, F., Aziz, A., Abbas, A., Zehra, K. E., Bhutto, A. A., Ahmed, T., Rehman, F. U. (2023). Ecological fabrication of copper oxide nanoparticles for enhanced photocatalytic degradation of methylene blue and *rhodamine* B. Dye, *Inorganic Chemistry Communications*, 158, 1, doi.org/10.1016/j.inoche.2023.111547.

Matei, E., Predescu, A. M., Râpă, M., Țurcanu, A. A., Mateș, I., Constantin, N., & Predescu, C. (2022). Natural Polymers and Their Nanocomposites Used for Environmental Applications. *Nanomaterials (Basel, Switzerland)*, *12*(10), 1707. https://doi.org/10.3390/nano12101707.

Mikušová, V., & Mikuš, P. (2021). Advances in Chitosan-Based Nanoparticles for Drug Delivery. *International Journal of Molecular Sciences*, *22* (17), doi.org/10.3390/ijms22179652.

Okogwu, O. I., Elebe, F. A., & Nwonumara, G. N. (2021). Fish types, breeding grounds and migratory routes in Akwa Ibom State, Nigeria. *The Zoologist*, 19: 38 – 45, http://dx.doi.org/10.4314/tzool.v19i1.6.

Pădurețu, C. C., Isopescu, R., Ră'u, I., Apetroaei, M. R., &Schröder, V. (2019). Influence of the parameters of chitin deacetylation process on the chitosan obtained from crab shell waste. *Korean Journal of Chemical Engineering*, 36, 1890-1899.

Santos, V. P., Marques, N. S. S., Maia, P. C. S. V., Lima, M. A. B., Franco, L. O., & Campos-Takaki, G. M. (2020). Seafood Waste as Attractive Source of Chitin and Chitosan Production and Their Applications. *International Journal of Molecular Sciences*, 21(12), doi.org/10.3390/ijms21124290.

Siddiqui, V. U., Ansari, A., Chauhan, R., & Siddiqi, W. A. (2021). Green synthesis of copper oxide (CuO) nanoparticles by Punicagranatum peel extract. *Materials Today: Proceedings*, 36, 751-755.

Bacteriological Analysis of Water from Poultry Farms within Dutsin-Ma Town

*Tasiu Sulaiman, Bishir Muhammad and Khalifa Jamil Saleh

Department of Microbiology, Faculty of Life Science, Federal University Dutsin-ma, Katsina State.
*Corresponding author's email address: <u>teesulyman@gmail.com</u>

ABSTRACT
This study aimed to investigate the bacteriological quality of poultry water from different poultry farms within Dutsin-ma, Katsina State, Nigeria. Samples of poultry water were collected from seven different locations within the area used for rearing poultry. The Water samples were analyzed for Total Bacterial count, Total coliform count and Isolation and Identification of Indicator organisms using standard microbiological techniques. The results for Bacterial count showed that Unguwar Alkali, Unguwar Abba Jaye, Kadangaru and Hayin Gada had the highest bacterial load of $(8.25 \times 10^1 \text{cfu/ml})$, $(7.96 \times 10^1 \text{ cfu /ml})$, $(7.2 \times 10^1 \text{ cfu /ml})$, and $(6.72 \times 10^1 \text{ cfu /ml})$ respectively. While FUDMA Farm had $(1.0 \times 10^3 \text{ cfu /ml})$, Isah Kaita Farm $(1.72 \times 10^2 \text{ cfu /ml})$, and Dangani Farm $(2.02 \times 10^2 \text{ cfu /ml})$ recorded the least bacterial load respectively. The total viable bacterial count ranged from $(4.7 \times 10^3 \text{-} 5.9 \times 10^3 \text{cfu/ml})$ while the Total Coliform count ranged from $(1.3 \times 10^3 \text{-} 3.9 \times 10^4 \text{cfu/ml}$. *Staphylococcus aureus* and *Escherichia coli* were the most prevalent bacteria species in the samples with prevalence of (23.33%) each, while *Salmonella* spp. had the prevalence of (21.62%). There was no significant difference in the viable count of bacteria between the five locations. The results reveal that the water quality for poultry rearing within these locations are above the WHO acceptable limits. This suggests that interventions such as adequate chlorination and proper treatment of the samples should be employed to meet the standards set by the World Health Organization.
Keywords: Water, Water Quality, Water borne Pathogens, *Escherichia coli*

INTRODUCTION
Over the past decade, meat consumption increased significantly, worldwide. This was mainly driven by the poultry meat sector, which represents two-thirds of the additional meat consumed. Nowadays, the breeding of poultry is a huge market: in 2021 about 100 million tons of chicken meat were produced worldwide, and in 2022 a slight increase is expected. A similar trend was observed in Europe, as represented in Fig. on the right. After the USA, which in 2021 produced 20.4 million tons of chicken meat, the other largest producers are Brazil and China, with 14.5 and 14.7 million tons respectively. In Europe, the first producer is Poland (20% of total European production) followed by Spain, France, Germany and Italy, as shown in Fig. on the right. Egg production is equally relevant for poultry breeding: between 2000 and 2015, the world egg production increased of about 39%, reaching 1338 bilion eggs consumed per year (Abdullahi et al.2010).

In industrialized countries, every year 30% of the population is affected by diseases transmitted by food. Just in Italy, the estimates are 300 000 cases per year but the statistics underestimate the real incidence of these diseases (World Health Organization, report data 2008). In order to protect public health, the food authorities put a huge effort in reducing these human infections caused by different microorganisms. Food safety management is implemented through the adoption of preventive measures aimed at minimizing, as far as possible, contamination and development of pathogenic microorganisms at every stage of the food chain. These methodologies are collected in general food safety management systems - the most common are the Hazard Analysis and Critical Control Points (HACCP) and the Good Hygiene Practices (GHPs). Food safety is only guaranteed if these measures are applied in every phase of the production process: breeding, transport, processing, distribution, sale and last but not least the preparation for consumption. Indeed, since it takes several steps to bring food from farm to fork, the contamination with zoonotic agents can occur at any point in the process (Agada et al. 2014).

Poultry is a source of food that has been accepted worldwide through the ages. The consumption of poultry products is increasing every year and consumers want a safe product, thus it is pertinent that the poultry producers achieved this goal .Often, poultry products are involved in human foodborne poisoning/diseases posing a considerable cost and threat to public health (International Consultative Group on Food Irradiation, 2000; Ventura daSilva, 2016; Sule and Ilori, 2018). Increase in contacts of poultry with microbes lead to increased contact rates with humans and open new avenues for introduction, proliferation, and transmission of pathogens; and ultimately more threats to public health (The PEW Charitable Trusts, 2016). Two major poultry systems in Nigeria and Sokoto in particular are the Deep litter (DL), where birds are reared in restricted houses; and Battery cage (BC), where birds are reared in cages (Adam, 2019). Therein, quality water is essential for proper production and safety of poultry health and consequently public health (Folorunso et al., 2011; Abbas et al., 2008). Water make up large proportion of the body of chicken, from 55-

75 percent, they cannot thrive without it comparatively to the feed for a long time; that is why they consume circa 1.5-2 fold of water than feed (Abbas et al., 2019). Water is used in electrolyte replacement therapy, treatment with drugs, and cleaning among others. But the quality of drinking water in poultry can be jeopardized as a result of diverse things .Parable, the source (well or pipe), poor cleaning and maintenance of drinkers, regurgitated feed by the birds, chicken feed, chicken conduct, rearing sites, faeces, antimicrobials or drugs ,and knowledge of rearers (Folorunso *et al*., 2016; Oviasogie *et al*., 2018). Consequently, the objective of this paper was to determine the bacterial quality of drinking water for layer chicken managed under deep litter (DL) and battery cage (BL) systems in Sokoto, Nigeria (Aderson et al. 2019).

Statement of the research problem
Poultry farming, raising of birds domestically or commercially, primarily for meat and eggs but also for feathers. Chickens, turkeys, ducks, and geese are of primary importance, while guinea fowl and squabs (young pigeons) are chiefly of local interest. This article treats the principles and practices of poultry farming. For a discussion of the food value and processing of poultry products, see egg and poultry processing.
Recently. the incidence of Salmonellosis have become prevalent among poultry farm which result in high mortality rate, reduce egg production and Wight loss (Scallan and Hoekstra, 2019) thus the occurrence of salmonellosis has affect the goal set by poultry farmer and hence give rise to decrease in meat and egg production.

Justification of the research
Poultry production accounts for a significant percentage of the economic output of some Nigerians, and it is estimated that almost 70% of people derive their protein from poultry. Thus, it is necessary for poultry to be free from dangerous pathogens such as *Salmonellae*. Usually, the water given to poultry is not microbiologically safe, and such contaminated water creates an avenue for health risks, when the poultry utilize the water, subsequently getting infected with the pathogens that ultimately get transmitted to humans.
Worldwide, more chickens are kept than any other type of poultry, with over 50 billion birds being raised each year as a source of meat and eggs. Traditionally, such birds would have been kept extensively in small flocks, foraging during the day and housed at night. This is still the case in developing countries, where the women often make important contributions to family livelihoods through keeping poultry. However, rising world populations and urbanization have led to the bulk of production being in larger, more intensive specialist units. These are often situated close to where the feed is grown or near to where the meat is needed, and result in cheap, safe food being made available for urban communities. Profitability of production depends very much on the price of feed, which has been rising. High feed costs could limit further development of poultry production.

Aim of the research
The aim of this study is to isolate and identify bacterial species from poultry water within Dutsin-ma, katsina state.

Objectives of the research
1. To isolate and identify bacterial species from the sampling location
2. To enumerate total bacterial count of the sample collected
3. To carry out biochemical tests of the isolates

MATERIALS AND METHODS
Study Area
Dutsin-ma is a local government Area (LGA) in katsina state, Nigeria. Dutsin-ma is situated at 12°27'18 N latitude, 7°29'29 E longitude and is 605 meters elevation. The LGA has an area of 527 square km and a population of 169,671 at the 2006 census, the postal code of the area is 821. It is one of the respected LGA of katsina State and it's the current learning center of Katsina State. Thus significant amount food produce in other parts of the country found their way to this town for sales and consumption purposes. The vegetation is basically tropical and the climate is characterized by dry November to March and wet April to October seasons. The mean annual rainfall of 1150-1500 mm occurs mainly between May and September with major peak in August.

Sample Size
A total of 50 samples were collected at 8 different farms, within Dutsin-ma area. Incuding Fudma Farm (10 samples), Isah Kaita Farm (10 samples), Dangani Farm (10 samples), Unguwar Abba Jaye (5 samples), Kadangaru (5 samples), Ungyuwar Alkali (5 samples), Hayin Gada (5 samples).

Sample Collection and Processing
Sterile container was used to collect the sample of poultry water and labeled for bacteriological studies the sample was analyzed at FUDMA microbiology laboratory within six hours from time of collection.

Enumeration of Coliforms
Bacteriological analysis was carried out for indicator organisms; total and fecal coliform (*E. coli*) by most probable number (MPN) method (APHA, 2004). This was carried out according to the three-stage process of presumptive test, confirmed test and completed test.

Presumptive Test
The presumptive test was carried out to screen the water sample for the presence of coliforms. Ten tubes of lactose broth were arranged in two rows. The water sample was in a 100ml screw capped bottle. Both single and double strength lactose broth was prepared. In the preparation of the double strength lactose broth, twice the amount of media required (according to the manufacturer's instructions) was introduced into the appropriate volume of water. The single strength lactose broth was prepared according to manufacturer's instruction (Willey *et al*., 2011). First row containing five tubes of 10ml double strength lactose broth was inoculated with 1ml of the water samples, and the second row containing 5ml single strength lactose broth was also inoculated with 0.5ml of the water samples (Rijal, 2021). The tubes were incubated in an incubator at 44°C for 24 hours. After incubation, the number of bottles in which lactose fermentation with acid coupled with gas formation occurred, considered and counted. Finally, by referring to the probability table (Macrady table), the MPN of coliforms in 100ml water sample was estimated (Cheesbrough, 2006).

Confirmed Test
This test was carried out to determine whether acid and gas production was due to coliform alone and other bacteria. From the tubes which were positive for gas production in presumptive test, a loopful was withdrawn and used to inoculate lactose broth, nutrient agar slants and tryptone water (Cheesbrough, 2006). Lactose broth tubes were incubated at 37°C for 24 hours, and observed for gas formation. If no gas was observed after 24 hours, incubation was extended to 48 hours. Growths obtained from nutrient agar slants were used to prepare smears for Gram staining.

Completed Test
This test was carried out to rule out any false positives from the confirmatory test. Inocula from the tubes positive for gas production were obtained and streaked using a sterile wire loop, onto the surface of two plates of Eosin-Methylene Blue (EMB) Agar. One plate was incubated at 37°C and another at 44°C, both for 24 hours. All plates were observed for the formation of colonies. Coliforms produce colonies with a greenish-metallic sheen, while non-coliforms do not produce any sheen. The presence of colonies with greenish metallic sheen on the plate incubated at 44°C shows the presence of thermo-tolerant *E. coli* (Rijal, 2021).

Isolation and Identification
The bacteria present in the water samples were characterized by following these steps: serial dilution, inoculation on suitable media, culture and incubation, Gram's staining and biochemical tests. These were explained in details below:

Serial Dilution
The water samples were serially diluted using the procedure adopted from Cheesbrough (2006). Six tubes were arranged in a test tube rack and used for the dilution. From the water samples, 1ml was withdrawn using a sterile syringe and introduced into a test tube containing 9ml of sterile distilled water, to make the 10^{-1} dilution. The test tube was gently homogenized to ensure even mixing of the aliquot and the diluent. Thereafter, successive dilutions were made into 5 subsequent tubes, by withdrawing 1ml from each tube, and introducing it into the next, until 10^{-2}, 10^{-3}, 10^{-4} and 10^{-5} dilutions were obtained (Willey *et al*., 2011).

Cultural Identification
Sterile wire loops were used to withdrawn 0.1ml of each dilution from the 10^{-6} dilutions of the samples, which were subsequently inoculated onto the prepared solid culture plates. The prepared culture plates were inoculated onto the prepared media. The plates were incubated aerobically at 37°C for 24 or 48 hours, depending on the medium used. Formation of colonies and the physical appearances were observed and recorded.

Morphological Identification

The morphological features of the organism were observed by assessing the colonies appearance, such as form, texture, consistency, shape, pigmentation, margin and elevation of the obtained colonies.

Gram stain

The procedure of Cheesbrough (2006) was used, as follows: smears of the isolates were prepared from the overnight culture plates on a clean glass slide, and allowed to air dry. These were then fixed by passing the slide three (3) times through the flame of a Bunsen burner. The slide was then allowed to cool before staining. Crystal violet stain was added to the smear for 30-60 seconds. The plates were then washed using tap water. Lugol's iodine was added for 1 minute, and then washed using tap water. The slides were decolorized rapidly for 15 seconds with acetone alcohol and then immediately washed using tap water. The back sides of the slides were wiped clean and placed in a staining rack for the smear to air dry. Drops of oil immersion (100x) was added to the dried smears and examined under the electron microscope (Wiegel, 1992).

RESULTS AND DISCUSSION

Table 1: Occurrence prevalence of bacteria isolated from the samples

ORGANISMS	OCCURRENCE	PREVALNECE (%)
Staphylococcus aureus	20	22.72
Salmonella spp.	26	29.54
Klebsiella pneumoniae	6	6.81
Staphylococcus epidermidis	8	9.09
Escherichia coli	26	29.54
Staphylococcus saprophyticus	2	2.27
TOTAL	88	100%

The table below shows the number of colony count from each farm, where the Unguwar Alkali has the highest number of colony which is 8.25×10^1 CFU/ML, and Fudma farm have the lowest number of colony count which is 1.0×10^3 CFU/ML. These result shows that the poultry found in different locations not from the farm have the highest occurrence of bacterial species.

Table 2: Bacteria colony count in relation to farm

S/No.	Sample location	Number of samples	Mean bacterial count (cfu/ml)
1	Fudma Farm	10	1.0×10^3
2	Isah Kaita farm	10	1.72×10^2
3	Dangani farm	10	2.04×10^2
4	Unguwar abba jaye	5	7.96×10^1
5	Kadangaru	5	7.2×10^1
6	Unguwar alkali	5	8.25×10^1
7	Hayin gada	5	6.72×10^1

Table 3: Isolates

Isolates	Morphology	Gram reaction	IN	MR	VP	C	CAT	COG	H2S	GLU	SUC	FRU	GAS	MOT	Suspected organism
1	Cocci	+ve	-ve	-ve	+ve	NA	+ve	+ve	-ve	+ve	+ve	-ve	+ve	+ve	*Staphylococcus, E coli*
2	Cocci	+ve	+ve	-ve	-ve	NA	-ve	-ve	+ve	+ve	-ve	+ve	-ve	-ve	*Staphylococcus,corynebacterium*
3	Cocci	+ve	-ve	+ve	+ve	NA	+ve	+ve	-ve	+ve	+ve	+ve	+ve	+ve	*Staphylococcus, salmonella*
4	Cocci	+ve	NA	-ve	NA	-ve	-ve	+ve	NA	-ve	NA	NA	NA	+ve	*Staphylococcus, E coli.*
5	Rod	+ve	NA	NA	NA	NA	-v	-ve	NA	NA	NA	NA	NA	+ve	*Staphylococcus pyogens*
6	Cocci	-ve	+ve	-ve	+ve	+ve	NA	NA	-ve	+ve	+ve	+ve	-ve	+ve	*Klebsiellapneumoniae, salmonella*
7	Cocci	+ve	NA	NA	NA	NA	+ve	+ve	NA	NA	NA	NA	NA	NA	*Staphylococcus, corynebacterium*
8	Chain	-ve	+ve	-ve	+ve	-ve	-ve	-ve	-ve	+ve	-ve	-ve	+ve	-ve	*Klebsiellapneumoniae*
9	Baccili	+ve	NA	NA	NA	NA	+ve	+ve	NA	NA	NA	NA	NA	NA	*Corynebacterium*
10	Cocci	-ve	+ve	-Ve	+ve	+ve	NA	NA	-ve	+ve	+ve	+ve	-ve	+ve	*Klebsiellapneumoniae, E coli*
11	Chain	-ve	-ve	-ve	+ve	+ve	-	-	-ve	+ve	+ve	+ve	-ve	+ve	*Klebsiellapneumoniae, Salmonella*
12	Cocci	+ve	+ve	+ve	-ve	-ve	-ve	-ve	-ve	+ve	-ve	-ve	NA	+ve	*Salmonella, E coli, S epidemidis.*
13	Cocci	+ve	+ve	-ve	+ve	+ve	-ve	-ve	+ve	+ve	+ve	+ve	NA	+ve	*Klebsiellapneumoniae, staphylococcus*
14	Cocci	+ve	NA	NA	NA	NA	-ve	-ve	NA	NA	NA	NA	NA	+ve	*s.epidemidis s.saprophyticus*
15	Rod	+ve	+ve	+ve	+ve	-ve	-ve	-ve	-ve	+ve	-ve	+ve	NA	-ve	*Salmonella, staphylococcus.*
16	Cocci	+ve	-ve	-ve	+ve	+ve	-ve	-ve	NA	+ve	-ve	+ve	-ve	-ve	*Klebsiellapneumoniae, E coli*
17	Cocci	+ve	NA	NA	NA	NA	-ve	-ve	NA	NA	NA	NA	NA	NA	*s.epidemidis s.saprophyticus*

Keys

1. I- Indole
2. H2S- Hydrogen sulfide
3. TSI- Triple Sugar Iron
4. + = Positive
5. - = Negative
6. GR- Gram Reaction
7. MR- Methyl Red
8. C- Citrate
9. CAT- Catalase
10. COG- Coagulase
11. FRU- Fructose
12. MOT- Motility
13. VP- Vogue-Proskauer

Discussion

This research was conducted isolation and identification of bacterial species from poultry water of different poultry farms within Dutsin-ma Town. Sampling and detection was predominantly by research. The result for each sample and overall was recorded. Isolation and identification of bacterial species from poultry water Substantial economic losses were manifested through mortality and poor growth of infected animals as well as the hazard of transmission to humans either through food chain or direct animal contact (Radkowski, 2011).

The finding reveals the higher bacterial count in some poultry farms which is almost similar with the findings of (Radkowski, 2011). The higher bacterial observed indicate high level of contamination. Although some farms were found to have low bacterial count this is similar to the findings (LI *et al*., 2015). This might be due to improvement in sanitations of the poultry farms as indicated by (Gordana *et al*., 2018).

 The research shows that most of the poultry water investigated is conducted isolation and identification of bacterial species from poultry water. to some extent (either slightly or highly contaminated). The isolates are similar to the findings of Agada (2018).

CONCLUSION

The result of this study revealed that higher level of isolation and identification of bacterial species from poultry water, also the presence of *Salmonella* spp and Campylobacter from water sample means that the direct consumption of such water without treatment may be very risk. Also is one of the major pathogen both in developing and developed countries. The role of animals particularly food animals in *Salmonella* and Campylobacter cycle have been recognized (Ashblot, 2017).It is well established that poultry are the major reservoirs and most infections in animals are symptomless. The rate of occurrence of infections in poultry is reflected by the frequency with which the organisms can be detected in poultry and their products.

RECOMMENDATION

Base on the research conducted, the following recommendations were given:
   i.   Avoid cross contamination or used of untreated water which is source of the bacterial infection in a poultry
   ii. The area in which the water is collected and containers through which the water is fetched and stored should always be clean to avoid the harmful microorganism.
   iii. Proper treatment of water to consumption.
   iv. Avoid overcrowding of poultry and isolate the infected once.
   v.   Use of antibiotics such as fosfomycin (FOS), tetracycling, ciprofloxacin, norflaxacin, and ampicillin is administrate for treatment of bacterial species especially *salmonella* spp.
   vi. Introduction health education for farm workers and promoting good hygiene in poultry farms
   vii. Treating infected animals that may be the source of infection within the hatchery and husbandry farm
   viii. .Further studies are needed to investigate the relation between bacterial species and public health in Dutsinma LGA of Katsina State.
   ix. The application of quick diagnostic procedures (e.g. PCR) are needed to trace sources of infection and help in quick diagnosis

REFERENCES

Abdullah, K., Bedik, O., Kocak, N., Levent, B., Eyigun,C., Tekbas, O., Gorenek, L., Baylan, O. and Basustaoglu, A., (2010). Analysis of an outbreak of Salmonella enteritidis by repetitive sequence based PCR and pulsed. *Field gel electrophoresis international medicine,* 49:458-498.

Advisory Committee on the Microbiology Safety of Food (2001). Second report on Salmonella in egg. London: *The stationary office.*

Agada, G. Abdullahi, I. O., Odugbo, M., Chollom, S.C., Kumblish, P.R and Okwori, A.J.(2014). Prevelance and Antibiotic Resistance Profile of Salmonella isolate from commercial poultry and poultry handle in Jos, *Plateau State Nigeria. Microbiology* 4: 462-479.

Anderson, N.L., et al. cumitect 3B: Quality System in the Clinical Microbiology Laboratory. Coordination ed., A.S Weissfeld. American Society for Microbiology, Washington, D.C.

Ashblot NJ (2004) Microbial contamination of drinking water and disease outcome in developing region. *Journal of Toxicology* 1989 (1-3):229-238.

Available at: http//www.who.int/entity/foodsafety/publications/micro/en/Salmonella.pdf

Binder, E.M, Tan, L.M, Chin, L.J, Handl, J., and Richard, J. (2007) "Worldwide occurrence of mycotoxins in commodities, feeds and feed ingredients. Animal Feed Science and Technology, 136(3-4), 265-282. Borland, E.D. (2002). Salmonella infection in poultry. *Veterinary Record*, 97, 406-408.

Boyer, C.L, Burner, D.W. and Brown, J.A. (1985). Salmonella organisms isolated from poultry feed. Avian Diseases, 2, 396-401. Brown, P. Will, R. Brandley G, Asher D.M. and Detwiler, L. (2001). Bovine spongiform encephalophathy and variant creutzfeilt jacob disease, background, evaluation and current concerns. *Emerging Infectious Diseases,* 7(1), 6-16.

Bryan, F.L. and Doyl, M.P. (1995). Health risk and consequences of Salmonella and Campylobacter jejuni in raw poultry. *Journal of Food Protection*, 58, 326-344.

Callaway, T. R., Keen, J. E., Eddington, T. S., Baumgard, L. H., Spicer, L., Fonda, E.R., Griwoid, K. E., Overtones, T.R., Van Amburgh, M. E., Anderson R.C., (2005) fecal prevalence and diversity of *Salmonella* species in lactating dairy cattle in Four State. *J. Dairy sci.* 88, 3603-3608.

Center for Disease and Control. (2002). Investigation Update: Multistate Outbreak of human Salmonella Enteritidis by repetitive sequence based PCR and pulsed. *Field gel electrophoresis .medicine* 49:31-36.

Cheesebrough, M (2002). District laboratory manual for tropical countries part 2. *Cambridge low price edition pp 172*-184.

Cheesebrough, M (2006). District laboratory manual for tropical countries part 4. *Cambridge low price edition pp* 29-36.

Ebel E., and Schlosser W., (2000). Estimating the annual fraction of egg contaminated with Salmonella enteritidis in the United State. *International Journal of Food Microbiology.* 61:51-62.

Ecoli and *Salmonella* Isolated from cattle and man .proceeding of the 4th Int. *Sci Cong. Mansoura; 2005 April 5-6*; *Mansoura, Egyp: Mansoura University;* 303-310.

European Commission. (2004). Trends and source of zoonotic agent in animal, feeding stuffs, *food and man in the European Union and Norway in 2002*. SANCO/29/2004

European Food Safety Authority. (2004). Opinion of the scientific panel on biological hazard on a request from the commission related to the use of vaccine for the control of Salmonella in poultry. *The European Food Safety Authority Journal.*114-174.

Food and Agriculture Organization/World Health Organization (2002) Microbiology Risk Assessment Series No.2 *Risk Assessment of Salmonella in Eggs and Broiler Chicken.*

Gordane, M., Bogdanka, A., Dragica, T., Milena, L and Brankica, D. (2012). Antibiotic Susceptibility of Salmonella spp; A comparison of two survey with a 5 years interval. *J Imab. Annual proceeding (scientific paper).* 18:216-219.

Jay J., (1991). Food borne gastro enteric caused by Salmonella, Shigella and Escherichia in: *Modern food microbiology*, 4th: edition, chapman and Hall, New York, 553-582.

Kleven SH and Yoder HW (1998). A laboratory Manual for the Isolation and Identification of Avian Pathogen. 4th edn. *American Association of Avian Pathology Kennett Square. pp* 74-88.

MacFaddin J. F. (1980). Biochemical test for Identification of Media Bacteria. Williams and Wilkins Edition. *Williams and Wilkins Publishers, Baltimore.* Pp. 1293.

Maciorowski, K. G., Jones, F. T., Pillai, S. D. and Ricke, S. C. (2004). Incidence, sources and control of foodborne Salmonella spp. in poultry feed. *World's Poultry Science Journal.* 60:465:765

Mead, G.C., Hudson, W.R., and Hinton, M.H. (1993). *Microbiological survey of five poultry processing plants in the UK. British Poultry Science,* 34, 497-503.

Mullner, P., Jones, G., NSoble, A., Spencer,S. E., Hathaway, S. and French, N. P. (2009). Source attribution of food.borne zoonoses in *New Zealand: a modified half model. Risk Analysis* 29:970-984

Nyamongo, J., and Okioma, M. (2005). The aflatoxin outbreaks in Kenya in 2004 and 2005: a case study, *in Proceedings of the Conference on Reducing Impact of Mycotoxins in Tropical Agriculture with Emphasis on Health and Trade in Africa, Accra, Ghana. 3. Ogbulie, J.N*

Oyeleke, S.B and Manga S.B (2008). *Essential of laboratory practical in microbiology (1st edition) tobes publisher niger state*. Pp 36-58.

Popoff M., Bockemuhl J., Brenner F., (2001). Supplement 2000 (no. 44) to the Kauffmann. *White scheme. Research in Microbiology.* 152: 907-909.

Radkowkis M. (2001). Occurrece of Salmonella spp. In consumption egg in Poland. International *Journal of Food Microbiology*. 64:189-909.

Salman, A.M., Tanios A.T (2004). Biological and immunological studies on heat- labile enterotoxins of salmonella recovered from diarrheic calve. Proceeding of the 1st international conference Vet. Res. Div. Feb 15-17; *Cairo, Egypt National Research Center,* pp. 149-160.

Scallan, E.and Hoekstra, R.M., (2011). *Food borne illness acquired in the United State. mojor pathogens. Emerged. Infect.* Dis.17:7-15.

Stotzky, G. (1997). Soil as an environment for microbial life. In: Van Elsas, J. D., Trevors, J. T., Wellington, E. M. H. (Eds), *Modern Soil Microbiology. Marcel Dekker, Inc., New York, NY, pp.* 1-20

Taylor R., Sloan D., Cooper T., (2002). A waterborne outbreak of S. saintpaul. *Communicable Disease Intelligence.* 24:336-240.

Taylor, S. E., Klein, L. C., Lewis, B. P., Gruenewald, T. L., Gurung, R. A. R., & Updegraff, J. A. (2000). Biobehavious response to stress *Psychological Review*, 107-411-429.

Utrarachkij, F.,/pornraungwong, S.,/ siripanichgon, K.,/ Nakajima, C.,/ Suzuk Y. and Suthienkul. O (2012). Possible horizontal transmission of *Salmonella* via reusable. *International. Journal FoodMicrobiology*. 154:73-78.

Yan S., Pendrak M. and Abela. Ridder B., (2003). An overview of salmonella typing public health perspective. *Clinical and Applies Immunology* Review. 4:189-204.

Antimalarial and Antioxidant Activities of Lumefantrine Formulation on *Plasmodium Berghei* Infected Mice

*[1]Aderounmu Ibrahim Ganiyu, [1]Benjamen Maina Yohanna, [1]Ali Siddiq Idoko, [1]Balkisu O. Abdulrahman and [2]Jubril Olayinka Akolade

[1]Department of Biochemistry and Molecular Biology Federal University Dutsin-Ma, Katsina State, Nigeria.
[2]Biotechnology Advanced Research Centre, Sheda Science and Technology Complex, Sheda, Abuja.
*Corresponding author. E-mail: gaibrahim@fudutsinma.edu.ng Phone: +2347032779391

ABSTRACT
Antimalarial drug resistance is one of the greatest challenges towards eradicating malaria. Exploring new combination therapies can overcome the challenges of antimalarial resistance. The present study examined the antimalarial and antioxidant activities of lumefantrine formulated with polyethylene glycol (LUM-PEG) on *Plasmodium berghei* infected mice. Mice weighing 27 ± 2.5g were randomized into five groups of seven mice per group. Group 1 received dimethyl sulphoxide, group 2 (infected 1×10^7 *Plasmodium berghei* and untreated), 4 and 5 were infected and treated with chloroquine, lumefantrine and LUM-PEG respectively. Thin blood smears were prepared 72 hrs after inoculation with parasites and after 3 days' treatment, blood samples were collected for biochemical analyses. Data obtained were subjected to statistical analysis. There was no significant ($p>0.05$) difference in percentage parasitaemia in all the groups compared to the control after 72hrs inoculation. Parasitaemia reduced significantly ($p<0.05$) in the treatment groups producing 22.89%, 26.27%, and 18.81% parasitaemia in chloroquine, lumefantrine and LUM-PEG respectively compared to untreated group and corresponding parasitaemia inhibition recorded were 50.94, 44.14 and 59.64 in treated groups respectively. Untreated groups showed significant increased ($p<0.05$) in white blood cell count, lymphocyte and granulocyte while decrease hemoglobin, red blood cell count, haematocrit, mean corpuscle haemoglobin and mean corpuscle haemoglobin concentration were recorded. Significant decrease in superoxide dismutase and catalase with increased malondialdehyde in untreated compared to the control. Results indicate that lumefantrine formulation has antimalarial properties and can be used in the treatment of malarial after clinical trials.
Keywords: Antioxidant, antimalarial, polyethylene glycol, lumefantrine, *Plasmodium berghei*

INTRODUCTION
Malaria is an infectious disease that is acquired by the bite of a mosquito vector and is caused by the parasite organism Plasmodium. Plasmodium species include *P. falciparum*, *P. vivax, P. ovalae, P. knowelsi,* and *P. malariae* (Zhang et al., 2016). *P. falciparum* is the pathogen that causes the highest rates of morbidity and mortality. Two key species that are necessary for the malaria life cycle: mosquitos and humans (Woldearegal et al., 2018). The most common clinical symptoms of malaria include shivering, fever, diaphoresis, general discomfort, cephalalgia, and myalgia. After a parasite invasion, the aforementioned symptoms often start to show up one to four weeks later (Kondillis et a*l., 2013)* The most widely used techniques for diagnosing malaria at the moment include microscopy (using either light or fluorescence), immunochromatographic lateral flow assays (commonly referred to as rapid diagnostic tests or RDTs), serology, and nucleic acid amplification techniques (NATs), such as polymerase chain reaction (PCR) and isothermal amplification (WHO, 2012).
In 2019, around 228 million cases of malaria were recorded worldwide. It is estimated that over 90% of all malaria deaths occur in Sub-Saharan Africa (WHO, 2020). One reason for these deaths is that malaria parasite causes life-threatening illnesses and is very common in many Sub-Saharan African countries because of the habitable climate (Antonella et al., 2016). The lack of healthcare access in many areas of Sub-Saharan Africa also leads to an increased number of malaria deaths (CDC, 2020). About 191,106 deaths attributed to malaria were recorded in Nigeria in 2019. In contrast, there were no deaths attributed to malaria in the United States that same year (Max et al., 2019). In 2020, just 4 Sub-Saharan African countries (Nigeria, the Democratic Republic of the Congo, Tanzania, and Mozambique) accounted for over half of all malaria deaths globally (WHO, 2021).
Antimalarial drug resistance is becoming the most difficult hurdle for the success of antimalarial therapy, so scientists are continuously move researching to overcome the problem. Resistant parasite strains will always emerge, requiring the continual generation of new molecules. The novel drugs with a new mechanism of action are entering into clinical trials (Kumar *et al.*, 2018). A polymer-drug conjugate increases bioavailability and biodegradability. Also, polymer-based Nano carriers offer several advantages such as enhanced bioavailability, good biocompatibility, increased drug solubility, and reduced toxicity (Mhlwatika & Aderibigbe, 2018). Pharmacodynamics, pharmacological and pharmacokinetic properties of drugs thus improved when administered as polymer-drug conjugate (Mvango et al.*,*

2018). Polyethylene glycol (PEG) is a synthetic polymer that is well-suited for biomedical applications due to its high solubility in aqueous media, biocompatibility, and good tolerance (Sawant et al., 2008). Because of various drawbacks of present malaria treatment as highlighted above. Hence, this study carried out nanoparticle-based combination therapy of *Plasmodium berghei* infected mice

MATERIALS AND METHOD
Materials
Lumefantrine, PEG and DMSO are products of Sigma-Aldrich Company (USA). The experimental mice and Chloroquine -sensitive *P. berghei* (ANKA strain) donor mice were obtained from ABU Zaria.

Methods
Processing in Supercritical-CO_2 by PGSS
Supercritical fluid apparatus for PGSS were set up as previously described by (Labuschagne et al., 2011). Processing in sc-CO2 was carried out in a Separex pilot-scale reactor (Separex Equipment, Champigneulles, France). Blends of liquefiable PEG were mixed with LUM of varying weight ratios (0.1–0.5). At different times, PEG (24 g), LUM (24 g) and PEG–LUM blends (24 g) were transferred into the PGSS autoclave (0.5 L capacity) which were pre-heated with electrical heaters to 45Ċ and fitted with a mechanically driven stirrer. For polymer-drug processing, was autoclaved and sealed. CO_2 gas was drawn from a standard commercial gas cylinder, and pumped through a chamber, preset to the same temperature of 45Ċ as the autoclave. The autoclave pressure was then set to 80 bar. The polymer–LUM mixture was allowed to liquefy for 30 min and was further stirred for 30 min at 150 rpm. The liquefied product was sprayed and micronized through a 500 mm capillary with a length of 5 mm, into a 10 L expansion chamber at atmospheric pressure. The PGSS-micronized particles were then collected for characterization and further studies.

Experimental Animals
The experimental mice weighing between 22-30g were used for this study. Animals were housed in standard cages placed in well-ventilated housing conditions. They were allowed to be acclimatized for 7 days and were allowed to have access to food and water ad libitum. Animals were properly handled following the criteria outlined in the guideline for the care and use of Laboratory Animals prepared by the institute of Laboratory Animal Research (ILAR, 2011).

Parasite inoculation
Sodium citrate (3.8 g) and 0.5 g of glucose were weighed and dissolved in 100 ml distilled water and kept in a refrigerator until required. 0.2 ml blood was obtained from the tail of a donor mouse of known parasitemia into a sample bottle containing 1ml citrate/glucose solution and mice were infected with an inoculum of 1.5×10^7 of parasitized erythrocytes intraperitoneally.

Animal grouping and extract administration
Thirty-five (35) mice were randomized into five (5) groups containing seven (7) mice each and treated as follows group 1: (Control) received DMSO, group 2 (Negative control infected and received DMSO, group 3: infected and received 25 mg/kg b. w. chloroquine, group 4: infected and received 40 mg/kg b. w. lumefantrine, group 5 infected and received 40 mg/kg b. w. LUM-PEG. Administration was done orally for three days using oral gavage.

Serum preparation
At the end of the administration, the mice were sacrificed after an overnight fast under diethyl ether anesthesia. Blood samples were collected through the abdominal aorta into plain sample container and EDTA containers for Biochemical analysis.

Curative test
The curative test was conducted according to the Rane's test as described by Ryley et al. (1970). Treatment began within 72hrs after intraperitoneal inoculation of mice with the parasite (D3), allowing parasitaemia to be established. The tail blood smears were stained with 10% Giemsa in phosphate buffer (pH 7.2). Percentage parasitemia, and percentage suppression of the parasite multiplication, were determined in line with Peters' test and after the treatment.

Preparation of smear and determination of parasitemia
The tail of the donor mouse was sterilized with cotton wool soaked with ethanol. Citrate glucose solution 1 ml was dispensed into a sterile bottle, and another 1ml in a 2ml syringe. The volume in the syringe were used to collect drops

of blood from the donor mouse and be transferred to the sterile bottle. The syringe and its contents were kept on ice all through the procedure. Appropriate volume was introduced into the Haemocytometer counting chamber and viewed under 100 X magnification. % Parasitaemia and % Inhibition

% parasitaemia $= \dfrac{Number\ of\ parasitized\ RBC}{Total\ number\ of\ RBC}\ X\ 100$

% Chemosuppression $= \dfrac{\%\ Parasitaemia\ in\ Negative\ control - \%\ Parasitaemia\ in\ study\ group}{\%\ Parasitaemia\ in\ negative\ control}\ X\ 100$

Evaluation of haematological indices
The haematological parameters in *Plasmodium berghei* infected mice were done using an automated machine (SYSMX.KX-2ln) haematology analyzer.

Biochemical Analyses
Catalase (CAT), superoxide dismutase (SOD) and malondialdehyde were assays using kits from Randox Laboratories (Antrim, UK) and other reagents.

Statistical analysis
The data were analyzed using Graph pad prism version 5. Then one-way Analysis of Variance (ANOVA) was used to test the statistical differences for the doses within a group, followed by Bonferroni's test for multiple comparisons (p< 0.05) were considered significant in all tests.

RESULTS AND DISCUSSION
Percentage parasitaemia and % inhibition of *Plasmodium berghei* infected mice treated with Lumefantrine formulation
There was no significant difference (p>0.05) in % parasitaemia in all the treatments groups at 72 hours post inoculation of *P. berghei* parasites. However, after 3 days of treatment with CQ, lumefantrine and LUM-PEG, significant decreases were observed in the % parasitaemia (p<0.05) of lumefantrine and LUM-PEG compared to the untreated group. Lumenfantrine-PEG group showed lowest % parasitaemia and the highest % inhibition of parasite multiplication throughout the experimental period (Table 1)

Table 1: Mean percentage parasitaemia and % Inhibition of *Plasmodium berghei* infected mice treated with Lumefantrine formulation

Group	% Parasitaemia					% Inhibition			
	72HRS	Day 1	Day7	Day 14	Day 21	Day 1	Day 7	Day 14	Day 21
Infected untreated	28.43±2.70[a]	40.33±3.29[a]	44.71±3.05[a]	46.10±3.04[a]	47.76±2.97[a]	0.00	0.00	0.00	0.00
Infected + CQ	30.10±2.39[a]	27.89±2.39[b]	25.67±2.33[b]	24.71±2.38[b]	22.89±2.37[b]	31.42	40.61	44.88	50.94
Infected + LUM	28.27±1.62[a]	31.79±1.89[c]	31.14±2.12[c]	29.26±2.20[c]	26.27±2.12[c]	29.21	29.78	35.36	44.14
Infected+ LUM-PEG	31.53±1.33[a]	28.81±1.09[b]	27.21±1.06[b]	25.71±0.88[b]	18.81±1.17[b]	25.21	32.83	42.85	59.64

Values are in means ± SEM three replicates. Means with the same superscripts alphabet within a column are not significantly different P>0.05

Haematological parameters of *Plasmodium berghei* infected mice treated with Lumefantrine formulation
The total white blood cell (WBC) count, lymphocyte (LYM) and total granulocyte (GRAND) in the untreated group showed a significant increase (p<0.05) compared to the control. However, chloroquine and LUM-PEG treated groups show significant decreases (p<0.05) in WBC, LYM, and GRAND compared to the untreated group. There were significant decreased (p<0.05) in red blood cell (RBC), heamoglobin (HGB), heamatocrit (HCT), mean corpuscle hemoglobin (MCH) and mean corpuscle haemoglobin concentration (MCHC) in the untreated group compared to the control. However, RBC, HGB, HCT, MCH, MCHC and PLT in the treatment groups were significantly (p<0.05) higher compared to the untreated group. There was no significant difference (p> 0.05) in MCV level of the untreated group compared to the control group (Table 2).

Table 2: Haematological parameters of *Plasmodium berghei* infected mice treated with lumefantrine formulation

Group	Control	Infected untreated	Infected + Chloroquine	Infected + Lumefantrine	Infected + LUM-PEG
WBC(10³/uL)	4.83±0.17[a]	6.83±0.33[b]	4.63±0.13[a]	5.90±0.00[b]	4.40±0.20[a]
LYM (%)	6.77±0.13[a]	7.600±0.20[b]	5.67±0.17[c]	5.10±0.10[d]	5.47±0.13[e]
GRAND	3.30±0.20[a]	3.77±0.20[b]	2.60±0.1[b]	2.67±0.10[b]	2.80±0.10[a]
RBC(10⁶/Ul)	7.67±0.13[a]	6.10±0.10[b]	5.97±0.03[c]	5.93±0.07[d]	6.17±0.07[b]
HGB(g//dL)	14.40±0.10[a]	13.57±0.13[b]	11.77±0.07[c]	12.27±0.07[d]	11.57±0.03[e]
HCT (%)	44.33±0.1[b]	40.67±1.67[b]	38.33±2.85[a]	34.33±1.33[b]	38.00±1.00[b]
MCV(FL)	88.53±0.43[b]	89.33±0.33[b]	87.73±0.13[a]	85.73±730.23[c]	78.97±0.07[d]
MCH(pg)	30.57±0.47[b]	28.33±0.33[b]	87.73±0.13[a]	85.73±730.23[c]	37.40±0.03[b]
MCHC(g/dL)	31.50±0.20[b]	30.27±0.47[a]	33.13±0.37[c]	34.13±0.32[d]	33.43±0.07[a]
PLT(10³/uL)	188.7±0.33[a]	165.7±0.67[b]	168.3±0.67[c]	187.0±1.00[d]	187.0±1.00[d]

Values are in means ± SEM in three replicates and means with the same superscripts alphabet within a row are not significantly $P>0.05$

Antioxidant parameters of *Plasmodium berghei* infected mice treated with lumefantrine formulation

There was a significant decrease ($p<0.05$) in SOD and CAT activities with increased MDA concentration in the untreated group compared to the control. However, significant increases ($p<0.05$) were observed in SOD and CAT activities with decreased MDA concentration in chloroquine, lumefantrine and LUM-PEG treated groups compared to the untreated group (Table 3).

Table 3: Antioxidant parameters of *Plasmodium berghei* infected mice treated with lumefantrine formulation

GROUP	SOD (U/ml)	CAT(U/ml)	MDA(nmol/ml)
Control	22.27±0.43[a]	11.47±0.23[a]	100.4±0.67[a]
Infected untreated	20.97±0.63[b]	10.30±0.30[b]	183.6±0.30[b]
Infected +chloroquine	50.17±0.30[c]	21.67±1.03[c]	161.6±2.97[c]
Infected +lumefantrine	31.33±0.43[b]	22.27±0.43[b]	121.7±1.20[d]
Infected +LUM-PEG	21.67±0.17[d]	11.03±0.67[d]	173.9±3.97[e]

Values are in means ± SEM in three replicates and means with the same superscripts alphabet within a column are not significantly different $P>0.05$

Discussion

The current study examined the antimalarial and antioxidant activities of lumefantrine formulation on *Plasmodium berghei* infected mice. Unekwuojo et al. *(*2011) reported that *P. berghei* is used in predicting the treatment outcomes of an antimalarial candidate, due to its sensitivity to chloroquine making it an important parasite for this antimalarial study The observed decreased in % parasitaemia with an increase in % inhibition of *P. berghei* parasite in LUM-PEG treated group may be due to the presence of PEG in lumefantrine as PEG has been reported to improve drug efficacy via PEGylation (Xia et al., 2019). This finding agrees with Bobasa et al. (2018) who reported that suppressive and curative tests are effective in the antiplasmodial evaluation of candidate drugs on early and established infections respectively.

White blood cells play a crucial role in the body's immune response to foreign substances. This defence mechanism is commonly facilitated by processes such as leucocytosis and antibody formation (Marrieb, 1995). The observed increase in WBC, LYM and GRAND in the untreated group may be due leuckocytosis and antibody production. This observation is consistent with the findings of Marrieb (1995), who discovered that the presence of leucocytosis in the untreated mice infected with *P. berghei* NK65 may be attributed to many factors such as bone marrow tumour, leukaemia, tissue damage, and inflammatory diseases in mice. However, the observed substantial reduction in WBC, LYM, and GRAND in the treatment groups may be attributed to the antiplasmodial activities of LUM-PEG. The observed significant reduction ($P<0.05$) in the levels of RBC, HGB, HCT, MCH and MCHC in the untreated group may be due to anemia. This study is in line with the findings of Nardos and Makonne (2017), who observed that *P. berghei* is susceptible to anaemia as a result of erythrocyte destruction. This destruction occurs due to the multiplication of the parasite or the action of spleen reticuloendothelial cells, which leads to the production of phagocytes by the spleen in response to abnormal erythrocytes (Nardos and Makonne, 2017).

Erhirhie et al. *(*2021) and Gabriele et al. (2017) reported that antioxidant enzymes such as superoxide dismutase (SOD) and catalase (CAT), as well as serum ascorbate and reduced-glutathione, are main to protect the biological system

from oxidative stress by maintaining a normal level of free radicals. In this study, the observed significant decrease in SOD and CAT activities with increased MDA concentration (p<0.05) in the untreated group may be due to oxidative stress attacked by the free radicals. This finding is in consonant the work of Tyagi *et al.* (2017), which observed a decrease in the levels of SOD, CAT, and GST with increased in level of MDA in untreated malaria mice. Subsequently, the observed increase in SOD and CAT with decreased MDA in the treatment group may be due to the antimalarial activities of LUM-PEG. Overall, the effective antimalarial activity of lumenfantrine formulation recorded in this study might be due to the properties of PEG which have been proven to enhance bioavailability, good biocompatibility, increased drug solubility, and reduced toxicity (Mhlwatika & Aderibigbe, 2018).

CONCLUSION

The study demonstrated that LUM-PEG has the best antimalarial activity as characterized by decreased percentage parasitaemia and increased percentage inhibition during 21 days of the experimental period. Therefore, lumenfantrine formulated with polyethylene glycol can be used for malaria treatment after undergoing clinical trials.

REFERENCES

Antonella, R (2016). "Climate,Environment and Transmission of Malaria,"InfezMed 2:93–104.

Bobasa, E. M, Alemu B. G., Berkessa, ST, Gemechu Y, Fufa FG, & Cari GZ (2018). Antimalarial activity of selected Ethiopian medicinal plants in mice. Journal of Pharmacy & Pharmacognosy Research, 6 (1), 57-64.

Centers for Disease Control and Prevention. (2020) "Malaria,"

Erhirhie E., Ikegbune C., Okeke A., Onwuzuligbo C., Madubuogwu N., Chukwudulue U. & Okonkwo O. (2021). Antimalarial herbal drugs: a review of their interactions with conventional antimalarial drugs. Clin Phytosci 7(4):1e10

Gabriele, P., Natasha I., Mariapaola C., Giovanni P., Federica M. & Vincenzo A. (2017). Oxidative stress: harms and benefits for human health. Oxid Med Cell Longev (13):345e55.

Institute for Laboratory Animal Research (ILAR). Guide for the care and use of laboratory animals. 8th ed. Washington DC: National Academic Press; 2011.

Kondilis E, Giannakopoulos S, Gavana M, Ierodiakonou I, Waitzkin H. & Benos A. (2013). Economic crisis, restrictive policies, and the population's health and health care: the Greek case. Am J Public Health.103 (6):973–979.

Kumar S., Bhardwaj T., Prasad D., & Singh R. K. (2018). Drug targets for resistant malaria: historic to future perspectives. Biomed Pharmacother.104:8–27.

Marieb, E. N. (1995). Human Anatomy and Physiology. 3rd ed. Benjamin and Cummnings Pub Co, California 585-611.

MaxRoser&HannahRitchie,(2019)"Malaria,"OurWorldinData,November12,https://ourworldindata.orgmalaria.

Mhlwatika, Z., & Aderibigbe, B. A. (2018). Polymeric nanocarriers for the delivery of antimalarials. *Molecules*, *23*(10), 2527.

Mvango S., Matshe WM., Balogun AO, Pilcher L. & Balogun MO. (2018). Nanomedicines for malaria chemotherapy: encapsul.ation vs. polymer therapeutics. Pharmaceutical research. 35(12):237.

Nardos A, & Makonnen E. (2017). In vivo antiplasmodial activity and toxicological assessment of hydroethanolic crude extract of Ajuga remota. Malaria Journal. 16:25; 1-8

Ryley, J.F, & Peters, W. (1970). The antimalarial activity of some quinolone esters. Journnals of Tropical Medicine

Sawant, R. R., Sawant, R. M. & Torchilin, V. P. (2008). Mixed PEGPE/vitamin E tumor-targeted immunomicelles as carriers for poorly soluble anti-cancer drugs: improved drug enhanced in vitro cytotoxicity. *European Journal of Pharmaceutics and Biopharmaceutics* (70) 517.

Unekwuojo EG, James O, & Olubunmi AR. (2011). Suppressive, curative and prophylactic potentials of Morinda lucida (Benth) against, erythrocytic stage of mice infected with Chloroquine sensitive Plasmodium berghei. British Journal of Applied Science and Technology. 1(3):131-40

World Health Organization (WHO) (2012). World malaria   report Geneva, World Health Organization, *18*, 3229–32

World Health Organization, (2020) https://www.who.int/news/item/who-urges-countries-to-move-quickly-to-save-lives-from-malaria-in-sub-saharanafrica:According%20to%20the%20World%20malaria,under%20the%20age%20of%20five.

WorldHealth Organization, "World Malaria Report (2021)," accessed February 7, 2023, https://www.who.int/teams/global-malariaprogramme/reports/ world-malaria-report-2021.

Xia Q., Zhang Y., Li Z., Hou X. and Feng N.(2019). Red blood cell membrane-camouflaged nanoparticles: A novel drug delivery system for antitumor application. *Acta Pharm. Sin. B. 9*, 675–689.

Zhang Y., Xie L., Xie L. and Bourne P. (2016). The Plasmodium falciparum dru- gome and its olypharmacological implications. bioRxiv.042481.

Antibacterial Potential and Phytochemical Analysis of Aqueous and Ethanolic Extracts of Guava Leaf (*Psidium Guajava*)

*Abdulmalik, U., Shehu, I. and Sulaiman, T

Microbiology Department Federal University, Dutsinma P. M. B 5001 Dutsinma, Katsina State Nigeria.
*Corresponding author: <u>umaruabdulmalik449@gmail.com</u>

ABSTRACT

The guava (Psidium guajava) is a plant used in folk medicine that is believed to have active components that help to treat and manage various diseases. The many parts of the plant have been used in traditional medicine to manage conditions like malaria, gastroenteritis, vomiting, diarrhea, dysentery, wounds, ulcers, toothache, coughs, sore throat, inflamed gums, and several other conditions. This study aimed was to determine the phytochemical constituents, antibacterial activities, Gas Chromatography-Mass Spectrophotometer (GCMS) analysis and Fourier Transform Infrared Spectrometer (FTIR) (FTIR) analysis of aqueous and ethanolic extracts of guava leaf on E. coli and Salmonella species. The extracts component was subjected to Phytochemical screening using standard procedure. The leaf of Psidium guajava was Extracted using ethanol and water as solvents. The leaf extracts were tested for in vitro antibacterial activity against Salmonella and E.coli using different concentrations (50 mg/ml, 100 mg/ml and 200 mg/ml) using agar well diffusion method. The gas chromatography mass spectrophotometer (GC-MS) analysis of the extract and furrier transfer infrared (FTIR) analysis of aqueous and ethanolic extracts was analyzed. The ethanolic and aqueous leaf extracts were inhibitory to the test organisms (Salmonella and E. coli) with the highest inhibition recorded at 24 mm and least zone of inhibition at 12 mm at 50 mg/ml. With twenty (20) components were identified in the ethanolic extract. The Fourier Transform Infrared Spectrometer (FTIR) analysis of ethanolic extract indicate six (6) chemical compound with different peak numbers, wave length and intensity while the aqueous extract reveals three (3) chemical compounds. The presence of the various compounds confirms the use of the leaf extracts of Psidium guajava for the treatment of various ailments by traditional methods of medicine.

Keywords: Psidium guajava, Antibacterial activities, GC-MS analysis, FTIR analysis and Extracts

INTRODUCTION

Pathogenic bacteria cause many illness and death. Although different pharmaceutical companies have introduced several new antibacterial in the last years, resistance to these agents has also increased and has now become a worldwide problem (Gratus *et al*., 2009). World Health Organization has recognized herbal medicine as an important building block for primary health care in vast countries like India (WHO; 2018).The leaves of the plant have been used as an herbal remedy for their medicinal properties since ancient times. Some bioactive compounds (alkaloids, tannin, flavonoids and phenolic etc.,) of these plants are responsible for their medicinal value (Thirumurugan *et al.,* 2010). Drugs are found in every plant part such as leaves, stems, bark, roots, flowers, seeds, etc. Medicinal plants are important sources of therapeutic help in reducing human illness. The leaves of the guava plant are well documented in the treatment of diarrhea, stomach upset, toothache, fever, and inflammation (Richard *et al.,* 2013). The guava (*Psidium guajava*) is a phytotherapeautic plant used in folk medicine that is believed to have active components that help to treat and manage various diseases. The many parts of the plant have been used in traditional medicine to manage conditions like malaria, gastroenteritis, vomiting, diarrhea, dysentery, wounds, ulcers, toothache, coughs, sore throat, inflamed gums, and several other conditions. The genus *Psidium* belongs to the family *Myrtaceae*, which is considered to have originated in tropical South America. Guava crops are grown in tropical and subtropical areas of the world like Asia, Egypt, Hawaii, Florida, Palestine, and others. The genus *Psidium* comprises approximately 150 species of small trees and shrubs in which only 20 species produce edible fruits and the rest are wild with inferior quality fruits. The most commonly cultivated species of *Psidium* is L *P. guajava*. Which is the common guava? Other species are utilized for regulation of vigor, fruit quality improvement and resistance to pest and disease (Yadav *et al*., 2011). Guava fruit today is considered minor in terms of commercial world trade, but it is widely grown in the tropics, enriching the diet of hundreds of millions of people in those areas of the world. The guava tree is an evergreen small tree. The guava leaves are 2 to 6 inches long and 1 to 2 inches wide, aromatic when crushed and appear dull-green with stiff but coriaceous with pronounced veins. There are bioactive components in the guava leaf that can fight against pathogens, regulate blood glucose levels, and even aid in weight loss. The leaves of guava contain an essential oil rich in cineol, tannins, triterpenes, flavonoids, resin, eugenol, malic acid, fat, cellulose, chlorophyll, mineral salts, and several other fixed substances. The leaves of guava trees have a long history of medicinal uses. Various part of the guava tree has been traditionally used as a cough sedative (Joseph and Priya, 2011). Guavas are free from fat and

cholesterol. They are also an excellent source of fiber, potassium and vitamin A (Mishra *et al.,* 2017). Leaf extracts have show to have in vitro toxic action against numerous bacteria. In studies, guava leaf and bark have shown activity against *S. aureus*. *Shigella*, *Salmonella, Bacillus* and *E. coli* are causative agents of diarrhea (Mohammad *et al.,* 2011).

MATERIALS AND METHODS
Study area
The work was carried out in Federal University Dutsinma, Katsina State. Nigeria.

Collection, Identification and authentification of the plant
The plant material (Leaves) of *Psidium guajava* was collected by scraping the tree branch using sterile knife within Darawa Dutsin-Ma LGA katsina state. Nigeria. Identification and authentification was confirmed at the Department of Plant Science and Biotechnology Department of Federal University Dutsinma, Katsina.

Test Organisms
The test bacteria used in this study*, Salmonella* spp and *E.coli*. The stock cultures of the organisms were obtained from Federal University Dutsin-Ma, Katsina State, Nigeria. Gram staining of the stock cultures was done and some biochemical test was carried out to confirm the test organisms.

Gram staining
The bacterial isolates were subculture onto prepared nutrient agar and blood agar plates and incubated at 37ºC for 24hrs after which the smear of each isolate was prepared by emulsifying it is colony in 2-3 drops of sterile distilled water on a clean microscopic slide. The smear was left to air dry and then fixed by passing over the Bunsen burner flame about three times. The fixed smear was covered with crystal violet staining reagent for 30-60 seconds. It was washed with clean water and then drops of logos iodine were added. This was later washed with clean water and decolorized using drops of 95% ethanol followed by washing with clean water immediately. Safranin stain was then applied for 2 minutes after which it was washed with clean water and allowed the smear to air-dry. Microscopic examination was done using 10x and 40x objectives. (Cheesebrough, 2002)

Citrate utilization test
Using a sterile wire loop, 2-3 well-isolated colonies of pure culture of the test organism were streaked first at the slope surface of the Simmons citrate medium contained in a bijou bottle and then stabbed the butt. The inoculated medium was incubated for 24hrs at 37ºC after which the result was noticed (Cheesebrough, 2002).
Urea test
The test organism was inoculated in to 3 ml of urea agar medium in bijou bottles. The inoculated medium was the incubated for about 24 hrs at 37ºC changes occur from red to pink for positive tests (Cheesebrough, 2002).

Indole test
The test organism was inoculated into a Bijou bottle containing about 3ml of sterile peptone water. The inoculated peptone water was then incubated for about 24 hrs at 37ºC.Test for Indole was achieved by the addition of about 0.5 ml of Kovac's s reagent (composed of 75ml Amyl alcohol, 25 ml 37% concentrated Hydrochloric acid and 5g kovac's reagent powder),shaken gently and examined for the results within 10 minutes. Red purple coloration indicates positive reaction (Cheesebrough, 2002).

Preparation of Plant for Extraction
The fresh plant materials (leaves) were obtained and allowed to dry at room temperature for 7 days. The leaves were then pulverized using Pestle and Mortar. The following extractions were carried out as described in (Daniels *et al*., 2013) with some variation. Aqueous and Ethanol. For aqueous extraction, 50 g of guava leave samples were weighed separately into bama bottle containing 500 ml each of distilled water and for the ethanolic extraction 50 g of guava leaf samples were weighed separately into bama bottle containing 500 ml each of ethanol respectively. The mixtures were initially shaken rigorously and left for 5 days. All mixtures were filtered using filter paper and the filtrates were collected directly into a conical flask. All filtrates obtained were introduced into sterile reaction tubes and heated continuously using a water bath at the following temperatures: 78°C for ethanol extraction, and 105°C for distilled water. The residues obtained were kept at room temperature.

Preparation of the stock solution of the Extracts

Using an aseptic condition, the extracts were reconstituted by adding 2 g of each extract with 2 ml of Dimethylsulphoxide (DMSO) to form stock solutions of the extracts.

Preparation of media

Mueller Hinton agar was used and was prepared from ready-to-use agar powder according to the manufacturer's specifications. The agar was prepared by dissolving 38 g in 400 ml of distilled water in a conical flask and was heated gently to dissolve the agar. The media was then autoclaved at 121°C for 15 minutes. The sterilized media was allowed to cool to a temperature of 45°C and then approximately 25 ml was poured into sterile Petri dish and allowed to gel.

Standardization of the inoculums

The inoculums were standardized using 0.5 McFarland standards, where Barium sulphate ($BaSO_4$) was used as a standard for the preparation of the broth culture of the organisms. 1 g of $BaCl_2$ was added to 5 mls of distilled water. 1 ml of tetra oxosulphate (VI) acid was added to 5 ml of distilled water. 0.5 ml of the 1% Sulphuric acid (H_2SO_4) was added to the 5 ml of $BaCl_2$ solution to form $BaSO_4$.

Antibacterial screening/testing

The sensitivity test was carried out using the agar well diffusion method according to National Committee for Clinical Laboratory Standards (NCCLS 1993). The Petri dishes were inverted and incubated overnight to observe for contamination. Sterile cotton swabs were dipped into the standardized inoculums. The swab was used to swab the surface of the set agar plates. Cork borer of 6 mm diameter was used to bore holes equidistant from each other on the agar. Extracts of the different solvents and concentration (100 mg/ml, 50 mg/ml, 25 mg/ml, and 12.5 mg/ml) were prepared from the stock solution and used to fill the bored holes with o.1ml of the various concentrations of the two extracts. Doxycycline solution was filled in the bored hole at the center of the culture plate which serves as control. The plates were allowed to stand for 1 hour so that the extracts could percolate the medium and incubated at 37°C for 24 hrs after which the plates were observed for a zone of inhibition.

Gas Chromatography Mass Spectrometry (GCMS) Analysis

The Gas chromatography-Mass spectrometry (GC-MS) analysis of ethanol and aqueous extracts of Psidium guajava were performed using a GC-MS analysis, and was done at NARICT, Zaria-Nigeria laboratory using GC-MS QP2010 PLUS Shimadzu, Japan. The Column Oven Temperature 70.0°C Hold Time 2.0 min, Injector Temperature 250.0°C, Pressure 116kPa, Total Flow 40.8mL/min, Linear Velocity 49.2cm/sec, Column Flow 1.80mL/min, Purge Flow 3.0 Ml/min and Carrier Gas was off. The Gas chromatography-Mass spectrometry (GC-MS) analysis of petroleum ether, ethanol and aqueous extracts of Psidium guajava were performed using a GC-MS (Model; QP 2010 series, Shimadzu, Japan) equipped with a VF-5ms fused silica capillary column of 30m length, 0.25mm diameter and 0.25μm film thickness. The column oven temperature was programmed from 80°C to 280°C for 2°C min-1. Ionization of the sample components was performed in electron impact mode (EI, 70 eV). The temperature of the injector was fixed to 250.00°C and one of the detector to 200°C. Helium (99.9995% purity) was the carrier gas fixed with a flow rate of 1.5 ml min-1. The mass range from 40-1000 m/z was scanned at a rate of 3.0 scans/s. 1.0μl of the extracts was injected with a Hamilton syringe in to the GC-MS manually for total ion chromatographic analysis in a split injection technique. The total running time of GC-MS is 35 min. The relative percentage of each extract constituent was expressed as a percentage with peak area normalization.

RESULT AND DISCUSSIONS

Table 1 shows the phytochemical tests of ethanol and the aqueous leaf of guava (*psidium guajava*) leaf.. The results of the phytochemical test reveal the presence of alkaloids, flavonoids, saponins, phenols, tannin and glycosides while in the aqueous extracts tannin was absent with the presence of alkaloids, flavonoids, saponins, phenols and glycoside. Aqueous is the only one that showed the presence of all the phytochemical, whereas the ethanolic solvent failed to have show the presences of Tannins and Glycosides chemical compounds. The presence of phytochemical which are known to exhibit medical and physiological activities. For example, tannins are polyphenolic compounds that bind to protein that interferes with protein synthesis (Sanches 2005) and has shown to have antibacterial activity (Akiyama 2001). Flavonoids are hydroxylated polyphenolic compounds known to be produced by plants in response to microbial infections which this aspect has been extensively studied and found to have antimicrobial activity against an array of microorganisms in vitro (Cowan, 1999). Their ability has been attributed to their ability to form complexes with extracellular and soluble proteins and bacterial cell walls. Saponins which are glycosides have been found to have inhibitory effects on gram-positive organism, *S. aureus.* Therefore, the phytochemical analysis revealed that the

methanol, ethanol, and distilled water extract have chemical compounds that have been found to possess antibacterial activities, which could contribute to the results obtained from antibacterial activities.

The usage of plants as remedies has been practiced a long time ago. The WHO has catalogued more than 20,000 plant species with medicinal properties providing treatments for diseases (Goncalves *et al*., 2008). *P. guajava* is a medicinal plants used in tropical and subtropical countries to treat many disorders such as diarrhoea, cough and gastrointestinal disorders (Hirudkar *et al*., 2019). Hirudkar *et al*., (2019) have reported that quercetin is the main flavonoid of *P. guajava* leaves that has many pharmacological activities. According to Parekh *et al.,* (2005), the most commonly used solvents for investigations of antibacteria activity in plants are organic compounds (methanol and ethanol) and aqueous (water), but among these two, organic solvents have been found to give more consistent antibacteria activity compared to aqueous extracts. In this study, ethanol and aqueous had been used as the extraction solvent. In this present study, it was found that the ethanolic and aqueous extracts of *P .guajava* leaf was active against the test microorganisms (*E .coli* and *Salmonella*) at different concentrations as shown in Table 2 -5 respectively. In *E. coli* the aqueous extract was found to have inhibitory activity with 15 mm and 6 mm been the highest and lowest values at 50 mg/ml and 25 mg/ml respectively, In *E. coli* the ethanolic extract have the maximum and minimum of 16 mm and 6 mm zone of inhibition against the organism at 50 mg/ml and 25 mg/ml respectively. The aqueous extract possesses a 12 mm and 6 mm zone of inhibition as the highest and lowest values recorded at 50 mg/ml and 12.5 mg/ml against Salmonella respectively. While the ethanolic extract of the used against the salmonella exhibited 12 mm zone o inhibition at 50 mg/m/ and 6 mm at 100 mg/ml.

The findings of this work on guava extracts of different concentrations correlated with the findings of Goncalves *et al.,* 2008, who applied guava extracts against food borne pathogens and spoilage bacteria. This was confirmed by Malaviya *et al.,* 2011. The observations in the case of guava extracts matched with the findings of Hoque et al., 2007 who showed that the antibacterial activity of guava and guava leaf extracts mostly attributed to the action of its principal phenolic components and both of these exhibit significant bactericidal activities when tested separately. However, the studies provide evidence that phenolic compounds, particularly flavonoids, are responsible for antibacterial properties of guava same was also reported by Hoque *et al.,* 2007. These observations also correlated with the work of Ismail *et al.,* 2012 which exhibited the antibacterial activity of guava against food- borne pathogens. The control shows the highest inhibiting activity for all the two bacteria under study ranging between 18mm – 22mm zone of inhibition. Other research work that agreed with this finding includes, Sanches *et al.,* 2005 who found that the aqueous extract of guava was effective against *Staphylococcus* and *Bacillus*. Also the methanolic extracts of guava were reported by Lin *et al.,* 2002 that showed significant inhibitory activity against the growth of 2 isolates of *Salmonella* and enteropathogenic *E. coli*. In other studies by Mohammad et al., 2011 guava leaf has show activity against *S. aureus*. *Shigella*, *Salmonella, Bacillus* and *E. coli* that are causative agents diarrhea

The Gas chromatography mass Spectrophotometer (GC-MS) analysis results clearly show the retention time (RT), molecular formula, molecular weight (MW), area % and compound name presented, for the ethanolic crude extracts (Table 8) reveals a total number of twenty (20) peak indicating compound, ethanol crude extract the major compound include Cyclohexanone, Heptane, Propanetriol, 1,3-Dioxolane, 4-Heptane 3-1, 4-methyl, Resorcinol, Isopinocampheol, 1,3 Propanediol, 2-ethyl, 3-O-Methyl-d-glucose, methyl ester, n-hexadecanoic acid, 9,12-Octadecadienoic acid, 11-Octadecenoic, Decanoic, Oleic Acid, 3-Trifluroacetoxy-6-ethyldecane, 2-Decyn-1-o1, 9,12-Octadecadienoyl chloride, Nonadecyl alcohol and Hexadecanoic acid. Similar work on The GC-MS method confirms that *P. guajava* contains the compounds such as, 2-Isopropoxyethylamine, Bicyclo (7.2.0) undec-4- Ene,4,11,11-Trimethyl-8-methylene-, Caryophyllene, Alpha-Farnesene, Trans-Z, alphaBisaboleneepoxide, Alpha-bisabolol, B-carotene, Propanoic acid, 2-(Aminooxy)- and 2,4,6 Cycloheptatrien-1-one,3,5-Bis-Trimethylsilyl. Fu *et al.,* 2009. identified nine compounds such as, ursolic acid, 2 alpha-hydroxyoleanolic acid, 2 alphahydroxyursolic acid, quercetin, hyperin, 1- O- galloylbeta- D- glucose morin- 3- O- alpha- L- arabopyranoside, myricetin- 3- O- beta- D- glucoside and quercetin- 3- Obeta- D-glucuronopyranoside were identified from the leaf extract of *P. guajava*. Jebashree *et al.,* 2011 carried out GC-MS analysis using ethyl acetate extract to find the anticancer molecules. Thirteen compounds were identified from the extract of *P. guajava* and caryophyllene is a known compound for its curative efficiency as an antibacterial activity and antiinflammatory and remarkable Gertsch *et al.,* 2008 which also agreed with this findings.

The furrier transfer infrared (FTIR) analysis of ethanolic extract indicate six (6) chemical compound with different peak numbers, wave length and intensity while the aqueous extract reveal three (3) chemical compounds

Table 1: Phytochemical Activity of Ethanolic and Aqueous Leaf Extract of *Psidium Guajava*

S/NO	CHEMICALS	Ethanolic	Aqueous
1.	Alkaloids	+	+
2.	Flavonoids	+	+
3.	Tannin	+	-

4.	Saponins	+	+
5.	Phenols	-	+
6.	Cardiac glycosides	-	+
7.	Glycoside		

Key: + indicates present, - indicates absence

Table 2: Antibacterial activity of aqueous leaf extract of *Psidium Guajava* zone of inhibition (mm)

S/N	ORGANISIMS	CONCENTRATIONS (mg/mm)				
		100	50	25	12.5	CONTROL
1	*E. coli*	8	13	8	6	18
2	*E. coli*	8	15	7	6	20
3	*E. coli*	9	14	6	6	20

Table 3: Antibacterial activity of ethanolic leaf extract of *Psidium Guajava* zone of inhibition (mm)

S/N	Organisms	CONCENTRATIONS (mg/mm)				
		100	50	25	12.5	CONTROL
1	*E. coli*	8	15	8	6	18
2	*E. coli*	8	16	7	7	22
3	*E. coli*	9	16	8	6	20

Table 4: Antibacterial activity of aqueous leaf extract of *Psidium Guajava* zone of inhibition(mm)

S/N	Organisms	CONCENTRATIONS (mg/mm)				
		100	50	25	12.5	CONTROL
1	*Salmonella*	7	10	8	9	20
2	*Salmonella*	7	10	10	8	20
3	*Salmonella*	6	12	8	8	20

Table 5: Antibacterial activity of ethanol leaf extract of *Psidium Guajava* zone of inhibition(mm)

S/N	Organism	CONCENTRATIONS (mg/mm)				
		100	50	25	12.5	CONTROL
1	*Salmonella*	6	10	8	9	19
2	*Salmonella*	7	10	8	8	20
3	*Salmonella*	6	12	10	7	20
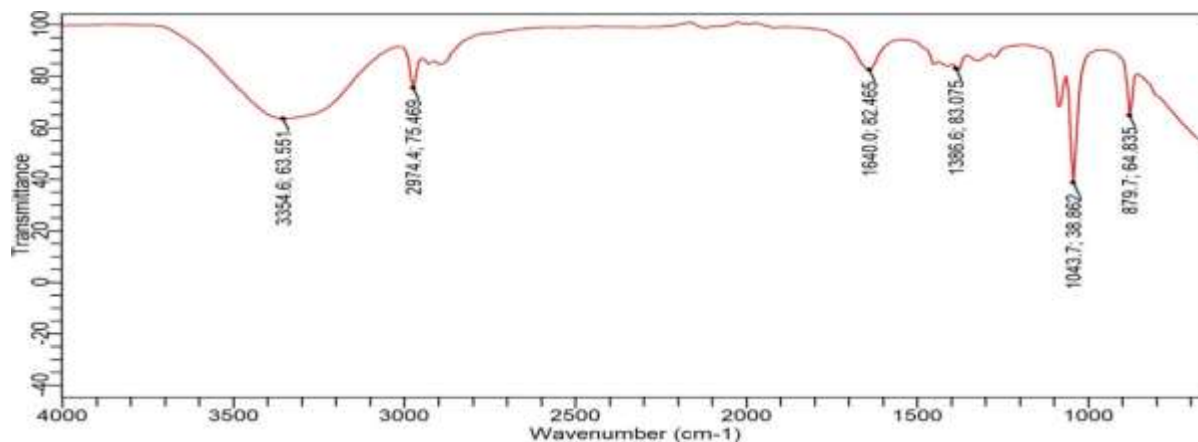
Figure 1: Show Fourier transform Infrared Spectrometer (FTIR) analysis of aqueous extract

Table 6: Fourier Transform Infrared Spectrometer (FTIR) analysis of ethanolic extracts

Peak Numbers	Wave number (cm^{-1})	Intensity
1	879.65173	64.83477
2	1043.65459	38.86219
3	1386.56968	83.07497

4	1640.02865	82.46537
5	2974.41559	75.46868
6	3354.66355	70.43347

Table 7: Fourier Transform Infrared Spectrometer (FTIR) analysis of aqueous extracts

Peak Numbers	Wave number (cm^{-1})	Intensity
1	1632.57397	65.31512
2	2117.12789	95.98839
3	3324.78535	44.30647
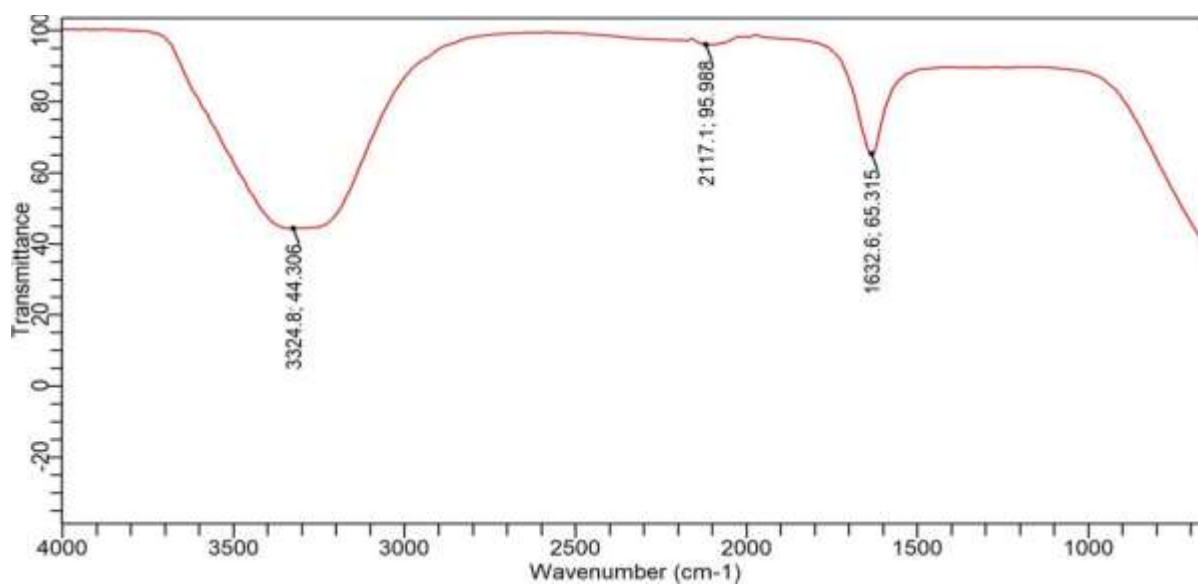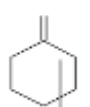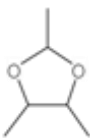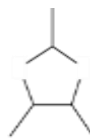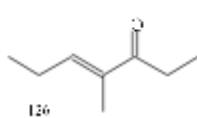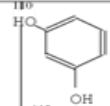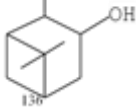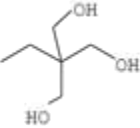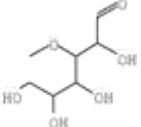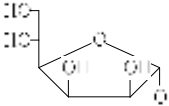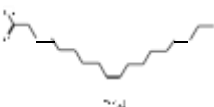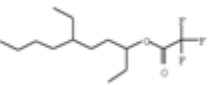
Figure 2: Showing Fourier Transform Infrared Spectrometer (FTIR) analysis of aqueous extract

Table 8:.Phytochemical components identified from *Psiudium Guajava* ethanolic leave extract

S/NO	Reaction Time	Molecular Structure	Component Formular	Molecular Weight	Molecular Name	Area %
1	3.683		C6H10O	98	Cyclohexanone	0.83
2	3.917		C7H14	98	Heptane	1.89
3	4.525		C3H8O3	92	Propanetriol	3.46
4	6.342		C6H12O2	116	1,3-Dioxolane, 2,4,5, trimethyl	0.42
5	7.750		C8H14O	126	4-Heptane 3-1, 4-methyl	1.31

6	9.400		C6H6O2	110	Resorcinol 1,3 Benzenediol	4.62
7	10.517		C10H18O	158	Isopinocampheol	0.47
8	10.983		C6H14O3	134	1,3 Propanediol, 2-ethyl 1-2-(hydroxymethyl)	4.39
9	14.233		C7H14O6	194	3-O-Methyl-d-glucose	7.00
10	15.708		C14H28O2	228	Tridecanoic acid, methyl ester, methyl tridecanoate	1.08
11	17.050		C16H32O2	256	n-hexadecanoic acid	7.03
12	18.925		C19H34O2	294	9,12-Octadecadienoic acid	2.58
13	18.992		C19H36O2	296	11-Octadecenoic acid, methyl ester	2.20
14	19.350		C11H22O2	186	Decanoic acid, methyl ester	0.41
15	20.175		C18H34O2	282	Oleic Acid, 9-Octadecanoic acid	37.80
16	21.700		C14H25F3O2	282	3-Trifluroacetoxy-6-ethyldecane	1.05
17	23.108		C10H18O	154	2-Decyn-1-o1	1.20
18	23.567		C18H31ClO	298	9,12-Octadecadienoyl chloride	5.93
19	23.783		C19H40O	284	1-Nonadecanol, Nonadecyl alcohol	1.63
20	24.108		C19H38O4	330	Hexadecanoic acid, 2,3-dihydroxypropyl ester	3.14

CONCLUSION

At the end of the experiment, extracts from *P. guajava* leaves inhibited the test microorganisms (*Salmonella* and *E .coli*) been tested but not in the extracts from *P. guajava leaf.* Results revealed that the guava leaf extract can be used as the source of natural antimicrobial agents which can be applied to treat diseases caused by the Gram-negative bacteria (*Salmonella* and *E.coli)* and validate its use in traditional medicine.

RECOMMENDATIONS

For the leaf of *Psidium guajava* to be scientifically recommended for public consumption, more research should be undertaken in the area of the phytochemical constituents and nutritional constituents of the leaf, as well as other various parts of the plant. It is also recommended that more research should be done in the area of antifungal, antiviral and anti-protozoan activity of the plant using various solvent to order to ascertain whether the plant is capable of inhibiting the growth or killing some fungi, protozoan and viruses that causes major public health crisis also the use of local herbs or medicinal plant should be encouraged by individuals.

REFERENCES

Daniels A.O., Famurewa O. and Malomo O., and Alamu E.A. (2013). Screening of *Daniella oliveri* against Three Bacteria and One Fungus. *Research Journal of Pharmaceutical, Biologicaland Chemical Sciences*, 4(**1**):93.

Fu H., Luo Y., Zhang D. Studies on chemical constituents of leaves of Psidium guajava. Zhongguo Zhong Yao Za Zhi, **34**(5); 577-579, (2009).

Gonçalves, F. A.; Andrade Neto, M.; Bezerra, J. N. S.; Macrae, A.; Sousa, O. V.; Fonteles-Filho, A. A. & Vieira, R. H. S. F. - Antibacterial activity of guava, Psidium guajava Linnaeus, leaf extracts on diarrhea-causing enteric bacteria isolated from Seabob shrimp. Xiphopenaeus kroyeri (Heller). Rev. Inst. Med. trop. S. Paulo, **50** (1): 11-15, 2008.

Goncalves, F.A., Neto, M.A., Bezerra, J.N.S., Macrae, A., Sousa O.V., Fonteles-Filho, A.A. & Vieira, R.H.S.F. (2008). Antibacterial activity of guava, *Psidium guajava L.*, leaf extracts on diarrhea-causing enteric bacteria isolated from seabob shrimp, Xiphopenaeus kroyeri (HELLER), Rev. Inst. Med. Trop. S. Paulo, **50**(**1**):11-15.

Gratus, Christine, Sue Wilson, Sheila M., Damery, S. L., Warmington, S. A., Grieve, R. &Routledge, P. (2009). The use of herbal medicines by people with cancer: a qualitative Study. *BMCComplementary and Alternative Medicine,* **9**(**1**), 1-7.

Gertsch J., Leonti M., Raduner, S. et al. Betacaryophyllene is a dietary cannabinoid. Proceedings of the National Academy of Sciences of the United States of America. **105**(26); 9099– 9104, (2008

H. Akiyama, K. Fujii, O. Yamasaki, T. Oono, and K. Iwatsuki, "Antibacterial action of several tannins against Staphylococcus aureus," Journal of Antimicrobial Chemotherapy, vol. 48, no. 4, pp. 487–491, 2001..

Hoque, M. M.; Bari, M. L.; Inatsu, Y; Vijay, K; Juneja and Kawamoto, S. - Antibacterial Activity of Guava (*Psidium guajava L.*) and Neem (*Azadirachta idica A. Juss.)* extracts Against Foodborne Pathogens and Spoilage Bacteria. National Food Research Institute, Japan. **4** (4):481-488, 2007.

Hirudkar, J. R., Parmar, K. M., Prasad, R. S., Sinha, S. K., Jogi, M. S., Itankar, P. R., & Prasad, S.K. (2019). Quercetin a major biomarker of *Psidium guajava L.*   Inhibits SepA protease

Ismail, M; Minhas, P. S.; Khanum, F; Sahana, V. M. and Sowmya, C. - Antibacterial Activity of Leaves Extract of Guava (Psidium Guajava). International Journal of Research in Pharmaceutical and Biomedical Sciences. **3** (1): 1, 2012.

Joseph, B., & Priya, M. (2011). Review on nutritional, medicinal and pharmacological properties of guava (*Psidium guajava* Linn.). *International journal of pharmaceutical and biological sciences,* **2**(**1**), 53-69.

J. Lin, T. Puckree, and T. P. Mvelase, "Anti-diarrhoeal evaluation of some medicinal plants used by Zulu traditional healers," Journal of Ethnopharmacology, vol. 79, no. 1, pp. 53–56, 2002.

Jebashree, H.S., Kingsley S.J., Sathish E.S., Devapriya D. Antimicrobial Activity of Few Medicinal Plants against Clinically Isolated Human Cariogenic Pathogens—An In Vitro Study. ISRN Dentistry, 2011; Article ID 541421, 6 pages, (2011).

Mishra R, Tiwari P, Srivastava M, Singh CS, Ghoshal S. (2017). A comprehensive review on psidium guajava Linn (Amaratafalam). *International journal of Ethnobiology and Ethnomedicine*, **4**(**1**):1-6

Mohammed, S. J., Al–Mousawi, T., & Al-Fraji, S. A. (2020). A Review of Salmonella types on food source. *International Journal of Psychosocial Rehabilitation.*

M. M. Cowan, "Plant products as antimicrobial agents," Clinical Microbiology Reviews, vol. **12**, no. 4, pp. 564–582, 1999.

Malaviya, A and Mishra, N. - Antimicrobial activity of tropical fruits. Biological Forum – An International Journal, 3(1): 1-4: 2011

N. R. Sanches, D. A. G. Cortez, M. S. Schiavini, C. V. Nakamura, and B. P. D. Filho, "An evaluation of antibacterial activities of Psidium guajava (L.)," Brazilian Archives of Biology and Technology, vol. 48, no. 3, pp. 429–436, 2005.

NCCLS. Performance Standards for Antimicrobial Disc Suspectibility TestsApproved Standard NCCLS Publication M2-A5, Villanova, PA, USA, 1993.t

Parekh. J., Jadeja, D., & Chanda, S. (2005). Efficacy of aquoues and methanol extracts of some medicinal plants for potential antibacterial activity. Turk. J. Biol. **29**:203-210.

Thirumutugan, Kavitha, MS., Shihabudeen, PD Hansi- Steroids. (2010). Research gate.net

WHO (2018). Antibiotic resistance: Fact sheet [online]. http://www.int/news-room/fact-sheets/details/antibiotic-resistance. Accessed on (08 Dec. 2018).

Simulation of Nuclear Cross Sections for Cs-130 and Cs-131 Production using (a,n) and (a,g) Reactions on Stable I-127 (from 1 to 20MeV)

*[1]Zubaida Gali Habib, [2]Idris Ahmad and [1]Abdulkadir M. Nura

[1]Department of Physics, Federal College of Education, Kano, Nigeria
[2]Department of Physics, Bayero University, Kano, Nigeria
Corresponding author's email: zubaidagh92@gmail.com

ABSTRACT
Use of radionuclides in diagnoses and therapies of many diseases is becoming a routine part of national and even local healthcare systems around the globe in recent times. Commonly employed nuclear diagnostic procedures such as Positron Emission Tomography (PET) and Single Photon Emission Computed Tomography and many other specialist imaging procedures are now becoming choice means for detecting cancer of many organs and other anomalies just as radiotherapy is being utilized to treat cancers like that of the thyroid with Iodine-131. This research investigates the excitation function calculation for the production of Caesium-130 and 131 via the (a,n) and (a,g) reactions on stable Iodine-127 within energy range of 1 to 20 MeV using EXIFON Code. Cs-130 and 131 are important radionuclides for radiotherapies of several vital organs as Cs-130 serve as intracavity implant while Cs-131 provides soft X-rays for Brachytherapy. A new dataset has been established and compared with evaluated nuclear data file (ENDF) and experimental data EXFOR with good agreement.
Keywords: Excitation Function, EXIFON, PET, Radionuclide, SPECT

INTRODUCTION

Nuclear reaction parameters such as nuclear cross section and excitation function provide fundamental information that facilitates the prediction of the probability of production and purity of radionuclides. Hence they play a crucial role in the course of nuclear energy and development of fusion and fission reactors (Zubaida & Ahmad, 2019). As a consequence of this principle, nuclear reaction data describes the interactions of various projectiles such as protons, neutrons or alpha particles with target nuclei. These data are becoming increasingly important for various reasons such as optimizing radionuclide production, analysis of impurities as well as ascription of the most suitable method for radionuclide production with high efficiency (Iwamoto, 2007).

In nuclear theory, quantum mechanics is used to predict the probability that a specific nuclear reaction will occur under certain conditions (Hibstie et al., 2018). This quantitative prediction is the nuclear cross section which can be measured in the laboratory with the use of experimental techniques veritably developed to investigate nuclear reactions involving radioactive nuclei and playing a crucial role in many areas of basic and applied nuclear sciences over the past few decades (Ahmad & Koki, 2017).

Radioisotope production for use in nuclear medicine has already become one of the most important contributions of nuclear physics because radionuclides play a central role in life saving applications especially nuclear diagnostics and therapeutics (Elbinawi et al., 2016). An example of radionuclide therapy is treatment of thyroid disease with radioiodine, while nuclear diagnostics involves application of short half life nuclide attached to suitable radiopharmaceutical. The nuclide emission as a result of accumulation and movement of activity would be measured from outside the body (Qaim, 2012) with the use of external detectors, to capture and form images from the emission of radiation by the radiopharmaceutical. This process is called emission tomography which includes Positron Emission Tomography (PET) and Single Photon Emission Computed Tomography (SPECT).

Nuclear diagnostics are now routinely applied throughout the developed world and in many developing nations to detect disorders of the human body's vital organs such as the heart, liver, brain, kidney and glands (Ahmad & Koki, 2017). Bone and joint disorders as well as anomalies of the spinal cord are also detected with the same principles. However, as the medical cases requiring nuclear diagnosis and therapy such as cancers of different organs are on steady rise, there appears vulnerability to failure of nuclear medical services in the event of radioisotope shortage. Thus if anything hitches the availability of radioisotope, a lot of nuclear medical services may halt leading to the cause of fatalities. This has happened in the United States during the shortage of Molybdenum which is used in producing Technetium 99. The shortage was due to stoppages of nuclear reactors that produce the radionuclide (Ruth, 2014). Hence with the teeming morbidity of the Nigerian population a crisis may unfold if steps are not taken to ensure radioisotope availability, this is the foundation behind exploring the various routes of radionuclide production including particle induced reactions, use of cyclotrons, particle accelerators as well as low enrichment.

Radioisotopes produced from (a,n) and (a,g) reactions with Iodine-127 have been found to play important medical roles. [127]I (a,n) produces Caesium-130. This radionuclide has a half life of 30 minutes and is used as a localizing

agent (Volkert & Huffman, 1999) . [127]I (a,g) reaction yields Caesium-131 which has a half life of 10.2 days and is a gamma emitter. Cs-131 is used in intracavity implantation for radiotherapy and also produces soft X-rays, which makes it very suitable for Brachytherapy (Volkert, 2003).

Production routes of medical radionuclides need to be optimized in order to produce higher yields and to achieve high purity in production (Ahmad & Koki, 2017). For this to be accomplished, nuclear data which encompasses reaction cross section, excitation function, reaction energetic and angular distribution etc need to be evaluated (Chadwick, 1995). This underlines the theoretical and experimental calculations of excitation functions and other various nuclear parameters which the International Atomic Energy Agency (IAEA) has been undertaking for the past five decades for the purpose of research, innovation and nuclear information dissemination (Yamoah & Asamoah, 2013). Moreover, it's through such nuclear data evaluations that such parameters (cross section, excitation function etc) are validated through comparison with experimentally generated data.

Hence the fundamental objectives of this research are to obtain the threshold energy and reaction cross sections for (a,n), and (a,g) reactions on stable [127]I, and to evaluate the excitation functions for the reactions. This is to facilitate the production of Cs-130 and Cs-131 using other routes (such as cyclotrons) apart from the use of nuclear reactors. This will go a long way towards preventing medical crisis due to nuclear radionuclide shortage.

Theoretical Background

Description of nuclear reactions are usually achieved with the use of several nuclear models which are linked together to calculate nuclear cross sections. One of the most important models however, is the Statistical (or Compound nuclear) model which belongs to the group of reaction models in the slow order along with the pre-equilibrium model (Hilaire, 2000). This model has been receiving attention over the years for description of reactions in the low and intermediate region up to 20 MeV. The models provides that a compound nucleus is formed with high enough excitation energy so that the incident particle – target nucleus interaction may excite many states (Ahmad et al., 2017). In addition, it assumes the incident energy is shared among individual components of the nucleus which equilibrate fully before nuclear decay takes place (Griswold et al., 2018).This implies no correlation of compound nucleus formation with the decay process and hence the existence of independent expressions to describe the ingredients of the process as summed up in equation (I). These processes include Statistical Multistep Direct (SMD) and Multistep Compound (SMC).

Same residual interaction was utilized in computing both the formation and decay within SMD and SMC (Hilaire, 2000). Thus reference is not tenable to the optical model (OM) reaction cross section. OM cross section for charged particles was used for simulation of Coulomb effects in the threshold region (Ahmad & Koki, 2017).

Multiple particle emission (MPE) calculation is generalized and up to three decays of the compound nucleus are considered. The statistical model is formulated in detail for predicting emission spectra for neutrons, protons, alpha particles and photons with inclusion of equilibrium, pre-equilibrium, direct and MPE processes with high degree of consistency (Artun & Aytekin, 2015). One physical parameter set for several energies and reaction types was employed in performing calculations.

Statistical multistep models are very successful in describing nuclear reactions at energies up to about 100 MeV (Kalka, 1992). These models enable the description of direct, pre-equilibrium and equilibrium processes in a constant way for a wide number range and various reaction channels e.g. neutrons, protons, alpha particles, and gamma rays (Ahmad & Koki, 2017). The application of Statistical Multistep Model to heavy nuclei requires the consideration of fission as a competing process to particle and gamma-ray emissions. Therefore, Statistical Multistep Models should be extended to the fission channel.

Statistical Multistep Model

In the Statistical Multistep Model, the total emission spectrum of the process (a, xb) is divided into three main parts (Ahmad & Koki, 2017).

$$\frac{d\,\sigma_{a,xb}(E_a)}{dE_b} = \frac{d\,\sigma_{a,b}^{SMD}(E_a)}{dE_b} + \frac{d\,\sigma_{a,b}^{SMc}(E_a)}{dE_b} + \frac{d\,\sigma_{a,xb}^{MPE}(E_a)}{dE_b} \qquad (1)$$

Where $d\sigma_{a,xb}$ is the probability for (a,xb) process, $d\sigma_{a,b}SMD$ is the probability for direct reaction for production of b from a and E_b is the excitation energy for the formation of b.

The first term on the right-hand side of the equation (1) represents the statistical multistep direct (SMD) part which contains from single step to five-step contributions. Besides particle-hole excitations also collective photon excitations are considered. The second term represents the statistical multistep compound (SMC) emission which is based on a master equation. Both terms together (SMD+SMC) represent the first chance emission process (Pandey et al., 2011). The last term of the equation (1) represent multiple particle emission (MPE) reaction which includes the second chance, third chance emissions, etc. These terms are summarized below:

$$\frac{d\,\sigma_{a,xb}^{MPE}(E_a)}{dE_b} \;=\; \sum \frac{d\,\sigma_{a,cb(E_a)}}{dE_b} \;+\; \sum \frac{d\,\sigma_{a,cdb(E_a)}}{dE_b} \;+\;\ldots\ldots \qquad\qquad (2)$$

MATERIALS AND METHODS

Computer Code EXIFON 2.0

Theoretical calculations of nuclear cross-sections were performed using nuclear model code EXIFON which is a FORTRAN based computer program that outputs nuclear reaction data for a wide range of incident energies.

EXIFON code is based on an analytical model for the description of excitation function of particle induced reactions within a statistical multistep direct and multistep compound reactions (SMD/SMC) model. The computer code is very important for several technical applications if the experimental data are not available or unable to measure the reaction cross-sections due to the experimental difficulties. This code is capable of calculating equilibrium and pre-equilibrium emission cross-section, and valid for excitation energy of the compound nucleus up to 100 MeV.

EXIFON code provides continuous and smooth description of nuclear reactions over a wide energy and mass range which is based on an analytical model for statistical multistep direct and multistep compound reactions (SMD/SMC model). It predicts emission spectra, angular distribution and activation cross-section for neutrons, protons, alpha particles and photons. Multiple particle emissions are considered for up to three decays of the compound system. EXIFON is a fast, easy to handle code which predicts cross-sections from one global parameter set. The only adjustable quantity is the pairing shift. The INPEXI code creates input files for EXIFON 2.0 from mass and shell – correction tables. The MAKE6 code transforms EXIFON output into an ENDF-6 format file (Ebiwonjumi, 2014).

General Features of EXIFON Code

Computer: PC/AT, Programming language: FORTRAN 77, Characters: ASC II (IBM International Graphic), Memory size: 300kbyte, Number of subroutines: 13, Records; about 1600, running time: about 20 seconds per incident energy.

Standard Parameters Set

The following global parameters are used

Strength of surface – delta interaction:	F0 = 27.5MeV
Radius Parameter:	r0= 1.21 +4.0A$^{-2/3}$ – 15A$^{-4/3}$
Fermi energy:	Ef = 33MeV
Potential energy:	V0 = 52 – 0.3Eα MeV
Pairing shift:	Δ = 12.8A$^{-1/2}$ MeV
Phonon (Breit-Weigner) width:	Δw = 14MeV
Optical Model Potential OM:	for protons, neutrons and alpha (Kalka, 1992)

In the calculations, the following parameters can be changed; Strength of surface-delta interaction F0, Radius parameter r0, Fermi energy Ef, Phonon width Δw and global OM parameter for protons.

Procedure

Inputting data in Exifon code involves target nucleus specification in which user add mass number A of the target nucleus. This is followed by specifying the incident particle (neutron, proton or alpha), the first incident energy, and then the incident energy step. Subsequently, the cross-section corresponding to each particular energy step will be generated.

The output data (OUTEXI) for the calculation are then stored in the output directory, also DAT file name are stored in the set output directory. The computer program Python was used to generate a code that can convert the results which comes in complex notepad format into a simple format for easy processing.

Input Data and Output Data files

For each target nucleus, input data files are necessary. They contain all binding energies BC and shell correction energies dW, as well as phonon parameters. They can be created with code INPEXI.EXE. One input data file contains all the information for neutron, proton and alpha induced reactions. Output data files are equally necessary for each target nucleus. The emission spectra of neutrons, protons and alpha particles are stored in the file AXN.DAT, AXP.DAT, AXA.DAT and AXG.DAT respectively. A short documentation is written to OUTEXI after each run.

Data Analysis Procedure

The data of this work has been arranged in proper order and organized by using tabulation method. These organized data was analyzed and described graphically with the help of spreadsheet (Microsoft Excel). Results generated from

this analysis were then compared with the experimental (EXFOR data library) and evaluated nuclear data libraries (ENDF), from the International Atomic Energy Agency (IAEA), to validate the calculated result.

RESULTS AND DISCUSSION

The nuclear reaction cross-sections generated from EXIFON code based on the proton interaction with Iodine nucleus are given in Tables (I & II) as well as in figures (I & II) below, with incident energies 1 to 20 MeV, along with the available experimental EXFOR and evaluated ENDF data. All cross-sections are expressed in millibarns (mb) and energies in Mega electron Volt (MeV).

Table 1: Datasets for I-127 (a,n) Cs-130 reaction

Incident Energy (MeV)	EXIFON (mb)	ENDF (mb)	EXFOR (mb)
8	0	0	0
9	0	0	0.013
10	0	0.001	0.045
11	0	0.2	0.59
12	0	1.39	4.31
13	42.7	8.48	17.7
14	107.3	36.62	68.6
15	191.3	106.78	167.6
16	294.5	204.33	
17	416.5	254.33	
18	552.1	270.89	
19	675.4	300.8	
20	785.1	450.5	

Table 1 is the nuclear cross section data obtained for the production of ceasium 130 through iodine-170 (a,n) channel. The results from this research (I.e EXIFON) are all zero for the energy range from 1 to 12 MeV; therefore the threshold energy is 13 MeV with 42.7 mb cross section. But for EXFOR the threshold energy is 9 MeV with cross section 0.013 mb, while for ENDF the threshold energy is 10 MeV with cross section of 0.001mb.

Table 2: Datasets for I-127 (a,g) Cs-131 reaction

Incident Energy (MeV)	EXIFON (mb)	ENDF (mb)	EXFOR (mb)
9	0	0	0
10	0	0.000045	0.0018
11	0	0.00059	0.0039
12	0	0.00501	0.021
13	0.3	0.0172	0.042
14	0.5	0.0686	0.0966
15	0.7	0.1676	0.1477
16	0.9	0.2657	0.2051
17	1.1	0.3554	0.3322
18	1.2	0.4789	0.5383
19	1.4	0.5876	0.9308
20	1.5		

Table 2 is the nuclear cross section data obtained for the production of ceasium 131 through iodine-170 (a.g) channel. The results from EXIFON are also zero for the energy range from 1 to 12 MeV; therefore the threshold energy is 13 MeV with 0.3 mb cross section. But for ENDF and EXFOR the threshold energy is 10 MeV with cross section 0.000045 mb, and 0.0018mb respectively.
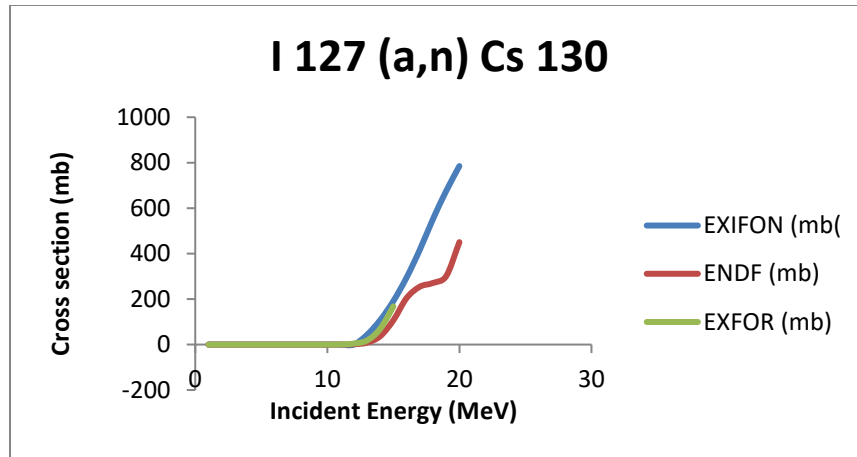
I 127 (a,n) Cs 130

Figure 1: Excitation function of I-127 (a,n) Cs-130 reaction
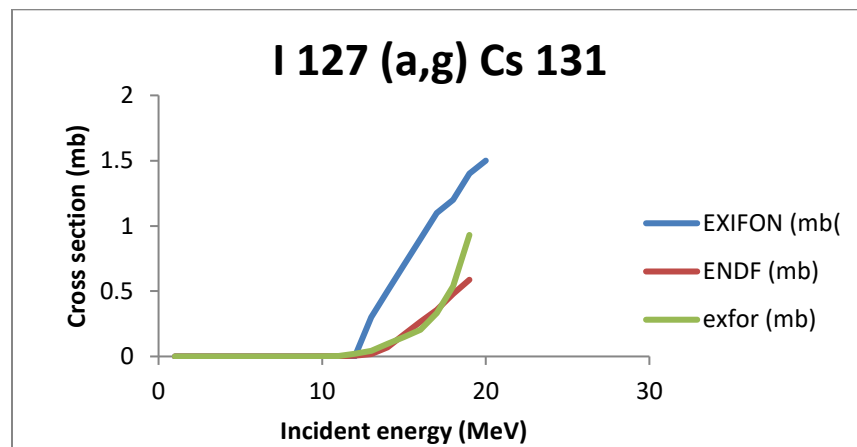
I 127 (a,g) Cs 131

Figure 2: Excitation function of I-127 (a,g) Cs-131 reaction

Figure 1 indicates the reaction I-127(a,n) Cs -130 for the production of Caesium- 130. This is a break up reaction; Caesium 130 has a half life 30 minutes and decays by positron and gamma emission while reaction threshold stands at 13 MeV and cross-section rise from threshold proportionately. The graph shows good agreement between calculated values and evaluated (ENDF) as well as experimental (EXFOR) data files.

Figure 2 show excitation function for the reaction I-127(a, g) Cs-131. Cs-131 is important for Brachytherapy; a form of topical tumor treatment Threshold for this reaction is 13MeV which exhibits the radiative capture of alpha particle by I-127 to produce caesium -131 at excited state. This radioisotope has half life of 10.2days and decays through k-capture and positron emission. The calculated values also show agreement with both ENDF and EXFOR nuclear data files.

CONCLUSION

Owing to the original goal, a new data set for the production cross sections of the Cs130 and Cs131 radionuclides through the alpha particle bombardment on natural Iodine have been reported in the energy range of 1 - 20 MeV using the EXIFON Code. The evaluated cross sections have much importance in several fields such as nuclear medicine, trace elemental analysis and improvement of model calculations.

Cs130 is an important radionuclide whose gamma emission could be useful for SPECT in nuclear medicine and the evaluation would be very instrumental in optimizing production conditions. Cs131 is an important therapeutic radionuclide that is useful for PET and Brachytherapy and its evaluation herein will facilitate its optimized production as well as help in predicting and evaluation of its radiochemical purity.

Indeed these evaluations will go a long way to enhancing the supply and availability of these radionuclides and as well avoid the hazardous route of reactor production as well as the unbecoming consequences of their shortage for nuclear medical procedures.

REFERENCES

Ahmad, I., & Koki, F. S. (2017). Calculation of Reactions Cross Section for Neutron-Induced Reactions on 127 I Isotope. *International Journal of Medical Physics, Clinical Engineering and Radiation Oncology.*, *6*(No 3), 344–359. https://doi.org/10.4236/ijmpcero.2017.63031

Ahmad, I., Yola, Y. I., & Koki, F. S. (2017). *Evaluation of Excitation Functions of Reactions Used in Production of Some Medical Radioisotopes*. 290–303. https://doi.org/10.4236/ijmpcero.2017.63026

Artun, O., & Aytekin, H. (2015). Calculation of excitation functions of proton, alpha and deuteron induced reactions for production of medical radioisotopes 122-125I. *Nuclear Instruments and Methods in Physics Research, Section B: Beam Interactions with Materials and Atoms*, *345*. https://doi.org/10.1016/j.nimb.2014.12.029

Chadwick, M. B. (1995). Medical and industrial applications of nuclear reaction physics. *Acta Physica Hungarica New Series Heavy Ion Physics*, *2*(3–4), 333–346. https://doi.org/10.1007/BF03055117

Elbinawi, A., Al-Abyad, M., Abd-Elmageed, K. E., Hassan, K. F., & Ditroi, F. (2016). Proton induced nuclear reactions on natural antimony up to 17 MeV. *Radiochimica Acta*, *104*(4). https://doi.org/10.1515/ract-2015-2483

Griswold, J. R., Jost, C. U., Stracener, D. W., Bruffey, S. H., Denton, D., Garland, M., Heilbronn, L., & Mirzadeh, S. (2018). Production of Th 229 for medical applications: Excitation functions of low-energy protons on Th 232 targets. *Physical Review C*, *98*(4). https://doi.org/10.1103/PhysRevC.98.044607

Hibstie, Y., Mathuthu, M., & Derso, M. (2018). Analysis of reaction cross-section production in neutron induced fission reactions on uranium isotope using computer code COMPLET. *Journal of Applied Radiation and Isotopes*, *139*, 81–85.

Hilaire, S. (2000). Statistical Nuclear Reactions. *Workshop of Nulear Data and Nuclear Reactor Physics, Design and Safety, Trieste, April, 2000*.

Iwamoto, O. (2007). Development of a Comprehensive Code for Nuclear Data Evaluation , CCONE , and Validation Using Neutron-Induced Cross Sections for Uranium Isotopes Development of a Comprehensive Code for Nuclear Data Evaluation ,. *Journal of Nuclear Science & Technology*, *44*(5), 687–697.

Kalka, H. (1992). Statistical Multistep Reacions from 1 to 100MeV. *Hadrons and Nuclei*, *341*, 289–299. https://doi.org/10.2139/ssrn.2737990

Pandey, K., Agrawal, H. M., & Kumar, A. (2011). Excitation functions of (n, α) reaction cross-sections for some important isotopes from threshold to 20 MeV. *Annals of Nuclear Energy*, *38*(5), 1084–1087. https://doi.org/10.1016/j.anucene.2011.01.002

Qaim, B. S. M. (2012). *The present and future of medical radionuclide production*. *651*, 635–651. https://doi.org/10.1524/ract.2012.1966

Ruth, T. J. (2014). The Medical Isotope Crisis: How We Got Here and Where We Are Going. *Journal of Nuclear Medicine Technology*, *42*(4), 245–248. https://doi.org/10.2967/jnmt.114.144642

Volkert, W. A. (2003). Handbook of radiopharmaceuticals, radiochemistry and applications. *Nuclear Medicine and Biology*, *30*(7), 791. https://doi.org/10.1016/s0969-8051(03)00057-x

Volkert, W. A., & Huffman, T. J. (1999). Therapeutic radiopharmaceuticals. *Chemical Reviews*, *99*(9), 2269–2292. https://doi.org/10.1021/cr9804386

Yamoah, S., & Asamoah, M. (2013). Calculations of Excitation Functions of (n , p), (n , a) and (n , 2n) Reaction Cross-Sections for Stable Isotopes of from Reaction Threshold to 20 MeV. *Journal of Nuclear and Particle Physics*, *3*(4), 100–107.

Zubaida G. H. & Ahmad, I. (2019). Theoretical Calculation of Excitation Function of (p.n), (p,na), (p,np) & (p 2n) Reactions on Stable I-127 from 1 to 20 MeV. *Journal of the Nigerian Association of Mathematical Physics*, *50*(March), 253–258.

Smoked Fish Quality and Safety: A Review

*Kaan I. U., Okunola O. J. and Saulawa A.I

Department of Chemistry, Federal University Dutsin-Ma, Katsina State.
*Corresponding author's email: kaanisaac88@gmail.com

ABSTRACT
Fish is an important source of proteins to human that help to improve human nutrition and economic growth. However, many communities and poor rural households relying on fish to meet their end needs are still constrained by postharvest losses of fish and fish products in the value chain due to spoilage, expensive processing technologies and inability to start a fish business venture. Hence, fish smoking has become the most common method of preservation. To address the issue of quality and safety of the smoked fish, this study provided a comprehensive review of acceptable practices to address potential hitches threatening the safety of fish and fish products, specific factors influencing the smoking process and the reward for adopting improved techniques as well as eight stimuli for safe food processing and production in developing countries.
Keywords: Fish, Smoked, Quality, Safety

INTRODUCTION

Without any processing or preservation methods, fish is extremely prone to deterioration. (Okonta & Ekelemu, 2005) and requires proper handling and preservation to increase its shelf life, quality and nutritional value (Ye, 1999).

Despite its importance, the fishing sector experiences massive postharvest losses, which are estimated to be between 35 and 40 percent of landed weight. Food and Agriculture Organization [FAO], 1994). According to FAO (1994), postharvest losses still account for around 25% of the annual global catch. Fishing communities, whose status and income frequently depend on post-harvest activities, are severely harmed by these losses.

The quality of fish and fisheries products has grown to be a major problem for the global fish business. (Huss et al., 2003). Despite technological advancements in fish production, fish is one of the most perishable foods, and as a result of the globalization of food trade, fish products tend to be more susceptible to rejection due to poor quality, especially if the initial raw materials are of poor quality.

For producers and end users alike, worries about the quality of fresh and processed fish products are a real worry that never goes away. Since fish is one of the essential diets required for optimal human health performance, this reality will never change. Fish is a major source of protein and a source of money for many low-income rural communities (Béné et al., 2009).

When consumed once per week or more (He et al., 2004), or consumed at approximately 900 mg/day (Kris - Etherton et al., 2002) if possible, fish has the potential to reduce mortality from coronary heart disease (He et al., 2004), supply omega-3 fatty acid, protein, vitamins, selenium and iodine (Odeyemi et al., 2020) particularly nutritionally digestive proteins such as lysine and methionine among other amino acids, lipid soluble vitamins A and D, and microelements such as calcium among others (Medina et al., 2009)

Fish after harvest is highly perishable because of its high susceptibility to microbial attack (Ashie et al., 1996). As a perishable food item, fish has shelf life ranging from several days to about three weeks (Amit et al., 2017). The losses of fish after harvest are described by Akande and Diei-Quadi (2010) as physical loss (i.e., damages to body parts), quality loss (i.e., unacceptability or spoilage) and market force loss (i.e., monetary).

Exacerbated by poor road infrastructure, seasonal changes, improper packaging and storage among others, the magnitudes of annual post-harvest losses of landed fish weight were estimated at 35-40% regionally and 25% globally (Adeyeye & Oyewole, 2016). These losses vary by type of species, size and hygiene status. As a result, people managed to develop innovative approaches to break through the hurdles. For example, hanging fish over fire to dry gained more attention and the smoke improves the flavor with extended storage time. Consequently, fish smoking became a universal method for preserving fish (Tys et al., 2009). In spite of this adaptation to smoking as a drying method to preserve fish products for longer period of time and improved flavor, many communities and poor rural households relying on fish to meet their end needs are still constrained by post-harvest losses of fish and fish products in the value chain in developing countries due to spoilage, expensive processing technologies and inability to start a fish business venture.

To address the issue of quality and safety of the smoked fish. This study provided a comprehensive review on acceptable practices to address potential hitches threatening safety of fish and fish products, specific factors influencing the smoking process and the reward for adopting improved techniques as well as eight stimuli for safe food processing and production in developing countries.

Potential Hitches Warrant Careful Attention

The most important thing when handling fish is personal cleanliness. One of the main causes of the decline in the quality of fish and many other food products is poor personal hygiene. The first step in good hygiene procedures is always to wash your hands properly using one of the twelve stages laid out by the World Health Organization (WHO, 2009). The steps were demonstrated using visual aids.

Because nothing can be done to improve the quality of the fish before or after smoking, handling it properly before smoking is extremely important. Fish can also get damaged after smoking due to inadequate cleanliness, cross-contamination, breakage, etc. (Training Division of the Sea Fish Industry Authority [TDSFIA], 1987d). Given that most people have germs on their skin and in their respiratory tracts, this is quite plausible.

Microbes, autolysis, and cross-contaminations are frequently prevalent main causes of fish and food deterioration or spoilage beginning at the time of harvest. Conditions for storage and processing can also have an impact on spoilage, which can start right after harvest or at the time of slaughter (Odeyemi et al., 2020). When microbial load reaches between 10^7 and 10^9 cfu/g, there is a high likelihood that it will result in the production of off-odor or off-flavor, making the fish product undesirable due to a decline in quality, palatability, and shelf-life as well (Mik-Krajnick et al., 2016; Odeyemi et al., 2018; Odeyemi et al., 2020), which will adversely affect efforts to curb food wastage and food security.

According to Medina et al. (2009), the development of off-flavor as well as quality loss of fish products in cold storage is typically brought on by the influence of lipid oxidation. This is because radical attacks on unsaturated fatty acids cause the formation of hydro peroxides, which then release new radicals freely to produce low molecular weight volatiles like aldehydes, ketones, and alcohols, or are frequently catalyzed by hemoglobin. There are a number of well-documented obstacles in the manufacture of smoked fish used in processed fish products.

According to Salvi and Barnes (2010), several researchers have previously issued health advisories regarding the dangers of exposing people to harmful fumes such carbon monoxide, sulfur dioxide, and poly-aromatic hydrocarbons. In addition, Kodgule and Salvi (2012) listed respiratory tract infections, particularly in children and the elderly, and asthma as additional complications associated with smoke inhalation. Chronic obstructive pulmonary disease is also referred to as an emerging killer disease (Umoh & Etete, 2014) in most developing countries. Nigeria has reported to be experiencing similar issues (Umoh & Etete, 2014). If the heating procedure is applied incorrectly, the smoked fish products may end up losing practically useful elements like protein, vitamin C, and other important nutrients (Amit et al., 2017).

Improved Fish Handling and Smoking Rewards Better Quality

In the realm of fish processing and safety, there is an increasing need for improved fish handling and smoking (IFHAS). Quality assurance is one of the areas targeted for guaranteeing the safety of fish or food.

It has been defined by International Standards (Sciortino & Ravikumar, 1999) as a planned, methodical action designed to ensure confidence regarding the caliber of a certain good or service. Fish quality assurance necessitates precise yet comprehensive scientific information (FAO & WHO, 2001), which also takes into account controls and dangers related to fish and fisheries products (Food and Drug Administration [FDA], 2011). It has been advised to take steps to reduce microbial spoilage and delay lipid oxidation, including controlling the storage temperature, applying brine solution, packing methods, and using supplemental or natural antioxidants (Medina et al., 2009).

Appropriate policies and technologies that can be applied correctly during the processing and storage stages should also serve as a reference for such efficient methods or strategies intended to prevent food spoiling (Odeyemi et al., 2020). Fish must be preserved properly for a prolonged amount of time in order to maintain its nutritional value, color, texture, and flavor (Amit et al., 2017)

With increasing consumers' demand for fresh food and growing efforts to keep or maintain the freshness of raw fish upon harvest, strategies such as efficient storage of fish in the forms of chilled and frozen products are examples of highly recommended practices which have also dominate the proportion of fish production and consumption in areas with developed technologies driven by rising demand for high quality products and the impact of distant markets and the need for long -term storage (Medina et al., 2009). Application of ice in ice -cooler boxes as the only method of fresh fish storage by fish retailers in the local markets in the developing countries (Alosias, 2019) is an example of chilled storage for fresh fish preservation commonly practiced in developing countries, albeit the use of refrigerators for storage of all types of fresh and other processed foods can be found in supermarkets. The term chilling and freezing are sometimes used interchangeably when cooling is conducted below 5ºCelsius as described in the physical principles of food preservation (Amit et al., 2017).

In an effort to withhold the sensory and nutritional qualities of fish products, several technologies such as modified atmosphere packaging, freeze - chilling, chilling by use of slurry ice, irradiation and many other ground breaking

practices have been proposed and employed (Medina et al., 2009). Data from a report published by the Food and Agricultural Organization of the United Nations have also shown the total production and consumption of fresh and frozen fish products above 10 million tones (Medina et al., 2009).

A number of procedures, including the use of heat, salting, and the supply of cold systems, are some complimentary recommendations targeted at bolstering efforts to manufacture high quality fish products. However, some of these preservation techniques, like cold chain, have a financial cost associated with them even though they help the food last longer (Gokoglu & Yerlikaya, 15). Such techniques or approaches could not be feasible in regions without ice production unless new technology is implemented (Wang & Wang, 2005), especially in developing nations.

Application of heat is one of the oldest and universal methods of preserving perishable food products (FAO, 2012). Even if the application of heat on fresh fish is effective against pathogenic and spoilage microorganisms as well as inactivation of enzymes and enhancement of desirable flavor and taste, producers and processors should be mindful of possible detrimental effects of thermal sensitivity due to cooking and sterilization (Medina et al., 2009). Smoking fish products, categorized by Flick (2010) as cold smoking (usually below 30℃) having long smoking time & shelf-life or hot smoking (greater than 80℃) having short smoking time & shelf-life using hardwood & other materials, is one example. Hardwood is generally a preferred source of fuel because it imparts a milder flavor rather than softwoods which have a more resinous flavor. However, careful selection of wood is very crucial because fuel woods that have previously been exposed to chemicals or hazardous materials are a major source of Benzo [a] pyrene (Stolyhwo & Sikorski, 2005) – a marker of carcinogenic polycyclic aromatic hydrocarbons that can precipitate in smoked products and lead to intoxication or food borne diseases. After an assessment of the association between personal exposure to benzo [a] pyrene from indoor air pollution and leukocyte mitochondrial DNA copy number, Wong et al. (2017) revealed that such an exposure may alter mitochondrial dynamics. These serious concerns were acknowledged but argued with an assumption that consumers' choices or preferences are more noticeable than concerns over intoxication from certain woods. Consumers' preferences are generally linked to flavor, aroma, and preservative effect (Tull, 1997). Although Benzo [a] pyrene has been categorized as carcinogenic to human health (International Agency for Research on Cancer [IARC], 2012) which targets organs such as lung, breast and gastrointestinal tracts (Hamidi et al., 2016), its existence solely cannot seemly be indicative of the incidence and critical harmfulness of polycyclic aromatic hydrocarbons in foods (European Food Safety Authority [EFSA], 2008).

In smoking, the process combines the effects of smoke, heat and drying simultaneously (Salvi & Brashier, 2014). The smoke always deposits chemicals such as Phenols and Formaldehyde in the forms of vapors (TDSFIA, 1987a), which either kill or prevent microbial growth in stored smoked products for an extended shelf-life (Salan et al.,2006), though they can increase with time and temperature (Hood et al., 1983). It helps reduce the water content of fish flesh via evaporation (TDSFIA, 1987a) due to the movement of gases in the smoke and the rising temperature over the surface fish flesh. The speed at which water is lost from the surface of fish flesh, termed as drying rate (TDSFIA, 1987a), increases with increase in velocity of air in the oven which is also influenced by the speed at which water can move from within the flesh to its surface. Besides reduction of water content, penetration of heat and the chemical components formed a barrier layer (TDSFIA, 1987a) which reduces the oxygen that enters the flesh from the surrounding air and reduces rancidity of the fat content as well. Both smoke and heat components (FAO CXS 311e, 2013) can potentially allow the smoked products to be transported and stored without refrigeration. After 7 days of storage (Kumolu et al.,2010), significant differences in texture, appearance, odor, flavor and taste are also noticeable. As smoked fish started to dominate the demand for fish products in the market, concerns over polycyclic aromatic hydrocarbon levels could be curbed or mitigated by increasing the distance between the fish and the producing source of smoke as well as optimizing microbiological food safety temperature (Hokkanen et al., 2018) and other probable options.

Hot smoking mostly cooked fish (TDSFIA, 1987a) which helps destroy autolytic spoilage and reduce water activity within the flesh, while cold smoking provides smoke-chemicals that can significantly terminate spoilage microorganisms. Hot smoking is a popular fish processing and preservation method practiced traditionally.

While traditional fish smoking is widespread throughout Africa, local fish processors and producers use a variety of processing and preservation methods that differ from location to location (Adeyeye & Oyewole, 2016). It's still outdated and typically linked to heat/smoke waste, accidents, and other issues (Motorykin et al., 2015). Additionally, the items put consumers' health at risk because of inadequate cleanliness and the potential buildup of carcinogenic substances (Essumang et al., 2012), as was previously highlighted (Stolyhwo & Sikorski, 2005).

Paying close attention to improved handling, packaging, and storage is one of the best ways to address the aforementioned concerns in order to minimize losses (International Labor Organization - World Employment Program [ILO - WEP], 1982). This serves as a basis for better managing and smoking behaviors. Furthermore, specific guidelines for IFHAS have already been created for hot-smoked fish processors (Bannerman, 2001). Additionally, the United States Department of Agriculture (USDA), in 2015, established safe minimum internal temperatures for fish

and other food products. Efforts to encourage and support IFHAS technologies in Africa have been captured as essential tread of the African Network on Fish Technology and Safety (ANFTS) (ANFTS, 2017). But in practice, selection of the best quality raw fish is the first step (TDSFIA, 1987b) that ensures the best quality smoked fish products. Subsequently, good & acceptable quality can be ensured via proper handling of fish and fish products right from the production site till consumed (Sciortino & Ravikumar, 1999). The process is then complemented by grading based on species, sizes, qualities and prices. If preferred, the raw fish products can be salted using dry salt or brine solution prior to smoking. Salting helps improve flavor & texture (TDSFIA, 1987a) of the final smoked fish products and plays a preservative role in reducing water content as salt is observed into the flesh and draws out water in form of drips or vapor.

Quality and Safety Status of Smoked Fish
Traditional smoking methods entail applying wood smoke to pre-salted, whole, or filleted fish, allowing smoke from incomplete wood burning to come into direct contact with the product. If the process is not sufficiently regulated or extremely intense smoking methods are used, it has been discovered that PAHs will contaminate the fish (Guill´en and Sopelana, 2005, Gómez-Estaca et al., 2011).

Smoked fish is one source of polycyclic aromatic hydrocarbons (PAHs), which are a broad class of organic molecules with two or more fused aromatic rings composed of carbon and hydrogen atoms (Guillen, Sopelana, & Partearroyo, 1997). The incomplete combustion or thermal degradation of the organic components occurs when fish is smoked, roasted, barbecued, or grilled, leading to the formation of PAHs (WHO, 2006). Pyrolysis of the fats in the meat/fish generates PAHs that become deposited on the meat/fish. PAHs production by cooking over charcoal (barbecued, grilled) is a function of both the fat content of the meat/fish and the proximity of the food to the heat source (Kazerouni, Sinha, Hsu,Greenberg, & Rothman, 2001; Phillips, 1999).

Several analyses of charcoal roasted/grilled common fish by several researchers (Ogbadu and Ogbadu, 1989; Akpan et al., 1994; Guill´en and Sopelana, 2005; Akpambang et al., 2009; Linda et al., 2011) have proven the presence of PAHs such as benzo [α] pyrene, anthracene, chrysene, benzo[α]anthracene, indeno [1,2,3-c,d] pyrene. Several researchers (Bababunmi et al., 1982; Alonge, 1988; Lijinsky, 1999; Fritz and Soos, 1980; Borokovcova et al., 2005) reported that most of these PAHs have been found to be carcinogenic while some are not. Emerole (1980) studied and screened for the presence of PAH in local foodstuffs available in Nigerian market. He discovered that appreciable amounts of benzo[a] anthracene and benzo [α] pyrene were found present in three varieties of smoked fish and smoked meat (suya) purchased from a popular market in Ibadan, Nigeria. High levels of PAHs have been reported to be associated with the dark colourations in intensively heated fish products. Research has also revealed the existence of aflatoxins in fish and fish feed. Aflatoxin-producing microsclerotial species of Aspergillus section Flavi, Aspergillus flavus, and Aspergillus parasiticus naturally create these extremely deadly substances. (Adebayo-Tayo et al., 2008; Almeida et al., 2011; Barbosa et al., 2013).

Furthermore, the detrimental impacts of aflatoxin-contaminated feeds on fish health and productivity have been well-documented (Jantrarotai & Lovell, 1990; Abdelhamid, Salem, Mehrem, & El-Shaarawy, 2007; Zaki, Sharaf, Mostafa, & Fawzi, 2008). Despite the wealth of information on aflatoxin contamination of different foods and livestock feeds, as well as the health consequences associated with it, little to no data are available regarding the prevalence of Aspergillus species and aflatoxin in fish in Nigeria and many other developing nations, despite the fact that fish is a common food item in these countries. A good fish smoking plan (FAO, 2005) should not only consider applying IFHAS approach but also improved smoking kiln or fish drier.

The Prospect on Improved Food Safty and Incentives
Adeyeye (2016) states that the prospect for increased food safety outlines the requirement for the creation of strategic food policies meant to improve food product safety and take advantage of globalization opportunities, such as the encouragement of trading these food products domestically or internationally. Policies aimed at enhancing safety and quality control in order to attain profitable and sustainable trade ought to be devised in compliance with regional and global accords. These include the Sanitary and Phytosanitary (SPS) agreement, which acknowledged the Codex Alimentarius Commission (CAC) for standardizing food standards, and the Technical Barriers to Trade (TBT) agreement, among other significant accords, in order to achieve the World Trade Organization's (WTO) goal of market globalization for safe food production.

Improving the safety of food items may encounter challenges during implementation in many developing nations if incentives are not given to food processors and producers. According to Adeyeye (2016), encouraging the adoption of measures targeted at enhancing the sanitary quality of the products as well as raising awareness of the medium- and long-term benefits will help improve food product safety. These incentives or measures were grouped and termed in

this study as the *eight stimuli for safe food processing and production in developing countries*. Policy and influential decision makers should consider:

1. Preferential rates of water and electricity fees. Charging local processors and producers specified preferential rates can help prevent them from relying on free or cheap water harvested from wells or open - surface water bodies which are potential sources of contamination of food products. This may also attract local food processors and producers to start using electric dryers and refrigerators, among others, to produce good quality food

   products that guaranteed safety of consumers.

2. Provision of technical assistance via adequate training sessions on critical processing and preservation steps by competent and/or certified trainers for sensitization of fish processors and all players actively engaged in the fish value chain as well. Technical assistance should also include promotion of food safety awareness on hygiene, contamination, economic, social   and   health benefits as well as consumption patterns via the available sources of communications.

3. Facilitating technology transfer (e.g., infrastructure, transportation, electricity, water supply   etc.) from household level to small or medium industrial scale coupled with tax reduction and relevant business plan for economic growth.

4. Facilitation of loans to groups or associations as startup capital at reduced rates for acquisition of small equipment and machinery.

5. Subsidizing products locally produced as motivation and encouragement to local cooperatives or associations.

6. Provision of supports to local women groups or associations actively engaged in food processing to balance gender economic growth in developing countries.

7. Encouraging the role of NGOs in collaboration with relevant stakeholders to promote safety and quality food processing and production. Organizations such as WHO and FAO, to mention a few, can play critical roles in promoting safe processing and production of food products. These organizations are expected to be engaged with stakeholders in defining national food safety policies under appropriate food safety standards and provide appropriate technical guidance for economic growth.

8. Tapping annual prizes for individuals, groups or associations processing and producing competitive food products that meet safety standards.

CONCLUSION

The study addressed significant topics that demonstrate the range of IFHAS strategies to guarantee high-quality, safe food products. An endeavor of this kind can be effectively accomplished if fishermen, fish processors, traders, and everyone else involved in handling fish until it is consumed in developing nations where customary hot fish smoking has been documented as a widespread practice, are better prepared for any obstacles they may face and are aware of the acceptable or recommended practices, the necessary skills, and the potential rewards in terms of quality and profits. Eight stimuli have been identified as incentives to boost safe fish processing and production. Good hygiene, improved handling, and smoking are important drivers that reward improved quality of fish products within developing countries. Other factors that affect the smoking process, such as the addition of salt and other fuels and smoking kiln selection, play a significant role in extending the shelf life of the products and luring consumers' preferences.

REFERENCES

Abdelhamid, A. M., Salem, M. F. I., Mehrem, A. I., & El-Shaarawy, M. A. M. (2007). Nutritious attempts to detoxify aflatoxic diets of tilapia fish. *Egyptian Journal of Nutrition and Feeds,* 10(1), 205–223.

Adebayo-Tayo, B. C., Onilude, A. A., & Patrick, U. G. (2008). Mycoflora of smoke-dried fishes sold in Uyo, Eastern Nigeria. *World Journal of Agricultural Science,* 4(3): 346-350.

Adeyeye, S. A. O. (2016). Safety Issues in Traditional West African Foods: A Critical Review. *Journal of Culinary Science & Technology,* doi: 10.1080/15428052.2016.1225533.

Adeyeye, S. A. O., & Oyewole, O. B. (2016). An overview of traditional fish smoking in Africa. *Journal of Culinary Science & Technology,* 14(3), 198-215.

Affel R., & Smith, N. (2017). Report on a campaign and durbar on improved fish smoking technology and best hygienic fish handling and advocacy practices awards. The SAID/Ghana Sustainable Fisheries Management Project

(SFMP). Narragansett, RI: Coastal Resources Center, Graduate School of Oceanography, University of Rhode Island and Central and Western Fish Mongers Improvement Association. GH2014_COM028_CEWEFIA.12pp.http://www.crc.uri.edu/download/GH2014_COM028_CEWEFIA_FIN508.pdf Accessed 6 June 2018.

Akande, G., & Diei-Ouadi, Y. (2010). Post-harvest losses in small-scale fisheries: case studies in five sub-Saharan African countries. FAO Fisheries and Aquaculture Technical Paper, RomeIss.50:I,III,IV,V,IX,X,XI,XII,XIII,1-13,15-39,41-59,61-65,67-69,71
72https://search.proquest.com/openview/74897e1dad1d1c44c7c3577cdd930604/1?pqorigsite=gscholar&cbl=23732 0 Accessed 8 February 2018.

Akpambang, V. O. E., Purcao, G., Lajide, L., Amoo, I. A., Conte, L. S., & Moret, S. (2009). Determination of polyaromatic hydrocarbons in commonly consumed Nigerian smoked/grilled fish and meat. Food Additives and Contaminants, 26(07), 1090–1103.

Akpan, V., Lodovici, M., & Dolara, P. (1994). Polycyclic aromatic hydrocarbons in fresh and smoked fish samples from the three Nigerian cities. Bulletin on Environmental Contaminants and Toxicology, 53, 246–253.

Almeida, I. F. M., Martins, H. M. L., Santos, S. M. O., Freitas, M. S., Da Costa, J. M. G. N., & Bernardo, F. M. A. (2011). Mycobiota and aflatoxin B1 in feed for farmed Sea Bass (Dicentrarchus labrax). Toxins, 3, 163–171. doi:10.3390/toxins3030163

Alosias, J. K. B. (2019). A pilot survey on retail fish marketing in Juba, South Sudan: perceptions on motivation and challenges. *African Journal of Tropical Agriculture,* 7(12), 001-011.

Alosias, J. K. B. (2018). Building research infrastructures is key to developing South Sudan's fishery sector. Africa Portal, South African Institute of International Affairs https://www.africaportal.org/features/building-research-infrastructures-key-developing-south-sudans-fisheries-sector Accessed 6 June 2018.

Amit, S. K., Uddin, M. M., Rahman, R., Islam, S. R., & Khan, M. S. (2017). A review on mechanisms and commercial aspects of food preservation and processing. Agriculture & Food Security, 6(1), 51.

Ashie, I. N. A., Smith, J. P., Simpson, B. K., & Haard, N. F. (1996). Spoilage and shelf-life extension of fresh fish and shellfish. Critical Reviews in Food Science & Nutrition, 36(1-2),87-121.

Bababunmi, E. A., Emerole, G. O., Uwaifo, A. O., & Thabrew, M. I. (1982). The role of aflatoxins and other aromatic hydrocarbons in human carcinogenesis. In H. Bartsch & N.Armstrong (Eds.), Host factors in carcinogenesis (Vol. 39, pp. 395–403). *IARC Scientific Publications.*

Bannerman, A. Mck. (2001).Hot smoking of fish. Torry Advisory Note No. 82 (revised), Torry Research Station. Ministry of Agriculture, Fisheries and Food http://www.fao.org/3/x5953e/x5953e01.htmAccessed 8 February 2018.

Barbosa, T. S., Pereyra, C. M., Soleiro, C. A., Dias, E. O., Oliveira, A. A., Keller, K. M., & Rosa, C. A. R. (2013). Mycobiota and mycotoxins present in finished fish feeds from farms in the Rio de Janeiro State, Brazil. International Aquatic Research, 5, 3. doi:10.1186/2008-6970-5-3

Béné, C., Steel, E., Luadia, B. K., & Gordon, A. (2009). Fish as the "bank in the water"–Evidencefrom chronic-poor communities in Congo. Food policy,34(1), 108-118.

Borokovcova, I., Dofkova, M., Rehurkova, I., & Ruprich, J. (2005). Polycyclic aromatic hydrocarbons in the Czech Foodsstuffs in the Year 2004. Chemical Listings, 99, 268–270.

Elbashir, S., Parveen, S., Schwarz, J., Rippen, T., Jahncke, M., &DePaola, A. (2018). Seafood pathogens and information on antimicrobial resistance: A review. Food Microbiology, 70, 85-93.

Emerole, G. O. (1980). Carcinogenic PAHs in some Nigerian Foods. Bulletin of Environmental Contaminants and Toxicology, 24, 641–646. doi:10.1007/BF01608167

Essumang, D. K., Dodoo, D. K., &Adjei, J. K. (2012). Polycyclic aromatic hydrocarbon (PAH) contamination in smoke-cured fish products. Journal of Food Composition and Analysis, 27(2), 128-138.

European Food Safety Authority (EFSA). (2008). Polycyclic Aromatic Hydrocarbons in Food-Scientific Opinion of the Panel on Contaminants in the Food Chain. EFSA Journal, 6(8),724.

FAO. (1994). Utilization of Bonga (Ethmalosa fimbriata) in West Africa. A. Jallow. Rome.

FAO.(2016).The state of World Fisheries and Aquaculture 2016. Contributing to food security and nutrition for all. Rome. 200 pp. http://www.fao.org/3/a-i5798e.pdf Accessed 8 February 2018.

FAO. (2012). Second international congress on seafood technology on sustainable, innovative and healthy seafood. Food and Agriculture Organization Fisheries and Aquaculture Proceedings 22, Rome. ISBN 978-92-5-107108-3 (Ryder, J and Balaban, M.O, 2011) http://citeseerx.ist.psu.edu/viewdoc/download?doi=10.1.1.401.582&rep=rep1&type=pdf Accessed 27 May 2016.

FAO. (2005). Report and papers presented at the seventh FAO expert consultation on fish technology in Africa. FAO Fisheries Report No. 712. http://www.fao.org/3/y9155b/y9155b0k.htm Accessed 8 February 2018.

FAO CXS311e. (2013). Standards for smoked fish, smoke-flavored fish and smoke-dried fish. http://www.fao.org/input/download/standards/13292/CXS_311e.pdf Accessed 23 May 2016.

FAO and WHO. (2001). Hazard analysis and critical control point (HACCP) system and guidelines for its application. Annex to CAC/RCP 1-1969, Rev. 3 (1997) http://www.fao.org/docrep/005/y1579e/y1579e03.htm Accessed 23 May 2016.

Flick, G. J. (2010). Smoked fish: old product with new appeal offers enhanced taste & shelf-life. Global Aquaculture Alliance http://agris.fao.org/agrissearch/search.do?recordID=US201301852147 Accessed 20 June 2016.

Food and Drug Administration (FDA). (2011). Fish and fishery products hazards and controls guidance. Fourth Edition. U.S. Department of Health and Human Services, Food and Drug Administration, Center for Food Safety and Applied Nutrition https://www.fda.gov/media/80637/download Accessed 14 May 2018.

Fritz, W., & Soos, K. (1980). Smoked Food and Cancer. Journal of Bibliographic Nutrition and Dietetics, 29, 57–64.

Gokoglu, N., &Yerlikaya, P. (2015). Seafood chilling, refrigeration and freezing: Science and Technology. John Wiley & Sons. https://www.wiley.com/enss/Seafood+Chilling,+Refrigeration+and+Freezing:+Science+and+Technology-p-9781118512234 Accessed 8 February 2018.

Gómez-Estaca, J, Gómez-Guillén, MC, Montero, P, Sopelana, P, & Guillén, MD. (2011). Oxidative stability, volatile components and polycyclic aromatic hydrocarbons of cold smoked sardine (sardina pilchardus) and dolphin fish (coryphaena hippurus). Lwt – Food Sci. Technol., 44, 1517-1524.

Guillén, M. D, & Sopelana, P. (2005). Headspace solid-phase microextraction as a tool to estimate the contamination of smoked cheeses by polycyclic aromatic hydrocarbons. *Journal Of Dairy Science,* 88, 13–20.

Guillen, M. D., Sopelana, P., & Partearroyo, M. A. (1997). Food as a source of polycyclic aromatic carcinogens. Reviews on Environmental Health, 12, 133–146. doi:10.1515/REVEH.1997.12.3.133

Hamidi, E. N., Hajeb, P., Selamat, J., &Razis A. F. A. (2016). Polycyclic aromatic hydrocarbons (PAHs) and their bioaccessibility in meat: a tool for assessing human cancer risk. *Asian Pacific Journal of Cancer Prevention,* 17 (1), 15-23.

Håstein T, Hjeltnes B, Lillehaug A, Utne Skåre J, Berntssen M, Lundebye A. Food safety hazards that occurduring the production stage: *Rev. sci. tech. Off. int. Epiz* 2006; 25:607-625

He, K., Song, Y., Daviglus, M. L., Liu, K., Van Horn, L., Dyer, A. R., & Greenland, P. (2004). Accumulated evidence on fish consumption and coronary heart disease mortality: a meta-analysis of cohort studies. Circulation, 109(22), 2705-2711.

Hood, M. A., Ness, G. E., Rodrick, G. E., & Blake, N. J. (1983). Effects of storage on microbial loads of two commercially important shellfish species, Crassos-treavirginica and Mercenaria campechiensis. Appl. Environ. Microbiol.,45(4), 1221-1228.

Hokkanen, M., Luhtasela, U., Kostamo, P., Ritvanen, T., Peltonen, K., &Jestoi, M. (2018). Critical effects of smoking parameters on the levels of polycyclic aromatic hydrocarbons in traditionally smoked fish and meat products in Finland. *Journal of Chemistry,* 2018. http://downloads.hindawi.com/journals/jchem/2018/2160958.pdf Accessed 19 September 2019

Huss H, Ababouch L, Gram L. Assessment and Management of Seafood Safety and Quality, FAO Fisheries Technical Paper 444, Rome, 2003, 230.

International Agency for Research on Cancer (IARC). (2012). Chemical agents and related occupations. A review of human carcinogens. IARC Monographs on the evaluation of carcinogenic risks to humans, ISBS-13 (PDF): ISBN 978-92-832-0138-0 https://publi-cations.iarc.fr/123

International Labor Organization-World Employment Program (ILO-WEP). (1982).Small-scale processing of fish. International Labor Office, CH-1211 Geneva 22, Switzerland <http://www.nzdl.org/gsdlmod?e=d-00000-00---off-0cdl--00-0----0-10-0---0---0direct-10---4------0-1l--11-en-50---20-about---00-0-1-00-0--4----0-0-11-10-0utfZz-8-00&cl=CL1.91&d=HASH9e9f8f99212e7c3ee056a4>=2>Accessed 8 February 2018.

Jantrarotai, W., & Lovell, R. T. (1990). Subchronic toxicity of dietary aflatoxin B1 to channel catfish. Journal of Aquatic Animal Health, 2, 248–254. doi:10.1577/1548-8667(1990) 002<0248:STODAB>2.3.CO;2

Kazerouni, N., Sinha, R., Hsu, C. H., Greenberg, A., & Rothman, N. (2001). Analysis of 200 food items for benzo[a]pyrene and estimation of its intake in an epidemiologic study. Food Chemical Toxicology, 39, 423436. doi:10.1016/S0278-6915(00)00158-7

Kodgule, R., &Salvi, S. (2012). Exposure to biomass smoke as a cause for airway disease in women and children. CurrOpin Allergy ClinImmunol,12, 82–90.

Kris-Etherton, P. M., Harris, W. S., &Appel, L. J. (2002). Fish consumption, fish oil, omega-3 fatty acids, and cardiovascular disease. Circulation,106(21), 2747-2757.

Lijinsky, W. (1999). The formation and occurrence of polynuclear aromatic hydrocarbons associated with foods. *Journal of Muttagenic Research,* 259(3–4), 251–261.

Medina, I., Gallardo, J. M., &Aubourg, S. P. (2009). Quality preservation in chilled and frozen fish products by employment of slurry ice and natural antioxidants. *International Journal of Food Science & Technology*, 44:1467-1479.

Mikš-Krajnick, M., Yoon, Y. J., Ukuku, D.O., & Yuk, H. G. (2016). Volatile chemical spoilage indexes of raw Atlantic salmon (Salmosalar) stored under aerobic condition in relation to microbiological and sensory shelf lives. Food Microbiology, 53, 182-191.

Motorykin, O., Schrlau, J., Jia, Y., Harper, B., Harris, S., Harding, A., et al. (2015). Determination of parent and hydroxy PAHs in personal PM2. 5 and urine samples collected during Native American fish smoking

Ndiaye, O., SodokeKomivi, B., & Diei-Ouadi, Y. (2014). Guide for developing and using the FAO-Thiaroye processing technique (FTT-Thiaroye). Rome, FAO. 67 pp. http://www/fao.org/3/a-i4174e.pdf Accessed 8 February 2018.

Odeyemi, O. A., Alegbeleye, O. O., Strateva, M., &Stratev, D. (2020). Understanding spoilage microbial community and spoilage mechanisms in foods of animal origin.Comprehensive Reviews in Food Science & Food Safety, 19(2), 311-331.

Odeyemi, O. A., Burke, C. M., Bolch, C. J., & Stanley, R. (2018). Evaluation of spoilage potential and volatile metabolites production by Shewanellabaltica isolated from modified atmosphere packaged live mussels. Food Research International, 103, 415-425.

Ogbadu, G. H., & Ogbadu, L. J. (1989). Levels of benzo (a) pyrene in some smoked ready-to eat Nigerian foods. Lebensmittel- Wissenschaft Und Technologie, 22(5), 313–314.

Okonta, A. A., & Ekelemu, J. K. (2005). A preliminary study of micro-organisms associated with fish spoilage in Asaba, Southern Nigeria. Proceedings of the 20th Annual conference of fisheries society of Nigeria (FISON), Port-Harcourt 14th-18th November, 2005-557-560.

Phillips, D. H. (1999). Polycyclic aromatic hydrocarbons in the diet. Mutagen Research, 443, 139–147.

Salan, O. E., Galvao, J. A., &Oetterer, M. (2006). Use of smoking to add value to salmonid trout. Braz. Arch. Biology. Technol. 49(1), 57-62.

Salvi, S., & Barnes, P. J. (2010). Is exposure to biomass smoke tech biggest risk factor for COPD globally? Chest, 138, 3–6.

Sciortino, J. A., &Ravikumar, R. (1999). Fishery harbor manual on the prevention of pollution –Bay of Bengal Programme. Chapter 5: Fish quality assurance http://www.fao.org/docrep/X5624E/x5624e08.htm Accessed 17 January 2019.

Stolyhwo, A., & Sikorski, Z. E. (2005). Polycyclic aromatic hydrocarbons in smoked fish – acritical review. Journal of Food Chemistry, 91(2), 303-311.

Training Division of the Sea Fish Industry Authority (TDSFIA). (1987a). Preservative action by salting and smoking. Seafish Open Learning. Seafood Training Academy. http:// seafoodacademy.org/pdfs/fsolm-seg-2.pdf Accessed 8 February 2018.

Training Division of the Sea Fish Industry Authority (TDSFIA). (1987b). Raw material selection and preparation. Seafish Open Learning. Seafood Training Academy. http://seafoodacademy.org/pdfs/fsolm-seg-3.pdf Accessed 8 February 2018.

Training Division of the Sea Fish Industry Authority (TDSFIA). (1987c). Smoking Kiln. Seafish Open Learning. Seafood Training Academy. http://seafoodacademy.org/pdfs/fsolm-seg-5.pdf Accessed 8 February 2018.

Training Division of the Sea Fish Industry Authority (TDSFIA). (1987d). Product handling and packaging. Seafish Open Learning. Seafood Training Academy http://seafoodacademy.org/pdfs/fsolm-seg-6.pdf56.

Tull, A. (1997). Food and Nutrition. Second Edition, Oxford University Press, (pp104-109) Oxford, UK

Tys, D., Pieters, M., Sicking, L., & Abreu Ferreira, D., (Ed.). (2009). Understanding a medieval fishing settlement along the southern Northern Sea: Walraversijde, c. 1200-1630. Beyond the Catch: Fisheries of the North Atlantic, the North Sea and the Baltic, 91–122.

Umoh, V. A., & Etete, P. (2014). The relationship between lung function and indoor air pollution among rural women in the Niger Delta region of Nigeria. Lung India, 31, 110–5.

Wang, S. G., & Wang, R. Z. (2005). Recent developments of refrigeration technology in fishing vessels. Renewable Energy,30(4), 589-600.

WHO. (2006). Polycyclic aromatic hydrocarbons. WHO food additives series 55: Safety evaluation of certain contaminants in food. International Programme of Chemical Safety (IPCS) (pp. 563–743). Geneva: World Health Organization.

WHO.(2009). Clean hands protect against infection. Clean Care is Safer Care https://www.who.int/gpsc/clean_hands_protection/en/Accessed 8 February 2018.

Wong, J. Y., Hu, W., Downward, G. S., Seow, W. J., Bassig, B. A., Ji, B. T., ... & Liu, C. S. (2017). Personal exposure to fine particulate matter and benzo [a] pyrene from indoor air pollution and leukocyte mitochondrial DNA copy number in rural China. Carcinogenesis, 38(9), 893-899.

Ye, Y. (1999). Historical consumption and future demand for fish and fishery products, exploration calculations for the years 2015, 2030. FAO Fisheries Circular No 949 Rome.

Zaki, M. S., Sharaf, N. E., Mostafa, H. S., & Fawzi, O. M. (2008). Diminution of aflatoxicosis in Tilapia niloticus fish by dietary supplementation with fix in toxin and Nigella sativa oil. American-Eurasian Journal of Agriculture and Environmental Science, 3(2), 211–215.

Investigation and Analysis of White LED for Visible Light Communication Using Blue Filtering and Equalization Techniques

*[1]Magaji, A.B., [2]Ikechiamaka, F. N. and [2]Akinbolati, A.

[1]Department of Physics, Umaru Musa Yar'adua University Katsina, Nigeria.
[2]Department of Physics, Federal University Dutsin-Ma, Nigeria.
*Corresponding Author's e-mail: abdulrasheed.magaji@umyu.edu.ng

ABSTRACT

One of the most difficult issues in VLC with white LEDs is modulating the optical signal to carry data while maintaining acceptable levels of light. On-Off Keying non-return to zero (OOK-NRZ) modulation is a popular technique in VLC systems that switch the LED intensity between two states to represent binary data. The suggested method incorporates blue filtering and equalization techniques, the latter tries to lessen the impact of the phosphor coating while improving the modulation capabilities of the white LED's blue component. Equalization techniques were used to adjust for transmission medium-induced signal degradation, such as multipath interference or noise. OOK-NRZ modulation signal generated with the light beam intensity, the relative eye-opening percentage decreases from 5 Mbps to 10 Mbps, and the eye-opening drops dramatically to 50% at a data rate of 3.5 Mbps. With the 20MHz of bandwidth the white and blue light's shows a relatively flat line at lower frequencies, at 9.0 mV and gradually decreasing to 10.5 mV at 6.5 MHz. The decline continues as the frequency increases, there is drop in signal strength between 10 MHz and 11 MHz for Equalization1 across the entire frequency range. Quality factor was obtained with driver current of 100mA at 34.5°C with Q-factor 13.2 and it decreases as temperature increases. Beyond 100°C, 300mA starting Q-factor at 34.8°C is around 14.2, and it decreases as the temperature rises. Findings have broad implications for the adoption and improvement of VLC technology, as it demonstrates the viability of OOK-NRZ modulation for VLC systems.

Keywords: On-off-keying non-return to zero (OOK-NRZ), LED (visible light communications)

INTRODUCTION

Over the past several years there has been an increase in research into visible light communication (VLC) and the notion of using light emitted diodes (LEDs) for both illumination and data communication. The widespread adoption of the white light emitting diode as the next-generation green lighting has led to the development of visible light communication, a subtype of optical wireless communication (Shi et al., 2020). Due to its better brightness and longevity than other common light sources like incandescent light bulbs, as well as its data security, high bandwidth/data rate, lack of any health dangers, and low power consumption, solid state lighting has become more and more popular (Heoher, 2019). Higher power is needed for the majority of applications, including display in communications, backlighting, and medical.

VLC technology is being explored for various applications, including indoor positioning, wireless internet access, underwater communication, and even integration into vehicular communication systems. Researchers and engineers continue to work on improving modulation techniques, developing more robust systems, and addressing the challenges associated with VLC to make it a viable communication technology for various scenarios (Heoher, 2019).

From the same high brightness LEDs, visible light communication has offered numerous uses for lighting and data exchange. They also produce areas of applications such car-to-car communication, high-speed connection in airplane cabins, in-train data transfer, home networking, and traffic light management and communications (Zafar et al., 2017). High brightness white LEDs used in solid state lighting are more expensive than compact fluorescent lamp or incandescent lamp, however, the level of dependability and power efficiency provided by LEDs is by far superior to that of common incandescent light sources used for lighting (Ghassemlooy et al., 2019).

The idea of employing visible light as a communication channel dates back to the 1870s, when Alexander Graham Bell successfully demonstrated the transmission of an audio signal using a mirror that was made to vibrate by a person's voice (Ghassemlooy et al, 2019). In June 1880, sunlight was used as the light source for the first actual demonstration of visible light communication, known as the photophone. In the photophone experiment, Bell and his assistant Tainter were successful in maintaining a clean line of communication at a distance of around 213 meters. But because it relies on sporadic sunshine, the Bell system has certain obvious limitations.

MATERIALS AND METHOD
Table 1: VLC transmitter and its Electrical characteristics are shown in

Part number	Junction temperature	Forward Voltage V_f		Dynamic resistance $(\Omega)R_D$	Temperature coefficient of forward Voltage (Mv/°C)
LXHL-MWIB	Tj = 25°C	$V_f\ min$= 2.79	$V_f\ maz$= 3.99	1.0	-2.0

Bandpass filters were used in this study because they are adaptable and may be tailored to match specific VLC wavelength requirements. They have high spectral selectivity. Central wavelength and breadth of the blue filter: The center wavelength of the filter affects which parts of the electromagnetic spectrum it lets to flow through and which it reflects. The center wavelength of a blue filter corresponds to the blue portion of the spectrum, which is typically around 450-470 nanometers (nm) (Minh & Allen, 2021). It ensures that only blue light is transmitted while blocking or attenuating other wavelengths. In VLC systems, this feature is critical for isolating and transmitting the desired blue light for data transfer. A PIN photodiode is a highly sensitive photodetector with a large active area that consists of three layers: a p-type layer, an intrinsic (i) layer, and an n-type layer. PIN photodiodes are suitable for high-speed VLC applications due to their high sensitivity and low noise characteristics (Minh & Allen, 2021).

The MAX3664 TIA is a critical component in VLC systems, amplifying and converting the feeble electrical current created by the photodetector in response to incoming optical signals. Amplification, transimpedance conversion, signal conditioning, noise reduction, and impedance matching are among its primary purposes. These functions work together to improve the identification and decoding of optical data signals in VLC communication (Minh & Allen, 2021).The equalization capacitor is a component of the VLC receiver circuit that is used to optimize frequency response, adjust for signal losses, and improve overall system performance. This capacitor's proper selection and integration aid in ensuring dependable data reception and high-quality signal demodulation in VLC applications. Because of their small size, low cost, and outstanding high-frequency performance, ceramic capacitors are recommended. Load (Oscilloscope - input impedance): Choosing an oscilloscope with the right input impedance is crucial in VLC experiments and system development to accurately measure and analyze optical signals. To avoid loading effects on VLC circuits, high input impedance oscilloscopes are frequently preferred (Minh & Allen, 2021).

The beam angle in VLC influences how wide or narrow the coverage region is. The choice of LED beam angle in VLC systems is based on the desired coverage area, signal directionality, interference mitigation, data rate requirements, ambient light conditions, system design constraints, and regulatory considerations. A wider beam angle can cover a larger area but may result in lower optical power density, while a narrower beam angle provides a concentrated signal but with limited coverage. Choosing the proper beam angle 45 is a significant design issue that affects the VLC system's performance and dependability (Minh & Allen, 2021).

Table 3.2 shows the specific parameter values used in the investigation.

The work on the investigation and analysis of white led for visible light communication using blue filtering and equalization techniques is divided in to three (3) stages as follows:

A. Generation of white light

1. Phosphor-converted white LEDs use a blue LED as the primary light source, was adopted and selected in this investigation and a phosphor coating is applied to the LED chip. When the blue light from the LED chip acts as a transmitter interacts with the phosphor, it excites the phosphor, causing it to emit light in a broader spectrum, including white light. The blue LED emits high-intensity blue light and the phosphor coating converts a portion of this blue light into longer wavelengths, including green and red, which together create white light. The phosphor's composition determines the quality of white light, including its color rendering index (CRI) and color temperature. Phosphor-converted white LEDs in this study investigation and analysis of white LED for VLC systems due to their efficiency and simplicity. They offer stable and consistent white light output, making them suitable for a wide range of applications, including VLC (Minh & Allen, 2021).

The VLC system was setup and assembled with the transmitter and receiver. The transmitter is capable of modulating OOK-NRZ which is connected to a light source (LED) as shown in the Fig3.1 the receiver comprised of a PD as the photodetector (PIN), trans-impedance amplifier (TIA) and the oscilloscope. The setting of OOK-NRZ and 4-Pulse amplitude modulation (4-PAM) signals generated with the light beam intensity and modulated to represent the data rate up to 10 Mbps, the quality factor (Q-factor) was investigation using white LED (Luxeon star) to achieved this, the driver current was set at 100mA, 200mA and 300mA respectively, as shown in fig.3.1. The AC input voltage set

at 5V (peak-to-peak) and the frequency of the sequence begins with 1 KHz- 20MHz. OOK-NRZ and 4-PAM signal was transmitted separately from the transmitter, allowing it to propagate through the VLC channel to the receiver. The output of the VLC receiver were connected to an oscilloscope with the 20MHz to capture the optical signal waveform and capture the eye diagram of the relative eye-opening (NRZ) and 4-PAM. In the oscilloscope screen eye diagram is a graphical representation of the signals quality for both the eye-opening and the eye of the diagram. The oscilloscope was triggered to ensure that the eye diagram is stable and provides meaningful information. The result of measurement is presented in table 3 and 4 respectively.
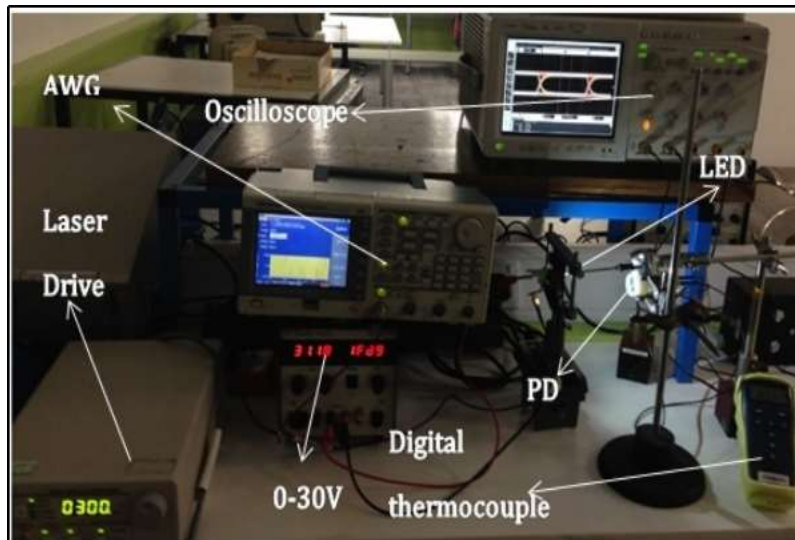
Figure 1: Set-up for the VLC system

Table 2: VLC parameters specifications

Parameters	Values
Luxeon LED Part number	LXHL-MW1B
Receiver concentration lens diameter	30mm
Blue filter central wavelength and width	450nm, 40nm (60% through)
Photodetector (PIN) area	$15mm^2$
LED driver current (Low current)	300mA (Low data rate in indoor application)
Preamplifier (Max 3664) TIA	6000Ω
Equalizer capacitor (Ceramic X7R)	15PF
Equalizer resistor (Surface-Mount Resistor)	750Ω
Load (Oscilloscope – input impedance)	50Ω
Receiver input dynamic range	28dB
LED beam angle	45^0

Blue filtering in VLC systems is essential for selecting, enhancing, and isolating the blue portion of the visible spectrum for data transmission. It helps improve the system's signal quality, spectral purity, and resistance to interference from other light sources, ultimately enhancing the reliability and performance of VLC communication (Minh & Allen, 2015). Blue filtering techniques can include optical filters, coatings, or materials that selectively transmit the desired blue wavelengths while blocking other colors of light. By filtering out unwanted colors, the receiver can focus on the modulated blue signal, reducing the risk of interference from other light sources and improving the system's robustness (Minh & Allen, 2015).

In this experiment, the VLC systems were modulation techniques, such as On-Off Keying non-return to Zero (OOK-NRZ) was employ to encode data onto the light signal. Filtering out other colors of light ensures that the receiver can accurately detect and decode the modulated blue light, reducing interference and improving the signal-to-noise ratio (SNR). The VLC system was setup as shown in Fig.1 with the drive LED and the setting of DC level at 300mA. To transmit white light, a sine wave signal was applied to the LED and the frequency signal was varied from min of 0.5MHz to Max of 20MHz at the distance of 10cm to obtain the corresponding received signal amplitude from the

Scope (white light). To transmit the blue light the photodetector was covered using a blue filter, the measurement for white light was repeated and received signal amplitude was recorded for the blue signals as shown in table 4.

Equalization is an important technique in Visible Light Communication (VLC) to compensate for frequency-dependent losses and distortions in the communication channel. One common method of equalization use in this work is an RC (Resistor-Capacitor) circuit in parallel, which is often referred to as a "parallel RC equalizer" or "parallel RC filter (Mukherjee at al., 2020). "This equalization technique helps improve the frequency response of the VLC system setup.

The parallel RC equalizer is designed to address frequency-dependent signal distortions, particularly in VLC systems where data is transmitted through optical channels. Its primary functions include: The parallel RC circuit introduces frequency-dependent impedance that can compensate for the frequency-dependent losses in the VLC channel.VLC channels may exhibit variations in attenuation at different frequencies, causing distortion and signal degradation. The parallel RC equalizer helps flatten the frequency response, ensuring that all frequency components of the signal are treated more equally (Mukherjee at al., 2020). Significance of Parallel RC Equalization in VLC: It helps enhance the quality and fidelity of the received signal, ensuring that data can be accurately recovered.

In VLC systems, the parallel RC equalizer is an essential tool for compensating the frequency-dependent channel effects, reducing distortion, and improving overall system performance. Its design and implementation should be carefully considered to match the channel characteristics and system requirements (Minh & Allen, 2015). Equalization: the R//C circuits was chosen as the equalizer to improve the frequency response of the VLC system, the frequency response measurement was repeated as in method B above with the frequency range form 0.5 – 20 MHz. The difference between the EQ1 and EQ2 that the latter has to improve the frequency response of the VLC system to the overall performance, the equalization was measure and recorded as shown in table 5.

RESULTS AND DISCUSSION

All the measurement and results were presented and discussed including experimental findings.

To optimize the performance of modulation in VLC system to measure the values of relative eye-opening (NRZ) using on-off-keying non-return-to-zero and 4-pulse amplitude modulation (4-PAM), white LED was modulated using OOK-NRZ and 4-PAM the result is presented in table 4.

Table 3: The result for the measurement values of the relative eye-opening (NRZ) using On-Off-keying Non-Return-to-Zero (OOK-NRZ) Modulation

Data rate (Mbps)	Relative eye –opening (%)
1.0	100
2.0	96
3.0	92
4.0	89
5.0	81
6.0	77
7.0	71
8.0	66
9.0	58
10.0	50

The relative eye-opening is a measure of the separation between the signal levels corresponding to the high and low states of the NRZ signal. A larger eye-opening indicates better signal quality and robustness against noise and other impairments. It is essentially a measure of how well-defined the transitions between signal levels are.
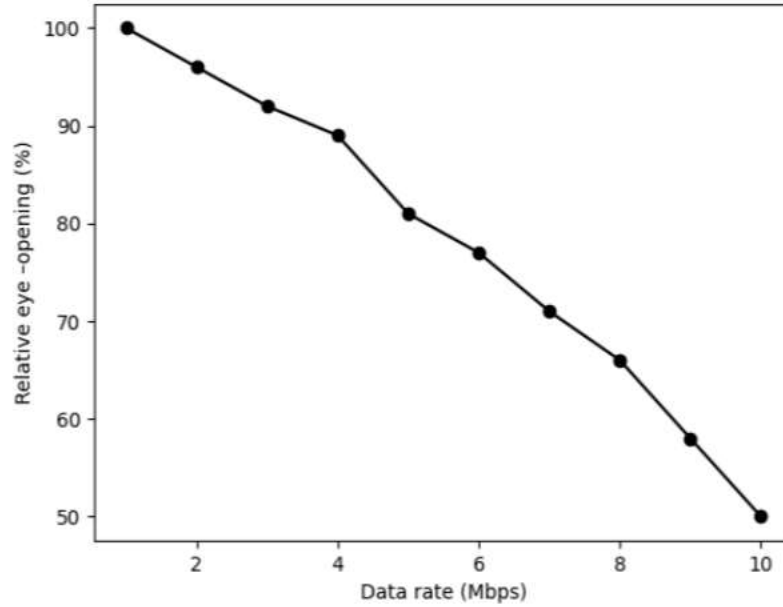
Figure 2: Relative eye-opening Vs Data rate (Mbps) for OOK-NRZ

From Fig 2 the following deduction were made:
1. The relative eye-opening percentage gradually drops as the data rate rises from 1 Mbps to 3 Mbps. This shows that although the initial decline is relatively tiny, the eye-opening percentage decreases as the data rate increases.
2. There is a more noticeable decline in the relative eye-opening percentage from 3 Mbps to 5 Mbps. Increasing the data rate appears to have a more pronounced effect on lowering the eye-opening percentage above a specific threshold.
3. The relative eye-opening percentage decreases from 5 Mbps to 10 Mbps, but the rate of reduction slows down. This suggests that at greater speeds, the diminishing returns of raising the data rate become more obvious.
The plot as a whole shows that the association between data rate and relative eye-opening is non linear. It implies that as the data rate rises, the improvement in the percentage of eyes opening reduces. Understanding the trade-offs between data rate and eye-opening in real-world applications, such as communication systems or data transmission scenarios, can be facilitated by this information.
The result obtained from the 4-PAM modulation is presented in table 4

Table 4: Measurement values of the relative eye-opening (4PAM)

Data rate (Mbps)	Smallest relative eye –opening (%)
0.5	100
1	99
1.5	90
2	88
2.5	77
3	65
3.5	50
4	35
4.5	25
5	0.5

The table 4 above contains data rate (in Mbps) and the corresponding values for the smallest relative eye-opening (%). These values are indicative of the signal quality at different data rates. The smallest relative eye-opening is a measure of the signal-to-noise ratio (SNR) margin required for reliable data transmission.
The analysis of the smallest relative eye-opening and data rate shows in Fig 3:
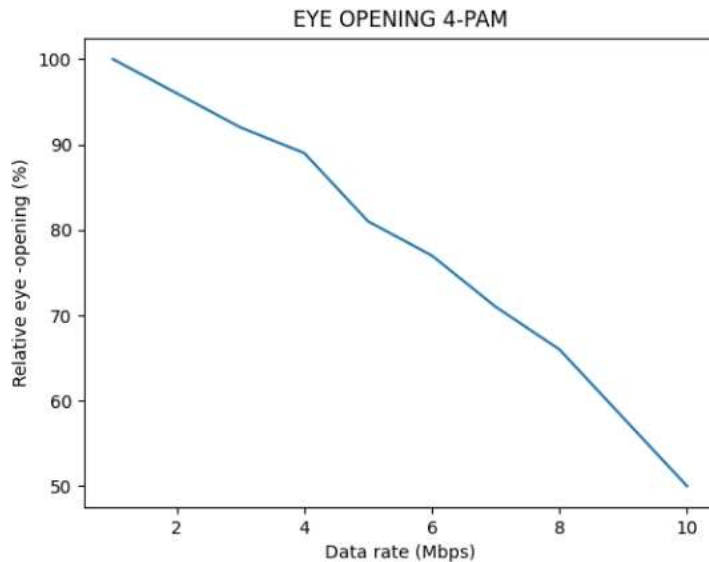
Figure 3: The smallest relative eye-opening (%) Vs Data rate (Mbps)

As data rate increases, the smallest relative eye-opening generally decreases as shown in fig.3 above. This means that as data transmitted at higher rates, we need a higher SNR margin to maintain reliable communication. This is consistent with the general behavior of digital communication systems: higher data rates are more sensitive to noise and interference.

At the lowest data rate (0.5 Mbps), you can see that a 100% relative eye-opening is achievable. This suggests that even in the presence of noise and interference, there is a considerable margin between the signal and noise levels. The communication system is highly robust at this rate.

As the data rate increases to 1 Mbps, the smallest relative eye-opening drops slightly to 99%, which is still quite robust. However, as the data rate continues to increase, the eye-opening decreases more significantly. This is due to the fact that at higher data rates, the signals are more susceptible to noise and require a larger SNR margin to maintain reliability.

The eye-opening drops dramatically to 50% at a data rate of 3.5 Mbps. This suggests that at this point, the system is operating on the edge, and a 50% SNR margin is the minimum required for reliable communication. Beyond this point, the system's performance degrades rapidly.

As the data rate exceeds 3.5 Mbps, the system performance continues to degrade significantly, reaching 0.5% eye-opening at 5 Mbps. At this point, the system is extremely sensitive to noise, and maintaining a reliable communication link becomes very challenging.

The result of investigation of how blue filtering will improve the modulation bandwidth at the receiver to filter out the slow yellow component and to investigate how equalization for the VLC system will improve the frequency response using R//C circuits.

Table 5: Results for the received signal response to the frequency change (White light and blue light.

Frequency (MHZ)	Receive signal (mV) White Light	Receive signal (mV) Blue Light
0.5	68	9.0
1	64	9.0
1.5	60	9.2
2	56	9.2
2.5	52	9.3
3	49	9.5
3.5	46	9.6
4	43	9.8
4.5	42	10.0
5	40	10.1
5.5	39	10.3

6	38	10.5
6.5	37	10.9
7	36	11.4
7.5	35	11.7
8	35	11.9
8.5	35	12.1
9.0	35	12.7
9.5	35	13.0
10.0	35	13.3
11.0	33	13.3
12.0	25	11.4
13.0	18	9.3
14.0	14	8.0
15.0	12	7.1
16.0	10	6.1
17.0	7	5.5
18.0	9	6.3
19.0	7	5.1
20.0	6	4.8

The table 5: above shows the received signal strength in millivolts (mV) for two different light sources, white light, and blue light, at various frequencies (in MHz).
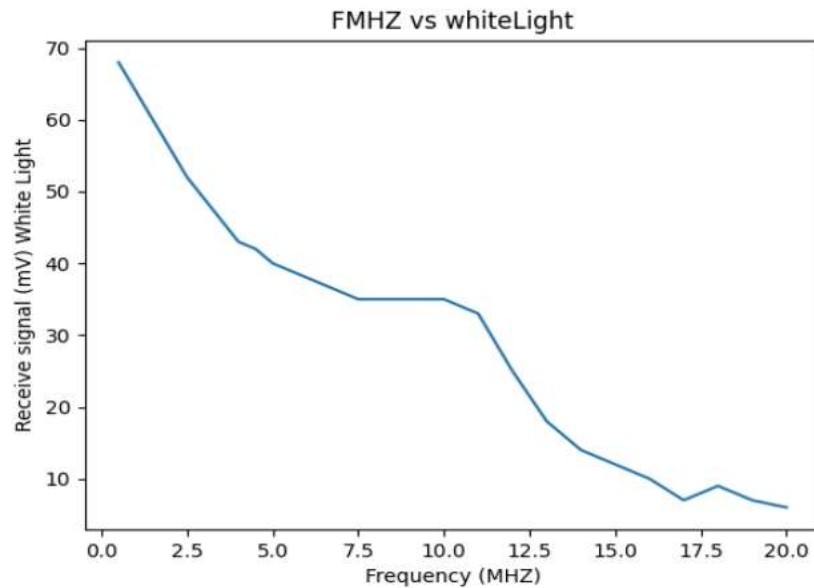
Figure 4: Graphs for the received signal response to the frequency change for white light

White Light in Fig.4 above shows that at lower frequencies (0.5 - 5.5 MHz), you will see a relatively flat line with received signal strength starting at 68 mV and gradually decreasing to around 38 mV. There is a gentle decline in signal strength. From 6 MHz onwards, you'll notice a steeper decline in signal strength. The line for white light is consistently higher than that for blue light, indicating that white light provides stronger signals at all frequencies.
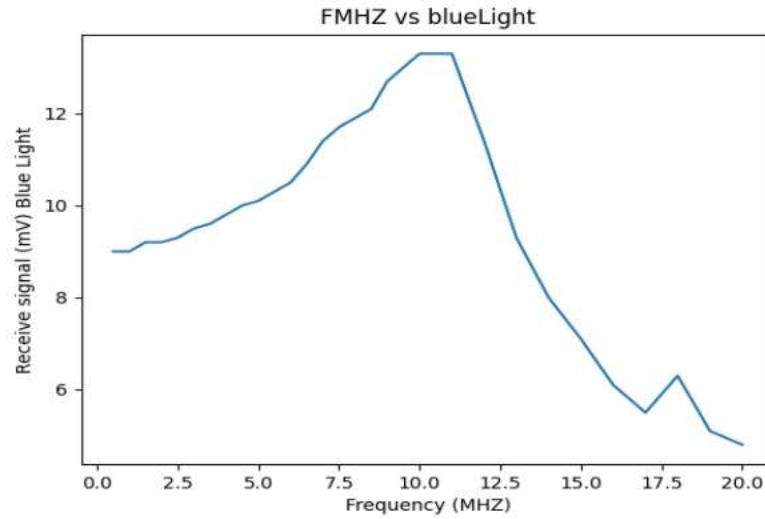
Figure 5: Graphs for the received signal response to the frequency change for blue light

Blue Light in the Fig.5 above is similar to the white light graph, blue light's graph shows a relatively flat line at lower frequencies, starting at 9.0 mV and gradually decreasing to around 10.5 mV at 6.5 MHz. The decline in signal strength for blue light is slightly steeper compared to white light, especially beyond 6.5 MHz. After 6.5 MHz, there's a noticeable drop in signal strength for blue light. The decline continues as the frequency increases.
Both white and blue light have stronger signals at lower frequencies. White light maintains higher signal strength throughout the entire frequency range. Blue light starts with lower signal strength and experiences a more significant drop at higher frequencies, indicating that it is more susceptible to frequency-related signal degradation.

Table 6: Results for the received signal response to the frequency change (Equalization)

Frequency (MHZ)	Receive signal (mV) EQ1	Receive signal (mV) EQ2
0.5	8.2	14.3
1.0	7.9	14.7
1.5	7.6	15.7
2.0	7.6	15.9
2.5	7.4	16.5
3.0	7.4	16.5
3.5	7.4	16.7
4.0	7.2	16.9
4.5	7.1	17.5
5.0	7.1	17.9
5.5	7.1	18.5
6.0	7.2	19.5
6.5	7.4	20.9
7.0	7.6	22.7
7.5	7.9	24.3
8.0	8.2	25.1
8.5	8.4	28.1
9.0	8.7	30.4
9.5	9.0	32.8
10.0	9.5	34.0
11.0	10.0	33.0
12.0	9.5	26.5
13.0	8.7	19.7
14.0	8.0	15.1
15.0	7.6	12.3

16.0	7.2	9.6
17.0	6.9	7.2
18.0	7.7	8.0
19.0	7.1	6.0
20.0	6.9	5.6

Table 6: above shows the received signal strength in millivolts (mV) for the Equalization at frequencies 0.5 – 20 MHz.
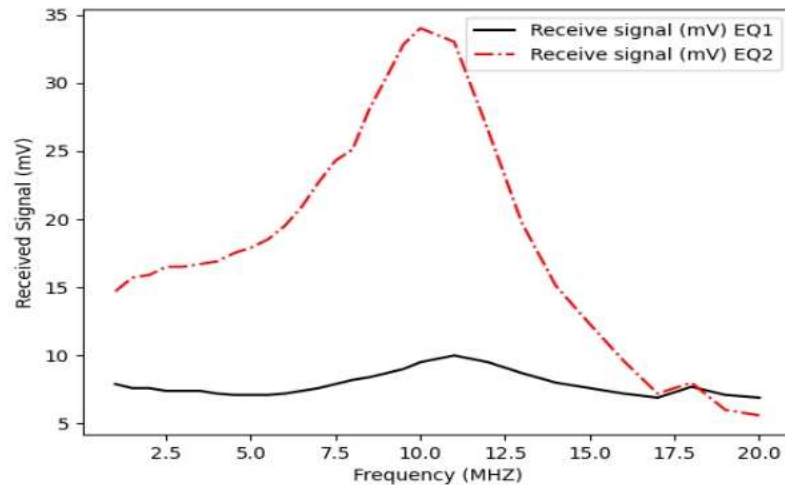
Figure 6: Received signals (mV) for Equalizations EQ1 AND EQ2 Vs Frequency (MHz)

EQ1: The received signal strength for EQ1 generally decreases as the frequency increases. This indicates that EQ1 is less sensitive to higher frequencies. There is a noticeable drop in signal strength between 10 MHz and 11 MHz for EQ1. EQ1 generally has lower signal strengths compared to EQ2 across the entire frequency range. EQ2: The received signal strength for EQ2 exhibits a different trend. It increases as the frequency rises up to a certain point. Between 0.5 MHz and 11 MHz, EQ2 shows a consistent increase in signal strength. Beyond 11 MHz, there is a slight drop in signal strength, but it remains higher than EQ1.

In conclusion, the field of Visible Light Communication (VLC) is a promising technology with a range of practical applications, and the use of On-Off Keying - Non-Return-to-Zero (OOK-NRZ) modulation techniques offers distinct advantages and some challenges such as Simplicity and Energy Efficiency, Suitability for Specific Applications and Reliability and Signal Quality.

REFERENCES
Ghassemlooy, Z., Popoola, W., & Rajbhandari, S. (2019) *Optical wireless communications: system and channel modelling with Matlab*®: CRC Press.

Hoeher, P.A (2020) Visible Light Commuinations, theoretical and Practical Foundations, Book

Minh, H & Allen, J. (2015) Optical Communication System Design. Laboratory Experiment, Northumbria University, Newcastle United Kingdom.

Minh, H & Allen, J. (2021) Optical Communication System Design. Laboratory Experiment, Northumbria University, Newcastle United Kingdom.

Mukherjee, B., Tomkos, I., Tornatore, M., Winzer, P., & Zhor, Y. (2020). Springer Handbook of Optical Networks. Springer Nature.

Shi, D., Li, J., Liu,Y., Shi, L., Huang, Y., Wang, Z., Zhang, X. & Vladimirescu., A. (2020) Effect of Illumination Intensity on LED Based Visible Light Communication System. IEEE International Symposium on Broadband Multimedia Systems and Broadcasting

Zafar, A; Khalid & Asif,. (2017). *[IEEE 2017 International Conference on Electrical and Computing Technologies and Applications (ICECTA) - Ras Al Khaimah (2017.11.21-2017.11.23)] 2017 International Conference on Electrical and Computing Technologies and Applications (ICECTA) - Equalization techniques for visible light communication system. , (), 1–5.* doi:10.1109/ICECTA.2017.8251941

Unsteady MHD Free Convection Flow with Thermal Radiation in a Porous Channel Saturated with Porous Materials

*Yusuf A.B. and Umar A.

Department of Mathematics, Federal University Dutsin-ma, Katsina State. Nigeria
*Corresponding author's email address: <u>ayusuf@fudutsinma.edu.ng</u> Phone: +2349130824575

ABSTRACT
This paper investigates unsteady magnetohydrodyamic (MHD) free convection flow with thermal radiation in a vertical porous channel saturated with porous materials. The partial differential equations (Pdes) modeling the flow behavior together with appropriately defined dimensionless quantities are given. These Pdes are changed into dimensionless forms using the defined quantities after which their solutions are obtained with the aid of regular perturbation and the method of undetermined coefficients. The solutions gotten via these methods are coded into MATLAB where responses of the parameters of interest are presented on graphs and discussed. Results of this investigation show that the fluid velocity in the porous channel increases with increase in Gr, Pr, R, S and M. It is worthy to mention that the present work coincides with that of Jha et al. (2015) when Da tends to infinity (i.e. Da $\rightarrow$ ∞).
Keywords: Unsteady flow, MHD flow, free convection flow, thermal radiation, Porous material, porous channel.

INTRODUCTION
The study of fluid flow under the influence of MHD in a channel with thermal radiation has attracted the interest of many investigators and researchers. This is due to its importance in sciences and engineering, particularly in heat exchangers, environmental control, ground spread of pollutants and so on. In addition, it has application in the field of chemical engineering for filtration, purification processes in petroleum industries, drying of porous solids and thermal insulation. Aruna *et al.* (2012) studied the effect of heat transfer on MHD oscillatory flow in a channel with slip effect at a lower wall where the solutions for the velocity and temperature are obtained analytically.
In the work of Makinde and Mhone (2005), they investigated MHD oscillatory flow in a channel filled with porous medium and later Mahmood and Ali (2007) extended this work by considering the fluid slip at the lower wall. In the study of Kavita and Kumari (2012) investigate the influence of heat transfer on MHD oscillatory flow of Jeffery fluid in a channel where they concluded that, the axial velocity increases with increasing of Jeffery fluid and the maximum velocity occurs at the centerline of the channel with minimum velocity at the channel walls. The effect of viscous dissipative heat on three dimensional oscillatory flows with periodic suction velocity has been studied by Sahim (2010). Al-Khafajy (2016) investigates the effect of heat transfer on MHD oscillatory flow of Jeffrey fluid with variable viscosity through porous medium. Ahmad and Ishak (2017) studied steady two-dimensional mixed convection boundary layer flow and heat transfer of a Jeffrey fluid over a stretched sheet immersed in a porous medium in the presence of a transverse magnetic field. Hamza *et al.,* (2011) investigated the transient heat transfer to MHD oscillatory flow through porous medium under slip conditions, magnetic field condition and oscillating temperature, but the authors has not addressed the influence of a Jeffrey fluid parameters in their work. Idowu *et al.,* (2013) studied the effect of heat and mass transfer on unsteady MHD oscillatory flow of Jeffrey fluid in a horizontal channel with chemical reaction. In the work of Afify A.A (2023) explored the impacts of changing viscosity on non-Darcy MHD natural convection in a thermal stratified permeable medium.
But the work of Uwanta and Hamza (2012) investigated unsteady heat transfer flow of a viscous, incompressible, electrically conductive fluid through porous medium with periodic suction and temperature oscillation. Yale *et al.,* (2019) studied the influence of Jeffery fluid, slip condition, magnetic field and radioactive heat transfer on unsteady flow of conducting optically thin fluid through a channel filled with porous medium and surface temperature oscillating.
In a preliminary study, Hamza *et al*. (2021) investigated steady-state MHD natural convection slip movement in a vertical geometry and discovered that increasing the contaminant reactivity parameter had no effect on fluid momentum. Studies of flow of viscous with thermal radiation by numerous investigators find abundant applications in human endeavors, especially in heating and cooling processes. It also has significance importance in the context of space technology and processes involving high temperature; this is due to effective system performance and maintenance for human existence. For example, thermal radiation is being used in our hospitals for sterilization of medical instruments, treatment of cancer and tumor. It is also used in bakery for toasting of bread, cake and meat pie.

In engineering technology, the concept is used in manufacturing of air conditioners, boilers, heaters and crude oil refining. Ajibade *et al.* (2021) investigate the effect of dynamic viscosity and nonlinear thermal radiation on free convective flow through a vertical porous channel in their model. Shah *et al.* (2022) provided and idea of Maxwell fluid flow between vertical plates with damped shear and thermal flux a free convection phenomenon. While in the study of Cao *et al.* (2022) investigated the steady flow of Maxwell fluid over a porous medium.

It is in view of this that unsteady MHD free convection flow with thermal radiation in a porous channel saturated with porous materials is investigated using regular perturbation method. This article is an extension of Jha *et al.* (2015) while considering the channel to be filled with porous materials.

MATERIALS AND METHODS
Mathematical formulation of the problem
The physical problem under consideration (figure 1) consists of a vertical channel formed by two vertical parallel porous plates place in distance apart. The channel is saturated with porous materials filled with viscous incompressible optically thick fluid in the presence of thermal radiation. The fluid physical properties are all assumed constant except for its viscosity which is temperature dependent. Since the fluid is optically thick, the radiative heat flux given by Roseland is adopted.
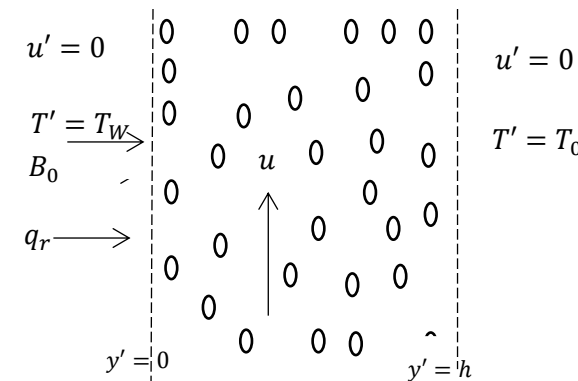
Figure 1: Flow configuration

Under these assumptions along with Boussinesq's approximation, the governing equations for the momentum and energy can be written as follows:

$$\frac{\partial U'}{\partial t'} + V_0 \frac{\partial U'}{\partial y'} = v \frac{\partial^2 U'}{\partial y'^2} + g\beta(T'-T_0) - \frac{\sigma_1 B_o^2 U'}{\rho} - \left(\frac{v}{K*}U'\right) \tag{1}$$

$$\frac{\partial T'}{\partial t'} + V_0 \frac{\partial T'}{\partial y'} = \alpha\left[\frac{\partial^2 T'}{\partial y'^2} - \frac{1}{k}\frac{\partial q_r}{\partial y'}\right] \tag{2}$$

Subject to the initial and boundary conditions:

$$t \leq 0; \quad U' = 0, \; T' = 0, \qquad\qquad for \; all \; y \tag{3}$$

$$t' \geq 0; \quad U' = U, \; T' = T_\omega, \qquad at \qquad y' = 0 \left.\right\}$$
$$U' = 0, \; T' = T_0, \qquad at \qquad y' = H \tag{4}$$

With the dimensionless quantities:

$$y = \frac{y'}{H}, \quad t = \frac{t'v}{H^2}, \quad u = \frac{u'}{U}, \quad Pr = \frac{v}{\alpha}, \; Da = \frac{K}{H^2}$$
$$M^2 = \frac{\sigma_1 B_o^2 H^2}{v\rho}, \; Gr = \frac{g\beta H^2(T_\omega - T_0)}{Uv}, \tag{5}$$
$$\theta = \frac{T'-T_0}{T_\omega - T_0}, \quad \Gamma = \frac{v_{eff}}{v}, \quad R = \frac{4\sigma(T'-T_0)^3}{k^* K}, \quad S = \frac{V_0 H}{v}$$

using equation (5), equations (1), (2), (3) and (4) are changed into dimensionless differential equations to have:

$$\frac{dU}{dt} + S\frac{dU}{dy} = \Gamma\frac{d^2U}{dy^2} + Gr\theta - bu \tag{6}$$

$$\Pr\left[\frac{d\theta}{dt} + S\frac{d\theta}{dy}\right] = \left[1 + \frac{4R}{3}(C_T + \theta)^3\right]\frac{d^2\theta}{dy^2} + 4R(C_T + \theta)^2\left(\frac{d\theta}{dy}\right)^2 \tag{7}$$

In this equations $\Pr, Da, Gr, \theta, v_{eff}T', R, T_0$ and T_w represent Prandtl number, Darcy number, Grashof number, radiation, temperature and wall temperature respectively.

where $\qquad b = m^2 - \dfrac{1}{Da}$

with the initial and boundary conditions:

$$t \leq 0; \quad U = 0, \ \theta = 0, \qquad\qquad for\ all\ y \tag{8}$$

$$\left.\begin{array}{l} t \geq 0; \quad U = 1, \ \theta = 1, \qquad at\ y = 0 \\ \qquad\qquad U = 0, \ \theta = 0, \qquad at\ y = 1 \end{array}\right\} \tag{9}$$

Similarly, through equation (1-9) $u', t', v_0, y', g, \beta, \delta, \alpha, \rho, k^*, k, T'$ and q_r represent dimensional velocity, dimensional time, suction velocity, dimensional length, gravitational force, thermal radiation, density, thermal conduction, dimension of porous space, dimensional temperature and radiative heat flux respectively.

Method of Solution

The model equations (6-7) under the conditions in equations (8-9) are highly nonlinear differential equations which cannot be solved easily. To solve them, we therefore reduce the complexity of these equations by considering steady flow case $\left(i.e.\dfrac{du}{dt} = \dfrac{d\theta}{dt} = 0\right)$ so that they can be solved easily. In doing so, the emanating equations are thus:

$$0 = \Gamma\frac{d^2u}{dy^2} - S\frac{du}{dy} + Gr\theta - bu \tag{10}$$

$$0 = \left[1 + \frac{4R}{3}(C_T + \theta)^3\right]\frac{d^2\theta}{dy^2} + 4R(C_T + \theta)^2\left(\frac{d\theta}{dy}\right)^2 - s\Pr\frac{d\theta}{dy} \tag{11}$$

subject to the boundary conditions:

$$\left.\begin{array}{l} u = 1, \ \theta = 1, \quad at\ y = 0 \\ u = 0, \ \theta = 0, \ at\ y = 1 \end{array}\right\} \tag{12}$$

By the perturbation method, we assume the solutions of equation (9-12) as:

$$\left.\begin{array}{l} u = u_0 + Ru_1 \\ \theta = \theta_0 + R\theta_1 \end{array}\right\} \tag{13}$$

On using equation (13) into equation (9-12) and equating the coefficient of R^0 and R^1 we get:

$$\left(\begin{array}{l} R^0 : \dfrac{d^2u_0}{dy^2} - \dfrac{s}{\Gamma}\dfrac{du_0}{dy} - \dfrac{c}{\Gamma}u_0 + \dfrac{Gr\theta}{\Gamma} = 0 \\[3mm] R^1 : \dfrac{d^2u_1}{dy^2} - \dfrac{s}{\Gamma}\dfrac{du_1}{dy} - \dfrac{c}{\Gamma}u_1 + \dfrac{Gr\theta}{\Gamma} = 0 \end{array}\right) \tag{14}$$

$$\begin{cases} R^0 : \dfrac{d^2\theta_0}{dy^2} - s\,\Pr\dfrac{d\theta_0}{dy^2} = 0 \\ R^1 : \dfrac{d^2\theta_1}{dy^2} + \dfrac{4}{3}(c_T + \theta_0)^3 \dfrac{d^2\theta_0}{dy^2} + 4(c_T + \theta_0)^2\left(\dfrac{d\theta_0}{dy}\right)^2 - Sp\,r\dfrac{d\theta_1}{dy} = 0 \end{cases} \tag{15}$$

Subject to the conditions:

$$\begin{aligned} u_0 = 1, \quad u_1 = 0, \quad at\ y = 0 \\ u_0 = 0, \quad u_1 = 0, \quad at\ y = 1 \end{aligned} \tag{16}$$

Solving equation (15) by the method of undetermined coefficients we get.

$$u_0(y) = c_1 e^{yr1} + c_2 e^{yr2} + c_3 e^{yspr} + c_4 \tag{17}$$

$$u_1(y) = D_1 e^{yr1} + D_2 e^{yr2} + D_3 + D_4 e^{yspr} + D_5 e^{yspr} + D_6 e^{2yspr} + D_7 e^{3yspr} + D_8 e^{4yspr} \tag{18}$$

$$\theta_0(y) = A_2 e^{yspr} - A_1 \tag{19}$$

$$\theta_1(y) = B_1 + B_2 y e^{yspr} + B_3 e^{yspr} + B_4 e^{2yspr} + B_5 e^{3yspr} + B_6 e^{4yspr} \tag{20}$$

So that when R tends to zero, the final solution is:

$$u(y) = c_1 e^{yr_1} + c_2 e^{yr_2} + c_3 e^{yspr} + c_4 + R(D_1 e^{yr_1} + D_2 e^{yr_2} + D_3 e^{yr_3} + D_4 e^{yspr}$$
$$+ D_5 e^{yspr} + D_6 e^{2yspr} + D_7 e^{3yspr} + D_8 e^{4yspr}) \tag{21}$$

$$\theta(y) = A_2 e^{yspr} - A_1 + R(B_1 + B_2 y e^{yspr} + B_3 e^{yspr} + B_4 e^{2yspr} + B_5 e^{3yspr} + B_6 e^{4yspr}) \tag{22}$$

Where $= A_1 = 1 - A_1$, $B_1 = -(B_3 + B_4 + B_5 + B_6)$, $B_2 = \dfrac{k_5}{e^{spr}}$, $B_3 = 0$, $B_4 = \dfrac{-k_2}{3S^2\Pr^2}$

$B_5 = \dfrac{-k_3}{6S^2\Pr^2}$, $B_6 = \dfrac{-k_4}{12S^2\Pr^2}$, $c_1 = 1 - c_1 - c_2 - c_3 - c_4$, $c_2 = \dfrac{q_2}{q_1}$, $c_3 = -\dfrac{GrA_2}{S^2 pr^2 - S^2 pr - c}$, $c_4 = -\dfrac{A_1 Gr}{c}$,

$D_1 = -D_2 - D_3 - D_4 - D_5 - D_6 - D_7 - D_8$, $D_2 = \dfrac{k_6}{k_7}$, $D_3 = \dfrac{GrB_1}{r}$, $D_4 = \dfrac{-GrB_2}{S^2\Pr^2 - S^2\Pr - r}$,

$D_5 = \dfrac{-GrB_3}{S\Pr - S - r} - \dfrac{D_4(2S\Pr - S)}{S\Pr - S - r}$, $\qquad D_6 = \dfrac{-GrB_4}{4S^2 r^2 - 2S^2\Pr - r}$, $\qquad D_7 = \dfrac{-GrB_5}{9S^2 Pr^2 - 3S^2\Pr - r}$,

$D_8 = \dfrac{-GrB_6}{16S^2 Pr^2 - 4S^2\Pr - r}$,

$K_2 = \dfrac{4}{3}(3c_T{}^2 A_2^2 S^2\Pr^2 - 2C_T A_1 A_2^2 + 3A_1^2 A_2^2) + 4(c_T{}^2 A_2^2 S^2\Pr^2 - C_T A_1 A_2^3 S^2\Pr^2 + A_1^2 A_2^2 S^2\Pr^2$,

$K_3 = \dfrac{4}{3}(3c_T{}^2 A_2^3 - 3A_1 A_2^3) + 4A_2^4 S^2\Pr^2 A_2^2)$, $K_4 = \dfrac{4}{3}(A_2^4 S^2\Pr^2) + A_2^2 S^2\Pr^2$,

$K_5 = B_3(1 - e^{spr}) + B_4(1 - e^{yspr}) + B_5(1 - e^{2yspr}) + B_6(1 - e^{3yspr})$,

$K_6 = -D_3(1 - e^{x_1}) - D_4(e^{spr} - e^{x_1}) - D_5(e^{spr} - e^{x_1}) - D_6(e^{2spr} - e^{x_1}) - D_7(e^{3spr} - e^{x_1}) - D_8(e^{4spr} - e^{x_1})$,

$K_7 = (e^{x_2} - e^{x_1})$, $q_1 = e^{x_2} - e^{x_1}$, and $q_2 = e^{x1} - c_3(e^{Spr} - e^{r_1}) - c_4(1 - e^{r_1})$

RESULTS AND DISCUSSION

The solutions obtained using the regular perturbation technique (equation 21-22) are simulated into MATLAB programming to depict the influence of different values of M, R, Da, Gr, Pr, R, S and C_T on the velocity profile and skin friction between fluid and the channel plates. The following values are fixed throughout the calculations except where otherwise stated: Pr = 7, M = 1, R = 0.01, Da = 1, S=0.5, Gr =3, C_T = 0.001, y = 0.1, 0.2, 0.3.
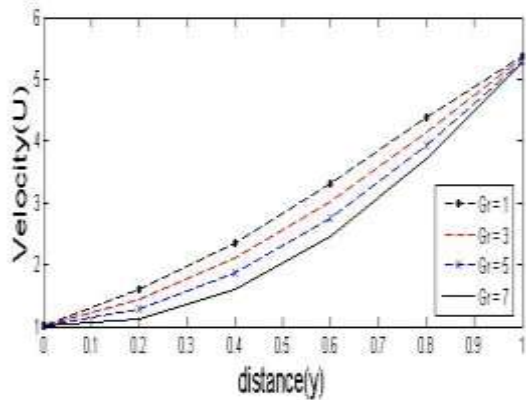
Figure 2: Effect of various value of Gr on velocity profile
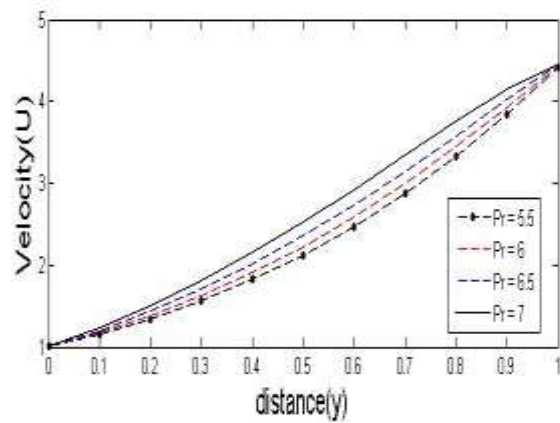
Figure 3: Effect of various value of Pr on Velocity profile
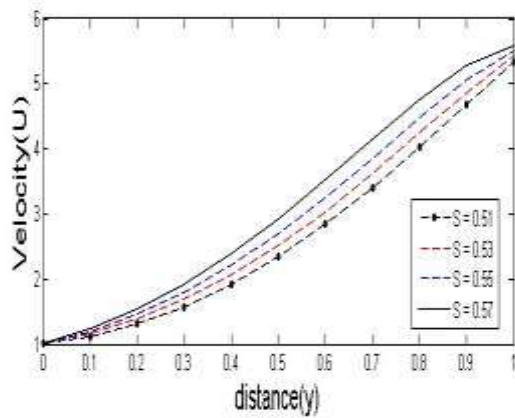
Figure 4: Effect of various value of R on Velocity profile
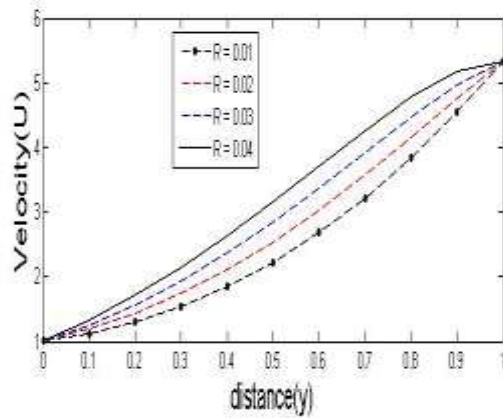
Figure 5: Effect of various value of S on Velocity profile
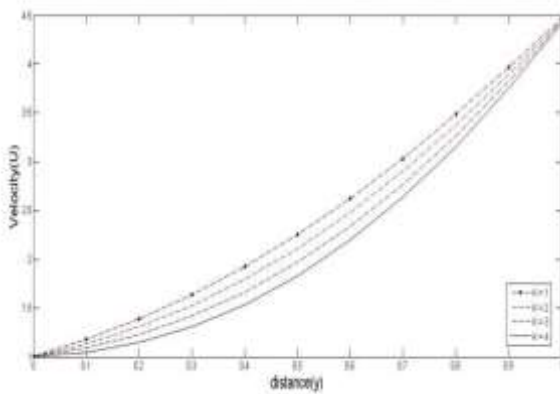
Figure 6: Effect of various value of Da on Velocity profile
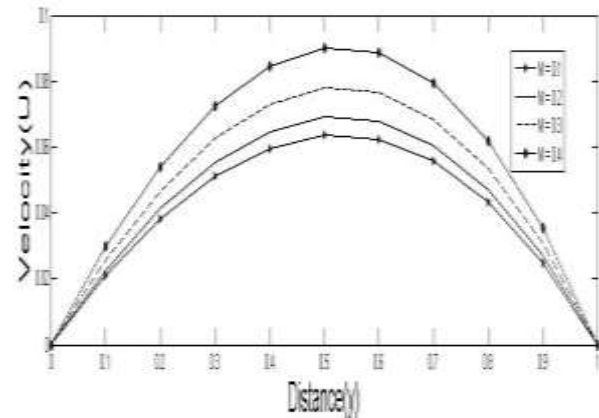
Figure 7: Effect of various value of M on Velocity profile
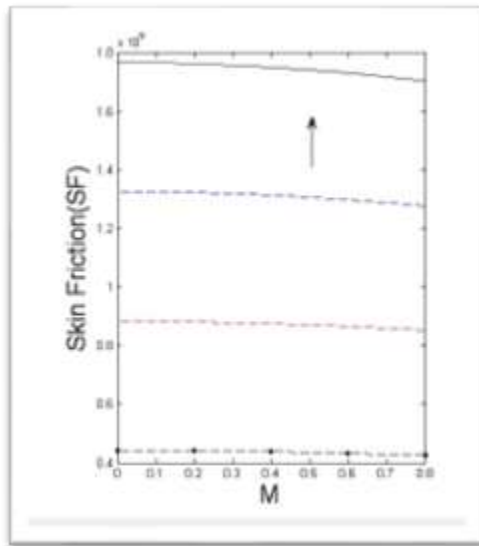
Figure 8: Effect of skin friction with M = 1, and R = 0.01, at y = 0.4 and y
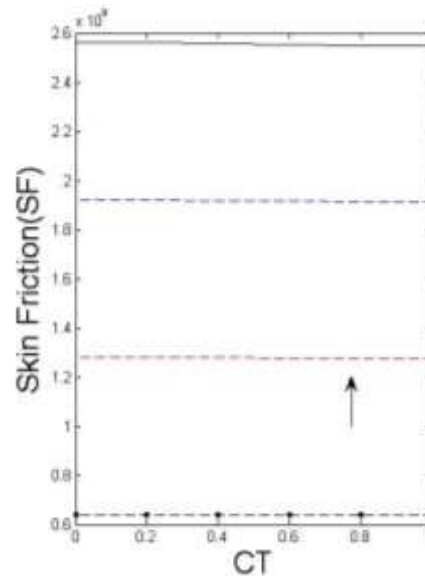
Figure 9: Effect of skin friction with CT = 0.001 at y = 0.6 and y = 0

Figures 2 - 6 illustrates the velocity profiles for various values of Grashof number (Gr = 1, 3, 5, 7), Prandtl number (Pr = 5.5, 6, 6.5, 7), Radiation (R = 0.01, 0.02, 0.03, 0.04), Suction/Injection (S = 0.51, 0.53, 0.55, 0.57), and Darcy number (Da = 1, 2, 3, 4). It is sighted from Figure 2 that the velocity decreases with increasing Grashof number parameter (Gr). Figure 3 indicates that, the velocity increase with rising Prandtl number parameter (Pr). The increase of velocity in this case is inclined to the reduction of thermal diffusion into the fluid. The velocity of the fluid in the channel increase with increasing radiation Parameter (R) and this can be viewed from figure 3. This culture is caused by the decrease of thermal conduction of the fluid. Furthermore, figure 4 displays that, the velocity increase with fluid injection parameter (S) while figure 6 describes that, the velocity decrease with boosting Darcy number (Da). Figure 8 portrays that the fluid velocity intensified with increase in magnetic field parameter (M).

Validation of the results

In order to validate the accuracy of our results, we assume $Da \rightarrow \infty$ so that $\frac{1}{Da} \rightarrow 0$ and v_{eff} becomes v $(i.e. \Gamma = 1)$ which represents a clear fluid (no porous materials). On the consideration of this phenomenon our work coincides with that of Jha *et al. (2015).*

CONCLUSION
The present work analyzes unsteady MHD free convection flow with thermal radiation in a porous channel saturated with porous materials. Semi-analytic solutions of the problem are obtained via regular perturbation method and the attained solutions are finally solved using the method of undetermined coefficients. The realized final solutions are coded into MATLAB programing with output presented on graphs. The investigation found that the velocity of the fluid in the channel increase with intensification of Gr, Pr, R, S, and M. It is recommended that the present work can be extended while considering non-porous channel and with the fluid viscosity to be temperature dependent.

REFERENCES
Afify A.A (2023). Effect of viscosity on non-Darcy MHD free convection along a non-isothermal vertical surface in a thermally stratified porous medium. *Apply math model,* 31 (8) (2007) pp. 1621-1634.

Ahmad, K. and Ishak, A. (2017). Magnetohydrodynamics (MHD) Jeffrey Fluid over a Stretching Vertical Surface in a Porous Medium. *Propulsion and Power Research,* 6(4):269-276.

Ajibade O.A, Jha B.K., Jibril H.M and Yusuf A. B. (2021). Investigate the effect of dynamic viscosity and nonlinear thermal radiation on free convective flow through a vertical porous channel. *International journal of thermo fluids 9:1-9.*

Al-khafajy, D.G.S. (2016). Effect of Heat Transfer on MHD Oscillatory Flow of Jeffrey Fluid with Variable Viscosity through Porous Medium. *Advances in Applied Sciences Research,*7(3):179-186.

Aruna, K. B., Ramakrishna, P. K. and Kavita, K. (2012). Slip Effects on MHD Oscillatory Flow of Jeffrey in a Channel with Heat Transfer. *International Journal Math. Arch,*3(8):2903-2911.

Cao L. M., Si X. H. and Zheng L. C. (2020). Convection of Maxwell fluid over over stretching porous surface with heat source/sink in presence of nanoparticles. *Appl. Math. Mech.,* 11 (2020), 433-442.

Hamza, M. M., Isah, B. Y. and Usman, H. (2011). Unsteady Heat Transfer to MHD Oscillatory Flow through Porous Medium under Slip Condition. *International Journal of Computer Application*, 33(4):0975-8887.

Hamza, M.M., Usman H, I. J Uwanta (2021). Investigated steady-state MHD natural convection slip movement in a vertical geometry and discovered that increasing the contaminant reactivity parameter had no effect on fluid momentum. *International Journal Engineering Science,* 23: 544–553.

Idowu, A. S. and Daniel, S. (2013). Effect of Heat and Mass Transfer on Unsteady MHD Oscillatory Flow of Jeffery Fluid in Horizontal Channel with Reaction. *Journal of Mathematics (IOSR-JM)*, 3(4):74-87.

Jha B. K., Isah B. Y., and Uwanta I.J. (2015). Unsteady MHD free convective Couette flow between vertical plates with thermal radiation. *Journal of King Saud University – Science* 3(3):276-283.

Kavita, K. and Kumari, A. (2012). Influence of Heat Transfer on MHD Oscillatory Flow of Jeffrey Fluid in a Channel. *Advances in Applied Science Research,*3(4):2312-2325.

Mahmood, A. and Ali, A. (2007). The Effect of Slip Condition on Unsteady MHD Oscillatory Flow of a Viscous Fluid in a Planner Channel. *Romanian Journal of Physics,*52(1-2):85-91.

Makinde, O. D. and Mhone, P. Y. (2005). Heat Transfer to MHD Oscillatory Flow in a Channel Filled with Porous Medium. *Romanian Journal Physics*, 50(9-10):931-938.

Na W., N.A. Shah, I. Tlili, I. Siddique (2022) Maxwell fluid flow between vertical plates with damped sear and thermal flux: free convection, *Chinese J. Phys.,* 65 (2020), 367-376.

Sahin, A. (2010).The Effect of Viscous Dissipative Heat on three Dimensional Oscillatory flows with periodic Suction Velocity. *Indian Journal Science Technology,*3(3):276-283.

Uwanta, I. J. and Hamza, M. M. (2012). Transient Heat Transfer Flow in a Channel with Porous Medium and Periodic Suction. *Research Journal of mathematics and Statistics,*4(4):89-93.

Yale, I. D., Aisha, A. H., Mustapha, I. and Muhammad, M. H. (2019). Unsteady Heat Transfer to MHD Oscillatory Flow of Jeffrey Fluid in a Channel Filled with Porous Material. *International Journal of Science*, 9 (7):641-645.

Measurement of Natural Radioactivity of Baobab (Adonsonia Digitata) Plant in Katsina Metropolis, Katsina State Nigeria

*[1]Idris, H. Y. and [2]Joseph, E.

[1]Nigerian Nuclear Regulatory Authority, North West Zonal Office Katsina, Katsina State - Nigeria
[2]Department of Physics, Federal University Dutsin-Ma, Katsina State – Nigeria
*Corresponding author's email: yaxfta2005@gmail.com

ABSTRACT
Natural radioactivity sources are mostly soil, water, plants and vegetation. The major isotopes of concern from these sources are potassium, uranium and the decay product of uranium, such as thorium and radium. In this study, radioactivity estimation of baobab plants was carried out in Katsina metropolis, Katsina State, Nigeria. Samples of soil, roots, and leaves were collected, prepared and analyzed to estimate the activity concentration of the natural radionuclides of U-238, Th-232, and K-40 using a low background detector of NaI (TL) Gamma-ray spectrometer. The results obtained showed that the activity concentration ranged from 0.1 Bq/kg to 33.26 Bq/kg, 1.98 Bq/kg to 64.98 Bq/kg and 65.89 Bq/kg to 1009.69 Bq/kg with overall mean values of 11.35, 18.87 and 545.14 in Bq/kg for ^{238}U, ^{232}Th and ^{40}K respectively. The mean values obtained for U-238 and Th-232 are lower than the world average values of 30 Bq/kg for U-238 and 35 Bq/kg for Th-232, while K-40 was found to be higher than the world average of 420 Bq/kg; high activity level of K-40 could be due to continual deposition of the organic manure and public waste generated by the locals in the study area which might lead to radiation health effects. Base on the activities of these natural radionuclides and the radiological hazards evaluations; this current study indicates that there is no radiological health risk in using the roots and leaves of Baobab plants for any purposes. Moreover, the measured soil around the study area was found to be safe and will not pose any radiation exposure to the population. Hence, this radioactivity estimation will serve as a baseline for detection of any future released activities of related natural radionuclides, especially around the consumable plants. However, effort should be made to ensure that the radiological parameters of the study area are kept as low as reasonably achievable.
Keywords: Katsina State, Natural Radioactivity, Baobab plant, Soil, Root, Leaves, NaI (Tl)

INTRODUCTION

Originally from human existence, people have been in search of food for nutritional and medicinal purposes. After going round many parts of sub-Saharan Africa discussing with native healers in rural societies, had found great significance in the baobab plants which a surprising amount of constituents with nutritional and medicinal benefits that cover their needs. However, it is unaware that human beings are exposed to radiation from different sources such as intakes of naturally occurring radionuclides through inhalation and ingestion in water, air, soil and plants (UNSCEAR, 2020, Augustine, 2011). Radionuclides are abundant in the soil; the concentrations of these radionuclides in the soil are determined by the radioactivity of the rock and the nature of the process of the formation of the soil (Elijah, 2016). Therefore, radionuclides in soil generate a significant component of the background radiation exposure to the population (UNSCEAR, 2000). Radioactivity in the environment is mainly due to the presence of long-lived radionuclides of the ^{238}U, ^{232}Th series and ^{40}K. Baobab plants grow in semi-arid regions and local communities consider their roots, fruits and leaves as potentially rich sources of nutrients including minerals, vitamins, and other nutraceuticals. However, consumption of natural radioactivity in the root or leaves part of baobab trees may endanger human health and causes radiation health effects as they being used for the sources of food and medicinal purposes (Isaac *et al,* 2013). Different methods and techniques have been used to measure the amount of natural radioactivity in plants. The use of a Sodium Iodide (TL) Gamma Spectrometry detector has been adopted for this study to investigate natural radioactivity present in the baobab plant to ascertain the possible radiological effects associated with the use of the roots, leaves and soil samples in the baobab plant. Moreover, evidence from available literature has shown that no such work has been carried out in this study area, as such; this research will help to contribute to data that can be used for further studies.

In the northern part of Nigeria, the baobab plant is regarded for its multipurpose uses in different aspects of life. The plant is said to be growing almost in all part of the region which is as a result of the favorable climatic condition of the area. Its fruits and leaves are believed to have high potential rich source of nutrients including minerals, vitamins and other nutraceuticals benefits. The mode in which the roots and leaves parts of this plant are pre-prepared for food and medicinal purposes calls for concern as there are possibility of contamination with natural radioactivity in the soil and uptake by plant. Baobab roots and stems served as the main storage of water; as such this may lead to radioactivity

movement in the soil contaminated with the molecules of water and uptake by baobab plant. Based on the available literatures, no work of this nature has been done on the study area, and from the reviewed of the literature, there is lack of comprehensive compositional data regarding the radioactivity estimation of baobab on the samples of soil, roots and leaves in the study area. Therefore, this research attempted to address the radiation exposure due to Norm's deposition in the study area.

The study aims to assess the level of radioactivity in baobab tree around Katsina metropolis, Katsina State Nigeria, using thallium activated sodium iodide gamma spectrometry detector. The objective of this study is to estimate the activity concentration of the natural .radionuclides ^{238}U, ^{232}Th, and ^{40}K in soil, root and leave samples of baobab plant from the study area.

Location of the Study Area

Katsina State was created out of the defunct Kaduna State on 23rd September 1987 and like the former Katsina Province of Old Northern Nigeria, the State comprises Katsina and Daura Emirates. It borders Kaduna State to the South, Jigawa and Kano States to the East; Zamfara State to the West and shares an international border with the Republic of Niger to the North, it occupies an area of about 24,192 square kilometers (km), with an estimated population of about 5.8 million people as per 2006 projection. The study was carried out in Katsina metropolis located between the geological coordinate of latitude 12°15'N and longitude of 7°30'E in the North West Zone of Nigeria, with an area of 24,192km^2 (9,341 sq meters). Katsina State has two distinct seasons: rainy and dry. The rainy season begins in April and ends in October, while the dry season starts in November and ends in March. This study was undertaken during the dry season. The average annual rainfall, temperature and relative humidity of Katsina State are 1,312 mm, 27.3°C and 50.2%, respectively (Katsina State Investor's Handbook, 2016).
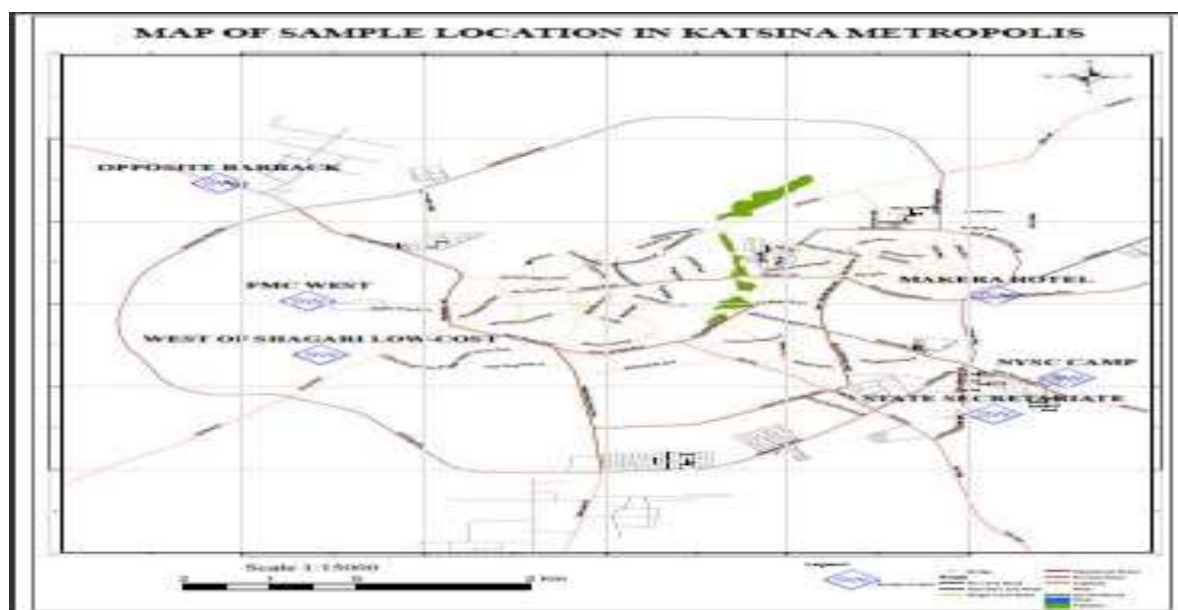
Figure 1. Map of Katsina showing the sampling locations

Sample Collection

Sample of soil, roots and leaves was collected from six (6) selected locations across the study area in Katsina Metropolis. All the samples were labeled at the point of collection and coordinate was recorded using global poisoning system (GPS) with geological information giving a total of 18 samples (soil, roots and leaves). The entire sample was transported to the laboratory for analysis at the National Institute of Radiation Protection and Research (NIRPR), University of Ibadan (UI) Oyo State. These samples were analyzed using NaI (Ti) gamma spectrometry to determine the activity concentration of radionuclides.
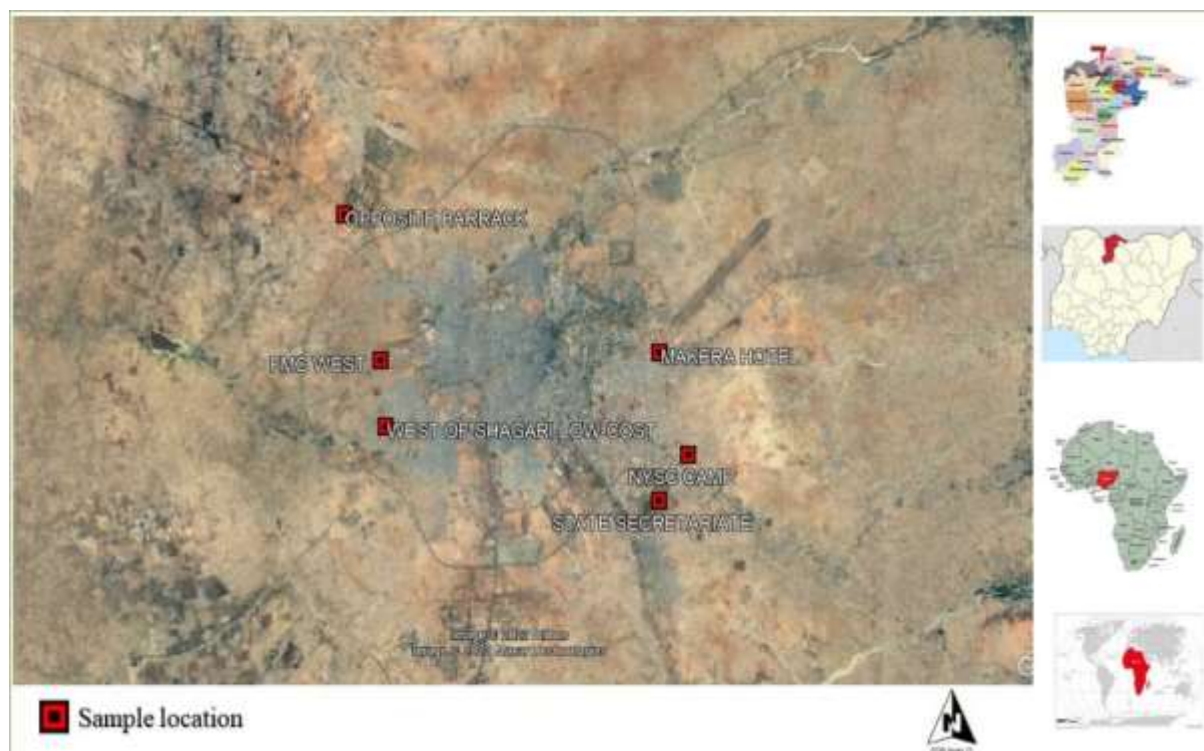
Figure 2. Satellite maps showing the sampling site and it geographical position

Experimental
The specific radioactivity concentration values of ^{40}K, ^{232}Th and ^{226}Ra measured in the samples collected are presented in Table 3.0 below, the measured data were obtained from the NaI (Ti) Gamma Ray spectrometry analysis carried out at the national institute of radiation protection and research, University of Ibadan, Oyo State. The value of the Radionuclides activity Concentrations at each sample point for ^{40}K, ^{226}Ra and ^{232}Th were measured in **(Bq/kg)**

RESULTS AND DISCUSSION
Table 1: Measured activity concentration of U-238, Th-232 and K-40

SAMPLE CODE	K-40	Ra-226	Th-232
A L01	1009.69	16.88	3.150
A L02	872.310	6.830	1.980
A L03	344.810	1.990	3.450
A L04	736.440	9.680	31.74
A L05	758.160	4.970	25.11
AL06	619.810	0.220	8.420
BR01	740.780	21.85	29.37
BR02	750.650	33.26	64.98
BR03	616.160	10.98	48.84
BR04	486.160	20.33	25.16
BR05	398.550	12.87	9.090
BR06	332.29	11.69	61.83
CS01	762.320	17.24	16.09
CS02	986.980	15.90	26.23
CS03	65.8900	1.870	10.45
CS04	136.960	7.570	2.130
CS05	122.320	0.100	6.500
CS06	82.3100	10.19	14.07
Range	**1009.69-65.89**	**33.26-0.100**	**64.98-1.980**

Mean	545.14	11.35	18.87

Table 1 presents the activity concentration of the naturally occurring radioactive materials in eighteen (18) different samples of leaves, root and soil. Mean average dose values of activity concentration obtained were estimated at 545.14 Bq/kg, 11.35 Bq/kg, and 18.87 Bq/kg for K-40, Ra-226 and Th-232 respectively.
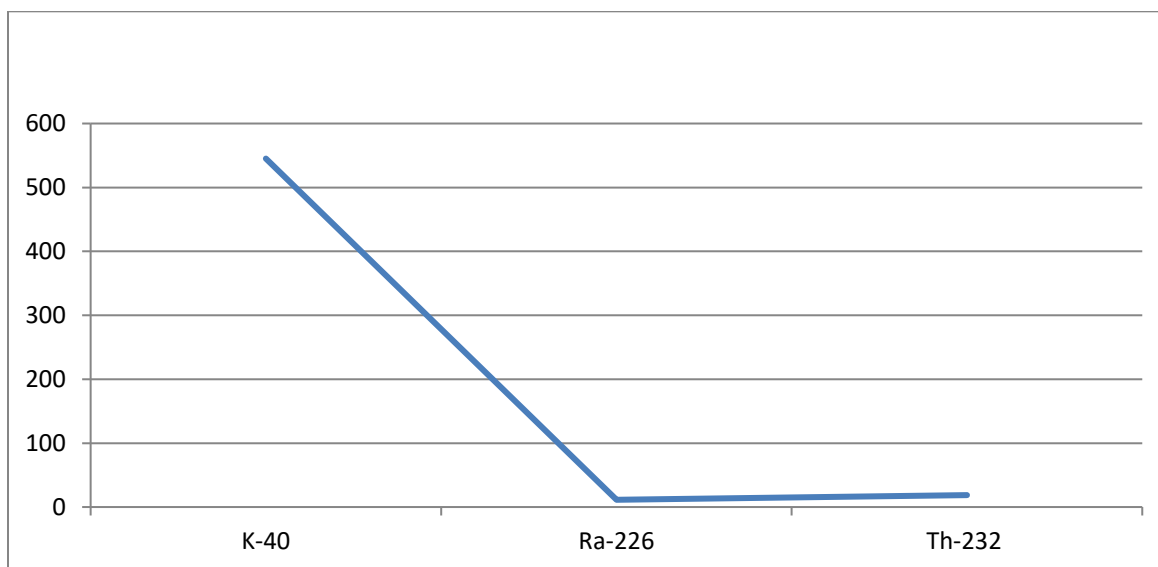
Figure 3: Graph of measured activity concentration of K-40, Ra-226 and Th-232.

Discussion

The Radioactivity Concentration of U-238, Th-232 and K-40 in Katsina Metropolis in this present study showed that the activity concentration of ^{238}U, ^{232}Th and ^{40}K in the eighteen (18) different samples of leaves, roots and soil have been measured and presented in table 1. The maximum activity concentration of U-238, Th-232 and K-40 is 33.26 Bq/kg, 64.98 Bq/kg and 1009.69 Bq/kg while the minimum values are 0.1 Bq/kg, 1.98 Bq/kg and 65.89 Bq/kg respectively; their mean values are: 11.35 Bq/kg, 18.87 Bq/kg and 545.14 Bq/kg respectively. These mean values were below the world recommended standard of 35Bq/kg and 30Bq/kg for ^{238}U and ^{232}Th which is defined by UNSCEAR, 2000; the activity concentration of potassium (K-40) was found to be higher than the UNSCEAR recommendation of 420 Bq/kg. However, the result of the current study indicated that there is not much deposition of ^{238}U in the geological formation of the Katsina metropolis and environs. Moreover, there are fewer industrial activities that might contribute to triggering NORM in the study area. Katsina Nigeria (study area) is considered to have a lower value for the mean activity concentration of Th-232 with a mean value of 18.87 Bq/kg; the mean value obtained in the study area is below the UNSCEAR recommendation of 30Bq/kg; the lower value for the mean activity concentration of Th-232 in the study area might be due to less industrial activities such as mining and mineral explorations that could contribute trigger NORMs. However, value obtained for Th-232 in the geological formation of the Katsina metropolis and the environs (control areas) was slightly higher than the value obtained for U-238, this indicated that thorium is almost two times as abundant as uranium in the study area. The presence and the release of Th-232 in the environment may be harmful to aquatic plants and animals when inhaled or ingested.

The study area contained a higher deposition of K-40 with a mean activity concentration value of 545.14Bq/kg; this value is above the world recommended limit of 420Bq/kg established by UNSCEAR 2000, 2018. Higher depositions of K-40 in the study areas could be due to the continual deposition of natural organic manure generated from waste by the local communities; K-40 is an important nutrient for man and is naturally available in abundance; baobab plant contained natural radioactivity of K-40, as reported by food standard agency, 2002; the plants are rich in nutrient and also important in the fight against cancer and heart diseases (food standard agency, 2002 and SCUC, 2006). Consumption of the leaves, roots and fruits pulp can help in fighting infections, urinary tract diseases, and diarrhea and heal wounds (Food Standard Agency, 2002 and SCUC, 2006). However, when K-40 exceeded the recommended dose limit established by regulatory bodies such as UNSCEAR, ICRP and WHO could lead to

radiation health effects (Yuki et al., 2014). K-40 might pose health hazards from both beta particles and gamma rays, when injected or inhaled; it's completely absorbed, moving quickly from the gastrointestinal tract to the bloodstream which is quickly distributed to all organs or tissues. The health hazards of K-40 are associated with cell damage caused by the ionizing radiation that results from the radioactive decay with the general potential for subsequent cancer induction (Yuki et al., 2014).

CONCLUSION

This work aims to assess the radioactivity estimation of the baobab tree in Katsina, Katsina state. Samples were collected in different locations of west Shagari low-cost, State Secretariat, Makera Daura road, NYSC Camp, Opposite Barrack and FMC West. All these samples were prepared and analyzed to estimate the extent of annual effective dose rates and the risk associated with the exposure due to natural radionuclides in baobab plants using a Sodium iodide (Tl) Gamma Spectrometry device. It is possible to see from the findings that the activity concentration of Uranium-238, Thorium-232 and Potassium-40 in the soil, leaves and roots samples were found to be in the range of (33.26-0.10) Bq/kg, (64.98-1.98) Bq/kg and (1009.69-65.89) Bq/kg respectively. The mean activity of ^{238}U, ^{232}Th and ^{40}K in the soil leaves and roots samples were fund to be 11.35 Bqkg^{-1}, 18.87 Bqkg^{-1} and 545.14 Bq/kg respectively. The concentrations of ^{238}U and ^{232}Th are lower than the world average value while a concentration of ^{40}K was found to be higher compared to the world average established by UNSCEAR, 2000 this might be possible when there is much continuous application of potassium fertilizers and much deposition of natural organic manual generated from waste by the local communities in the study area. A study can be made to determine the levels of activity concentrations of heavy metals in the seed and pulp parts of baobab plant from the area. These parts of the plant are reported to have high nutritional value and play important role in human nutrition.

REFERENCES

Abdul Galil, N. (1985). Evaluation of baobab (gonglase) solution for home management of diarrhoea in suddenness children's: a thesis submitted to the University of Khartoum, faculty of medicine.

Augustine, F. (2011). Assessment of public exposure to naturally occurring radioactive materials from mining and mineral processing activities of tarkwa goldmine in Ghana. A thesis submitted to the Department of Chemistry, College of Science, Kwame Nkrumah University of Science and Technology, Kumasi.

Gwana A., Effiong E., Muhammad A., Buhari B., Shetima U., Abubakar M., Bukar M. (2016). Determinations of Some Selected Heavy Metals and Elements in Baobab Tree Leaves. *Academic Journal of Life Sciences* (Adonsonia digitata) Grown in College of Agriculture, Maiduguri, North – Eastern Nigeria. ISSN (e): 2415-2137, Vol. 2, No. 12, pp: 89-95.

Habte, K. (2018). Metaphysical analysis of nutritional and therapeutic value of baobab (adasonia digitata), a research submitted to the department of international nutrition, institute of human nutrition, justus-liebig university Giessen, Germany.

IAEA (2000). Postgraduate Educational Course in Radiation Protection and the Safety of Radiation Sources (PGEC), Training Course Series 18, IAEA, Vienna (2002).

ICRP (2000). Limits for intakes of Radionuclides by workers. International Commission on Radiological protection Committee II. Pergamon Press New York. Pp277.

Isaac, K., (2013). Major, Minor and Trace Element Analysis of Baobab Fruit and Seed by Instrumental Neutron Activation Analysis Technique, Food and Nutrition Sciences, 2013, 4, 772-778 *http://dx.doi.org/10.4236/fns.2013.48100* Published Online August 2013 (*http://www.scirp.org/journal/fns*).

Jonah, S. (2015). Preliminary investigation of naturally occurring radionuclides in some traditional medicinal plants used in Nigeria; Department of Physics, Ahmadu Bello University, Zaria.

Jwanbot, D., Izam, M., Nyam, G., John, H. (2014). Radionuclides analysis of some soil and Food Crops in Barkin Ladi LGA, Plateau State-Nigeria; *Journal of Environment and Earth Science* ISSN 2224-3216 (Paper) ISSN 2225-0948 Vol. 3, No.3, 2013 www.iiste.org.

Katsina investors guide (2016). Katsina State Investors handbook. www.katsinastate.gov.ng.

Mujahid S., & Hussain, S. (2011). Measurement of Natural Radioactivity from soil samples of Sind, Pakistan, Radiation Protection Dosimetry 145(4): page 351–355.

Nobuyiki, H., yuki F. (2014). Classification of radiation effects for dose limitation purposes; History, current situation and feature prospect. Radiation safety research centre, nuclear technology research laboratory, Tokyo *201-8511, Japan.*

SCUC (2006). Baobab Manual, Field Manual for Extension Workers and Farmers. University of Southampton, Southampton, UK. ISBN 0854328173 Printed at RPM Print and Design, Chichester, England.

Shuaibu, I. (2022). Map of katsina metropolis showing the study area.

Tilde, U., Gana, A. (2010). Assessment of Naturally Occurring Radionuclides in Soil and their Annual Dose Rate in Bornu Basin. *Journal of Radiation and Health Physics*, 92(1), 34.

UNSCEAR (2018). Effect and risk of ionizing radiation, United Nations, New York.

UNSCEAR (2000). Exposures from Natural Sources, 2000 Report to General Assembly, Annex B, New York.

Vanusa M. (2009). Soil-to-Plant Transfer Factors for Natural Radionuclides in the Brazilian Cerrado Region. 2009 International Nuclear Atlantic Conference - INAC 2009Rio de Janeiro, RJ, Brazil, September27 to October 2, 2009 ASSOCIAÇÃO BRASILEIRA DE ENERGIA NUCLEAR – ABEN ISBN: 978-85-99141-03-8.

Mathematical Model for the Dynamics of Kalare Crime with Rehabilitation Programme in Gombe State

*[1]Usman Garba, [2]Muhammad Abdullahi, [1]Ibrahim Adamu Mohammed and [3]Isa Ibrahim Mohammed

[1]Department of Mathematics and Computer Science, Gombe State College of Education Billiri, Gombe State, Nigeria
[2]Department of Mathematics, Federal University Dutsin-Ma, Katsina State, Nigeria
[3]Department of General Studies, Gombe State College of Health Sciences and Technology, Kaltungo, Gombe State, Nigeria
*Corresponding author: usmangarbapantami@gmail.com

ABSTRACT
Like the rest of Nigeria, Gombe state is home to a sizable population of young males without jobs who have few chances to better their socioeconomic standing. Some of these teenagers in Gombe have developed Kalare Boys, loosely organized criminal gangs. The study developed a mathematical model based on a set of ordinary differential equations to analyze the dynamics of Kalare crime while considering a Gombe state rehabilitation plan. The study used Lipchitz condition to test for the existence and uniqueness of the solution for the model, determining the solution's positivity and the invariant region, respectively. The basic reproduction number A was calculated using a next-generation matrix technique. According to the study, the Kalare Crime-free equilibrium (KCFE) is unstable whenever it exceeds one and locally asymptotically unstable (LAS) whenever it is less than 1. The Kalare Crime Free Equilibrium (KCFE)'s global stability was also attained. Numerical investigations illustrated that reduction in the Kalare conversion rate, an increase in the arrest rate of Kalare boys, and a boost in the rehabilitation programme will significantly help reduce and eradicate Kalare thuggery.It is recommended that rehabilitation programme should be improved.
Keywords: Kalare, Crime, Gombe, Positivity of solution, Rehabilitation, invariant region

INTRODUCTION
The term *Kalare* is said to be the name of a gangster who was a hunter from a Village called Miya in Bauchi State. Kalare was famous; he rarely missed occasions organized by his fellow hunters in northern Nigeria. In 1994, the hunters of the Bolari district in Gombe sometimes organized an event (a ceremony) led by the head of Bolari called *Barde* and *Yan Dawa*, to which they invited Kalare as a result of his visit *Barade* and *Yan Dawa*'s names changed to *Yan Kalare*. Yan Kalare are known to be hunters, and they mostly live in the bush during their festivals. Their activities were characterized by hunting, and the traditional hunters' play was similar to that of Yan Gunda of Bauchi. During festivals, they come to the Emir's plot and entertain people with their play, using sticks, daggers, dogs, etc. The young men were peaceful (initially) as hunters but gradually started clashing with their fellow hunters at festivals (as in Sallah celebrations and annual hunters' gatherings). Rotten eggs started joining the Kalare, and within a period, the group lost bearing, turning into thuggery. The Kalare boys of Jakadafari fought the Kalare boys of Pantami, those of Bolari fought those of Tudun Wada and so on. In the 2003 general elections, politicians invited them to serve as their guards whenever they embarked on a campaign. As a result of that, more jobless youth continue involving themselves in one form of political violence or the other (Umar, 2013).

Alhaji Muhammad Danjuma Goje, the executive Governor of Gombe State from 2003-2011, introduced a squad of a task force called Anti Kalare to end the thuggery of Kalare, but the initiative recorded an insignificant success. The Talba Empowerment Scheme (TES), implemented by the administration of His Excellency Dr. Ibrahim Hassan Dankwambo, who presided from 2011 to 2019, was designed to address the needs of the teeming youth and reduce the network of violence expected from them. By hiring the youngsters who were left behind from the Anti Kalare squad, the TES was designed to supplement it in terms of reducing crime. Additionally, it was anticipated to facilitate the work of the Squad by lowering the crime committed by young people due to unemployment (Bashir, 2017).

Bashir (2017) conducted research on the assessment of *Kalare* Eradication Policies in Nigeria: A Study of Anti *Kalare* Squad and Talba Empowerment Scheme (TES) governmental organizations. He found that Gombe state government in Eastern Northern Nigeria in its response to the numerous complaints by its citizens over the political violence activities perpetrated by youth groups known as Kalare in the state has formulated two policies with the intention to eradicate these violence activities. These policies include Anti Kalare Squad and Talba Empowerment Scheme (TES) but unfortunately these policies achieved limited success especially in eradicating the violent activities perpetrated by the youth. Therefore, his paper assessed the factors responsible for the limited success of the two policies. The findings

of his paper revealed that the implementation of these policies was marred by political interference influenced by personal interest and political sentiments. In his study, he recommended that a monitoring and evaluation and mediating committees should be set up which will function as mediator among the different Kalare groups to ensure proper implementation of the policies.

Mathematical models of crime have played a significant role in providing grounds to study and control social vices. The following are a few examples of existing works on crimes: Sanda *et al.* (2019) developed a mathematical model in which they studied the dynamics of Kalare crime within the Gombe Metropolis. In their work, they had two categories of susceptible classes. Additionally, they were able to determine the basic reproduction number and the existence and uniqueness of the model equations' solutions. According to their calculations, the crime-free equilibrium is unstable if the threshold exceeds one and locally asymptotically unstable if it is less than 1. They ran a numerical simulation in three alternative situations to demonstrate how crime in Kalare may decrease significantly.

MATERIALS AND METHODS
Model Formulation

The population is divided into seven (7) compartments: the Susceptible educated S_E, the Susceptible uneducated S_U, the Exposed class E, the Kalare crime class K_C, the Jail class J, the Rehabilitated class R_1, and the recovered class R_2 and the total population is equal to the sum of all the compartments. The susceptible educated class is the class of people who can be exposed to Kalare crime due to illicit acts by the kalare individual(s). That is, when the Kalare gang attacks one of the relatives of the susceptible class such that the victim or a relative may go for revenge, in the process of doing so, he may join the gang. The susceptible uneducated class is the class where people are capable of being exposed to Kalare crime due to contact with the Kalare crime individuals; these include people who have closed relationships with the Kalare crime and those who live in the same area with Kalare crime individuals; the exposed class contains individuals that exposed to Kalare crime but do not encourage people to practice; kalare crime class consists of those who practice Kalare crime and capable of influencing other people to join the kalare crime either willingly or otherwise; jailed course consists of those who practice kalare crime and convicted; rehabilitated class consists of those who have been engaged into rehabilitation programmed (Talba Empowerment Scheme (TES)) and the recovered course consists of those that have been fully recovered from the Kalare activities.

Assumption of the model

The following presumptions form the basis of the model:
1. All susceptible individuals are equally likely to join Kalare crime individuals when they come in contact.
2. Those in the uneducated class are more vulnerable to being infected.
3. Rehabilitated individuals are moved into recovered classes for a particular period.
4. It is assumed recovered individuals can join either the susceptible educated class or the susceptible uneducated class after recovery.

Table 1: Parameters of the model

VAR/PAR	DESCRIPTION	Value	Source
π	Recruitment rate of susceptible	1000	Sanda A. et al
ρ	Proportion of youth that have been enrolled in school	0.70	''
β_1	Rate of moving from educated class into the exposed class	0.9	''
β_2	Rate of moving from susceptible uneducated class into the exposed class	0.9	''
α	Rate of moving from exposed class into the kalare class	0.30	''
μ	Natural death rate in all the classes	0.019	''
δ_1	Death induced by been exposed to kalare crime	0.1	''
δ_2	Death induced by kalare crime	0.1	''
ω_1	Rate of moving from recovered class into the susceptible educated class	0.65	Assumed
ω_2	Rate of moving from recovered class into the susceptible uneducated class	0.35	''
ξ	Rate of moving from exposed class into the rehabilitated class	0.02	''
σ	Rate of moving from kalare crime class into the rehabilitated class	0.73	''
η	Rate of moving from exposed class into the jail class	0.15	Sanda A. et al
γ	Rate of moving from jail class into the rehabilitated class	0.68	Assumed

τ	Rate of moving from kalare crime class into Recovered class	0.37	''
Ψ	Rate of moving from rehabilitated class into the recovered class	0.82	''
Φ	Rate of moving from jail class into the recovered class	0.15	Sanda A. et al
Y	Rate of moving from jail class into the kalare crime class	0.32	Assumed
θ	Rate of moving from Kalare Crime class into the Jail crime class	0.15	Sanda A. et al

Table 2: Variables of the model

VAR/PAR	DESCRIPTION
S_E	Number of susceptible educated individuals at time t
S_U	Number of susceptible uneducated individuals at time t
E	Number of Exposed individuals at time t
K_C	Number of Kalare crime individuals at time t
J	Number of Jail individuals at time t
R_1	Number of Rehabilitated individuals at time t
R_2	Number of Recovered individuals at time t

Model equations

$$
\begin{aligned}
\frac{dS_E}{dt} &= \pi\rho + \omega_1 R_2 - (\beta_1 K_C + \mu)S_E \\
\frac{dS_U}{dt} &= \pi(1-\rho) + \omega_2 R_2 - (\beta_2 K_C + \mu)S_U \\
\frac{dE}{dt} &= \beta_1 K_C S_E + \beta_2 K_C S_U - (\xi + \alpha + \eta + \delta_1 + \mu)E \\
\frac{dK_C}{dt} &= \alpha E + \upsilon J - (\theta + \tau + \sigma + \delta_2 + \mu)K_C \\
\frac{dJ}{dt} &= \theta K_C + \eta E - (\upsilon + \phi + \gamma + \mu)J \\
\frac{dR_1}{dt} &= \xi E + \sigma K_C + \gamma J - (\psi + \mu)R_1 \\
\frac{dR_2}{dt} &= \tau K_C + \psi R_1 + \phi J - (\omega_1 + \omega_2 + \mu)R_2
\end{aligned} \tag{1}
$$

Model Analysis

The fundamental components of the system (1) are examined in this section. It was possible to achieve the equilibria's existence and stability. The basic reproduction number was also obtained.

Positivity of the solution

By expressing and demonstrating the following theorem, we demonstrated the positivity of the solutions to model (1).

Theorem 1:

Let the initial solution set

$$\{S_E(0) > 0, S_U(0) > 0, E(0) > 0, K_C(0) > 0, J(0) > 0, R_1(0) > 0, R_2(0) > 0\} \in \Re^7_+,$$

If t>0, the solution set is then positive forever.

Proof:

From $\frac{dS_E}{dt} = \pi\rho + \omega_1 R_2 - (\beta_1 K_C + \mu)S_E$ $\hspace{2cm}$ (2)

$\frac{dS_E}{dt} \geq -(\beta_1 K_C + \mu)S_E$ $\hspace{2cm}$ (3)

By separating the variables in problem (3), we have

$\frac{dS_E}{S_E} \geq -(\beta_1 K_C + \mu)dt$ $\hspace{2cm}$ (4)

Integrating (4) we have

$\int \frac{1}{S_E} dS_E \geq \int -(\beta_1 K_C + \mu)dt$

$\ln S_E \geq \int -(\beta_1 K_C + \mu)dt$ $\hspace{2cm}$ (5)

Taking exponential of both side of (5)

$S_E(t) \geq e^{\int -(\beta_1 K_C + \mu)dt} \geq 0$

Similarly, for $\frac{dS_u}{dt}, \frac{dE}{dt}, \frac{dK_C}{dt}, \frac{dJ}{dt}, \frac{dR_1}{dt}$ and $\frac{dR_2}{dt}$. The solution to equation (1) is therefore positive for all times t>0 according to the second theorem.

Existence of invariant region

From the model equation, the population estimate is provided by

$$N = S_E + S_U + E + K_C + J + R_1 + R_2 \tag{6}$$

That is $\frac{dN}{dt} = \frac{dS_e}{dt} + \frac{dS_u}{dt} + \frac{dE}{dt} + \frac{dK_C}{dt} + \frac{dJ}{dt} + \frac{dR_H}{dt} + \frac{dR}{dt}$

Consequently, when the differential equations are included, we have $\frac{dN}{dt} = \pi - \mu(S_E + S_U + E + K_C + J + R_H + R) - \delta_1 E - \delta_2 K_C$

$$\frac{dN}{dt} = \pi - \mu N - \delta_1 E - \delta_2 K_C$$

$$\frac{dN}{dt} \leq \pi - \mu N \tag{7}$$

Integrating this, we obtain $N(t) \leq \frac{\pi}{\mu}$ as $t \to \infty$

Consequently, the area where the model makes biological sense is indicated by $\Omega = \Big\{ S_E, S_U, E, K_C, J, R_1, R_2 \in$

$$\mathbb{R}^7_+ : S_E + S_U + E + K_C + J + R_1 + R_2 \leq \frac{\pi}{\mu} \Big\} \tag{8}$$

Accordingly, every solution with initial condition(s) in Ω continues to be in Ω. Our model is thus mathematically sound, positively invariant, and physiologically plausible in region Ω.

Kalare Crime Free Equilibrium (KCFE) Point

In the absence of Kalare crime, we obtain the following KCFE, denoted by E_O

$$E_0 = \left(\frac{\pi\rho}{\mu}, \frac{\pi(1-\rho)}{\mu} 0,0,0,0,0 \right) \tag{9}$$

Endemic Equilibrium (EE) Point

Lemma 1. The Kalare Crime model has a unique endemic equilibrium if and only if $R_0 > 1$.

Proof. When we compute the endemic equilibrium point, we get,

$$\left. \begin{array}{l} S_E^* = \frac{A_4\pi\rho\alpha^2 + \pi\rho\eta\upsilon\alpha + K_C^*\omega_1 G_1}{\alpha(A_4\alpha + \eta\upsilon)(\beta_1 K_C^* + \mu)}, S_U^* = \frac{A_1 A_4 A_6\alpha^2 + A_1 A_2\eta\upsilon\alpha + K_C^*\omega_2 G_2}{\alpha A_6(A_4\alpha + \eta\upsilon)(\beta_1 K_C^* + \mu)}, E^* = \frac{K_C^* G_3}{A_6(A_4\alpha + \eta\upsilon)} \\ K_C^* = K_C^*, J^* = \frac{K_C^*(\theta\alpha + A_3\eta)}{(\alpha A_4 + \eta\upsilon)}, R_1^* = \frac{K_C^* G_1}{\alpha(\alpha A_4 + \eta\upsilon)}, R_2^* = \frac{K_C^* G_2}{A_6\alpha(\alpha A_4 + \eta\upsilon)} \end{array} \right\} \tag{10}$$

where:

$$G_1 = A_3 A_4\xi\alpha + A_3\xi\eta\upsilon + \sigma\alpha^2 A_4 + \sigma\alpha\eta\upsilon + \gamma\theta\alpha^2 + \gamma\eta\alpha A_3 - \upsilon\theta\alpha\xi - A_3\upsilon\eta\xi$$
$$G_2 = A_4\tau\alpha^2 + \tau\alpha\eta\upsilon + \psi G_1 + \phi\alpha^2\theta + \phi\alpha\eta A_3$$
$$G_3 = A_3 A_4\alpha + A_3\eta\upsilon - \upsilon(\theta\alpha + A_3\eta)$$

Basic Reproduction Number of the Model

Adopting from Van, Driessche & Wantmough, (2002), given the disease-free equilibrium, if F_i represents the rate at which new infections emerge in the compartment and V_i represents the rate at which people move from i, , then R_0 is the spectral radius (biggest Eigen value) of the subsequent generation matrix represented by $G = \rho F V^{-1}$ Diekmann & Heesterbeek (2000). In order to determine F and V, which are their respective Jacobian matrices at a disease-free equilibrium E_0, Therefore, the basic reproduction number is given below

$$R_0 = \frac{\pi\left(\beta_1\rho + \beta_2(1-\rho)\right)\left(\eta\upsilon + \alpha(\upsilon + \phi + \gamma + \mu)\right)}{\mu(\xi + \alpha + \eta + \delta_1 + \mu)\left((\theta + \tau + \sigma + \delta_2 + \mu)(\upsilon + \phi + \gamma + \mu) - \theta\upsilon\right)} \tag{11}$$

4.6 Local Stability Analysis of the Kalare Crime Free Equilibrium (KCFE)

$$\begin{vmatrix} -\mu & 0 & 0 & 0 & 0 & \omega_1 & 0 \\ 0 & -\mu & 0 & 0 & 0 & 0 & \omega_2 \\ 0 & 0 & -a_1 - \lambda & a_2 & 0 & 0 & 0 \\ 0 & 0 & \alpha & -a_3 - \lambda & \upsilon & 0 & 0 \\ 0 & 0 & \eta & \theta & -a_4 - \lambda & 0 & 0 \\ 0 & 0 & \xi & \sigma & \gamma & -a_5 - \lambda & 0 \\ 0 & 0 & 0 & \tau & \phi & \psi & -a_6 - \lambda \end{vmatrix} = 0 \tag{12}$$

where

$$a_1 = (\xi + \alpha + \eta + \delta_1 + \mu), a_2 = \frac{\beta_1\pi\rho + \beta_2(1-\rho)\pi}{\mu}, a_3 = (\theta + \tau + \sigma + \delta_2 + \mu), a_4 = (\upsilon + \phi + \gamma + \mu),$$

$$a_5 = (\psi + \mu), a_6 = (\omega_1 + \omega_2 + \mu)$$

The four eigenvalues of above are $\lambda_1 = -\mu, \lambda_2 = -\mu, \lambda_3 = -a_6$ and $\lambda_4 = -a_5$ while the remaining three eigenvalues are obtained from 3 by 3 matrix below.

$$G = \begin{vmatrix} -a_1 & a_2 & 0 \\ \alpha & -a_3 & v \\ \eta & \theta & -a_4 \end{vmatrix} \tag{13}$$

Thus, the eigenvalues of K are real and negative if the Routh-Hurwitz condition is satisfied. Applying the Routh-Hurwitz condition: (i) $Tr(G) < 0$ (ii) $Det(G) > 0$.

Thus,

$Tr(K) = -a_1 - a_3 - a_4 = -(a_1 + a_3 + a_4) < 0$ and $\qquad Det(K) = \theta v a_1 + v\eta a_2 + \theta a_2 a_4 - a_1 a_3 a_4 = \theta v a_1 + v\eta a_2 + \theta a_2 a_4 - a_1 a_3 a_4$

$$= (\xi + \alpha + \eta + \delta_1 + \mu)\big(\theta v - (\theta + \tau + \sigma + \delta_2 + \mu)(v + \phi + \gamma + \mu)\big)(1 - R_0) \tag{14}$$

Following theorem 2 of Sanda, et al, we conclude that KCFE point is locally asymptotically stable.

Global stability Analysis of the Kalare Crime Free Equilibrium (KCFE)

We employ the theorem by Castillo-Chavez, Feng & Huang (2002) to prove the global stability of the Kalare Crime free equilibrium of the model (1). Achieving the requirements is necessary.

$H_1: \frac{dX}{dt} = H(X, 0), X^0$ is globally asymptotically stable (GAS)

$H_2: G(X, Z) = PZ - \hat{G}(X, Z), \hat{G}(X, Z) \geq 0$ for $(X, Z) \in \Omega$, where $P = \Delta_z G(X^0, 0)$ is an $M-matrix$ (the off diagonal elements of P are non-negative) and is also Jacobian of $G(X, Z)$

We write the model equation given by (1) as

$$\frac{dX}{dt} = H(X, Z) \tag{15}$$

$$\frac{dZ}{dt} = G(X, Z), G(X, 0) = 0$$

$$E_0(X^0, 0) = \left(\frac{\pi\rho}{\mu}, \frac{\pi(1-\rho)}{\mu}, 0\right) \tag{16}$$

Where $X = (S_E, S_U, R_2) \in R^3$ denotes the number of un-infected individuals and $Z = (E, K_C, J, R_1) \in R^4$ denotes the number of infected individuals.

$E_0 = (X^0, 0)$ denotes the DFE of the system.

Take (E, K_C, J, R_1) and evaluated at $E_0(S_E, S_U, R_2) = \left(\frac{\pi\rho}{\mu}, \frac{\pi(1-\rho)}{\mu}, 0\right)$. If the system satisfies the conditions H_1 and H_2 above, then according to Carlos Castillo-Chavez (2002), the following theorems hold.

Theorem 2: The fixed point $E_0 = (X^0, 0)$ is a globally asymptotic stable (GAS) provided that $R_0 < 1$ (L.A.S) and those assumptions H_1 and H_2 are satisfied.

Proof: The two functions $H(X, Z)$ and $G(X, Z)$ are given by

$$H(X, Z) = \begin{bmatrix} \pi\rho + \omega_1 R_2 - (\beta_1 K_C + \mu)S_E \\ \pi(1-\rho) + \omega_2 R_2 - (\beta_2 K_C + \mu)S_U \\ \tau K_C + \psi R_1 + \phi J - (\omega_1 + \omega_2 + \mu)R_2 \end{bmatrix} \tag{17}$$

$$G(X, Z) = \begin{bmatrix} \beta_1 K_C S_E + \beta_2 K_C S_U - (\xi + \alpha + \eta + \delta_1 + \mu)E \\ \alpha E + vJ - (\theta + \tau + \sigma + \delta_2 + \mu)K_C \\ \theta K_C + \eta E - (v + \phi + \gamma + \mu)J \\ \xi E + \sigma K_C + \gamma J - (\psi + \mu)R_1 \end{bmatrix} \tag{18}$$

We then consider the reduced system $\frac{dX}{dt} = H(X, 0)$ from condition (1)

$$H(X, 0) = \begin{bmatrix} \pi\rho - \mu S_E \\ \pi(1-\rho) - \mu S_U \\ 0 \end{bmatrix} \tag{19}$$

$$\frac{dS_E}{dt} + \mu S_E = \pi\rho$$

To integrate let use the integrating factor.

$$\Rightarrow S_E . IF = \pi\rho \int IF dt$$

At $t \to \infty$

$$S_E(0) = \frac{\pi\rho}{\mu} + C \tag{20}$$

$C = S_E(0) - \frac{\pi\rho}{\mu}$

By putting the value of C into (20)

$S_E(t) = \frac{\pi\rho}{\mu} + \left(S_E(0) - \frac{\pi\rho}{\mu}\right)e^{-\mu t}$, As $t \to \infty$ an $S_E(t) \to \frac{\pi\rho}{\mu}$.

Similar for $S_u(t) \to \frac{\pi(1-\rho)}{\mu}$ and $R(t) \to 0$.

convergence of X^0 is therefore global in Ω. This implies $X^0 = \left(\frac{\pi\rho}{\mu}, \frac{\pi(1-\rho)}{\mu}, 0\right)$ is g.a.s equilibrium of $\frac{dX}{dt} = F(X, 0)$.

Considering the second equation, we have

$G(X, Z) = PZ - \hat{G}(X, Z), \hat{G}(X, Z) \geq 0$ (21)

Therefore (21) gives,

$$P = \begin{bmatrix} -(\xi + \alpha + \eta + \delta_1 + \mu) & \beta_1 S_E + \beta_2 S_U & 0 & 0 \\ \alpha & -(\theta + \tau + \sigma + \delta_2 + \mu) & \upsilon & 0 \\ \eta & \theta & -(\upsilon + \phi + \gamma + \mu) & 0 \\ \xi & \sigma & \gamma & -(\psi + \mu) \end{bmatrix} \text{ and } Z = \begin{bmatrix} E \\ K_C \\ J \\ R_1 \end{bmatrix}$$

Therefore, $\hat{G}(X, Z) = \begin{bmatrix} 0 \\ 0 \\ 0 \\ 0 \end{bmatrix}$ (22)

But it is clear that $\therefore, \hat{G}(X, Z) = PZ - G(X, Z) \geq 0$. This implies that $\hat{G}(X, Z) = 0$, hence the kalare crime free equilibrium of the system is globally asymptotically stable implying that kalare crime will be eradicated if transmission rate is low in the environment and rehabilitation programmed is effectively employed.

Numerical Simulation
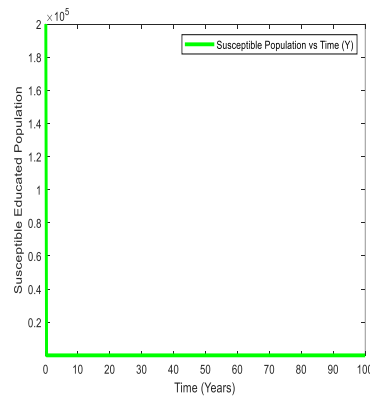
Figure 2
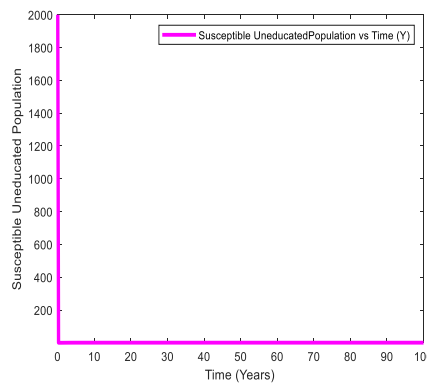
Figure 3
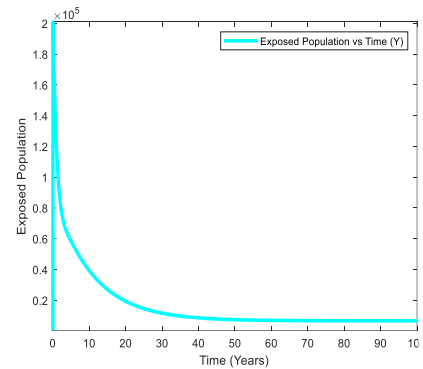
Figure 4
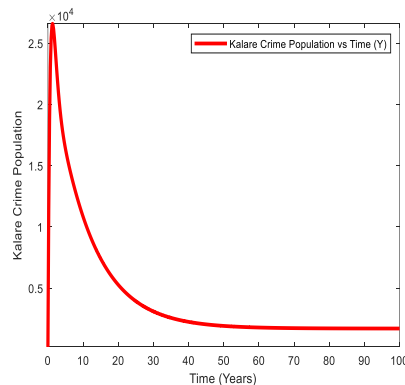
Figure 5
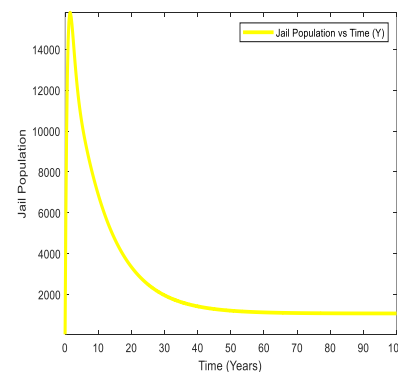
Figure 6
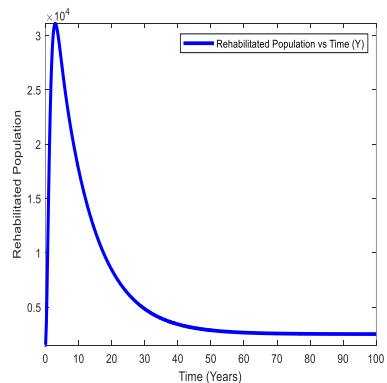
Figure 7
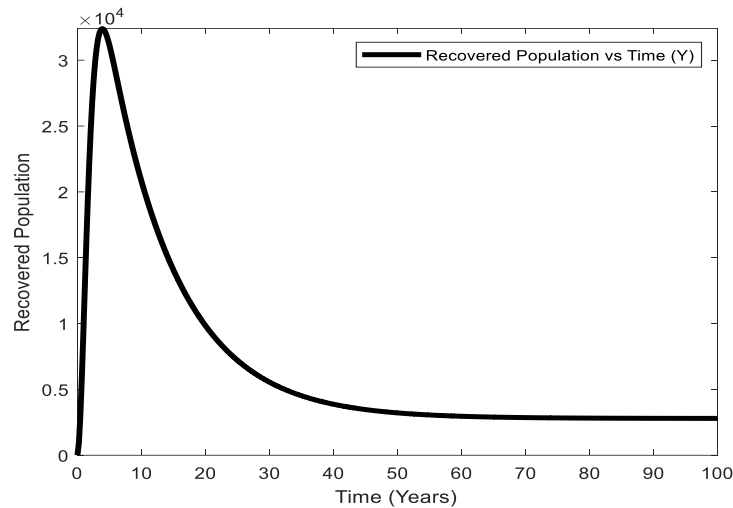
Figure 8

Discussion

To investigate how Kalare crime spreads, we created a deterministic $S_E, S_U, E, K_C, J, R_1, R_2$ and R model. The findings from our model analysis show that the model is appropriately posed mathematically and epidemiologically, with positive and bounded solutions. We investigated and computed the basic reproduction number and evaluated the stability of the equilibrium point. Based on Lyapunov's theory, our findings show that when $R_0 < 1$ is formed, the equilibrium point where Kalare crime is absent is globally asymptotically stable. Figures (2) and (3) revealed that susceptible educated and susceptible uneducated individuals dropped sharply over time. Based on the result, individuals exposed to kalare and kalare crime influence the potential ones, thereby reducing the number of susceptible ones. From figures (4) and (5), we observe that the population of primary infectious individuals increased exponentially and dropped drastically to a steady point because of treatment efficacy. In figures (6) and (7), it was observed that the population of drug-resistant individuals increased exponentially and later decreased to some certain level because of treatment efficacy. Figure (8) shows that the people of recovered individuals also increased exponentially over time and later slightly reduced due to proper treatment.

CONCLUSION

To find potential tactics for lowering and managing Kalare crime activity in Gombe state, the dynamic of Kalare crime was divided into seven distinct compartments. Compartmental models have been used to examine how sociological and economic factors have shaped the emergence of Kalare crime and criminal behavior in society. Using the trace approach, the local stability analysis of the Kalare crime equilibrium point and the Kalare present free equilibrium point were determined. The reproduction number demonstrates the controllability of the Kalare crime. The given numerical simulations of the Kalare criminal class, exposed class, jail class, rehabilitated class, and recovered class demonstrate how Kalare criminality activity in Gombe can eventually stabilize at each scenario.

REFERENCES

Bashir, U. M. (2017). The Assessment of Kalare Eradication Policies in Nigeria: A Study of AntiKalare Squad and Talba Empowerment Scheme (TES). *Journal of Research in Humanities and Social Science, 5*(3), 01-13.

Castillo-Chavez, C., Feng, Z., & Huang, W. (2002). On the computation of R_0 and its role on.
Mathematical approaches for emerging and reemerging infectious diseases: an introduction, 1,229.

Diekmann, O., & Heesterbeek, J. P. (2000). DiekmannMathematical Epidemiology of Infectious Diseases: Model Building, Analysis and Interpretation. *Diekmann, O., & Heesterbeek, J. P. (2000). Mathematical Epidemiology of Infectious Diseases:Wiley Series in Mathematical and Computational Biology, 1*, 23-24.

Sanda, A., Ibrahim, A., Yahaya, A., Adamu, I., Garba, I., & Abubakar, A. (2019). Modeling the Dynamics of Kalare Crime in Gombe Metropolis. *Bima Journal of science and Technology, 3*(1), 165-174.

Umar, M. (2013). An Assessment of the activities of Kalare in political violence in Gombe State, Nigeria. *International Journal of innovative research and develpoment, 2*, 2278-0211.

Van, D., Driessche, P., & Wantmough, J. (2002). Van, Reproduction numbers and sub-threshold endemic equilibria for compartmental models of diseases transmission. *Math. Biosci, 188*, 29-28.

Modelling the Dynamics of Tuberculosis Mathematically with Vaccination and Quarantine

*[1]Usman Garba, [2]Isa Ibrahim Mohammed, [3]Muhammad Abdullahi and [1]Raihanatu Mohammed Hamid

[1]Department of Mathematics and Computer Science, Gombe State College of Education Billiri, Gombe State, Nigeria
[2]Department of General Studies, Gombe State College of Health Sciences and Technology, Kaltungo, Gombe State, [3]Department of Mathematics, Federal University Dutsin-Ma, Katsina State, Nigeria
Nigeria
*Corresponding author's email: usmangarbapantami@gmail.com

ABSTRACT

This study examines the effects of an imperfect vaccine and quarantine by extending a deterministic mathematical simulation of the dynamics of TB transmission. The study examined the qualitative aspects of the model, including various unique aspects of disease transmission. The next-generation matrix technique presents the effective reproductive number, gauging TB's potential spread. We look into the endemic equilibrium point, TB-free equilibrium point, and sensitivity analyses' local and global stability. Furthermore, the findings show that quarantine and imperfect tuberculosis vaccines are consistently successful at halting the transmission of infectious diseases among people, even though the overall impact grows as efficacy and coverage rise. It has been demonstrated that a small proportion of those who receive vaccinations at steady-state and vaccine effectiveness play a comparable effect on lowering disease burden. A population can efficiently control tuberculosis by using a subpar vaccination and quarantine. The numerical simulation results reveal that employing an imperfect vaccine and implementing quarantine measures can effectively manage tuberculosis within a population as long as the vaccine's effectiveness, vaccination coverage, and the rigour of quarantine are maintained at moderately high levels.

Keywords: Tuberculosis, Imperfect, Quarantine, Vaccination, Effective Reproduction Number

INTRODUCTION

Tuberculosis (TB) is an infectious illness that primarily impacts the respiratory system. Yet, it can target various body organs, such as the brain, kidneys, spinal cord, lymphatic system, brain, and central nervous system Khajanchi, Das & Kar (2018); Ullah, Khan, Farooq & Gul (2019); WHO (2018). According to some estimates, the sickness may have affected up to one-third of people worldwide WHO (2018). Mycobacterium tuberculosis (Mtb) is a family of bacteria that causes tuberculosis WHO (2018). This infectious disease that spreads through the air poses a public health threat everywhere, including the USA (Hill, Becerra, & Castro, 2012), European countries (Abubakar et al. (2012); Behr (2004), and developing nations Fatima, Kumari, & Das (2020); WHO (2018). In 2018, there were up to 1.5 million more fatalities due to tuberculosis (TB) than due to HIV/AIDS worldwide (WHO 2018). Tuberculosis (TB) can spread by encounter with an infected person, either directly or indirectly (Bhunu et al 2008). The signs of TB consist of chest pain, fever, and night sweats, as well as an ongoing a bloody or mucus-producing cough that comes from deep inside the lungs (WHO 2018). It is challenging to comprehend how the disease progresses since the Mtb bacteria protracted latent period delays the onset of its active phase. The most effective and commonly used TB vaccine now available is BCG (Bacillus Calmette-Guerin) (Andersen & Doherty 2005), It effectively prevents more than 80% of TB types in children and offers greater than 50% protection against pulmonary infections. Most importantly, TB is spread by adults, not youngsters (Nadolinskaia, Karpov & Goncharenko 2020). Sadly, BCG has proven inconsistent TB protection in adults, primarily subpar. Therefore, new vaccines aimed at adult and pediatric populations are required (Fine, Carneiro, Milstien, & Clements 1999).

Several researchers have used mathematical models to analyze the importance of exogenous variables, including exogenous reinfection and reinfection in patients who have received treatment and inadequate immunizations in TB epidemics (see, for example, (Anderson, Anderson, & Robert 1992); Khajanchi, Das & Kar 2018); Song, Castillo-Chavez, & Aparicio 2002); Olaniyi et al. 2020); (Van Rie et al. 1999); (Vynnycky, & Fine 2000)). Bhunu et al. (2008) investigation of an expanded TB model with exogenous reinfection. In order to assess the possible impact of a flawed vaccine on reducing the rate at which TB spreads, Over the past several decades, a number SEIR models with vaccine compartments have been developed and described in the literature from a mathematical standpoint (Egonmwan, & Okuonghae 2019); (Gerberry 2016); (Nkamba 2019); (Renardy, M.; Kirschner 2019).

Typical Diagram
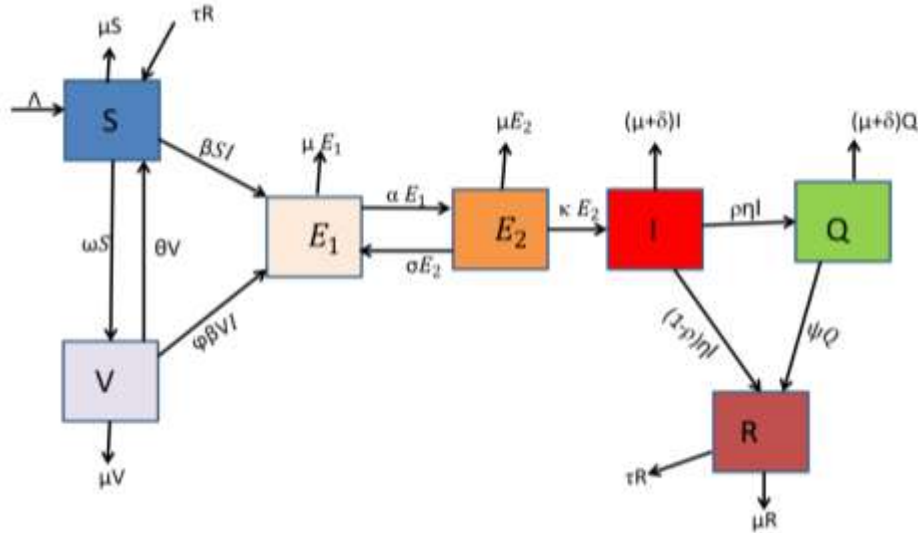
Figure 1: Model Diagram

The entire host population can be divided into seven compartments using a compartmental approach: susceptible individuals (S), vaccinated (V), early exposed (E_1), late exposed (E_2) individuals, individuals with active TB disease (I), quarantined individuals (Q) and recovered individuals (R). Only individuals in compartment I and Q are infectious, but quarantined individuals have been kept in a special place to avoid contact with other individuals. The susceptible compartment is increased by the incoming of individuals into the population by birth or immigration at a constant rate of Λ, and a natural death decreases each subpopulation at a rate of μ. The susceptible individuals get the infection at the rate of βI The administration of the BCG vaccine transfers individuals from susceptible populations to the vaccinated population at the rate of ω; however, the protection provided by the vaccine wanes overtime at the rate of θ. The model assumes the vaccination to be less than 100% effective. Therefore, vaccinated people in this compartment can get the disease through contact with people in the infected individuals, but less frequently φ where $0 \leq \varphi \leq 1$. The early exposed individuals progressed to the later exposed class at the rate α. The later exposed individuals moved to the early exposed and infected classes at the rates σ and κ, respectively. The proportion of Infected individuals move to quarantined and recovered classes at the rate $\rho\eta$ and $(1-\rho)\eta$, respectively. The quarantined individual progresses to the recovered class due to efficient treatment at the ψ. Finally, the recovered individual moves to the susceptible class due to its nature of temporary immunity at the rate τ.

Table 1: The model's parameters

Parameter	Description	Value	Source
Λ	Recruitment rate	10	Nkamba et l. (2019)
ψ	recovered rate of Quarantined Individuals	0.1	Assumed
β	Transmission Rate	1	Sulayman & Abdullah (2022)
κ	Rate of progression of later exposed class to infectious	0.00375	Sulayman, Abdullah, & Mohd (2021)
ρ	Proportion of infected individual that are moving into the Quarantined class	0.65	Assumed
σ	Progression Rate of later exposed individuals into early exposed class	0.02	Assumed
η	Progression of infected individuals into Quarantined and recovered classes	1.5	Sulayman, Abdullah, & Mohd (2021)
τ	Progression of individuals from recovered class into the susceptible class	0.129	Tunde, Yusuf & Afeez (2023)
δ	Disease-induced death rate	0.12	Sulayman, Abdullah, & Mohd (2021)
μ	Natural death rate	0.01874	Nkamba et l. (2019)
φ	Rate of Vaccine inefficacy	0.50	Nkamba et l. (2019)

α	Rate of progression of early exposed to later exposed class	0.21	Assumed
θ	Rate of vaccine waning	0.067	Sulayman, Abdullah, & Mohd (2021)
ω	Vaccination coverage	0.9 8	Nkamba et l. (2019)

Model Equations

$$\left.\begin{aligned}
\frac{dS}{dt} &= \Lambda + \theta V + \tau R - (\beta I + \omega + \mu)S \\
\frac{dV}{dt} &= \omega S - (\varphi\beta I + \theta + \mu)V \\
\frac{dE_1}{dt} &= \beta SI + \varphi\beta IV + \sigma E_2 - (\alpha + \mu)E_1 \\
\frac{dE_2}{dt} &= \alpha E_1 - (\kappa + \sigma + \mu)E_2 \\
\frac{dI}{dt} &= \kappa E_2 - (\mu + \delta + \eta)I \\
\frac{dQ}{dt} &= \rho\eta I - (\psi + \delta + \mu)Q \\
\frac{dR}{dt} &= (1 - \rho)\eta I + \psi Q - (\tau + \mu)R
\end{aligned}\right\} \qquad (1)$$

Invariant Region

Lemma 1: let $(S, V, E_1, E_2, I, Q, R)$ be the solution of the model (1) with initial conditions and biological feasible region given by the set Ω where:

$$\Omega = \left\{(S, V, E_1, E_2, I, Q, R) \in R^7 : \frac{\Lambda}{\mu}\right\}$$

Proof:

$$dN \leq (\Lambda - \mu N)dt$$
$$N(t) \leq \frac{\Lambda}{\mu}(1 - e^{-\mu t}) + N(0)e^{-\mu t} \qquad (2)$$
$$\lim_{t \to \infty} N(t) \leq \frac{\Lambda}{\mu}$$

The region in which the models make biological sense is given by

$$\Omega = \left\{(S, V, E_1, E_2, I, Q, R) \in R^7 : S, V, E_1, E_2, I, Q, R \leq \frac{\Lambda}{\mu}\right\} \qquad (3)$$

This means that every solution with initial condition(s) in Ω remain in Ω. Therefore, our model is biologically feasible, mathematically well posed and positivity invariant Ishaku et al. (2020).

Disease Free Equilibrium (DFE) Point

$$(S^*, V^*, E^*, E^*, I^*, Q^*, R^*) = \left(\frac{\Lambda(\theta+\mu)}{\mu(\omega+\theta+\mu)}, \frac{\omega\Lambda}{\mu(\omega+\theta+\mu)}, 0, 0, 0, 0, 0\right) \qquad (4)$$

Basic Reproduction Number: We applied the same next generation matrix procedure as in (Faniran et al. 2022); Faniran & Adewole 2021) to calculate the Basic Reproduction Number.

$$\lambda = R_{ef} = \frac{\beta\Lambda\kappa\alpha(\theta+\mu+\varphi\omega)}{\mu(\eta+\delta+\mu)(\omega+\theta+\mu)((\alpha+\mu)(\kappa+\sigma+\mu)-\sigma\alpha)} \qquad (5)$$

Local Stability of DFE

As adopted in (Saputra, Darti & Suryanto 2023); Chitnis, Cushing & Hyman 2006), the local stability of the DFE is illustrated by the Jacobian of the suggested model system (1). The characteristic equation is then derived using the Jacobian to produce the eigenvalue outcome.

Theorem 1: When $R_{ef} < 1$, the system (1)'s disease-free equilibrium is locally asymptotically stable and unstable if $R_{ef} > 1$.

Proof: The Jacobian of system (1) at $J(E_0)$, which is provided by: is examined to demonstrate the system's local stability.

$$J(E_0) = \begin{bmatrix} -(\mu+\omega) & \theta & 0 & 0 & -\dfrac{\beta\Lambda(\theta+\mu)}{\mu(\omega+\theta+\mu)} & 0 & \tau \\ \omega & -(\theta+\mu) & 0 & 0 & -\dfrac{\beta\varphi\omega\Lambda}{\mu(\omega+\theta+\mu)} & 0 & 0 \\ 0 & 0 & -(\alpha+\mu) & \sigma & \dfrac{\beta\Lambda(\theta+\mu+\varphi\omega)}{\mu(\omega+\theta+\mu)} & 0 & 0 \\ 0 & 0 & \alpha & -(\kappa+\sigma+\mu) & 0 & 0 & 0 \\ 0 & 0 & 0 & \kappa & -(\eta+\delta+\mu) & 0 & 0 \\ 0 & 0 & 0 & 0 & \eta\rho & -(\psi+\delta+\mu) & 0 \\ 0 & 0 & 0 & 0 & (1-\rho)\eta & \psi & -(\tau+\mu) \end{bmatrix}$$

Adopted from [25]

$Tr(P) = -A_1 - A_2 - A_3 - A_4 - A_8 - A_{10} - A_{11}$

$= -(A_1 + A_2 + A_3 + A_4 + A_8 + A_{10} + A_{11}) < 1$

$Det(P) = A_{10}A_{11}(A_1A_2 - \theta\omega)(A_8(A_3A_4 - \alpha\sigma) - A_7\alpha\kappa)$

$= (\psi+\delta+\mu)(\tau+\mu)((\omega+\mu)(\theta+\mu) - \theta\omega)(\eta+\delta+\mu)((\alpha+\mu)(\kappa+\sigma+\mu) - \alpha\sigma)(1 - R_0) > 0$

Based on the findings in Faniran et al. (2022), we can deduce that the local asymptotic stability of the DFE point is established.

Global Stability of the Disease-Free Equilibrium Point

Using the condition of Cohen et al. (2007), we examine the disease-free equilibrium's global asymptotic stability for the model (1).

Lemma 2: Consider a model system written in the form

$$\left. \begin{array}{l} \dfrac{dX}{dt} = F(X,Z) \\ \dfrac{dZ}{dt} = G(X,Z), (X,0) = 0 \end{array} \right\} \tag{6}$$

Where $X = (S, V, R())$ and $Z = (E_1, E_2, I, R())$ with the components of $X \in \Re^3$ denoting the uninfected population and the components of $Z \in \Re^4$ denoting infected population.

The disease-free equilibrium is now denoted as

$E_0 = (X^0, 0)$

Where;

$$X^0 = \left(\frac{\Lambda(\theta+\mu)}{\mu(\omega+\theta+\mu)}, \frac{\omega\Lambda}{\mu(\omega+\theta+\mu)}, 0 \right) \tag{7}$$

The following conditions must hold to guarantee global asymptotic stability. Assume that, H_1: $\frac{dX}{dt} = \boldsymbol{F}(\boldsymbol{X}, \boldsymbol{0})$, $\boldsymbol{X^0}$ is globally asymptotically stable.

H_2: $\boldsymbol{G}(\boldsymbol{X}, \boldsymbol{Z}) = \boldsymbol{PZ} - \hat{\boldsymbol{G}}(\boldsymbol{X}, \boldsymbol{Z}), \hat{\boldsymbol{G}}(\boldsymbol{X}, \boldsymbol{Z}) \geq \boldsymbol{0}$ For $(X, Z) \in \Omega$ (8)

where $P = D_z G(X^0, 0)$ is an M-matrix (the off-diagonal elements of P are non-negative) and Ω is the region where the model makes biological sense; Then, E^0 is globally asymptotically stable provided that $R_0 < 1$ Cohen et al. (2007).

Theorem 2: The model (1) is globally asymptotically stable provided that $R_0 < 1$.

Proof: We need to show that the conditions (H_1) and (H_2) hold when $R_0 < 1$.

From our model (1), (2) and (6) we have, for the uninfected population.

$$F(X,0) = \begin{pmatrix} \Lambda + \theta V + \tau R - (\beta I + \omega + \mu +)S \\ \omega S - (\varphi\beta I + \mu + \theta)V \\ (1-\rho)\eta I + \psi Q - (\mu + \tau)R \end{pmatrix} \tag{9}$$

From the above equation, we have

$$X^0 = \left(\frac{\Lambda(\theta+\mu)}{\mu(\omega+\theta+\mu)}, \frac{\omega\Lambda}{\mu(\omega+\theta+\mu)}, 0 \right) \tag{10}$$

is globally asymptotically stable. This can be proved below, thus,

$$S(t) = \left(\frac{\Lambda(\theta+\mu)}{\mu(\omega+\theta+\mu)}, 0 \right) + \left(S(0) - \left(\frac{\Lambda(\theta+\mu)}{\mu(\omega+\theta+\mu)} \right) \right) e^{-(\mu+\tau)(\mu+\theta+\varphi\beta I)t},$$

$$V(t) = \frac{\omega\Lambda}{\mu(\omega+\theta+\mu)} + \left(V(0) - \frac{\omega\Lambda}{\mu(\omega+\theta+\mu)} \right) e^{-(\mu+\theta+\varphi\beta I)t}, R(t) = 0$$

As $t \to \infty$, $S \to \frac{\Lambda(\theta+\mu)}{\mu(\omega+\theta+\mu)}, V \to, \frac{\omega\Lambda}{\mu(\omega+\theta+\mu)}, R \to 0,$ (11)

convergence of X^0 is therefore global in Ω. This implies $X^0 = \left(\frac{\Lambda(\theta+\mu)}{\mu(\omega+\theta+\mu)}, \frac{\omega\Lambda}{\mu(\omega+\theta+\mu)}, 0 \right)$ is globally asymptotically stable and satisfied H_1.

Thus, using the second condition of the theorem

$H_2 \colon \hat{G}(X,Z) = PZ - G(X,Z), \hat{G}(X,Z) \geq 0$ for $(X,Z) \in \Omega$. Therefore, $\hat{G}(X,Z) = PZ - G(X,Z), \hat{G}(X,Z) \geq 0$. Where P is an $n_\circ \times n$ matrix, Z is a column vector and $G(X,Z)$ is a column vector formed from the infectious classes; Recall

$$\hat{G}(X,Z) = PZ - G(X,Z) = \begin{pmatrix} 0 \\ 0 \\ 0 \\ 0 \end{pmatrix} \tag{12}$$

Since $\overset{\wedge}{G_1}(X,Z), \overset{\wedge}{G_2}(X,Z), \overset{\wedge}{G_3}(X,Z), \overset{\wedge}{G_4}(X,Z) = 0$

However, it is evident that $(X,Z) = PZ - G(X,Z) \geq 0$. This suggests that $\hat{G}(X,Z) = 0$ and that the system's tuberculosis disease-free equilibrium is globally asymptotically stable, suggesting that the disease will be wiped out provided transmission rates are low and vaccine delivery is used successfully.

Endemic Equilibrium (EE) Point

The Endemic Equilibrium Points of the Model $\left(S^*, V^*, E_1^*, E_2^*, I^*, Q^*, R^* \right)$ is expressed as follows:

$$\left. \begin{array}{l} S^* = \frac{\eta(\varphi\beta I^* + \mu + \theta)\left((\mu+\delta+\psi)(\mu+\tau) + I^*(\mu+\delta+\psi-\rho(\mu+\delta))\right)}{\Gamma}, V^* = \frac{\omega\left(\eta(\mu+\delta+\psi)(\mu+\tau)+\eta I^*(\mu+\delta+\psi-\rho(\mu+\delta))\right)}{\Gamma} \\[2mm] E_1^* = \frac{(\mu+\delta+\eta)(\mu+\sigma+\kappa)I^*}{\alpha\kappa}, E_2^* = \frac{(\delta+\eta+\mu)I^*}{\kappa}, I^* = I^*, Q^* = \frac{\rho\eta I^*}{(\psi+\delta+\mu)}, R^* = \frac{\eta I^*(\mu+\delta+\psi-\rho(\mu+\delta))}{(\mu+\delta+\psi)(\mu+\tau)} \end{array} \right\} \tag{13}$$

where;

$$\Gamma = (\mu+\delta+\psi)(\mu+\tau)(\mu^2+\theta\mu+\mu\omega+\beta I(\theta+\mu+\mu\varphi+\varphi\omega+\beta\varphi I).$$

Figure 2: Effect of transmission rate on quarantine individuals
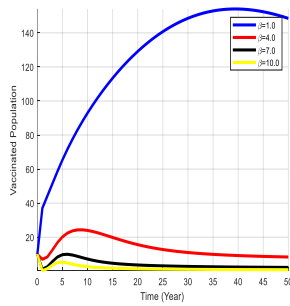
Figure 3: Effect of transmission rate on vaccinated individuals
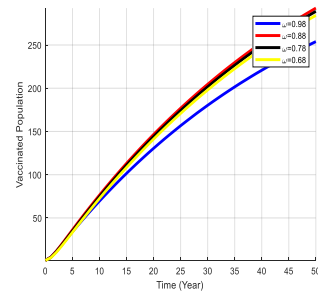
Figure 4: Effect of vaccine coverage on Vaccinated Individuals
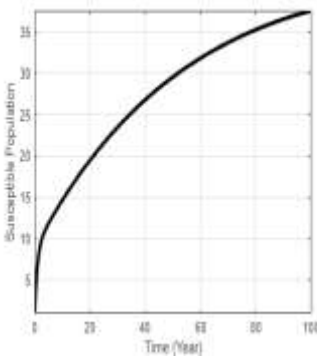
Figure 5(a)
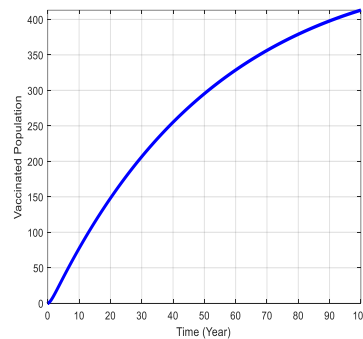
Figure 5(b)
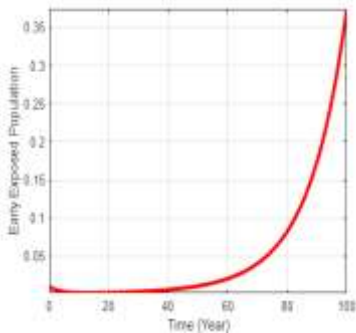
Figure 5(c)
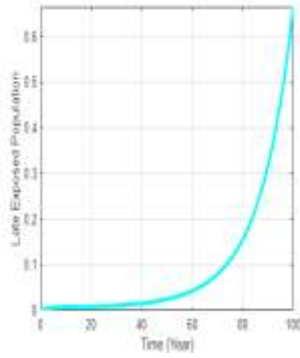
Figure 5(d)
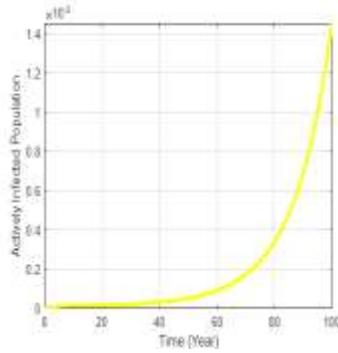
Figure 5(e)
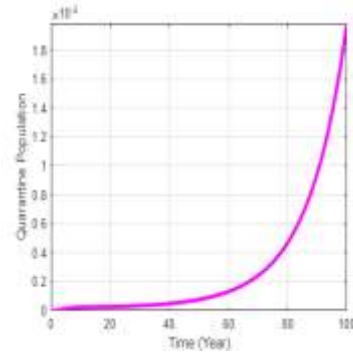
Figure 5(f)
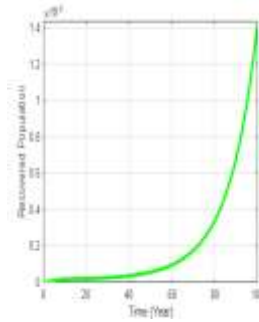
Figure 5(g)

Discussion

To investigate how TB spreads, we created a deterministic SVE_1E_2IQRS model. The results of our model study demonstrate that the model is mathematically and epidemiologically well stated, with both positive and bounded solutions. We investigated and computed the basic reproduction number and evaluated the stability of the equilibrium point. Based on Lyapunov's theory, our findings show that when $R_0 < 1$ is formed, the equilibrium point where tuberculosis illness is absent is globally asymptotically stable. We investigated the impact of different parameters on the quarantined and vaccinated population within the model, as shown in Fig.2, 3, and 4. From Fig. 5a, we observed that the susceptible population increased exponentially because of the influx of individuals. The number of people vaccinated increased and later stabilized, rising gradually, as shown in Fig.5b, resulting from failure in treatment efficacy. From Fig.5c-5g, we observe that the population of early latent, late latent, active, quarantined, and recovered individuals stabilized, increased exponentially, and dropped drastically to a steady point because of treatment efficacy.

Conclusion

The study examined the qualitative aspects of the model, including various unique aspects of disease transmission via the next-generation matrix technique that presents the effective reproductive number, gauging TB's potential spread. The findings show that quarantine and imperfect tuberculosis vaccines are consistently successful at halting the transmission of infectious diseases among people, even though the overall impact grows as efficacy and coverage rise. The numerical simulation results reveal that employing an imperfect vaccine and implementing quarantine measures can effectively manage tuberculosis within a population as long as the vaccine's effectiveness, vaccination coverage, and the rigour of quarantine are maintained at moderately high levels.

REFERENCES

Abubakar, IDara, M.; Manissero, D.; Zumla, A. Tackling the spread of drug-resistant tuberculosis in Europe. *Lancet* **2012**, *379*, e21–e23.

Anderson, R.M.; Anderson, B.; Robert, M.M. *Infectious Diseases of Humans: Dynamics and Control*; Oxford University Press: Oxford, UK, 1992.

Andersen, P.; Doherty, T.M. The success and failure of BCG—Implications for a novel tuberculosis vaccine. *Nat. Rev. Microbiol.* **2005**, *3*, 656–662.

A. Ishaku, A. M. Gazali, S. A. Abdullahi, and N. Hussaini, "Analysis and optimal control of an HIV model based on CD4 count," *J Math Biol*, vol. 81, no. 1, pp. 209–241, Jul. 2020, doi: 10.1007/s00285-020-01508-8.

Behr, M.A. Tuberculosis Due to Multiple Strains: A Concern for the Patient? A Concern for Tuberculosis Control? *Ann. Am. Thorac. Soc.* **2004**, *1*69, 554–555.

Bhunu, C.P.; Garira, W.; Mukandavire, Z.; Zimba, M. Tuberculosis transmission model with chemoprophylaxis and treatment. *Bull. Math. Biol.* **2008**, *70*, 1163–1191.

Bloom, B.R.; Murray, C.J. Tuberculosis: Commentary on a reemergent killer. *Science* **1992**, *257*, 1055–1064.

Buonomo, B.; Della Marca, R. Oscillations and hysteresis in an epidemic model with information-dependent imperfect vaccination. *Math. Comput. Simul.* **2019**, *162*, 97–114.[Online]. Available: http://math.asu.edu/˜mbe/

Cohen, T.; Colijn, C.; Finklea, B.; Murray, M (2007). Exogenous re-infection and the dynamics of tuberculosis epidemics: Local effects in a network model of transmission. *J. R. Soc. Interface*

Egonmwan, A.O.; Okuonghae, D. Mathematical analysis of a tuberculosis model with imperfect vaccine. *Int. J. Biomath.* **2019**, *12*, 1950073.

Fatima, S.; Kumari, A.; Das, G.; Dwivedi, V.P. Tuberculosis vaccine: A journey from BCG to present. *Life Sci.* **2020**, *252*, 117594.

Feng, Z.; Castillo-Chavez, C.; Capurro, A.F. A model for tuberculosis with exogenous reinfection. *Theor. Popul. Biol.* **2000** *57*, 235–247.

Fine, P.E.; Carneiro, I.A.; Milstien, J.B.; Clements, C.J (1999. *Issues Relating to the Use of BCG in Immunization Programmes: A Discussion Document (No. WHO/V and B/99.23);* World

Gerberry, D.J. Practical aspects of backward bifurcation in a mathematical model for tuberculosis. *J. Theor. Biol.* **2016**, *388*, 15–36.

Hill, A.N.; Becerra, J.E.; Castro, K.G. Modelling tuberculosis trends in the USA. *Epidemiol. Infect.* **2012**, *257*, 1862–1872.

H. L. Saputra, I. Darti, and A. Suryanto, "Analysis of an SVEIL Model of Tuberculosis Disease Spread with Imperfect Vaccination," 2023, doi: 10.31764/jtam. v7i1.11033.

Khajanchi, S.; Das, D.K.; Kar, T.K. Dynamics of tuberculosis transmission with exogenous reinfections and endogenous reactivation. *Phys. A* **2018**, *497*, 52–71.

Nkamba, L.N.; Manga, T.T.; Agouanet, F.; Mann Manyombe, M.L. Mathematical model to assess vaccination and effective contact rate impact in the spread of tuberculosis. *J. Biol. Dyn.* **2019**, *13*, 26–42. [CrossRef]

N. Chitnis, J. M. Cushing, and J. M. Hyman, "Bifurcation analysis of a mathematical model for malaria transmission," *SIAM J Appl Math*, vol. 67, no. 1, pp. 24–45, 2006, doi: 10.1137/050638941.

Nadolinskaia, N.I.; Karpov, D.S.; Goncharenko, A.V. Vaccines against Tuberculosis: Problems and Prospects. *Appl. Biochem. Microbiol.* **2020**, *56*, 497–504.Health Organization; Geneva, Switzerland, 1999.

Renardy, M.; Kirschner, D.E. Evaluating vaccination strategies for tuberculosis in endemic and non-endemic settings. *J. Theor. Biol* **2019**, *469*, 1–11.

Song, B.; Castillo-Chavez, C.; Aparicio, J.P. Tuberculosis models with fast and slow dynamics: The role of close and casual contacts. *Math. Biosci.* **2002**, *180*, 187–205.

S. Olaniyi, O. S. Obabiyi, K. O. Okosun, A. T. Oladipo, and S. O. Adewale, "Mathematical modelling and optimal cost-effective control of COVID-19 transmission dynamics," *Eur Phys J Plus*, vol. 135, no. 11, Nov. 2020, doi:10.1140/epjp/s13360-020-00954-z.

T. Faniran, A. Ali, M. O. Adewole, B. Adebo, and O. O. Akanni, "Asymptotic behavior of Tuberculosis between smokers and non-smokers," *Partial Differential Equations in Applied Mathematics*, vol. 5, Jun. 2022, doi: 10.1016/j.padiff.2021.100244.

T. S. Faniran and M. O. Adewole, "Analysis of a cholera model with treatment noncompliance," *International Journal of Nonlinear Analysis and Applications*, vol. 13, no. 1, pp. 29–43, Mar. 2022, doi:10.22075/ijnaa.2021.23626.2568.

Tunde T. Yusuf and Afeez Abidemi" Effective strategies towards eradicating the tuberculosis epidemic: An optimal control theory alternative. *Health care Analytics* 3 (2023) 10013

Ullah, S.; Khan, M.A.; Farooq, M.; Gul, T. Modeling and analysis of Tuberculosis (TB) in Khyber Pakhtunkhwa, Pakistan. *Math. Comput. Simul* **2019**, *165*, 181–199.

Van Rie, A.; Warren, R.; Richardson, M.; Victor, T.C.; Gie, R.P.; Enarson, D.A.; van Helden, P.D. Exogenous reinfection as a cause of recurrent tuberculosis after curative treatment. *N. Engl. J. Med.* **1999**, *341*, 1174–1179.

Vynnycky, E.; Fine, P.E. Lifetime risks, incubation period, and serial interval of tuberculosis. *Am. J. Epidemiol.* **2000**, *152*, 247–263.

Wangari, I.M.; Davis, S.; Stone, L. Backward bifurcation in epidemic models: Problems arising with aggregated bifurcation parameters. *Appl. Math. Model.* **2016**, *40*, 1669–1675.

World Health Organization. *Global Tuberculosis Report*; WHO: Geneva, Switzerland, 2018; p. 214.

Sulayman, F. Abdullah, F. A. and Mohd, M. H. An SVEIRE model of tuberculosis to assess the effect of an imperfect vaccine and other exogenous factors. Mathematics. 2021. 9(4):327.

Sulayman, F and Abdullah, F.A. "Dynamical Behaviour of a Modified Tuberculosis Model with Impact of Public Health Education and Hospital Treatment" *axioms* **2022**, *11*, 723

Soft BCK/BCI-EXT-Implicative Ideal of Soft BCK/BCI-EXT-Algebra

*Yusuf, A. O., and Sanusi, B.

Department of Mathematical Science, Faculty of Physical science, Federal University Dutsinma, Katsina. Katsina Nigeria.
*Corresponding author's email: oyusuf@fudutsinma.edu.ng

ABSTRACT

This article introduces the concept of soft BCK/BCI-ext-implicative ideals and BCK/BCI-ext-implicative idealistic soft BCK/BCI-ext -algebras, and explores their elementary properties. The affairs between soft ideals and soft BCK/BCI-ext-implicative ideals in soft BCK/BCI-ext-algebras are also examined. Additionally, the connection between idealistic soft BCK/BCI-ext -algebras and BCK/BCI-ext-implicative idealistic soft BCK/BCI-ext-algebras is recognized. The article establishes the intersection, union, "AND" operation, and "OR" operation of soft BCI-implicative ideals and BCK/BCI-ext-implicative idealistic soft BCK/BCI-ext-algebras. Finally, the paper contributes a deeper understanding of soft BCK/BCI-ext-algebras and their ideals.

Keywords: Implicative, implicative ideal, BCK/BCI-ext-implicative.

INTRODUCTION

Soft set theory is a relatively new mathematical framework that deals with uncertainty and vagueness in decision-making and data analysis. It provides a flexible and robust mechanism to handle imprecise information. Soft set theory has found applications in various fields, including pattern recognition, image processing, data mining, and decision support systems.

In recent years, there has been an increasing interest in combining soft set theory with other algebraic structures to develop new mathematical frameworks. One such combination is the assimilation of soft set theory with BCK/BCI-algebra, which are important algebraic structures used to study logic and reasoning in computer science and mathematics. Molodtsov (1999) Defined soft sets as a parameterized family of a soft sets. Some years ago, the idea of a soft set was studied by many researchers. Maji *et al* Offered a detailed investigation of soft sets which includes the type's set theories and basic operation of set among others, they also deliberate and conferred the fundamental properties of set. Pie and Miao (2005) Redefined a soft set and joint of soft set and discourse the bond between soft sets and informants systems.

Extended BCK/BCI-EXT-Implicative Algebras

The BCK/BCI-algebras are considered to be a very important class of logical algebras and these algebras were introduced by Imai and Iseki (1996) and were widely studied by various researchers.

Definition 1 Malik and Touqeer, (2014)

An algebra $(X, *, 0)$ of type $(2, 0)$ is called a BCK/BCI-algebra if it satisfies the following conditions:

i. $\big((d * e) * (d * f)\big) * (f * e) = 0$

ii. $\big(d * (d * e)\big) * e = 0$

iii. $d * d = 0$

iv. $d * e = 0$ and $e * d = 0 \Rightarrow d =$

v. $0 * d = 0$, for all $d, e, f \in Y$. If

Definition 2

A BCK/BCI-ext-algebra, denoted by BCK/BCI-ext-algebra is an algebra $(Y, *, /, 0)$ of form $(3, 0)$ that meets all the requirements BCK/BCI-ext-algebras, and also fulfills the condition

vi. $d * \frac{(d \, * \, e)}{d \, * \, e} * e = 0, \forall \, d, e \in$

vii. $\frac{(d \, * \, e)}{e} = e$

viii. $d \leq e \iff d * e = 0$

Definition 3

A non-empty subset M of an extended BCK/BCI-ext-algebra Y is called a sub-ext-algebra of Y, if $d * e \in M$ and $d/e \in M$ for all $d, e \in M$.

In other words, a sub-ext-algebra of an extended BCK/BCI-ext-algebra Y is a subset M that preserves closure under multiplication and division within Y.

Justification of definition of sub-ext-algebra of Y.

$d * e$ is in M for any d and e in M:

For M to be a sub-ext-algebra of Y, it needs to be closed under the operation of multiplication (denoted by "$*$"). For any two element $d, e \in M$, their product $d * e$ must also be in M. This condition ensures that the subset M inherits the closure property from the original BCK/BCI-ext-algebra Y.

2. If d divide e is in M for any d and e in M:

In addition to closure under multiplication, M must also be closed under the operation of division (denoted by "divide"). The divide operation represents the inverse of multiplication in the BCK/BCI-ext-algebra. So, for any two elements d and e in M, their division d divide e must also be in M. This condition guarantees that M preserves the inverse operation within itself.

By satisfying both conditions, the subset M fulfills the necessary criteria to be considered a sub-ext-algebra of Y.

Definition 4
Implicative
An ideal A of a BCK/BCI-ext-algebra Y is called implicative if for any elements $d, e \in Y$, whenever the expression $\left((d * e) * e\right) * (0 * e) \in A$ the expression $d * \left(\left(e * (e * d) * \left(0 * (e * e)\right)\right)\right)$.

Theorem 1
In a BCK/BCI-ext-algebra Y, an ideal A is implicative if and only if $\left((d * e) * e\right) \in A$ implies
Proof: Assume Y is a BCK/BCI-ext-algebra and let $A \in Y$.
Assume A is implicative. We want to show that $\left((d * e) * e\right) \in A$ implies $d * \left(e * (e * d)\right) \in A$.
We know that an ideal A is implicative if for all $d, e \in Y, (d, e) \in A \to d * (e * e) \in A$.
Let's consider $d, e \in Y$, such that $\left((d * e) * e\right) \in A$ From implicative ideals, $(d * e) \in A$ implies $d * (e * e) \in A$.
Therefore we have $\left((d * e) * e\right) \in A$ implies $d * \left(e * (e * d)\right) \in A$
Since Y is a BCK/BCI-ext-algebra, we may have a condition that $d * (e * f) = (d * e) * c \; \forall \, a, b, c \in Y$
Using this property, we can rewrite the above equation as $d * \left(e * (e * e)\right) \in A$.
we can simplify it further to $d * \left(e * (e * d)\right) \in A$.
Therefore, we have shown that if $\left((d * e) * e\right) \in A$ then $d * \left(e * (e * d)\right) \in A$.
Thus A is implicative

Definition 5 A non-empty subset I of an extended BCK/BCI-ext-implicative ideal of Y is called an extended BCK/BCI-ext-implicative ideal of Y if it satisfies.
   i.   Non- emptiness $0 \in l$
   ii.   Consistency with Y: The subset l which BCK/BCI-ext-implicative $Y. l \in Y$
   iii.   If $d \in l$ and $e \in Y$ for any $f \in Y$ any operation $^e/_f \in l$

Fusion of this conditions together define an extended BCK/BCI-ext-implicative ideal of Y.
Example 1: Assume that Y defines an operation $(*,/)$ on Y Demonstrated by the following table.

Table 1 Cayley table

$*$	O	e_1	e_2	e_3	e_4
O	O	O	o	e_3	e_3
e_1	e_1	0	0	e_3	e_3
e_2	0	e_2	o	0	e_3
e_3	e_3	e_3	e_3	0	0
e_4	e_4	e_4	e_3	e_2	0

Table 2: Caley table

/	O	e_1	e_2	e_3	e_4
O	O	0	e_1	e_3	e_2
e_1	e_1	e_2	0	e_3	e_4
e_2	0	e_3	e_3	e_4	e_2
a_3	O	0	e_1	0	0
e_4	e_2	e_4	e_3	e_1	0

The definition $(Y; /,*,O)$ is a BCK/BCI-ext- algebra and $A \subset Y$. The sub-algebra $A = \{0, e_3\}$ therefore shows that A is implicative. However, is not a BCK/BCI-implicative ideal

$$\left(\left(\frac{e_1}{e_1} * \frac{e_2}{e_2}\right) * \frac{e_2}{e_2}\right) * \left(\frac{0}{0} * \frac{e_2}{e_2}\right) = 0 \in \{0, e_3\} \text{ this implies } \frac{e_1}{e_1} * \left(\left(\frac{e_2}{e_2} * \left(\frac{e_2}{e_2} * \frac{e_1}{a_1}\right)\right) * \left(\frac{0}{0} * \left(\frac{e_2}{e_2} * \frac{e_1}{e_1}\right)\right)\right) = e_2 \notin \{0, e_3\}$$

Definition 6: Let $(P, N) \ and \ (Q, S)$ be a couple of soft sets over a common universal U. The intersection of $(P, N) \ and \ (Q, S)$ denoted by $(P, N) \bowtie (Q, S)$ is defined to be the soft set (HC) satisfying the following four conditions

    i. $C = A \cap B$
    ii. $C \subset NUS$
    iii. $H \subset U$
    iv. $C \subset U$

Theorem 2

Suppose that soft set (P, N) over a common universe U. The complement of the set is defined to be (H, C).

To prove the theorem, we need to show that the complement of a soft set (P, N) over a common universe U, which is defined to be (H, C) satisfies the properties of a soft set.

    Recall that a soft set (P, N) over U satisfies the following properties:

$P \subset U$ Every positive set in the soft set is a subset of the universe U. Also $N \subset U$ Every negative set in the soft set is a subset of the universe U.

Now, let's study the complement of the soft set (P, N) denoted as (H, C) We define the complement operation as follows:

$H = U \backslash P$ The positive set in the complement (H, C) is the set difference between the universe U and the positive set P.

$C = U \backslash N$ The negative set in the complement $(H, C))$ is the set difference between the universe U and the negative set N.

To prove that (H, C) is a soft set, we need to show that it satisfies the properties of a soft set:

$H \subset U$ The positive set H in the complement is a subset of the universe H. This is true since H is defined as the set difference $U \backslash P$ and set differences preserve subset relationships.

$C \subset U$: The negative set C in the complement is a subset of the universe U.

    This is true since C is defined as the set difference $U \backslash N$ and set differences preserve subset relationships.

Therefore, (H, C) satisfies the properties of a soft set, and the theorem is proved.

Definition 7

Two difference soft set over a common universe U, (P, N) and (Q, S). There difference is defined as $(P \backslash Q, N \backslash S)$ where $(P \backslash Q)(e) = P(x) - Q(e)$.

Definition 4

Let (P, N) be a soft extended BCK/BCI-ext- algebra over Y. A soft set (Q, l) over Y is called a soft ideal of (P, N), denoted by $(Q, l) \widetilde{\bowtie} (P, N)$, if it satisfies the following conditions.

    i. $l \subset_{ext} A$
    ii. $Q(x) \bowtie_{ext} P(x) \ \forall \ d \in l$

Example 1: Consider an extended BCK/BCI-ext-algebra $Y = \{0, e_1, e_2, e_3, e_4, e_5$ which is given in example 1 above. Let (P, N) be a soft set over Y, where $A = Y$ and $F: A \to P(x)$ is a set valued function defined by: $F(x) = \{u\} \cup \{y \in X/y * \left(\frac{y}{x}\right) \in \{0, a, b\}$ for all $x \in A$.

We can see that $F(0) = F(e_2) = F(e_3) = Y$, $F(e_1) = F(e_4) = F(e_5) = \{0\}$ which are sub-algebras of Y. Hence, (P, N) is a soft BCK/BCI-ext-algebra over Y.

Let $I = \{0, e_1, e_2, e_3\} \subset A$ and $Q: I \to P(x)$ to be a set-valued function defined by: $Q(x) = \begin{cases} \{x \in X | 0 * (0/x) \in \{0, e_1, e_2\} \ if \ e_1 = e_2 \\ \{0\} \quad\quad\quad\quad\quad if \ x \in \{0, e_1, e_2\} \end{cases}$

Then $Q(0) = \{0\} \bowtie_{bck/bci - ext -i} Y = P(0)$

$Q(e_1) = \bowtie_{bck/bci - ext -i} \square Y = P(e_1)$

$G(e_2) = \{0\} \bowtie_{bck/bci - ext -i} \square_\square Y = F(e_2)$

and $\quad G(e_3) = \{0\} \bowtie_{bck/bci - ext -i} Y = F(e_3)$.

Hence (Q, l) is a soft BCK/BCI-ext-implicative ideal of (P, N)

Example 2: Let $Y = \{0, e_1, e_2, e_3, e_4, e_5, e_6\}$ be an extended BCK/BCI-ext-algebra with the following Cayley table.

Let (P,N) be a soft set over Y, where $A = Y$ and $F: A \to P(x)$ is a set valued function defined by $F(x) = \{0\} \cup \{y \in X|\ y * (y/x) \in \{0, e_1, e_2, e_3\}$ for all $x \in A$.

Then $P(0) = P(e_1) = Y$, $P(e_2) = \{0, e_1, e_2, e_4, e_5\}$, $P(e_3) = \{0, e_1, e_2, e_3\}$, $P(e_4) = \{0, e_1, e_3, e_4, e_5\}$, $P(e_5) = \{0, e_2, e_4\}$, $P(e_6) = \{0, e_5, e_6\}$ which are all sub-algebras Y. Hence (P,N) is a soft extended BCK/BCI-ext-algebra on Y.

Let (Q,S) be a soft set on Y, where $l = \{e_1, e_3\} \subset A$. And $Q: S \to P(x)$ be a set-valued function defined by $G(x) = \{y \in X|(x/y) * (x/z)\}$ for all $x, z, \in I$. Then $G(e_1) = \{e_1, e_3\} \bowtie_{ext} Y = F(e_1)$, $G(e_3) = \{0, e_1, e_2, e_5\} \bowtie_{ext} F(e_3) = \{0, e_1, e_2, e_3\}$. Hence (Q,S) is a soft ideal of (P,N) and it is a soft BCK/BCI-ext-implicative ideal of (P,N).

Theorem 3

Let $(G_1 M_1)$ and $(G_2 M_2)$ be two Soft set over Y. Where the Cartesian product $M_1 \times M_2 = O$ and for any (P,A) is a soft BCK/BCI-ext-algebra over Y.

$$\therefore (G_1 M_1)\ \widetilde{\bowtie}_{bck/bci-i}\ (P,A), (G_2 M_2)\ \widetilde{\bowtie}_{bck/bci-i}\ (P,A).$$

It implies that $(G_1 M_1)\ \widetilde{\times}\ (G_2 M_2) = (G,M)$.

Proof

Obviously $M \subset A$ and $M = M \times M$ for any $x \in M$. $G(x) = G_1(x)\ and\ G_2(x)$ and a mapping $G: M \to \beta(x)$ and $M \subset A$ evidently. Hence $(G.I)$ is a soft set over Y. Since

$$(G_1 M_1)\ \widetilde{\bowtie}_{bck/bci-i}\ (P,A), and\ (G_2 M_2)\ \widetilde{\bowtie}_{bck/bci-i}\ (P,A).$$

It follows that $G(x) = G_1(x) \bowtie_{bck/bci-i} f(x) \times G(x) = G_2(x) \bowtie_{bck/bci-i} f(x)$ for all $x \in M$. Hence $(G_1 M_1)\ \widetilde{\times}\ (G_2 M_2) = (G,M)\ \widetilde{\bowtie}_{bck/bci-i}\ (P,A)$.

Soft BCK/BCI-EXT- Implicative Idealistic Soft BCK/BCI-EXT-Algebras

Example 4: Let $Y = \{0, e_1, e_2, e_3, e_4, e_5, e_6$ be a BCK/BCI-ext-algebra a,b,d hence a BCK/BCI-ext-algebra with the following Cayley tables.

Table 3: Caley table

*	0	e₁	e₂	e₃	e₄
0	0	O	0	0	0
e₁	e₁	0	e₁	e₂	e₃
e₂	e₂	e₁	0	e₂	e₃
e₃	e₃	e₁	e₂	0	e₃
e₄	e₄	e₂	e₃	e₃	0

Table 4: Caley table

/	O	e₁	e₂	e₃	e₄
0	0	e₁	e₂	e₃	e₄
e₁	e₁	0	e₁	e₂	e₃
e₂	e₂	e₃	0	e₃	e₄
e₃	e₃	0	e₃	0	e₅
e₄	e₄	0	e₁	e₂	0

Let (P,N) be a soft set on Y, where $A = Y$ and $F: A \to P(x)$ is a set valued function defined by $F(x) = \{0\} \cup \{y \in X|y * (y/x) \gets \{0, e_1, e_2, e_3, e_4, e_5\}$ for all $x \in A$. Then $F(0) = Y, F(e_1) = P(e_2) = \{0, e_1, e_2, e_3\}, P(e_3) = \{0, e_2, e_3, e_4\}, P(e_4) = \{0, e_3, e_4,\}$ which are all sub-algebras of Y. Hence, (P,N) is a soft extended BCK/BCI-ext-algebra over Y.

Let (Q,S) be a soft set over X, where $J = \{0, e_1, e_2, e_3, e_4\} \subset A$ and $(F,A)\ H: J \to P(x)$ be a set-valued function defined by; $Q(x) = \{y \in X|(x/y) * (x/z)\}$ for all $x, z \in J$. Then $G(0) = \{0, e_1, e_2, e_3, e_4\} \widetilde{\bowtie}_{ext} Y = P(0), Q(e_1) = \{0, e_1, e_2, e_3, e_4\} \widetilde{\bowtie}_{ext} \{0, e_1, e_2, e_3, e_4\} = P(e_1), Q(e_2) = \{e_1, e_2, e_3, e_4\} \widetilde{\bowtie}_{ext} \{0, e_1, e_2\} = P(e_2), Q(c) = \{0, e_3\} \widetilde{\bowtie}_{ext} \{0, e_2, e_3, e_4\} = P(e_3), Q(e_4) = \{0, e_2, e_3, e_4\} \widetilde{\bowtie}_{ext} \{0, e_4\} = P(e_4)$. Hence (Q,S) is a soft ideal of$(P,N))$ and also it is a soft BCK/BCI-ext-implicative ideal of $(P,N))$.

Now let us consider $J = \{e_1, e_2, e_3\}$ which is a sub-algebra of I I and let $H: J \to P(x)$ be a set-valued function defined by $H(x) = \{y \in X|y * (y/x) \in \{0, a\}$ for all $x \in J$.

Then $H(a) = \{0, e_1, e_2\} \bowtie_{bck/bci-ext-i} \{0, e_2, e_3, e_4\} = P(a), H(b) = \{0, e_3, e_4\} \bowtie_{bck/bci-ext-i} \{e_1, e_2, e_3, e_4\} = F(e_2), H(e_3) = \{e_3, e_4\} \bowtie_{bck/bci-ext-i} \{0, e_3\} = F(e_3)$. Hence (H,J) is a BCK/BCI-ext-implicative ideal (P,N).

But if $(P,N) = (Q,S) \ \tilde{\cup} \ (H,J)$ then $P(e_3) = Q(e_3) \ \tilde{\cup} \ H(e_3) = \{0, e_3, e_4\}$ which a BCK/BCI-ext-implicative ideal Y related to $P(c)$ sinc $\left.\dfrac{((e_2 * e_3) * e_2) * (0 * e_3)}{}\right/_{e_3} = e_3 \in P(e_3)$ also

$e_2 * \left(\left(e_3 * (e_3 * e_2) * \left(o * (e_3 * e_2)\right)\right)\right) = o \in P(x)$. Hence $(P,N) = (Q,S) \ \tilde{\cup} \ (H,J)$ is a soft extended BCK/BCI-ext-implicative ideal (F,A).

CONCLUSION

In this paper, the concept of a soft set is presented as a novel mathematical tool for handling uncertainties. This concept, initially proposed by Molodtsov overcomes the challenges encountered in traditional theoretical approaches. Soft sets exhibit a strong connection with fuzzy sets and rough sets. Furthermore, we introduce the notion of soft BCI-implicative ideals and BCI-implicative idealistic soft BCI-algebras and delve into their properties. Specifically, we explore the intersection, union, "AND" operation, and "OR" operation of soft BCI-implicative ideals and BCI-implicative idealistic soft BCI-algebras

REFERENCES
Molodtsov, D. (1999). Soft Sets Theory, Computer, Mathematic Application. 37:19 – 31.

Maji, P. k., Biswas, A. R., Roy, A. R. (2003). Soft Sets Theory Computer, Mathematic Application. 45:555 – 562.

Pie, D. and Miao, D.(2005). From soft set to information system, in Proceeding IEEE International comference on Granuler Computing, PP, 617-621'

Imai, Y. and Iseki K. (1966). On axiom of proportional calculi. XIV Proc., Jpn. Acad. 42, 19-22.

Zhang & Cao (2012) investigates soft BCI-implicative ideals of soft BCI-algebras

Zhu, D., & Ma, X. (2018). Brain computer ideal framework for brain research. 12, 806.

Jun Y. Bao and Jin Zou (2015), "Notes on soft BCI-implicative ideals of BCK-algebras," Journal of Intelligent & Fuzzy Systems, 29(5), 1973-1979).

Feng Feng (2015), "Soft BCK-implicative ideals in BCK-algebras," Iranian Journal of Fuzzy Systems, 12(2), 21-30)

Guoqing wei and xueying yang (2016), "soft bci-implicative ideals based on soft lattice theory," indian journal of pure and applied mathematics, 47(4), 493-509

Path Loss Modeling of FM Radio Channel (Express FM 90.3MHz) over the Urban City of Kano, Nigeria

[1]Akinsanmi Akinbolati, *[2]Muftahu Suleiman, [1]Shafiu Umar, [1]Badmus Muktar and [1]Oluwole Seyi

[1] Department of Physics, Federal University Dutsin-Ma, Nigeria
[2]Department of Electrical/Electronic Engineering, Katsina State Institute of Technology and Management.
*Corresponding Author's e-mail: madugu694@gmail.com

ABSTRACT

This study investigated the Received Signal Strength (RSS) of Express Radio (90.3 MHz) in the urban City of Kano, Nigeria, through drive test protocol. Two different routes with the base station as reference point were considered in the measurement campaigns. The RSS was measured with a signal meter while a Global Positioning System (GPS) receiver was used to determine the elevation above sea level, the geographic coordinates and the line of sight of the various data points from the base station. The measurement was done at interval of 1 km up to about 15 km for each route through. Path loss was calculated using empirical models and the results were then used to generate the variation of path loss with distance and a set of path loss models by employing the least squares algorithm, with the aim of estimating the path loss of future Radio Networks in the city. Average path loss of 108.96 dB and 114.68 dB were recorded along routes A; FM Transmitter to Madobi Road and B; FM Transmitter to Hadejia Road respectively. The results reveal that the environment of the urban city of Kano has an effect on the propagation of the radio signal. It is expected that the proposed models will be useful for designers of future wireless networks in the urban city of Kano.
Keywords: FM Radio Signal, Path Loss Model, Drive Test Protocol and Received Signal Strength

INTRODUCTION

Path loss in radio communication signifies the decline in the intensity of a signal, brought about by an array of elements such as terrain characteristics and atmospheric circumstances encountered along the transmission route or channel (Armoogum e*t al.,* 2010). This phenomenon illustrates the reduction in signal magnitude due to several factors, including the dissipation of energy as radio waves travel through open space, the reflection of surfaces, the bending of waves around obstacles, and the scattering of waves due to objects in the environment (Ayatunji *et al*, 2011). Path loss refers to the typical reduction in signal strength encountered by a transmitted Radio Frequency (RF) signal during its propagation. This reduction becomes evident as the signal covers a distance equivalent to several wavelengths and ultimately arrives at the receiver. This phenomenon is encapsulated by the formula provided by (Agbo *et al*., 2011).

$$P_L\,(dB) = \, 10\log\frac{Pt}{Pr} \hspace{4cm} (1)$$

Where P_t and P_r are the transmitted and received power respectively.

Path loss is used in the calculation of link budget of communication systems. It serves as a tool for forecasting and enhancing coverage areas in radio communication. Furthermore, it finds utility in anticipating spatial areas for TV and accommodating secondary users, as highlighted by (Faruk, 2016).

Path loss prediction encompasses the capability to accurately anticipate the attenuation of a radio signal as it traverses a communication channel. This entails the computation of the power reduction that occurs from the point of transmission, usually at a base station, to the point of reception at the receiver. Essentially, path loss prediction quantifies the power dissipation encountered by the transmitted signal during its journey between the origin and the destination (Adediji *et al.,* 2008).

In both radio wave propagation theory and equipment design, the propagation profile is a crucial variable. It is the change in a radio signal's electric field intensity across a range of distances (Akinwumi. *et al*., 2015). Ultra High Frequency (UHF) Propagation Profiles and Signal Strength Variation as well as the Received Signal Strength (RSS) from far places may be predicted with the aid of the radio wave channel (Akinbolati *et al.,* 2016).

Diverse prediction models have been formulated for wireless channels. Some of these models are established through statistical analyses of field measurements, while others are developed analytically, taking into consideration factors like diffraction effects. These models are equipped with specific parameters tailored to achieve a reasonable level of accuracy in their predictions (Akinbolati *et al.,* 2017). Path loss modeling collectively comprise a repertoire of mathematical equations and algorithms designed to prognosticate the behavior of radio signal propagation within defined regions. The need to incorporate local content in path loss modeling to enhance accuracy has been stressed by many literatures (Akinbolati. *et al.,* 2020).

According to Ranvier (2004). Path loss models have been classified as Deterministic Model, Stochastic Model and Empirical Model. Deterministic and stochastic models represent theoretical approaches to predict transmission losses

by employing mathematical and computational analyses of the geometric characteristics of the terrain between the transmitter and the receiver, along with considering the refractivity of the troposphere, as outlined by Standard path loss models, particularly empirical ones, are built upon measurements gathered from specific environments. While these models may not achieve the highest level of accuracy, they offer notable advantages in terms of time and cost efficiency. The primary focus of this study is directed towards the empirical model, given that the research exclusively relies on observations and measurements, without incorporating additional influencing factors (Buildings, Device calligraphy etc).

MATERIALS AND METHOD

This section focuses on the study area, the instruments used for field work, transmission parameters of the experimental station and statistical tools. This study was carried out in Kano City, Nigeria. Kano lies on the latitude of 12.0022°N and Longitude 8.5920°E located in the northern region of the country. Table 1 presents the list of instruments and their uses while Table 2 presents the transmission characteristics of the experimental station.

Table 1: Materials used for data collection

S/N	Instrument	Uses
1	GPS Garmin Map 78s	Used to measure the locations longitude and latitude, the elevations above sea level and distance.
2	Dipole Antenna	Used for reception of signal
3	Signal Level Meter	Used to effectively and accurately measure the analogue and digital channels of TV and satellite signal strengths
4	Coaxial Cable	To connect the antenna to the Signal Level Meter

Table 2: Transmission Parameters of the experimental station

S/N	Parameters	Values
1.	Base Station's coordinates	(Lat.11°56.737" N Long. 008°29.414 E
2.	Transmitted power	3 kW
3.	Base station's frequency (MHz)	90.3
4.	Height of transmitting antenna(m)	182.5

Method of data collection

The measurement of RSS of Express Radio (90.3) Kano was conducted in February, 2022 along two selected routes using the station as reference using drive test. Measurements were done at an interval of 1 km up to 15 km using a field strength meter and an antenna; a VHF dipole antenna mounted on a receiver pole of 1.5 m. A Global Positioning System (GPS) hand held receiver was also used to monitor the elevation, distance from the station and used to log the geographic coordinates of the data points by drive test protocol. The data was recorded in each 1 km of the 15 km (distance covered away from the station) along each route. Route A; FM Transmitter base station to Madobi Road and route B; FM Transmitter base station to Hadejia Road respectively.

Empirical Tools and Data Analysis

The transmitted power and measured RSS values are in kW and dBμV respectively. Equation (2) was used to convert transmitted power to dBm. Equation (3) was used to convert RSS in dBμV to P_r (dBm) while equation (4) was used to calculate the difference between the two, which is the path loss in dBm.

$$P_t (dBm) = 10 \log_{10} (P_t (kW) * 1000) + 30 \qquad (2)$$
$$P_r (dBm) = P_r (dB\mu V) - 107 \qquad (3)$$
$$L_{dBm} = P_t(dBm) - P_r(dBm) + G_t (dBm) \qquad (4)$$

where G_t (dBm) is the transmitting antenna gain assumed to be equals to unity

RESULTS AND DISCUSSION

Figures 1and 2 present the path loss variation with distance for routes A and B respectively.
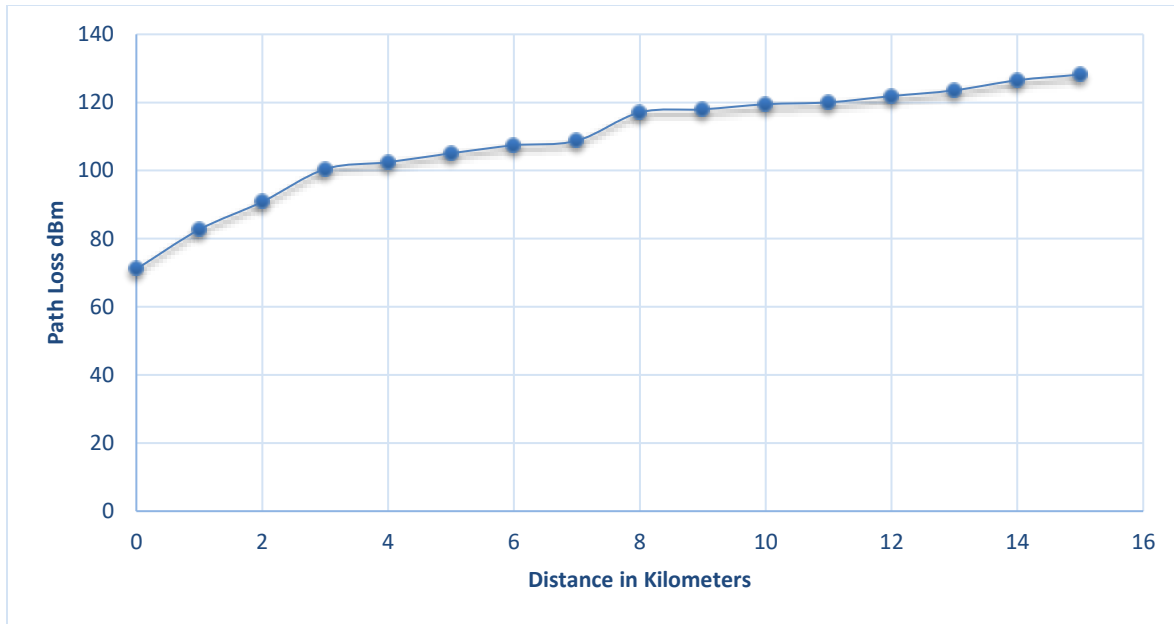
Figure 1: Path Loss Variation with distance (Route A) from base station to Madobi road Kano.
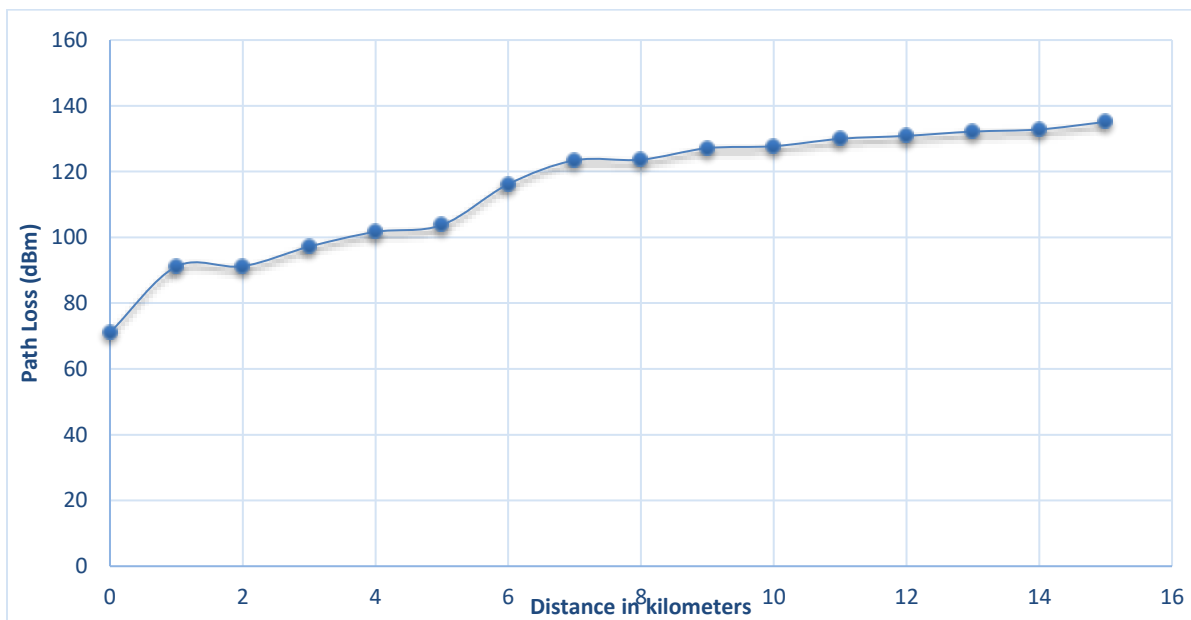
Figure 2: Path Loss Variation with distance (Route B) from base station to Hadejia road Kano.

For the first route; base station to Madobi road Kano. The average path loss of 108.96 dBM was recorded while average path loss of 114.68 dBM was recorded for the second route; base station to Hadejia road Kano. It was observed that path loss increases as the LOS separation distance from the base station increases for both routes. The path losses for the two routes, however, did not significantly differ from one another. Path loss was shown to rise with increasing LOS away from the base station. For the first and second routes, regression analysis was done between the Path Loss (PL), Line of Sight (LOS), and Elevation (ELV) from Base Station. The greater the elevation of locations for the research area, the higher the RSS value. In comparison to the second path, locations along the first route will thus receive better signals. The overall findings of this research will improve FM Radio transmission and reception within Kano city, Nigeria.

The implication of this is reduction in the signal strength and quality of the FM signal received by radio audience of the channel in Kano especially at distances of 8 km and above from the base station. The station is advised to increase the transmitted output power of their transmitter to increase coverage area. In order to further strengthen the findings

of this study, simple regression analysis was carried out on the data using Path Loss P_L as the dependent variable while LOS (km) and the Elevation (m) as the independent variables. Path loss model (s) that incorporate these two parameters were generated. They are as presented in equations (5) and (6) for the two routes A and B respectively. Equation (7) is the generalized model proposed for use in the urban city of Kano over FM Radio channel being the average for the two routes.

$$P_{LA(dBm)}= \qquad -528.605 + 4.12323LOS + 1.23477 \; ELV \qquad\qquad (5)$$
$$P_{LB(dBm)}= \qquad -347.875 + 6.6889LOS + 0.867907 \; ELV \qquad\qquad (6)$$
$$P_{L(dBm)} = \qquad -438.24 + 5.406LOS + 1.0515 \; ELV \qquad\qquad (7)$$

Where $P_{LA(dBm)}$ and $P_{LB(dBm)}$ are generated path loss model for routes A and B respectively. $P_{L(dBm)}$, is the mean path loss for the two routes which is recommended for use over the study location and channel. ELV (m) and LOS (km) are the elevation of data location and line of sight distance from the base station respectively.

CONCLUSION

This study has successfully investigated the path loss associated with FM Radio channel in Kano City Nigeria. The path loss profiles and quantitative values of the two routes considered were well presented. The Path loss models that incorporated the elevation of data location and line of sight distance from the base station were developed and recommended for use over the study location and channel. The overall findings of this research will improve FM Radio transmission and reception within Kano city, Nigeria.

REFERENCES

Adediji, A. T., & Ajewole, M. (2008). Vertical Profile of Radio Refractivity Gradient in Akure South-West Nigeria. *Progress In Electromagnetics Research C*, *4*, 157-168.

Agbo, G. A. (2011). Tropospheric refractivity dependence on atmospheric weather conditions in Jos-Nigeria. *Journal of Basic Physical Research*, *2*(2), 2-6,

Akinbolati, A., Adediji,A. T. and Ojo, J. S (2016). "Precipitation Effect on the Coverage Areas of Terrestrial UHF Television Stations in Ondo State, Nigeria", International Journal of Engineering and Technology, 4(9), 524 – 535.

Ajewole, M. O., Akinbolati, A., Adediji, A. T., & Ojo, J. S. (2014). Precipitation effect on the coverage areas of terrestrial UHF television stations in Ondo state, Nigeria. *International Journal of Engineering and Technology*, *4*(9), 524-535.

Akinbolati, A., & Ajewole, M. O. (2020). Effect of some radio climatic factors on digital terrestrial television signal in a Sahel savannah city of Nigeria. *FUDMA Journal of Sciences*, *4*(2), 111-118.

Akinbolati, A., Oludare, A. M., Titus, A. A., & Sunday, O. J. (2017). The influences of meteorological parameters on digital terrestrial television (DTT) signal in the tropics. *International Journal of Digital Information and Wireless Communications (IJDIWC)*, *7*(3), 161-172.

Akinwumi, S. A., Omotosho, T. V., Willoughby, A. A., Mandeep, J. S., & Abdullah, M. (2015, August). Seasonal variation of surface radio refractivity and water vapour density for 48 stations in Nigeria. In *2015 International Conference on Space Science and Communication (IconSpace)* (pp. 106-110). IEEE.

Armoogum, V. K. M. S., Soyjaudah, K. M. S., Mohamudally, N., & Fogarty, T. (2010). *Propagation models and their applications in digital television broadcast network design and implementation*. IntechOpen.

Ayantunji, B. G., Okeke, P. N., & Urama, J. O. (2011). Diurnal and seasonal variation of surface refractivity over Nigeria. *Progress In Electromagnetics Research B*, *30*, 201-222.

Faruk. (2016), "Climate Change: Fact, Fiction and Faction", An Inaugural Lecture delivered at Federal University Dutsin- Ma, Katsina State, p9-25.

Investigation of Radio Refractivity and its Effects on Radio Wave Propagation over Abuja, using Forty-One Years Atmospheric Data

*[1]Usman, S. L., [2]Ikechiamaka, F. N. and [2]Akinbolati, A.,

[1]Department of Physics, Nigerian Defence Academy, Kaduna, Nigeria.
[2]Department of Physics, Federal University Dutsin-Ma, Nigeria.
*Corresponding Author's E-mail; usmansakinat885@gmail.com

ABSTRACT

Secondary radio climatic factors play a significant role in shaping wireless communication system design and can have detrimental effects on signal quality and coverage. This study focuses on assessing surface radio refractivity, refractivity gradient, and their implications for wireless communication in the Federal Capital Territory (FCT) of Abuja, Nigeria. Secondary Data of meteorological parameters spanning 41 years (1980-2020) were retrieved from the European Center for Medium-Range Weather Forecasts (ECMRF). Data analysis involved computing the radio refractivity for surface (12 m), 100 m and 250 m Above Ground Levels (AGL) using the latest International Telecommunication Union Radio Study Group (ITU-R, 2019-2021) model. Seasonal variations were also investigated with findings showing higher values during wet compared to dry season months. Result reveals that radio refractivity decreases with increase in height (AGL). The mean values of 356.9533N-units, 344.966N-units, and 332.3189N-units were obtained for the surface, 100m and 250m respectively. The overall findings will be useful for terrestrial radio link over the study area.

Keywords: Terrestrial radio links; Meteorological variable; Radio refractivity.

INTRODUCTION

Radio waves constitute a form of electromagnetic radiation found at the longer wavelength end of the electromagnetic spectrum. They encompass frequencies ranging from 3 kHz to as high as 300 GHz. These waves are utilized in various applications, including frequency modulated (FM) radio in the megahertz (MHz) range and amplitude modulated (AM) radio, commonly functioning within the kilohertz (kHz) range. The behavior of electromagnetic waves, especially within the troposphere, the lower atmospheric layer where meteorological phenomena occur, is substantially influenced by the atmospheric composition (Adediji and Adewole 2008). The troposphere's dynamic nature, characterized by fluctuations in temperature, pressure, and relative humidity, plays a pivotal role in wave propagation. Variations in these factors lead to changes in the refractive index of air within this layer, which in turn affects the velocity of radio waves. (Isaac-Onerime et al., 2019). Consequently, the non-uniformity of the atmosphere causes radio waves to experience curvatures during transmission, resulting in signal distortions and potential interference. A key determinant of radio wave behavior is the refractive index denoted by 'n,' a function of refractivity 'N.' This refractive index causes the bending of propagation paths, leading to disparate arrival times for identical signals traversing different routes (O.O. Ajileye et al 2016). Such bending is responsible for the phenomenon of sub-refraction, super-refraction, and ducting in radio wave propagation. Central to atmospheric behavior is the surface radio refractivity, referred to as 'N.' Profiles of N values offer insights into propagation characteristics, aiding in the prediction of signal paths and aiding in the construction of communication stations for varying radio frequencies (Naveen et al., 2011). The accurate understanding of the surface radio refractivity, particularly when it relates to the atmosphere's radio refractivity, is crucial for radio engineers. This understanding facilitates precise forecasts of electromagnetic radio wave signals and informs the design of communication stations for different frequency ranges. Consequently, the utilization of meteorological data collected over years, specifically between 1980 and 2020, supports the examination of the surface refractivity within Abuja.

Several research works have been carried out in different regions of Nigeria on Radio Refractivity. In this review of related literature, studies on the radio refractivity by different researchers were reviewed.

Adediji and Adewole (2008) studied the vertical refractivity gradient in Akure, Nigeria, by measuring atmospheric variables using integrated sensor suits (ISS) at various heights above ground level. The measurements were made every 30 minutes using wireless weather stations positioned at different heights. The study showed that propagation conditions varied throughout the year, with sub-refraction prevalent between January and July, and super-refraction and ducting occurring mostly between August and December. Further research using long-term data and additional locations in the South Local Government Area of Ondo could provide more insights.

Ayanntuniji et al. (2011) conducted a study on the seasonal and diurnal variations of surface radio refractivity in Akure, Nsukka, Minna, Sokoto, and Jos, Nigeria. The results revealed higher surface refractivity values during the

wet season compared to the dry season. Additionally, it was observed that surface radio refractivity increases from the arid regions in the north to the southern parts of Nigeria.

Emetere et al. (2015) developed a model for analyzing radio refractivity in selected locations in the north-central region of Nigeria. A tropical model was derived and tested using data from the National Oceanic and Atmospheric Agency (NOAA) Climatology Center (1973-2012) for six stations within the North-Central part of Nigeria. The study emphasized the need to reassess the existing 1T0 model due to climate change, as the tropical model detected tropospheric perturbations caused by the extensive influx of aerosols.

Akinwunmi et al. (2015) conducted a study on the seasonal variation of surface radio refractivity and water vapor density across 48 stations in Nigeria. Meteorological data from NOAA covering a span of 39 years (1973-2012) were used for analysis. The results demonstrated that surface refractivity and water vapor density generally exhibited higher values during the rainy season compared to the dry season in all the stations studied. Additionally, the study revealed that the values of surface refractivity and water vapor density varied across the different regions of Nigeria, ranging from approximately 263 N-units and 3 g/cm³ in the northeastern parts of the country to about 393 N-units and 23 g/m³ in the coastal areas of Southwest Nigeria. The research emphasized the importance of considering the variability of surface radio refractivity and water vapor pressure when designing terrestrial radio links throughout Nigeria.

Adediji et al. (2017) conducted a study on the variability of microwave radio refractivity and field strength across seven cities in Nigeria. They utilized two years of data from the Tropospheric Data Acquisition Network (TRODAN) in Ayingba, Nigeria. The results showed that surface radio refractivity was higher during the rainy season compared to the dry season and was also higher in coastal areas than in other locations.

Theoritical Framework

Source of Data

Monthly and yearly summaries of temperature, pressure, and humidity data for Abuja were obtained from microwave links and weather stations affiliated with the European Center for Medium-Range Weather Forecasts (ECMWF-ERA 5). It is important to note that certain limitations in the systems configurations were considered due to their specific implementation to meet particular business requirements. These observatories or data sites, a comprehensive suite of weather measurement instruments is available, encompassing rain gauges for precipitation measurement, thermometers for temperature assessment, barometers for air pressure evaluation, and hygrometers for relative humidity measurement. ECMRF-ERA5 collected data throughout the year. The secondary data utilized in this study consists of raw yearly and monthly temperature, atmospheric pressure, and relative humidity data collected over a period of 41 years (1980-2020) for the city of Abuja. The data was obtained from the European Centre for Medium Range Weather Forecast (ECMRF - ERA 5), a renowned institution known for its high-resolution satellite data.

The ECMRF-ERA 5 satellite data has been widely used in various research studies, and its results have been widely accepted and acknowledged. For this research, the secondary data includes weather parameters such as temperature, relative humidity, and atmospheric pressure measured at three different heights: surface (12m), 100m, and 250m above ground level. This involves arranging the raw data obtained in a meaningful order to make it easier to understand analysis and visualize.

The data were calculated and sorted out accordingly based on months, yearly and seasonal. The secondary radio climatic factors were computed based on the obtained weather parameters using (ITU-R 2019) equations. The obtained values of the radio climatic factors were compared with acceptable range to determine the possible degree of effects on radio propagation.

Computation of Radio Refractivity

The distinction between the speed of radio energy in a vacuum and its speed in a specific medium is referred to as the radio refractive index. This index, denoted as 'n,' decreases from 1.0003 at the near-Earth troposphere's surface to a value of unity (n = 1.0) at the uppermost layer of the atmosphere. Alternatively, the refractive index can be expressed more conveniently using the dimensionless parameter of refractivity, 'N.' This parameter quantifies the deviation of the refractive index from unity in terms of parts per million (Bean B.R. and Dutton E. J. 1996).

$$N = (n - 1) \times 10^6 \qquad\qquad (1)$$

The radio refractivity N can be expressed in terms of meteorological variables as:

$$N = \frac{77.6}{T}\left(P + 4810\frac{e}{T}\right)(N - units) \qquad\qquad (2)$$

Where N depends on pressure P (hPa), temperature T (K) and water vapour pressure e (hPa) (Ayantuji et al., 2011; Adediji and Ajewole, 2008). Meteorological activity in the atmosphere is dynamic in nature which often leads to the variation of its refractive index. As the height of the atmosphere increases, the refractive index changes resulting in a refractive attenuation effect on the electromagnetic signal being propagated. There is a standard procedure for finding

the refractive index variation with height, which ITU-R provides (Afullo et al., 1999; ITU-R , Rec. P.453, 2019).The refractivity gradient, on the other hand, is a measure of how the refractive index varies with increasing height (Adelakun et al., 2020, Freeman, 2007).This is given as:

$$\frac{dN}{dh} = 77.6\frac{1}{T}\frac{dP}{dh} - \left(\frac{77.6}{T^2} + \frac{746512e}{T^3}\right)\frac{dT}{dh} + \frac{373256}{T^2}\frac{de}{dh} \tag{3}$$

Where e, is the water vapor pressure (hPa) and h, is the height (m).

But the water vapor pressure *e* cannot be acquired directly, hence using its relationship with relative humidity (%RH), we can have:

$$e = \frac{H}{100}e_s \tag{4}$$

where e_s is the saturated vapor pressure at a particular temperature t (°C), and it is defined as:

$$e_s = EF.a.exp\left[\frac{\left(b-\frac{t}{d}\right)t}{t+c}\right] \tag{5}$$

and:

$$EF = 1 + 10^{-4}[7.2 + P.(0.0320 + 5.9 \times 10^{-6}t^2)] \tag{6}$$

where:

   t, is temperature(^oC)
   P, is total atmospheric pressure(hPa)
   H, is relative humidity (%),
   es is saturation vapor pressure(hPa) at the temp t(^oC)
   a=6.1121
   b=18.678
   c=257.14
   d=234.5

$$e_s = EF \times 6.1121 \times exp\left(\frac{\left(18.678 - \frac{t}{234.5}\right) \times t}{(t+257.14)}\right) \tag{7}$$

and:

$$EF_{water} = 1 + 10^{-4}[7.2 + P \times (0.0320 + 5.9 \times 10^{-6} \times t^2)] \tag{8}$$

Equations (7) was used to calculate the saturated vapour pressure e_s, at a given temperature t (°C), with the substitution of (8). Equations (4) and (2) were used to calculate the water vapour pressure and the radio refractivity values respectively.

RESULTS AND DISCUSSIONS

Analyzing the monthly and yearly mean variations in radio refractivity (Ns, N100, and N250) changes across the city of Abuja, from 1980 to 2020 resulted in the findings illustrated in Figures 1 to 6 respectively.
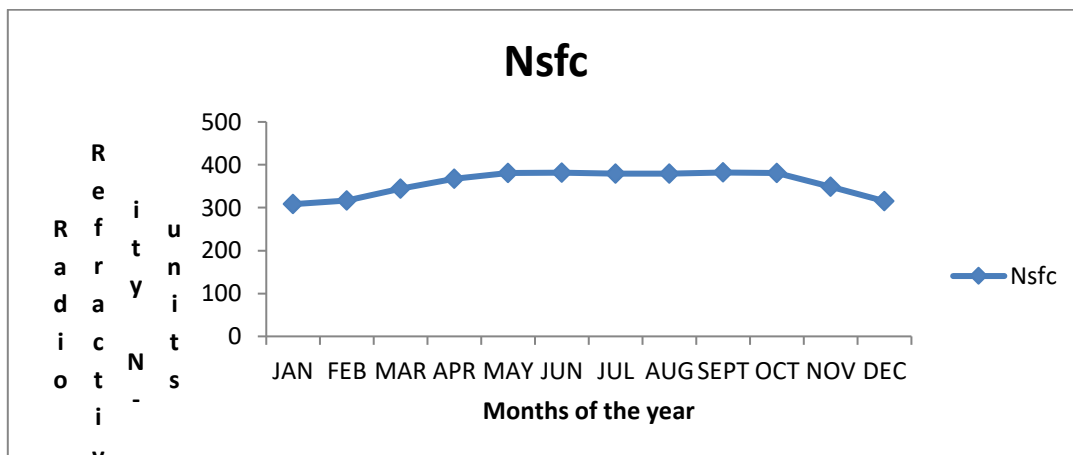
Figure 1: Monthly Average Variation of Radio Refractivity over Abuja in the year (1980-2020).

Fig 1 shows surface (12m) radio refractivity (N) values showing a general increasing trend from January to September, with a peak in September (382.0630N-units). From October to December, the values decrease, reaching the lowest

point in December (315.3370N-units). This shows a seasonal variation in surface refractivity, with higher values in the middle of the year and lower values towards the end of the year.
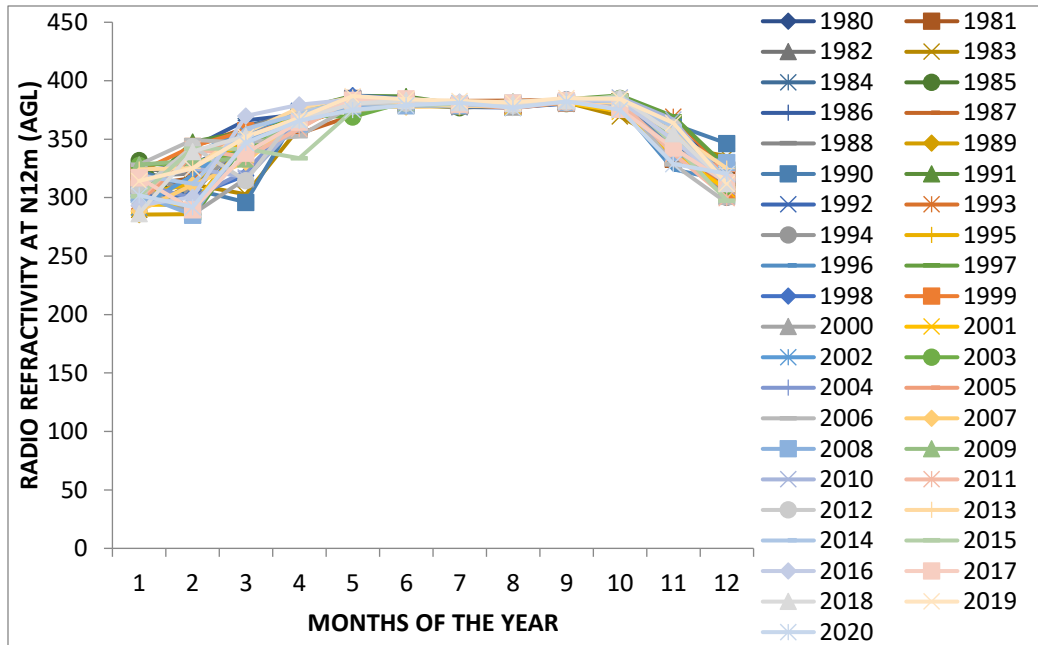
Figure 2: Yearly Variation of Vertical Radio Refractivity over Abuja in the year (1980-2020).

Fig.2 shows yearly variations in vertical radio refractivity (N) at 12m of height in Abuja from 1980 to 2020, with 41 years of data. It gives an understanding of how radio wave behaves in the atmosphere, especially for long-range and high-frequency transmissions. It reveals that vertical radio refractivity experiences annual fluctuations, likely due to changing in the atmospheric conditions, and suggests recurring patterns, possibly linked to seasonal changes, like shifts between dry and wet seasons. To better comprehend these variations, it's essential to investigate correlations with meteorological factors such as temperature, humidity, and atmospheric pressure, as these fluctuations can significantly impact radio communication systems, especially signal propagation over long distances. Ultimately, comprehending the patterns and trends in refractivity can play a vital role in optimizing radio networks and enhancing the reliability of radio signals.

Figure 3: Monthly Average Variation of Radio Refractivity over Abuja in the year (1980-2020).

Fig3 represents the monthly average values of radio refractivity (N) at 100m for the city of Abuja over a 41-year period, from 1980 to 2020. The values are provided for each month of the year, from January to December. The graph shows clear seasonal variations in N_100 values over Abuja. Lowest values typically occur in January and February (300.0110 and 307.5952)N-units. N_100 values start to rise from March (332.8510N-units) and reach their peak around June and July (367.8774 and365.7013)N-units. After July, there's a gradual decline in N_100 values through the end of the year. The N_100 values exhibit an annual cycle, indicating that these variations are influenced by the changing in atmospheric conditions and typical weather patterns for the region. There's a noticeable decrease in N_100 values in November and December (338.2561 and 306.8747)N-units. These decreases linked to specific meteorological events, weather patterns, or atmospheric conditions during those months.
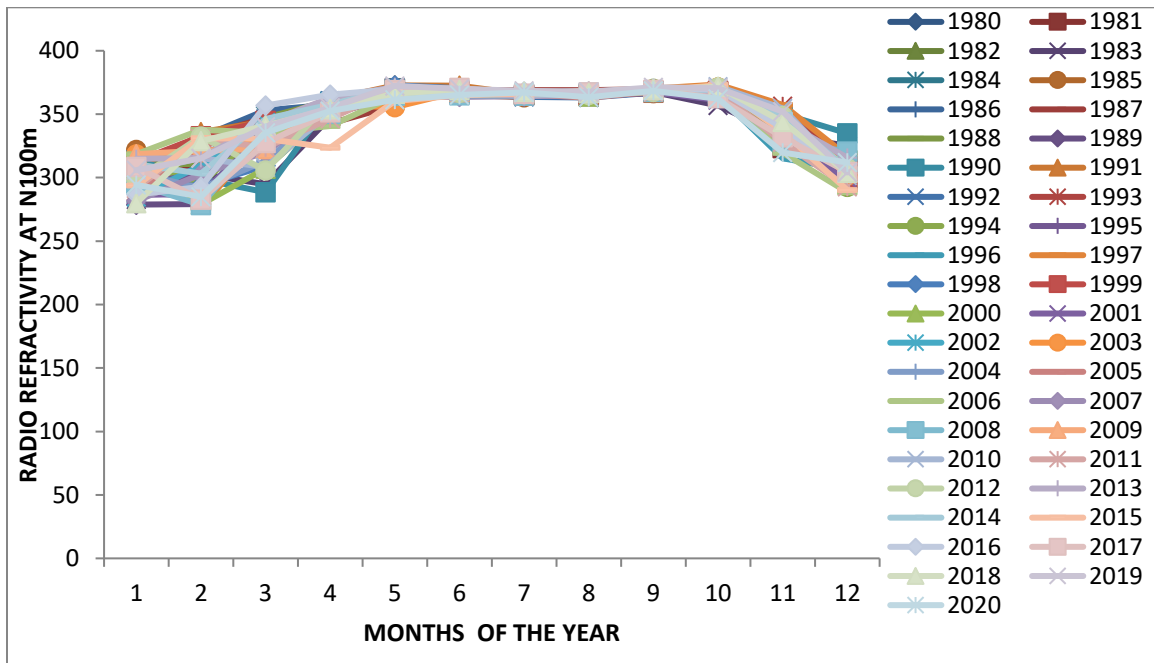
Figure 4: Yearly Variation of Vertical Radio Refractivity over Abuja in the year (1980-2020).

Fig4 shows significant yearly fluctuations in the vertical radio refractivity at a height of 100 meters over Abuja from 1980 to 2020. There is no clear linear trend over this period, indicating that the refractivity values do not consistently increase or decrease. However, there are noticeable periods of higher and lower refractivity, such as in the mid-1980s and the mid-1990s, suggesting the possibility of seasonal patterns or weather-related influences. The wide range of values indicates a degree of variability, which could be attributed to factors like seasonal variations, changing weather conditions, or meteorological influences affecting radio refractivity at this specific height. Further analysis, including statistical methods and correlation studies with meteorological variables, may help uncover underlying patterns and factors influencing these variations. Understanding these fluctuations is crucial for assessing the behavior of radio refractivity in Abuja, which is essential for radio communication and related applications in the region.
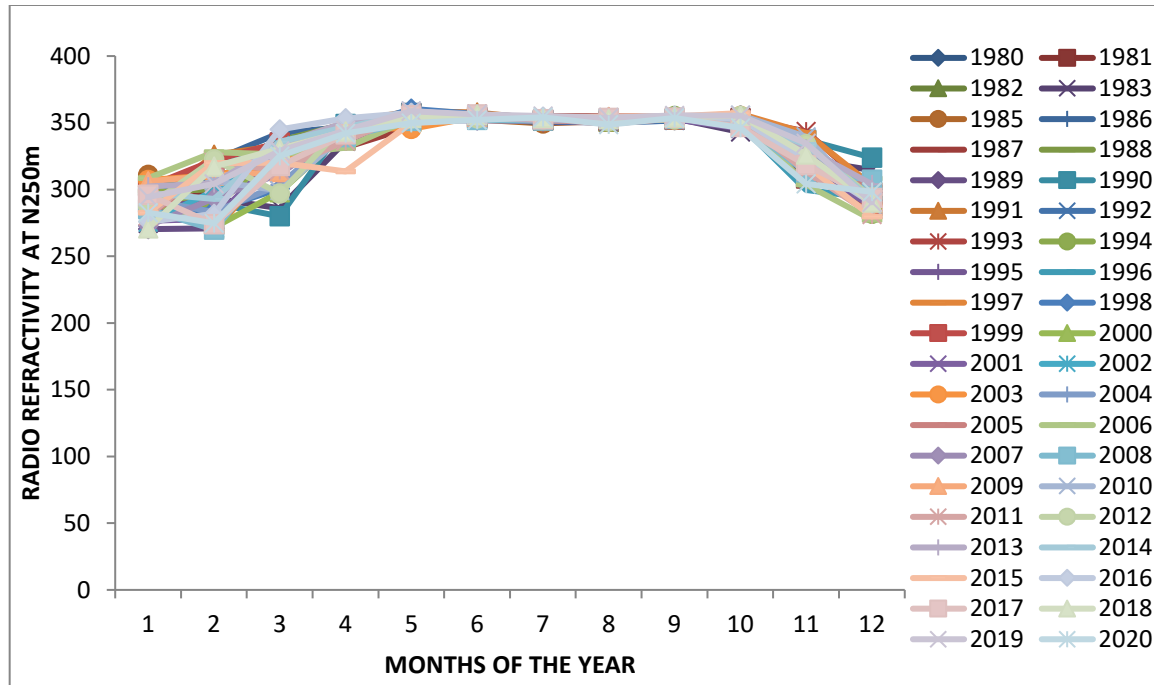
Figure 3: Yearly Variation of Vertical Radio Refractivity over Abuja at N250m in the year (1980-2020).

Analyzing the annual changes in vertical radio refractivity at a 250-meter altitude over Abuja from 1980 to 2020 reveals significant variations in atmospheric conditions, which can affect radio communication and signal propagation. The data shows a wide range of refractivity values over the 41-year period, from approximately 268N-units to over 357N-units. This indicates substantial changes in the atmosphere over the years. Year-to-year fluctuations are apparent, with some years experiencing significant increases or decreases in refractivity. For instance, there was a sharp drop in refractivity in 1983 (around 274.50N-units), followed by a substantial increase in 1985 (around 310.90N-units). Although there are yearly fluctuations, it's crucial to identify any long-term trends. Some years exhibit extreme refractivity values, such as 1983 (around 274.50N-units) and 2017 (around 357.15N-units), which could be attributed to exceptional weather or atmospheric conditions. Certain periods show relatively stable refractivity values, while others display more significant variations. Recognizing periods of stability or consistency can be valuable for planning radio communication. High variability in vertical radio refractivity can have a significant impact on radio signal propagation. Years with lower refractivity may lead to reduced radio communication range, while higher refractivity could enhance signal propagation. Radio operators and planners should take these variations into account when designing and optimizing communication networks.
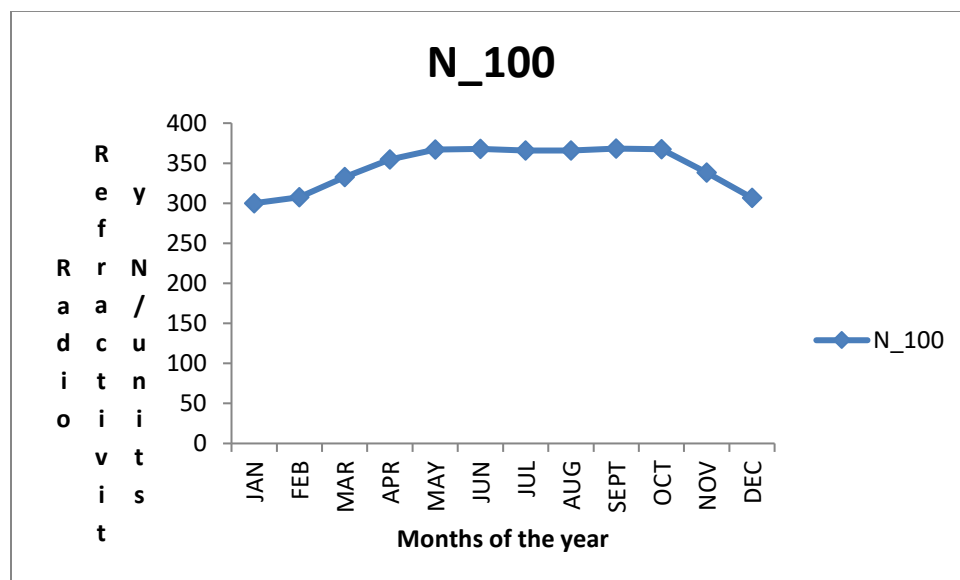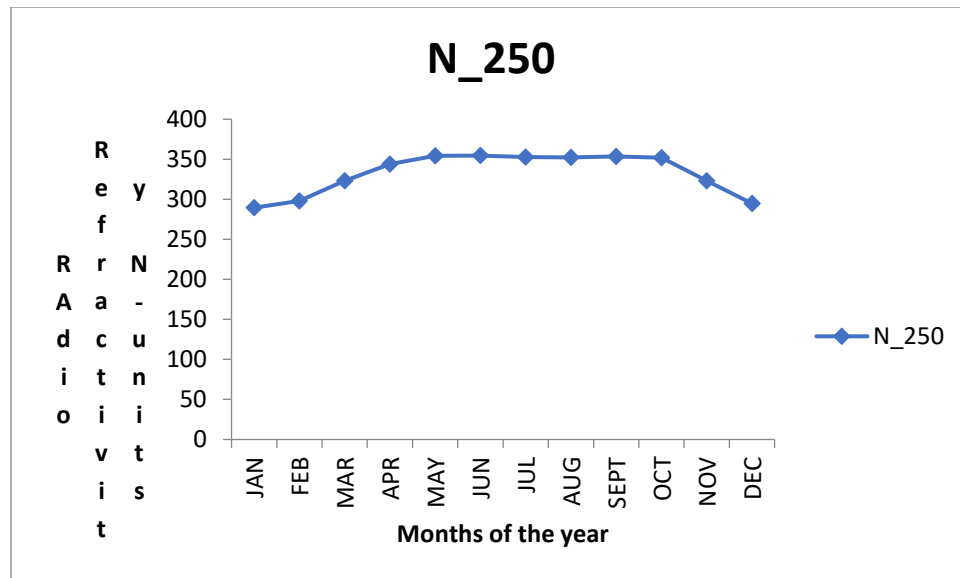
Figure 5: Monthly Average Variation of Radio Refractivity over Abuja in the year (1980-2020).

Fig5 represents the monthly average values of surface radio refractivity at N_250m (N_250) for the city of Abuja over a 41-year period, from 1980 to 2020. The values are provided for each month of the year, from January to December. Lowest values typically occur in January and February. N_250 values start to rise from March and reach their peak around May and June. After June, there's a gradual decline in N_250 values through the end of the year. The N_250 values exhibit a clear annual cycle, indicating that these variations are influenced by the changing atmospheric conditions and typical weather patterns for the region. There's a noticeable decrease in N_250 values in November and December. These decreases may be linked to specific meteorological events, weather patterns, or atmospheric conditions during those months. The highest N_250 values from March to June suggest that this period corresponds to relatively dry and stable atmospheric conditions in Abuja, which are conducive to higher radio refractivity at 250 meters above ground level. The decline in N_250 values from July through December is likely due to the rainy season, which often brings increased humidity and precipitation. These conditions can lower radio refractivity as the atmosphere's electrical properties change.

CONCLUSION
In conclusion, this research has provided valuable insights into the behavior of radio refractivity in the lower atmospheric layer of Abuja Federal Capital of Nigeria. The analysis focused on Abuja spanning the years 1980 to 2020. The consistent patterns observed in the monthly average refractivity changes reflect the influence of seasonal variations and atmospheric conditions on radio wave propagation. Overall, the research underscores the intricate relationship between atmospheric conditions and surface radio refractivity. This relationship has far-reaching implications for radio wave propagation and communication systems. The findings contribute to a deeper comprehension of how atmospheric factors influence radio signals' behavior and propagation paths, thus aiding in the optimization of communication networks and signal reliability under varying meteorological conditions. The mean values of 356.9533N-units, 344.966N-units, and 332.3189N-units were obtained for the surface (12m), 100m and 250m respectively. The overall findings will be useful for improving the design of terrestrial radio link over the study area.

REFERENCES
Adediji A.T and Ajewole M.O (2008) Vertical profile of radio refractivity gradient in Akure south-west nigeria . progress in Electromagnet Research C, vol.4,157-168.

Afullo,T. J.,T. Motsoela, and D. F. Molotsi,2019. "Refractivity Gradient and K-factor in Botswana, Radio Africa.

Ayantunji B. G., Okeke P.N., Urama J. O. and Najib Y.(2011). A semi-empirical model for vertical extrapolation of surface refractivity over Nigeria.The African Review of Physics, 6:0014.

Bean B. R. and Dutton E. J. (1996). "Radio Meteorological" Us Department of Commerce National Bureau of Standard Monograph 92.

ITUR (2019) .The radio refractivity index its formula and refractivity data recommendation ITU-R,453-456.

Naveen, K.C., Trivedi, DK, Roopam, G., (2011). The impact of k-factor on wireless link in Indian semi desert terrain International Journal of Advanced Networking and Applications.

Oyedum O.D., igwe K.C., Echie J.O. and Moses A.S., (2010). Reduce –to-sea-level refractivity in Minna, central Nigeria. Natural and Applied Science Jounal (2).

Steady MHD Free Convection Flow with Temperature Dependent Viscosity, Viscous Dissipation and Joule Heating in a Vertical Porous Channel

*Yusuf A. B. and Abdullahi F.

Department of Mathematics, Federal University Dutsin-ma, Katsina State, Nigeria.
*Corresponding author's email: ayusuf@fudutsinma.edu.ng Phone: +2349130824575,

ABSTRACT

The present work investigate steady MHD free convection flow with temperature dependent viscosity, viscous dissipation and Joule heating in a vertical porous channel. Due to consideration of these parameters, the governing flow equations which represent the flow formation are highly nonlinear coupled whose solutions cannot be obtained easily through analytical method. This therefore called the use of Adomian decomposition method of solution (ADM). The ADM is a powerful tool capable of decomposing the coupled differential equations into series form and the series solutions are then simulated via computer algebra package of MAPLE where results under varying situations are presented on graphs with conclusions drawn. Some of the finding reveled that decrease in viscosity causes increase in velocity and decrease in the temperature of the fluid. This philosophy is due to increase in cohesive force between the fluid molecules. Furthermore, it was found that rising Joule heating causes increase in both the velocity and temperature of the fluid. These trends are as a result of the decrease of thermal conduction of the fluid, which in return increase the kinematic viscosity of the fluid. This investigation may have numerous importance in the aspect of crude oil extraction as the components of crude oil are extracted under varying temperatures.

Keywords: Temperature-dependent viscosity, viscous dissipation, Joule heating, MHD fluid, porous channel and Adomian decomposition method

INTRODUCTION

Magnetohydrodynamic (MHD) is the study of the magnetic properties of electrically conducting fluids such as plasma, liquid metals and electrolytes. This phenomenon is based on the concept that when a magnetic field passes through a fluid, it induces an electric current in that fluid. This electric current polarized the fluid, which in return changes the magnetic field and reciprocal force that changes the magnetic is called the Lorent force. Alfven (1942) was the first person who studied MHD where he described the class of MHD waves called Alfven waves. The study of Sinha (2015) identified some uses and applications of magnetic and electromagnetic field therapies which are used to relief pain, to accelerate fracture healing in bones, to control blood flow particularly during surgery and it is also being used to treat some various health disorder in human arthritis. Kumar and Singh (2015) revealed that, there is significant drop in velocity and temperature with rising the magnetic parameter in the transient MHD free convective flow through a semi-infinite vertical plate.

Joule heating effect and viscous dissipation on MHD flow has application in electric heating devices like electric heater and boiler electric iron, bread toaster and other high temperature devices. Altunkaya *et al.* (2017) studied the role of viscous dissipation on mixed convection flow in a vertical micro channel with asymmetric heat fluxed. The found that increasing rarefaction parameter decreases the effect of viscous dissipation on the Nusselt number. Joule heating and viscous dissipation on effects of MHD flow over a stretching porous sheet subjected to the power law heat flux in the presence of heat sources was studied by Jaber (2016). He concluded that increasing the magnetic parameter lead to the increases the temperature and the local Nusselt number and decreasing the velocity and the local sin friction, whereas increasing in the Joule heating parameter increase the temperature profile and local Nusselt number and its does not affect the skin friction. Mohammad and Nazma (2021) investigated free convection flow with Joule heating, heating generation and viscous dissipation along a vertical wavy surface. Their studied show that, the temperature within the boundary layer increase for increasing value of Joule heating parameter.

Temperature dependent viscosity was firstly studied by Reynold (1883) where he stated that, the viscosity of liquid decreases exponentially with increase in temperature. Borah and Hazaria (2013) studied the effects of variable viscosity, thermal conductivity and magnetic field on free convective flow through porous medium with constant suction and heat flux, where their work revealed that, temperature decreases with increase in both viscosity and thermal conductivity. Some other research studies such as Singh and Shwefa (2013), Vajravelu *et al.* (2013) and Isaac and Anselm (2014) show that, the velocity profiles decrease with increasing viscosity, while the temperature profiles increase with increase in viscosity.

This investigation is motivated by the study of Ajibade *et al.* (2021) while neglecting the effect of thermal radiation in their model. In this work, the effects of Joule heating and MHD flow are now added to investigate the flow behavior. Under this condition, the equations modelling our problem are highly nonlinear coupled differential equations which

are difficult to solve using analytical means and we therefore resort to Adomian decomposition method of solution (ADM) because of its capability to handle equations of this nature.

Mathematical Formulation of the Problem

Figure 1 below shows the flow configuration of the problem. It consists of a vertical channel formed by two infinite parallel vertical porous plate stationed h distance apart. It is assumed that a magnetic fluid of strength B_0 flow in the channel under the influence of gravity g. It is also assumed that all the properties of the fluid are constant except for the viscosity which is temperature dependent. The x-axis is taken along the channel in the vertically upward direction, which is the direction of the flow while the y-axis is taken normal to it. The temperature of the plate kept at $y = 0$ is raised to T_w and thereafter remained constant while the other plate at $y = h$ is fixed and maintained at temperature T_0.
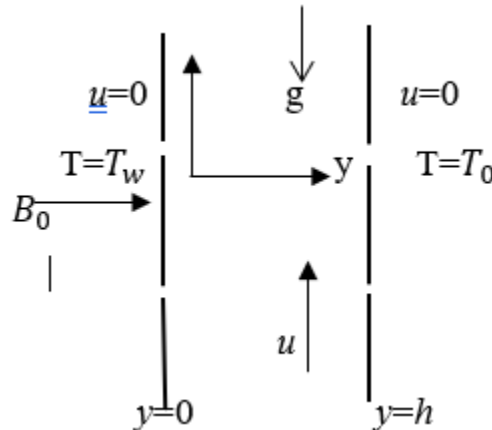
Figure 1: Diagram of the problem

Where y is the dimensionless length, u is the dimensionless velocity, B_0 is the magnetic strength, h is the dimensional channel width, g is the force of gravity, T_w is the wall temperature and the T_0 is the ambient temperature.

Under these assumptions, the appropriate equations representing the flow are thus:

$$V_0 \frac{du'}{dy'} - \frac{1}{\rho} \frac{d}{dy'} \left(\mu \frac{du'}{dy'} \right) - g\beta \left(T' - T_0 \right) - \frac{\mu}{\rho} \sigma B_0^2 u' = 0 \tag{1}$$

$$V_0 \frac{dT'}{dy'} - \frac{k}{\rho Cp} \frac{d^2 T'}{dy'^2} - \frac{\mu}{\rho Cp} \left(\frac{du'}{dy'} \right)^2 - \frac{\delta B_0^2 u'^2}{\rho Cp} = 0 \tag{2}$$

With the boundary conditions for the momentum and energy fields as:

$$u' = 0, T' = T_w \qquad at \ y' = 0 \tag{3}$$
$$u' = 0, T' = T_0 \qquad at \ y' = h \tag{4}$$

The varying viscosity (μ) is assumed to adopt the one given by Carey and Mollendorf (1978) which has the form:

$$\mu = \mu_0 \left(1 - \lambda \left(\frac{T' - T_0}{T_w - T_0} \right) \right) \text{ for } \lambda \in (0,1) \tag{5}$$

Equation (1) represents the momentum equation with the first, second, third and fourth terms representing the fluid velocity due to suction, variable viscosity, force of gravity and magnetic effect accordingly. Also equation (2) represents energy equation having first, second, third and fourth terms donating heat due to fluid suction, thermal conduction, viscous dissipation and Joule heating effect respectively. The meaning of the physical quantities through equations (1-5) are as follow: V_0 is the dimensional suction velocity, μ is the dynamic fluid viscosity, ρ is the parameter of the fluid density, σ Stefan-Boltzman constant, u' is dimensional velocity, T' is the dimensional temperature, k is the thermal conductivity, and C_p is the temperature difference parameter. λ is the viscosity variation parameter and μ_0 is the initial fluid viscosity.

MATERIALS AND METHODS

Non-dimensionalization of the Problem

The quantities involved in equations (1 - 5) are all in dimensional form and these equations need to be changed to dimensionless form. To achieve this, we use the quantities adopted in Ajibade *et al. (*2021) which are:

$$u = \frac{u'}{g\beta(T'-T_0)h^2}, y = \frac{y'}{h} , \ \theta(y) = \frac{T'-T_0}{T_w-T_0}, \tag{6}$$

By using equations (5) and (6) in equations (1) and (2), the following equations are achieved:

$$u'' = = c(1 + \lambda\theta)u' + \lambda(1 + \lambda\theta)\theta'u' - (\theta(1 + \lambda\theta)) - Mu \tag{7}$$

$$\theta'' = c\theta' - Bru'^2 - Ju^2 \tag{8}$$

Similarly using equation (6) in equations (4) and (5), the boundary conditions become:

$$u(0) = 0, \theta(0) = 1 \text{ at } y = 0 \tag{9}$$

$$u(1) = 0, \theta(1) = 0 \text{ at } y = 1 \tag{10}$$

The single prime ($'$) denotes the first derivative with respect to y and double primes ($''$) indicate the second derivative with respect to y.

$$c = \frac{V_0 h}{v}, M = \sigma\beta_0^2 h^2, J = \frac{\sigma\beta_0^2 vC_p}{k}, Br = P_r E_c, P_r = \frac{v}{\alpha} \text{ and } E_c = \frac{h^4 g^2 \beta_0^2 (T_w - T_0)}{vC_p}, u \text{ is the dimensionless velocity}$$

and θ is the dimensionless temperature

Principle of Adomian Decomposition Method (ADM):

Adomian decomposition is a semi-analytical method of solution which consists of splitting a given differential equations into two parts; namely the linear and nonlinear parts. Then inverting the highest order derivative operator in the linear operator on both sides, decomposing the nonlinear terms using Adomian polynomial and then finding the successive terms using recursive relation. The principle of ADM is as follows:

Assume the differential equation

$$Fy(x) = r(x) \tag{11}$$

Where F is a general nonlinear ordinary differential equation containing both linear and nonlinear terms with r(x) as a given function. Fy(x) is decomposed into Ly +Ry where L is the highest order derivative which is also invertible and R is the remainder of the linear operator.

So, equation (11) can now be written in the form:

$$Ly + Ry + Ny = r \tag{12}$$

Where Ny indicates the nonlinear terms in Fy.

Solving for Ly $= r - Ry - Ny$ $\tag{13}$

Since L is invertible, we take L^{-1} to the both sides of equation (13) to have:

$$L^{-1}Ly = L^{-1}r - L^{-1}Ry - L^{-1}Ny \tag{14}$$

Which is equivalent to

$$y = \varphi - L^{-1}r - L^{-1}Ry - L^{-1}Ny \tag{15}$$

Where φ is a constant achieved from integration of r(x).

Next, due to ADM we assume $y = \sum_{n=0}^{\infty} y_n$, and $N_y = \sum_{n=0}^{\infty} A_n$ $\tag{16}$

Using equations (15) and (16) we get:

$$\sum_{n=0}^{\infty} y_n = \varphi + L^{-1}r - L^{-1}R\sum_{n=0}^{\infty} y_n - L^{-1}N\sum_{n=0}^{\infty} A_n \tag{17}$$

They A_n are calculated via the Adomian polynomial

$$A_n = \frac{1}{n!}\frac{d^n}{d\lambda^n}f\left(\sum_{i=0}^{\infty}\lambda^i y_i\right)_{\lambda=0}, n = 0, 1, 2 \ldots \tag{18}$$

To get the solution, we set:

$$y_0 = \varphi + L^{-1}r \tag{19}$$

$$y_{n+1} = -L^{-1}Ry_n - L^{-1}A_n, n \geq 0 \tag{20}$$

Since we have an infinite series and all the terms cannot be computed, we assume the final solution to be $y = \sum_{n=0}^{\alpha} y_n$

, where α is a truncation point for which the ADM solution converges.

ADM Solution of the Problem

Having described the principle of ADM, the solution of equations (7−8) is as follow:

Let L $= \frac{d^2}{dy^2}$ and $L^{-1} = \iint_0^y (.)dydy$ so that equation (7) and equation (8) can be written as:

$$L u = c(1+ \lambda \theta)u' + \lambda (1+ \lambda \theta)\theta' u' - (\theta (1+ \lambda \theta)) - M u \tag{21}$$

$$L \theta = c\theta' - Br u'^2 - J u^2 \tag{22}$$

Taking $L^{-'}$ to both sides of the equations (21) and (22)

$$L^{-'}L u = cL^{-'} ((1+ \lambda \theta))u' + \lambda L^{-'}((1+ \lambda \theta)\theta' u') - L^{-'}(\theta (1+ \lambda \theta)) - ML^{-'}u \tag{23}$$

$$L^{-'}L u = cL^{-'}\theta' - BrL^{-'}(u'^2) - JL^{-'}(u^2) \tag{24}$$

But $L^{-'}L u = \iint_0^y u'' dy dy = u(y) - yu'(0) - u(0) \tag{25}$

and $L^{-'}L u = \iint_0^y \theta'' dy dy = \theta(y) - y\theta'(0) - \theta(0) \tag{26}$

Substituting equation (25) into equation (23) and rearranging:

$$u(y) = u(0) + yu'(0) + c\iint_0^y u' \, dy dy + c \lambda \iint_0^y \theta u' \, dy dy + \lambda \iint_0^y \theta' u' + \lambda^2 \iint_0^y \theta \theta' u' \, dy dy - \lambda \iint_0^y \theta \, dy dy - M \iint_0^y u \, dy dy - \iint_0^y \theta \, dy dy \tag{27}$$

But $u(0) = 0$, so that equation (27) is now:

$$u(y) = Ay + c\iint_0^y B_z \, dy dy + c \lambda \iint_0^y C_z \, dy dy + \lambda \iint_0^y D_z + \lambda^2 \iint_0^y E_z \, dy dy - \lambda \iint_0^y F_z \, dy dy - M\iint_0^y G_z \, dy dy - \iint_0^y K_z \, dy dy \tag{28}$$

Similarly, by substituting equation (26) into equation (24) and rearranging:

$$\theta(y) = \theta(0) + y\theta'(0) + c\iint_0^y \theta' \, dy dy' - Br \iint_0^y u'^2 \, dy dy - J \iint_0^y u^2 \, dy dy \tag{29}$$

But $\theta(0) = 1$, so equation (29) becomes:

$$\theta(y) = yH + 1 + c \iint_0^y L_z' dy dy' - Br \iint_0^y P_z \, dy dy - J \iint_0^y Q_z \, dy dy \tag{30}$$

Where $A = u'(0)$, $H = \theta'(0)$ are assumed values to be obtained using equation (10) and $B_z, C_z, D_z, E_z, F_z, G_z, L_z, P_z$ and Q_z for $z \geq 0$ are to be determined via equation (18) to have the following few terms:

$B_0 = u_0'$, $B_1 = u_1'$, $B_2 = u_2'$, $C_0 = \theta_0 u_0'$, $C_1 = \theta_0 u_1' + \theta_1 u_0'$, $C_2 = \theta_0 u_2' + \theta_2 u_0'$

$D_0 = \theta_0' u_0'$, $D_1 = \theta_0' u_1' + \theta_1' u_0'$, $D_2 = \theta_0' u_2' + \theta_1' u_1' + \theta_2' u_0'$, $E_0 = \theta_0 \theta_0' u_0'$,

$E_1 = \theta_0 \theta_0' u_1' + \theta_0 \theta_1' u_0' + \theta_1 \theta_0' u_0'$, $E_2 = \theta_0 \theta_0' u_2' + \theta_0 \theta_2' u_0' + \theta_2 \theta_0' u_0'$, $F_0 = \theta_0$, $F_1 = \theta_1$, $F_2 = \theta_2$

$G_0 = u_0$, $G_1 = u_1$, $G_2 = u_2$, $K_0 = \theta_0$, $K_1 = \theta_1$, $K_2 = \theta_2$ $L_0 = \theta_0'$, $L_1 = \theta_1'$, $L_2 = \theta_2'$,

$P_0 = u_0' u_0'$, $P_1 = u_0' u_1' + u_1' u_0' + u_0' u_0'$, $P_2 = u_0' u_2' + u_1' + \theta_0 u_2' u_0' + u_0' u_1' + u_1' u_0' + u_0' u_0'$

$Q_0 = u_0 u_0$, $Q_1 = u_0 u_1 + u_1 u_0$, $Q_2 = u_0 u_2 + u_1 u_1 + u_2 u_0$

Now assume $u = \sum_{n=0}^{\infty} u_n$, $\theta = \sum_{n=0}^{\infty} \theta_n$ and substitute into equations (29) and (30) to have the recurrence relation:

$$u_0 = yA \tag{31}$$

$$u_{z+1} = c \iint_0^y B_z \, dy dy + c \lambda \iint_0^y C_z \, dy dy + \lambda \iint_0^y D_z + \lambda^2 \iint_0^y E_z \, dy dy - \lambda \iint_0^y F_z \, dy dy - M \iint_0^y G_z \, dy dy \text{, for } z \geq 0 \tag{32}$$

$$\theta_0 = yH + 1 \tag{33}$$

$$\theta_{z+1} = c \iint_0^y L_z' dy dy' - Br \iint_0^y P_z \, dy dy - J \iint_0^y Q_z \, dy dy \text{, for } z \geq 0 \tag{34}$$

The final solution is:

$$u(y) = u_0 + u_1 + u_2 + \ldots + u_s \tag{35}$$

$$\theta(y) = \theta_0 + \theta_1 + \theta_2 + \ldots + \theta_s \tag{36}$$

Where S is a truncation point for which the ADM solution converges.

Convergence of the ADM Solution of the Problem

Convergence of ADM solution has been assured to be rapidly in the Adomian (1994) and Cherruault (1990). So because of this, we need not to test the convergence of the solution of our problem.

RESULTS AND DISCUSSION

The article investigates steady MHD free convection flow with temperature dependence viscosity, viscous dissipation and Joule heating through a vertical porous channel. The important parenthesis in this study are the varying viscosity (λ), suction parameter (c), Brinkman number (Br), Joule heating term (J) and magnetic parameter (M). Using a computer software algebra package of Maple, simulation of the flow equations is carried out while considering the

values of λ , Br, J, M and c as: (0.1, 0.3 , 0.6), (-1, 1 , 1.5), (1, 5 , 10), (0.1, 0.5 , 0.8) and (-1, 0.1 , 1) respectively. Results are displayed on graphs (2 – 11) and table 1 below.

Fig. 2. Velocity propiles for different values of λ
.........λ=0.1, ————λ=0.3, .-.-.-.-.-.-λ=0.6

Fig. 3. Temperature profiles for different values of λ
.........λ=0.1, ————λ=0.3, .-.-.-.-.-.-λ=0.6

Fig. 4. Velocity profiles of different values of J
.........J=1, ————J=5, .-.-.-.-.-J=10

Fig. 5. Temperature profiles for different values of J
.........J=1, ————J=5, .-.-.-.-.-J=10

Fig. 6. Velocity profiles for different values of c
.........c=0.1, ————c=0.5, .-.-.-.-.-c=0.9

Fig. 7. Temperature profiles for different values of c
.........c=0.1, ————c=0.5, .-.-.-.-.-c=0.9

Fig. 8. Velocity profiles for different values of M
..........M=0.2, ---------M=0.4, .-.-.-.-.-.-.-M=0.9

Fig. 9. Temperature profiles ofr different values of M
..........M=0.2, ---------M=0.4, .-.-.-.-.-.-M=0.9

Fig. 10. Velocit profiles for different values of Br
..........Br=0.1, ----------Br=0.5, .-.-.-.-.-.-Br=0.9

Fig. 11. Temperature profiles for different values of Br
..........Br=0.1, ----------Br=0.5, .-.-.-.-.-.-Br=0.9

Figure 2 and 3 exposed the response of reducing viscosity on the velocity and temperature within the channel. It is seen that decrease in viscosity causes increase in velocity and decrease in the temperature of the fluid. This philosophy is due to increase in cohesive force between the fluid molecules. The effects of changing Joule heating is graphed in figure 4 and 5 where it illustrate that, both the velocity and temperature of the fluid within the channel increase with increase in J. These trends are as a result of the decrease of thermal conduction of the fluid, which in return increase the kinematic viscosity of the fluid. It is viewed form figure 6 and 7 that rising fluid suction (c) on both the velocity and temperature within the channel results to the decrease in both the temperature and velocity of the fluid in the channel. These culture are the consequential effect of the decrease in the kinematic viscosity of the fluid which attributed to the increase of the force of attraction between the fluid molecules. The response of changing magnetic effect (M) is mirror in figure 8 and 9, the figures show an increases of velocity of the fluid within the channel with insignificant effect on the temperature profiles. The effect of changing Brinkman number (Br) is presented in figure 10 and 11 where it mirror that, an increase in Brinkman number in both the temperature and velocity profiles are insignificant.

Validation of the results

Since equations (7-8) are highly nonlinear coupled differential equations whose solutions cannot be easily obtained through analytical means, we therefore reduce the complexity of these equations by neglecting the effects of varying viscosity (i.e. $\lambda = 0, Br = 0$) in order to validate our results. In doing this, the emerging equations are thus:

$$u'' - cu' + Mu + \theta = 0 \tag{37}$$

$$\theta'' - c\theta' - Ju^2 = 0 \tag{38}$$

In order to ascertain the validity of our results here, we use differential transformation method of solution (DTM) to solve the equations (equations 37-38) for the purpose of validation with result displayed in table 1 below.

Table 1. Comparison between ADM and DTM Solution

y	ADM		DTM		Error (ADM – DTM)	
0.02	$u = 0.99134$	$\theta = 0.98139$	$u = 0.99979$	$\theta = 0.99997$	$u = 0.00845$	$\theta = 0.03690$
0.04	$u = 0.98222$	$\theta = 0.96301$	$u = 0.99919$	$\theta = 0.99991$	$u = 0.01697$	$\theta = 0.03690$
0.06	$u = 0.97265$	$\theta = 0.94459$	$u = 0.99819$	$\theta = 0.99981$	$u = 0.02554$	$\theta = 0.05522$
0.08	$u = 0.96261$	$\theta = 0.92612$	$u = 0.99679$	$\theta = 0.99967$	$u = 0.03418$	$\theta = 0.07355$

The table shows the comparison between Adomian decomposition method (ADM) and the differential transformation method (DTM) of solution of our problem. It is viewed from the table that there is good agreement between the two.

CONCLUSION

Steady MHD free convection flow with temperature dependent viscosity, viscous dissipation and Joule heating in a vertical porous channel have been studied using ADM and DTM method of solutions with computer simulations. The results are presented in graphs and table with the discussion of the outcomes. The following are the outcome of the investigation:

1. The finding reveled that decrease in viscosity causes increase in velocity and decrease in the temperature of the fluid. This philosophy is due to increase in cohesive force between the fluid molecules.
2. When Joule heating parameter increase, both the velocity and temperature of the fluid within the channel also increase.
3. Rising fluid suction on both the velocity and temperature within the channel results to the decrease in both the temperature and velocity of the fluid in the channel.
4. An increase in magnetic effect parameter causes an increases of velocity of the fluid within the channel with insignificant effect on the temperature profiles.
5. The effect of changing Brinkman number (Br) is presented where the result in both the velocity and temperature profiles mirror to be insignificant.

REFERENCES

Adomian, G., (1994) Solving frontier problems of physics: the decomposition method, MA Kluwer, Boston

Ajibade, O.A., Jha, B.K. and Jibril, M.H., Bichi, Y.A., (2021). Effects of dynamic viscosity and nonlinear thermal radiation on free convective flow through a vertical porous channel. *International journal of thermofluids 9:1-9*

Alfvén, H., (1942). Existence of Electromagnetic-Hydrodynamic Waves. Nature, *150:405- 406*

Altunkaya, A.N., Avci, M. and Aydin, O., (2017). Effect of viscous dissipation on mixed convection in a vertical parallel plate micro channel with asymmetric uniform wall heat flux: the slip regime, *Int. j. Heat Mass Tran. iii (8):495-499.*

Borah, G. and Hazaria, G.C., (2013). Effects of variable viscosity and thermal conductivity and magnetic field effect on the free convection and mass transfer flow through porous medium with constant suction/heat flux, *J. comput. Math. Sci. 4(6):407-418.*

Carey, V.P. and Mollendorf, J. C. (1978). Natural convection in liquid with temperature dependent viscosity. *In proceedings of the 6th International Heat Transfer Conference.Toronto, 2:211-217.*

Cherruault, Y., (1990) Convergence of Adomians method, J. Math. Comput. Model. (14): 83-86

Isaac, L.A. and Anselm, O.O., (2014). Effects of variable viscosity, Dofour, Soret and thermal conductivity on free convective heat and mass transfer of non-darcian flow past porous flat surface. *AM. J. Comput. Math 4:357-365.*

Jaber, K.K., (2016). Joule Heating and Viscous Dissipation on Effects on MHD Flow over a Stretching Porous Sheet Subjected to Power Law Heat Flux in Presence of Heat Source. *Open Journal of Fluid Dynamics, 6:156-165.*

Kumar, A. and Sigh, A., (2015). Unsteady MHD free convective heat and mass transfer in a boundary layer flow past a vertical permeable plate with thermal radiation and chemical reaction. *Procedia Eng. 127:791-79.*

Mohammad Nurul Amin and Nazma Parveen, (2021). Free convection flow with joule heating, heat generation and viscous dissipation along a vertical wavy surface. *Conference paper in AIP Conference Proceedings: February 2021.*

Reynold, O., (1883). An experimental investigation of the circumference which determine whether the motion of water shall be director sinusoidal and of the law of resistance in parallel channels, *Philos. Trans. R. Soc. 174: 935-982.*

Singh, V. and Shweta, A., (2013). Flow and heat transfer of maxwall fluid with variable viscosity and thermal conductivity over an exponentially stretching sheet, *Am. J. Fluid Dyn. 3(4): 87-95.*

Sinha, A., (2015). MHD flow and heat transfer of a third order fluid in a porous channel with stretching wall: Application to hemodynamics: *Alexendria Engineering journal*

Vajravelu, K., Prasad, K.V. and Chiu-on, N., (2013). Unsteady convective boundary layer flow of a viscous fluid at a vertical surface with variable fluid properties, *Nonlinear Anal. 14: 455-464.*

Thermodynamic Studies and Influence of pH on Nickel (II) Adsorption from Aqueous Solution Using Banana Peel

*Ashiru Auwal Mairuwa, Jibrin Abubakar Maje, Lirwan Salisu And Usman Muhammad Kabir

Al-Qalam University Katsina,
*Corresponding Author's E-mail: ashiruauwalmairuwa15@gmail.com; Phone: +2347068139849,

ABSTRACT
This study examines how effectively banana peel may remove Ni (II) ions from aqueous solutions using comparative adsorptive removal. The design of the experiment was used to identify the ideal adsorption conditions on operational parameters, posthoc significant statistical tests were also carried out. Adsorbent dose, pH, contact time, particle size, and temperature were each independently changed for their parametric effects, and their effects on the percentage of Ni (II) ion removal were estimated. At a pH of 8.0, both adsorbents reached the maximum % removal. The ideal conditions were 4.5 g of adsorbent dose, 120 minutes contact time, and 25^0C reaction temperature.
Keywords: Banana peel, Adsorption, Adsorbent Dose, pH, Temperature

INTRODUCTION

According to the World Health Organization (IARC Monographs on the Evaluation of Carcinogenic Risks to Humans IARC Monographs Vol 49, 1990), the carcinogenic risk to humans posed by industrial exposure to nickel and its components which are metallic nickel and nickel alloys, nickel oxides and hydroxides, nickel sulfides and nickel salts . Nickel carbonyl is identified as the most acutely toxic nickel compound, causing severe damage to the respiratory system in experimental animals and in humans. On the basis of evidence from human and animal studies, welding fumes are classified as possibly carcinogenic to humans (Abbas *et al.,* 2014). Nickel are widely use in industrial include rechargeable (NiCad) batteries, pigments for paints or ceramics, electroplating, electroforming and sintered metal coatings. These various applications are introduced into aquatic ecosystems as by-products of industrial processes and acid-mine drainage residues. The presence of toxic heavy metals contaminated in aqueous streams, arising from the discharge of untreated metal containing effluent into water bodies, is one of the most important environmental issues, (Ajayi *et al.,* 2016). Their presence in aquatic eco system poses human health risks and causes harmful effect to living organisms the effluents from metal finishing processes may contain up to 10 mg/L of copper, chromium, nickel and zinc. Nickel is a major concern because the larger usages in developing countries and their no degradability nature (Amer *et al.,* 2015).

Therefore, it is important to develop new methods for metal removal and for the reduction of heavy metal ions to very low concentrations. Biosorption, a biological method of environmental control can be an alternative to conventional physicochemical technologies waste-treatment facilities such as ion exchange, chemical precipitation, reverse osmosis and evaporative recovery. This conventional method for this purpose is often inefficient and/or very expensive, (Abbasi, *et al.,* 2013); Biomaterials that are available in large quantities may have a potential to be used as low cost adsorbents, because they represent unused resources that are widely available and environmentally friendly past recent research was still searching of an effective biosorbent that can be use to remove nickel from aqueous solution. According to the percentage sorption Ni (II) ability of C. fistula (Golden Shower) from seven industries are in the following order: TILHU (99.88 %) >GI (99.85%) ≈BMI (99.85%) > TIFU (99.80%) > TIHHU (99.78%) > TIDU (99.77%) Ni–Cr PI (90.59%). Water pollution due to toxic heavy metals has been a major cause of concern for environmental engineers. The industrial and domestic wastewater is responsible for causing several damages to environment and adversely affecting people's health. There are several cases due to heavy metal contamination in aquatic environment, increase the awareness about the heavy metal toxicity such as "Minamata" tragedy due to mercury poisoning and "Itai-itai" disease in Japan due to cadmium toxicity. Metals can be distinguished from other toxic pollutants since they are non-biodegradable and can accumulate in living tissues thus becoming concentrated throughout the food chain. A variety of industries are responsible for the release of heavy metals into the environment through their wastewater, (Gonen, and Serin, 2012), which include iron and steel production, the non-ferrous metal industry, mining and mineral processing, pigment manufacture, the painting and photographic industries and metal working and finishing processes (electroplating). Moreover, considerable quantities of heavy metals can be released into the environment through the routes other than wastewater. For example, lead is widely used in metallic form and copper is used in electric equipment, water pipes, alloy as chemical catalyst and in anti-fouling paints on ship hulls (Annadurai *et al.,* 2012).

MATERIALS AND METHODS

The materials and methods section of this study outlines the apparatus and reagents used, as well as the procedures followed to collect samples and conduct the adsorption experiments. The materials included a mesh sieve, Buck Atomic Absorption Spectrophotometer (AAS), electric water bath, oven, graduated beakers and cylinders, filter paper, electronic weighing balance, pH meter, furnace, funnels, stopwatch, and distilled water. The reagents used were analytical grade nitric acid (HNO3), sodium hydroxide (NaOH), and nickel(II) nitrate hexahydrate salt [Ni(NO3)2.6H2O]. For sample collection, banana peels from Musa Acuminata were collected from the Central market in Katsina, Nigeria. The peels were then prepared by washing them with distilled water, drying them in sunlight for five days, and further drying them in an oven at 70°C. The dried peels were cut into small pieces, ground, sieved, and dried again at 50°C before being stored in desiccators. The adsorbate used in the experiment was nickel (II) nitrate hexahydrate, which was obtained from GeetexLab, Bacha, Kano. It was prepared by diluting a stock solution of Ni(NO3)2.6H2O with distilled water to achieve desired concentrations ranging from 10 to 200 mg/L. The adsorption experiments were conducted by adjusting the initial pH of the solution using either 0.1 M NaOH or 0.1 M HNO3. The experiments were carried out at room temperature, and the initial and final metal ion concentrations were determined using AAS. Each run was repeated three times, and the average values were calculated. The percentage removal of Ni(II) ions and the amount of adsorbed banana peel were determined using specific equations.

$$Removal\ (\%) = \frac{100\ (C_o - C_e)}{C_o} \ldots\ldots\ldots\ldots\ldots.\ldots\ldots (1)$$

$$q_e = \frac{C_o V_o - C_e V_e)}{m} \ldots\ldots\ldots\ldots\ldots.\ldots\ldots (2)$$

RESULTS AND DISCUSSIONS

The results and discussion section of the study investigated the effects of various parameters on the adsorption of nickel (II) ions using banana peel as the adsorbent. The analysis focused on the adsorbent dose, pH, contact time, temperature, adsorbate concentration, and particle size. The study found that the percentage removal of the adsorbent increased with an increase in adsorbent dosage but tended to plateau at around 1.3 g. This may be due to overcrowding of the adsorbent particles, leading to overlapping of adsorption sites. Similar observations were reported in the biosorption of Ni(II) ions using Araucaria cookie leaves. The pH of the solution had a significant effect on adsorption. Higher pH values resulted in a higher percentage removal, with the optimal range being between pH 6 and 8. This is attributed to the solubility of metal ions, the concentration of counter ions on the adsorbent's functional groups, and the degree of ionization of the adsorbate during the reaction. Adsorption was found to be limited in highly acidic and alkaline conditions due to competition between hydrogen ions and hydroxyl ions for active sites on the adsorbent surface. Increasing contact time favored adsorption using banana peel as the adsorbent. The maximum uptake capacity of banana peel was observed to be higher compared to other studies, indicating its effectiveness as an adsorbent. Temperature had an adverse effect on adsorption, as an increase in temperature led to a decrease in the percentage removal of nickel ions. This can be attributed to desorption, where the ions do not attach properly to the adsorbent surface due to increased kinetic energy. The adsorbate concentration slightly reduced the percentage removal of nickel ions by banana peel. Super saturation of active sites occurred when more ions were provided for adsorption without increasing the adsorbent quantity, limiting the adsorption capacity. The particle size of the adsorbent influenced adsorption, with a decrease in percentage removal observed with increased particle size. This is due to the reduction in available surface area for adsorption. The findings of this study provide insights into the effects of various parameters on the adsorption of nickel (II) ions using banana peel as an adsorbent, contributing to the understanding of the adsorption process and the optimization of adsorption conditions.

CONCLUSION

This study investigated the adsorption of nickel (II) ions using banana peel as an adsorbent. The results provided valuable insights into the effects of different parameters on the adsorption process. The findings indicated that the adsorbent dose had an impact on the percentage removal of nickel ions, with an optimal dosage of around 1.3 g. Higher pH values within the range of 6 to 8 resulted in a higher percentage removal, while extreme pH conditions hindered adsorption due to competition for active sites on the adsorbent surface. The study also revealed that increasing contact time favored adsorption using banana peel as the adsorbent, demonstrating its potential as an effective adsorbent material. However, an increase in temperature led to a decrease in the percentage removal of nickel ions, indicating the influence of desorption processes. Additionally, the adsorbate concentration and particle size of the adsorbent were found to affect the adsorption efficiency, with higher concentrations leading to reduced removal percentages and larger particle sizes hindering adsorption. These findings highlight the importance of considering various factors when designing adsorption processes using banana peel as an adsorbent for nickel ions. The results contribute to the

optimization of adsorption conditions and can guide future research in developing sustainable and cost-effective approaches for the removal of metal ions from aqueous solutions.

REFERENCES

Abbas, I., Ismail, I. M., Ismail, N., & Abdel-Mottaleb, M. S. A. (2014). Effect of Welding Fumes on the Health of Welders in Alexandria City. Egyptian Journal of Occupational Medicine, 38(2), 185-199.

Abbasi, T., Anwar, A., & Bajwa, R. (2013). Biosorption of Heavy Metals—An Overview. Journal of Chemistry, 2013, 941021.

Ajayi, O. O., Adetunji, M. T., & Oloyede, I. O. (2016). Metal Pollution Status in Surface Water of Osun River, Nigeria: Human Health Risk Assessment. Chemistry and Ecology, 32(6), 556-574.

Amer, N., El-Bindary, A. A., Diab, M. A., El-Sonbati, A. Z., & El-Gammal, O. A. (2015). Heavy Metal Ions Removal from Industrial Waste Water Using New Adsorbent Polymer. Arabian Journal of Chemistry, 8(5), 692-699.

Annadurai, G., Ling, L. Y., Lee, J. F., & Selvaraju, N. (2012). Biosorption of Heavy Metals by Bacillus Thuringiensis Strain OSM29 Originating from Industrial Effluent Contaminated North Indian Soil. Journal of Hazardous Materials, 209-210, 240-247.

Gonen, F., & Serin, S. (2012). Treatment of Industrial Wastewaters Containing Heavy Metals Using Biosorbents. Environmental Monitoring and Assessment, 184(12), 7599-7612.

IARC Monographs on the Evaluation of Carcinogenic Risks to Humans. (1990). IARC Monographs Vol 49. World Health Organization. Retrieved from https://publications.iarc.fr/Book-And-Report-Series/Iarc-Monographs-On-The-Evaluation-Of-Carcinogenic-Risks-To-Humans/Iarc-Monographs-Vol-49-1990

Development of a Mathematical Model for Optimal Response of Lowland Rice Production to Furrow Irrigation and Fertilizers Application

*[1]Hakimi, D., [3]Batagi, S., A., [1]Lawal, A., [2]Daniya, E. [4]Yahaya, A., A., [5]Hassan, S.

[1]Department of Mathematics, Federal University of Technology, Minna, Niger State Nigeria.
[2]Department of Crop Production, Federal University of Technology, Minna, Niger State, Nigeria.
[3]Department of Statistics,Niger State Polytechnic Zungeru, Nigeria.
[4]Department of Mathematics, Federal polytechnic Bida
[5]Niger State Polytechnic Zungeru, Nigeria.
*Corresponding Author's E-mail: danladihakimi2016@gmail.com

ABSTRACT

In this work, we developed a mathematical model for optimal response of lowland rice production using furrow irrigation and fertilizers application as a system of second order (degree) of variables such as F (furrow irrigation), N (nitrogen fertilizer), W (NPK fertilizer), R (Lowland rice), Z (Zinc fertilizer), Se (Selenium fertilizer) which was solved and expressed as a product of matrices to optimize growth and yield of lowland rice production to give a bumper harvest to Nigerians.

Keywords: Lowland, Second order degree, Matrices, Furrow irrigation and Fertilizers

INTRODUCTION

In every aspect of life, the question of obtaining optimal result is important but it is even better in the production of food, because, it is a basic need which also promotes an economy of a country, and Nigeria is not an exception. Farmers are engaged in farming in order to maximize yields. The yield is therefore essential. Some farmers stabilize and become successful while others fail even before they begin (Perdani *etal.,* 2020).

Irrigation modeling and predictions are essential aspects in agricultural production and management of water resources. Irrigation is the principal phenomenon driving food production during the dry season. Proper planning of irrigation system is very imperative for crop production to boost the economy of Nigeria. Irrigation pattern system is fundamental for the cropping system and for effective soil water management plans. Such information could be beneficial in determining the best adapted crop species and optimum time of seedling to re-establish vegetation on deteriorated rangelands. Irrigation system and application of fertilizers are becoming increasingly in demand (Ping *e tal.,* 2020).In view of this, it has become imperative to assist the farmers and the policy makers within the immediate environment with information that could be utilized to boost crop production in Nigeria, especially in North Central region. This follows the fact that the majority of the farmers in North Central Nigeria rely on irrigation system as an alternative to source of water for crop production during the dry seasons. This research work will provide the use of analytical method, optimization method; matrix and differential solutions that can help farmers in enhancing upland rice production and improve their yields.

Statement of the Problem

Water shortages have become a major problem to the farmers in Niger State as well as other States in Nigeria. As the problem of water shortages increases, there is a need to an alternative source of water for food production. Lowland rice is one of the most widely cultivated crops globally, with over one million hectares planted annually. However, its productivity can be affected by various factors such as soil water availability, temperature and nutrients. Lowland rice requires a lots of water for its optimum production yield unlike upland rice production. Experiences and experiments have confirmed that lowland rice production yield maximally where there is availability of water throughout incubation period. Lowland rice production also depends on the availability of nutrients in the soil. If fertilizers are not properly applied, the soil fertility can decline over time, making it more challenging to the farmers to achieve sustainable and profitable rice production at the time of harvest. Inadequate application of fertilizers leads to nutrient deficiencies in the soil which affects growth and yield of lowland rice production. Insufficient fertilizers application also affects the quality of rice and without the necessary nutrients to the soil, the rice yields may be smaller, which will also have lower nutritional value, and may not meet the desired goals of Nigerians. The implication of not applying enough water through furrow irrigation for lowland rice production in Nigeria is that, the crop yield is reduced, it means water is essential for crop or plant growing, and without enough water, it is led to little or no yield. Nutrients deficiency may cause improper growth thereby reducing crop yields and quality.

Low crop yields and poor quality results in economic losses for farmers who struggle to recover their investment in the crop. Poor irrigation practices and improper application of fertilizers is a critical problem to food security, it compromises food availability, promotes hunger and malnutrition. If applications of fertilizers are too much in the first three weeks, it also affects the growth of lowland rice production. Agricultural revolution in Niger State will not be completed until the socio-economic importance of irrigation farming is recognized more and more. This is because, the use of irrigation is to complement the rainfall to increase the food production and boost the economy of the State. The researcher is therefore, intending to develop a mathematical model for lowland rice using furrow irrigation and fertilizers application to meet up with food production in Nigeria.

Aim of the study
This research work is aimed at developing a mathematical model that will optimize the growth and yield of lowland rice production using furrow irrigation and fertilizers application.

Objectives of the Study
The objectives of the research work are to:
  i.   develop a mathematical model for optimal response of lowland rice production using furrow irrigation and fertilizers application.
  ii. analyze the system of the developed model as a product of matrices and reduce its nth order determinant to $(n - 1)^{th}$ order using pivotal condensation method.
  iii. explore the model to enhance lowland rice production through furrow irrigation.
  iv. examine the experimental treatment of the model and its replication.
  v.   determine the optimal yield of lowland rice production .
  vi. provide graphical simulation of the system responses.
  vii. Sensitivity Analysis will be used to test the model developed for the lowland rice production.

Justification for the Study
Nigerians are being confronted with the problem of food insecurity since 2015 to date, especially the poor who are living from hand to mouth. This is due to poor output of rice production. Different researchers (Pardani *etal,* 2020 *and Ping etal.,* 2020)explained that the application of direct irrigation system without fertilizer has little effect on crop production. However, none of these researchers has applied NPK fertilizer, Zinc fertilizer and Selenium fertilizer into their mathematical models. Based on this, the present work seeks to apply NPK fertilizer, Zinc fertilizer and Selenium fertilizer together with interaction of furrow irrigation to give a bumper harvest in the production of lowland rice to Nigerians.

MATERIALS AND METHODS
Achieving the Objectives of the Study
We will develop a mathematical Model for Optimal Response of Lowland Rice Production using furrow irrigation and fertilizers application as a system of second order (degree) of variable such as $\{F_I, N, W, Z \text{ and } Se\}$by extending the work of Ping*et al.* (2020) described as:

$$Y_i = \beta_1 X_{n1} + \beta_2 X_{n2}, + \beta_3 X_{n3} + \beta_4 X_{n4} + \beta_5 X_{n5} + \mu \qquad (1)$$

Where $i = 1, 2, 3 \ldots \ldots \ldots n$
$y_i = $ Average MFV of a particular upland rice
$X_{n1} X_{n5} = STI_s$of RFW, RL, SFW, SL and n^{th} of upland rice respectively
$\mu = $is the constant
$\beta = $ Unstandardized coefficient

The system of the mathematical model for optimal response of Lowland Rice Production using furrow irrigation and fertilizers application would be differentiated with respect to $F_I, N, W, Z \text{ and } Se$ which would then be expressed as a product of matrices as:

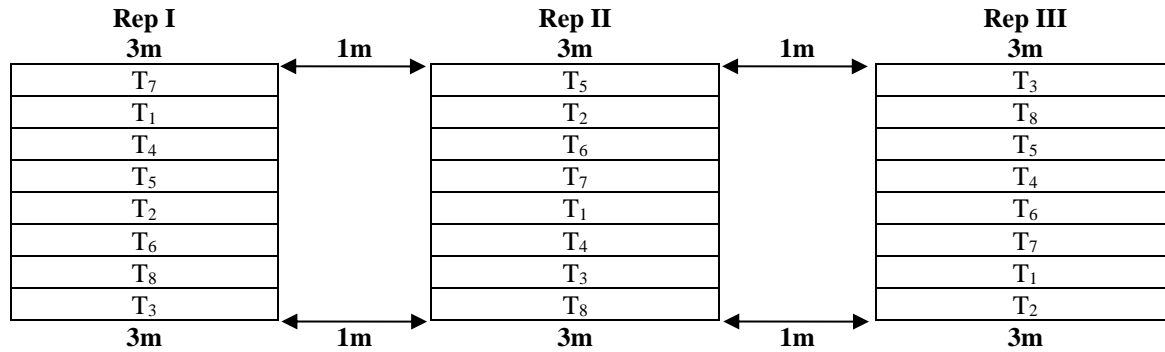$$A^* x = \beta^* \qquad (2)$$

Where

$$x = A^{*-1} \cdot \beta^* \qquad (3)$$

$$A^{*-1} = \frac{Adjoint\ (A^*)}{Det(A^*)} \qquad (4)$$

The determinant of A^*would be achieved by the process of reducing n^{th} order determinant to $(n - 1)^{th}$order determinant using pivotal condensation method. We would also find the cofactor of the matrices as

$$Cofactor = (-1)^{i+j} minor \qquad (5)$$

Where i is the number of rows of the element and j is the number of columns of the element.

We will achieve the objective three through furrow irrigation scheduling or intervals. The furrow irrigation interval would be "I_A" and "I_B" interval I_A would be continuous flooding (CF) control while interval I_B would be normal control. The treatment will be a factorial combination of two furrow irrigation schedules and four fertilizer applications (N, NPK, Z and Se) which would be arranged in a Randomized Complete Block design and replicated three times

This would be achieved through experimental layout of replication as Rep I, Rep. II and Rep III. Each replication would have eight treatments in a Randomize Complete Block Design (RCBD: Figure 1)

Rep I 3m		Rep II 3m		Rep III 3m
T_7		T_5		T_3
T_1		T_2		T_8
T_4		T_6		T_5
T_5	1m	T_7	1m	T_4
T_2		T_1		T_6
T_6		T_4		T_7
T_8		T_3		T_1
T_3		T_8		T_2
3m	1m	3m	1m	3m

The optimal yield points would be achieved by considering the continuous function of (F_I, N, W, Z and Se) and its first partial derivatives $\frac{dy}{dF_I}, \frac{dy}{dN}, \frac{dy}{dw}, \frac{dy}{dz}, \frac{dy}{dSe}$ at every point in the region R. And this can also be gotten from the graph simulations at the point as the curve changes signs. At the point where $\frac{dy}{dF_I} = 0, \frac{dy}{dN} = 0, \frac{dy}{dw} = 0, \frac{dy}{dz} = 0, \frac{dy}{dSe} = 0$ called stationary points. The stationary points fall into three categories:

(a) Those in which $\frac{dy}{dF_I}, \frac{dy}{dN}, \frac{dy}{dw}, \frac{dy}{dz}, \frac{dy}{dSe}$ change sign from positive through zero to negative are called maximum points.

(b) Those that change sign from negative through zero to positive are called minimum point

(c) Those that do not change signs are called point of inflexion.

This would be achieved through graphical simulation by using math-type software application which dictates the points on the graphs

MATERIALS AND METHODS

The following assumptions are made in developing a mathematical model for optional response of lowland rice preproduction using furrow irrigation and fertilizers application

i.   Weather condition is assumed normal

ii.   Soil type is assumed constant

iii. Furrow irrigation flows normal in two intervals

The model equation is developed as

$$Y = \lambda_0 + \lambda_1 F_1 + \lambda_2 N + \lambda_3 R + \lambda_4 W + \lambda_5 Z + \lambda_6 Se + \lambda_{11} F_I^2 + \lambda_{12} F_I N + \lambda_{13} F_I R + \lambda_{14} F_I W + \lambda_{15} F_I Z + \lambda_{16} F_I Se + \lambda_{22} N^2 + \lambda_{23} NR + \lambda_{24} NW + \lambda_{25} NZ + \lambda_{26} NSe + \lambda_{33} R^2 + \lambda_{34} RW + \lambda_{35} RZ + \lambda_{36} RSe + \lambda_{44} W^2 + \lambda_{45} WZ + \lambda_{46} WSe + \lambda_{55} Z^2 + \lambda_{56} ZSe + \lambda_{66} Se^2 + e$$

Where: (6)

Y = yield response

λ_i = estimated parameters ($i = 0,1,2,3,4,5$ and 6)

F_I = furrow irrigation

N = Nitrogen fertilizer

R = Lowland rice

W = NPK fertilizer (nitrogen, phosphorus and potassium)

Z = Zinc fertilizer

S_e = Selenium fertilizer

e = random error (i.e. constant)

These parameters are chosen in this research because of their benefits to crops as well as man after consumption of the crops. They will also help farmers to minimize the cost of production of crops, thereby, maximizing the outputs (yields). Crops need NPK fertilizer to live and grow, nitrogen fertilizer fuels vegetative growth, phosphorus is a stimulant for strong root growth and potassium promotes root and bud growth, and it also enhances disease resistance as well as to drought, heat and freezing.

Zinc helps in increasing crop production and nutritional status for consumption and it also helps crop tissues to withstand cold.

Furrow irrigation is a method of laying out water channels in such a way gravity plays the role of providing enough water for suitable crops to grow.

Method of Solution

The surface is obtained by taking the partial derivatives with respect to F_I (Furrow irrigation), N (Nitrogen fertilizer), R (Lowland rice), NPK (NPK Fertilizer), Z (Zinc fertilizer) and Se (Selenium fertilizer). Then, setting them equal to zero, we have.

$$\frac{\partial Y}{\partial N} = \lambda_2 + \lambda_{12}F_I + 2\lambda_{22}N + \lambda_{23}R + \lambda_{24}W + \lambda_{25}Z + \lambda_{26}Se \tag{7}$$

$$\frac{\partial Y}{\partial V} = \lambda_3 + \lambda_{13}F_I + \lambda_{22}N + 2\lambda_{33}R + \lambda_{34}W + \lambda_{35}Z + \lambda_{36}Se \tag{8}$$

$$\frac{\partial Y}{\partial W} = \lambda_4 + \lambda_{14}F_I + \lambda_{24}N + \lambda_{34}R + 2\lambda_{44}W + \lambda_{45}Z + \lambda_{46}Se \tag{9}$$

$$\frac{\partial Y}{\partial Z} = \lambda_5 + \lambda_{15}F_I + \lambda_{25}N + \lambda_{35}R + \lambda_{54}W + 2\lambda_{55}Z + \lambda_{56}Se \tag{10}$$

$$\frac{\partial Y}{\partial se} = \lambda_6 + \lambda_{16}F_I + \lambda_{26}N + \lambda_{36}R + \lambda_{46}W + \lambda_{56}Z + 2\lambda_{66}Se \tag{11}$$

The solutions of equation (7), (8), (9), (10), and (11) will provide information where Y is local maximum, local minimum or a local stationary value.

Solving Equation (7), (8), (9), (10), and (11) to obtain the points of optimum values for F_I, N, V, W, Z and Se

$$\lambda_1 + 2\lambda_{11}F_I + \lambda_{12}N + \lambda_{13}R + \lambda_{14}W + \lambda_{15}Z + \lambda_{16}Se = 0 \tag{12}$$

$$\lambda_2 + \lambda_{12}F_I + 2\lambda_{22}N + \lambda_{23}R + \lambda_{24}W + \lambda_{25}Z + \lambda_{26}Se = 0 \tag{13}$$

$$\lambda_3 + \lambda_{13}F_I + \lambda_{22}N + 2\lambda_{33}R + \lambda_{34}W + \lambda_{35}Z + \lambda_{36}Se = 0 \tag{14}$$

$$\lambda_4 + \lambda_{14}F_I + \lambda_{24}N + \lambda_{34}R + 2\lambda_{44}W + \lambda_{45}Z + \lambda_{46}Se = 0 \tag{15}$$

$$\lambda_5 + \lambda_{15}F_I + \lambda_{25}N + \lambda_{35}R + \lambda_{54}W + 2\lambda_{55}Z + \lambda_{56}Se = 0 \tag{16}$$

$$\lambda_6 + \lambda_{16}F_I + \lambda_{26}N + \lambda_{36}R + \lambda_{46}W + \lambda_{56}Z + 2\lambda_{66}Se = 0 \tag{17}$$

$$2\lambda_{11}F_I + \lambda_{12}N + \lambda_{13}R + \lambda_{14}W + \lambda_{15}Z + \lambda_{16}Se = -\lambda_1 \tag{18}$$

$$\lambda_{12}F_I + 2\lambda_{22}N + \lambda_{23}R + \lambda_{24}W + \lambda_{25}Z + \lambda_{26}Se = -\lambda_2 \tag{19}$$

$$\lambda_{13}F_I + \lambda_{22}N + 2\lambda_{33}R + \lambda_{34}W + \lambda_{35}Z + \lambda_{36}Se = -\lambda_3 \tag{20}$$

$$\lambda_{14}F_I + \lambda_{24}N + \lambda_{34}R + 2\lambda_{44}W + \lambda_{45}Z + \lambda_{46}Se = -\lambda_4 \tag{21}$$

$$\lambda_{15}F_I + \lambda_{25}N + \lambda_{35}R + \lambda_{54}W + 2\lambda_{55}Z + \lambda_{56}Se = -\lambda_5 \tag{22}$$

$$\lambda_{16}F_I + \lambda_{26}N + \lambda_{36}R + \lambda_{46}W + \lambda_{56}Z + 2\lambda_{66}Se = -\lambda_6 \tag{23}$$

We write equation (18), (19), (20), (21), (22) and (23) in the Matrix Form

$$Ax = \lambda \tag{24}$$

Where

x= {F_I,N,R,W,Z and Se}

$$\begin{pmatrix} 2\lambda_{11} & \lambda_{12} & \lambda_{13} & \lambda_{14} & \lambda_{15} & \lambda_{16} \\ \lambda_{12} & 2\lambda_{22} & \lambda_{23} & \lambda_{24} & \lambda_{25} & \lambda_{26} \\ \lambda_{13} & \lambda_{22} & 2\lambda_{33} & \lambda_{34} & \lambda_{35} & \lambda_{36} \\ \lambda_{14} & \lambda_{24} & \lambda_{34} & 2\lambda_{44} & \lambda_{45} & \lambda_{46} \\ \lambda_{15} & \lambda_{25} & \lambda_{35} & \lambda_{45} & 2\lambda_{55} & \lambda_{56} \\ \lambda_{16} & \lambda_{26} & \lambda_{36} & \lambda_{46} & \lambda_{56} & 2\lambda_{66} \end{pmatrix} \begin{pmatrix} F_I \\ N \\ V \\ W \\ Z \\ Se \end{pmatrix} = \begin{pmatrix} -\lambda_1 \\ -\lambda_2 \\ -\lambda_3 \\ -\lambda_4 \\ -\lambda_5 \\ -\lambda_6 \end{pmatrix} \tag{25}$$

Expected Results

Some of the results expected are:

i. The new mathematical model would be developed for Optimal Response of Lowland Rice Production using furrow irrigation and fertilizers application as a second order (degree) of variables such as (F_I, N, W, Z and Se).

ii. The system of the new mathematical model for optimal response of lowland rice production using furrow irrigation and fertilizers application would be reduced from nth order determinant to $(n-1)^{th}$ order using pivotal condensation method.

iii.   The furrow irrigation intervals would be "I_A"and "I_B". Interval "I_A" would be the data of continuous flooding while interval "I_B"would be the normal control and both interval "I_A" and "I_B" would be arranged in a table of complete factorial design.

These are the data of experimental replication as Rep I, Rep II and Rep III with eight treatments in a complete Block Design (RCBD)

iv.   The optimal yields would fall into stationary points such as maximum, minimum and inflexion points of $\frac{dy}{dF_I}, \frac{dy}{dN}, \frac{dy}{dw}, \frac{dy}{dz}, \frac{dy}{dSe}$. It would also be gotten from the graph simulations.

v.   This would be graphical simulations using math-lab software application

REFERENCES

Perdani A. Y.,Dewi, T. K.,Widowati, T., Zulfitri, A. and Praharyawan, S. (2019) Utilization of bio organic fertilizers for increasing upland riceproduction. IOP Conference Series: Earth and Environmental Science, 439

Ping, M.,Xiu, J.,Jianrong, G.,Xianzhi, X. &Baoshan, W. (2020) A Mathematical Model Predicts Salt Tolerance in Upland Rice at the Germination Stage. *Journal of Plant Biology and Crop Research, 2637-7721*

Phytochemical Screening, Antimicrobial Activity and FTIR Analysis of the Stem of *Kalanchoe pinnata* Plant

*1Sada Maryam Hassan, 2Abdulazeez Lawal Maigoro and 1Abdussalam Shehu Shema

1Department of Chemistry, Faculty of Physical Sciences, Federal University Dutsinma, Katsina State, PMB 5001, Nigeria.
2Department of Industrial Chemistry, Faculty of Physical Sciences, Federal University Dutsinma, Katsina State, PMB 5001, Nigeria
*Corresponding Author's E-mail**: mhassansada@fudutsinma.edu.ng

ABSTRACT

In some regions of Nigeria, *kalanchoe pinnata*, often known as the "Life" or "Miracle plant" and also known by the scientific name *Bryophyllum pinnatum*, is utilized in traditional medicine. This study's primary goal is to assess the stem bark of *Kalanchoe pinnata* for the presence of phytochemicals, antimicrobial activity and FTIR analysis. Using 300 ml of n-hexane and ethanol, the plant's stem was extracted, and the crude extract was tested for phytochemical screening that revealed the presence of phenols, alkaloids, flavonoids, saponins, terpenoids, and a variety of other compounds, except for tannins and fatty acids for hexane, and the absence of tannins for ethanol. Antimicrobial activity *Aspergillus niger, Klebsiella pneumonia, Pseudomonas aeruginosa, Staphylococcus aureus, Echerichia coli*, and *Bacillus cereus* were among the microorganisms that responded favorably to the stem bark's antimicrobial susceptibility test, but *Salmonella typhi* and *Candida albicans* did not and the crude extract produced the most significant cytotoxic activity against brine shrimp *Artemia salina* (LC_{50}: 0.181mg/mL). FTIR results confirmed the existence of C-H, C=O, $-CH_2$, $-NO_2$, and C-O. In conclusion, the results of this study have given the local people's long-standing use of the herb to fight illnesses a scientific justification and the plant studied can be a potential source of biologically active compounds as antitumor agent, antibacterial and pesticide.
Keywords: *Kalanchoe pinnata,* cytotoxic, FTIR, antimicrobial

INTRODUCTION

Plants have been utilized as remedies for hundreds of years because they are a priceless gift from nature. According to the World Health Organization, over 25% of modern medicines that are widely used around the world contain compounds extracted from medicinal plants. 80% of the world's population relies primarily on indigenous medicine, and the majority of traditional therapies use plant extracts or their active ingredients. (Chowdhury *et al*., 2016)
Increasing interest in "natural" therapies as a result of rising antibiotic resistance has led to an increase in interest in the therapeutic properties of natural products in recent years, but despite these claims, few products have undergone thorough evaluations for their antimicrobial activity. (Iqbal *et al*., 2006). Plants are a source of bioactive natural products that can be improved upon to treat diseases by increasing their effectiveness and lowering their toxicity. (Duraipandiyan *et al*., 2006: Mostofa 2017). The Crassulaceae family includes the *Kalanchoe pinnata* plant, often known as the "Miracle plant" or "Life plant," or *Bryophyllum pinnatum*. When young plantlets start to emerge from the leaf, it is also known as the "Mother of Thousand". (Rajsekhar *et al.*, 2016).

MATERIALS AND METHODS

The stem bark of *Kalanchoe pinnata* plant was obtained from Katsina state, Nigeria. The sample identified was done by the herbarium of Federal University Dutsinma. The fresh stems were cut, cleaned and air dried, grounded into powder using mortar and pestle and stored in a sterile container and finally kept for further analysis.

Extraction

The crushed stem bark (100 g) was macerated using 300 ml n-hexane with regular stirring to improve the extraction efficiency. The extract was filtered and concentrated using a rotary evaporator to obtain a solvent-free crude extract. Calculations were made to determine the extract's % yield.

Phytochemical analysis

The extracts were tested for the presence of phytochemical substances like alkaloids, flavonoids, terpenoids, saponins, and phenols using the following methodology (Banu et al., 2015).

Antimicrobial activity

Standard and clinically isolated strains of the following bacteria were collected from the university clinic in FUDMA, Katsina State: *Salmonella typhi, Bacillus cereus, Echerichia coli, Pseudomonas aeruginosa, Klebsiella pneumonia, Candida albicans,* and *Aspergillus niger.* These were utilized to evaluate the crude extract's in vitro antibacterial effectiveness. As described by (Sanchez *et al.*, 2005: Ochei and Kolhatka 2007).

Brine Shrimp Lethality Assay (BSLA)
The assay was carried out according to the principle and protocol previously described by (Sarah *et al.*, 2017 and Biswas *et al.*, 2011) with slight modifications. Brine shrimp eggs weighing around 50 mg were then sprinkled over the simulated seawater that had been collected in the beaker after it had been covered with aluminum foil. A few tiny pores were made to enhance the material's ability to conduct heat and light. The beaker was then allowed to sit at room temperature for 48 hours while being exposed to the radiation from the 60-watt bulb and used for the assay. 2 mg of the extract was weighed out, and 2 mL of DMSO (Dimethyl Sulfoxide) was added to it to create a stock solution with a 1000 ppm (mg/mL) concentration. By using the serial dilution procedure, we were able to produce solutions with concentrations of 1 mg/mL, 0.5 mg/mL, 0.25 mg/mL, 0.125 mg/mL, and 0.0625 mg/mL, all derived from the initial stock solution. Three test tubes for each concentration received the 2 mL solutions from each of the 5 solutions. Three test tubes each contained 2 mL of DMSO (as a blank). After they were labeled the tubes were maintained for 24 hours from this data the percentage of the lethality of the brine shrimp nauplii was calculated and the lethal concentration (LC_{50}) of the hexane extract was determined.

% mortality = (no. of dead nauplii/ initial no. of live nauplii) x 10

FT-IR Analysis
The FTIR spectroscopic analysis is a useful method for determining the kind of bonding in organic molecules, particularly the functional group. The infrared region absorption spectra for the extract were produced using a Perkin Elmer IR SUBTECH spectrum ASCII PEDS spectrometer in the 4000 to 400 cm $^{-1}$ range. The presence of functional groups, the -bond conjugate system, and aromatic and aliphatic structures in the constituents can be determined using FTIR spectra.

RESULTS AND DISCUSSION
Table 1: phytochemical screening test

S/NO	Phytochemical Constituents	Hexane	Ethanol
1	Alkaloids	+	+
2	Flavanoids	+	+
3	Saponins	+	+
4	Terpernoids	+	+
5	Fatty Acid	−	−
6	Phenolic	+	+
7	Tannins	−	+

Key: + = presence, - = absence.

The phytochemical profile of the stem-bark crude n-hexane and ethanol extracts revealed the presence of phytochemical components such alkaloids, flavonoids, saponins, terpenoids, and phenols except for tannins and fatty acids for hexane and the absence of tannins in ethanol as shown in Table 1. Although this result support the findings reported by (Kendeson *et al.*, 2021) except for saponins, but differs from the reports of Mora-Pérez and Hernández-Medel 2016; Kendeson *et al.*, 2021). Where they reported the absence of alkaloids and flavonoids in the methanol extracts of the stems and roots; Similarly, (Nwadinigwe 2011) observed that there were no saponins in the aqueous and methanolic extracts of the stem; this could be due to differences in the solvents used as well as external influences.

Table 2: Antimicrobial Activity

Test organisms	Zone of inhibition (mm) Concentration of extract (mm/gL)						(Mg/ mL)		
	200	100	50	25	1.25	C	MIC	MBC	MFC
Aspergillus niger	30	25	21	-	-	20	50		100
Candida albicans	8	6	-	-	-	11	-		-
Klebsiella pneumonia	28	20	13	6	-	26	100	200	

Pseudomonas aeruginosa	21	16	10	7	-	23	200	-
Staphylococcus aureus	25	21	14	-	-	24	200	-
Salmonella typhi	-	-	-	-	-	-	-	-
Echerichia coli	25	19	11	-	-	23	200	200
Bacillus cereus	22	17	15	8	-	22	50	200

Key: - implies no sensitivity

MIC = Minimum Inhibitory Concentration MBC = Minimum Bactericidal Concentration

MFC = Minimum Fungicidal Concentration C = Control (standard drug) Ciprofloxacin (10 mg/ mL) for bacteria and Ketoconazole (10 mg/ mL) for fungi.

Aspergillus niger, Klebsiella pneumonia, Pseudomonas aeruginosa, Staphylococcus aureus, Echerichia coli, and *Bacillus cereus* were among the test organisms which the stem bark revealed significant antimicrobial activity against, while *Salmonella typhi* and *Candida albicans* were found to be resistant to the extract. The antimicrobial activity of the stem was also found to be concentration dependent as shown in Table 2. This reported antimicrobial activity suggests that the extract could be effective in the management of infections caused by susceptible microorganisms and therefore, it may be determined how effective these plant species extracts are as antimicrobial agents, which is in accorders with the report (Kendeson *et al*., 2021). The LC_{50} value for the hexane extract was determined as shown in the table below:

Table 3: Calculation of mortality % of hexane extract.

Concentration (mg/mL)	No. of dead nauplii			% Mortality
1	10	10	10	100
0.5	9	10	10	69.997
0.25	5	6	6	56.667
0.125	4	2	4	33.333
0.0625	1	3	1	16.667
LC50 = 0.181 mg/mL				

Brine Shrimp Lethality Assay (BSLA) After the freshly hatched live nauplii were exposed to concentrations of 1 mg/mL, 0.5 mg/mL, 0.25 mg/mL, 0.125 mg/mL, and 0.0625 mg/mL, respectively, the LC_{50} value of hexane extract was computed. The most and least number of brine shrimp larvae perished at doses of 1 mg/mL and 0.0625 mg/mL, respectively.

Table 4: FTIR analysis

Absorption (cm^{-1})	Types of stretching	Appearance
2952.05	C-H	Strong
1871.12	C=O	Strong
1438.75	-CH$_2$	Medium
1364.20	-NO$_2$	Medium
1173.47	C-O	Medium

The results were compared using an infrared chart of FTIR analysis to confirm the presence of functional groups such as the strong band observed at 2952.05 cm^{-1} corresponds to C-H stretching. The strong band at 1871.12 cm^{-1} indicates the presence of C=O stretching assigned to carbonyl group. The medium band at 1438.75 cm^{-1} corresponds CH_2, CH_3 and C-H bond alkanes. The medium band at 1364.20 cm^{-1} corresponds to –NO_2 stretching. The medium band at 1173.47 cm^{-1} corresponds to C-O group. In the hexane extract of *K. pinnata* stem; these functional groups are connected to the bioactive phytochemicals. (Kendeson *et al*., 2021).

CONCLUSION

Finally, it could be suggested that the hexane and ethanol extracts of *Kalanchoe pinnata* stem possess phytochemical, pharmacological and FTIR activities. The plant studied can be seen to be a potential source of useful antimicrobial drugs. Further studies are however recommended on the plant to determine the pharmaceutical potentialities of the plant as a medicine and to isolate and elucidate the structure of the bioactive compounds.

REFERENCES.

Banu, K. S., & Cathrine, L. (2015). General Techniques Involved in Phytochemical Analysis. International Journal of Advanced Research in Chemical Science, 2(4).

Biswas, S. K., Das, J., Karmakar, U. K., and Shill, M. C., Assessment Of Cytotoxicity And Antibacterial Activities Of Ethanolic Extracts Of *Kalanchoe Pinnata* Linn. (Family: Crassulaceae) Leaves And Stems . *IJPSR*, Vol. 2(10): 2605-2609. ISSN: 0975-8232

Chowdhury, K. A. A., Huq, M. E., Ali, S., Huq, I., Royhan, M. J., Adnan, Md., Chy. N. U., *et. al*., (2016) Antioxidant, cytotoxic and thrombolytic activity of leaves of *Kalanchoe pinnata* (LAM.) PERS. *Journal of Pharmacognosy and Phytochemistry.* 5(4): 309-315

Duraipandiyan, V., Ayyanar, M. and Ignacimuthu, S., (2006). Antimicrobial activity of some ethnomedicinal plants used by Paliyar tribe from Tamil Nadu, India. *BMC Complementary Alternative Medicine*. 6: 35 – 41.

Iqbal, A., Farrukh, A., and O. Mohammad, O., (2006). Modern Phytomedicine: Turning Medicinal Plants into Drugs. WILEY-VCH Verlag GmbH & Co. KGaA, Weinheim. Pp: 20 –21.

Kendeson, C. A., Kagoro, M. L., and Adelakun, E.A., (2021). Phytochemical And Pharmacological Evaluation Of Nigerian *Kalanchoe Pinnata* (Lam.) Stem-Bark *J. Chem. Soc. Nigeria,* Vol. 46, No.4, Pp 0751 – 0756

Mostofa, R, Ahmed, S., Begum, M., Rahman, S. M., Begum, T., Ahmed, U. S., Tuhin, H. R., Das, M., Hossain, A., Sharma, M., Begum, R., (2017). Evaluation of anti-inflammatory and gastricanti-ulcer activity of *Phyllanthus niruri* L. (Euphorbiaceae) leaves in experimental rats. *BMC Complement Altern Med*. 17:267

Mora-Pérez, A & Hernández-Medel, M. R., (2016). Anticonvulsant activity of methanolic extract from *Kalanchoe pinnata* (Lam.) stems and roots in mice a comparison to diazepam. *Neurología*. 31: 161 – 168.

Nwadinigwe, A. O., (2011). Antimicrobial activities of methanol and aqueous extracts of the stem of *Bryophyllum pinnatum* Kurz (Crassulaceae), Afr. J. Biotechnol. 10 (72): 16342 – 16346.

Ochei, J. and Kolhatkar, A., (2007), Medical laboratory science. Theory and Practice. 6th Ed. Tata McGraw-Hill publishing company ltd. Pp. 801 – 807

Sanchez, N. R., Garcia, D. A., Shiavini, M. S., Nakamura, C. V., and Filho, B .P. D., (2005). An evaluation of antibacterial activities of *Psidium guajava*. *Brazilian Journal of Biotechnology*, 48: 429 – 436.

Sarah, Q. S., Fatema C. A., and Misbahuddin, M., (2017) Brine shrimp lethality assay, *Bangladesh J Pharmacol*. 12: 186-189

Phyto-Pharmacological Activities of *Phyllantus amarus*: A Brief Overview

*[1,2]Garba, I. L., [2]Garga, M. A., and [1]Okunola, O. J.
[1]Department of Chemistry, Federal University Dutsin-Ma, Katsina State, Nigeria.
[2]National Biotechnology Development Agency, Bio-resources Development Centre, Katsina, Nigeria.
Corresponding Author's E-mail: iladan34@gmail.com Phone: +2348034708230

ABSTRACT
This study provides an overview of the phyto-pharmacological activities of *Phyllanthus amarus*. The plant is reported to have a lot of phytochemicals including alkaloids, flavonoids, terpenoids, saponins, and tannins etc. which are responsible for its pharmacological activities. Examining its medicinal properties reveals a spectrum of bioactive compounds with potent anti-inflammatory, antiviral, antileptospira, hepatoprotective effects, nephrotic effects, and other pharmacological effects. The plant's diverse therapeutic potential extends to many medicinal applications, making it a subject for various health applications. Understanding the multi-faceted phytochemistry and pharmacology of *Phyllanthus amarus* is crucial for harnessing its beneficial effects in the development of therapeutic functions. More than 510 compounds have been isolated, the majority of which are lignins, triterpenoids, flavonoids, and tannins. The researches of their remarkable antiviral, antioxidant, antidiabetic, and anticancer activities have become hot topics.
Keywords: Hepatoprotective, Antiviral, Anti-leptospira, Pharmacology.

INTRODUCTION
Herbs have long been essential to human health and are used to cure a wide range of illnesses (Verma *et al*., 2014). Since 80% of people worldwide still primarily rely on herbal remedies, the World Health Organization (WHO) has mandated that countries support and incorporate traditional medicine into their national healthcare systems (Salisu *et al*., 2022). Therefore, it is encouraged to use medicinal plants and herbs to treat both infectious and non-infectious disorders.
The plant *Phyllanthus amarus* (PA) belongs to the Euphorbiaceae family, which includes about 800 species that grow in tropical and subtropical regions of the globe. In Nigeria a country with three major languages, which involve Hausa, Igbo and Yoruba. *Phyllanthus amarus* (PA) is called "Geron tsuntsaye" (Hausa), "Eyin Olobe" (Yoruba), and "Ngwu" (Igbo) (Zubair *et al*., 2016). PA is an annual glabrous herb that branches, growing to a height of 30 to 60 cm. Its leaves are sub-sessile, elliptic-oblong, obtuse, and round in base. Its branching leaves are slender and leaf-bearing. The auxiliary flowers are yellowish, whitish, or greenish. The male flowers are grouped in groups of one to three, while the females are solitary. Fruits resemble longitudinal parallel ribs on the back and are depressed-globose in shape (Verma*et al*., 2014).

Figure 1: *Phyllantus amarus* (Patel *et al*., 2011)

The study of phytochemistry, a subfield of chemistry that evaluates the chemical makeup of plants and plant products (natural products chemistry), has revealed that many of the chemicals found in plants, such as lignans, carbohydrates, alkaloids, glycosides, terpenoids, and other secondary metabolites, are either therapeutically active or inactive (Ghosh *et al*., 2022). Flavonoids, one of the secondary metabolites found in PA, are polyphenolic compounds with different classes including flavones, chalcones, catechins, and their derivatives; in humans, they help prevent and treat a variety of pathologies that have been scientifically documented (Agati*et al*., 2012). Alkaloids, yet another secondary metabolite found in plants in PA, exhibit a range of pharmacological actions. Numerous alkaloids, such as securinine, epibubbialine, isobubbialine, and others, are found in PA. The compounds primarily carry out various antibacterial and other pharmacological actions (Ghosh *et al*., 2022). Using various methodologies, some additional phytochemicals found in PA are home to several classes of secondary metabolites that have been identified and demonstrated to have therapeutic benefits all around the world (Ghosh *et al*., 2022). Numerous medicinal uses for PA's therapeutic properties have been demonstrated, including hepatoprotective, antiviral, anti-inflammatory, anti-oxidant, anti-leptospira, anti-malaria, and anti-diabetic benefits among others (Islam *et al*., 2008).

Antiviral Activity

There have been reports of *Phyllanthus amarus* having antiviral properties against HIV, hepatitis B, and other viruses. The most effective mediators of the antiviral action were found to be ellagitannins, specifically geranin and corilagin. *In vitro*, tests were used to determine the methanolic extracts of PA's roots and leaves inhibitory effect on the NS3 and NS5B enzymes of the hepatitis C virus (Patel *et al*., 2011).

Anti-SARS-CoV2 (Covid-19)

A selected group of researchers have reported on the possibility of PA in inhibiting COVID-19 following the 2019/2020 pandemic. One study used molecular dynamics simulations to test 198 bioactive compounds from five chosen medicinal plants, including PA, which was previously shown to have antiviral properties against SARS-Cov-2 protease and two co-receptors. Astragalidin was found to be a superior candidate among the evaluated compounds for COVID-19 inactivation, suggesting that it would be a good option for the activity (Adejoro *et al*., 2020).

Antiamnesic Activity

In male Swiss albino mice, the effects of an aqueous extract of PA's leaves and stems were assessed for cognitive abilities and brain cholinesterase activity. Both young and old mice's memory scores improved in a dose-dependent manner when given PA at 50, 100, or 200 mg/kg. Additionally, PA effectively corrected the amnesia brought on by diazepam (1 mg/kg, i.p.) and scopolamine (0.4 mg/kg, i.p.). Remarkably, there was a decrease in brain cholinesterase activity by phyllanthin, an active ingredient of PA. The positive control was piracetam 400 mg/kg, intraperitoneally (Joshi and Parle, 2007).
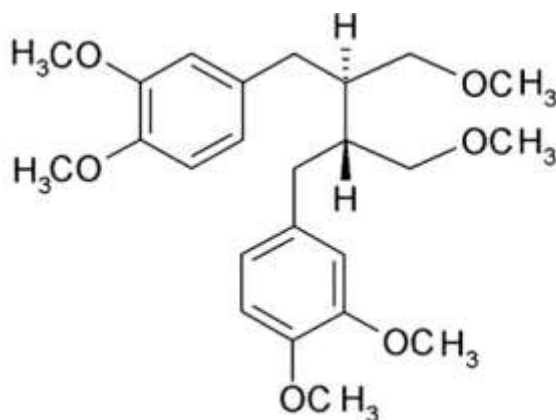

Figure 2: Chemical Structure of Phyllanthin Compound (Source: Huang et al., 2001)

Anticancer Activity

The MTS (3-(4,5-dimethyl thiazole-2-yl)-5(3-carboxymethoxyphenyl)-2-(4-sulfopheny)-2H-tetrazolium) reduction test was used to screen for cytotoxicity of the crude extracts (aqueous and methanolic) and their two fractions of PA. According to Patel *et al*. (2011), it was demonstrated to suppress the growth of MCF-7 (breast carcinoma) and A549 (lung carcinoma) cells, with IC_{50} values ranging from 56 to 126 µg/mL and 150-240 µg/mL for methanolic and aqueous extracts, respectively.

Figure 3: Showing the structure of Tetrazolium compound as Anticancer
Agent (Source: Huang et al., 2001)

Anti-leptospiral Activity

Leptospirosis is a serious disease that affects people worldwide and is primarily contracted through exposure to animal feces or environments contaminated with urine. By using the tube dilution technique or the microdilution test, PA's anti-leptospiral action has been studied. The outcome shows that the entire plant extract of PA, both in a methanolic and aqueous form, inhibits leptospira (Chandan and Sirasakthivelan, 2012). The underneath figure showed antileptospiral agent known as niranthin.
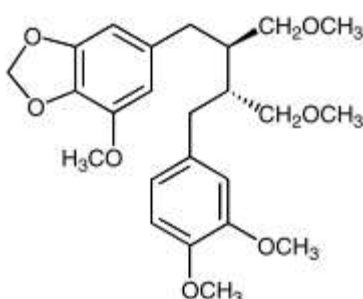
Figure 4: Niranthin Compound Isolated from *Phyllantus amarus*
(Source: Huang et al., 2001)

Hepatotoxicity Effect of *Phyllanthus amarus*

According to early research, the main lignin found in large quantities in PA leaves, phyllathin, is what reduces liver toxicity (Ogunmoyole*et al*., 2020). When the herb powder was administered to rats with ethanol-induced fatty liver, the efficiency of PA was seen. One study's findings demonstrated that giving mice aqueous leaf extracts of PA for a week significantly reduced the cytotoxic effects of lead nitrate and aluminum sulfate (Ghosh *et al*., 2022). The following structures are compounds isolated from PA that have hepatoprotective activities.
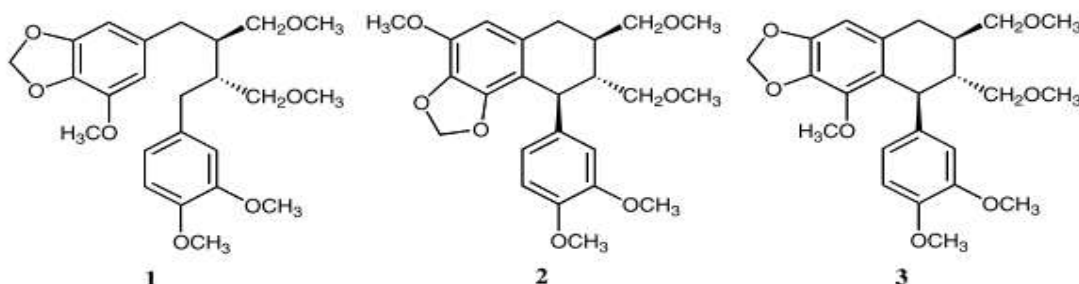
Figure 5: Showing Hepatoprotective Isolated Compounds (1) niranthin, (2) hypophyllanthin, and (3)   nirtetralin. (Source: Huang et al., 2001)

Effects of PA on Kidneys

The effects of oral administration of *Phyllantus amarus* aqueous extract, which is extensively used in African ethnomedical practice to treat urological disorders and kidney stones, on the kidneys of adult Wistar rats were meticulously examined in terms of histology. For 28 days, the rats in the treatment groups were given oral doses of 500 mg/kg and 1000 mg/kg body weight of PA aqueous extract. The kidneys were closely examined on the 29th day following the rats' sacrifice. According to the histological results, treated kidney sections displayed different degrees of tubular necrosis, mild-to-severe chronic inflammatory cell infiltration, and blood vessel hypertrophy in comparison to the control sections. According to the study's conclusion, adult Wistar rats' kidneys are negatively impacted by PA extracts in some ways (Eweka and Enogieru, 2011). Additionally, it was discovered that PA extract has a strong and efficient non-concentration-dependent inhibitory effect on the development of calcium oxalate crystals, which are the precursors of the majority of kidney stones (Calixto, 2000). Kidney stone removal with PA has been proven to be 94% successful (Eweka and Enogieru, 2011).

***Phyllanthus amarus* as anti-asthma**

Phyllanthin and hypophyllathin were detected in the methanolic extract of PA by HPLC analysis, with retention times of 25.243 and 26.832 minutes, respectively. The findings of this study demonstrated that, in a maurine model of asthma, the presence of phyllanthin and hypophyllathin in PA reduces the Th2 response in OVA-induced AHR by altering endogenous markers. Phyllanthin and hypophyllathin, therefore, may provide a novel therapeutic strategy for the treatment of asthma (Wu *et al*., 2018).

Antidiabetic Activity of PA

Monitoring hypo- and hyperglycemia is critical for the management of diabetes. A study conducted on 21 diabetic individuals who were not insulin-dependent and were administered aqueous extracts of PA demonstrated the plant's efficacious hypoglycemic properties. Additionally, it was discovered that methanolic extracts of PA exhibited antioxidant activity and, when given for 15 days to rats with alloxan-induced diabetes, produced a significant ($p<0.001$) drop in blood sugar (Ghosh *et al*. 2022). Aqueous preparations of the whole PA plant were tested for their hypoglycemic properties in diabetic Wistar rats who had been given alloxan. After 24 hours of oral treatment, the extracts at a dose of 260 mg/kg significantly ($p<0.05$) reduced blood glucose levels by 112%. At doses of 130 to 260 mg/kg of extract, there was a substantial ($p<0.01$) drop in blood glucose levels of 81 and 61% (day 7) respectively (Patel *et al*., 2011).

CONCLUSION

Decades of thorough clinical trials and the necessity to standardize *Phyllanthusamarus's* therapeutic potential have prompted an extensive scientific study on the plant. The plant may have significant biological medicinal potential, according to a compilation of studies on PA. It is firmly believed that all of the detailed information about PA included in this overview offers insight into how this plant can be used to treat a variety of illnesses and also investigates its potential applications in the pharmaceutical industry.

REFERENCES

Adejoro, I. A., Babatunde, D. D., and Tolufashe, G. F. (2020). Molecular Docking and Dynamic Simulations of some Medicinal Plants Compounds against SARS-Cov-2: An *in silicoistudy, Journal of Taibah University Science,* 14(1): 70-1563 DOI: 10.1080/16583655.2020.1848049

Agati, G., Azzarello, E., Pollastri, S., and Tattini, M. (2012). Flavonoids as Antioxidants in Plants: Location and Functional Significance, *Journal of Plant Science,* 196: 67-76

Calixto, J. B. (2000). Efficay, Safety, Quality Control, Marketing and Regulatory Guidelines for Herbal Medicines (Phytotherapeutic Agents), *Brazilian Journal of Medicines and Biological Research,* 3: 179-189.

Chandan, S., Sirasakthivelan, P. (2012). Screening of Antibacterial Activity of the Medicinal Plant *Phyllanthus amarus* against UTI causing Bacterial Pathogens, *Applied Journal of Hygiene* 1(3): 19-24

Eweka, A. O. and Enogieru, A. (2011). Effects of Oral Administration of *Phyllanthus amarus* Leaf Extracts on the Kidneys of Adult Wistar Rats: A Histological Study, *African Journal of Traditional and Complementary Alternative Medicine,* 8(3):307-311 DOI: 10.4314/ajtcam.v8i3.65294.

Ghosh, A. B. M., Banerjee, A. and Chathopadhyay, S. (2022).An Insight into the Potent Medicinal Plant, *Phyllanthus amarus*Schum. and Thonn., *Journal of The Nucleus,* 65: 437-472

Huang, R., Huang, Jun-Chih, Y., C., Chen, Feng-Lin H., and Chungming C. (2003) Screening of 25 Compounds Isolated from *Phyllanthus* Species for Anti-Human Hepatitis B Virus *In Vitro, Phytother. Res.* 17: 449–453

Islam, A., Mazumder, U. K., Gupta, M., and Ghosal, S. (2008). Phyto-Pharmacology of *Phyllanthus amarus,* an overview, *Pharmacologyonline,* 3: 202-209.

Joshi, H., Parle, M. (2007). Pharmacological Evidences for Antamnesic Potentials of *Phyllanthus amarus* in mice, *African Journal of Biomedical Research,* 10: 165-173.

Ogunmoyole, T., Awodooju, M., Idowu, S., and Daramola, O. (2020). *Phyllanthus amarus* Extract Restored Deranged Biochemical Parameters in Rat Model of Hepatotoxicity and Nephrotoxicity, PMCID: PMC7753912, 6(12): 1-10 DOI: 10.1016/j.heliyon.2020. e05670.

Patel, J. R., Tripathi, P., Sharma, V., Chauhan, N. S., and Dixit, V. K. (2011). Phyllanthus amarus: Ethnomedicinal uses, Phytochemistry and Pharmacology: A Review, *Journal of Ethnopharmacology,* 138: 286-313.

Salisu, A., M. Y. Iliyasu, M. R. Sahal, I. Titus, S. Isma'il, R. D. Umar, H. Tahir, Z. M. Kabeer, A. H. Idris, H. S. Musa and Agbo, E. B. (2022). Antimicrobial Potential of Syzygiumaromaticium (CLOVE) Extracts on Multidrug-Resistant (MDR) Uropathogenic Bacteria Isolated from Clinical Specimens in Bauchi, Nigeria, *Journal of Advances in Medical and Pharmaceutical Sciences,* 24(11-12): 41-57, 2022; Article no.JAMPS.95522 ISSN: 2394-1111

Wu, W., Li, Y., Jiao, Z., Zhang, L., Wang, X. and Qin, R. (2018). Phyllanthin and hypophyllathin from *Phyllanthus amarus* ameliorate immune inflammatory response in Ovalbumin-induced asthma: Role of IgE, NrF2, iNos, TNF-α, and IL's, Immunopharmacological and Immunotoxicology, 41(1): 1-10 DOI: https://doi,org/10.1080/08923973.2018.1545788.

Zubair, M., F., Atolani, O., Ibrahim, S., O., Adebisi, O., O., Hamid, A., A., and Sowunmi, R., A. (2017). Chemical Constituents and Antimicrobial Properties of Phyllanthus amarus (SCHUM & THONN), *Bayero Journal of Pure and Applied Sciences, 10 (1): 238-246.*

Physicochemical Parameters and Heavy Metals Analysis in Boreholes Water of Selected Locations in Dutsin-Ma Local Governmnent Area, Katsina State, Nigeria.

*Hassan Abdulkadir, Isah Yusuf Shinkafi and Ilyasu Gambo
Department of Chemistry, Federal University Dutsin-ma, Katsina State, Nigeria.
*Corresponding Author: nhassanabdulkadir@gmail.com Phone: +2349064924650

ABSTRACT
This study assessed the levels of some physicochemical parameters and determined the heavy metal concentrations of borehole water from some locations in Dutsin-ma local town. The water samples were collected from Bayan Area, Unguwar Kudu, and Unguwar Yamma and labeled as A, B, and C respectively. Physicochemical parameter such as pH, Electrical conductivity, TDS, Turbidity, and TSS was determined using standard analytical methods and compare with the permissible limit of WHO. The results obtained as pH (6.5 ± 0.10, 5.7 ± 0.10 and 6.5 ± 0.33), Electrical conductivity (9.9 ± 0.13 μs/cm, 27.8 ± 0.1 μs/c and 88.2 ± 0.31 μs/cm), TDS (5.03 ± 2.76 mg/L 14.10 ± 1.83 mg/L and 44.10 ± 0.14 mg/L), Turbidity (0.323 ± 1.50 NTU, 0.313 ± 2.41 NTU and 0.130 ± 2.15 NTU) and TSS (23.3 ± 2.49 mg/L, 16.1 ± 1.80 mg/L, and 13.1), Hardness (210 ± 5.9 mg/L, 196 ± 5.58 mg/L, and $179. \pm 7.21$ mg/L) for all the locations A, B and C respectively and found to be within the permicible limit, except pH level of sample B, and Hardness in sample C, which are below the standard limit set by WHO for drinking water. Heavy metals concentrations of (Cu, Cr, Mn, Zn) was also investigated using Atomic Absortion Spectrophotomer (AAS). The results obtained shows that the mean concentrations of Cu were (0.73 mg/L, 0.78 mg/L, and 0.71 mg/L), Cr (0.02 mg/L, 0.04 mg/L, and 0.10 mg/L), Mn (0.54 mg/L, 0.32 mg/L and 0.18 mg/L), and Zn (0.52 mg/L, 0.78 mg/L and 0.00 mg/l). Both metals concentratios are not within the permissible limit set by WHO with the exception of Cu, and Zn. Hence, the need for further investigations.
Keywords: Physicochemical Parameters, Borehole water, Heavy metals, WHO.

INTRODUCTION

Water supply systems and drinking water inaccessibility in developing countries is a global concern that calls for immediate action. About 884 million people in the world still do not get their drinking water from approved sources, and almost all of these people are in developing regions. Providing quality drinking water to all citizens who are deprived of access to water will serve as the breaking point of poverty alleviation in most developing countries, especially in Africa, where substantial amounts of national budgets are used to treat preventable water-borne diseases. Having reliable drinking water is now recognized by the United Nations as a human right (Samuel *et al.,* 2015). The major source of drinking water for the inhabitants of Dutsin-ma Local Government Area is the untreated groundwater obtained from drilled boreholes across the entire study area by non-governmental agencies and individuals. Hence, quality assessment of these borehole water samples has become necessary to provide firsthand information on their quality to ascertain their suitability as drinking water. Water is precious and necessary for a the sustainable economic development of an area as it is the next major support to life after air. In the urban areas where pipe-borne water, borehole water and hand-dug wells are available is an indication that water is a vital component of human existence. Groundwater is of major importance and is intensively exploited for private, domestic and industrial use Pollution of groundwater is an impairment of water quality by chemicals heat or bacteria to a degree that does not necessarily create public health hazards, but does adversely affect such water for domestic, farm, municipal or industrial use. Trace elements are generally present in small concentration in natural water systems, their occurrence in groundwater and surface water can be due to natural sources such as the dissolution of naturally occurring minerals containing trace elements in the soil zone or the aquifer material or to human activities such as mining, fuels, smelting of ores and improper disposal of industrial wastes (Musa *et al.,* 2013). Heavy metal is a generic term that describes the group of metals and metalloids with an atomic density greater than 4g/cm3 or 5 times or more, greater than water. Heavy metals have little to do with density but concern chemical properties. However, lead, cadmium, mercury and arsenic are the main threats to human health when exposed to them (Njar *et al.,* 2012). Some metals are essential to sustain life-calcium, magnesium, potassium and sodium must be present for normal body functions. Also, cobalt, copper, iron, manganese, molybdenum and zinc are needed at low levels as catalyst for enzyme activities, however, excess exposure to heavy metals can result in toxicity (Adumanya *et al.,* 2013). Pollution of water bodies with heavy metals from a variety of sources is becoming a matter of global concern. Though the effects of chemical contamination of drinking water are not felt on a short-term basis (except nitrate), their accumulation over a long period in the body has significant health effects (Raji *et al.,* 2010).

MATERIALS AND METHODS
Water Sample Collection and pre- treatment
Water samples were collected from designated sampling points as indicated in the Table 1 below at 5 mins intervals. Before sampling, the bottles were rinsed with deionized water and then three times with the sample water. The Samples were labeled with the date of collection and sampling points, transported to the laboratory, and kept for analysis (Kumar *et al.,*2015).The water samples for heavy metals determination were preserved by the addition of $5cm^3$ diluted HNO_3 acids to each liter of sample to adjust pH to 2 and also to prevent metals from adhering to the wall of the containers. The samples were stored in a refrigerator at about 4°C before analysis (Anuo *et al.,* 2012).

Table 1: Sample Locations

Sample location	Labeled
Bayan Area Borehole	A
Unguwar Kudu	B
UnguwarYamma	C

Determination of the Physicochemical Parameters
Determination of pH
The samples were transferred into a clean dried glass beaker, then the electrodes of the standardized pH meter were immersed and the meter was allowed to be standardized, after which the reading was taken. The electrode was rinsed well with distilled water and tabbed slightly with tissue paper after each test as described by Geotechnical Engineering Bureau, 2007.

Determination of conductivity and total dissolved solid (TDS)
Electrical conductivity was measured using a combined TDS/Conductivity meter by shifting one of the four buttons of the instrument. Before measuring, the probes were rinsed with distilled water. Then the probe was immersed in a beaker containing the water sample and moved up and down taped on the beaker to be free from any bubbles. The data was recorded for each sample. (ASTM,2004).

Determination of Turbidity
The sample of the borehole water was transferred into the sample cell turbidity meter up to the horizontal mark, then wiped with tissue paper and subsequently placed in the turbidity meter such that the vertical mark in the sample cell coincided with the mark in the turbidity meter, after which it was covered. The reading was displayed on the screen and was recorded, as described by (NITTRC, 2009)

Determination of Total Suspended Solids   (TSS)
A Whatman (125 mm) filter paper was weighed accurately and place in a funnel; 50 ml of water sample was measured using a measuring cylinder and filter, transferring all the solids to the filter paper. The residue was washed with about 20 mL of distilled water. The filter paper was removed carefully and dried in an oven at $103-105^0C$ to a constant weight and the filter paper was allowed to cool in a desiccator and weighed.

Determination of total hardness of water
2 ml of ammonia buffer solution and 1 tablet of Erichrom black T were aadded to each of the 100 ml of the samples of the borehole water. The mixture was titrated against EDTA, until a blue end point was observed (APHA, 2005).

Determination of Chloride (Cl)
2 drop of potassium chromate indicator was added to each of the 100 ml of the borehole water samples and titrated with 0.01 N $AgN0_3$ until pinkish yellow colour was observed. The pH of the water samples can be adjusted with dilute H_2SO_4 (If not between 7 and 10). Or adjusted up with 2N NaOH (APHA, 2005)

Heavy Metals Determination
Sample digestion
5.0 ml of nitric acid was added to 100 mL of water sample in a 250 mL conical flask, the mixture was evaporated to half of its volume on a hot plate after which it was allowed to cool and then filtered as described by Momodu *et al.,* 2009. The digested water samples were analyzed for the presence of lead (Pb), Manganese (Mn), Chromium (Cr), Zinc (Zn), and Copper (Cu). Using Atomic Absorption Spectrophotometer (AAS) (BULK Scientific/210VGP model).

Where the machine gives out the absorbencies of each metal, the concentration of each metal was then determined by interpolation from its standard calibration curves (Alghamdi *et al*., 2023).

RESULTS AND DISCUSSION
Table 2: Physicochemical Parameters of Borehole Samples Collected from A, B and C Locations

Parameters	Units	Samples			WHO Limit
		A	**B**	**C**	
pH		6.5$\pm$0.10	5.7$\pm$0.10	6.5$\pm$0.33	6.5 8.5
Conductivity	μs/cm	9.9$\pm$0.13	27.8$\pm$0.10	88.2$\pm$0.31	400
TDS	mg/L	5.03$\pm$2.76	14.10$\pm$1.83	44.10$\pm$0.14	1000
Turbidity	NTU	0.323$\pm$1.50	0.313$\pm$2.41	0.130$\pm$2.15	<5
TSS	mg/L	23.3$\pm$2.49	16.1$\pm$1.80	13.1$\pm$1.82	50
T Hardness	mg/L	210$\pm$5.97	196$\pm$5.58	179.$\pm$7.21	200

pH
pH is classified as one of the most important water quality parameter as it relates to the acidity or alkalinity of the water. The results of pH levels in samples A, B and C were presented in Table 1.0, the result showed that all the samples pH level falls within the WHO recommended range value of 6.5-8.5. With the exception of samples collected at Unguwar Kudu, in which the pH level was found to be 5.7, which is slightly below the recommended level set by WHO. This could be attributed to acid rain, sewage, and industrial waste dumping through leaching into the soil which ultimately increases the soil acidity and consequently lowers the pH.

Conductivity
Electrical conductivity is the measure of the dissolved ionic components in water which indicates the electrical characteristics of the total dissolved components in water. The conductivity measurements showed that all the sampling sites have conductivity lower than the maximum level of 400 μs/cm set by the WHO. This could be attributed to less accumulation and leaching of dissolved inorganic solid materials (Adnan *et a.,* 2010). The highest and lowest conductivities are 88.2 and 9.9 recorded in Unguwar Yamma and Bayan Area respectively.

Total Dissolved Solids (TDS)
Total dissolved solid is due to the presence of dissolved salts which consequently causes undesirable taste. According to the result, all sampling sites have TDS levels lower than the maximum allowable level set by WHO of 1000 mg/l. The highest TDS value of 44.10 mg/l and the lowest TDS value of 5.03 mg/l correspond to samples from Unguwar Yamma C and Bayan Area A respectively.

Turbidity
Higher level of turbidity is associated with disease-causing bacteria, and suspended materials due to soil runoff. (United States Environmental Protection Agency 2017). The turbidity recorded in all the water samples is within the recommended level of 5 NTU as set by WHO for drinking water.

Total Suspended Solid (TSS)
The maximum recommended Total Suspended Solid (TSS) safe limit set by the World Health Organization (WHO) is 50 mg/L. The TSS values of all the samples were found to be within the permissible limit set by WHO. The TSS values of all the samples as illustrated in Table 1.0, are 23.3 mg/L, 16.1 mg/L, and 13.1 mg/L for Bayan Area, Unguwar kudu, and Unguwar Yamma samples respectively. The average TSS value of the samples under study is 13.1 mg/L which is also within the WHO (2011) set limit. The water in the area is therefore good for drinking and other purposes based on the content of TSS.

Total Hardness
The Hardness of water is a measure of its capacity to form precipitates with soap and scales with certain anions presents in the water. The hardness concentration values ranged from 210 $-$179 mg/L. According to WHO international standard for drinking water classified water with a total hardness of $CaCO_3$ less than 50 mg/L as soft water and 50$-$150 mg/L as hard water. Based on this classification, the total hardness of the analyzed water sample

from the borehole in Dutsin Ma Town could be grouped as hard water considering the values obtained in the analysis even though it is within the WHO permissible limits of 200 mg/L.

Heavy Metals Determination
Table 3: Mean Concentrations of Heavy Metals

Metals	Units	Samples			WHO Limit (2011)
		A	B	C	
Cu	mg/L	0.73±0.12	0.78±0.34	0.71±0.02	1.0
Cr	mg/L	0.02±0.03	0.04±0.06	0.10±0.06	0.05
Mn	mg/L	0.54±0.07	0.32±0.07	0.18±0.07	0.05
Zn	mg/L	0.52±0.53	0.78±0.15	0.73±0.11	5.0

Copper (Cu)
The concentrations of copper in all the water samples were found to be 0.73 mg/L, 0.78 mg/L, and 0.71 mg/L for A, B and C locations respectively. All water samples from the areas are within the 1.0 mg/L standard limit for drinking water, as recommended by the WHO. This agrees with the finding of Hassan and Mohammed (2023), who reported lower concentration of Zn and Cu. This element is present naturally with iron deposits but more often its presence in water is due to an attack on copper pipes (Uchhariya, *et al*, 2012) A higher level of copper in drinking water may impart a stringent taste and can cause a gastrointestinal disorder.

Chromium (Cr)
The concentration of chromium determined in the water samples from the study areas were 0.02 mg/L, 0.04 mg/L, and 0.10 mg/L. Water samples analyzed from Unguwar Yamma had values above the WHO standard limit for drinking water which is 0.05 mg/L. This may be as a result excessive dying and other agricultural activities in the area. Water samples from Bayan Area and Unguwar Kudu are good for drinking as the level indicated. Higher level of chromium in drinking water is found to cause cancer and are lethal to the healthy well-being of human especially at the a concentration above 1.0 mg/L.

Manganese (Mn)
Manganese is An ores and rocks was constituent which is widely distributed naturally. It is a vital element for biological system whose chemical behavior is a function of pH, oxidation and reduction reactions. The concentration of manganese in all the water samples was found to be 0.54 mg/L, 0.32 mg/L and 0.18 mg/L for Bayan Area, Unguwar Kudu, and Unguwar Yamma respectively. All water samples from the study area are not within the 0.05 mg/L standard limit for drinking water as recommended by the WHO. Effects of high manganese concentration in water include (1) metallic and unpleasant taste to water, (2) blackish staining of laundry and plumbing fixtures and (3) formation of darkish scales in water pipes. However, no record of excess manganese health risk has been recorded in humans.

Zinc (Zn)
The concentration of Zn in the samples was found to be 0.52 mg/L and 0.78 mg/L in samples A and B). This is in agreement with the finding of Dohare *et al*, (2014) reported approximately 0.5 g/kg of zinc to be present naturally in the earth crust All values obtained were within the 5.0 mg/L standard limit for drinking water, as recommended by the world health organization. This could be becouse the zinc in its natural mineral form (sphalerite) did not dissolve into underground water bodies via leaching in all the study areas. However, medical experts have reported electrolyte imbalance, vomiting, acute renal failures and abdominal pain as symptoms of excessive exposure of humans to zinc.

CONCLUSION
The findings of this study show that, several parameters tested were within the standard permissible limit set by WHO except for pH level at (Unguwar Kudu sample B) and hardness level at (Bayan Area which is sample A). it was also found that the heavy metals concentrations investigated shows (Cu, Mn, Cr and Zn,) are above the permissible limits except for Cr and Zn at (Unguwar Yamma sample C) which are below the standard limit set by WHO for drinking water. Hence routine monitoring and public enlightenment should be enforced to ensure adherence to drinking water standards, and other sources of potable water for domestic uses should be provided to the community.

REFERRENCES

Alghamdi, M. A., Hassan, S. K., Al Sharif, M. Y., Khoder, M. I., and Harrison, R. M. (2023). Pollution characteristics and human health risk of potentially toxic elements associated with deposited dust of sporting walkways during physical activity. *Atmospheric Pollution Research,* 101649https://doi.org/10.1016/j.apr.2023.101649

Anuo,A.U,Egereonu U.N.J, and Egereonu, J.C. (2012). Comparative Analysis of the Degree of Pollution of Okintankwo River along Border Communities, Mbaitoli, Ekeduru, Emekuku, and Ultra of Imo State Nigeria. *Analytical Science Journal*. **1**(1):9-14.

ASTM(2004). American society for testing materials Annual book of Standard Water and environmental technology. Vol.11 Pg 22-132.

Geotechnical Engineering Bureau (2007):Test Method for Determination of pH Value of Water or Soil by pHMeter.NewYork.

Hassan, N. E., and Mohammed, S. J. (2023). Assessment of Ground Water Pollution by Heavy Metals in Some Residential Areas in Kurdistan Region of Iraq. *Environmental Science and Architecture*.**2**. Pp. 35-44.

Ibrahim,Y.E. Nuraddeen,A.M.(2014): An Assessment of Some Water Quality Properties of Groundwater in Dutsin-MaMetropolis.

Kumar, S.N.C. Ghosh, R.P. Singh, M.M. Sonkusare, S. S., and Sanjay M., (2015). Assessment of Water Quality of Lakes for Drinking and Irrigation Purposes in Ibom State, Nigeria. *African Journal of Environmental Science and Technology*.**8** (7),

Musa, O.K., Shaibu, M.M., and Kudamnya, E.A., (2013). Heavy Metal Concentration in Groundwater around Obajana and its Environs, Kogi State, North Central Nigeria. *American International Journal of Contemporary Research*.Vol.3 No.8.

Njar, G.N., Iwara, A.I., Offiong, R.A., and Deekor, T.D., (2012). Assessment of Heavy Metal Status of Boreholes in Calabar South Local Government Area, Cross River State, Nigeria. *Ethiopian Journal of Environmental Studies and Management*. Vol.5 No1.

Raji, M. I. O, Ibrahim, Y. K. E and Ehinmidu, J. O.,(2010). Physico-Chemical Characteristics and Heavy Metal Levels in Drinking water Sources in Sokoto Metropolis in North Western Nigeria. *Journal of Applied Sciences and Evironmental Management*.ISSN1119-8362.Vol.14 (3) Pp81-85

WHO, (2011). Drinking Water Quality Guideline 4th Edition. World Health Organization Geneva, Switzerland. Pp. 1-28.

Role of Effective Earth Radius Factor in Radio Communication in Dutse, Nigeria

[1]Akinsanmi Akinbolati, *[1,2]Sabiru Aminu Yaradua, and [1]Florence N. Ikechiamaka

[1]Department of Physics, Federal University Dutsin-ma
[2]Department of Physics, Umaru Musa Yaradua University Katsina
 *Corresponding Author's E-mail: aminusabiru@gmail.com, aminu.sabiru@umyu.edu.ng Phone:+2347036043538

ABSTRACT
When planning and designing a radio system, it encounters a setback that makes the signals weaker and limits their range. To avoid or minimize these issues, it's crucial to carefully consider certain secondary radio climatic factors. This research studied the effective earth radius factor (k-factor) and its propagation effect on satellite communication over the city of Dutse, Jigawa State.Secondary data of forty-one years (1980-2020) of temperature, pressure rainfall and humidity at the surface 12, 100 and 250 m above ground level retrieved from the European Centre for Medium-Range Weather Forecasts (ECMRWF) ERA-5. The k-factor was computed and analyzed using the latest ITU-R Models. The range of the mean values of the k-factor of the twelve months at the location of the study is 4.44395-1.82210 where the largest and least values are obtained at September and February. It was observed that secondary radio-climatic variables exhibit seasonal type dependence, during the dry season, the k-factor varies from 2.38011 to 1.82210, with maximum and minimum values in November and February, respectively. The average dry season k-factor over forty-one years is 1.97818, pointing to significant super-refraction in radio signal propagation during these seasons. During wet season months, the k-factor varies from 4.44395 to 2.08349, with maximum and minimum values occurring in September and April. The average wet season k-factor over forty-one years is 3.21266, implying a predominantly super-refractive situation in radio signal propagation. This indicates that k-factor values were observed to be higher during the wet season compared to the dry season months, indicating significant variations in the regions' moisture conditions.
Keywords: k-factor, Dry Season, Wet Season, and Super Refraction

INTRODUCTION

In an era defined by unprecedented technological advancements, radio transmission remains a fundamental component of worldwide interconnectedness. But as much as we may take it for granted, signal transmission is not always smooth, especially in light of today's obstacles. The landscape of radio communication is evolving at an astonishing pace, bringing forth challenges that demand innovative solutions (Abu-Almal and Al-Ansari, 2010; Ojo et al., 2017). The modern radio engineer confronts several challenges, ranging from dealing with signal interference in crowded metropolitan settings to fending off disturbances from the environment. The climatic conditions in the troposphere have a significant impact on radio signal transmission. Radio transmissions are significantly impacted by meteorological events, which are frequently powerful and unpredictable. The quality and dependability of radio transmission may be greatly impacted by variables including temperature fluctuations, air pressure, relative humidity, atmospheric moisture content and effective earth radius factor. Resilient communication systems depend on an understanding of the complex interaction between climatic conditions and signal transmission. (Akinbolati and Ajewole, 2020; Ukhurebor, and Azi, 2018, Adelakun et al., 2020 and Faruk et al., 2013).

The effective earth radius factor (k-factor) is one of the key variables affecting radio wave propagation. This characteristic is crucial in influencing the power and range of radio broadcasts since it is closely related to the Earth's curvature and atmospheric conditions. It is yet another crucial factor in determining how radio wave propagation will behave. Additionally, climatic parameters are used to obtain it. Examining the subtleties of this component reveals the complex interplay between the natural world and artificial technology, providing information about how to best optimize communication networks for dependability and efficiency .In the places where the value of the k-factor is unknown, k-factor is taken to be the 1.33 as it is recommended by ITU-R (2019). Numerous studies have demonstrated that its worth varies depending on the area and shouldn't be taken for granted everywhere. (Ojo et al., 2017).

Knowing the Effective Earth Radius Factor for a study location is crucial in the field of radio communication engineering. Adapting communication systems to the physical and climatic characteristics of a certain region guarantees the smooth exchange of information as well as the ability to endure unfavorable circumstances. (Afullo et al.1999)

This research employed secondary data spanning forty years that included air temperature, relative humidity, and atmospheric pressure at three distinct altitude levels. The information comes from city of Dutse, Jigawa States. The k-factor over the territory and its use for wireless communication over the region were determined and analyzed using the collected data.

MATERIALS AND METHODS
Input Data
This study was conducted in Dutse that is located at North-Western parts of Nigeria. Secondary atmospheric data of temperature, pressure and humidity at the surface 12m, 100m and 250m above ground levels for Dutse was retrieved from the European Centre for Medium-Range Weather Forecasts (ECMWF) ERA-5 in December 2021. The data of the Meteorological parameters are of the period of forty years (1980-2020).

Theoretical Background
Radio refractivity N is a measure of changes in refractive index n of air from unity. N is a dimensionless quantity defined in (1) and measured in N-units.

$$N = (n - 1) \times 10^6 \tag{1}$$

The radio refractivity N can be expressed in terms of meteorological variables as (Varma et al., 2011):

$$N = \frac{77.6}{T}\left(P + 4810\frac{e}{T}\right)(N\text{-}units) \tag{2}$$

The k-factor can be derived from the vertical refractivity gradient, ΔN, in the first kilometer above the ground; ΔN is obtained from two refractivity values as:

$$\frac{dN}{dh} = \frac{N_2 - N_1}{h_2 - h_1} \tag{3}$$

where N_1 and N_2 are the refractivity values at heights h_1 and h_2, respectively. In this study h_1 and h_2 are at the surface (12 m) and 100 m Above Ground Level respectively. The k-factor can be expressed as indicated in equation (4) amd (5) (Abu-Ahmal and Al-Ansari, 2010; Ojo et al., 2017)

$$k = \frac{1}{\left(1 + a\left(\frac{dN}{dh}\right)\right)} \tag{4}$$

where a is the radius of the earth given in either kilometers km or nautical miles (nmi), (a = 6371 km = 344 mni) and $\frac{dN}{dh}$ is the rate of change of refractivity indices with height. k-factor can also be expressed as indicated (8). This was used for k-factor computations in this work.

$$k = \frac{1}{1 + \frac{\left(\frac{dN}{dh}\right)}{157}} \tag{5}$$

Equations (3) and (5) were used to determine the values of refractivity gradient, and effective earth radius factor (k-factor) in the study location.

ITU-R Recommendation on k-factor
The ITU-R Recommendation on k-factor, and associated propagation effects are as presented in Table 1. The determined values of k-factor obtained for the years and seasons were compared with ITU-R standard such as to predict the refractive propagation effects over the study areas.

Table 1: ITU-R standards on k-factor and the associated propagation effects (ITU-R, 2019); (Ukhurebor et al., 2018)

k – factor's range of values	Refractive Condition of the atmosphere	Propagation effect on radio communications
$k = 1.33$	Normal refraction or standard atmosphere	In This case, radio signals are transmitted along a straight line part on the earth's surface and go into space unimpeded
k<1.33 but k>0	Sub-refraction	Here, the radio wave (signal) propagates abnormally away from the earth surface, resulting to interference and coverage limitation
$\infty > k > 1.33$	Super-refraction	Here, the radio wave signals (e. g microware link, signals, GSM signals, satellite signals) spread irregularly toward the earth's surface, thus, extending the radio horizon and merge the path

		clearance giving rising to irregular huge waves above the line of view due to multiple reflection
$-\infty < k < 0$	Ducting condition	Here, there is ducting which make the radio waves to bend downwards with a curvature greater than the earth's. The radio signals can become trapped between a layer in the lower atmosphere and the surface duct which is the earth's or sea's surface which is the elevated duct.

RESULT AND DISCUSSION
k-factor at Study Location
The k-factor was computed for the period of forty one years. Figure 1, shows the k-factor of the study location. The k-factor starts with steady values at the first three months i.e., from January to March, then it increased steadily from March up to September or October where it reaches its peaks level, some few trends reaches its peak at November. The k-factor then rapidly decreases and by December it returns back to values that are approximately similar with the initial one of the first three months of the year.
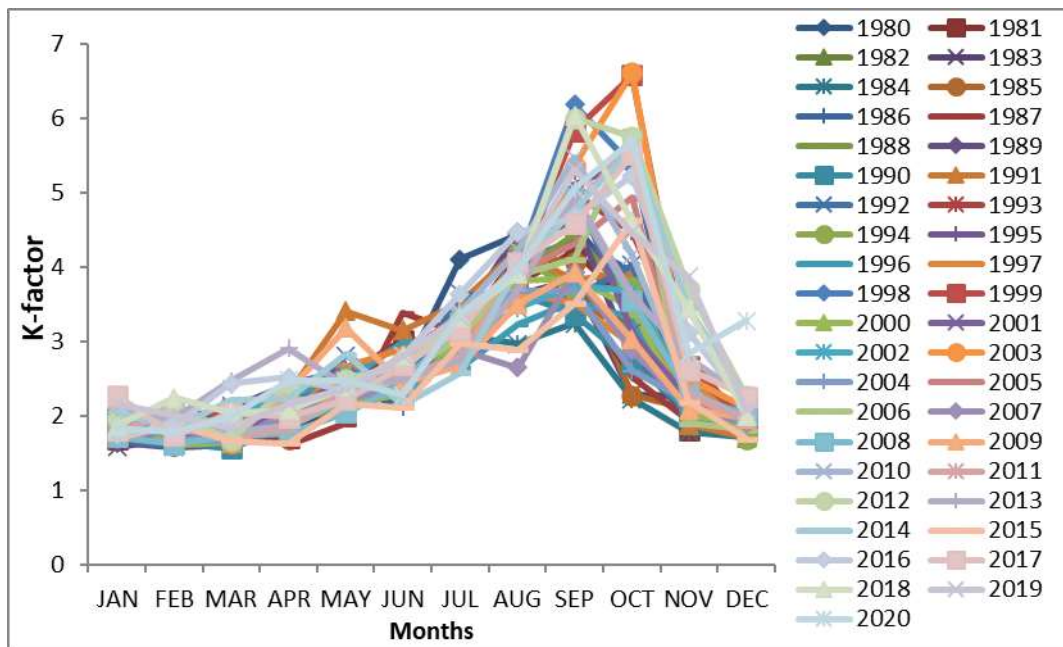

Figure 1: Monthly k-factor for the period of forty one years at the Study Location

Mean Climatic Variation of k-factor
The mean effective earth radius factor (k-factor) of Dutse, is depicted in Figure 2 below. The figure shows that k-factor remains constant during the first two months of the year followed by continuous increases until September. Subsequently, it starts to decrease for the remaining months.
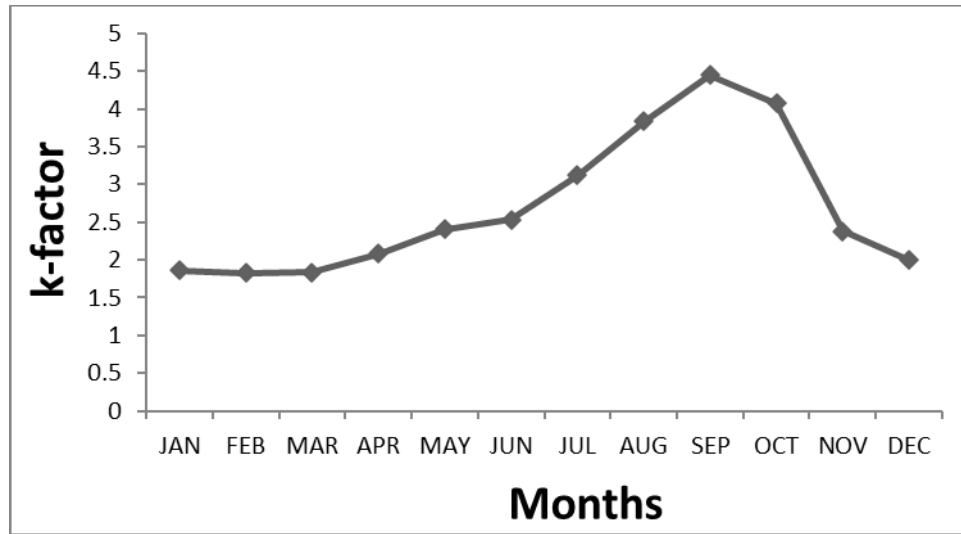
Figure 2: Mean k-factor at (the Study location

The range of the mean values of k-factor of the twelve months at the location of the study is 4.44395- 1.82210 where the first and second highest values are 4.44395 and 4.07410 of the month of September and October, then followed by 3.83212 of August respectively. The least mean value is 1.82210 and it is acquired in February.

Seasonal Variation of k-factor

Figure 3(a) shows the variation of k-factor during dry season of the study area. The k-factor varies from 2.38011 to 1.82210, with maximum and minimum values in November and February, respectively. The average dry season k-factor over forty-one years is 1.97818, pointing to significant super-refraction in radio signal propagation during this season.

These variations at different periods of time are essential in understanding the dynamics of the study location`s dry seasons and their radio signal communication implications.
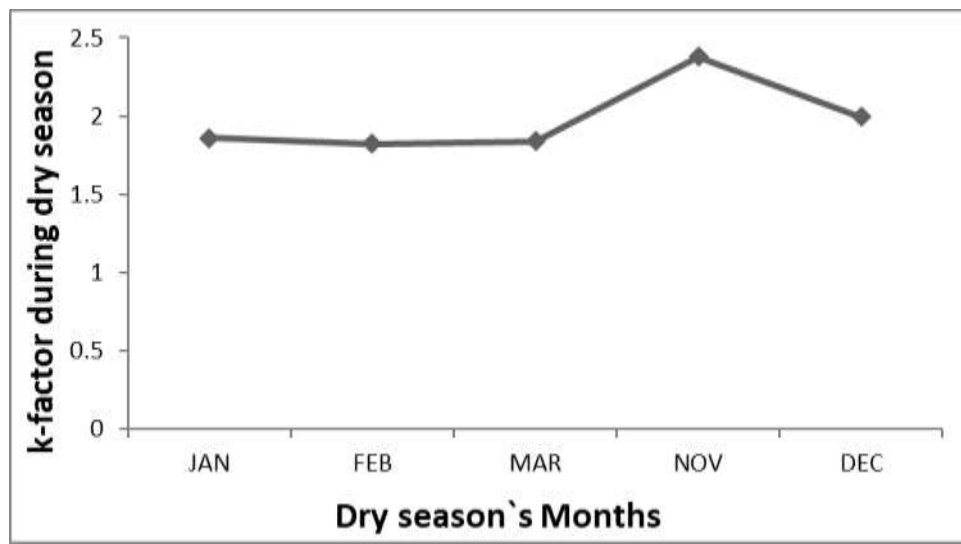
(a)
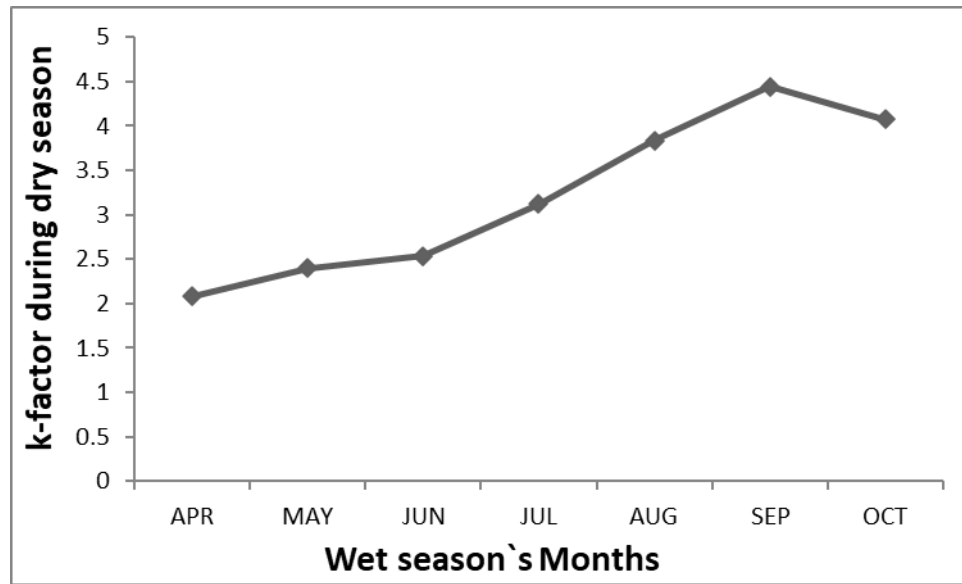
(b)

Figure 3: The mean values of k-factor during (a) the dry season months and (b) wet season months over each of the study Area

Figure 3(b) shows the results of the k-factor mean values for wet season months over the study area. The k-factor varies from 4.44395 to 2.08349, with maximum and minimum values occurring in September and April. The average wet season k-factor over forty-one years is 3.21266, implying a predominantly super-refractive situation in radio signal propagation.

Notably, higher k-factor values were observed during the wet season compared to the dry season months, indicating significant variations in the regions' moisture conditions.

CONCLUSION

In the pursuit of establishing robust and efficient radio communication systems, this study delved deep into the secondary radio climatic factors, particularly focusing on the effective earth radius factor (k-factor) over the city of Dutse, Jigawa State. The meticulous analysis of forty-one years of meteorological data, spanning a range of altitudes, offered valuable insights into the seasonal nuances that govern radio signal propagation dynamics. The careful examination of 41 years' worth of meteorological data over the surface 12m, 100m and 250m above ground levels for Dutse provided insightful information on the seasonal variations that control radio signal propagation dynamics. The k-factor demonstrated a seasonal pattern, ranging from 2.38011 to 1.82210 during dry months, indicating super-refractive conditions, and from 4.44395 to 2.08349 during wet months, denoting predominantly super-refractive propagation. These findings emphasize the critical impact of moisture content on signal efficiency. By understanding these nuanced variations, radio engineers can design adaptive systems, ensuring reliable communication in diverse climatic conditions. This research not only enriches our understanding of radio signal dynamics but also provides essential data for the strategic development of communication networks.

REFERENCES

Abu-Almal, A. and Al-Ansari, K. (2010) "Calculation of effective earth radius and point refractivity gradient in UAE". *International Journal of Antennas and Propagation.* Vol.2010, Article ID 245070.

Adelakun. A.O., Ojo, J.S., and Edward, V.O., (2020) "Quantitative analysis of Complexity and non- linear trend of radio refractivity gradient in the troposphere" *Advances in Space Research*, 59 (12), 2611-2515

Afullo, T. J., T. Motsoela, and D. F. Molotsi, (1999) "Refractivity Gradient and K-factor in Botswana, Radio Africa," 107-110.

Akinbolati, A., and Ajewole, M. O. 2020. "Investigation of Path Loss and Modeling for Digital Terrestrial Television over Nigeria," *Elsevier Heliyon, e04101*, , https://doi.org/10.1016/j.heliyon.2020.e04101

Faruk, N., Ayeni, A.A., and Adediran, A.Y., (2013) "On the study of empirical path loss modelsfor accurate prediction of TV signal for secondary users*." Progress in Electromagnetic Research B,* pg 1–5.

International Telecommunications Union Recommendation, ITU-R, (2019) The Refractive Index: It's Formula and Refractivity Data, ITU Radio Communication Assembly, ITU-R P—Series, No. 453-14.

Ojo, O. L., Ojo J. S. and Akinyemi, P. (2017) "Characterization of Secondary radioclimatic variables for microwave and millimeter wave link design in Nigeria", *Indian Journal of Radio and Space Physics,* vol.46, pp.83-90

The European Centre for Medium-Range Weather Forecasts (ECMWF) ERA5, (2021)

Ukhurebor, E.K. and Azi S.O (2018)"Review of Methodology to Obtain Parameters for Radio Wave   Propagation at Low Altitudes from Meteorological Data: New Results for Auchi Area in Edo State, Nigeria, "*Journal of King Saud University – Science,*. (doi: https://doi.org/10.1016/j.jksus.20 18.03.001).

Valma, E., Tamosiunaite, M. Tamosiunas, Stasys & Tamosiuniene, M & Zilinskas, M. (2011). "Variation of Radio Refractivity with Height above Ground." *Electronics and Electrical Engineering.* 111. 10.5755/j01.eee.111.5.349.

Assessment of Health Risks Associated with Heavy Metals in Sediment from Hand- Dug Wells in Katsina Metropolis, Nigeria

[1]Uduma, A. U., [1]Okunola, O. J., [1]Aminu Kabir and [2]Jacob A. G.

[1]Chemistry Department, Federal University Dutsin-Ma, P.M.B. 5001, Katsina State, Nigeria
[2] Industrial Chemistry Department, Federal University Dutsin-Ma, P.M.B. 5001, Katsina State, Nigeria

ABSTRACT
The present study was conducted to evaluate the level of contamination of heavy metals   concentration (Zn, Pb, Fe, Cu, Mn, Ni, Co and Cr) in the sediment samples using Atomic Absorption Spectrophotometer (AAS) from 5 selected hand-dug wells within Katsina metropolis. Results revealed that concentrations of the heavy metals in sediment ranged from 0.06 ± 0.001 to 2.86 ± 0.15mg/Kg for Zn, 0.10 ± 0.008 to 0.33 ± 0.014 mg/Kg for Pb, 13.73 ± 0.27 to 552.43 ± 13.55mg/Kg for Fe, 0.15 ± 0.001 to 5.85 ± 0.012mg/Kg for Cu, 0.11 ± 0.001 to 10.73 ± 0.11mg/Kg for Mn, 0.05 ± 0.008 to 0.60 ± 0.006mg/Kg for Ni, 0.02 ± 0.004mg/Kg for Co and 0.29 ± 0.19 to 5.02 ± 0.017mg/Kg for Chromium. These metal concentrations were within the permissible limits set by WHO and other regulatory agencies. Descriptive statistics was applied on the data set generated to analyze the mean and standard deviation. Other statistical tools such as analysis of variance (ANOVA), Pearson Product Moment Correlation, Cluster analysis and Duncan's Multiple Range Test (DMRT), were utilized in evaluating the significant differences within the parameters evaluated. The human health risk assessment in this study classifies the selected hand dug wells as safe with regards to human exposure to the heavy metals in which the Hazard Quotient (HQ) and Hazard Index (HI) were < 1, indicating that there is no health risk associated with the hand dug wells. However, despite the low levels of the metals in this work compared to other literatures, they could still lead to serious health hazard in future if not checked, considering their bioaccumulation effects in humans and other living organisms in the environment.
Keywords: Heavy Metals, Sediment, Health Risk Assessment, Hand Dug Wells, Katsina Metropolis

INTRODUCTION

Heavy metals refer to any metabolic chemical element that has a relatively high density of 5 g/cm^3 and is poisonous at low concentration (Alizaveya *et al*., 2006). Heavy metals are some of the major chemical pollutants that have lasting effects on the natural balance in aquatic ecosystem. They are serious environmental problem in the aquatic environment and sediment is the ultimate sink of that contaminant (Huang *et al*., 2009; Emara *et al*., 2015). The chemical pollutants are not biodegradable, so they can affect the environment adversely for a long time. Biodegradability means the ability for the pollutants to be removed from the environment overtime through natural biological processes (Travizani *et al*., 2016). In the aquatic system, heavy metals tend to accumulate in the bottom sediment and become concentrated in biota, in other words, they bio accumulate in aquatic organisms.

The aquatic ecosystem is the ultimate recipient of almost everything including heavy metals. Pollution of heavy metals in aquatic environments is a growing problem worldwide and currently it has reached an alarming rate. Conversely, metals also occur in small amounts naturally and may enter into the aquatic systems through leaching of rocks, air-bone dust, forest fires and vegetation (Fernandez *et al*., 2008).

Also as heavy metals cannot be degraded, they are continuously being deposited and incorporated in water, sediment and aquatic organisms (Zheng *et al*., 2008). Thus causing heavy metal pollution in water bodies. The pollution of heavy metals is an important cause of soil degradation. The danger of heavy metals, unlike other pollutants lies in their being non-degradable and the accumulation in the earth's surface may pile up in the body of human body directly or indirectly. Trace elements may be immobilized within the stream sediments and thus could be absorbed, co-precipitated involved in complex formation (Mohiuddin *et al*., 2010). The contamination of soil/sediment by heavy metals from different activities has gained worldwide attention especially among environmental stakeholders. Metals are intrinsic components of the earth crust, thus their contents in the ecosystem can be altered through different natural processes and anthropogenic inputs (Gopal *et al*., 2017). Also, lithogenic process such as rock weathering, water flow and natural erosion play significant roles in the concentration of metals in the sediment (Karthikeya *et al*., 2018).

 Many hand-dug wells exist in Nigeria and in many developing countries all over the world. They serve as an extremely effective water source for many economically developing countries. They are important to both urban and rural communities (Aina & Oshunrinade, 2016). However, a poorly maintained well is completely ineffective and can even serve to pollute the entire aquifer. It is imperative therefore, that all wells are constructed, operated and maintained appropriately to ensure clean drinking water for the life- time of the well (Collin, 2000).

Sediment entering storm- water degrades the quality of water for drinking, wildlife and the land surrounding the streams. Water polluted with sediment becomes cloudy, preventing aquatic animals from seeing food (Speneer & Maclead, 2002). The concentration of heavy metal is positively correlated to organic matter. That is, sediment with relatively high organic matter tends to be more polluted by heavy metals. It is previously suggested that organic matter in sediment can absorb heavy metals from the environment (Xu *et al*; 2016).

Sediments are important sinks for heavy metals in aquatic ecosystem. Heavy metal pollution may increase the susceptibility of aquatic animals to various diseases by interfering with the normal functioning of their immune, reproductive and developmental processes (Rainey *et al*., 2003).

Therefore, the prime objectives of this study are to quantify the concentration levels of some heavy metals (Pb, Cd, Cu, Fe, Zn, Mn, Co, Cr and Ni) in sediment and to assess the human health risk associated with heavy metals in sediment from selected hand-dug wells in Katsina metropolis.

MATERIALS AND METHODS
Study Area
The research study is focused in hand dug wells of selected areas within Katsina metropolis, Katsina State, Nigeria. Covering a land area of 3,370 square kilometers and lies between latitude 11° 08'N and 13° 22N'N and longitude 6° 52'E and 9° 20'E. It is bounded to the North by Kaita Local Government Area, East by Rimi Local Government Area, South by Batagarawa Local Government Area, and to the West by Jibiya Local Government Area. (Ladan, 2014).
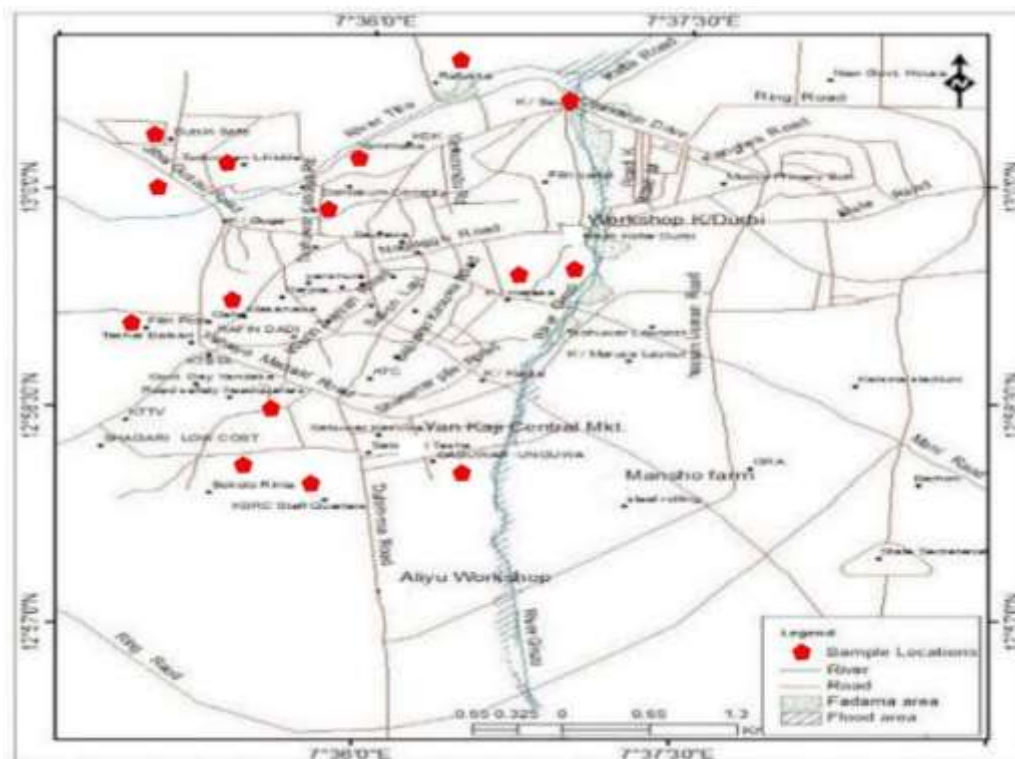

Figure 1: Map of Katsina Metropolis Showing Sample Locations
Source: National Aeronautic and Space Administration Spot Image 2020

Sediment Sampling and Sample Preparation
The sediment samples were collected from five (5) different hand dug wells within Katsina metropolis and stored in a labelled cleaned polyethene bag. The sampled sediments were spread on a different flat trays inside the laboratory to be air dried for 5 days at room temperature, after which they were ground using mortar and pestle and sieved for digestion process (Olafisoye *et al*., 2013).

Digestion and Preparation of Sediments Samples for Heavy Metals Analysis
One (1) gram was taken in a 250 cm^3 conical flask, 15 cm^3 of the mixture of per chloric, nitric and sulphuric acids in the ratio of 1:2:2 were added and heated in a fume chamber until dense white fumes appeared. Then the flask was

allowed to cool and the content was filtered and poured in to a 50 cm^3 volumetric flask and were made to mark with deionized water and then aspirated in to the flame of the Atomic Absorption Spectrophotometer (AAS) (Agilent Technologies model 200 series AA). The instrument was set at specific wavelength unique to each respective metal and between two readings, distilled-deionized water aspiration was conducted. The records of the absorbance were taken from the steady galvanometer in a moment of 1 min. For any sample, analysis was performed in triplicate and the concentration of metals was calculated with the aid of a standard calibration plot (Sani *et al.,* 2016).

Estimation of Health Risk Assessments
The potential risk from heavy metals in sediment are calculated based on recommendations proposed by United States Environmental Protection Agency (USEPA 2001; 2000). The Estimated daily intake (EDI) (mg/kg-day) of each heavy metal through ingestion and dermal contact pathways were calculated using the following equations.

$$EDI = \frac{C_{metal} \times IR \times ED \times CF}{BW \times AT}$$

(1)

Where, EDI = Estimated daily intake, IR=ingestion rate (2.2g/day), ED = Exposure duration (70 years), CF= Conversion factor (0.085), BW (60kg) = Body weight of the exposed individual, AT (days) = Estimated time period over which the dosed is estimated.

The potential health risk can be categorized by target hazard quotients (HQ) and hazard index (HI) as proposed by (USEPA 2001; 2000). HQ is a ratio of determined Estimated daily intake (EDI, mg/kg/day to reference dose RFD, (mg/kg/day) of individual element. All HQs were dded to generate a HI for the estimation of total potential health risks.

HI = ∑HQ --   (2)

Statistical Analysis
Data generated from this study were subjected to statistical analyses using SPSS statistical software version 20.0. Basic descriptive Statistic are presented as mean ± standard deviation. Furthermore, analysis of variance (ANOVA) was applied to estimate significant mean differences in heavy metals in sediment between the samples. Duncan's Multiple Range test (DMRT) was utilized in evaluating the significant difference within the levels of independent variables. Cluster analysis and Pearson Product Moment Correlation was used to ascertain the relationships between each heavy metal concentration in sediment. The results of heavy metals present in hand dug wells from Katsina metropolis is presented in Table 1. Table 1 indicates that in all the samples Zn was detected, with the estimated mean of (0.76±0.67 mg/kg). Sample A has the highest concentrations and sample L has the lowest concentration of Zn ranging from 0.12±0.01 to 2.86±0.15 mg/kg respectively.

RESULTS AND DISCUSSION
Results of the concentration of Heavy Metals Analysis.
Table 1: Concentrations levels of Heavy Metals in Sediment (mg/kg)

Sample	Zn	Pb	Cd	Fe	Cu	Mn	Ni	Co	Cr
A	2.86±0.15[a]	0.30±0.009[b]	-0.013±0.001[cde]	494.37±2.40[b]	0.27±0.003[k]	10.73±0.11[a]	0.60±0.006[a]	0.29±0.001[a]	4.76±0.014[b]
B	0.21±0.001[ef]	0.21±0.019[e]	-0.014±0.005[def]	330.23±1.63[d]	0.15±0.001[l]	0.94±0.003[g]	0.11±0.006[f]	0.06.±0.003[e]	3.75±0.014[c]
C	0.40±0.001[c]	0.33±0.014[a]	-0.006±0.002[a]	449.53±19.70[c]	0.27±0.002[k]	5.49±0.014[b]	0.14±0.010[e]	0.11±0.005[b]	2.06±0.028[g]
D	0.12±0.003[gh]	0.12±0.009[j]	-0.013±0.001[cde]	190.57±8.80[fg]	3.85±0.220[b]	0.11±0.001[k]	0.08±0.002[i]	0.02±0.005[i]	1.49±0.031[j]
E	0.19±0.001[efg]	0.28±0.014[c]	-0.010±0.002[bc]	552.43±13.55[a]	0.91±0.017[f]	1.13±0.003[f]	0.18±0.003[c]	0.08±0.003[d]	5.02±0.017[a]

Therefore, this high concentrations of zinc in sample A could be attributed to Zn loading in acquifire. Furthermore, the values reported in this study were low when compared with a research by Sani *et al*., (2016) in the determination of heavy metals in sediment and water sample from River Challawa, Kano State. The maximum permissible limit of Zinc in sediment/soil recommended by WHO is 50 mg/kg (WHO, 2002). Thus the concentration of Zinc in all the sediment samples is within the permissible limit. Similarly, analysis of variance (ANOVA) revealed that the concentration of Zn is statistically different among the samples at 5% level of significance. Furthermore, samples with the same superscripts statistically have the same concentration of Zn at 5% level of significance while samples with different superscripts have statistically different Zn contents, as shown by Duncan multiple comparison test.

For lead (Pb) metal concentrations from Table 1, sample D was found to have the lowest concentration and C has the highest concentrations of Pb ranging from (0.12±0.008 mg/kg to 0.33±0.014 mg/kg) respectively, with an estimated mean of (0.25±0.74 mg/kg) This high concentration of Pb in sample C may be due to lead loading in acquifires. The Permissible limit of lead in sediment/soil recommended by WHO is 0.3 mg/kg and the concentration of lead was below ANZECC (2000) recommended level of 50 mg/kg. Therefore, in this study the concentrations of lead in the sediments were within the permissible limit. Although the concentration of Pb in this study was low when compared to heavy metals analysis in sediment from River Ngada, Maiduguri metropolis by (Akan *et al*., 2011).

The results from Table 1 showed that cadmium (Cd) concentrations in the analyzed sediments from hand dug wells under study ranged from (-0.006±0.002 to -0.014±0.05 mg/kg) with a mean of (-0.012±0.003 mg/kg), indicating that sample B has the highest concentrations while sample C has the lowest concentration of Cd among the samples. The low concentration of Cd in this study may be as a result of Cd loading of acquifire in the studied area. However, Cd concentration in this study is below the permissible limit (0.03±0.3 mg/kg) set by (WHO, 2002). This concentration of Cd is similar to a research by Musa *et a*l. (2007) which determed the concentration of cadmium in borehole and well waters in Zaria, Nigeria (ranged from 0.001 to 0.28 mg/kg).

 For Iron (Fe) concentrations, although it was detected in all the samples as shown in Table 1 with a mean of (403.45±150.93 mg/kg) ranging from (190.57±8.80 to 552.43±13.55 mg/kg) in which sample E has the highest concentration and sample D has the least concentration of Fe in the sediment. This high concentration of iron may be due to Fe loading in acquifire. Moreover, iron has the highest concentration in each sediment sample , this is because Fe has been earlier stated by good number of researchers that iron occurs in high proportion in Nigeria soil, implying that the concentration is contributed from both anthropogenic and natural origin (Okoye, 2008). The findings reported in this study were similar to those reported by Said *et al*, (2012) for similar metals (Pb, Ni, Cd, Fe, Zn, Cu) accumulated in the sediments of Titiwangsa lake as well as those reported by Wasiu *et al*. (2016) in their study of heavy metal contamination in stream water and sediments of gold mining areas in south western Nigeria.

 For copper (Cu), the total copper (Cu) mean concentration detected for the sediment samples was (1.09±1.52 mg/kg), and this ranged from (0.15±0.001 to 3.85±0.012 mg/kg). Sample B have the lowest concentration and sample D had the highest concentrations of Cu respectively. The concentration of copper may be due to copper loading of acquifire in the area. The permissible limit of copper concentration in sediment/soil is 36 mg/kg. The concentration of copper in all the sediment samples were within the permissible limit. Also this concentration of copper in this study was below the ANZECC (2000) limit of 65 mg/kg. Similar result with the work of Emmanuel *et al*, (2018) in Assessment of heavy metals in New Calabar River, Nigeria, in which Cu has a value ranged from 1.43±0.01 to 4.90±0.02 mg/kg. The Manganese (Mn) concentration in the sediment samples recorded highest in sample C (5.49±0.014 mg/kg), while the lowest concentration was recorded in sample D (0.11±0.001 mg/kg). The cumulative mean concentration for the samples was (3.68±2.77 g/kg). The concentration of Mn may be from both anthropogenic sources and natural origin because based on literature, manganese is found naturally in ground water, but levels can be increased by human activities (ATSDR, 2000). This study revealed low concentration of Manganese (Mn) when compared to a research by Yunusa *et al*, (2022) in evaluation of heavy metals contamination in the sediment of selected water of South Senatorial District, Niger State, Nigeria. It was found that Manganese (Mn) was detected with the concentration ranging from (55.00±16.94 to 89.15±16.60 mg/kg).

 For Nickel, the total mean concentration recorded for the sediment samples were (0.22±0.12 mg/kg) ranging from 0.08±0.02 to 0.18±0.003 mg/kg. Sample E and D showed the highest and lowest Nickel (Ni) concentrations. Therefore, this high concentration in sample E may be due to waste disposal in the landfills and fertilizers that are used through the irrigation farming in the area, which may enter ground water from the farm runoff. The permissible limit of Nickel is 35 mg/kg. The concentration of Nickel in this study were within the permissible limit. When compared to a research of the assessment of some heavy metals of selected borehole water samples in Dutsin-Ma, it was found that Nickel was detected with the concentration level ranged from 0.00 to 0.01mg/l (Mansur and Suleiman, 2022).

 Moreover, for Cobalt (Co) concentration from the sediments indicates that Sample A has the highest concentration of (0.29±0.001 mg/kg) and sample D has the lowest concentrations of (0.02±0.004 mg/kg) with the estimated mean

value of (0.12±0.66 mg/kg) respectively. The concentration of cobalt could be as a result of improper fertilizer management and use of some pesticides. this implies similar result of Cobalt (0.79±0,56 mg/kg) determine by Ajani *et al*, (2020) in health risk assessment of heavy metals from soil in Mayo-Dallah southern area of Chad.

The Chromium (Cr) concentration in the sediment samples was recorded highest at sample E (5.02±0.017 mg/kg), while the lowest was recorded at sample D (1.49±0.031 mg/kg) and the cumulative mean concentration for the samples was (3.42±1.31 mg/kg). Therefore, this high concentration may be from leather tanning in that area.

Table 2: **Correlations Results among the Concentration Heavy Metals for Sediment**

H.M	Zn	Pb	Cd	Fe	Cu	Mn	Ni	Co	Cr
Zn	1								
Pb	0.466**	1							
Cd	0.063	0.584**	1						
Fe	0.461**	0.743**	0.244	1					
Cu	-0.103	-0.266	0.177	-0.273	1				
Mn	0.914**	0.668**	0.267	0.561**	-0.072	1			
Ni	0.955**	0.626**	0.142	0.575**	-0.153	0.894**	1		
Co	0.935**	0.709**	0.268	0.584**	-0.070	0.959**	0.965**	1	
Cr	0.535**	0.663**	0.164	0.872**	-0.169	0.511**	0.670**	0.634**	1

*Correlation is significant at 0.05 level (2-tailed)
**Correlation is significant at 0.01 level (2-tailed)

The result of this study from Table 2, shows that (Zinc) Zn has a significant positive correlation with Pb, Fe, Mn, Ni, Co and Cr in the sediment samples. This means that the higher concentration of Zn results in higher concentrations of Pb, Fe, Mn, Ni, Co and Cr for sediment and vice versa. It also indicates that Zn has no significant correlation with Cd and Cu among the Sediment samples which means that they are not correlated.

Lead(Pb) has a significant positive correlation with Cd, Fe, Mn, Ni, Co and Cr for the sediments. This means that the higher concentration of Pb results in higher concentrations of Cd, Fe, Mn, Ni, Co and Cr for the sediments and vice versa. It also indicates that Pb has no significant correlation with Cu for the sediment which means that they are not

correlated. Cd has no significant correlation with Fe, Cu, Mn, Ni, Co and Cr for sediment. This means the concentration of Cd does not affect concentrations of Fe, Cu, Mn, Ni, Co and Cr for sediment and vice versa. Significant positive correlations are as a result of human activities and they work together to alter the well water quality.

Iron (Fe) has significant positive correlation with Mn, Ni, Co and Cr for sediment. This means higher concentration of Fe results in higher concentrations of Mn, Ni, Co and Cr for sediment and vice versa. It also indicates that Fe has no significant correlation with Cu for Sediment which means that they are not correlated. Cu has no significant correlation with Mn, Ni, Co and Cr for sediment. This means the concentration of Cu does not affect concentrations of Mn, Ni, Co and C for sediment and vice versa.

Manganese (Mn) has significant positive correlation with Ni, Co and Cr for sediment. This means the higher concentration of Mn results in higher concentrations of Ni, Co and Cr for sediment and vice versa. Also Nickel (Ni) has significant positive correlation with Co and Cr for sediment. This means the higher concentration of Ni results in higher concentrations of Co and Cr for sediment and vice versa. Co has significant positive correlation with Cr for sediment. This means the higher concentration of Co results in higher concentrations of Cr for sediment and vice versa.
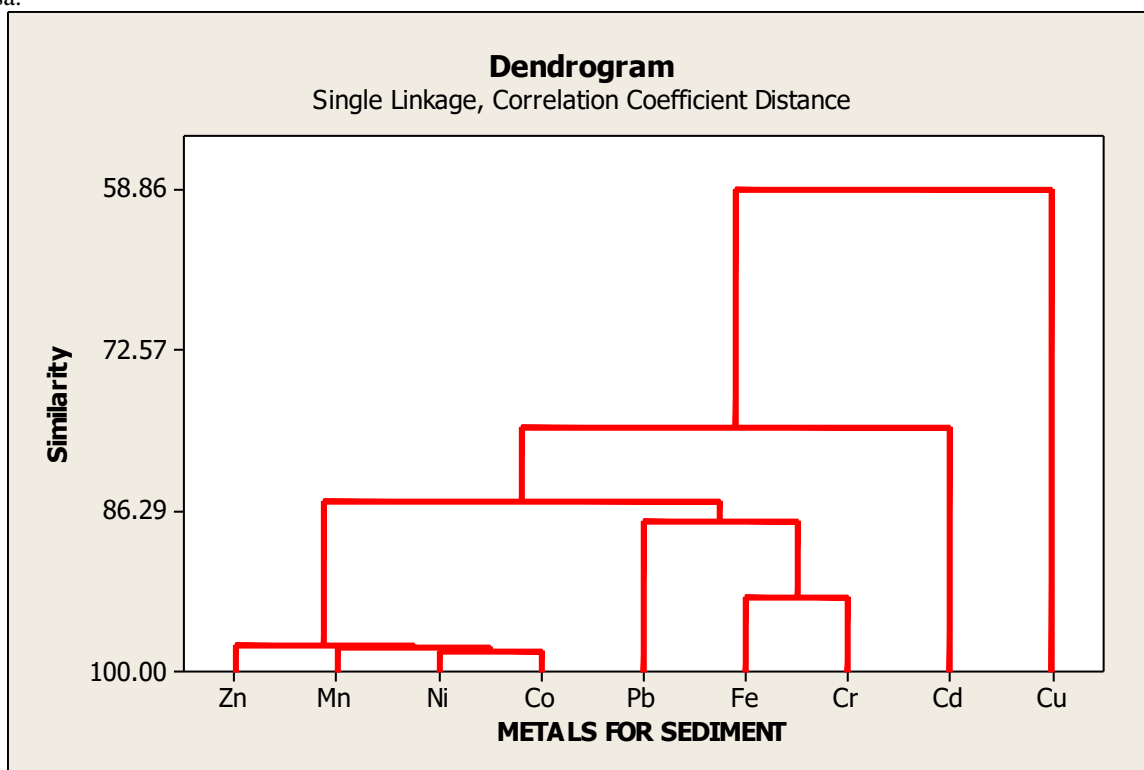

Figure 2: Cluster Analysis of Heavy Metals for Sediment

Figure 2 is a dendrogram that shows the hierarchical relationship between the metals. It is most commonly created as output from hierarchical clustering. The results of this study revealed a final portion of 7 clusters, which occurs at different similarity levels. The first cluster is composed of Zn metal only. The second cluster is composed of Mn metal only. The third cluster is composed of two metals for sediment namely Ni and Co. The fourth cluster is composed of Pb metal only. The fifth cluster is composed of two metals for sediment namely Fe and Cr. The sixth cluster is composed of Cd metal only and the seventh cluster is composed of Cu metal only. Metals for sediment within a cluster are very similar and variables outside a cluster are very dissimilar.

Health Risks Estimations for Exposure to metals in Sediments

The estimated human health risks due to ingestion exposure to heavy metals in the sediment from the hand dug wells of selected areas within Katsina metropolis are presented in Tables 3, the hazard quotient (HQ) of each metal in the sediment samples from each location was less than one (< 1). This implies that the level of exposure is not likely to cause any obvious adverse health effects (USEPA 2000; Wang & Gardinal 2013). Accordingly, the hazard index (HI) of each sample was (<1), implying that no any non- carcinogenic adverse health effects is implied.

Table 3: Estimated Human Health Risks of Heavy Metals in the Sediment Sample A

HM	EDI	HQ
Zn	0.000027	0.00009
Pb	0.000029	0.0072
Fe	0.047459	0.0678
Cu	0.000026	0.00065
Mn	0.001031	0.00736
Ni	0.000058	0.0029
Co	0.000028	0.00094
Cr	0.000457	0.15233
		H I = 0.24

HM = Heavy metals, EDI = Estimated daily intake, HQ = Hazard quotient, HI= Hazard index

Table 3 represents the estimated human health risks of heavy metals present in the sediment sample A. From Table 3, it indicates that the Hazard Quotient (HQ) of each of the metals were found to be less than one (<1) in the sample. Accordingly, the Hazard Index (HI) was also found to be 0.24. This implies that level of exposure to heavy metals is not likely to cause any health effects in the hand dug wells.

Table 4: Estimated Human Health Risks of Heavy Metals in Sediment Sample B

HM	EDI	HQ
Zn	0.000021	0.00007
Pb	0.000021	0.00525
Fe	0.03170	0.04529
Cu	0.000014	0.00035
Mn	0.000091	0.00065
Ni	0.000012	0.00060
Co	0.000058	0.00193
Cr	0.00036	0.120
		H I = 0.2

HM = Heavy metals, EDI = Estimated daily intake, HQ = Hazard Quotient, HI = Hazard index

The results of the estimated Human health risks due to dermal exposure to heavy metals is presented in Table 4. Therefore, Table 4 revealed that the calculated Hazard Quotient (HQ) of each of the metals were found to be less than one (<1) in the sediment sample B. Accordingly, the Hazard Index (HI) was also found to be 0.20, implying that non-carcinogenic adverse effects due to exposure of heavy metals are not likely to cause any obvious health effects.

Table 5: Estimated Human Health Risks of Heavy Metals in Sediment Sample C

HM	EDI	HQ
Zn	0.000038	0.00019
Pb	0.000032	0.00079
Fe	0.043155	0.06165
Cu	0.000026	0.000648
Mn	0.000527	0.00376
Ni	0.00004	0.000672
Co	0.000011	0.000352
Cr	0.000198	0.06592
		H I = 0.13

HM = Heavy metals, EDI = Estimated daily intake, HQ = Hazard Quotient, HI = Hazard index

Table 5 shows the result of the estimated human health risks due to exposure to heavy metals in sediment sample C. The result indicates that the calculated Hazard quotient (HQ) were found to be less than one (<1). However, the Hazard

index (HI) was 0.13, which is also less than one (<1). This implies that the consumption of water from the studied hand dug well is not likely to cause any toxic risk associated with the heavy metals (USEPA, 2000).

Table 6: Estimated Human Health Risks of Heavy Metals in Sediment Sample D

HM	EDI	HQ
Zn	0.000012	0.000038
Pb	0.000012	0.00288
Fe	0.01825	0.026614
Cu	0.00037	0.00924
Mn	0.000011	0.00007
Ni	0.000007	0.00004
Co	0.000002	0.000064
Cr	0.00014	0.0478
		H I = 0.08

HM =Heavy metals, EDI= Estimated daily intake, HQ = Hazard Quotient, HI= hazard index

The estimated human health risks of heavy metals due to consumption from sediment sample D are as presented in Table 6. The results showed that the Hazard Quotient (HQ) of each of the metals was found to be less than one (<1) in the sample. However, as seen in Table 6, the Calculated Hazard Index (HI) was 0.08, which implies that the level of exposure to heavy metals is not likely to cause any adverse health effects.

Table 7: Estimated Human Health Risks of Heavy Metals in Sediment Sample E

HM	EDI	HQ
Zn	0.000018	0.000046
Pb	0.000027	0.00672
Fe	0.053033	0.07576
Cu	0.000087	0.002184
Mn	0.000108	0.00077
Ni	0.000017	0.000123
Co	0.00008	0.000256
Cr	0.000482	0.016064
		H I = 0.10

HM = Heavy metals, EDI= Estimated daily intake, HQ = Hazard Quotient, HI= hazard index

Table 7 represents the estimated human health risks exposure to heavy metals in sediment sample E. Table 7 shows that the Hazard Quotient (HQ) of each of the metals were found to be less than one (<1) in the sample. Accordingly, the Hazard Index (HI) was 0.10 which implies that the level of exposure to heavy metals is not likely to cause any toxic effects. These findings are similar to a research carried out by (Wang and Gardinal, 2013).

CONCLUSION
The results of the study have revealed the presence of heavy metals like Zn, Pb, Fe, Cu, Mn, Ni, Co, and Cr in the samples and also revealed that the concentration of all metals under investigation were found to be within the permissible/recommended values set by relevant authorities, except Cd which has a negative concentration meaning that it is below the detection limit in all the samples. Therefore, from the results, it could be concluded that the investigated heavy metals occurred at various concentration levels in the sediment and are within acceptable limits. The human health risk assessment in this study classifies the selected hand-dug wells as safe with regards to dermal exposure to the heavy metals in which each of the Hazard quotient (HQ) and Hazard index (HI) was <1; indicating that there is no health risk associated with the heavy metals in the sediment. However, despite the low levels of the metals in this work compared to the various literatures in the other researches, they could still lead to serious health hazard considering their cumulative effects in the environment over time.

REFERENCES

Aina A.T, and Oshunrinade O.O .(2016). Comparison of water quality from boreholes and hand dug wells around and within the University of Lagos, Lagos Nigeria. *Int J Res Environ*, Stud 3:93-100.

Ajani U.M, Ajani P.P, Maleka I.T and Usman S.P .(2020). Assessment of Heavy Metals and Associated Health Risks from Soil in Mayo-Dallah, Southern area of Chad. *Journal of Environmental Management,* 43 (2) (2020) p.70.

Akan, J.C., Abdulrahman F.I, Mamza P.T, and Aishatu N (2011). Effect of Environmental pollution on the quality of River Ngada, Maiduguri Metropolis, Borno State, Nigeria. Global Science Books. *Terrestrial and Aquatic Environ. Toxicol*.6 (1): 40-46.

Alizarveya A, Streck T, Richer J. (2006). Characterization of atmospheric trace element on particulate matter over the New York-New jersey harbor estuancy, 2:3-15.

ATSDR 2000.*Toxicological Profile for Manganese*. U.S. Department of Health and Human Services, public Health service, Agency for Toxic substances and Disease Registry, Atlanta, GA.

Australian and New Zealand Environment and Conservation Council (ANZECC). (2000). Australian and New Zealand. *Guidelines for Sediment, Fresh and Marine Water Quality*. New Zealand, Canberra.

Collins S (2000) hand dug shallow wells. series of manuals on drinking water supply, Vols.swiss centre for Development co-operation in Technology managem.ent, Hand dug shallow SKAT, Switzerland.

Emara M, Faraq K.S, Dawuh A.A and Fathi M (2015). Assessment of heavy metals concentration in water and edible tissue of Nile tilapia (oreochromics nitoticus) from two fish farms irrigated with different water sources. Egypt Int J Environ 4(1):105-115.

Emmanuel E, Terver S, Jonathan U (2018). Assessment Heavy Metals Concentration in shore Sediments from the Bank of River Benue, North-Central Nigeria. *Journal of Geoscience and Environment.* Vol.6 No.4, April 2018.Doi: 10'4236/gep.2018.64003

Fernandez C, Fontaihas –fernandes A, Cabral D, Salgado MA (2008). Heavy metals in water, sediment and tissues of liza sallens from Esmoriz-paramos lagoon, *Portugal, Environ monit Assess* 136:267-275.

Gopal., V., Hema, A., Jayaprakash, M. (2017). Assessment of trace elements in Yercard lake sediments, southern India. Environmental Earth Sciences. *76:63. https:doi.org/10.1007/S12 665-6390-6.*

Huang XF, Hu JW, Deng JJ, Li CX. Qin FX (2009) Speciation of heavy metals in sediments from Baihua and Aha lake, Asia-pacific.J Chem Eng 4:635-542

Karthikeyan, P., Vennila, G., Venkatachala pathy, R.et al., (2018). Assessment of heavy metals in the surface sediments of the Emerald Lake using of spatial distribution and multivariate techniques. Environmental Monitoring Assessment *190: 168.https://doi/10,1007/s10611-081-7073-0.*

Ladan SI. (2014). Composting as sustainable waste management method in katsina metropolis, Northern Nigeria. *International journal* of Bioscience Biochemistry and Bioinformatics Vol.4.no.1, pp.11-13 Jan 2014.

Mansur A, Suleiman A (2022). Quality Assessment of some Selected Borehole Water Samples in Dutsinma Town, Katsina State, Nigeria. *International Journal of Research Publication and Reviews,* Vol 3, no 9, pp 110-116.

Mohiuddin, K, M., Zakir H.M., Otomo, K. Sharmin, S., Shikezoro N. (2010). Geochemical distribution if trace metal pollutants in water and sediments of downstream of an urban River-*International journal of Environmental Science and Technology.,* **7**(1):17-28.

Musa H, Yakasai IA, Musa HH, Musa KY and Gwarzo MS. (2007). The concentration of cadmium in Borehole and well waters in Zaria. Journal of Applied Sciences **7**(22):3572-3575.

Okoye BCO. (2008) Nutrients and selected chemical analysis in Lagos lagoon surface waters. *International environmental studies journal* of. 38:131-135.

Olafisoye, O.B, Adefioye, T., Osibote, O.A. (2013). Heavy metals contamination of water, soil, and plants around an electronic waste dumpsite. *Pol J Environ Stud.* 22(5), 1431-1439.

Rainey M.P., Tyler, A.N; Gilver, D.J., Bryant, R.G., McDonald. (2003). Mapping intertidal Estuarine Sediment Grain Size Distributions through Airborne Remote sensing. Remote sensing of Environment, 86:480-490.

Sani, A., Bello. M.G., Abubakar, A.F., (2016). Determination of heavy metals in selected coosmetics sold in Kano metropolis. Toxicol. Rep. 3, 866-869.

Speneer, K.L., Maclead, C.L (2002). Distribution and partitioning of heavy metals in Estuarine sediment cores and implications for the use of sediment Quality standards. *Hydrology and Earth system Sciences*, 6**:**989-998.

Travizani T.H, Figueira R.C, Ribeiro A.P, oreopholo C.Y, major A.P, Petti M.A, Corbusier T.N and Montone R.C .(2016). Bioaccumulation of heavy metals in marine organisms and sediments from admirably Bay. King George Island, Antactica Marine pollution. Bulletin 755-756.

USEPA (United State Environmental Protection Agency) .(2000). Guidelines for assessing chemical contaminant data for use in fish advisories: Fish sampling and analysis. 3rd edition Washington DC

USEPA (United State Environmental Protection Agency) .(2001). Framework for ecological risk assessment EPA/630R.92/001. Risk assessment forum, USEPA. Washington DC

Wang C, Gardinal PR (2013). Detection and occurrence of micro constituents in reclaimed water used for irrigation – a potentially over-looked source. *Analytical and Bioanalytical Chemistry* 405(18):5925-5935.https://doi.org/10.1007/s00216-013-6799-

Wasiu, M. O., Ayodele, O.E., Ayodele, T. l., Olurumi, O. l., Temitope, O. K., and Temitope, F.O (2016). Heavy metal contamination in stream water and sediments of gold mining areas of south Western Nigeria. *African journal of Environmental Science and Technology*, 10(5), 150-161.

WHO (2002) The world health report: reducing risks, promoting healthy life. *World Health Organization ;2002.* Available: https://apps.who.int/iris/handle/10665/4251035.

Xu, G., Liu, J., Pei, S., Hu, G., Kong, X., (2016). Sources and geochemical background of potentially toxic metals in surface sediments from the Zhenjiang coastal mud area of the East China Sea. *J, Geochem Explor,* 168:26-35.

Yunusa J A, Aliyu DA, Naomi J and Mahmud D. (2022). Evaluation of Heavy metals contamination in the sediment of some selected water of South Senatorial District of Niger State, Nigeria. *Science World Journal* Vol.17 (No.4) 2022.*www.scienceworldjournal.org*.

Zheng, Y. (2008). Multivariate geostatistical analysis of heavy metals in top soils from Beijing china, Journal of soil sediments. 8, pp 51-58.

Theoretical Calculation of Radiation Shielding Parameters in Parkia Pods

*[1]Usman Sani and [2]Rilwan U.

[1]Department of Physics, Umaru Musa Yar'adua University, Katsina-Nigeria.
[2]Deparment of Physics, Nigerian Army University, Biu, Borno State-Nigeria
*Corresponding Author's E-mail: usman.s@umyu.edu.ng Phone: +2348067595770

ABSTRACT
Investigations and researches on the photons and radiation shielding capacity of materials focus mostly on rocks, soil, concretes and glasses. The investigations are silent on some biological samples such as plants and trees. In this study, the investigation focuses on the elemental composition and theoretical shielding parameters in Parkia pods using PHY-X software. The elemental composition of the sample was analyzed using Energy Dispersive X-ray Fluorescence (EDXRF). The linear attenuation coefficient, mass attenuation coefficient, tenth value layer, mean free path and effective atomic mass of the sample were computed by PHY-X software. The results showed that the linear attenuation coefficient decreases as the photon energy increases 1.00E-01 MeV, 25.689 cm^{-1} and 1.00E+01 MeV, 2.042 cm^{-1}. While the Half Value Layer and Tenth Value Layer are increasing with the increase in photon energy 1.00E-1 MeV, 0.012 cm, 1.00e+01, 0.339 cm. And the mass attenuation coefficient decreases as the photon energy increases. The results also showed that the photon energy and effective atomic mass (Z_{eff}) were 1.00E-01, 1.50E-01, 2.00E-01, 2.84E-01, 3.00E-01, 3.47E-01, 4.00E-01, 8.26E-01 to 8.00E+00 and 43.53, 34.39, 28.65, 24.00, 22.35, 21.53, 20.63, 20.14 and 19.95, respectively. The results showed that the sample is efficient for radiation shielding due to the presence of lead (Pb) and high effective atomic mass.
Keywords: Attenuation coefficient, value layer and shielding

INTRODUCTION

The advancement in nuclear science led to the high demand for various sources of radioactive substances. The ionizing radiations such as X-rays, gamma and neutron rays have a very high energy and penetrating power which travelling in the free air (Abdullahi et al., 2022).

Continuous exposure to ionizing radiations above the safety limits causes detrimental and stochastic effects which includes radiation sickness, cancer, genetic mutations and early death (Sayyed et al., 2022). Precautionary measures must be adhered to ensure the safety of workers, members of the public and the environment (Hajer, et al., 2020).

Among the safety precautions against the harmful effects of ionizing radiation is the use of protection barrier (Kawa and Sayyed, 2023). The materials that can attenuate the radiation and photon intensities when properly placed between the source and individuals exposed to the dose resulting from the said source is referred to as shielding (Kawa and Sayyed, 2023; Muhammad et al., 2020).

In order to have a proper radiation shielding, material with high attenuation parameters has to be employed (Gerken et al., 2022). The selection of radiation and photons shielding material needs a diligent computation regarding the elemental composition and atomic mass of the material (Prabhu et al., 2023). Lead is the best and most common shielding material due to its high density and atomic and mass (Kawa and Sayyed, 2023). However, several materials can be used as alternative shielding which includes rocks, concrete and glasses (Wu et al., 2023; Sakar et al., 2020; AbuAlroos et al., 2019).

PHY-X is a user-friendly electronic software designed to compute radiation shielding and dosimetry parameters constitute in a biological or geological material. It is designed to compute the average molecular weight, mass attenuation coefficient, linear attenuation coefficient, half value layer, tenth value layer, mean free path, atomic cross section, electronic cross section, effective atomic number and effective electronic density of the material (Sakar et al., 2020; Alhassan et al., 2022).

Parkia is a perennial tree that grows from 10 m to 20 m tall. It is mostly found in Africa. It produces seeds which is covered by the pods. Traditionally, the pod is used in fabricating soil in order to make it hard and strong (Termote et al., 2020).

Researches that involve direct contact with ionizing radiation are hazardous. To palliate the effects of exposure to ionizing radiation, the use of alternative model needs to be employed. Many researches were conducted on the shielding abilities of rocks, concretes, soil, and glasses as found in the following studies (El-khayatt, 2010; Shamsan et al., 2019; Mahmoud et al., 2019; Nabil et al., 2023; Shaaban et al., 2023; Zakaly et al., 2023; Ozkan and Gokmen, 2023; Afnah et al., 2023). However, the investigations remain silent on the shielding capacities of the geological samples such as plants and trees. In order to bridge the gap, this study is trying to investigate the shielding parameters in Parkia pods using theoretical model.

MATERIALS AND METHODS
Sample Collection and Preparation.
Parkia pods were collected from the Parkia Biglobosa tree. The pods were dried using muffle furnace at 200 ºc It was then grinded to powder.

Materials
The study is focused on the Investigation of radiation shielding parameters in Parkia pods. The following materials were used: Electronic beam balance, Container, Measuring cylinder, Mortar and pedal and Energy Dispersive X-ray Fluorescence (EDXRF) machine.

Methods
The sample was grinded using metallic mortar and pedal. Then the density of the sample was measured using measuring cylinder and electronic beam balance.

Energy Dispersive X-ray Fluorescence (EDXRF)
The sample was taken to Central Laboratory, Umaru Musa Yar'adua University, Katsina for elemental analysis using Energy Dispersive X-ray fluorescence (EDXRF) machine with a model number: ARL. QUANT'X. EDXRF ANALYZER and serial number: 9952120. The sample was grinded to powder and inserted in the small container. The sample was run in a vacuum for 10 minutes and then inserted in to the XRF spectrometer for the elemental analysis. The method was calibrated using geological calibration analysis.

PHY-X Software
The software is designed to calculate the shielding parameters of a sample. The elemental composition in the sample was used to determine the Mass attenuation coefficient (MAC), Linear attenuation coefficient (LAC), Half value layer (HVL), Tenth value layer (TVL) Mass free path (MFP) and Effective atomic mass (Z_{eff}) of the sample. The result obtained from the XRF analysis was normalized and inserted in the software. The software calculated the MAC, LAC, HVL, TVL, MFP and Z_{eff}.

Theory
The mathematical relationship between the LAC, MAC, HVL, TVL, MPF and Z_{eff}, can be derived from the Beer-Lambart law (Sayyed et al., 2023).

$$lx = loe - \mu x \tag{1}$$

$$LAC(\mu) = ln\left(\frac{lo}{lx}\right)/x \tag{2}$$

Where μ is the linear attenuation coefficient
I_O is the intensity
I_0 is the original intensity
X is the depth of the material in cm (Obaid et al., 2018)

$$MAC = \frac{\mu}{\rho} \tag{3}$$

Where μ is the linear attenuation coefficient and ᴾ is the density (Agar, 2018).

$$HVL = \frac{0.693}{\mu} \tag{4}$$

$$TVL = \frac{ln\,10}{\mu} \tag{5}$$

$$MFP = \frac{1}{\mu} \tag{6}$$

Where μ is the linear attenuation coefficient (Sayyed et al., 2020).

$$Zeff = \frac{\sum_{i=1}^{n} f_i Ai(\rho)i}{\sum_{j=1}^{n} f_j \frac{Aj}{Zj}(\rho)j} \tag{7}$$

Where f_i is the molar fraction,
A_i is the atomic weight,
Z_j is the atomic number
μ/p is the mass attenuation (Sayyed et al., 2020).

RESULTS AND DISCUSSION
The results obtained from the EDXF analysis and the PHY-X software were presented on the tables below:

Table 1. Elemental weight percentage of the sample

SN	Elements	Bagaruwa (Wt %)
1	Fe	0.26569
2	Cu	0.001646
3	Ni	0.00938
4	Zn	0.002362
5	Al	0.13402
6	Mg	0.01357
7	S	0.06613
8	P	0.10189
9	Ca	0.13890
10	K	0.8521
11	Mn	0.005494
12	Rb	0.00387
13	Sr	0.001734
14	Br	0.00239
15	Cl	0.12338
16	Cr	0.00
17	W	0.0209
18	Bi	0.087
19	Sn	0.07
20	Si	0.56
21	Nb	0.0239
22	Ta	0.00746
23	Pb	0.171

Table 1 shows the elemental composition of the sample which analyzed using Energy Dispersive X-ray Fluorescence (EDXRF). The results indicate that the sample consists of 22 elements which includes Potassium (K) 0.8521%, Iron (Fe) 0.2656%, Silicon (Si) = 0.5600%, and Lead (Pb) = 0.171% as the elements with the highest weight.

Table 2: Elemental Density percentage of the sample

SN	Elements	Density (g/cm³)
1	Fe	9.977783
2	Cu	0.061814
3	Ni	0.352259
4	Zn	0.088703
5	Al	5.033018
6	Mg	0.509611
7	S	2.483461
8	P	3.8264
9	Ca	5.216282
10	K	31.99996
11	Mn	0.206323
12	Rb	0.145335
13	Sr	0.065119
14	Br	0.089755

15	Cl	4.633441
16	Cr	0
17	W	0.784883
18	Bi	3.267218
19	Sn	2.628796
20	Si	21.03037
21	Nb	0.897546
22	Ta	0.280155
23	Pb	6.421773
	Sum	100

The table shows the elemental density of the sample. The elements with highest density are K, Si, Fe, Pb and Ca with a density of 31.99 g/cm^3, 21.03 g/cm^3, 9.97 g/cm^3, 6.42 g/cm^3 and 5.22 g/cm^3 respectively. Density plays an important role in radiation shielding.

Table 3: Mass attenuation Coefficient and Linear attenuation coefficient of the sample.

SN	Energy	MAC (cm^2/g)	LAC (cm^{-1})
1	1.00E-01	84.456	58.748
2	1.50E-01	36.931	25.689
3	2.00E-01	22.995	15.996
4	2.84E-01	14.937	10.390
5	3.00E-01	14.111	9.815
6	3.47E-01	12.352	8.592
7	4.00E-01	11.024	7.668
8	5.00E-01	9.432	6.561
9	6.00E-01	8.419	5.856
10	6.62E-01	7.948	5.528
11	8.00E-01	7.135	4.963
12	8.26E-01	7.008	4.875
13	1.00E+00	6.306	4.386
14	1.17E+00	5.778	4.019
15	1.33E+00	5.396	3.753
16	1.50E+00	5.076	3.531
17	2.00E+00	4.414	3.071
18	2.51E+00	3.998	2.781
19	3.00E+00	3.719	2.587
20	4.00E+00	3.372	2.346
21	5.00E+00	3.177	2.210
22	6.00E+00	3.064	2.132
23	8.00E+00	2.960	2.059
24	1.00E+01	2.935	2.042
25	1.50E+01	2.991	2.081

Table 3 shows the mass attenuation coefficient and linear attenuation coefficient of the sample at different photon energy level. The MAC and LAC are decreasing as the photon energy increases. For example, at 1.00E-10 MeV the mass attenuation and linear attenuation are 84.456 cm^2/g and 58.748 cm^{-1} respectively. And at 1.00E+01 MeV the mass and linear attenuation coefficients are 2.935 cm^2/g and 2.081 cm^{-1}, respectively. It is normal trend that as energy increases, the mass and linear attenuation of the material decrease.

Table 4. Half Value Layer (HVL) and Tenth Value Layer (TVL) of the sample

SN	Energy (MeV)	HVL (cm)	TVL (cm)
1	1.00E-01	0.012	0.039
2	1.50E-01	0.027	0.090
3	2.00E-01	0.043	0.144
4	2.84E-01	0.067	0.222
5	3.00E-01	0.071	0.235
6	3.47E-01	0.081	0.268

7	4.00E-01	0.090	0.300
8	5.00E-01	0.106	0.351
9	6.00E-01	0.118	0.393
10	6.62E-01	0.125	0.417
11	8.00E-01	0.140	0.464
12	8.26E-01	0.142	0.472
13	1.00E+00	0.158	0.525
14	1.17E+00	0.172	0.573
15	1.33E+00	0.185	0.614
16	1.50E+00	0.196	0.652
17	2.00E+00	0.226	0.750
18	2.51E+00	0.249	0.828
19	3.00E+00	0.268	0.890
20	4.00E+00	0.295	0.982
21	5.00E+00	0.314	1.042
22	6.00E+00	0.325	1.080
23	8.00E+00	0.337	1.118
24	1.00E+01	0.339	1.128
25	1.50E+01	0.333	1.107

Table 4 shows the HVL and TVL as a function of energy. As the energy of the photon increases, the HVL and TVL increase. The results showed that at 1.00E-01 MeV, the HVL and TVL are 0.012 cm and 0.039 cm, respectively. And at 1.00E+01 MeV, the HVL and TVL are 0.339 cm and 1.128 cm, respectively. The TVL is higher than the HVL at all the photon energies level. This is because HVL is 50% attenuation while TVL is 90% attenuation.

Table 5. Mean Free Path (MFP) and Effective Atomic Mass (Z_{Eff}) of the sample.

SN	Energy (MeV)	MFP (cm)	Zeff
1	1.00E-01	0.017	43.53
2	1.50E-01	0.039	34.39
3	2.00E-01	0.063	28.65
4	2.84E-01	0.096	24.00
5	3.00E-01	0.102	23.47
6	3.47E-01	0.116	22.35
7	4.00E-01	0.130	21.53
8	5.00E-01	0.152	20.63
9	6.00E-01	0.171	20.14
10	6.62E-01	0.181	19.95
11	8.00E-01	0.201	19.66
12	8.26E-01	0.205	19.62
13	1.00E+00	0.228	19.43
14	1.17E+00	0.249	19.32
15	1.33E+00	0.266	19.27
16	1.50E+00	0.283	19.25
17	2.00E+00	0.326	19.30
18	2.51E+00	0.360	19.42
19	3.00E+00	0.387	19.55
20	4.00E+00	0.426	19.83
21	5.00E+00	0.452	20.10
22	6.00E+00	0.469	20.34
23	8.00E+00	0.486	20.77
24	1.00E+01	0.490	21.11
25	1.50E+01	0.481	21.72

Table 5 shows the results of Mean free path (MFP) which is the process of interaction between the energy photons and the material. The results indicate that the MFP increases as the energy of the photon increases. Which is the normal trend. The results showed that the effective atomic mass was presented in the table. The result shows that the Z_{eff} is

dropping with the increase of the photon energy. The higher the Zeff, the more the attenuation. The material with high Z is best for radiation and photon shielding.
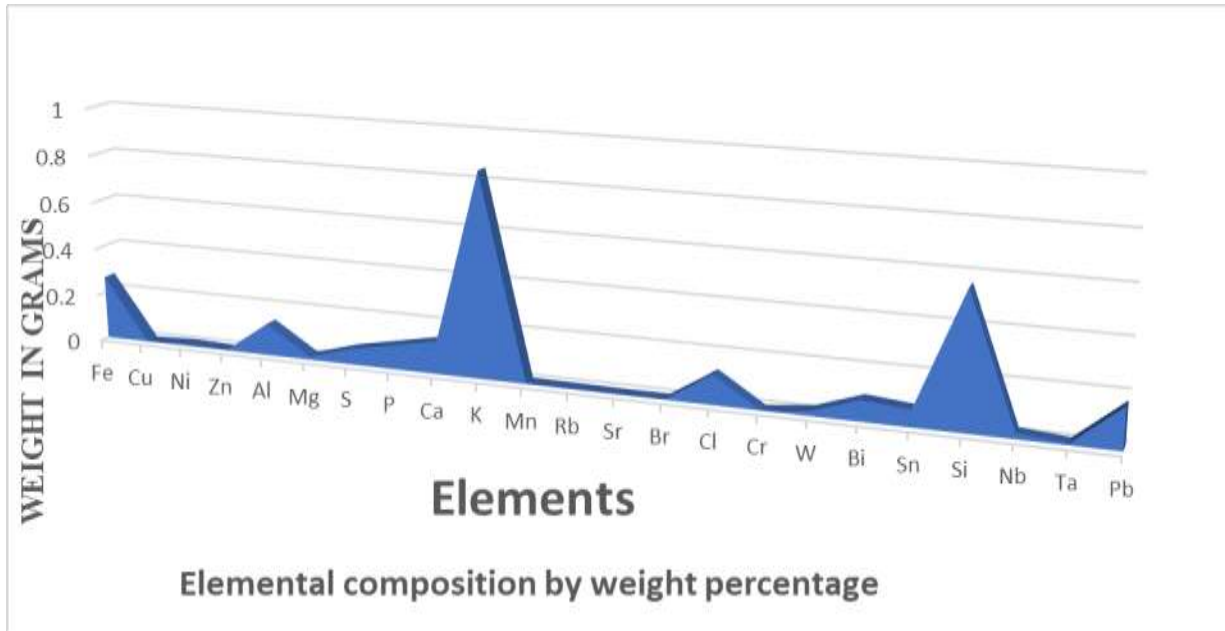

Figure 1. The chart of elemental composition by weight in percent
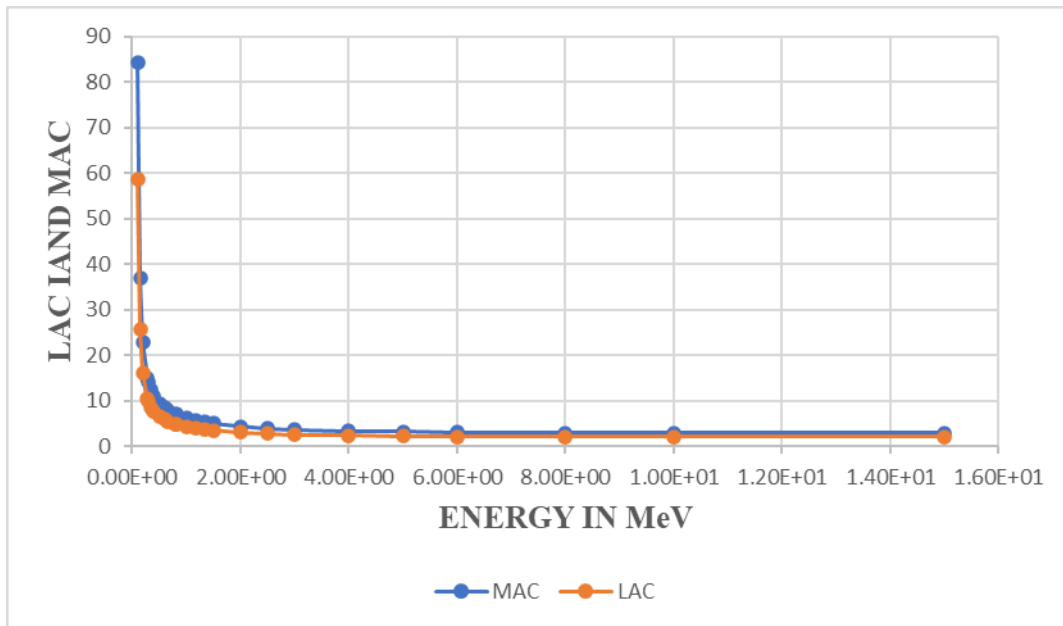

Figure 2: The chart of Linear and mass attenuation coefficient with relation to photon energy.
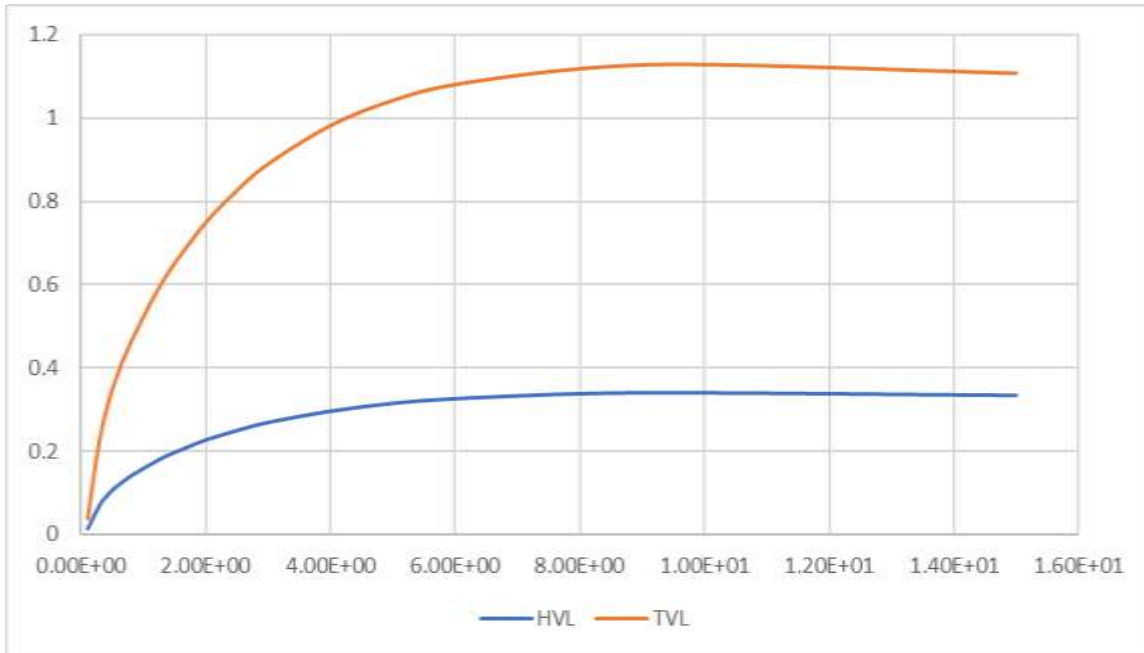
Figure 3: The chart of Half value layer and Tenth value layer in relation to photon energy.
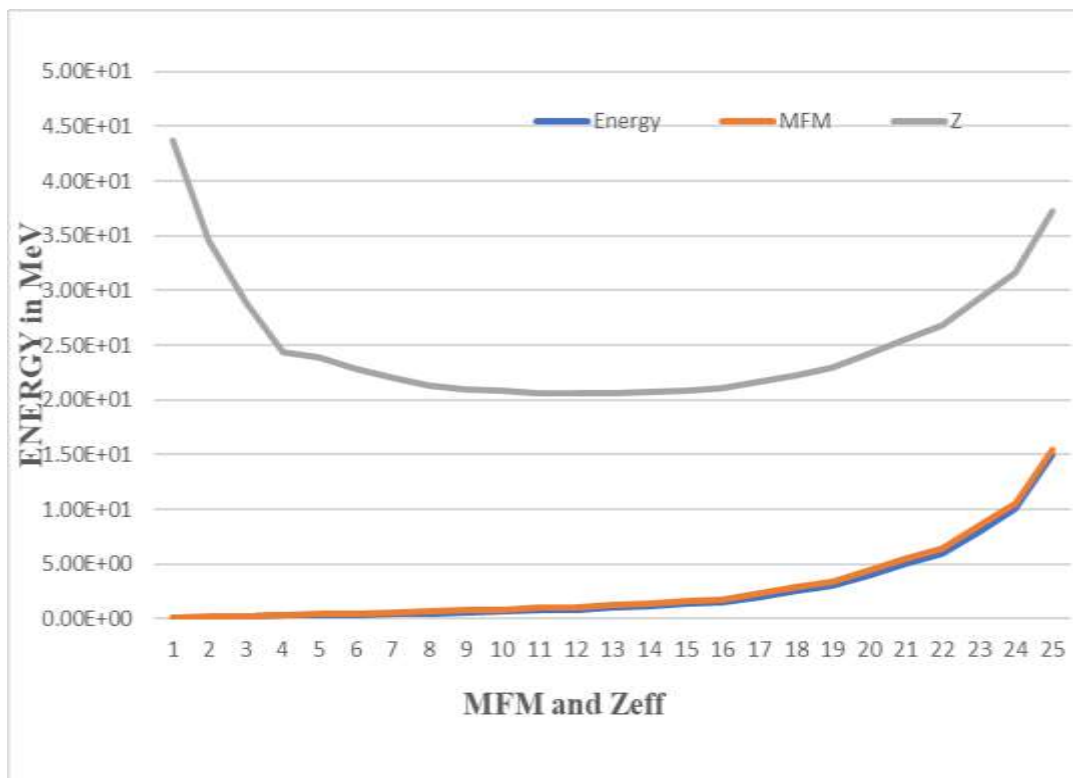
Figure 4: The chart of Mean free path and Effective atomic mass in relation to photon energy.

CONCLUSION

In this work, the shielding parameters of Parkia pods were computed theoretically using PHY-X software. The results of the Half value layer, Tenth value layer, Mass attenuation coefficient, Mean free path and Effective atomic mass of the sample were obtained. The results showed that the sample possessed high effective atomic mass and contained

some reasonable amount of lead (Pb). Based on these results and other finding from the previous literature, Parkia pods has all the qualities to attenuate radiation intensity defending on the energy and intensity of the photon.

REFERENCES
Afneh, F., Al-Ghamdi, H., Alsaif, N.A.M., Rammah, Y.S., and Khattari, Z.Y. (2023). *Elastic, mechanical and radiation shielding behaviors of copper-phosphate binary-glasses with diverse copper valence-state*. Journal of Radiation Physics and Chemistry.

Alhassan, A., Baraya, J.T, and Garba, A.S. (2023). *Accuracy of Phy-X/PSD Software Compared to XCOM in the Determination of Mass Attenuation Coefficient of Glass System*. African Journal of Applied Science and Environmental Management, 27(5), 985-988.

Abdullahi, M.A.H., Rashid, R.S.M., Amran, M., Hajazii, F., Azreen, N.M, Fediuk, R., Voo, Y.L., Vatin, N.I., and Idris, M.I. (2022). *Recent trends in advanced radiation shielding concrete for construction of facilities: materials and properties*. Journal of Polymers, 14(14),2830.

AbdulAlroos, N.D., Noorfatin, A.B.A., and Rafidah, Z. (2019*). Conventional and new lead-free radiation shielding material for protection in nuclear medicine. A review.* Journal of Radiation Physics and Chemistry, 165:108439.

Gerken, L.R.H., Alexander, G., Fabian, H.L., Helena, D., Maren, E., and Serena, P. (2022). *Catalytic activity imperative for nanoparticle dose enhancement in photon and proton therapy.* Journal of Nature Communications. 13(1).

Hajer, S.A., Mahmoud, A.H., and Tijani, S.A. (2020*). Use of rock in lieu of bricks and concrete as radiation shielding barriers at low gamma and medicine energies*. Journal of construction and building materials. 251:118908.

Kawa, M.K., and Sayyed, M.I. (2023). *The Radiation Shielding parameters of a standard silica glass system. Journal of Physics and Chemistry Solids*. 6(21), 175-186.

Khayatt, A.M. (2010). *Radiation shielding of concretes containing different lime/silica ratios.* Journal of Nuclear Energy. 37(7), 991-995.

Mahmoud, K.A., Sayyed, M.I., and Tashlykov, O.L. (2019). *Gamma Characteristics and Exposure Buildup Factor for Some Natural Rocks Using MCNP-5 Code,* Journal of Nuclear and Technology.

Muhammad, B.G., Sani, U., Usman, A.R., and Joseph, D.S. (2020). *Evaluation of shielding barrier of a computed tomography unit.* Journal of Science FUDMA. 4(1), 150-155.

Nabil, I.M., El-Samrah, M.G., Omar, A., Tawfic, A.F., and El-Sayed, A.F. (2023). *Experimental, analytical and simulation studies of modified concrete mix for radiation shielding in a mixed radiation field.* Journal of Scientific Reports.

Ozkan, Z., and Gokmen, U. (2023). *Radiation transmittance of Aluminium/Silicon matrix functionally graded hybrid composites reinforced with B4C/TiO2.* Journal of Radiation Physics and Chemistry.

Prabhu, S., Bubby, S.G., and Shivappa, B.G. (2023). *X-ray and Gamma ray shielding efficiency of polymer composites: choice of fillers, effect of loading and filler size, photon energy and multifunctionality.* Polymer review. 63(1), 246-288.

Shaaban, K.S., Tama, N., Alghastam, H.A., Alburiahi, M.S., and Ellakawa, T.E. (2023). *Thermal, optical, and radiation shielding capacity of B2O3-MoO3-Li2O-Nb2O5 glasses*. Journal of Materials and Communication.

Sakar, E., Ozpolat, O.F., Alim, B., Sayyed, M.I., and Kurudirek, M. (2020). *PHY-X/PSD: Development of a user-friendly online software for calculation of parameters relevant to radiation shielding and dosimetry.* Journal of Radiation Physics and Chemistry. 166:108496.

Shamsan, S.O., Sayyed, M.I., Gaikwad, D.K., and Pravina, P., (2019). *Attenuation Coefficients and Exposure Buildup by some Rocks for Gamma Ray Shielding Applications*. Journal of Radiation Physics and Chemistry.

Sayyed, M.I., Elbashir, B.O., Tekin, H.O., Altunsoy, E.E., and Gaikawad. D.K., (2020). *Radiation Shielding properties of pentaternary borate glasses using MCNPX code.* Journal of Physics and Chemistry Solids. 121:17-21.

Termote, C., Odongo, N.O., Dreyer, B.S., Guissou, Charles, C.B.P., and Vinceti, B. (2022). *Nutrient composition of Parkia biglobosa pulp, raw and fermented seeds: a systematic review.* Journal of food science and Nutrition, (64), 119-144.

Zakaly, H.M.H., Nabil, I.M., Issa, S.A.M., Khattari, Z.Y., and Rammah, Y.S. (2023). *Probing the Elasticity and radiation protection potential of neodymium (III) doped zinz and niobium tellurite glasses. An Integrated Simulated and Applied Physics Perspective.* Journal of Materials and Communication.

Outdoor Background Radiation Level and Radiological Hazards Assessment in Kaduna City, Kaduna State, Nigeria

*Kamal Muhammad Gonto, Otto Muhammed Sani, Faisal. U. Muhammad and Z. S. Liman

Federal University of Lafia
*Corresponding Author's E-mail: Kamalmuhammadgonto@gmail.com

ABSTRACT

This research reports on the background radiation assessment in Kaduna City, Kaduna State, Nigeria over several selected dumpsites where their background ionization radiation measurements. This was achieved by measuring the *micro-sievert per hour* (μSvhr^{-1}) radiation exposure rate by a radiation survey meter (Radex one Outdoor 55130719 NA). The detector was positioned at a height of roughly one (1) *meter* above ground level in four (4) sample locations to take readings. In the month of January 2023, the readings were taken three times a week in four different locations within each of the Dumpsites. The results showed that the annual effective dose rate measurements taken in the four dumpsites are Unguwan Rimi 0.23 *mSv/yr*, Hayin Danbushiya 0.25 *mSv/yr*, Badarawa Kaduna 0.31 *mSv/yr*, and Unguwan Shanu Kaduna 0.30 *mSv/yr* with a mean value of 0.27 *msv/yr*, while 0.95X 10^{-3} is the mean excess life cancer risk (ELCR). The results demonstrated that the total dumpsites' annual absorbed dose rate has not exceeded the 1.0 *mSv/yr* maximum permissible limit suggested by the InternationalCouncil on Radiological Protection (ICRP, 2000) for the general public and non-nuclear industrial environment. For the dumpsite personnel, scavengers, and nearby people (residents) around the dumpsite, it was found that the mean average exposure values from the site were discovered to be less than 1.16 x 10^{-3} (the typical background standard). This means that the exposure to the dumpsite is minimal and within safe limits.

Keywords: Absorbed Dose, Annual effective dose, Background radiation, Radiation survey meter

INTRODUCTION

The term "radioactive contamination of the environment" refers to a rise in natural background radiation caused mostly by human activities that entail the use of naturally occurring or man-made radioactive substances (Ogundare *et al.,* 2015). Radiation is very common in nature and everyone is exposed to radiation throughout their life. Human activities such as the smelting of metalliferous ores, manufacture of fertilizers, milling mining and processing of mineral sands and uranium ores, drilling, processing and burning of fossil fuels have increased the concentrations of naturally occurring radioactive materials in our environment (Olanrewaju *et al*., 2018). In the environment, naturally occurring radionuclides can enter the human body through ingestion and inhalation (Avwiri *et al.,* 1998). Cosmic rays, internal radioactivity, and terrestrial radioactivity are the three main sources of natural background radiation that the populace is exposed to. The terrestrial radioactivity which correlates with the geological condition of the site location and altitude is the major external source of radiation to the human body (UNSCEAR 2008, 2011). In addition, radiation from wastes (particularly when contaminated) is combined with natural background radiation from the environment. Waste disposal particularly of radioactive contaminants can expose the populace to radiation hazards if not properly managed. The hazard posed by these point sources of contamination offers a risk not just in terms of odor and presence of disease-causing microbes, but from radiations emanating from such landfills. Our natural environment is continuously bombarded with ionizing radiations from both natural and man-made sources (WHO, 2000). The most common radionuclide in the soil is the radioactive isotopes of the three natural decay series (238U, and 232Th and 40 *K*).

MATERIALS AND METHOD

A well-calibrated portable radiation survey meter with serial number 55130719 NA containing a Geiger Muller tube capable of detecting Alpha, Beta, X-rays and Gamma-rays was used to estimate the field's exposure level. Readings were taken at four (4) locations in each of the four dumpsites to spatially reflect the sites. Measurements were taken three times per week at each dumpsite for four (4) weeks in January, and average values were obtained. Each day, readings were taken between 11 a.m. and 4:00 p.m. The tube of the radiation meter was raised to a height of 1 *m* above the ground with its window facing first the Dumpsites and then vertically downward (Avwiri *et al.,* 2007). The detector was switched on to absorb radiation for a few seconds and the highest stable point was recorded. This was converted to the annual effective dose rate in milli-Sievert per year ($mSvyr^{-1}$) (Agbalagba *et al.,* 2013). Which was used to compute the ELCR equation (3) through (1) below.

Absorbed dose in air, D (nGy/hr) = Exposure in air, E ($\mu Sv/hr$) x 1000   (1)

AEDR (mSv/yr) = absorbed dose in air (D) (nGy/hr) x $8760\ hr/yr$ x $O.F$ x $C.C$ (2)

$ECLR\ =\ AEDR((mSv/yr)\ x\ DL\ x\ RF$ (3)

Where,

$\dfrac{8760hr}{yr}\ =\ the\ total\ hours\ per\ year$

$0.2\ =\ outdoor\ occupancy\ factor\ (OF)\ for\ outdoor\ radiation.$

$0.7\ =\ he\ conversion\ coefficient\ (CC)\ (Sv/yr).$

$D\ =\ Annual\ absorbed\ dose\ rate\ in\ micro\ sievert\ per\ year$

$ELCR\ =\ excess\ lifetime\ cancer\ risk$

$AEDR\ =\ annual\ effective\ dose\ rate$

$DL\ =\ average\ duration\ of\ life\ (70\ years)$

$RF\ =\ risk\ factor\ (0.05\ sv^{-1})$

RESULTS AND DISCUSSION

The purpose of the study was to examine the level of background radiation at specific dump sites in Kaduna Metropolis, Kaduna State and the results are presented in Tables 1 to 4, which show the average absorbed dose rates measured in $\mu Sv/hr$ at selected locations during morning and evening readings. Table 5 summarizes the radiological hazard indices that were computed based on the average absorbed dose rates, including the annual effective dose rate in mSv/yr and Excess Life Cancer Risk. The values presented in the tables represent the radiation levels at the dumpsites studied.

Table 1: Absorbed Dose Rate ($\mu Sv/hr$) in Unguwan Rimi Kaduna (L1)

Weeks	Absorbed Dose ($\mu Sv/hr$)		Annual Effective Dose Rate (mSv/yr)
	Morning	*Afternoon*	
1	0.22	0.24	0.28
2	0.19	0.21	0.24
3	0.17	0.20	0.22
4	0.14	0.18	0.19
AVERAGE	0.18	0.20	0.23

Table 2: Absorbed Dose Rate ($\mu Sv/hr$) in Hayin Danbushiya Kaduna (L2)

Weeks	Absorbed Dose ($\mu Sv/hr$)		Annual Effective Dose Rate (mSv/yr)
	Morning	*Afternoon*	
1	0.23	0.26	0.30
2	0.21	0.24	0.27
3	0.18	0.22	0.24
4	0.16	0.19	0.21
AVERAGE	0.20	0.23	0.25

Table 3: Absorbed Dose Rate ($\mu Sv/hr$) in Badarawa Kaduna (L3)

Weeks	Absorbed Dose (μSv/hr)		Annual Effective Dose Rate (mSv/yr)
	Morning	*Afternoon*	
1	0.28	0.33	0.37
2	0.25	0.29	0.33
3	0.24	0.27	0.31
4	0.21	0.24	0.27
AVERAGE	0.25	0.28	0.32

Table 4: Absorbed Dose Rate ($\mu Sv/hr$) in Unguwan Shanu Kaduna (L4)

Weeks	Absorbed Dose (μSv/hr)		Annual Effective Dose Rate (mSv/yr)
	Morning	*Afternoon*	
1	0.26	0.30	0.34

2	0.25	0.26	0.31
3	0.23	0.24	0.28
4	0.20	0.22	0.25
AVERAGE	0.24	0.25	0.29

Table 5: Summary of Indices of Radiological Hazard

Location	Average Dose Rate ($\mu Sv/hr$)	Mean Dose Rate. D (nGy/hr)	Annual Effective Dose Rate (mSv/yr)	ELCR X 10^{-3}
L1	0.19	190	0.23	0.80
L2	0.21	210	0.25	0.87
L3	0.26	260	0.31	1.08
L4	0.25	250	0.30	1.05
Average	0.22	227	0.27	0.95

The result presents the findings of a study conducted on four selected dumpsites to determine their absorbed dose rate, annual effective dose rate, and excess life cancer risk (ELCR). The minimum absorbed dose rate was found to be 0.19 $\mu Sv/hr$ in Unguwan Rimi and the maximum was 0.26 $\mu Sv/hr$ in Badarawa Kaduna, with 0.22 $\mu Sv/hr$ as the average value for all four (4) sites. The annual effective dose rate was calculated to be 0.27 mSv/yr, with Unguwan Rimi having a minimum average value of 0.23 mSv/yr and Badarawa Kaduna having a maximum average value of 0.31 mSv/yr. The ELCR values ranged from 0.80 x 10^{-3} – 1.08 x 10^{-3}, with an average value of 0.95 x 10^{-3}.

When compared with other authors' work, the study found that the annual effective dose rate and ELCR values in the current work were generally greater than in other studies, (Emelue *et al.,* 2013*,* Latif and Kehinde*,* 2004) except for one study conducted by Avwiri and Emmanuel. However, it is important to note that all the AEDR values reported by the other authors were below the 1 mSv/yr world standard (ICRP), and the ELCR values were also below the 1.16 x 10^{-3} standard, except for Avwiri and Emmanuel's study. Therefore, while the values obtained in the current work may be higher than those reported in some other studies, they still appear to be within acceptable limits according to the world standard.

CONCLUSION
Based on the findings of the study on the absorbed dose rate, annual effective dose rate, and excess life cancer risk (ELCR) associated with four selected dumpsites, it is concluded that the dumpsites in the study area have relatively low levels of radiation exposure, with the annual effective dose rate and ELCR values within acceptable limits according to the world standard. However, the values obtained in this study are generally higher than those reported in some other studies, which could be due to variations in the location, measurement techniques and waste management practices.

RECOMMENDATIONS
Therefore, to ensure the safety of the environment and public health, it is recommended that regular monitoring of radiation levels in the study area should be conducted to detect any possible increase in levels. Also, it is important to implement proper waste management practices that reduce radiation exposure to the public and the environment. Waste materials that are found to contain high levels of radioactivity should be disposed of properly to minimize the risk of exposure to the public. Finally, further research is needed to investigate the sources and extent of radiation exposure in the study area to provide a more comprehensive understanding of the issue.

REFERENCES
Agbalagba, E.O., Avwiri, G.O., Chadumoren, Y.E. (2013). Gross alpha and beta activity concentration and estimation of adults and infants dose intake in surface and groundwater of ten oil fields environment in western Niger Delta of Nigeria. Journal of Applied Science and Environmental Management, 17(2): 267-277.

Avwiri GO, Ebeniro JO (1998) Radionuclide Concentration in Soils and Rocks around Warri Refinery, Nigeria. Bulletin of Environmental Contamination and Toxicology 61:393-399.

ICRP (2000). Protection of public in situations of prolonged radiation exposure; ICRP Publication 82; Pentagon Press, Oxford. Ann .ICRP, 29 (1 -2).

Ogundare FO, Adekoya JA (2015) Radioactive Contamination of the Environment: A Review. Journal of Environmental Science and Public Health 2015:3.

Olanrewaju IO, Oluyemi EA, Oyekunle JAO, Balogun FA (2018) Environmental radioactivity and public exposure in Nigeria: A review. Journal of Radiation Research and Applied Sciences 11:383-394.

UNSCEAR (2008). Sources and effects of ionizing radiation. United Nations Scientific Committee on the Effects of Atomic Radiation, New York.

UNSCEAR (2011). Sources, effects and risks of ionizing radiation. United Nations Scientific Committee on the Effects of Atomic Radiation, New York..

WHO (2012) World Health Organization, *Ionizing Radiation in our Environment,* online. www.who.int/ionizing_radiation/env/en. (accessed 17-10-2021).

Production of Antimicrobial Soap Using Soya Beans Oil, Neem Seed Oil and Sesame Seed Oil

*[1]Umar, A., [2]Salisu, A. and [1]Siaka A. A.

[1]Department of Chemistry, Faculty of Physical Sciences, Federal University Dutsin-Ma (FUDMA), P.M.B. 5001, Dutsin-Ma, Katsina State, Nigeria
[2]Department of Pure and Industrial Chemistry, Faculty of Natural and Applied Sciences, Umaru Musa Yar'adua University katsina, P.M.B. 2218, Dutsin-Ma Road, Katsina State, Nigeria
*Corresponding Author's E-Mail: aumarkfr@gmail.com

ABSTRACT

In this study, a saponification reaction was used to create soap using sesame seed oil, neem seed oil, and soybean oil. A pH value of [10.34] was one of the parameters used to analyze the soap produced, indicating that it is not corrosive to the skin. Test results for foam ability [6.1 cm] indicate that the soap produced has a higher foam ability. The results of the solubility test [0.30g] indicate that the soap will not dissolve quickly in water. Corrosiveness test [3.0] results show that the soap has a low percentage of free alkali, which lessens the soap's corrosiveness to skin and qualifies it for bath use. Additionally, the disc agar diffusion method was used to evaluate the antimicrobial activity of the soap produced in vitro. Bacillus cereus and Staphylococcus aureus, two gram-positive and gram-negative bacterial species, are the reference microbes. Aspergillus nigar and Candida albicans, two fungal species, were tested at three different concentrations [500 mg/l, 250 mg/l, and 125 mg/l].

Keywords: Soyabean oil; Neem seed oil; sesame seed oil; Soap; Physiochemical; Antimicrobial.

INTRODUCTION

As a chemical substance or mixture of chemical compounds created by the reaction of fatty acids with an alkaline solution, soap is an alkali metal salt of a long-chain fatty acid. The lengthy hydrocarbon chain that makes up a soap molecule has a carboxylic acid group on one end that is ionically linked to a metal ion, typically potassium or sodium. (Acquanye *et al.,* 2001). Potassium hydroxide (KOH) and sodium hydroxide (NaOH), commonly referred to as caustic soda, are the two common alkaline solutions used in soap making. Typically, liquid soap is made with potassium hydroxide, and solid soap is made with sodium hydroxide. In contrast to soaps formed from divalent metals like calcium and magnesium, which are water-insoluble, NaOH and KOH are soluble in water.

Soaps are mainly used as surfactants for washing up liquids, bathing, and cleaning, but they are also used in textile spinning and are important components of lubricants. There are three main saponification reactions for producing soap which are;

  i.   Direct saponification of fats and oils(Cold method)
  ii. Neutralization of fatty acids(Hot method) and
  iii. Saponification of fatty acid methyl esters (Hot method)

However, only the soap business frequently uses the saponification of fats and oils and the neutralization of fatty acids. Triglycerides react with alkali during saponification to create metal soap and glycerine. Tallow and coconut oil are the traditional basic materials used to make soap. Other naturally occurring fats that can be profitably used to create soap include palm, olive, cottonseed, corn, and soybean oils. However, due to PKO's increased availability and roughly 47% dodecanoic (lauric) acid content, soap producers are increasingly using it in place of tallow and coconut oil in their current global production processes. Furthermore, the crucial fatty acids that are involved in soap making are C_{16}-C_{18} and C_{12}-C_{14} (Danielle *et al.,* 2016).

These fatty acids are crucial to the process of making soap because C16–C18 fatty acids help the soaps have detergency, while C12–C14 fatty acids help the soaps lather and wash well. Conversely, the strength and purity of the alkali, the kind of oil used, the degree of saponification, and the age of the soap all affect its chemical properties. For example, moisture content, total fatty acids (TFM), pH, free alkali, and percent chloride. (Ajekigbe, 2006).

In addition to cleansing dry skin and leaving it feeling smooth and silky, anti-microbial soaps also include biological or chemical ingredients that work specifically to fight bacteria. Due to their potent antibacterial properties, neem and sesame seed oils are frequently utilized biological ingredients; triclosan, trilocarbon, and chloroxylenol are examples of chemical components (Moody *et al.,*2004).

MATERIALS AND METHODS

Ethanol, sodium hydroxide, dimethyl sulfoxide, sodium carbonate, and sulfonic acid are all of the reagents that are used. A pH meter, weighing balance, hot plate, and oils from soybeans, sesame seeds, and neem were also utilized for the saponification process. All glassware is washed, cleaned, and dried at 105°c in an oven.

Method
Procedure for Preparation Antimicrobial Soap Using Cold Process
The method reported by (Wara *et al.,* 2009) was adopted.
STEP ONE
32 g of NaOH was measured and dissolved into 100 ml of distilled water, which gave a lye solution of 0.22 g/ml of NaOH.
STEP TWO
Then, 50 ml of neem oil and 50 ml of sesame oil was measured and combined with 100 ml of soya beans oil, and stirred to obtain a homogeneous mixture of the oils (blending).
STEP THREE
Then, 100 ml of 0.33 g/ml lye solution was added into the oil gently with continuous stirring until a homogenous mixture was obtained.
STEP FOUR
Then 15 ml of silicate and 15 ml of perfume were added and the mixture was stirred gently until it reached trace.
STEP FIVE
The soap solution was then poured into the mold and it was covered properly, and left undisturbed for 24 hrs.
STEP SIX
After 24 hours the soap was removed from the mold.
STEP SEVEN
Then, the soap was placed on polyethylene leather and allowed to dry and cure properly for 7 days by turning it over every 24 hours, so that any unsaponified lye can be evaporated from the soap.

Physicochemical Properties
Foam Ability Test
The method reported by (lunkeheimera and malysa, 2003), in a 500 ml measuring cylinder, 1g of soap was weighed and dissolved in 100ml of distilled water. After giving the mixture a good shake for two minutes, it was left to stand for an additional two minutes. After that, the height of the foam was measured and noted.

pH Analysis
The method reported by (*tur'yan et al., 1996*), An analysis was conducted on the soaps' pH values using a pH meter (JENWAY 3510). The pH was measured with the meter after 2.0 g of the produced soaps were dissolved in 50 ml of deionized water. For the soap sample, this was done three times, and the mean was determined.

Corrosiveness Test
The method reported by (Nkafamiya *et.al.,* 2002), a conical flask was filled with 2g of the thoroughly combined material after it had been precisely weighed. 10 ml of phenolphthalein and neutralized 95% ethanol were then added. After that, 0.1M NaOH was added and the mixture was shaken continuously until a pink color persisted for 30 seconds. Using the formula, the percentage of free fatty acid was determined.

$$\%FFA = \frac{V \times M \times 2.82mg}{Sample\ weigh\ (g)}$$

Where;
V= Volume of NaOH used for titration
M = Concentration of NaOH

Solubility Test
In the method reported by (Sadeghian *et al.,* 2007)   About 20g of the soap sample was weighed and dropped into a conical flask and about 150 ml of distilled water was added. Then the flask was shaken for 30 secs and it was allowed to settle for 1 min interval. The procedure was repeated about 3 consecutive times, then the soap sample was removed from the flask using forks and it was re-weighed and recorded.

Antimicrobial Susceptibility Test

The method was reported by (Osborne *et al.,* 2003*).* The well diffusion method was used to test for antibiotic susceptibility following national committee or clinical laboratory standards. Using the serial dilution method, soap stock solutions were made at concentrations of 500 mg/L, 250 mg/L, and 125 mg/L. Mueller Hinton Agar plates were used to test the soap samples for the presence of antimicrobial qualities. A sterile borer was used to create a 5 mm diameter well in the media before the plates were infected with bacteria. The 0.5 McFarland standard solution, a reference used to adjust the turbidity of bacterial suspensions so that the number of bacteria will be within a given range to standardize microbial testing, was applied to the plate prior to the test bacterium's inoculation. The surface of the agar plates was streaked over the entire sterile agar using a sterile swab. To remove any remaining moisture, the plates were left for three to five minutes. After the plates were inoculated with the bacteria, 500 mg/L, 250 mg/L, and 125 mg/L of each test soap solution were dispensed into each well and the incubator was set to 370C. Each plate was checked for inhibition zones after it had been incubated for 24 hours. The inhibition zones were measured in millimeters using a metric ruler.

RESULTS AND DISCUSSION
Weight Of The Soap Produced
While the total weight of the raw materials used to make the bar soap was 168 g, the total weight of the bar that was produced was 132g. Because "mass is not conserved in an open system," the result demonstrates that there is an increase in weight following the reaction. (Warra, 2015).

Table 1: Physicochemical properties
The table below shows the observed values and the physicochemical properties of the soap produced**.**

		Observed values
Sample A	pH	10.34
	Foam height(cm)	6.1cm
	Solubility (gram)	0.3g
	Corrosiveness (% of free acid)	3.0

Key: A represent antimicrobial soap produced.

According to E-E Mak (Mensah *et al.,* 2002), "the pH range of bathing soap should be between 9 and 11," the soap sample meets the standard for bathing soap based on the results above. As a result, the outcome demonstrates that the soap is safe for the skin.

It is evident from the above results that soap produced naturally has a high foaming ability because foaming agents, which are primarily used to increase a soap's foaming ability, are not present. Examples of these agents are texapon, sodium laureth sulfate, and sulfonic acid.

Based on the aforementioned results, a solubility test was carried out, and the soaps generated were made no more than two weeks before the analysis's commencement. The longer the soap sample is allowed to cure, the more water and free alkali it evaporates; in other words, the more air it is exposed before use, the more firmly it becomes, giving it its long-lasting qualities (Sadeghian *et al.,*2007).

Because neem oil, sesame oil, and soybean oil contain ingredients like oleic acids, carotenoids, stearic acid, palmitic acid, and linolenic acid, it is evident from the above result that an increase in the concentration of the oil's antimicrobial properties lowers the percentage of free alkali in the soap and, consequently, reduces the soap's corrosiveness to the skin, making the soap suitable for use (Chatterjee *et al.,* 1994).

So as the concentration of the antimicrobial content of these ingredients increases. These ingredients all have pH in the range of 6.5 -3.5 (Sampson *et al.,* 2002). Therefore, as their amount increases in the soap mixture which has pH in the alkaline region the pH of the soap solution tends to decrease (Sampson *et al.,* 2002).

Therefore, taking the pH results shown above into consideration it can be seen that as the pH value increases the corrosiveness also increases and vice versa. The Longer curing period they take before usage, allows it to evaporate all moisture and free alkali.

Antimicrobial Test
After the above analysis, soaps were found to be suitable best bar soap to use the soap sample was subjected to the antimicrobial test.

Table 2: Antimicrobial test result

Test Organism	Mean Zones Of Inhibition(mm)

	Conc. Of Soap A(mg/ml)		
	500mg/L	250mg/L	125mg/L
B. Cereus	30	25	16
S. aureus	34	29	24
A. nigar	40	27	21
C. albicans	35	28	23

Clinical isolates of bacteria and fungi were used as test organisms for an antimicrobial susceptibility test on the antimicrobial soap that was produced. (*Aspergillus nigar and Candida albicans*) are the fungal organisms, whereas Bacillus cereus and Staphylococcus aureus are the Gram positive and Gram negative bacterial species. As can be seen from the above results, which display the zones of inhibition of the soap sample against the test organisms to determine whether the soap sample affects the microorganisms used, the soap produced appears to have a greater effect on fungal organisms (*Aspergillus nigar*), suggesting that it has a significant impact on the functionality of microorganisms and can therefore be used as an antimicrobial.

CONCLUSION

In summary, the investigation demonstrated the three oils' potential for use in soap making. The soap can be referred to as "antimicrobial soaps" since the results indicate that it has antimicrobial activity and that it becomes more active as the concentration of the antimicrobial agent (neem and sesame oil) increases. But even though the activity increases with an increase in concentration the concentration should not be very much as it will affect other significant properties of the soap, and it also shows that the soap is not corrosive to skin, therefore this research work shows that the soap produced can effectively replace commercial antimicrobial soaps in treating skin diseases

RECOMMENDATION

i.   It would be beneficial to carry out additional research on the production of soap using neem, sesame, and soybean oils to fully utilize their potential and address Nigeria's unemployment issues.

ii. Additionally, this study focused only on two types of microorganisms: fungi and bacteria. Future research on other microorganisms could potentially be conducted more broadly than it was here.

iii. Other procedures for the preparation of antimicrobial soap should be employed in the next research for further study and improvement of educational creativity among scientists.

iv. From the above research conducted government should give the students /other people more effort and contribution to improved entrepreneurship among the people and increasing economics as well as evaluate the poverty of the nation.

REFERENCES

Acquanye, D., Smith, M., Letchamo, W., Angers, P., Simon. Y., (2001). "*Soap and Detergent Production*" Agro Business in Sustainable Natural African Production. Vol. 2(4):Pp1-3.

Ajekigbe, P.G., (2006). "Yoruba Traditional Soap Production" *The Nigerian Field.*vol 6(2): pp 33-40.

Danielle, M., Conover, Kristen, E.G., (2016). "Comparison of two Plain Soap Types for Removal of Bacteria and Viruses from Hands with Specific Focus on Food Service Environment". University .of Arkansas, Department of food science. Center for Food Safety, USA.

Lunkenheimere., K., Malysa, K., (2003). Simple and generally applicable method determination and evaluation of foam properties, *journal of surfactants and detergents*, 6:69-74

Mensah, Kwame D., Ike, Z., (2002). "Craft Traditions of Palestine". Sunbula. Archived from the original on March 21, 2008. Retrieved 2019/12/18.

Nkafamiya., I,I., Maina., H.M., Usemeahon, S.A., Modibbo., U.U., (2002). *African journal of science,*4(7) ISSN1996-0794: pp 418-421 available from   https://academicjournals.org/ajfs

Osborne, T., Nef, T,. John U., (2003). "A Comparison of Industrial Growth in France and England from 1540 to 1640: III". *The Journal of Political Economy*. **44** (5): 643-666 (660ff.). doi:10.1086/254976. JSTOR 1824135.

Sadeghian M., Allison, T., *et al* (2007) "Repeal of the Soap Tax". Hansard. UK Parliament.Archived from the original on 24 March 2013. Retrieved 2019/11/27

Tur'yan., Y.I., Berezin., Y.U., Kulselmen, I., Shenher., A., (1996). pH-metric determination of acid value in vegetable oils without titration *journal of the American oil chemist society*, 73 (3), pp 295-301 https://link.springer.com

Warra, A.A., (2009). Extraction and chemical analysis of indigenous sheanut oil proceeding of the 1st National Conference of the academic staff union of polytechnics. Waziri umaru federal polytechnic chapter ,Birnin Kebbi, Nigeria. Pp 160-162.

Warra, A.A., (2015). "A report on Soap Making in Nigerian Using Indigenous Technology and Raw Materials"'. African Journal of Pure and Applied Chemistry. Vol. 7(4):pp 139-145.

Enhanced Photocatalytic Degradation of Congo Red Over Nanosized C –ZnO and Cu-ZnO Under Visible Light Irradiation

*Auwal, Y., Siaka, A. A., Kamaluddeen, S. K. and Abdullahi, H.

Department of Chemistry, Faculty of Physical Sciences, P.M.B 5001, Federal University Dutsin-Ma, Katsina State, Nigeria.

*Corresponding Author's E-mail: ayushau21@fudutsinma.edu.ng; auwalyushau2018@gmail.com

ABSTRACT

This work presents a new, highly efficient visible-light responsive nanosized C-doped ZnO (C-ZnO) and Cu-doped ZnO (Cu-ZnO) synthesized by mechanochemical and co-precipitation methods for the heterogeneous photocatalytic removal of congo red (CR) from the wastewater. The prepared catalysts were characterized by x-ray diffraction (XRD), energy dispersive spectroscopy (EDS), ultraviolet-visible (UV-Vis) spectrophotometry and surface area analysis. The XRD patterns for the synthesized C-ZnO and Cu-ZnO nanoparticles were in good agreement with that of the standard wurtzite structure of the standard ZnO catalyst. The EDS analysis confirmed the presence of C, Cu, Zn and O atoms for the C-ZnO and Cu-ZnO respectively. Cu-ZnO photoresponsive catalyst was found to exhibit better visible light photocatalyic activity than C-ZnO under identical experimental conditions due to the larger surface area and low band gap of Cu-ZnO nanocrystalline. The photocatalytic degradation of congo red over the ZnO, C-ZnO and Cu-ZnO nanoparticles was follows pseudo-first kinetics scheme with the apparent rate constant (k) of 1.75×10^{-3} min^{-1}, 1.89×10^{-3} min^{-1} and 1.91×10^{-3} min^{-1} respectively. Therefore, C-doped ZnO and Cu-doped ZnO photocatalysts can be used to remove congo red dye from the wastewater

Keywords: Photocatalysis, ZnO, C-doped ZnO, Cu-doped ZnO, and Congo red

INTRODUCTION

Water pollution is the introduction of contaminants into the aqueous environment (Danwittayakul *et al*., 2015). The textile, paper, ceramic, plastic, paint and pharmaceutical industries use huge amounts of water and approximately two percent of azo dyes are discharged directly in industrial effluent of which, about 10% are lost during the dyeing process (Sayaya *et al.,* 2023). Azo-dyes are heterocyclic aromatic compounds that have –N=N- linkage and are released into the open water which can lead to adverse effects on the ecosystem due to the toxicity (Danwittayakul *et al*., 2015). Congo red (CR) is a well-known anionic azo-dye and is presently listed among the superior pollutants of wastewater (Hamza *et al*., 2013). Some of the adverse effects of CR include; difficulty in breathing, eye and skin irritation, vomiting, diarrhea, mild haemolysis, carcinogenic and reduced penetration of light and oxygen into the aqueous environment (Arul *et al.,* 2019). Therefore, the removal of CR from the wastewater is of great importance to human and aquatic life (Gaya *et al*., 2008; Hamza *et al.,* 2013). Several physical and chemical methods such as adsorption, filtration, reverse osmosis, precipitation, coagulation and decantation for wastewater treatment have been employed (Abdullahi *et al.,* 2019). These methods however, reported insignificant success in the removal of CR due to the large molecular structure of CR, cost, formation of secondary sludge, and require extra planning (Saeid *et al.,* 2019).

Today, photocatalysis has attracted the attention of many researchers as an effective technology in the degradation of pollutants from the environment (Danwittayakul *et al*., 2015). Heterogeneous photocatalysis is a light-induced catalytic process that reduces or oxidizes organic pollutants through redox reactions activated through the electron-hole pairs generated on the surface of metal oxide semiconductors upon beyond band gap light irradiation (Danwittayakul *et al*., 2015). Some of the major applications of heterogeneous photocatalysis include removal of trace metals, removal of organic and inorganic pollutants, purification of air, artificial photosynthesis, degradation of cancer, degradation of microorganisms, degradation of pathogens, water splitting, and self-cleaning (Hamza *et al*., 2013). The beauty of heterogeneous photocatalysis over the conventional methods is the absence of formation of secondary sludge and use of natural sunlight that can lead to the reduced cost of treatment (Gaya *et al*., 2008). Zinc oxide (ZnO) is a well- known photocatalyst is widely used for the degradation of organic pollutants including the CR from the environment (Elaziouti *et al.,* 2011). However, ZnO demonstrated ignificant success for the photocatalytic removal of contaminants in comparison to TiO_2, ZnS, Fe_2O_3, WO_3, SnO_2, ZrO_2, Cu_2O, and V_2O_3 (Daneshvar *et al.,* 2007) due to its low cost, availability, stable to light and environmentally friendly [(Roy *et al.,* 2023). Band gap, surface area and surface defects of ZnO are important factors for enhanced photocatalytic performance (Danwittayakul *et al*., 2015). The higher effective surface area leads to higher absorption of organic contaminants, while enhanced photocatalytic activities lead to its efficient degradation. Recently, ZnO catalyst has been prepared by different methods such as solvothermal, hydrothermal, fabrication, sol-gel, precipitation and co-precipitation. Co-Precipitation synthesis is preferred because the method does not require sophisticated instruments less time consumed and

inexpensive (Rohan *et al*., 2015). Moreover, the photocatalytic of organic pollutants over the ZnO nanoparticles is partly limited to ultraviolet light of the electromagnetic irradiation due to its wide band gap (3.2eV) (Hamza *et al.,* 2013). In addition ZnO is suffered by the electron recombination process and is prone to photocorrosion (Li *et al*., 2018).

Recently, different approaches have been used to extend the ultraviolet light to visible light absorption. This however, is achieve by the modification of the band gap for the semiconductors materials such as doping, coupling of semiconductors, dye sensitization, ion impregnation and metal deposition (*et al.,* 2019). Doping is preferred due its chemical stability and high electron mobility (Danwittayakul *et al*., 2015) which are essential for enhanced heterogeneous photocatalysis. The method however, involves the introduction of a small amount of impurity known as dopant (s) onto the surface catalyst (Gaya *et al.,* 2008). Doping is mostly employed by metal, non-metal, noble metal and transition metals. Furthermore, transition metal and non-metal dopants are the most important for the photocatalytic degradation of organic pollutants due their chemical stability and higher photocatalytic degradation efficiencies. C-doped ZnO (C-ZnO) and Cu-doped ZnO (Cu-ZnO) have been extensively used as photo catalysts with better activity for the degradation of organic contaminants in wastewater due to their chemical stability and present of dopant play an importance role in hindering the electron-hole recombination. Although a lot of research targeted to the development of novel catalysts to improve the efficiency, there are still very few reports on real world photocatalytic applications for the removal of pollutants from the wastewater.

The aim of this work was to synthesize nanosize C-ZnO and Cu-ZnO via mechanochemical and precipitation methods respectively and compare the effectiveness of visible light using congo red under identical experimental conditions. Characteristics of ZnO, C-ZnO and Cu-ZnO photocatalysts were examined and reported in this study. In addition, the mechanism of photocatalysis, degradation of congo red over C-ZnO and Cu-ZnO nanoparticles under UV and natural sunlight, reusability study and kinetics study are also evaluated in this work.

MATERIALS AND METHODS
Materials
All the chemicals required in this study were of analytical grade. Some of these chemicals includes Zinc nitrate [(Zn(NO$_3$)$_2$, 98%], urea NH$_2$)$_2$CO, 99%), zinc sulphate heptahydrate (ZnSO$_4$.7H$_2$O, 97%), copper sulphate hexahydrate (CuSO$_4$.6H$_2$O, 98%), hydrochloric acid (HCl, 98%) and Congo red (98%) were supplied by Sigma Aldrich Canada while potassium hydroxide (KOH, 98%) and ammonium hydroxide (NH$_4$OH, 98%) were obtained from BDH, Poole, England, 300 W xenon lamp and tungsten lamp obtained from Sabon Gari Kano. All experiments were carried out in a 30 cm long, 1.0 L capacity, round bottom batch photoreactor which maintained at 298K. The visible light source was a 300W Xenon lamp emitting at 400 nm. This lamp was jacketed in cylindrical quartz glass, dipping down the reactor bottom.

Methods
Synthesis of Zinc Oxide (ZnO) Nanoparticle
ZnO nanoparticles (NPs) was prepared by the precipitation method. Zinc nitrate heptahdydrate (Zn(NO$_3$)$_2$.7H$_2$O) (50.89 g) was dissolved in 500 ml of deionized water under vigorous stirring till homogeneous solution was obtained. Then 10.55 g of ammonium hydroxide (NH$_4$ OH) were added at constant rate to the solution with vigorous stirring at 80 °C and pH 9. The precipitate formed was aged for 24 h, recovered by centrifugation, washed several times with deionized water and filtered under vacuum to obtain uncalcined ZnO catalyst. The product formed was dried overnight in an oven at 140 °C, calcined in a muffle furnace at 500 °C for 3 h, and cooled to room temperature to obtain undoped ZnO NPs (Hamza *et al.,* 2013).

Synthesis of Carbon-doped Zinc Oxide (C-ZnO) Nanoparticles
The C-ZnO photocatalyst was prepared by mechanochemical grinding of ZnO (10.00 g) and urea (1-15.00 wt % versus ZnO) in an agate mortar for 4 h. The mixture was calcined in a muffle furnace at 500 °C for 3 h. The product formed was ground to fine powder and then labeled as C- ZnO nanoparticles (Auwal and Gaya 2023).

Synthesis of Copper-doped Zinc Oxide (Cu-ZnO) Nanoparticles
The Cu-ZnO photocatalyst was prepared by the chemical co-precipitation method. The doping of ZnO with Cu was carried out using 25.00 g of zinc sulphate heptahydrate (ZnSO$_4$.7H$_2$O) and 5.00 g of copper sulphate hexahydrate (CuSO$_4$.6H$_2$O). 5.00 g of CuSO$_4$.6H$_2$O (0.3M) was dissolved in 400 ml of deionized water under vigorous stirring till a homogeneous solution was obtained. Then an aqueous solution (200 ml) of potassium hydroxide (KOH) (0.5M) was added at a constant rate to the solution with vigorous stirring at room temperature until the pH of the solution reached to 9. The precipitate formed was aged for 24 h, recovered by centrifugation, washed several times with deionized

water until the pH was 7. This product was dried overnight in an oven at 140 °C and then finally it was calcined at 500 °C for 3 h in a muffle furnace and leveled as Cu-ZnO nanoparticles (Auwal *et al.,* 2023).

Characterization of Synthesized Photocatalysts
The prepared photocatalysts were characterized by x-ray diffraction (XRD) analysis using a Philips Xpert Pro diffractometer operated with a CuK_α radiation (λ= 1.54468 Å) in the 2θ range 5-70 ° at 30 kV, 30 mA and scanning rate of 2 min. The average crystallite size has been estimated using Debye-Scherer (Eq. 1). The surface areas for the synthesized photocatalysts were estimated from the equation 2 and 3 respectively.

$$r = \frac{k\lambda}{\beta \cos\theta} \tag{1}$$

$$SSA = \frac{S.A}{V \times \rho} \tag{2}$$

$$SSA = \frac{6000}{D \times \rho} \tag{3}$$

Where r is the average particle size, k is the Debye- Scherer constant (0.89), λ is the wavelength of the x-ray radiation, β is the full width of half maximum intensity (FWHM), θ is the diffraction angle at the position of peak maximum, SSA is the specific surface area, SA is the surface area, ρ is the density of the prepared catalysts.

The elemental analysis was done with a Phoenix proxy energy dispersive x-ray spectrometer (E-max-60 spectrometer). The facility was operated at the same scale (30 µm), magnification (2,500) and accelerating voltage (15 kV).

The band gap values of the catalysts were calculated using Schuster-Kubelka-Munk relation (Eq. 4) from the electronic data recorded over wavelength range 200-800 nm on the Lambda 35 Perkin Elmer UV-Visible spectrophotometer.

$$(\alpha h\nu)^{\frac{1}{n}} = K(h\nu - E_g) \tag{4}$$

Where α is the absorption coefficient obtained from Beer's law, h is the planck's constant, ν is the frequency of vibration, K is the proportionality constant and E_g is the band gap energy of the semiconductor photocatalysts.

Preparation of Stock Solution of Congo Red (CR) Dye
Stock solution of CR was prepared by dissolving 1.0 g of congo red in 1.0 L of deionized water to obtain a stock concentration of 1000 mg/L. Experimental CR solutions of desired concentrations (5, 10, 15, 20, 25 and 30 mg/L) were prepared by appropriate dilution of the mother solution.

Photocatalytic Experiments
The photocatalytic activity of the synthesized nanoparticles was evaluated using congo red (CR) dye as a model substrate. All experiments were conducted in a 30 cm long, 1.0 L capacity, round bottom batch photoreactor which was maintained at 298 K. The visible light source was a 300 W Xenon lamp emitting at 400 nm. This lamp was jacketed in cylindrical quartz glass, dipping down the photoreactor bottom (Yusuf & Gaya 2018). Typically, 500 ml aqueous solution of the desired amount of CR (10-30 mg/L) and desired amount of photocatalyst(0.1-0.8 g) were added to the photoreactor and the pH of the suspension was adjusted using 0.1 molL^{-1} NaOH and HCl. This mixture was magnetically stirred for 30 min in the dark to establish adsorption equilibrium, and then exposed to irradiation under continuous stirring at room temperature (25°C) for 160 mins At interval of 20 mins, aliquot of 4 ml was taken and filtered using 0.45 µm cellulose nitrate filter and analyzed for residual concentration of CR at 498 nm using a T60 UV-Vis spectrophotometer. The percent photodegradation (D %) was calculated using Eq. (5).

$$D\% = \frac{A_0 - A_t}{A_0} \times 100 \tag{5}$$

Where A_o and A_t are the initial and final absorbance of CR, and t is the irradiation time. Thereafter comparative studies such as dark adsorption and photolysis over the C-ZnO and Cu-doped ZnO nanoparticles were also determined. These were compared with photocatalysis over C-ZnO and Cu-ZnO under visible irradiation.

Control Experiments
A systematic control experiments for the photocatalytic degradation of congo red over the ZnO, C-ZnO and Cu-ZnO nanoparticles under ultraviolet (UV) (96W halogen lamp) irradiation and natural sunlight illumination were conducted and compared with the photocatalysis of CR using C-ZnO and Cu-ZnO photocatalysts under visible (300W Xenon lamp emitting at 400 nm) light irradiation. The power intensity of sunlight was measured by using a solarimeter (SL-200-KIMO) every half-hour and found to be 700 Wm^{-2} (the experiments were carried out in January 2023). The percentage photodegradation efficiencies were calculated using Eq. (5).

RESULTS AND DISCUSSIONS

Photocatalysts Characterization
Nanostructural Analysis
The x-ray diffraction (XRD) analysis for the as synthesized catalysts was conducted and the result is presented in Table 1.0. It can be seen that the x-ray diffraction patterns of the as prepared ZnO, C-ZnO and Cu-ZnO nanoparticles were matched with that of the hexagonal wurtzite structure of the standard ZnO photocatalyst. No additional peaks were demonstrated by the diffractogram of ZnO, C-ZnO and Cu-ZnO photocatalysts. This indicated the high purity of the synthesized catalysts. These results were consistent with the literature report (Elaziouti *et al*., 2011). The average crystallite size and surface area of the synthesized photocatalysts were shown in Table 1. It is seen from Table. 1.0, that the average crystallite size for the bare ZnO C-ZnO and Cu- ZnO nanoparticles were found to be 30.25, 26.52 and 22.63nm respectively, which is consistent with the literature report (Nouria *et al.,* 2021). These might to be attributed to large surface area (51.33 m^{2}g^{-1}) of the Cu-ZnO catalyst.

Table 1: Physiochemical properties of the ZnO, C-ZnO and Cu- ZnO photocatalyst

Catalyst.	Crystallite size, D (nm)	Specific surface area (m^{2}g^{-1})	Band gap (eV)
Bare ZnO	30.25	35.33	3.32
C-doped ZnO	26.52	40.78	3.02
Cu-doped ZnO	22.63	51.33	2.62

Nanoelemental Analysis
The energy dispersive x-ray (EDX) analysis was performed to obtained the elemental comoposition of the as synthesized catalysts   The weight and atomic percent composition of Zn and O atoms for the bare ZnO, C. Zn and O for C-doped ZnO and Zn, O and Cu atoms in the Cu-doped ZnO are displayed in Table 2. Even though usually ZnO is considered as an n-type semiconductor where most defects are interstitial zinc and oxygen vacancy, our results showed the deficiency of zinc and excess of oxygen which implies the existence of interstitial oxygen and the less observed p-type semiconducting ZnO nanoparticles.

Table 2: Weight and Atomic percentage of the constituents of bare ZnO, C and Cu-doped ZnO photocatalyst

Element	Bare ZnO		C-doped ZnO		C-doped ZnO	
	Wt%	At%	Wt%	At%	Wt%	At%
C K		1.00	4.94	2.50	-	-
Cu K	-		-	-	5.94	3.50
Zn K	18.98	51.52	23.02	53.88	23.02	54.88
O K	81.02	48.48	72.04	43.62	71.04	43.62
Total	100		100		100	

Evaluation of Photocatalytic Activities
Experiments were performed to evaluate the contribution of background reactions to the photocatalytic CR removal over synthesized C-ZnO and Cu-ZnO photocatalysts. The effects of irradiation time on the percentage removal of CR over bare ZnO, C-doped ZnO, Cu-doped ZnO, adsorption and photolysis over 160 min is shown in Fig. 1. From the figure, the adsorption of CR in a suspension of 0.2 g/L catalyst at pH = 12 in the dark results in the removal of less than 29.45 % of this chemical compound due to the non-availability of hydroxyl radicals on the surface of the catalyst. In the photolysis, the percentage removal of CR was 15.11% probably due to the absence of photocatalyst in the CR solution. Conversely, the percentage removal of CR by photocatalysis over the bare ZnO, C-doped ZnO and Cu-doped ZnO were 80.10%, 86.11% and 98.90%, respectively, which clearly demonstrates that the as-synthesized C-doped ZnO and Cu-doped ZnO photocatalysts has a better photoeffiency for the removal of CR than the bare ZnO catalyst.
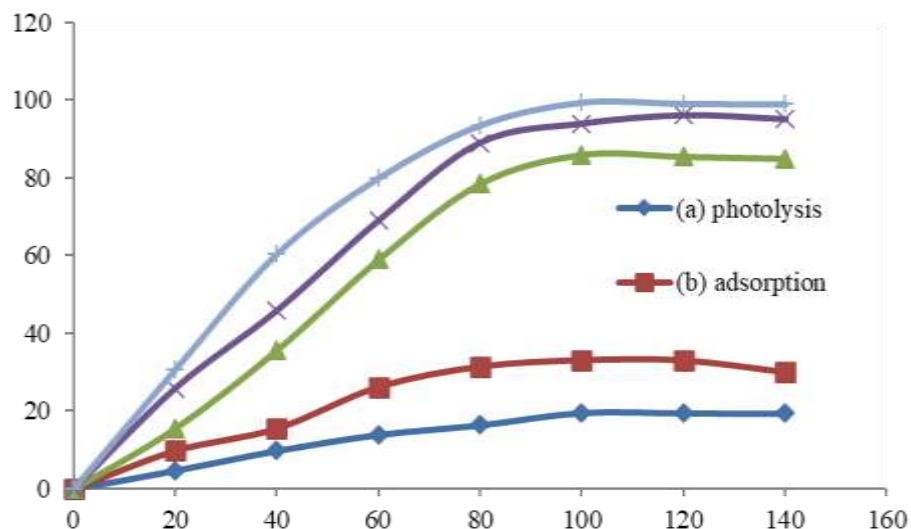
Figure 1: Effect of irradiation time on the photocatalytic degradation of CR under different processes. (a) photolysis. (b) adsorption (c) photocatalysis over bare ZnO. (d) photocatalysis with C-doped ZnO and (e) photocatalysis with Cu-doped ZnO nanoparticles.

Control experiments

In order to evaluate the effect of irradiation time on the photocatalytic removal of CR using the undoped ZnO and C-doped ZnO Cu-doped ZnO nanoparticles under visible light irradiation over 160 min, two further control experiments were conducted under two different conditions (1) under ultraviolet (UV) and (ii) under natural sunlight at optimal reaction variables (5.00 mg/L CR initial concentration, 0.1 g/L of catalysts and initial pH of 10 and their results were displayed in Fig. 2 and Fig. 3 respectively. From the Fig.2, the percentage removal of CR by photocatalysis over the undoped ZnO and C-doped ZnO nanoparticles were 72% and 80%, respectively, which clearly demonstrates that the as-synthesized C-doped ZnO photocatalyst has a better photoeffiency for the removal of CR than the undoped ZnO catalyst. The high photocatalytic activity of the C-doped ZnO can be attributed to the possible penetration and high stimulation of nanoparticles by ultraviolet (UV) lamps

.
Figure 2: Effect of irradiation time on the photocatalytic degradation of CR under UV light irradiation (a) C-doped ZnO (b) Cu-doped ZnO (c) bare ZnO.

Conversely, the Fig. 3 indicated that the percentage removal of CR by photocatalysis over the undoped ZnO and C-doped ZnO nanoparticles were 61 % and 70 %, respectively, which clearly demonstrates that the as-synthesized C-doped ZnO photocatalyst has a better photoeffiency for the removal of CR than the undoped ZnO catalyst. The high photocatalytic activity of the C-doped ZnO can be attributed to the possible penetration and high stimulation of nanoparticles by sunlight.
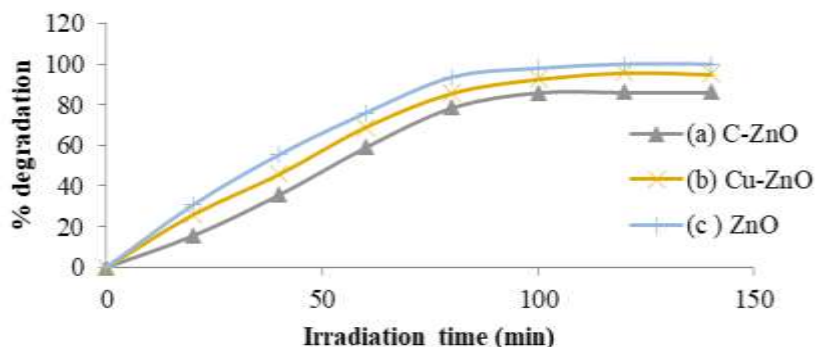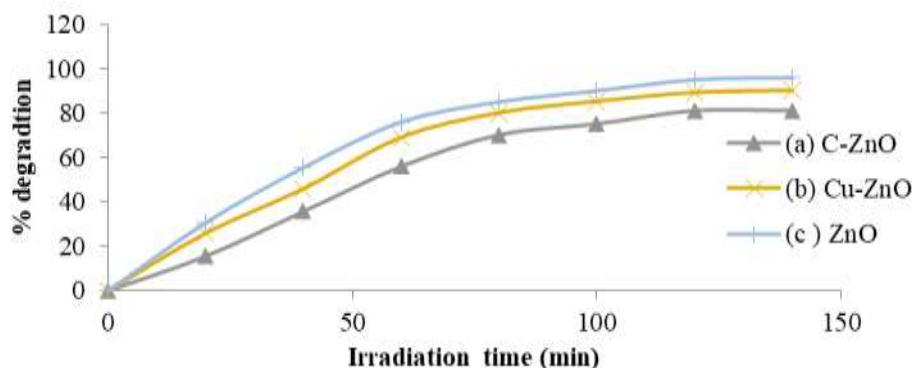
Figure 3: Effect of irradiation time on the photocatalytic degradation of CR under sunlight irradiation (a) Cu- ZnO (b) Cu-doped ZnO (c) bare ZnO

Stability of C-doped ZnO and Cu-doped ZnO photocatalysts
In order to determine the usability and stability of the C-doped ZnO and Cu-doped ZnO nanoparticles, a systematic experiment was performed at 0.2 g/L of desired catalyst, initial pH of 10, and 10.00 mg/L of CR initial concentration. Residual catalyst from degradation experiment was filtered, washed and dried and then recycled in fresh experiment and the result was depicted in Fig.4
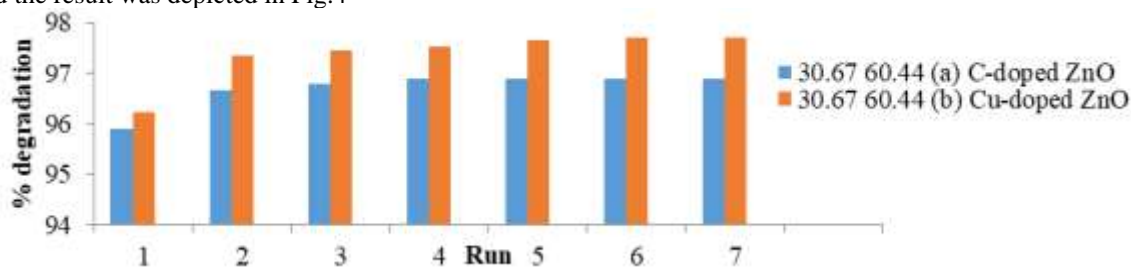
.
Figure 4: Stability of (a) C-doped ZnO (b) Cu-doped ZnO Nanoparticles.

From the Fig.4, it can be seen that the degradation of congo red increased steadily from the 1st and 2nd cycles but 3rd, 4th, 5th, 6th and 7th cycles remained the same. This clearly shows the stability and effectiveness of the C-doped ZnO and Cu-doped ZnO photocatalyst in the degradation of congo red.

Kinetics Profile
The kinetics of the photocatalytic removal of congo red over the bare ZnO , C-doped ZnO and Cu-doped ZnO photocatalysts under visible light were investigated and the results are presented in Fig. 5. It can be seen from the Fig.5 that the plot of $\ln \frac{[CR]_0}{[CR]_t}$ verse time gives a straight line graph that passing through the origin for ZnO, C-ZnO and Cu-ZnO nanoparticles. Therefore, the photocatalytic degradation of CR over the ZnO , C-doped ZnO and Cu-doped ZnO photocatalysts were nicely fitted pseudo-first order model when compared with the pseudo-zero and pseudo-second order plots.

Figure 5: Pseudo-first order plot for CR removal (a) over bare ZnO (b) over C-doped ZnO (c) over Cu-doped ZnO catalyst

The rate constant was obtained from the slope. The rate constant (k) obtained in this study is presented by the Table 3. The photocatalytic removal of congo red over the undoped ZnO, C-doped ZnO and Cu-doped was nicely fitted with the pseudo-first order kinetic scheme with rate constant (k) of 1.75×10^{-3} min^{-1}, 1.89×10^{-3} min^{-1} and 1.91×10^{-3} min^{-1} respectively.
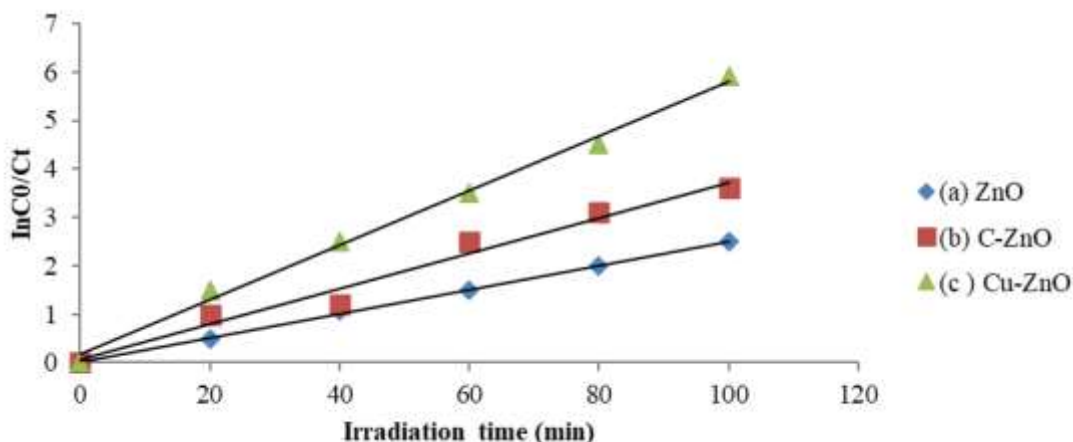
Table 3: Kinetic parameters for undoped ZnO, C-doped ZnO and Cu-doped ZnO photocatalyst

Catalyst	Pseudo-zero-order		Pseudo-first order		Pseud-second order	
	$k(10^{-3}$moldm^{-3}s^{-1})	R^2	$k(10^{-3}$ min^{-1})	R^2	k (10^{-3}moldm^{-3}s^{-1})	R^2
ZnO	2.14	0.956	1.75	0.998	1.09	0.894
C-ZnO	1.43	0.961	1.89	0.988	1.12	0.901
Cu- ZnO	3.11	0.958	1.91	0.995	1.18	0.898

CONCLUSION

The C-doped ZnO and Cu-doped ZnO nanoparticles were successfully synthesized and characterized using XRD, EDX and UV/Vis spectrophotometry. Cu-doped ZnO photocatalyst was found to exhibit better photocatalytic activitied than C-doped ZnO and ZnO catalysts under visible light irradiation due to the narrower band gap and larger surface specific area of Cu-doped ZnO when compared with ZnO and C-doped ZnO nanoparticles. The photocatalytic degradation of congo red was nicely follows pseudo-first order kinetics on both ZnO, C-doped and Cu-doped ZnO nanoparticles.

REFERENCES

Abdullahi, M.I. Irfan, A. S. Faheem, A. Ayesha, T. Muhammad, Z. I and Sayed, R. (2019). La and Mn-doped Bismuth Ferrite/Ti$_2$C$_2$ Mxene Composites for Efficient Photocatalytic Degradation of Congo red Dye. *Journal of Physical Chemistry,* 4:866-8668.

Akhund, A and Habibi-Yangjeh, A. (2016). Ternaary Magnetic g-C$_3$N$_4$/Fe$_3$O$_4$/AgI Nanocomposites: Novel Recyclable Photocatalysts with Enhanced Activity in Degradation of Different Pollutants under Visible Ligh: *Material Chemical Physics*, 174, 59-69.

Arul, S. Senthilnathan, T. (2019). Photodegradation of Congo Red Dye Using Heterogenous Photocatalysis Under Ultraviolet Irradiadation. *Rasayan Journal of Chemistry*, 12: 891-897.

Auwal, Y. and Gaya, U.I. (2023). Carbon tunable p-type ZnO Nanoparticles for Enhanced Phoocatalytic Removal of Eriochrome Black T. *Journal of Physical Chemistry and Functional Materials*, 6(1): 1-17. DOI:10.54565/jphcfum.1253804.

Auwal, Y, Abdullahi, M. and Kamaluddeen, S. K. (2023). Visible Light Induced Photocatalytic Degradation of Mehylene Blue Using Cu tunable p-type ZnO Nanoparticles. *Journal of Physical Chemistry and Functional Materials*, 6(2): 1-14. DOI:10.54565/jphcfum.1321022.

Danwittaykul, S. Jaisai, M. Dutta, J. ((2015) . Efficient Solar Photocatalytic Degradation of Textile Wastewater Using ZnO/ZTO Composites, *Applied Catalysis B: Environmental*, 163;1-8.

Deneshvar, N. Salari, Seyed D. M.S. Khataee, A.R and Rasoulifard, M.H. (2007). Photocatalytic Degradation of Azo-Dye ACID 14 in Water on ZnO as an Alternative Catalyst to TiO2. *Journal of Biochemistry and Photobiology,* A: Chem 162; 317-322.

Elaziouti, Laoued, N and Ahmed, (2011). ZnO-Assisted Photocatalytic Degradation of Congo Red and Benzopurpurine 4B in Aqueous Solution. *Journal of Chemical Engineering and Process*. 4: 201-214.

Escobar-Barrios, V.1. Rodrigueez, V.S. Rincon N. A and Salcedo, A. B. J. (2019).Modified Metallic Oxide for Efficient Photocatalysis, *Photocatalysts-Applications and Attributes, Books on Demand, Nor dersted, Germany*.

Gaya, U.I and Abdullah, A.H. (2008). Heterogeneous Photocatalytic of Organic Contaminants over TiO2. *Journal of Photochemistry and Photobiology*; 1: 1-12.

Gaya, U.I. (2014) Heterogeneous Photocatalysis using Inorganic Semiconductor Solids, *Springer. Dordrecht*, 2014

Gupta, V. K I. Ali, T. A. Saleh, A. Nayak and S. Agarwal. (2012). Chemical Treatment Technologies for Waste-water Recycling, An Overview: *RSC Advance*, 2 (16), 6380.

Hamza, A. Fatuase, J.T. Waziri,S. M and Ajayi, O.A. (2013) .Solar Photocatalytic Degradation of Phenol using Nanosized ZnO and α-Fe$_2$O$_3$, *Journal of Chemical Engineering Material Sci*ence, *4*(7), 87-92.

Li, T. Alazba A.A and Manzoor,U. A. A. (2014). Review of Removal of Pollutants from Water/Wastewater Using Different Types of Nanomaterials: *Advances in Materials Science and Engineering,* ID 825910, 24.

Nouasria, Z. Selloum, D. Henni, A. Tingry, S. and Hrbac J. (2022).Improvement of the Photocatalytic Performance of ZnO Thin Films in the UV and Sunlight Range by Cu Doping and Additional Coupling with Cu$_2$O: *Ceramic International*, 48(9); 13283-13294.

Parvulescus, V.I. Epron, F. Garcia, H and Grangers, P. (2021). Recent Progress and Prospect in Catalytic Water Treatment: *Chemical Reviews*, 122, 101-112.

Rajasulochana P and Preethy, V. (2016). Comparison on Efficiency of Various Techniques in Treatment of Waste and Sewage water-a Comprehensive Review: *Resource Efficient Technologies,* 2(4), 175-184.

Ray, T.K. Mondal, N. K. Mitra, P. (2023). Efficiency of Mn-doped ZnO Towards Removal of Congo Red Dye Under UV Exposure: Isotherm, Kinetics Thermodynamics and Optimization Study. *Pollution*, 9(2), 513-530.

Rohan, S. (2015). Removal of Congo Red Dye from Wastewater Using Orange Peel as Adsorbent, Department of Chemical Engineering. National Institute of Technology. *Journal Physical Chemistry.* 5: 128-133.

Saeid, T.F., Farzaned, M. Ali, R. (2019). Green Synthesis and Characterization of ZnMn$_2$O$_4$ Nanoparticles for Photocatalytic Degradation of Congo Red Dye AND Kinetics Study. *Indian Journal of Chemical Technology*, 4: 406-410.

Sayaya, S. M. Abdulfatah, S. M. Yunus, S.A. (2023). Photocatalytic Degradation of Congo Red Over 1w% CuO-ZnO Composite Catalyst. *International Journal of Noval Research in Physic, Chemistry and Mathematics*, 10(2), 18-31.

Shellofteh-Gohari, M and Habibi-Yangjeh, M. (2015). Novel Magnetically Separable Fe_3O_4@ZnO/AgCl Nanocomposites with Highly Enhanced Photocatalytic Activities under Visible Light Irradiation: *Sep Purifi Technol*, 147, 194-202.

Yang, G. Zhang, D. Zhu, G.A. (2022). Sm- MOF/GO Nanocomposite Membrane for Efficient Organic Dye Removal from Wastewater: *RSC Advance*, 10 (14), 8540-8547

Yusuf, A.H and Gaya, U. (2018). Mechanochemical Synthesis and Characterization of N-Doped TiO_2 for the Photocatalytic Degradation of Caffeine, *Nanochem. Res*, 3(1), 29-35.

Relationship between Meteorological Parameters and Effective Earth Radius Factor

[*1,2]Sabiru, Aminu Yaradua and [1]Muhammad, Ibrahim Bagudo

[1]Department of Physics, Umaru Musa Yaradua University Katsina
[2]Department of Physics, Federal University Dutsin-ma
*Corresponding author's email: aminusabiru@gmail.com

ABSTRACT
This research studied the impact of meteorological parameters (Rainfall, Humidity, Temperature and Pressure) on effective earth radius factor (k-factor) over the city of Dutse, Jigawa State. Forty-one years data of secondary data (1980-2020) of temperature, pressure rainfall and humidity were retrieved from the European Centre for Medium-Range Weather Forecasts (ECMRWF) ERA-5. The k-factor was computed and analyzed using the latest ITU-R Models (P.453-14 of 2019). The results indicate that while there's a pattern in rainfall similar to the k-factor, the k-factor is not directly influenced by the volume of rainfall. Instead, it is more closely associated with the high relative humidity typically observed during the rainy season. The presence of raindrops causes evaporative cooling as they fall through the air. This cooling effect can lead to a decrease in the temperature of the lower atmospheric layers. The correlation coefficient computation further reveals a very weak positive correlation between k-factor and temperature and pressure which reveal a slight positive relationship between them and a strong positive correlation between k-factor and rainfall and humidity which reveal that strong positive relationship between them. These indicates that changes in temperature and pressure are hardly related to changes in the k-factor while on the other hand changes in humidity and rainfall are related to changes in the k-factor.
Keywords: k-factor, Temperature, Pressure, Humidity and Rainfall

INTRODUCTION

A key component of radio signal transmission systems is the troposphere. Radio signal transmission and reception are greatly impacted by meteorological conditions and weather events in this lowest layer of the Earth's atmosphere. It has long been recognized that meteorological factors like temperature, pressure, relative humidity, and rainfall are essential to comprehending how radio waves behave in the troposphere. The study of these constantly changing elements is essential to the world of telecommunications because they play a significant role in shaping the complicated propagation of radio signals caused by natural atmospheric fluctuations (Eukhurabor and Azi, 2018) (Afullo et al., 1999).

The Effective Earth Radius Factor is one of the primary metrics used to evaluate radio wave propagation. This factor measures how much the Earth's curvature and atmospheric circumstances cause radio wave trajectories to deviate from a straight line. Meteorological factors are intrinsically connected to the Effective Earth Radius Factor. Temperature, pressure, humidity, and rainfall variations all have a direct impact on the Effective Earth Radius Factor. This can result in variations in signal pathways that affect the dependability and quality of communication (Abu-Almal and Al-Ansari, 2010) (Adediji and Ajewole, 2008).

Analyzing the correlation between climatic parameters and the Effective Earth Radius Factor is crucial for radio signal transmission. In order to address the difficulties caused by atmospheric changes, telecommunication engineers and researchers can create sophisticated technologies and predictive models by comprehending how meteorological aspects affect signal transmission. Precise evaluation of this connection leads to improved dependability of current communication systems and facilitates the creation of novel solutions that function flawlessly under a variety of weather scenarios (Ayantunji et al. 2011).

In this piece, we examine the complex interactions that occur between the Effective Earth Radius Factor and meteorological factors, as well as their importance and consequences for the changing face of radio signal transmission. (Ukhurebor, and Azi 2018).

This study used secondary data from three different altitude levels during a forty-year period, including air temperature, relative humidity, and atmospheric pressure. The data originates from the city of Dutse, Jigawa State.

MATERIALS AND METHODS

This study was conducted in Dutse, located at North-Western parts of Nigeria. Secondary atmospheric data of rainfall, temperature, pressure and humidity of Dutse is retrieved from the European Centre for Medium-Range Weather Forecasts (ECMWF) ERA-5 in December 2021. The data of the period of forty-one years (1980-2020) of the Meteorological parameters of temperature, pressure and humidity are obtained for three different height levels (12m, 100m and 250m) above ground levels.

Radio refractivity N is a measure of changes in refractive index n of air from unity. N is a dimensionless quantity defined in (1) and measured in N-units.

$$N = (n - 1) \times 10^6 \tag{1}$$

The radio refractivity N can be expressed in terms of meteorological variables as:

$$N = \frac{77.6}{T}\left(P + 4810\frac{e}{T}\right)(N\text{-}units) \tag{2}$$

The k-factor can be derived from the vertical refractivity gradient, ΔN, in the first kilometer above the ground; ΔN is obtained from two refractivity values as:

$$\frac{dN}{dh} = \frac{N_2 - N_1}{h_2 - h_1} \tag{3}$$

where N_1 and N_2 are the refractivity values at heights h_1 and h_2, respectively. In this study h_1 and h_2 are at the surface (12 m) and 100 m Above Ground Level respectively. The k-factor can be expressed as indicated in equations (4) and (5) (Abu-Ahmal and Al-Ansari, 2010; Ojo et al., 2017)

$$k = \frac{1}{\left(1 + a\left(\frac{dN}{dh}\right)\right)} \tag{4}$$

where a is the radius of the earth given in either km or nautical miles (nmi), (a = 6371 km = 344 mni) and $\frac{dN}{dh}$ is the rate of change of refractivity indices with height. k-factor can also be expressed as indicated in (5). This was used for k-factor computations in this work.

$$k = \frac{1}{1 + \frac{\left(\frac{dN}{dh}\right)}{157}} \tag{5}$$

Equations (3), and (5) were used to determine the values of refractivity gradient $\frac{dN}{dh}$, and effective earth radius factor (k-factor) in the study location.

For the determination of the degree of relationship between the variables, Karl Pearson's Product Moment Correlation Coefficient used for continuous data given by (6) as shown below:

$$r = \frac{n\sum xy - \sum x \sum y}{\sqrt{[n\sum x^2 - (\sum x)^2][n\sum y^2 (\sum y)2]}} = \frac{cov\,XY}{\sqrt{var\,X.var\,Y}} \tag{6}$$

Also, for statistical analysis correlation coefficient formula was used, regression and coefficient of multiple determinations which are described as follows:

Regression is a statistical method that attempts to determine the strength and character of the relationship between one dependent variable (usually denoted by Y) and a series of other variables (known as independent variables).

The general form of each type of regression is:

Simple linear regression: $Y = a + bX + u$ (7)

Multiple linear regression: $Y = a + b_1X_1 + b_2X_2 + b_3X_3 + ... + b_tX_t + u$ (8)

Where:

-      Y is the variable that you are trying to predict (dependent variable).
-      X is the variable that you are using to predict Y (independent variable).
-      a is the intercept.
-      b is the slope.
-      u is the regression residual.

The coefficient of multiple determinations measures the proportion of variation in the dependent variable that can be predicted from the set of independent variables in a multiple regression equation. When the regression equation fits the data well, R_2 will be large (i.e., close to 1); and vice versa.

The coefficient of multiple correlations can be defined in terms of sums of squares:

SSR = $\Sigma\,(\hat{y} - \bar{y})^2$

SSTO = $\Sigma\,(y - \bar{y})^2$

R_2 = SSR / SSTO

Where SSR is the sum of squares due to regression, SSTO is the total sum of squares, ŷ is the predicted value of the dependent variable, ȳ is the dependent variable mean, and y is the dependent variable raw score.

RESULT AND DISCUSSION

The mean effective earth radius factor (k-factor) of Dutse, is depicted in Figure 1 below. The figure shows that k-factor remains constant during the first two months of the year followed by continuous increases until September. Subsequently, it starts to decrease for the remaining months.
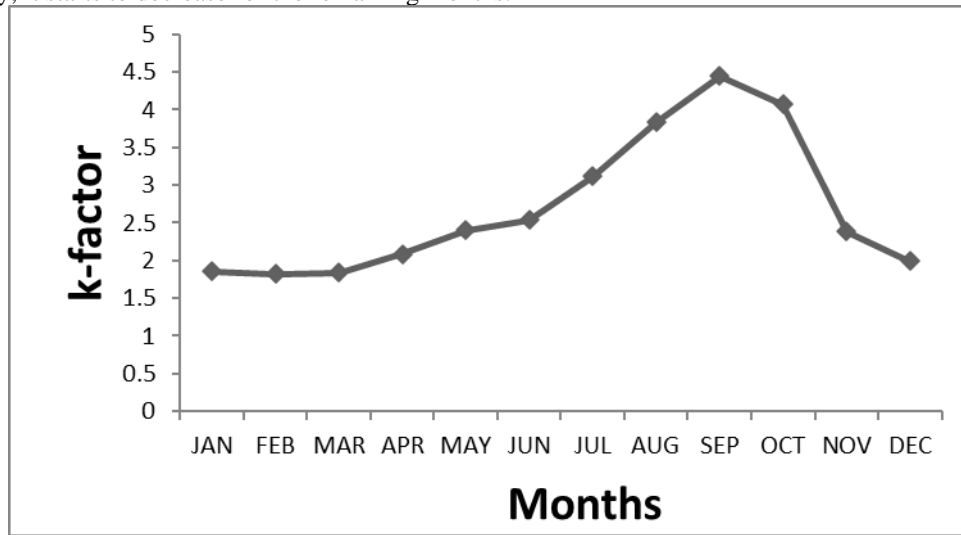
Figure 2: Mean k-factor at (the Study location

The range of the mean values of k-factor of the twelve months at the location of the study is 4.444- 1.822 where the first and second highest values are 4.444 and 4.074 of the month of September and October, then followed by 3.832 of August respectively. The least mean value is 1.822 and it is acquired in February.

Rainfall measurement refers to the process of quantifying the amount of precipitation that falls from the atmosphere onto a specific area within a given time period. Rainfall is a critical meteorological parameter that affects radio wave propagation. It influences the radio signal propagation in the troposphere and it was introduced into the analysis in order to confirm the relation between the k-factor and rainfall pattern. Figure 2 displays the relationship between mean rainfall and mean k-factor of forty- one years for the locations of the study.
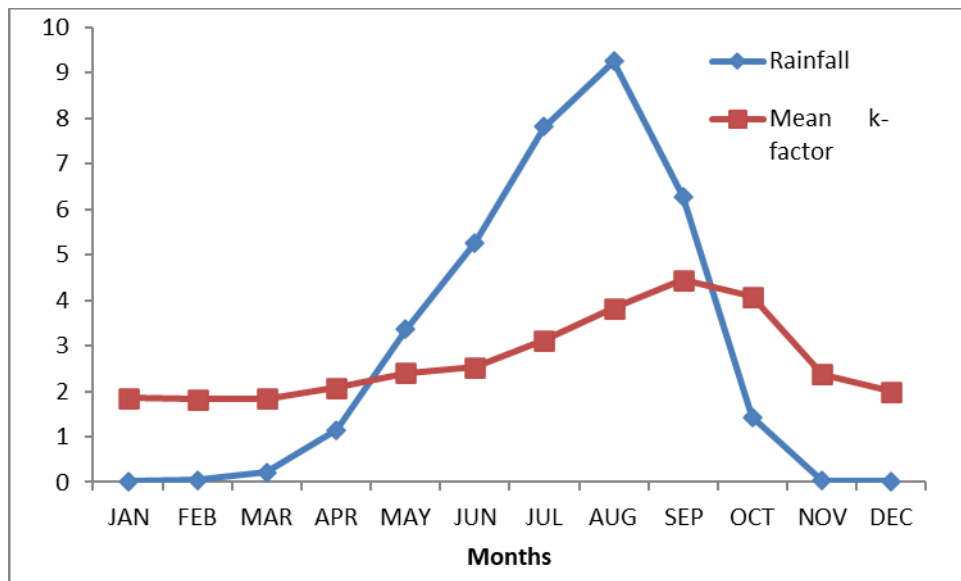
Figure 2: Relationship between Mean Monthly Rainfall and Mean k-factor at study Location

Figure 2 shows relationship between mean monthly rainfall and mean k-factor for the period study. From the figure it can be observed that the rainfall approximately followed the pattern of the k-factor. The rainfall curve shows a single peak in the month of August while the peak in the seasonal variation of k-factor is in August, September or October. It can be seen that the curve has same trend with the k-factor. This indicates a good relationship between the two.

Rainfall is associated with lower temperatures and higher humidity in the lower atmosphere. The presence of raindrops causes evaporative cooling as they fall through the air. This cooling effect can lead to a decrease in the temperature of the lower atmospheric layers. Additionally, the increased humidity from the evaporation of rainwater contributes to higher moisture content in the air. A correlation coefficient relationship between rainfall and k-factor is a moderate positive correlation, which is 0.601. It indicates a moderate strength of this relationship. As rainfall increases, the k-factor tends to increase moderately. Table 1 below shows the correlation relationship of Dutse between, k-factor, temperature, pressure and relative humidity.

Table 1: Correlation Coefficient between k-factor and Temperature, Pressure and Humidity for Dutse

	k-factor	Temperature	Pressure	Relative Humidity	Rainfall
k-factor	1				
Temperature	0.056	1			
Pressure	0.046	0.955	1		
Relative humidity	0.735	-0.007	0.017	1	
Rainfall	0.601	0.008	0.055	0.941	1

There is a very weak positive correlation between the k-factor and temperature. A correlation coefficient of 0.056 suggests an almost negligible positive relationship. This means that changes in temperature are hardly related to changes in the k-factor. Similarly, there is a very weak positive correlation between the k-factor and pressure. A correlation coefficient of 0.046 indicates a very slight positive relationship. Changes in pressure don't seem to be closely associated with changes in the k-factor. There is also a moderate positive correlation between the k-factor and relative humidity. A correlation coefficient of 0.735 suggests a high positive strength of this relationship. As relative humidity increases, the k-factor tends to increase.

CONCLUSION

In this study examining meteorological parameters' influence on the effective earth radius factor (k-factor) in Dutse, Jigawa State, was carried out. A meticulous analysis analysis of forty-one years of data revealed intriguing patterns. Rainfall, mirroring the k-factor, is directly linked, while high relative humidity during the rainy season emerges as a key factor.

Correlation analyses confirm a weak positive relationship between the k-factor and temperature/pressure, contrasting with a strong positive correlation with rainfall and humidity. Specifically, the k-factor ranges from [insert specific values from the abstract], showcasing the subtle yet impactful variations studied.

These findings emphasize the significance of humidity and rainfall in radio signal propagation. Engineers can leverage this understanding to design adaptive systems, ensuring robust communication networks that respond to the region's unique climatic dynamics. This research forms the foundation for resilient, weather-responsive communication technologies, ushering in a new era of reliable connectivity.

REFERENCES

Abu-Almal, A. and Al-Ansari, K. 2010. "Calculation of effective earth radius and point refractivity gradient in UAE". *International Journal of Antennas and Propagation.* Vol.2010, Article ID 245070.

Adelakun. A.O., Ojo, J.S., and Edward, V.O., 2020. Quantitative analysis of Complexity and non- linear trend of radio refractivity gradient in the troposphere. Advances in Space Research, 59 (12), 2611-2515

Afullo, T. J., T. Motsoela, and D. F. Molotsi,1999. "Refractivity Gradient and K-factor in Botswana, Radio Africa," 107-110.

Akinbolati, A., and Ajewole, M. O. 2020. "Investigation of Path Loss and Modeling for Digital Terrestrial Television over Nigeria," *Elsevier Heliyon, e04101*, , https://doi.org/10.1016/j.heliyon.2020.e04101

Ayantunji, B.G., Okeke P. N. and Urama, J. O. 2011. " Diurnal and Seasonal Variation of Surface Refractivity over

Nigeria", *Progress in electromagnetic research B,* vol 30, pp.201-222.

Faruk, N., Ayeni, A.A., and Adediran, A.Y., 2013."On the study of empirical path loss modelsfor accurate prediction of TV signal for secondary users*." Progress in Electromagnetic Research B,*pg 1–5.

Ojo, O. L., Ojo J. S. and Akinyemi, P. 2017. "Characterization of Secondary radioclimatic variables for microwave and millimeter wave link design in Nigeria", *Indian Journal of Radio and Space Physics,* vol.46, pp.83-90

The European Centre for Medium-Range Weather Forecasts (ECMWF) ERA5, 2021

Ukhurebor, E.K. and Azi S.O 2018."Review of Methodology to Obtain Parameters for Radio Wave   Propagation at Low Altitudes from Meteorological Data: New Results for Auchi Area in Edo State, Nigeria, "*Journal of King Saud University – Science*,. (doi: https://doi.org/10.1016/j.jksus.20 18.03.001).

Valma, E., Tamosiunaite, M. Tamosiunas, Stasys & Tamosiuniene, M & Zilinskas, M. (2011). Variation of Radio Refractivity with Height above Ground. Electronics and Electrical Engineering. 111. 10.5755/j01.eee.111.5.349.

A Mini Review on *Anisopus mannii:* its Phytochemistry and Antidiabetics Properties.

*Sada Maryam H. and Bello Oluwasesan M.

Department of Chemistry, Faculty of Physical Sciences, Federal University Dutsinma, Katsina State, PMB 5001, Nigeria.
Corresponding author's email: mhassansada@fudutsinma.edu.ng

ABSTRACT

Worldwide research is being done on new plants that may have medicinal properties, especially on Diabetes mellitus. Currently used in traditional Northern Nigerian medical compositions is the herb *Anisopus mannii* in managing Diabetes mellitus and its complications. The results of earlier research on *A. mannii* had to be compiled due to the species' significance in ethnopharmacology, demonstrating the species' potential uses. Using electronic databases including Science Direct, PubMed, Springer and Google Scholar, important data was taken from authentic scientific research publications. The aim of this research is to review the phytochemistry and anti-diabetes activity of *A. mannii* plant. Many studies attest to its leaves and stem possess the concerned activity but the roots has never been the aim of any research through the roots are mostly employed ethnobotanically against the disease and the compounds responsible for the activity has never been queried. These results validate the plant's traditional application and its use to manage this disease.
Keywords: Antidiabetics, Phytochemistry, Antioxidants, Medicinal plants

INTRODUCTION

Medicinal plants have been used for so long as therapeutic medications, so they are very valuable on a commercial basis. Many medicinal plants' kinds have been looked into, examined, and classified for their potential therapeutic uses according to the main biological components they contain. Almost 300 tribes in Africa, especially Nigeria, still primarily obtain their primary healthcare from medicinal plants. Many illnesses, including malaria, epilepsy, sickle cell anemia, bronchial asthma, and diabetes, have been treated with medicinal plants. (Manosroi *et al.,* 2011). The plant's chemical composition and biological activities have been the subject of several papers. The publications must be carefully read, and the most important discoveries that demonstrate the species' potential utility must be compiled. This study's goal was to investigate the biological evaluation, phytochemistry composition and the in-silico investigations on diabetes studies of *Anisopus manniiis* plant. A review of the scientific literature revealed that there are a number of traditional treatments for *A. mannii*. There have been reports of ethnomedical uses for various plant parts. In Nigeria, the herb has long been used to treat and control high blood pressure. Likewise, children's jaundice is treated with the plant's leaf. Diabetes is managed with extracts from the leaves, stem, bark, and roots (Abdulrahman 2021; Musa *et al*., 2015; Sani et al., 2019). *A. mannii* is used alone or in combination with other herbs to treat digestive diseases and diabetes, both of which involve biological oxidation as a prominent etiological factor (Atawodi *et al*., 2014). The plant was given the names Sakayau and Kashe Zaki, which translate to "sweet murderer" or "killing sweetness" in Hausa, a Hausa language that is widely spoken in Northern Nigeria (Manosroi *et al.,* 2011; Musa *et al*., 2009; Sani *et al.,* 2009). The entire plant, leaves, and stem decoctions are used for antibacterial, antiparasitic, analgesic, inflammatory, and infertile purposes (Ezuruike and Prieto, 2014). Breast milk is improved by consuming the powdered root (Kankara *et al*., 2015). Additionally, we handle infectious conditions including diarrhoea and piles (Musa *et al*., 2015).

Figure 1: Fresh *Anisopus mannii* leaves

MATERIALS AND METHODS

Science Direct, PubMed, Google Scholar, and Springer are just a few examples of the electronic databases that have been used to take valuable information out of original scientific research publications.. Requirements for inclusion: studies that met the following filters: toxicity, cytotoxic action, chemical composition, mineral elements, Gas Chromatography Mass Spectrometry (GCMS) analysis, antioxidant, antimicrobial, antidiabetic, antibacterial, drugs, antiviral, traditional medicine, ethnopharmacology, and any other related terms. Exclusion criteria: This investigation did not include the following data from dubious web sources, thesis reports, or review publications (Dogara 2022).

Antioxidants

According to Qader *et al*., (2011), antioxidants are substances that help postpone or prevent degenerative diseases that are brought on by free radical oxidative damage to the constituents of living cells.. Human systems are made up of a variety of cells, each of which contains a unique set of substances. Atoms that have been chemically linked together to form molecules (Abdulrahman *et al*., 2019). Normal conditions prevent the atoms' bonds from breaking, leaving the molecules with only one odd unpaired electron (Mahmoud 2021). A variety of techniques were employed to assess *A. mannii's* capacity as an antioxidant Table 1.

Table 1: Antioxidant activities *of A. mannii*

Method	Part of Plant	Solvent	Outcome of the Study	References
DPPH	Leaf	Aqueous	The ability to scavenge free radicals was shown using IC50 of 0.31 mg/mL.	(Manosroi *et al.,* 2011)
DPPH	Leaf	Ethyl acetate, methanol, and n-butanol	The antioxidant activity of methanolic, n-butanol crude extract, and ethyl acetate was 94.1, 94.3, and 88.7%, respectively, when free radicals were scavenged at 250 gmL^{-1}	(Aliyu *et al.,* 2010)
DPPH	Leaf, stem, and roots	de-ionized water	The activity was not detected at IC50 µL/3mL	Ene *et al.,* 2010
DPPH, FRAP	Leaf, bark and root	Ethanol	The highest capacity to convert Fe^{3+} to Fe^{2+} was found in the 100% ethanolic extract at 18.9 mmol/gm, and the maximum DPPH scavenging activities were observed at 75.5 µg/mL.	Usman, *et. al.,* 2022

Anti-diabetes

Among its many consequences, diabetes mellitus can lead to nephropathy, retinopathy, impotence, stroke, and heart attacks (Agofure *et al*., 2020). It is widely acknowledged to be ubiquitous in many underdeveloped and recently

industrialized countries, ranking as the fourth most common cause of death in the wealthiest nations (Naveen et al., 2021). Because they typically have no or few side effects, medicinal plants have been used for the treatment of diabetes mellitus for a very long time. In addition to their ability to counteract the toxicity of other drugs or toxic substances, the majority of these plants exhibit antioxidant activities, which helps them prevent or treat diseases that are difficult to cure. (Nasri *et al.,* 2015).

So plants have antioxidant property can be used to treat diabetes mellitus because of the most significant type of free radical in biological systems are radical derivatives of oxygen, or ROS. By consuming more natural antioxidants, one may be able to prevent oxidative stress, which has been linked to the pathophysiology of diabetes mellitus, and maintain a tolerable antioxidant status. Antioxidants have the potential to both improve glucose metabolism and uptake and shield against the harmful effects of hyperglycemia, making them a promising treatment option for diabetes mellitus. (Munir *et al*., 2017). Antioxidants that are effective in reducing diabetic complications include α-lipoic acid, vitamin C, and N-acetylcysteine. This suggests that dietary supplementation or ingestion of natural antioxidants may be beneficial. Antioxidants are showing to be vital tools in the study of diabetic pathologies linked to oxidative stress, and although replacement style therapy has clear potential benefits, the safety and effectiveness of antioxidant supplementation in any future treatment has not yet been determined. (Da Silver *et al*., 2010). Also the Table 2 further shows reports on the antidiabetes activities of different parts of *A. mannii*.

**Table 2: Antidiabetes Activities of *A. mannii***

Method	Part of Plant	Solvent	Outcome of the Study	References
in vivo	Stem	Aqueous	All of the crude stem extract dosages that were used were hypoglycemic, and 600 mg/kg had a very good antidiabetic effect when compared to the traditional medication (glibenclamide) used to treat diabetes mellitus.	(Tijjani *et al.*, 2012)
in vivo	Leaves and Stem	Aqueous	In comparison to the untreated diabetic group, the test groups exhibited significantly lower (P<0.05) levels of alanine transaminase, aspartate transaminase, lipid profile, creatinine, bilirubin, and fasting blood glucose. At 200 mg/kg, the extract successfully lowered total and LDL cholesterol.	(Matazu *et al.*, 2017)
in vivo	Leaves	Aqueous or methanolic	The traditional claim was confirmed by the discovery that 400 mg/kg had a hypoglycemic effect in animals with normal blood sugar and alloxan-diabetic animals.	(Shehu *et al.,* 2014)
in vivo	Stem	Methanolic/ Aqueous	This study found that the beneficial effects of metformin (50 mg/kg) and methanolic extract (200 mg/kg) on glucose homeostasis and lipid profile in diabetic rats may be counteracted by one another.	(Chika *et al.,* 2019)
B16 melanoma cells	Leaf		Although all of the compounds inhibited melanogenesis, compound 5 showed the strongest activity at 30 mol/L in terms of both cell viability (54.95%) and melanin content (27.43.5%), indicating that it may be further developed.	(Ye *et al*., 2018)
in vivo	Stem	Aqueous	When compared to diabetic controls, the extract significantly (P>0.05) lowered the fasting blood glucose levels in the diabetes-treated rats from week one to week three. In the fourth week, no significant (P>0.05) effect was found. Based on the research, it seems to have antihyperglycemic and hypolipidemic effects.	(Osibemhe *et al.,* 2017)
in vivo	Stem	Methanolic	The extract (200 mg/kg) and glibenclamide (0.6 mg/kg) counteracted each other's beneficial effects on glucose homeostasis and lipid profile in	(Chika and Yahaya 2019)

			streptozotocin/nicotinamide-induced diabetic mice.	
in vivo	Stem	Aqueous	The antidiabetic action was found to be dose dependent, with significant results at P < 0.05 and P < 0.01 for doses of 200, 400, 600, and 800 mg/kg.	(Tijjani *et al.*, 2012)
in vivo	Leaf	Methanolic	In normoglycemic and diabetic mice, the extract at 400 mg/kg bw caused a significant (P>0.05) decrease in fasting blood glucose (FBG) of 27.36 and 65.57 percent, respectively. The traditional use for diabetes mellitus was confirmed in this investigation.	(Zaruwa *et al.*, 2013)
in vivo	Leaf	Aqueous	The identification of Manosrin, a novel molecule, will add to the group of approved pharmaceutical hypoglycemic agents and represent a substantial breakthrough in the management of diabetes mellitus.	(Zaruwa *et al.*, 2018)
in vivo	Leaf	Aqueous	All extracts demonstrated strong hypoglycemic effects in diabetic mice induced with alloxan; however, *A. mannii* extract demonstrated the greatest reduction in fasting blood glucose (70.39%), which was equivalent to 1.54 and 0.98 times that of glibenclamide and human insulin, respectively.	(Manosroi *et al.,* 2011)
in vivo	Stem	Aqueous	At doses of 200, 400, 600, and 800 mg/kg, it demonstrated significant dose-dependent hypoglycemic and antidiabetic effects at P<0.05 and P<0.01, respectively.	(Tijjani *et al.*, 2012)
in vivo	Stem	Aqueous	After consuming various amounts of the plant extract for 28 days, they did gain weight, but the increase was not statistically significant (P>0.05). Repeatedly administering graduated extract dosages demonstrates the extract's folkloric use as a possible hypoglycemic medication and results in significant (P >0.05) increases in blood sugar levels in the treatment groups when compared to their respective day zero values.	(Sani *et al.,* 2009a)
in vivo	Stem bark	Methanol, n-hexane, ethylacetate and	In diabetogenic rats, the extract significantly (P>0.05) lowers the fasting blood glucose level. Throughout the entire study period, a significant (P>0.05) dose-dependent drop in fasting glucose levels was seen at 500 mg/kg, ranging from 7.66 ± 2.26 to 6.18 ± 2.14.	Adamu *et al.,* 2021
in vivo	Leaf	Aqueous	The percentage reductions observed in Anisopus manni aqueous extract were 59.4%, 61.0%, and 56.5%, respectively. These reductions indicate a maximum fasting blood glucose reduction and were all higher than the 32.27% reduction observed in diabetic rats given the standard medication, glibenclamide.	Gidado *et al.,* 2018

Phytochemistry

A. mannii, was found to contained: flavones, glycosides, saponins, and alkaloids in the plant. According to Manosroi *et al.,* (2011) findings. The results of the study by Abdulrahman *et al*., (2022) showed that there were high concentrations of glycosides, saponins, xanthone, alkaloids, flavonoids, terpenes, and steroids. Examples of some

Compounds found in *anisopus mannii* plant are shown in Fig 2 below: Anisopusin (**1**), is an alkaloids which are therapeutically well known as anaesthetics, cardioprotective, and anti-inflammatory agents. (Chabowska *et al.,* 2021). Lup-20(29)-en-3-ol, acetate, (**2**), Drogingerdione (**3**) and Gingerdione (**4**), are ginger constituent, which is known to have pharmacological activity. Ferulic acid (**5**) has numerous physiological properties, including anti-inflammatory, antioxidant, antimicrobial, anti-cancer, and anti-diabetic effects, and it is low in toxicity. The food, cosmetics, and pharmaceutical industries have all made extensive use of it. (Kamila *et al.,* 2018). hexadecyne (**6**), Flavanoid (**8**), possess a number of medical positive aspects, such as antiviral, anticancer, antioxidant, and anti-inflammatory qualities. They also have cardio- and neuroprotective properties. The kind of flavonoid, its (potential) mode of action, and its bioavailability all affect these biological activities. (Ullah *et al.,* 2020). Heptadecane, 9-octyl (**9**) and oxirane (**10**), is found in natural products such as psorospermin, which demonstrates efficacy against drug-resistant leukemia and AIDS-related lymphoma, azinomycins A and B, triptonid, epoxomicin, and cryptophycin A and B, which have anticancer properties.. 3-hexadecyne (**11**), anthraquinone (**12**) Current therapeutic indications include constipation, arthritis, multiple sclerosis, and cancer. (Malik and Müller, 2016). Phenols (**13**), they have anti-diabetic, antioxidant, anticancer, nueroprotective properties. (Venkata *et al.,* 2015). Phytol (**14**) Phytol has been studied for its possible effects on autophagy and apoptosis, anxiolytic, metabolism, cytotoxic, antioxidant, antinociceptive, anti-inflammatory, immune-modulating, and antimicrobial. (Islam *et al.,* 2018). Stigmasterol (**15**), lower cholesterol and also inhibit cancer cells. 9,12-Octadecadienoic acid (**16**), Hexadecenoic acid, methyl ester (**17**) were found to show excellent antioxidant activity. (Rahman *et al.,* 2014)
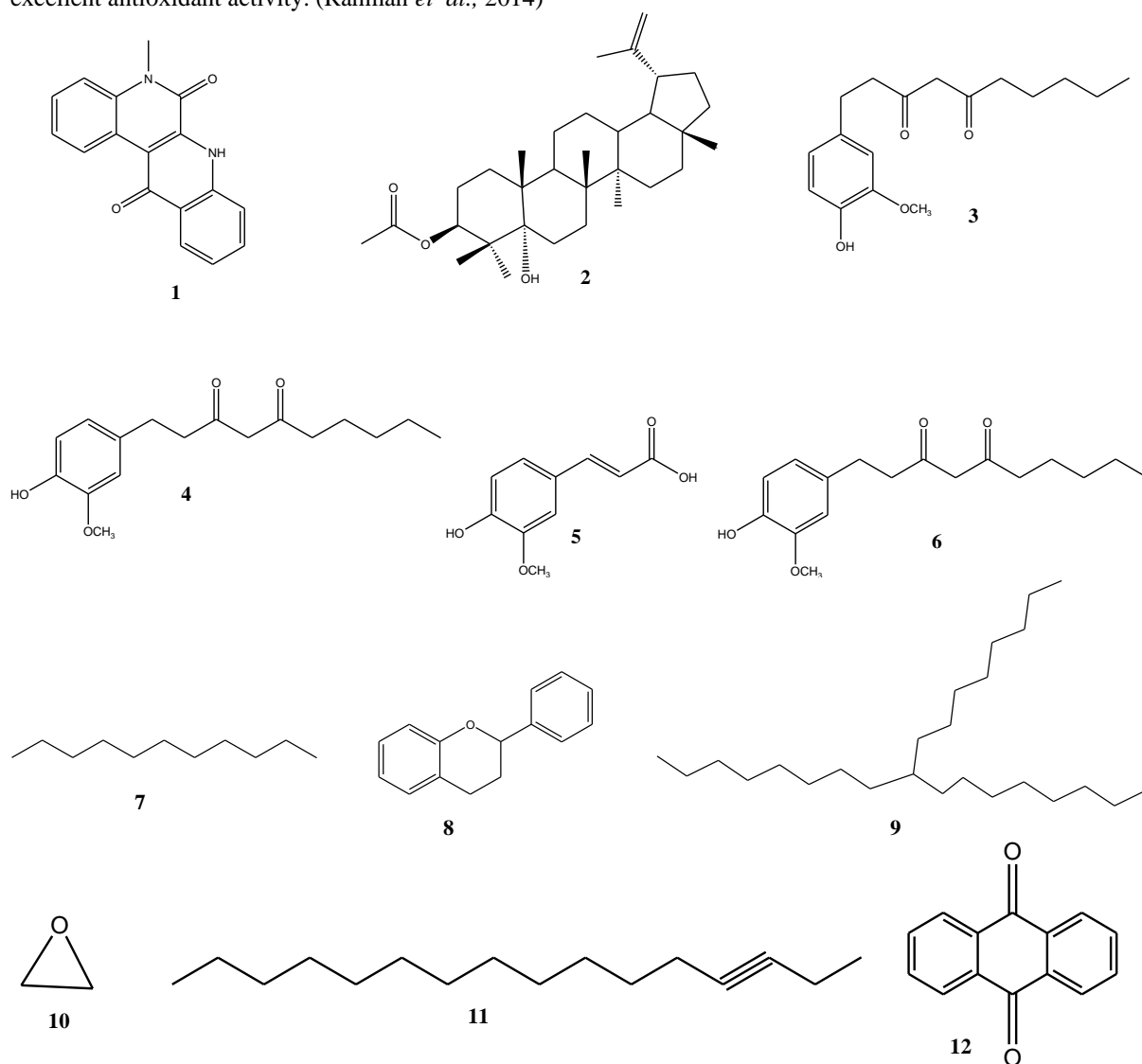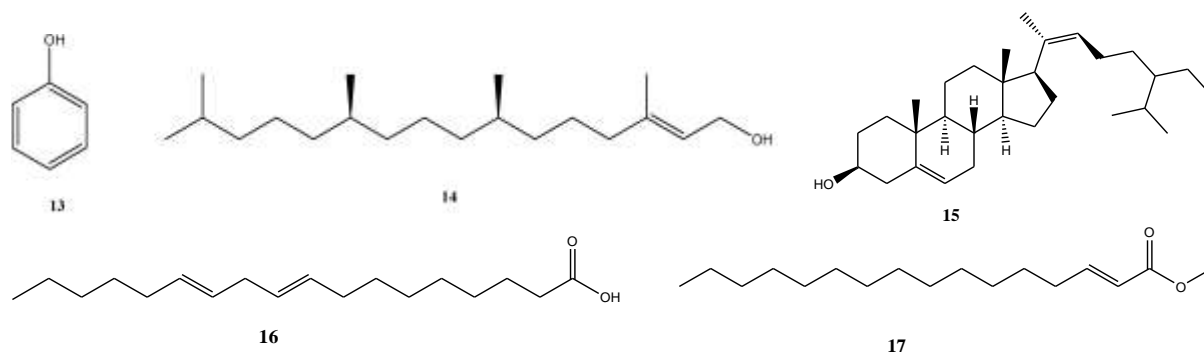
Figure 2: Isolated Compounds from different parts of *A. mannii*

CONCLUSION
Anisopus mannii is a well-known ethnomedicinal plant having a wide range of pharmacological effects in Nigeria. Numerous investigations on the plant have demonstrated its anti-diabetic potential and antioxidant activity according to this review, which supports the findings of the ethnobotanical studies on the plant. Nonetheless, no research has been done on the isolation of compounds responsible for the anti-diabetic activity, found in plants up to this point. This review is done in order for the researcher to work on the isolation of the compounds that are responsible for the anti-diabetes potential of the plant.

REFERENCES
Abdulrahman, M. D., Hasan Nudin, N., Khandaker, M. M., Ali, A. M., and Mat, N. (2019). *In vitro* biological investigations on *Syzygium polyanthum* cultivars. *International Journal of Agriculture and Biology,* 22(6), 1399-1406.

Abdulrahman, M. 2021. Ethnobotany of Medicinal Plants with Antidiabetic Potentials in Northern Nigeria. *Eurasian Journal of Science and Engineering,* 7(1), 46-58.

Abdulrahman, M. D., Bradosty, Hamad, S. W., Ibrahim, M. T., Lema, A. A., Sunusi, N., Usman, M., Ashiru, I., Ahmad, N. B., Wada, N., and Bussmann, R. W., (2022) Traditional Methods for Treatment and Management of Measles in Northern Nigeria: Medicinal plants and their molecular docking. *A journal of Plants, people and applied research.* http://dx.doi.org/10.32859/era.23.33.1-18

Adamu , I. zadva, Mustapha A. T., Hamidu, U., Abubakar, G., Ali, M. F., Fanna, I. A., (2021). Appraisal of Phytoconstituents and Anti-diabetic Properties of the stem extract of Anisopus mannii in alloxan induced Diabetic rats, *NAUB Journal of Science and Technolgy* Vol. (1), pp 236-252.

Agofure, O., Okandeji-Barry, O. R., and Ogbon, P., (2020). Pattern of diabetes mellitus complications and comorbidities in ughelli north local government area, Delta State, Nigeria. *Nigerian Journal of Basic and Clinical Sciences,* 17(2), 123-127.

Aliyu., A. B., Ibrahim, H., Musa, A. M., Oyewale, A. O., Amupitan, J. O., (2009). In vitro evaluation of antioxidant activity of Anisopus mannii N. E. Br., *Afr. J. Biotechnol.* Vol. 9 (16), pp 2437-2441.

Atawodi, S. E.-O., Olowoniyi, O. D., Obari, M. A., and Ogaba, I., (2014). Ethnomedical survey of Adavi and Ajaokuta local government areas of Ebiraland, Kogi State, Nigeria. *Annual Research and Review in Biology*, 4344-4360.

Chabowska G., Barg E., Wójcicka, (2021). A. Biological Activity of Naturally Derived Naphthyridines. *Molecules.* 26(14):4324.

Da Silva., S.B, Costa., J.P, Pintado., M.E, Ferreira., D. C, Sarmento B., (2010). Antioxidants in the Prevention and Treatment of Diabetic Retinopathy - A Review. *J Diabetes Metab.* 1:111.

Dogara, A., Hamad, S. W., Usman, M., Tahir, S. M., Sunusi, N., and Yunusa, A., (2021). Therapeutic plants used for Typhoid Fever treatment in Kaduna State. Nigeria. *Al-Qadisiyah Journal Of Pure Science,* 26(3), 9-21.

Dogara, M., (2022). Review of Ethnopharmacology, Morpho-Anatomy, Biological Evaluation and Chemical Composition of *Syzygium polyanthum* (Wight) Walp. *Plant Science Today,* 9(1), 167-177.

Ezuruike, U. F., and Prieto, J. M., (2014). The use of plants in the traditional management of diabetes in Nigeria: Pharmacological and toxicological considerations. *Journal of Ethnopharmacology,* 155(2), 857-924

Gidado, A., Abdulfattah, A. S., Mpato, J. ; Umar, B. ; Idris, A., (2018). Antidiabetic potentials of aqueous extracts of Acacia nilotica (Fabaceae), Anisopus manni (Asclepiadaceae) and a recipe comprising the two plants in experimental rats. *Tropical Journal of Natural Product Research*. Vol.2 No.5 pp.240-244 ref.29

Islam, M. T., Ali, E.S., Uddin, S.J., Shaw, S., Islam, M.A., Ahmed, M.I., Chandra Shill, M., et al., (2018). "Phytol: A review of biomedical activities". *Food and Chemical Toxicology*. 121: 82–94. doi:10.1016/j.fct.2018.08.032

Kamila Z., Agnieszka D., Anna K., Helena R., (2018). Antioxidant Properties of Ferulic Acid and Its Possible Application *Skin Pharmacol Physiol*. 31 (6): 332–336.

Kankara, S. S., Ibrahim, M. H., Mustafa, M., and Go, R., (2015). Ethnobotanical survey of medicinal plants used for traditional maternal healthcare in Katsina state, Nigeria. *South African Journal of Botany*, 97 (2015), 165-175.

Malik E. M, Müller C. E., (2016). Anthraquinones As Pharmacological Tools and Drugs. *Med Res Rev*. 36(4):705-48. doi: 10.1002/med.21391.

Manosroi, J., Zaruwa, M. Z., and Manosroi, A., (2011) "Potent Hypoglycemic Effect of Nigerian Anti-Diabetic Medicinal Plants," *Journal of Complementary and Integrative Medicine*: Vol. 8: Iss. 1, Article 6. DOI: 10.2202/1553-3840.1482

Murni N. S., Qamar U. A., Siti Zaiton M. S., Alhassan M. A., Suganya M., Vikneswari P., Sharifah N. M., Alfi Khatib, J. L., (2017) "Antioxidant and Antidiabetic Effects of Flavonoids: A Structure-Activity Relationship Based Study", *BioMed Research International*, vol. 2017, 14 pg. https://doi.org/10.1155/2017/8386065

Musa, A., Aliyu, A., Yaro, A., Magaji, M., Hassan, H., and Abdullahi, M., (2009). Preliminary phytochemical, analgesic and anti-inflammatory studies of the methanol extract of Anisopus mannii (NE Br)(Asclepiadaceae) in rodents. *African Journal of pharmacy and pharmacology,* 3(8), 374-378.

Musa, A. M., Ibrahim, M. A., Aliyu, A. B., Abdullahi, M. S., Tajuddeen, N., Ibrahim, H., and Oyewale, A. O., (2015). Chemical composition and antimicrobial activity of hexane leaf extract of Anisopus mannii (Asclepiadaceae). *Journal of intercultural ethnopharmacology,* 4(2), 129-133.

Nasri H, Shirzad H, Baradaran A, Rafieian-Kopaei M., (2015). Antioxidant plants and diabetes mellitus. *J Res Med Sci*. 20(5):491-502. doi: 10.4103/1735-1995.163977.

Naveen, Y., Urooj, A., and Byrappa, K., (2021). A review on medicinal plants evaluated for anti-diabetic potential in clinical trials: Present status and future perspective. *Journal of Herbal Medicine, https://doi.org/10.1016/j.hermed.2021.100436.*

Qader, S. W., Abdulla, M. A., Chua, L. S., Najim, N., Zain, M. M., and Hamdan, S., (2011). Antioxidant, total phenolic content and cytotoxicity evaluation of selected Malaysian plants. *Molecules,* 16(4), 3433- 3443.

Rahman, M. M., Ahmad, S. H., Mohamed M.T.M., Ab Rahman M.Z. (2014). Antimicrobial compounds from leaf extracts of Jatropha curcas, Psidium guajava, and Andrographis paniculata. *Sci. World J.* 2014:635240. doi: 10.1155/2014/635240.

Sani, D., Sanni, S., and Ngulde, S., (2009). Hypoglycaemic effect of aqueous stem extract of Anisopus mannii in normal rats. *African Journal of Pharmacy and Pharmacology,* 3(10), 481-484.

Sani, S., Aliyu, B., Haruna, M., Yahya, S. M., Yakasai, M. A., Hayatu, L. W., and Abba, H., (2019). Local plants and diabetes management; folkloric practices in Metropolitan Kano, Nigeria. *Bayero Journal of Pure and Applied Sciences,* 12(1), 268-273.

Ullah A, Munir S, Badshah SL, Khan N, Ghani L, Poulson BG, Emwas AH, Jaremko M., (2020). Important Flavonoids and Their Role as a Therapeutic Agent. *Molecules.* 25(22):5243.

Usman M., Mahmoud D. A., Saber W. H., Harmand A. H.,and Abubakar A. L., (2022). Antioxidants, Anti-inflammation, Anti-hyperglycemia and Chemical Evaluation of the whole plant extracts of Anisopus mannii N.E.Br. *Zanco Journal of Pure and Applied Sciences*, 34(5): 114-122. DOI: http://dx.doi.org/10.21271

Venkata Saibabu, Zeeshan Fatima, Luqman Ahmad Khan, and Saif Hameed, (2015). Therapeutic Potential of Dietary Phenolic Acids. *Advances in Pharmacological and Pharmaceutical Sciences.* (Vol) 2015. doi.org/10.1155/2015/823539

Yu, C., and Abbott, P. V., (2007). An overview of the dental pulp: its functions and responses to injury. *Australian Dental Journal,* 52(1), 4-6.

Sorption Properties of Modified and Unmodified Millet Husk on Aqueous Solutions of Cadmium II Ions

[1]Ikechukwu Ogadimma Alisi, [2]Sadauki Hamisu Garba and [2]Muhammad Suleiman Darma

[1]Department of Industrial Chemistry, Federal University Dutsin-Ma, Katsina State, Nigeria
[2]Department of Chemistry, Federal University Dutsin-Ma, Katsina State, Nigeria

ABSTRACT

Agricultural wastes of plant origin have been observed to possess great sorption capacity for heavy metal ions in aqueous solution. The contamination of water by heavy metals is a worldwide challenge. Unlike the organic pollutants in which most of them are susceptible to biological degradation, heavy metals are non-biodegradable. The sorption properties of modified and unmodified millet husk on aqueous solutions of Cd^{2+} via kinetic and thermodynamic studies were investigated in this research. Both modified and unmodified millet husk were processed and subjected to adsorption studies. Marcaptoacetic acid was employed in the thiolation of the modified millet husk. Both samples were subsequently subjected to thermodynamic and kinetic studies. Also Langmuir, Friendlich and Tempkin models were employed to investigate the interaction between metal ion in solution and the adsorbents. The thermodynamic studies revealed endothermic physisorption mechanisms for both modified and unmodified millet husk. Also, a spontaneous process was observed for modified millet husk, while non-spontaneous process was observed for the unmodified millet husk. An examination of the kinetics models indicated that the pseudo second order provided a better fit to the experimental data with highly encouraging R^2 values for both modified and unmodified millet husk. This search brings to light the possible use of millet husk as an adsorbent for heavy metal ions.

Keywords: Sorption properties; Millet husk; Cadmium (II) ions; Kinetics; Thermodynamics

INTRODUCTION

Agricultural waste is a general term for organic substances discarded by human beings in the process of agricultural production. With the rapid development of industry and the over-exploitation of natural resources, environmental pollution has caused serious harm to human health, so it is urgent to solve ecological problems. Conventional methods for removing contaminants from gaseous and aqueous phases are mainly biological treatment, flocculation (Jawad et al., 2015), membrane separation processes, chemical precipitation, adsorption (utilizing activated carbon) and ion exchange (Rosales et al., 2017). Among these methods, adsorption has been shown to be an effective and cost-effective method for removing many pollutants (Ashraf et al., 2015). Agricultural wastes have a loose, porous structure and contains carboxyl, hydroxyl and other reactive groups. They can be used as a biomass adsorption material in the field of pollution control, which can not only reduce the environmental burden but also achieve the effect of "treating waste by waste" (Huang, 2017). Soils may become contaminated by the accumulation of heavy metals and metalloids through emissions from the rapidly expanding industrial areas, mine tailings, disposal of high metal wastes, leaded gasoline and paints, land application of fertilizers, animal manures, sewage sludge, pesticides, wastewater irrigation, coal combustion residues, spillage of petrochemicals, and atmospheric deposition (Khan et al., 2008). Heavy metals constitute an ill-defined group of inorganic chemical hazards, and those most commonly found at contaminated sites are lead (Pb), chromium (Cr), arsenic (As), zinc (Zn), cadmium (Cd), copper (Cu), mercury (Hg) (Ling et al., 2007). Soils are the major sink for heavy metals released into the environment by aforementioned anthropogenic activities and unlike organic contaminants which are oxidized to carbon (IV) oxide by microbial action, most metals do not undergo microbial or chemical degradation, and their total concentration in soils persists for a long time after their introduction (Adriano, 2003). The adequate protection and restoration of soil ecosystems contaminated by heavy metals require their characterization and remediation.

The application of agricultural inputs such as fertilizers, pesticides, and biosolids (sewage sludge), the disposal of industrial wastes or the deposition of atmospheric contaminants increases the total concentration of Cd in soils, and the bioavailability of this Cd determines whether plant Cd uptake occurs to a significant degree (Weggler 2004). Cadmium is very biopersistent but has few toxicological properties and, once absorbed by an organism, remains resident for many years. Since the 1970s, there has been sustained interest in possible exposure of humans to Cd through their food chain, for example, through the consumption of certain species of shellfish or vegetables. Concern regarding this latter route (agricultural crops) led to research on the possible consequences of applying sewage sludge (Cd-rich biosolids) to soils used for crops meant for human consumption, or of using cadmium-enriched phosphate fertilizer (Campbell 2006). This led to the stipulation of highest permissible concentrations for a number of food crops (McLaughlin 2016). Cadmium in the body is known to affect several enzymes. It is believed that the renal damage

that results in proteinuria is the result of Cd adversely affecting enzymes responsible for reabsorption of proteins in kidney tubules. The major threat to human health is chronic accumulation in the kidneys leading to kidney dysfunction. Food intake and tobacco smoking are the main routes by which Cd enters the body (Manahan 2003). This research work is aimed to study the adsorption activity of millet husk for Cd^{2+} from aqueous solution, the effect in various operational parameters such as initial metal ion concentration, temperature, contact time and adsorption isotherm.

MATERIALS AND METHODS
The millet husk obtained from Dutsin-ma, Katsina State, Nigeria, was purified using distilled water and dried in an oven at 80 °C. The dried husk was grinded and sieved in a 1mm sieve to obtain particle sizes less than 1mm. The husk that passed through the 1 mm sieve was then used for sorption studies.

Activation of adsorbent
The millet husk activation was achieved using chemical activation method (Abia and Asuquo 2006), in this method, the screened fine adsorbent was soaked in excess 0.3M HNO_3 for 24 h. It was filtered through Whatman filter paper and rinsed with deionized water to remove any trace of debris and other soluble molecules that may interact with the metal ions during the sorption process.

Effect of initial metal ion concentration on adsorption
In accordance with the method described by Okafor *et .al*., 2012, batch adsorption was carried out using initial metal ion concentrations of 0.5, 1.0, 2.0, and 3.0, mg/l for aqueous solution of Cd^{3+} ions. 0.5 g adsorbent (millet husk) was weighed into (100 ml) beaker and 25 ml of 0.5 mg/l solution of metal was measured into beaker. The adsorption mixtures were uniformly and continuously agitated with the use of a platform shaker at a fixed temperature of 30ºC for 30 minutes after which the content of each beaker was filtered into clean sample bottles. A thermo stated water-bath was used to maintain the temperature. The concentration of residual metals ions in the filtrates was determined using AAS. The amount of metal ion adsorbed from the solution was determined by difference.

Effect of contact time on adsorption
This was studied at various time intervals of 30, 60, 90,120,150, 210 and 180 minutes. Also, 25 ml of metal ion solution with initial metal ion concentration of 0.5 mg/l containing 0.5 g of the adsorbent were employed.

Effect of temperature on adsorption
This was investigated at 30, 40 and 60 °C with the use of a thermostatic water bath. 25 ml of metal ion solution of initial concentration 0.5 mg/l were employed for a period of 30 minutes.

Data Analysis
Experimental readings were carried out in triplicate the average of each reading was used in the calculations. However, the amount of Cd^{2+} adsorbed from each metal solution at time, t, was computed using the equation shown below:

$$q_e = \frac{C_o - C_e}{v} \tag{1}$$

where qe is the amount of metal ion adsorbed at any given time, t, in mg/g; C_o is the initial metal ion concentration (mg/L); Ce is the metal ion concentration at equilibrium i.e. final concentration in solution (mg/L); v is the volume of initial metal ion solution used which is constant (25 ml); m is the mass of adsorbent used (0.5g). The percentage adsorptions were calculated using equation 2.

$$Adsorption(\%) = \frac{C_o - C_e}{C_o} \times 100 \tag{2}$$

Investigation of Cadmium ion /Millet husk interaction using Isotherm Models
Adsorption isotherm models have been used to describe the interaction between metal ion in solution and adsorbents (Liu *et al*., 2009 and Etim *et al*., 2012). In addition, the isotherm models can be used to explain the distribution of metal ion between the liquid and solid phase when equilibrium was reached (Etim *et al*.,, 2012). The most widely used isotherm models are Freundlich and Langmuir models. Freundlich Isotherm model deals with adsorption at multilayer heterogeneous surface (Heidari, *et al*., 2013). According to Freundlich isotherm model, during adsorption process stronger binding sites will occupy first. As more sites are occupied by metal ion, the binding strength becomes weaker (Etim *et al*., 2012). The linear form of the Freundlich equation is.

$$logq_e = logK_f + \frac{1}{n}logC_e \tag{3}$$

Where K_f (mg/g) and n re the Freundlich constants related to adsorption capacity and intensity, respectively. A linear plot of $\log q_e$ against $\log C_e$ will give K_f and n values. The Langmuir isotherm model assumes all sites on adsorbents have equal energy (Kwon, *et al*., 2010, and Liang, *et al*., 2011). During adsorption process, metal ion forms a monolayer on the adsorbent surface and when all sites are occupied, there will be no more binding can take place (Etim *et al*., 2012). The linear form of the Langmuir equation can be expressed as.

$$\frac{Ce}{qe} = \frac{Ce}{Q} + \frac{1}{Qb} \qquad (4)$$

where Q is the maximum adsorption at monolayer (mg/g), Ce is the equilibrium concentration of metal ion (mg/L), qe is the amount of metal ion adsorbed per unit weight of adsorbent at equilibrium concentration (mg/g) and b is the Langmuir constant related to the affinity of binding (mL/mg) and is a measure of the energy of adsorption. Q and b can be determined from the linear plot of C_e/q_e against C_e. Sites (ml/mg) and is a measure of the energy of adsorption. Q and b can be determined from the linear plot of C_e/q_e against C_e. The essential features of the Langmuir isotherm may be expressed in terms of equilibrium parameter which is a dimensionless constant referred to as separation factor or equilibrium parameter (Farooqui, 2004).

$$R_L = \frac{1}{1+K_L c_o} \qquad (5)$$

Where, C_o is initial concentration in ppm and K_L is Langmuir constant related to the energy of adsorption. R_L Value indicates the adsorption nature to be either unfavorable if $R_L > 1$, linear if $R_L = 1$, favorable if $0 < R_L < 1$ and irreversible if, $R_L = 0$ (Hamdaoni, 2006).

Tempkin isotherm: This isotherm is based on the assumption that the heat of adsorption decreases linearly with the increase of coverage of adsorbent. Tempkin isotherm assumes that the fall in the heat of sorption is linear rather than logarithmic (Hosseine *et al*., 2003). The linear form of the Langmuir equation can be expressed as:

$$q_e = \frac{RT}{b_t} \ln A_t + \frac{RT}{b_t} \ln C_e \qquad (6)$$

Where, A_t (L/g) is Temkin adsorption potential and b_t (J/mol) is heat of sorption. The linear plot of $\ln C_e$ versus q_e. From the slope and intercept of the straight line b_t and A_t can be calculated, respectively.

Investigation of Thermodynamic Parameter
Thermodynamic Parameters such as Gibb's free energy change, enthalpy change and entropy change were determined using the following equations (Vadivelan and Vasanthkumar, 2005).

$$K_c = \frac{C_{ad}}{C_e} \qquad (7)$$

$$\Delta G° = -RT \ln Kc \qquad (8)$$

Where

$$\Delta G° = \Delta H° - T\Delta S° \qquad (9)$$

$$\ln K_c = \frac{\Delta S°}{2.303R} - \frac{\Delta H°}{2.303RT} \qquad (10)$$

where, K_c is the equilibrium constant, Cad is the amount of metal ion adsorbed per liter of the solution at the equilibrium, C_e is the equilibrium concentration (mg/L) of the metal in the solution, T is the temperature in Kelvin and R is the gas constant (8.314 J/mole). The values of ΔH and ΔS were determined from the slopes and intercepts of the plot of $\ln K_c$ against $1/T$ respectively.

Investigation Adsorption Kinetics
Adsorption kinetics is used in order to explain the adsorption mechanism and characteristics. The pseudo first-order and pseudo second-order kinetic models were applied to the adsorption data. The adsorption rate constant using first-order reaction kinetics is given by equation 11.

$$\frac{dq}{dt} = k_1 (q_{qe} - q_t) \qquad (11)$$

Where K_1 is the adsorption rate constant for first-order adsorption, qt (mgg^{-1}) the amount of metal ions adsorbed at time t and qeq (mgg^{-1}) the amount of metal ions adsorbed at equilibrium or saturation Eq. 12 is the integrated form of Eq. 11.

$$\ln(q_{eq} - q_t) = -K_t + C_i \qquad (12)$$

Where c_i is the integration constant for first-order reaction kinetics. If it is supposed that $q_t = 0$ at t =0, then Eq. 12 transforms to Eq. 13

$$\ln(q_{eq} - qt) = lnq_{eq} - k_1 t \tag{13}$$

The adsorption rate proposed by Ho and McKay using pseudo second-order reaction kinetics is given by Eq. 14

$$\frac{dy}{dx} = k_2(q_{eq} - qt)^2 \tag{14}$$

Where k_2 is the rate constant for pseudo second-order reaction kinetics. With an algorithmic arrangement, Eq. 15 can be obtained from Eq. 14

$$\frac{t}{q_t} = \frac{1}{k_2 q_{eq}^2} + \frac{t}{q_{eq}} \tag{15}$$

The mathematical relation:

$$h = K_2 q_{eq}^2 \tag{16}$$

Can be used to calculate the initial sorption rate denoted by h (g mg-1 min-1). Eq. 15 was used to model the adsorption data by plotting t/q_t against t.

RESULTS AND DISCUSSION
Effect of Temperature on Adsorption of Cadmium Ion

Studies on the effect of temperature on adsorption of cadmium ions onto modified and unmodified millet husk were carried out at 30, 40 and 60°C using fixed quantities of millet husk (0.5g), volume of the adsorbent (25ml) and cadmium ion concentration (0.973ppm). These results are presented in Tables 1 and 2 for unmodified and modified millet husk respectively. The results revealed that adsorption capacity of Cd^{2+} has been observed to decrease from 0.2015mg/g to 0.02mg/g onto unmodified millet husk and decrease from 0.43 to 0.40 mg/g onto modified when the temperature increased from 30 to 60°C. These decreases in adsorption with increase in temperature were as a result of the tendency of heavy metal adsorbent ions to desorb from solid phase to the bulk phase or due to weak adsorptive forces between the active sites and the adsorbed species and also between close by molecules of adsorbed phase. This suggests that the adsorption process using Modified and unmodified millet husk is physisorption (Ladan *et al*., 2013).

Table 1: Thermodynamic parameters for Cd^{2+} adsorption onto unmodified and modified millet husk

T (°C)	C_O(ppm)	C_e (ppm)		(%) Adsorption		q_e (mg/g)	
		Unmod	Mod	Unmod	Mod	Unmod	Mod
30	0.973	0.570	0.123	41.410	87.360	0.202	0.430
40	0.973	0.834	0.124	14.280	87.260	0.070	0.420
60	0.973	0.934	0.159	4.000	83.650	0.020	0.400

Thermodynamic Parameters

Thermodynamic considerations of an adsorption process are necessary to conclude whether the process is spontaneous or non-spontaneous (Jing *et al.,* 2010). The changes of Gibb's free energy, enthalpy, and entropy were calculated presented in Tables 2 for unmodified and modified millet husk. The values of ΔH and ΔS were determined from the slopes and intercepts of the plot of lnK_c against $1/T$ respectively.

Table 2: Thermodynamic values for Cd^{2+} using unmodified and modified millet husk

ΔG(kJ/mol)		ΔH(kJ/mol)		ΔS	
Unmod	Mod	Unmod	Mod	Unmod	Mod
0.711	-4.87	0.8623	9.254	-0.8724	-31.052
4.66	-5.01	0.8623	9.254	-0.8724	-31.052
8.79	-4.52	0.8623	9.254	-0.8724	-31.052

The positive ΔG value as presented Table 2 for unmodified millet husk indicates that the reaction is nonspontaneous. The negative ΔG value for modified millet husk confirms the feasibility of the reaction and spontaneous nature of the adsorption. The ΔG values obtained in this study for the Cadmium metal ions are < -10 KJ/mole, which indicate that physical adsorption was the predominant mechanism in the adsorption process (Funtua and Ugbe, 2015). The decrease in the negative value of ΔG with an increase in temperature indicates that the adsorption process of heavy metal ions on modified millet husk becomes more favorable at higher temperatures (Zaki *et al*., 2000). Furthermore, the small absolute value for ΔG° obtained in this study indicates that physical adsorption is the predominant mechanism in the sorption process (Horsfall *et al.*, 2004). The positive value of ΔH suggests that the adsorption to be in agreement with

the endothermic. Whereas, positive values of enthalpy change (ΔH) for adsorption using modified and unmodified millet husk indicates an endothermic process. The negative values of entropy change (ΔS) for adsorption of heavy metal ions using unmodified husk indicates less randomness at the solid/solution interface during the sorption process. However, a negative value for ΔS was also reported for the adsorption of Methylene Blue by cereal husk (Han *et al.,* 2006), fallen phoenix tree's leaves (Han et al., 2007) and adsorption of heavy metals from aqueous waste water using unmodified and modified maize cobs (Funtua and Ugbe, 2015).

Effect of Initial Cadmium Metal Ion Concentration

These results on the effect of initial metal ions concentration on adsorption of cadmium ions onto modified and unmodified millet husk are presented in Table 3 for unmodified and modified millet husk respectively. According to these results adsorption capacity of Cd^{2+} has been observed to increase from 0.012 mg/g to 0.071 mg/g for unmodified millet husk and from 0.149 mg/g to 0.56 mg/g for modified millet husk. It is observed that as the initial concentration increases, the percentage removal efficiency increases because at low concentration, the number of active sites is more on the surface of the adsorbent. As the concentration increases the number of metal ions increases and hence adsorption increases. The adsorption processes simultaneously include liquid phase diffusion and solid phase adsorption process with increasing the probability of contact between metal ions and active sites is improved and a great adsorption capacity especially for modified millet husk is archived.

Table 3: Isotherm parameters for the adsorption Cd^{2+} Concentration using unmodified and modified millet husk

C_O (ppm)	C_e (ppm)		Adsorption (%)		q_e (mg/g)	
	Unmod	Mod	Unmod	Mod	Unmod	Mod
0.429	0.405	0.131	5.590	69.46	0.012	0.149
0.643	0.570	0.121	11.350	81.18	0.040	0.260
0.973	0.835	0.096	14.180	90.13	0.069	0.550
1.183	1.000	0.064	16.000	94.50	0.071	0.560

Isotherms Parameters

Linear plots of log q_e against log C_e for Freundlich Isotherm model for unmodified and modified millet husk respectively were generated. From the slope and intercept of the graphs, K_f and n values were obtained. On the other hand, linear plot of C_e/q_e against C_e for Langmuir isotherm model were plotted for unmodified and modified millet husk respectively, from the slope and intercept q_{max} and K_L were calculated. Linear plots of ln C_e versus q_e for Tempkin isotherm model is plotted for unmodified and modified millet husk respectively, from the slope and intercept of the straight line b_t and A_t were calculated, respectively. The isotherm parameters for the three isotherms models and their R^2 are presented in Table 4.

Table 4: Langmuir, Tempkin and Freundlich Isotherm Model Parameters for Adsorption of Cd^{2+} onto modified and unmodified millet husk

Isotherm parameters	Millet Husk Biomass Sample	
	Modified	*Unmodified*
Langmuir		
q_{max} (mg/g)	16.27	0.029
K_L (L/g)	0.992	0.8097
R^2	0.784	0.680
Freundlich		
n	0.6085	0.3966
K_F (Lmg/g)	0.00703	0.00944
R^2	0.803	0.954
Tempkin		
A_T (L/g)	5.2718	2.80
B_T (kJ/mol)	4.626	29.491
R^2	0.912	0.992

Table 5: Initial Concentrations and R_L values for Cd²⁺ adsorption onto modified and unmodified millet husk

Initial Concentration (ppm)	R_L Values for Adsorption onto Millet Husk	
	Modified (L/mg)	*Unmodified (L/mg)*
0.429	0.7012	0.7587
0.643	0.6106	0.6575
0.973	0.5088	0.5593
1.183	0.4602	0.5112

The essential characteristic of the Langmuir is a dimensionless constant separation factor R_L which was calculated and the values are presented in Table 5 for modified and unmodified millet husk. The separation factor R_L shows that the Langmuir isotherm for both modified and unmodified millet husk are favoured since the R_L values are less than 1 (Hamdaoni, 2006). High correlation coefficients (R^2) for modified millet husk which is 0.784 indicates that the Langmuir model is suitable for describing the adsorption equilibrium for the metal ion by modified as compare for unmodified which is 0.680. The high K_L value for modified millet husk had indicated a greater affinity to the metal ion.

Table 4 presented the Freundlich parameters and correlation coefficient R^2 for the fitting of the experimental data for both modified and unmodified. The calculated result shows that n is less than 1, thus, indicating that the millet husk is exhibited strong adsorption ability on cadmium ion. Modifying the millet husk with marcaptoacetic acid increased heavy metal ion adsorption significantly, the Regression coefficients (R^2) are 0.803 and 0.954 for unmodified and modified millet husk respectively.

Table 4 also shows Tempkin isotherms R^2 are 0.912 and 0.992 for modified and unmodified millet husk respectively, in comparison with Langmuir and Freundlich, the result of Tempkin isotherm model appears to be favorable for fitness to the experimental data of Cd²⁺ with high value of R^2 both for modified and unmodified. Similarly, El-Sayed *et al.*, (2011) also reported in their research that Tempkin isotherm model appears to be favorable for fitness to the experimental data of Cd (II).

The mercaptoacetic acid modification process led to the thiolation of the hydroxyl groups of the cellulosic biomass by the following reaction (Horsfall *et al.*, 2004).

$$\text{Biomass–OH} + \text{HSCH}_2\text{COOH} \longrightarrow \text{Biomass–SH} + \text{H}_3\text{CCO}_2^- + \text{H}^+$$

Effect of Contact Time

The effect of contact time on the adsorption of the metal ions by the modified and unmodified millet husk is presented in Table 6. It was observed that adsorption increases with increasing time. Sorption of metal ions is strongly dependent on the concentration of the adsorbate. Since the same initial concentration of the adsorbent was used, the availability of adsorption sites on the adsorbent may have led to the different rates observed for modified and unmodified husk and maximum adsorption was observed for modified husk. The modifying agent contributed COO⁻ linkages and also increased the H⁺ concentration, likely providing more adsorption sites.

Table 6: Kinetic Parameters for the Adsorption of Cd^{2+} using Unmodified and modified Millet Husk

t (min)	C_O(ppm)	C_e (ppm)		Adsorption (%)		q_t	
		Unmod	Mod	Unmod	Mod	Unmod	Mod
30	0.973	0.759	0.170	21.99	79.83	0.100	0.40
60	0.973	0.740	0.120	23.95	85.30	0.120	0.42
90	0.973	0.668	0.110	31.35	86.30	0.153	0.43
120	0.973	0.643	0.094	33.92	87.90	0.165	0.44
150	0.973	0.642	0.081	33.10	89.20	0.166	0.45
180	0.973	0.642	0.081	33.10	90.10	0.166	0.45

Kinetics study

Kinetic models were applied to the experimental data to study the mechanism of adsorption. The values of the constants were obtained by making necessary linear plots log (q_e-q_t) against t for pseudo first adsorption kinetics parameters and a linear plot 1/qe against t for pseudo second order adsorption kinetic parameters as guided by the kinetic models. The linear plots presented in Figure 1 and 2 represent pseudo first order adsorption kinetics of on

Cd^{2+} for modified and unmodified millet husk respectively. Also the pseudo second order adsorption kinetics of modified and unmodified millet husk on Cd^{2+} is presented in fig 3 and 4 respectively.

From the results presented in Table 7, the correlation coefficient (R^2) values for the pseudo-second-order model were higher than that of the Pseudo first order reaction and this suggests that the pseudo-second-order kinetic model fits the experimental data better. Similar result was reported by Aderibigbe *et al.*, (2017) for the adsorption studies of Pb^{2+} using unmodified and citric acid modified plantain peels. The insufficiency of the first order model to fit the kinetics may be due to the limitations of the boundary layer controlling the adsorption (Asim and Necip, 2012). For the pseudo-second-order kinetics, the experimental adsorption capacity values with those of the calculated were very close.
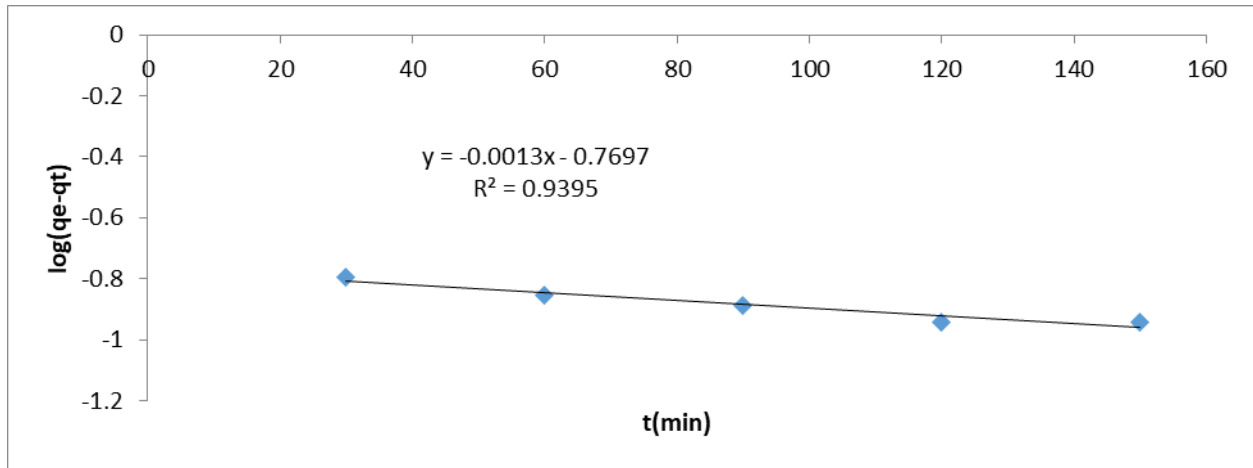
Figure 1: pseudo first order adsorption kinetics of modified millet husk on Cd^{2+}
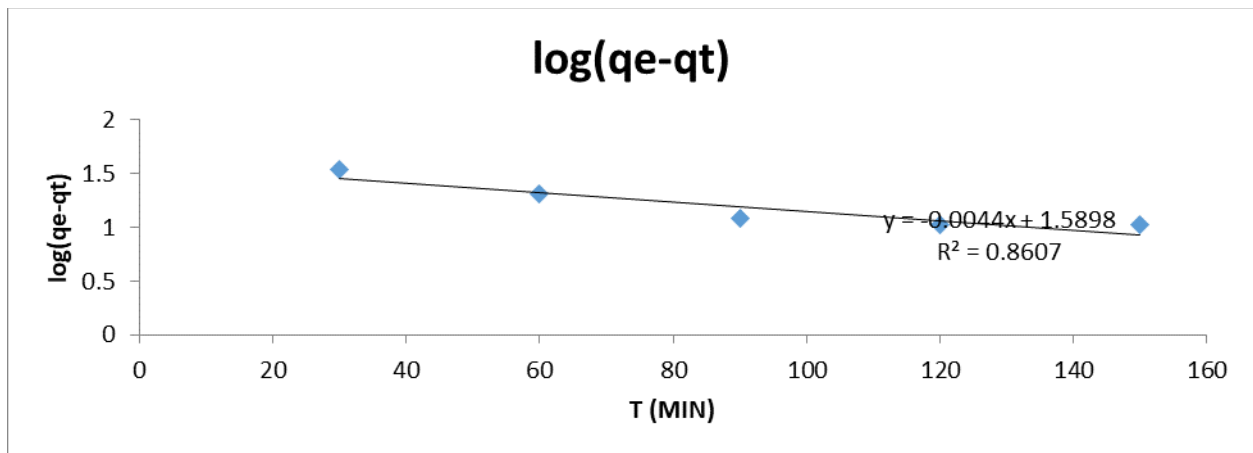
Figure 2: pseudo first order adsorption kinetic of unmodified millet husk on Cd^{2+}
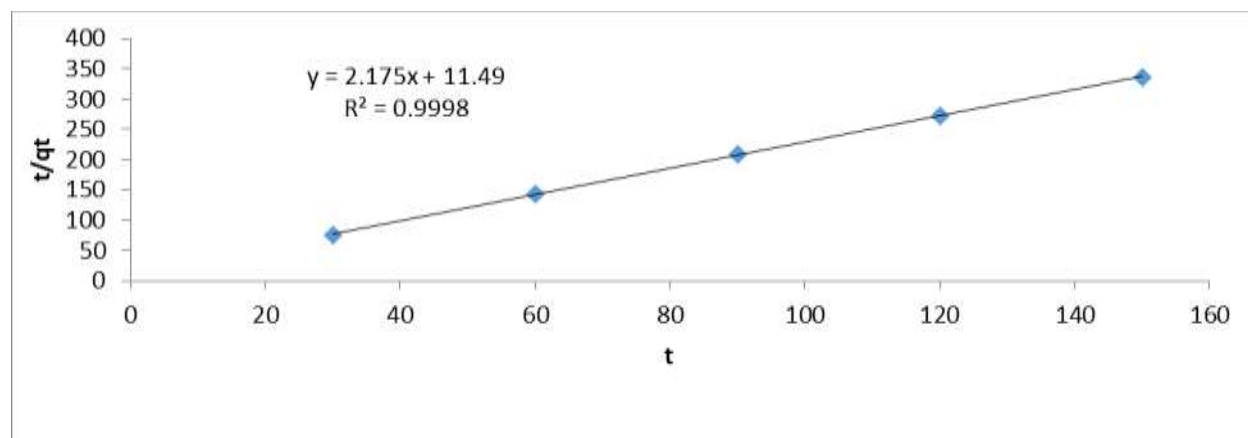
Figure 3: pseudo second order adsorption kinetic of modified millet husk on Cd^{2+}
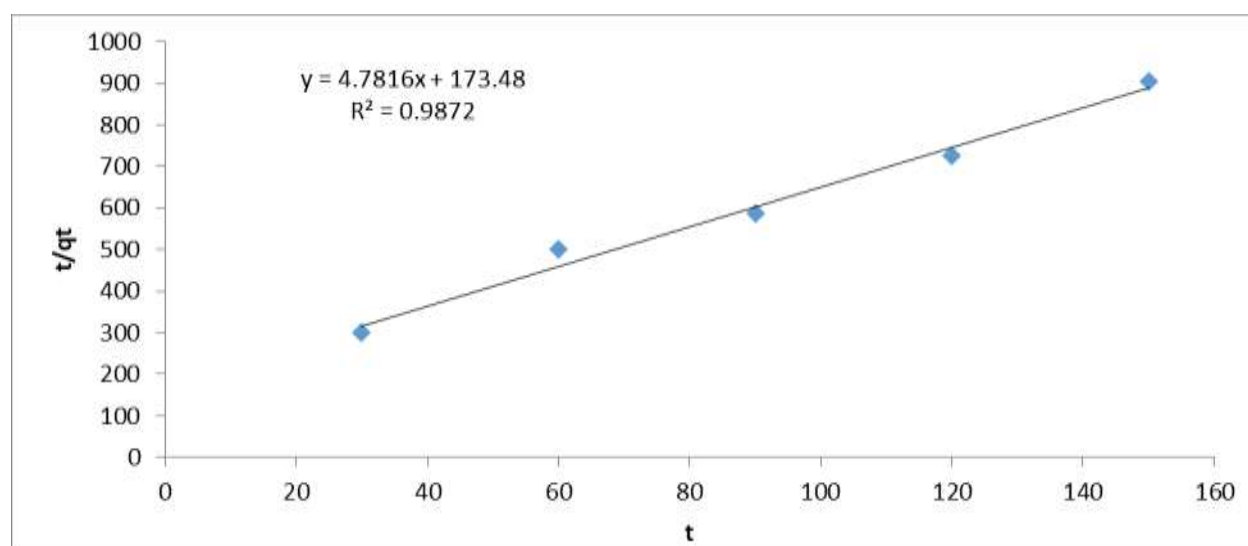
Figure 4: pseudo second order adsorption kinetic of unmodified millet husk on Cd^{2+}

Table 7: Pseudo first and second order kinetics Parameters for Adsorption of Cd^{2+} On modified and unmodified millet husk.

Pseudo first order kinetics	Millet Husk Biomass Sample	
	Modified	**Unmodified**
$k_1\ (min^{-1})$	0.0023	0.0010
R^2	0.939	0.860
Pseudo second order kinetics		
$k_2(gmg^{-1}min^{-1})$	0.4117	0.3110
q_e (mg/g)	0.459	0.209
h($gmg^{-1}min^{-1}$)	0.08674	0.01358
R^2	0.999	0.987

CONCLUSION

This work described the adsorption studies of heavy metal (Cd^{2+}) from the aqueous solution using modified marcaptoacetic acid and unmodified millet husk. The study shows the ability of millet husk to absorb cadmium from aqueous solution. The modification of the millet husk by Thiolation enhanced its sorption capacity. The thermodynamic study shows that the reaction is spontaneous for modified millet husk and non-spontaneous for

unmodified millet husk, the adsorption process was found to be endothermic. The sorption process was found to follow Pseudo-second kinetics. Freundlich and Tempkin adsorption models were applied successfully in the adsorption of cadmium (II) ions using modified and unmodified millet husk.

REFERENCES

Abia, A.A .and Asuquo, E.D. (2006). Lead (II) and nickel (II) Adsorption kinetics from aqueous Metal Solutions using chemically modified and unmodified. African Journal BiotechnologyVol.5 (16), pp.1475-1482,

Aderibigbe, A.D., Ogunlalu O.U., Oluwasina, O.O, and Amoo, I.A. (2017). Adsorption studies of pb^{2+} from aqueous solutions using Unmodified and citric acid – modified plantain *(musa paradisiaca)* peels adsorption studies of pb^{2+} from aqueous solutions using unmodified and citric acid – modified plantain *(musa paradisiaca)* peels. *IOSR Journal of Applied Chemistry (IOSR-JAC) e-ISSN: 2278-5736.Volume 10, Issue 2 Ver. PP 30-39.*

Adriano D. C., (2003); *Trace Elements in Terrestrial Environments: Biogeochemistry, Bioavailability and Risks of Metals*, Springer, New York, NY, USA, 2nd edition.

Anahan S.E., (2003); *Toxicological Chemistry and Biochemistry*, CRC Press, Limited Liability Company (LLC), 3rd edition.

Ashrafi, S.D., Kamani, H., Arezomand, H.S., Yousefi, N., Mahvi, A.H., (2015). Optimization and modeling   of process variables for adsorption of Basic Blue 41 on NaOH-modified rice husk using response surface methodology. Desalin. Water Treat. 57(30), 14051-14059.

Asim O. and Necip A. (2012). Equilibrium, thermodynamic and kinetic studies for the adsorption of lead (II) and nickel (II) onto clay mixture containing boron impurity, *Journal of Ind. and Eng. Chem*, *18*, 1751-1757.

Campbell P. G. C., (2006); "Cadmium-A priority pollutant," *Environmental Chemistry*, vol. 3, no. 6, pp. 387–388.

Etim, U.J., Umoren, S.A. and Eduok, U.M. (2012) Coconut Coir Dust as a Low Cost Adsorbent For the Removal of Cationic Dye from Aqueous Solution. *Journal of Saudi Chemical Society.*

Funtua M.A. and Ugbe F.A..(2015) Adsorption of Heavy Metals from Aqueous WasteWater Using Unmodified and EthylenediaminetetraaceticAcid (EDTA) Modified Maize Cobs. *International Journal of Current Research in Biosciences and Plant Biology ISSN: 23498080 Volume 2 Number 1pp. 98103*.

Han, R.P., Wang, Y.F., Han, P., Shi, J., Yang, J., Lu, Y.S., (2006). Removal of methylene blue from aqueous solution by chaff in batch mode... *J. Hazard. Mat. 137, 550-557*

Han, R.P., Zou, W.H., Yu, W.H., Cheng, S.J., Wang, Y.F., Shi, J., 2007. Bio sorption of Methylene blue from aqueous solution by fallen *Phoenix* tree's leaves. *J. Hazard. Mat. 141, 156 162.*

Hamdaoni O., J. (2006) Hazard. Mater, *B135, 264.*

Horsfall, M.; Spiff, A.I.; Abia, A.A. *(2004).* Studies on the influence of mercaptoacetic acid (MAA) Modification of cassava (Manihot sculenta cranz) waste Biomass on the adsorption of Cu2+And Cd2+ from aqueous solution. Bull. *Korean Chem. Soc., 25, 969–976.*

Hosseine, M., Merten, M., Ghorbani, M. and Arshadi, M.R. (2003). Asymmetrical Schiff bases

Houda, B., Moussa, B., 2017. Electrosorption removal of the zinc ions from aqueous solution on an artificial electrode based in the banana wastes. J. Electrochem. Sci. Technol. 8(1), 77-86.

Jawad, A.H., Rashid, R.A., Mahmuod, R.M.A., Ishak, M.A.M., Kasim, N.N., Ismail K., (2015). Adsorption of methylene blue onto coconut (Cocos nucifera) leaf: optimization, isotherm and kinetic studies. Desalin. Water Treat. 57(19), 8839-8853.

Jing, H., Song, H., Liang, Z., Fuxing, G., Yuh-Shan, H., (2010). Equilibrium and thermodynamic Parameters of adsorption of methylene blue onto rectorite. Fresen. *Environ. Bull. P 19(11a), 2651- 2656.*

Khan S., Cao Q., Zheng Y. M., Huang Y. Z., and Zhu Y. G., (2008); "Health risks of heavy metals in contaminated soils and food crops irrigated with wastewater in Beijing, China," *Environmental Pollution*, vol. 152, no. 3, pp. 686–692, 2008.

Kobya, m; demirbas, E; Senturk and ince m. (2005). Adsorption of heavy metal ions from Aqueous solution by activated carbon prepared from apricot stone, *Bioresources Technology 96(13), 1518-1521*

Kwon, J.S. Yun, S.T. Lee, J.H. Kim, S.O. and Jo, H.Y. (2010) Removal of Divalent Heavy Metals (Cd, Cu, Pb, and Zn) and Arsenic (III) From Aqueous Solutions Using Scoria: Kinetics and Equilibria of Sorption. *Journal of Hazardous Materials, 174, 307-313.*

Ladan, M., Ayuba, A.M., Bishir, U., Jamilu, A., Habibu, S., (2013). Thermodynamic properties of chromium adsorption by sediments of river water, Kano state. Chemsear. J. 4(1), 1-5.

Liang, S., Guo, X. and Tian, Q. (2011) Adsorption of Pb2+ and Zn2+ From Aqueous Solutions By Sulfured Orange Peel. *Desalination, 275, 212-216*

Ling W., Shen Q., Gao Y., Gu X., and Yang Z. (2007); "Use of bentonite to control the release of copper from contaminated soils," *Australian Journal of Soil Research*, vol. 45, no. 8, pp. 618–623,.

Liu, Y., Cao, Q., Luo, F. and Chen, J. (2009) Bio sorption of Cd^{2+}, Cu^{2+}, Ni^{2+} and Zn^{2+} Ions from Aqueous Solutions by Pretreated Biomass of Brown Algae. *Journal of Hazardous Materials, 163, 931-938.*

McLaughlin M. J., Hamon R. E., McLaren R. G., Speir T. W., and Rogers S. L. (2016) "Review: a bioavailability-based rationale for controlling metal and metalloid contamination of agricultural land in Australia and New Zealand," *Australian Journal of Soil Research*, vol. 38, no. 6, pp. 1037–1086.

Okafor, P.C., Okon, P.U., Daniel, E.F., and Ebenso, E.E. (2012). Adsorption Capacity of Coconut (Cocos nucifera L.) Shell for Lead, Copper, Cadmium and Arsenic from Aqueous Solutions. *.International Journal Electrochemical Science, 712354-12369.*

Rosales, E., Meijide, J., Pazos, M., Sanromán, M. A., 2017. Challenges and recent advances in biochar as low-cost biosorbent: From batch assays to continuous-flow systems. Bioresour. Technol. 246, 176-192.

El-Sayed, G. O., Dessouki, H. A., and Ibrahiem, S. S. (2011). Removal Of Zn(II), Cd(II) And Mn(II) From Aqueous solutions by adsorption on maize stalks. *The Malaysian Journal of Analytical Sciences, Vol 15 No 1: 8 – 21.*

Vadivelan V, Vasanthkumar K., *(2005). Journal of Colloid Interference Science, 91, 286.*

Weggler K., McLaughlin M. J., and Graham R. D., (2004); "Effect of Chloride in Soil Solution on the Plant Availability of Biosolid-Borne Cadmium," *Journal of Environmental Quality*, vol. 33, no. 2, pp. 496–504.

Zaki, A.B., El-Sheikh, M.Y., Evans, J., El-Softy, S.A., (2000). Kinetics and mechanism of the Sorption of some aromatic amines onto amberlite IRA-904 anion-exchange resin. *J. Coll. Interf. Sci. 221, 58-63.*

Enhancing Resource Optimization in Cloud Computing through Artificial Intelligence-Driven Fault Prediction Techniques

Bakare K. A. and *Abdulwasiu A. A.

Computer Science Department, Federal University Dutsin-Ma
*Corresponding Author's E-mail: ibnwasar@gmail.com

ABSTRACT

The majority of current fault tolerance techniques primarily focus on creating clones to replace a failing virtual machine (VM) rather than proactively predicting the failure in advance. Some of these techniques prioritize VM migration over recovery due to resource limitations and concerns about server availability. Examples of these one-dimensional approaches include fault tolerance, migration prediction, and simply expecting failure. Fault tolerance is a critical aspect of this research, where the research aims at identifying the most efficient strategy for transitioning from an underperforming system to a functional one. Timely prediction of VM failures is crucial to address issues like wasted resources, energy, and costs. The reliability of virtual machines (VMs), an integral part of fault tolerance systems has been a persistent challenge in cloud computing since its inception. Therefore, it is imperative to focus on enhancing and emphasizing the proactive prediction of VM failures. This effort is driven by the desire to reduce downtime and enhance scalability. This research work employs a technique to safely transfer predicted failing resources from one VM to another, effectively reducing migration time and optimizing resource usage. This article harnesses artificial intelligence to facilitate effective fault prediction techniques in cloud computing for improved resource optimization and to be specific in the novelty, the methodology is applied to specific scientific processes, such as small Ribonucleic Acid Identification Protocol using High-throughput Technology (SIPHT) and the Laser Interferometer Gravitational-Wave Observatory (LIGO), demonstrating its practical application in evaluating resource usage features against predefined thresholds.
Keywords: Fault prediction, Artificial intelligence, Fault tolerance, Cloud computing, CloudSim

INTRODUCTION

Cloud computing refers to the practice of using interconnected and virtualized computers to offer on-demand access to various computer resources, such as data storage and processing power. The term "cloud computing" encompasses this activity. While multiple servers are connected to the master server, only the master server can act as the master. The configuration of the cloud environment is adaptable and determined by the organization's needs, guiding the deployment of services. Cloud services can be categorized into three major configurations.

Software as a Service (SaaS) allows consumers to access cloud-based resources by paying a monthly membership fee (Taufiq-Hail *et al.*, 2021).

Platform as a Service (PaaS) empowers users to build, run, and develop their applications in the cloud, offering platform independence (Aldahwan and Ramzan, 2022).

Infrastructure as a Service (IaaS) grants access to internet-based computer resources like servers, networking devices, and storage spaces. Lin et al, (2023).

Cloud technology enhances efficiency and cost-effectiveness for service providers, offering various benefits such as improved quality and reliability. The pay-as-you-go model enables users to select suitable service levels, and cloud platforms enable users to run their applications by connecting to the internet. Metrics and service level agreements (SLAs) are used to assess service quality.

Virtualization allows the creation of a network of virtual machines (VMs), which serve as the computing units in a cloud environment. VMs can be moved or replaced without disrupting running applications, offering flexibility and efficiency. Virtualization also facilitates resource allocation, making it a key driver of cloud computing's popularity.

Cloud computing manages resources efficiently to prevent freezing or crashing of virtual machines. Load balancing can increase throughput, reduce effort, and enhance flexibility. Resources are divided into logical and physical categories, with distributed services improving fault tolerance and load balancing.

Scheduling workloads and allocating resources to customer workloads can be challenging. Evenly distributing jobs improves resource allocation and customer satisfaction, while maintaining multiple copies of resources minimizes failures. Fault tolerance ensures that system operations continue smoothly, even in the presence of faults or failures Lin et al, (2023).

Effective defect prediction approaches in cloud computing, driven by artificial intelligence, aim to enhance resource optimization and address issues related to system faults. These strategies aim to improve the overall efficiency of cloud computing environments.

Literature Review

To enhance the accuracy of predictions, many researchers have concentrated on improving fault prediction using various methods. However, cloud computing has not yet introduced methods for predicting failures in scientific processes. This research work conducted a comprehensive survey to identify the most effective methods for predicting and identifying job failures. Multiple approaches have been proposed to address fault detection and prediction, particularly in scenarios with dispersed faults.

For instance, Fu and Xu, (2017) developed a model employing supervised learning algorithms, achieving accuracy levels ranging from 70.1% online to 74% offline. Zhou et al., (2021) introduced a method to detect faults in workflow engines before they occur. Guan, et al., (2012) proposed using decision trees or Bayesian networks for healthcare data to identify and forecast failures. Zhao et al., (2010) established a heartbeat message protocol for identifying replica failures. Nevertheless, there is room for improving these methods, and new machine learning and statistical approaches are needed. Machine learning models have shown superiority over statistical methods in outcome anticipation (Catal, 2011). Researchers like Malhotra and Jain (2012) found Random Forest to be effective in predicting electrical failures, and Zhang et al., (2021) utilized multivariate analytic techniques for fault-prone class predictions. Artificial Neural Networks (ANNs) have been employed for resource use forecasting in cloud-based systems. Incorporating ANNs into cloud computing systems enhances resource provisioning forecasting accuracy. Catal's research suggests that the Naive Bayes Model is effective in forecasting software errors, but its performance compared to other machine learning algorithms like ANN, LR, and Random Forest has not been compared. Despite various machine learning algorithms, none of the approaches have precisely predicted job outcomes.

Accurate failure predictions could significantly mitigate the impact of failures in scientific applications, allowing for better resource arrangement and fault-tolerant strategies. Nevertheless, predicting failures in complex applications like workflows remains challenging. Glass et al. (2017) and others have noted that prior models typically consider one resource for each activity, neglecting connections between multiple resources and activities. Agent-based systems offer resilience through redundancy, allowing them to adapt to unforeseen events. Lohani et al., (2021) proposed using various techniques to improve the self-adaptive capabilities of software by eliminating discovered rules and graphical policy descriptions.

Conclusively, while many methods have been proposed for fault prediction in cloud computing, there is still room for improvement, especially in predicting failures in scientific processes and complex applications. Researchers are exploring various machine learning and statistical approaches to enhance accuracy and resilience in these prediction methods.

MATERIALS AND METHODS

The primary focus of this research paradigm is on the failure of tasks due to resource overutilization, including the central processing unit, memory, disk storage, and network bandwidth. The proposed methodology aims to build a model that tracks real-time data for scientific processes, identifying issues before they occur.

Data Collection

Data was obtained from the cloud computing environment, specifically focusing on scientific workflow applications. The initial features include Task ID, VM ID, Data Centre ID, CPU Utilization, Bandwidth Utilization, RAM Utilization, Disk Utilization, Task Size, and Status.

Data Preprocessing

This include data cleaning and feature selection to make sure the dataset are in well format to be used for the prediction.
Data Cleaning: Addressed any missing and inconsistent data values and impute missing values using the Pandas tool.
Feature Selection: in this the initial features were narrowed down to CPU Utilization, Bandwidth Utilization, RAM Utilization, and Disk Utilization using the Principal Component Analysis (PCA) algorithm technique for feature selection.

Machine Learning Models

In this research work, Linear regression, Random Forest, and Naive bayes were the algorithms used after when the data were split into 80% trained and 20% tested datasets.

Linear regression is one method used to predict a dependent variable based on independent variables, considering resource consumption characteristics.

Random Forest approach involves creating numerous individual trees, combining bagging and random selection methods. Each tree places a vote for classifying input vectors, and the forest selects the classification with the most votes. The Bayes theorem is used in data classification with Bayesian approaches, efficiently integrating various classification algorithms.

Naïve Bayes approach assumes a probabilistic model for numerical and categorical data, making it time-efficient. It is suitable for handling challenging data characteristics. Real-time data models focus on addressing missing values more than traditional models. The Naive Bayes classifier is used in sensor networks for accurate event outcome predictions. Figure 1 depicts the flowchart of the work step by step.
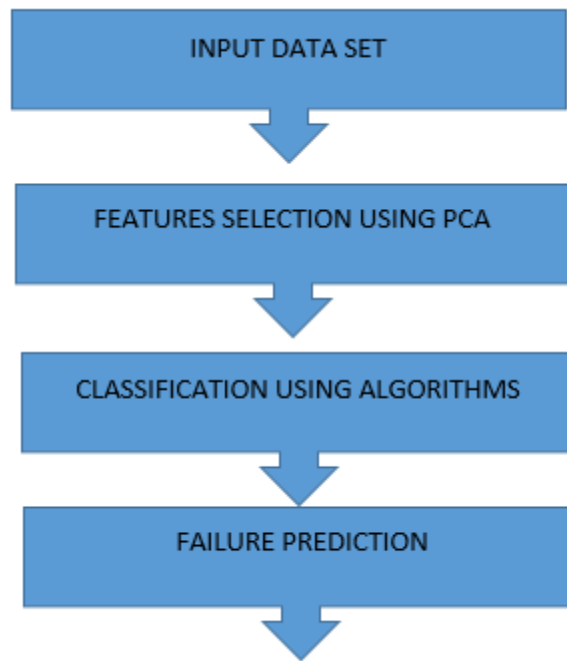
Figure 1: Methodology steps

Simulation Environment

This research work utilized Workflow Sim 1.0 for simulating scientific workflows. This allowed the creation of controlled environment to test the fault prediction techniques. And the work combines Workflow Sim 1.0 with CloudSim to replicate cloud computing conditions. This integration is crucial for emulating real-world cloud environments and their resource usage patterns. Then the work built applications for scientific workflows using XML schema and a workflow engine. This step simulates real-world applications and their interactions with cloud resources then integrated the processed and selected features (CPU Utilization, Bandwidth Utilization, RAM Utilization, and Disk Utilization) into the simulated scientific workflows and cloud computing environment. Then the research work conducts experiments using the simulated environment. Varied the parameters and conditions to observe how different factors influence fault prediction accuracy and resource optimization.

RESULTS AND DISCUSSION

The scientific process applications analyzed within the suggested approach include the small Ribonucleic Acid Identification Protocol using High-throughput Technology (SIPHT) and the Laser Interferometer Gravitational-Wave Observatory (LIGO). These applications involve the evaluation of resource usage features, such as CPU, bandwidth, random access memory, and disk usage, by comparing them to predefined threshold values. These thresholds are determined based on historical data of task failures caused by excessive virtual machine (VM) usage. If a utilization parameter exceeds the maximum threshold, the operation is considered unsuccessful; otherwise, it is deemed successful. Machine learning strategies were used to construct a failure prediction model with minimal Root Mean Square Error (RMSE), Mean Absolute Percentage Error (MAPE), and total accuracy errors.

Workflow Sim 1.0 and CloudSim were utilized to investigate, optimize, and enhance the patterns of failure in scientific workflow applications. Both static and dynamic schedulers were integrated to develop applications for scientific workflows using XML schema and a workflow engine. Clustering and fault tolerance were also incorporated into the analysis of scientific workflow applications. CloudSim and Workflow Sim were employed to analyze and document workflow applications within the scientific community.

The investigation employed data extraction and prediction-based outcome algorithms, which can be implemented using Python. Performance indicators and predicted task failures for various procedures were documented.

Resource consumption measures were analyzed using threshold values for CPU utilization, bandwidth utilization, random access memory utilization, and disk utilization. These thresholds were determined based on past task failures attributed to excessive VM usage. If a parameter value exceeds the predefined threshold, the task is marked as a failure; otherwise, it is labeled as "No Failure."

The input dataset comprises nine attributes: Task ID, VM ID, Data Centre ID, CPU Utilization, Bandwidth Utilization, RAM Utilization, Disk Utilization, Task Size, and Status.

The study evaluates and compares the performance of various algorithms based on criteria such as accuracy, sensitivity, RMSE, and specificity. Performance results are presented in Figures 2–5.
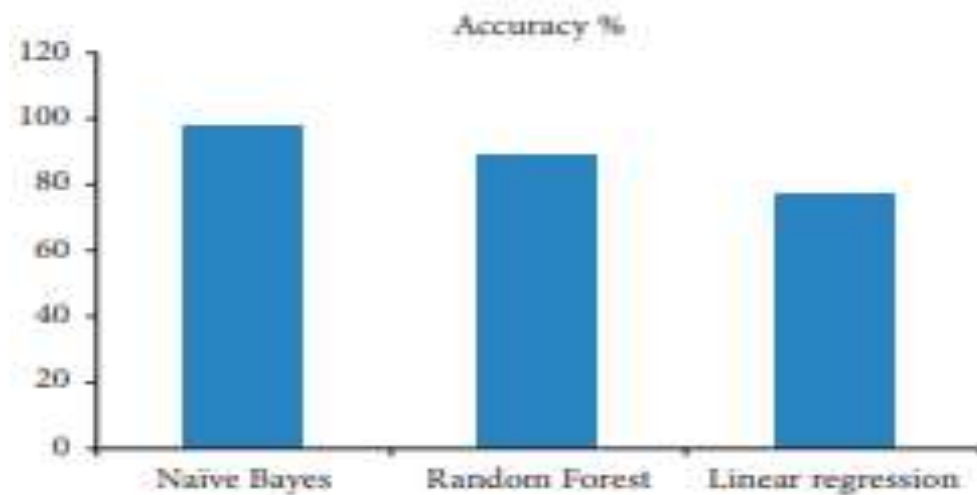
Figure 2: Accuracy result
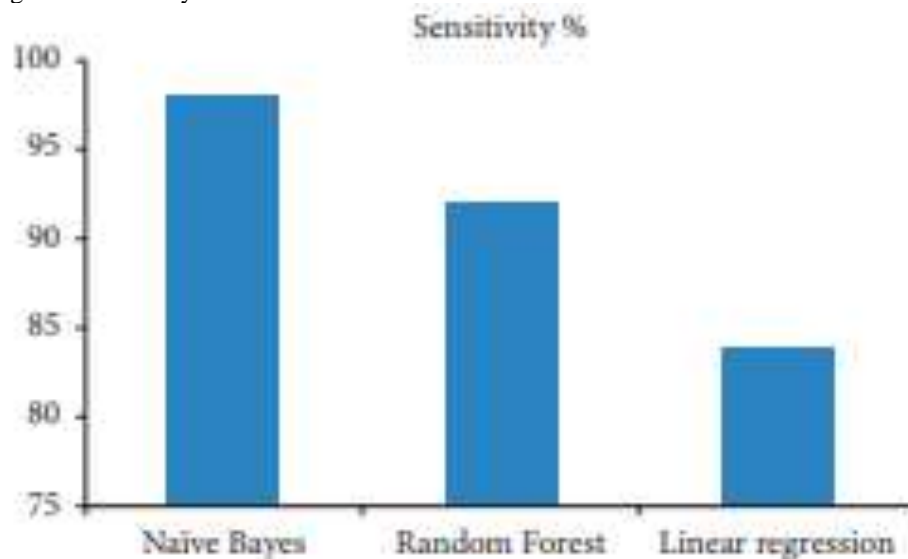
Figure 3: Sensitivity result
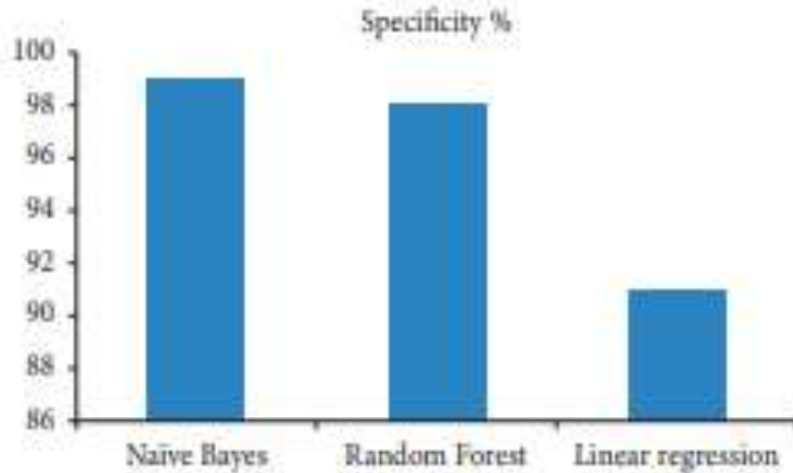
Figure 4: Specificity result
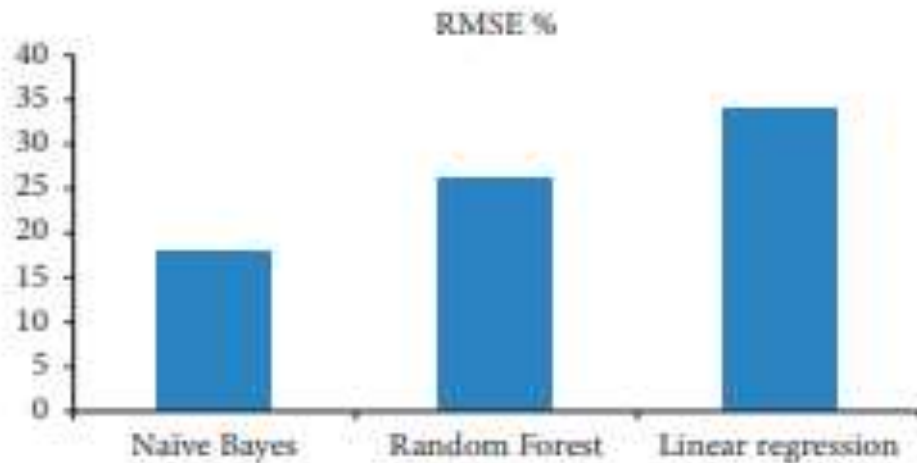
Figure 5: RMSE result

CONCLUSION

In conclusion, many current fault tolerance techniques primarily focus on creating clones to replace a virtual machine (VM) in case of failure rather than proactively predicting and preventing failures. Some of these techniques prioritize VM migration over recovery due to resource limitations and server availability concerns. Examples of single-objective algorithms include fault tolerance, migration prediction, and simply expecting failure. The goal of this research is to identify the most effective strategy for transitioning from a poorly performing system to a reliable one. Timely prediction of VM failures is crucial to address issues like resource wastage, energy consumption, and cost efficiency, which have been persistent concerns in cloud computing since its inception.

Proactive measures are essential to ensure uninterrupted service as part of a fault tolerance system. Therefore, there is a strong need to improve and emphasize the early prediction of VM failures. The primary motivations for this emphasis are reducing downtime and enhancing scalability. The article describes a technique for safely transferring predicted-to-fail resources from one VM to another, effectively reducing migration time and improving resource utilization through a compression strategy.

Ultimately, this article highlights the importance of leveraging artificial intelligence to enable effective fault prediction techniques in cloud computing, ultimately leading to enhanced resource optimization as the research addresses a critical gap in current fault tolerance techniques by focusing on proactively predicting virtual machine (VM) failures rather than relying solely on reactive measures such as creating clones. The emphasis on predicting failures before they occur is crucial for minimizing downtime and optimizing resource utilization. And the reseach work focuses on tracking real-time data for scientific processes within the cloud computing environment. This involves collecting and

preprocessing data related to CPU utilization, bandwidth utilization, RAM utilization, and disk utilization, and utilizing this information to predict and prevent resource overutilization and the study applies its methodology to specific scientific processes, including the sRNA Identification Protocol using High-throughput Technology (SIPHT) and the Laser Interferometer Gravitational-Wave Observatory (LIGO). By evaluating resource usage features in these applications and comparing them to predefined threshold values, the research demonstrates the practical application of its approach.

REFERENCES

Aldahwan, N. S., and Ramzan, M. S. (2022). Descriptive Literature Review and Classification of Community Cloud Computing Research. Scientific Programming, Volume 2022, Article ID 8194140, 12. https://doi.org/10.1155/2022/8194140

Catal, C. (2011). Software fault prediction: A literature review and current trends. Expert Systems with Applications, 38(4), 4626–4636.

Fu, S., and Xu, C. Z. (2017). Exploring event correlation for failure prediction in coalitions of clusters. In Proceedings of the 2017 ACM/IEEE conference on Supercomputing (Vol. 41, p. 112). Reno, NV, USA.

Glass, M., Lukasiewycz, M., Streichert, T., Haubelt, C., and Teich, J. (2017). Reliability-Aware System Synthesis. In Proceedings of the 2017 Design, Automation and Test Europe Conference and Exhibition (pp. 1–6). Nice, France.

Guan, Q., Zhang, Z., and Fu, S. (2012). A failure detection and prediction mechanism for enhancing dependability of data centers. International Journal of Computer Theory and Engineering, 4, 726–730.

Lohani, T. K., Ayana, M. T., Mohammed, A. K., Shabaz, M., Dhiman, G., and Jagota, V. (2021). A comprehensive approach to hydrological issues related to groundwater using GIS in the Hindu holy city of Gaya, India. World Journal of Engineering, ahead-of-print.

Malhotra, R., and Jain, A. (2012). Fault prediction using statistical and machine learning methods for improving software quality. Journal of Information Processing Systems, 8(2), 241–262.

Taufiq-Hail Ghilan Al-Madhagy, Ayed Alanzi, Shafiz Mohd Yusof, and Madallah M Alruwaili. (2021). Software as a Service (SaaS) Cloud Computing: An Empirical Investigation on University Students' Perception. Interdisciplinary Journal of Information, 16(1), 213-253. https://doi.org/10.28945/4740

Zhang, X., Rane, K. P., Kakaravada, I., and Shabaz, M. (2021). Research on vibration monitoring and fault diagnosis of rotating machinery based on the internet of things technology. Nonlinear Engineering, 10(1), 245–254.

Zhao, W., Melliar, P., and Moser, L. E. (2010). Fault tolerance middleware for cloud computing. In Proceedings of the 2010 IEEE 3rd International Conference on Cloud Computing (pp. 67–74). Miami, FL, USA.

Zhou, Y., Hu, X., and Shabaz, M. (2021). Application and innovation of digital media technology in visual design. International Journal of System Assurance Engineering and Management, 13(1).

Phytochemical Screening and In-Vitro Antimicrobial Activity of Extracts From *Citrullus lanatus* Rind Against Selected Bacteria

*[1]Hussaini Abdullahi Dangani, [2]Musa Abdullahi and [2]Shehu Shema Abdulsalam

[1]Department of Industrial Chemistry, Federal University of Dutsin-ma, Katsina state, Nigeria
[2]Department of Chemistry, Federal University of Dutsin-ma, Katsina state, Nigeria
*Corresponding author's email: ahdangani@fudutsinma.edu.ng

ABSTRACT

The emergence of antimicrobial resistance has necessitated the search for alternatives to traditional antibiotics, and phytochemicals from medicinal plants have attracted attention as a promising source. In this study, we investigated the antibacterial activity of different solvent extracts from *Citrullus lanatus* (watermelon) peel against *Escherichia coli* and *Staphylococcus epidermidis*. Phytochemical screening revealed the presence of alkaloids, saponins, steroids and reducing sugars in the crude methanol extract and its solvent fractions. In antibacterial tests using the agar well diffusion method, ethyl acetate fractions at different concentrations showed strong inhibitory activity against both bacterial strains, with a maximum inhibition zone diameter of 18 mm against E. coli and 20 mm. against S. epidermis. The methanol crude extract also showed significant antibacterial effects, particularly against Staphylococcus epidermidis (inhibition zone of 27 mm). The observed antibacterial properties may be due to the presence of saponins, alkaloids, and reducing sugars in the extract. These results indicate that *C. Lanatus* pericarp extract may serve as a potential source of novel antimicrobial agents and contribute to efforts to combat antibiotic resistance. This study highlights the importance of exploring plant-based alternatives to address the growing challenge of antibiotic resistance.

Keywords: *Citrullus lanatus* rind, antimicrobial activity

INTRODUCTION

Since their discovery in the early 1900s, antibiotics have played a crucial role in the treatment of infectious diseases. The excessive and improper utilization of antibiotics has led to the emergence of antimicrobial resistance (AMR), in which microorganisms have developed mechanisms to withstand the detrimental effects of antibiotics. Bacteria, specifically, undergo rapid evolution due to their small genome size, fast reproduction cycle, and high rate of mutation, resulting in the acquisition of resistant traits. The increase in AMR has generated an immediate necessity to explore alternative approaches in addressing bacterial infections. Phytochemicals obtained from medicinal plants have attracted attention as a potential reservoir of alternative medicine for addressing the challenge posed by AMR. (Ashraf et al., 2023)

Phyto, which are commonly referred to as plants, serve as a valuable reservoir of medicinal substances in traditional and contemporary medical practices, as well as in the production of nutraceuticals, pharmaceutical intermediates, dietary supplements, and synthetic reagents. Within medicinal plants, one can find chemically active components such as alkaloids, tannins, flavonoids, and phenolic compounds. (Patanayak et al., 2023)

Compounds derived from plants have exhibited antimicrobial properties in combating drug-resistant pathogens, like bacteria, fungi, and viruses. (Jadimurthy et al., 2023). Developing countries depend significantly on conventional medicines, specifically herbal plant remedies, as their primary form of medical therapy. The antioxidant, antibacterial, and antipyretic impacts of the phytochemicals contained within these plants can be attributed to their therapeutic properties. Throughout history, herbs have been utilized by the general public and traditional medicine practitioners across the globe owing to their perceived lack of toxicity. (Kumar & Singh, 2023).

Watermelon, originating from southern Africa, is a flowering plant, and Egypt is recognized as one of the leading five producers of this appetizing fruit. The pulp of watermelon is an excellent provider of phytochemical and lycopene, both of which function as antioxidants that safeguard against cancer. Typically considered as agro waste, the watermelon rind poses a challenge to ecological and environmental concerns.

Watermelon (Citrullus lanatus) is a fruit that is widely enjoyed and is known for producing a considerable amount of waste in the form of seeds and rind. The rind of the watermelon, which is often discarded, contains beneficial phytochemical compounds. Originally from tropical and subtropical regions, watermelon is a popular fruit crop and ranks as the second-largest fruit in terms of global production. In 2018, the worldwide production of watermelon reached an estimated 103 million tons. (Rezagholizade-shirvan et al., 2023).

Watermelon, scientifically known as Citrullus lanatus, is a melon variety that is widely cultivated for its delectable fruit. Belonging to the gourd family, it holds great economic importance within the Cucurbitaceae family. Watermelon

thrives as a trailing vine and was originally found in tropical Africa, specifically in the Kalahari Desert region. However, due to its immense popularity, it has been cultivated worldwide since ancient times. ("Watermelon," 2023, Britannica, 2023)

Watermelon consists of three major parts: pulp, rind, and seed (Zamuz et al., 2021). The rind can be consumed as pickles or used in various food formulations (Dane & Liu, 2007; Mandel et al., 2005; Milala et al., 2018). The inner rind contains citrulline, which can be converted to arginine and used to treat arginine deficiency. It also improves blood circulation. The improper disposal of watermelon rind raises environmental concerns (Collins et al., 2007).

The pericarp (rind) of Citrullus lanatus contains phytochemical compounds possessing significant nutritional ability. (Rezagholizade-shirvan et al., 2023). Both aqueous and ethanolic extractions derived from the rind of the watermelon displayed antibacterial properties against gram negative bacteria and fungi. (Neglo et al., 2021).

Watermelon is a nutritious fruit that contains macronutrients (Tabiri, 2016), vitamins, and minerals (Vinhas et al., 2021), and has therapeutic and pharmacological benefits due to its antioxidant components, particularly lycopene, which can protect against cancer and inflammation-related diseases, as well as aiding in the suppression of inflammation that can lead to different diseases such as atherosclerosis, asthma, diabetes, arthritis, and cancers, particularly prostate cancer (Ilic et al., 2011). Furthermore, watermelon has also gained significant popularity and cultivation in the northern region of Nigeria, particularly in central and northeast Nigeria. There exist over 1200 varieties of watermelon, varying in size, shape, flesh color, rind durability, and sweetness. (Gwana et al., 2014).

Bacterial infection poses a significant health problem worldwide, resulting in millions of deaths every year. The issue of antibiotic resistance is also escalating, causing growing concern. Researchers are exploring plant-based antibiotics as a potential solution to combat bacterial resistance. Extracts from watermelon have displayed promising antimicrobial properties, making them a viable alternative. Watermelon, especially its rind and seed extracts, has exhibited antibacterial, antimalarial, and anti-inflammatory effects. This suggests that it could be a potential treatment option for various infections. Thus, the aim of this research is to evaluate the crude methanolic, chloroform, hexane and ethylacetate and acetone extracts of rind of citrullus lanatus against gram-positive S*taphylococcus epidemidis* and gram-negative *Escherichia coli* and screen its phytochemicals.

MATERIALS AND METHODS
General
All solvents employed are of analytical grade, some of which are Methanol, Ethyl acetate, Chloroform, ethanol, acetone etc.

Collection and preparation of rind material
The rind was obtained by peeling off of the water melon fruit. The rind obtained was dried under shade for three days, and then ground to powder using a blender. Powdered rind material was weighed and kept in air-tight containers for further usage.

Preparation of crude extract
Extraction: The dried rind powder (200g) was placed in a closed beaker with 500ml of methanol and allowed to stand at room temperature for 2 days with occasional shaking in order to allow for maximum dissolution. The solution was decanted into a beaker, filtered using Whattman filter paper and was evaporated to dryness using a rotary evaporator and water bath at 40-50°C and then stored in air-tight containers for further use.

Fractionation of crude extract
The crude extract was prepared as mentioned above and labeled as F1 (fraction 1), and then it was macerated with 50ml of n-hexane and the soluble fraction was filtered and labeled as F2. The insoluble residue was macerated with chloroform in the same order as that of F1 and labeled as F3. The insoluble residue was macerated with ethyl acetate and labeled as F4, and then the residue was macerated with acetone and labeled as F5. All the soluble fractions were evaporated to dryness and stored for further usage.

Phytochemical Screening
Qualitative phytochemical screening of the various extracts was carried out according to standard procedure (Trease and Evans, 1989; Evans *et al*., 2002) to ascertain the qualitative composition of the rind. Phytochemicals screened include alkaloids, tannins, saponins, steroids, and flavonoids.

Test for Alkaloids

Dragendroff's test

The extract (0.5g) was stirred with aqueous hydrochloric acid (5ml, 1%) on a steam bath, the mixture was filtered; Dragendroff's reagent (potassium bismuth iodide solution) (1ml) was added to the filtrate (1ml). Turbidity or precipitation was taken as evidence for the presence of alkaloid in the extract.

Tests for Flavonoids

A portion of the extract was heated with ethylacetate (10ml) over a steam bath for 3min. The mixture was filtered and 1ml of dilute ammonia was added to 4ml of the filtrate. Formation of yellow precipitate indicates the presence of flavonoids.

Test for steroid

The dried extract (2mg) was shaken with chloroform. Sulphuric acid was added slowly by the sides of test tube to the chloroform layer. Formation of red colour indicates the presence of steroids.

Test for Tannins

The extract (0.5g) was dissolved in distilled water (10ml). The solution was filtered and iron (III) chloride solution was added to the filtrate, formation of a blue-black colour indicates the presence of tannin.

Test for saponin

Distilled water (5ml) was added to the extract (0.5g) with vigorous shaking. Persistence of frothing indicates the presence of saponin.

Reducing sugars

A portion of the extract was dissolved in distilled water followed by the addition of a mixture of Fehling's solution A & B and warmed. A brick brown precipitate appears which indicates the presence of reducing sugar.

In-Vitro Antibacterial Activity

Test microorganisms

In vitro antimicrobial test was conducted on two common pathogenic microorganisms, namely, *Escherichia coli* (gram negative) and *Staphylococcus epidemidis* (gram positive). The test organisms used were clinical bacterial isolates obtained from microbiology laboratory of Umaru Musa Yar'adua University, Katsina, Katsina State.

Preparation of test solution

The extracts (0.1g) F1, F2, F3, F4, and F5 was dissolved in dimethylsulfoxide (DMSO) (1ml) to yield a concentration of 0.1g/ml (100,000 μg/ml) solution which was labeled as stock solution from which other concentrations were formed (serial dilution)

From the stock solution, 1ml was transferred into a test tube containing dimethylsulfoxide (DMSO) (9ml) to effect 10 times dilution this gives a concentration of 10,000 μg/ml. subsequently 1ml was transferred into another test tube containing DMSO (9ml) which gives a concentration of 1000 μg/ml and this was further diluted to 100 μg/ml, 10 μg/ml and 1.0 μg/ml respectively.

Culturing and Sensitivity Testing (agar-well diffusion)

Microorganisms

The isolated bacteria were cultured on nutrient agar plates prepared by dissolving nutrient agar (28g) in one liter (1L) of distilled water and heated to boiling before autoclaving at 121mpa for 15min. about 10ml of the media was poured in each plate and allowed to solidify before inoculation.

The isolated bacteria were cultured on nutrient agar plates prepared by dissolving nutrient agar (28g) in one liter (1L) of distilled water and heated to boiling before autoclaving at 121mpa for 15min. about 10ml of the media was poured in plate and allowed to solidify before inoculation.

With the aid of sterile cock borer, wells of about 6mm in diameter were bored on the plates and about 0.5ml of the different concentrations of the extracts was dispensed into the wells and then allowed to stand for about 15mins. These were then incubated at 37^0C for 24hrs. At the end of the period, the diameter of zone of inhibition (mm) was measured using a meter rule.

RESULTS AND DISCUSSION
Phytochemical Screening
Phytochemical screening was employed as a guide in describing the large number of secondary metabolites found in various extracts of the plants. The result (table 1) revealed the presence of different secondary metabolites in the crude extract and ethylacetate fraction (F3).

Table 1: phytochemical screening for *Citrullus lanatus* rind

metabolite	Methanol extract	n-hexane	chloroform	Ethyl acetate	Acetone
Alkaloid	+	+	-	-	+
Flavonoid	-	-	-	-	-
Reducing sugar	+	-	+	-	-
Saponin	+	+	-	+	-
Steroid	+	-	-	+	-
Tannin	-	-	-	-	-

+ = present, - =absent

The results of phytochemical screening showed the presence of secondary metabolites such as alkaloids, flavonoid, reducing sugar, saponins and tannins in the crude methanolic extract, n-hexane, chloroform, ethyl acetate and acetone fractions of the rind of *Citrullus lanatus*. While alkaloids were found present in the crude methanolic extract, n-hexane and acetone, flavonoid and tannins were absent in all the fractions. Reducing sugar was found to be present in the crude methanolic extract and chloroform extracts. The presence of saponin was detected in the crude, n-hexane and ethyl acetate extracts but missing in the chloroform and acetone extracts. The presence of steroid was also detected in crude and ethyl acetate extracts but absent in n-hexane, chloroform and acetone fractions.

Antibacterial activity of *Citrullus lanatus* rind
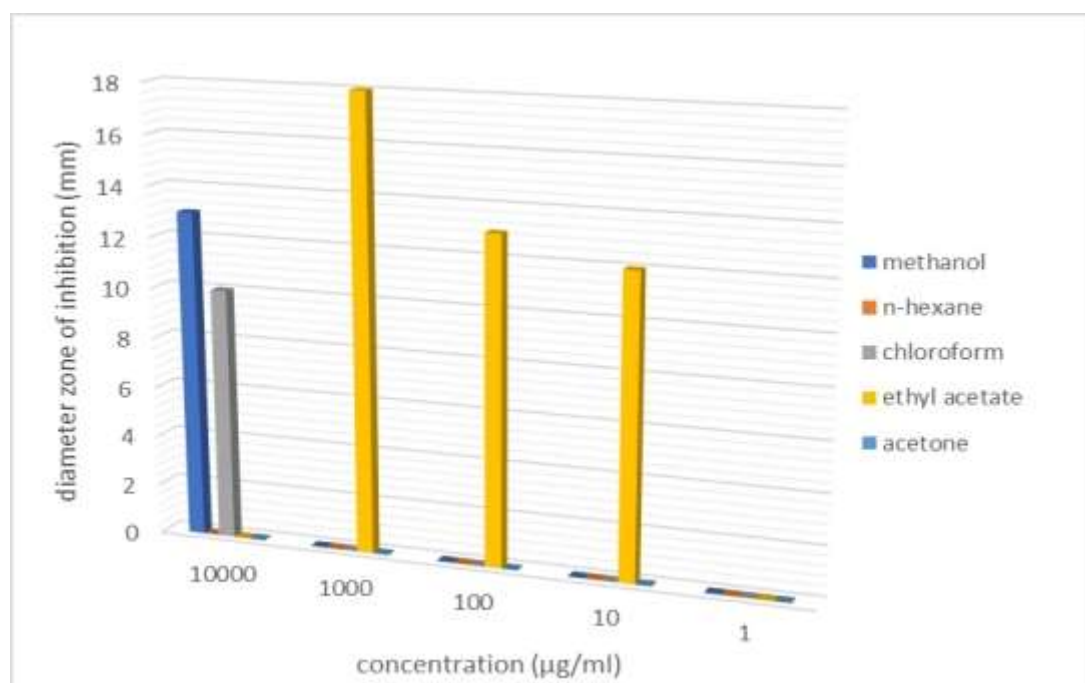
Figure 1: antibacterial activity of the various extract against *Escherichia coli*
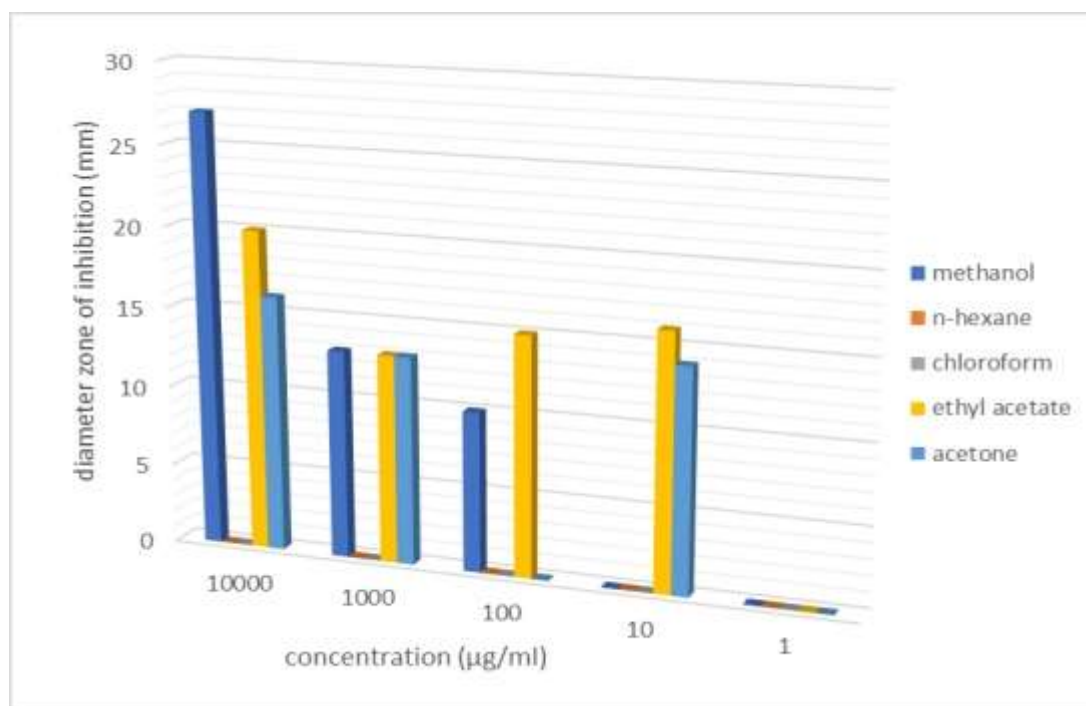
Figure 2: antibacterial activity of the various extract against *staphylococcus epidemidis*

Attempt have been made to screen the crude extracts of *Citrullus* lanatus for antimicrobial activity on two microorganisms; *staphylococcus epidemidis* (gram positive) and *escherichia coli (*gram negative)*,* and the result revealed promising bioactivities. The antimicrobial activity of the extracts against *escherichia coli* (figure 1) showed that ethyl acetate extracts exhibits activities at different concentrations with the highest rate of antibacterial activity with diameter zone of inhibition (18mm). While chloroform extract showed low antibacterial activity, n-hexane, ethyl acetate and acetone did not inhibit the bacterial growth.

As observed in the antibacterial activity against *staphylococcus epidemidis* (figure 2), the highest inhibitory activity (27mm) was exhibited by the crude extract followed by ethyl acetate extract (20 mm) then acetone (16mm) with the lowest. Overall, ethyl acetate extract exhibited the highest rate of activities against the two bacteria across the different concentrations.

Discussion

The study found that the rind of *Citrullus lanatus* possesses antibacterial properties against the bacteria tested, namely *Escherichia coli* and *staphylococcus epidemidis*. Previously, it has been reported that this plant has antibacterial activity (Babaiwa et al., 2017). The high rate of bacterial growth inhibition may be attributed to the presence of saponins in the ethyl acetate fraction of the extract. Saponins have been known to have significant antimicrobial activity against various microorganisms (Tagousop et al., 2018). For example, a study on *Allium chinense* demonstrated that total saponins from this plant exhibited significant antibacterial activity against *Staphylococcus aureus, Escherichia coli,* and *Salmonella typhimurium* (Xue-mei, 2013). Another study reported that saponins from *Melanthera elliptica* showed significant antimicrobial activity against pathogenic phenotypes (Tagousop et al., 2018). Additionally, alkaloids and reducing sugars have been reported to possess antibacterial activity, which could explain the antimicrobial activity observed in the extracts.

Suleiman et. al (2016) evaluated the phytochemical and antimicrobial activity of *Citrullus lanatus* (watermelon) seeds against selected bacteria. The result showed the presence of alkaloids, flavonoids, glycosides, tannins in the Water and ethanol extracts while were not detected in both aqueous and ethanolic extract. This is in contrast to the identified secondary metabolites detected in the crude methanolic extract of the rind which shows the presence of alkaloids, saponins, steroids and reducing sugars while flavonoids and tannins are absent. Antibacterial activity testing showed that S. aureus, E. coli, and P. aeruginosa were most susceptible to the extracts at concentrations ranging from 6.25mg/ml to 50mg/ml. However, in this study finding showed that the tested bacteria were mostly inhibited at concentrations range of 10 µg/ml to 1000 µg/ml with the ethyl acetate extract showing inhibition at almost all the concentration. Nevertheless, according to Sathya and shoba (2014) the effectiveness of watermelon seed extract as an

antimicrobial agent can be enhanced at high concentration levels. The findings from this research also agrees with the earlier reports by Neglo et al., (2021) that extracts from the rind possess antibacterial activity against gram-negative bacteria

CONCLUSION

The rind extracts of Citrullus Lanatus demonstrate antimicrobial effects against the bacteria that were studied, suggesting that the rind could serve as a potential source for antimicrobial agents. These agents would be efficient and safe, making a significant contribution to the ongoing search for new antimicrobial treatments against infectious diseases caused by antibiotic-resistant strains. The antimicrobial activities observed in the various rind extracts are likely attributed to the presence of secondary metabolites such as alkaloids, saponins, reducing sugars, and steroids.

REFERENCES

Adhikari, B. (2021). Roles of Alkaloids from Medicinal Plants in the Management of Diabetes Mellitus. *Journal of Chemistry*, *2021*, e2691525. https://doi.org/10.1155/2021/2691525

Ashraf, M. V., Pant, S., Khan, M. A. H., Shah, A. A., Siddiqui, S., Jeridi, M., Alhamdi, H. W. S., & Ahmad, S. (2023). Phytochemicals as Antimicrobials: Prospecting Himalayan Medicinal Plants as Source of Alternate Medicine to Combat Antimicrobial Resistance. *Pharmaceuticals*, *16*(6), Article 6. https://doi.org/10.3390/ph16060881

Assessment of antimicrobial efficacy of Citrullus lanatus methanolic seed extract | Semantic Scholar. (n.d.). Retrieved November 1, 2023, from https://www.semanticscholar.org/paper/Assessment-of-antimicrobial-efficacy-of-Citrullus-Sathya-Shoba/d781b57cd2744b301e7bfc6d526cadc2cc5c008e

Babaiwa, U. F., Erharuyi, O., Falodun, A., & Akerele, J. O. (2017). Antimicrobial activity of ethyl acetate extract of Citrullus lanatus seeds. *Tropical Journal of Pharmaceutical Research*, *16*(7), Article 7. https://doi.org/10.4314/tjpr.v16i7.23

Collins, J. K., Wu, G., Perkins-Veazie, P., Spears, K., Claypool, P. L., Baker, R. A., & Clevidence, B. A. (2007). Watermelon consumption increases plasma arginine concentrations in adults. *Nutrition*, *23*(3), 261–266. https://doi.org/10.1016/j.nut.2007.01.005

Comparative antioxidant and antimicrobial activities of the peels, rind, pulp and seeds of watermelon (Citrullus lanatus) fruit. (2021). *11*. https://doi.org/10.1016/J.SCIAF.2020.E00582

Dane, F., & Liu, J. (2007). Diversity and origin of cultivated and citron type watermelon (Citrullus lanatus). *Genetic Resources and Crop Evolution*, *54*(6), 1255–1265. https://doi.org/10.1007/s10722-006-9107-3

Dash, P., & Ghosh, G. (2023). In-vitro and in-vivo antimicrobial activity of Citrullus lanatus prolamin hydrolysates. *South African Journal of Botany*, *159*, 140–145. https://doi.org/10.1016/j.sajb.2023.06.011

Govindaraj, A., Paulpandian, S. S., & Shanmugam, R. (2022). Comparative Evaluation of The Effect of Rind and Pulp Extract of Citrullus Lanatus on Streptococcus Mutans. *Annals of Dental Specialty*, *10*(4), 34–39. https://doi.org/10.51847/OtdOtHZ09I

Gwana, A., Modu, B., Bagudu, B., Sadiq, A., & Abdullahi, M. (2014). Determinations of Phytochemical, Vitamin, Mineral and Proximate Compositions of Varieties of Watermelon Seeds Cultivated in Borno State, North – Eastern Nigeria. *International Journal of Nutrition and Food Sciences*, *3*, 238. https://doi.org/10.11648/j.ijnfs.20140304.12

Ilic, D., Forbes, K. M., & Hassed, C. (2011). Lycopene for the prevention of prostate cancer. *Cochrane Database of Systematic Reviews*, *11*. https://doi.org/10.1002/14651858.CD008007.pub2

Jadimurthy, R., Jagadish, S., Nayak, S. C., Kumar, S., Mohan, C. D., & Rangappa, K. S. (2023). Phytochemicals as Invaluable Sources of Potent Antimicrobial Agents to Combat Antibiotic Resistance. *Life*, *13*(4), Article 4. https://doi.org/10.3390/life13040948

Kumar, B., & Singh, J. (2023). A Review Study of Importance of Herbal Medicine. *IJFMR - International Journal For Multidisciplinary Research*, *5*(1). https://doi.org/10.36948/ijfmr.2023.v05i01.1667

Life | Free Full-Text | Phytochemicals as Invaluable Sources of Potent Antimicrobial Agents to Combat Antibiotic Resistance. (n.d.). Retrieved October 20, 2023, from https://www.mdpi.com/2075-1729/13/4/948

M, G. A. (n.d.). *Determinations of Phytochemical, Vitamin, Mineral and Proximate Compositions of Varieties of Watermelon Seeds Cultivated in Borno State, North – Eastern Nigeria | EndNote Click*. Retrieved October 20, 2023, from https://click.endnote.com/viewer?doi=10.11648%2Fj.ijnfs.20140304.12&token=WzQxNTM2MjcsIjEwLjExNjQ4L2ouaWpuZnMuMjAxNDAzMDQuMTIiXQ.DeZskE5fxJ7cKhDP7upkNzG1zKc

Mandel, H., Levy, N., Izkovitch, S., & Korman, S. H. (2005). Elevated plasma citrulline and arginine due to consumption of Citrullus vulgaris (watermelon). *Journal of Inherited Metabolic Disease*, *28*(4), 467–472. https://doi.org/10.1007/s10545-005-0467-1

Milala, M. A., Luther, A., & Burah, B. (2018). Nutritional Comparison of Processed and Unprocessed *Citrullus lanatus* (Watermelon) Seeds for Possible Use in Feed Formulation. *American Journal of Food and Nutrition*, *6*(2), 33–36. https://doi.org/10.12691/ajfn-6-2-1

Neglo, D., Tettey, C. O., Essuman, E. K., Kortei, N. K., Boakye, A. A., Hunkpe, G., Amarh, F., Kwashie, P., & Devi, W. S. (2021). Comparative antioxidant and antimicrobial activities of the peels, rind, pulp and seeds of watermelon (Citrullus lanatus) fruit. *Scientific African*, *11*, e00582. https://doi.org/10.1016/j.sciaf.2020.e00582

Panche, A. N., Diwan, A. D., & Chandra, S. R. (2016). Flavonoids: An overview. *Journal of Nutritional Science*, *5*, e47. https://doi.org/10.1017/jns.2016.41

Patanayak, S., Ninave, G., Mukherjee, M., Mukhopadhyay, J., Ragavendran, V., Paira, B. B., Samajdar, S., Dasgupta, S., Bose, D., & Mukhopadhyay, M. (2023). Phytochemicals as an Active Pharmaceutical Ingredient of Ocimum Sanctum and Azadirachta Indica: A Theoretical Screening Study. In A. Biswas, A. Islam, R. Chaujar, & O. Jaksic (Eds.), *Microelectronics, Circuits and Systems* (pp. 535–546). Springer Nature. https://doi.org/10.1007/978-981-99-0412-9_48

Phytochemicals as an Active Pharmaceutical Ingredient of Ocimum Sanctum and Azadirachta Indica: A Theoretical Screening Study | SpringerLink. (n.d.). Retrieved October 20, 2023, from https://link.springer.com/chapter/10.1007/978-981-99-0412-9_48

Rezagholizade-shirvan, A., Shokri, S., Dadpour, S. M., & Amiryousefi, M. R. (2023). Evaluation of physicochemical, antioxidant, antibacterial activity, and sensory properties of watermelon rind candy. *Heliyon*, *9*(6). https://doi.org/10.1016/j.heliyon.2023.e17300

Roles of Alkaloids from Medicinal Plants in the Management of Diabetes Mellitus. (n.d.). Retrieved November 1, 2023, from https://www.hindawi.com/journals/jchem/2021/2691525/

Sathya, J., & Shoba, F. (2014). *Assessment of antimicrobial efficacy of Citrullus lanatus methanolic seed extract*. https://www.semanticscholar.org/paper/Assessment-of-antimicrobial-efficacy-of-Citrullus-Sathya-Shoba/d781b57cd2744b301e7bfc6d526cadc2cc5c008e

Shelf-life-studies-guidelines.pdf. (n.d.). Retrieved October 20, 2023, from https://foodnutritionhaccp.tripod.com/sitebuildercontent/sitebuilderfiles/shelf-life-studies-guidelines.pdf

Suleiman Bello, H., Ismail, H., Goje, M., & Mangga, H. (2016). *Antimicrobial Activity of Citrullus Lanatus (Watermelon) Seeds on Some Selected Bacteria*.

Tabiri, B. (2016). Watermelon Seeds as Food: Nutrient Composition, Phytochemicals and Antioxidant Activity. *International Journal of Nutrition and Food Sciences*, *5*(2), 139. https://doi.org/10.11648/j.ijnfs.20160502.18

Tagousop, C. N., Tamokou, J.-D., Kengne, I. C., Ngnokam, D., & Voutquenne-Nazabadioko, L. (2018). Antimicrobial activities of saponins from Melanthera elliptica and their synergistic effects with antibiotics against pathogenic phenotypes. *Chemistry Central Journal*, *12*(1), 97. https://doi.org/10.1186/s13065-018-0466-6

Valgas, C., Souza, S. M. de, Smânia, E. F. A., & Smânia Jr., A. (2007). Screening methods to determine antibacterial activity of natural products. *Brazilian Journal of Microbiology*, *38*, 369–380. https://doi.org/10.1590/S1517-83822007000200034

Vinhas, A. S., Sousa, C., Matos, C., Moutinho, C., & Vinha, A. F. (2021). *VALORIZATION OF WATERMELON FRUIT (CITRULLUS LANATUS) BYPRODUCTS: PHYTOCHEMICAL AND BIOFUNCTIONAL PROPERTIES WITH EMPHASIS ON RECENT TRENDS AND ADVANCES*. *5*(1).

Wahdan, O., Bassuony, N., Abd El-Ghany, Z., & Ahmed, A. (2015). EVALUATION OF ANTIBACTERIAL ACTIVITY AND GAS CHROMATOGRAPHY-MASS SPECTROMETRY ANALYSIS OF WATERMELON WHITE RIND EXTRACTS. *Journal of Agricultural Chemistry and Biotechnology*, *6*(5), 117–125. https://doi.org/10.21608/jacb.2015.44097

Watermelon. (2023). In *Wikipedia*. https://en.wikipedia.org/w/index.php?title=Watermelon&oldid=1179473622
Watermelon / Nutrition, Health Benefits, Recipes / Britannica. (2023, September 21). https://www.britannica.com/plant/watermelon

Xue-mei, Y. Z. X. L. X. Z. S. S. (2013). Antimicrobial Activity and Mechanism of Total Saponins from Allium chinense. *FOOD SCIENCE*, *34*(15), 75. https://doi.org/10.7506/spkx1002-6630-201315016

Zamuz, S., Munekata, P. E. S., Gullón, B., Rocchetti, G., Montesano, D., & Lorenzo, J. M. (2021). Citrullus lanatus as source of bioactive components: An up-to-date review. *Trends in Food Science & Technology*, *111*, 208–222. https://doi.org/10.1016/j.tifs.2021.03.002

Seasonal Assessment of Cadmium and Lead in Soil Samples from Dutsin-Ma Irrigated Farmlands in Katsina State, Nigeria

*[1]Muhammad, F. and [2]Sa'eed, M. D.

[1]Department of Chemistry, Isa Kaita College of Education Dutsin-ma, Katsina State. Nigeria
[2]Department of Chemistry, Bayero University Kano, Kano State, Nigeria
*Corresponding Author's e-mail: fatimuhd99@gmail.com Phone: +2348032932834

ABSTRACT
Heavy metal pollution cause major changes in soil quality and ecological status of the environment, they are extremely persistent in the environment because of their non-biodegradable nature, long biological half-lives, and thermal stability hence becoming sources of pollution in the soil. Once soil is contaminated, it will not only affect the rapid growth of crops and quality yield of agricultural products but also pose a threat to human health via the food chain. This study was conducted to assess the seasonal variations of cadmium, and lead in soil sampled obtained from Dutsin-Ma irrigated farmlands, so as to evaluate the impact of using these soils for agricultural or pastoral farming. A total of ten (10) soil samples were collected from ten irrigated farmlands in the dry and wet season. The samples were ground, sieved, digested and analysed using flame atomic absorption spectrophotometer. Descriptive and inferential statistics were adopted for data interpretations. Mean levels of Cd and Pb in soils during dry season were 0.239 ± 0.022 and 0.21833 ± 0.011 mg/kg respectively and 0.134 ± 0.01 and 0.293 ± 0.021 mg/kg respectively during wet season . There was a significant difference in the levels of these metals across the sampling sites and seasons ($P < 0.05$). All the soil across the sampling location had Cd and Pb below WHO, and NESREA threshold limit except Daguda soil (DSL) and Makera soil (MSL) with Cd mean levels of 0.386 ± 0.02 mg/kg and 0.363 ± 0.030 mg/kg respectively during dry season. The contamination factor (CF), pollution load index (PLI), and geoaccumulation index (Igeo) of the soils were low across the sampling sites and therefore of acceptable quality for agricultural and pastoral farming as at the time of this study
Keywords: Analysis, Agricultural, Concentration, Pastoral, Pollution

INTRODUCTION
Metals such as cadmium (Cd), lead (Pb), arsenic (As) and mercury (Hg) are not required by man even in trace amount (Türkdoğan *et al.,* 2003). These metals are very toxic and excessive amount of these elements can lead to kidney, cardiovascular and nervous system diseases (Vousta *et al.,* 1996; Cui *et al.,* 2004) While copper (Cu), iron (Fe), nickel (Ni) zinc (Zn), and manganese (Mn) are considered as essential elements. But, when these essential elements are found higher than their permissible limits they can be toxic to living system (Edem *et al.,* 2009)

Heavy metals may enter the human system through consumption of contaminated water and consumption of food plants grown in metal contaminated soil. These metals are capable of causing human health problems if excess amount is ingested. Heavy metals are Non bio degradable and persistent, have a long biological half live, and can be bio-accumulated through biological chains (Zhou *et al.,* 2016)

Metal contamination may also occur in soil due to irrigation with contaminated water, Addition of fertilizers and metal-based pesticides, Industrial emission, Transportation, harvesting process and storage. Crops grown in soils contaminated with heavy metals have greater accumulation of heavy metals than those grown in uncontaminated soil (Sharmah *et al.,* 2008; Bempah *et al.,* 2010). Excessive accumulation of metals in agricultural soil through wastewater irrigation may not only result in soil contamination but also lead to elevated heavy metal uptake by crops and thus affect food quality and safety (Muchuweti *et al.,* 2006).

Reports showed that industrial and domestic effluents constitute the largest sources of heavy metals which contribute to the increasing metallic contaminant in aquatic and terrestrial environment in most parts of the world (Jibrin and Adewuyi, 2008). The specific problem associated with heavy metals in the environment is their accumulation through the food chain and persisted in nature (Dimari *et al.,* 2008)

Farming activities is well pronounced in Katsina State, especially in Dutsin-Ma local government area where they carried out intensive irrigated farming during dry season. Indiscriminate waste disposal coupled with bad land practices are common scene that can easily pollute surface water and soil consequently degrading the soil and water quality (Ndabula and Jidauna, 2010).

MATERIALS AND METHODS
Study Area
Dutsin-Ma is located at the central part of Katsina state, and lies on Latitude 12^0 26′N and longitude $07˚29′$ E With estimated area of 552,323 km, and it is bounded in the north by Kurfi, Charanchi and Kankia LGAs. Matazu in the south-east, Safana and Dan-musa from the west (Figure 1).

Soil Samples
A total of ten (10) samples were randomly collected from ten (Chediya, Garhi, Shantalawa, Tabobi, Katsaba, Badole, Daguda, Makera, Ruwangamji, and Walari) major farmlands in Dutsin-Ma local government area of Katsina state during dry and wet seasons. Surface scrapping of the soil were carried out at each point of collection so as to prevent accommodation of extraneous materials along with the samples collected. The samples were collected using plastic spatula from the surface (2- 20 cm), Soil samples were randomly sampled and bulked together to form a composite sample from each designated point , and immediately packed in pre-cleaned 500 cm^3 polythene containers, labelled and transported to the laboratory for further preparation and analysis. Each Soil sample was air dried under laboratory condition for two weeks, ground, sieved through 2 mm mesh sieve and dried to constant mass in an oven at 105^OC, and kept in a dessicator for further analysis.
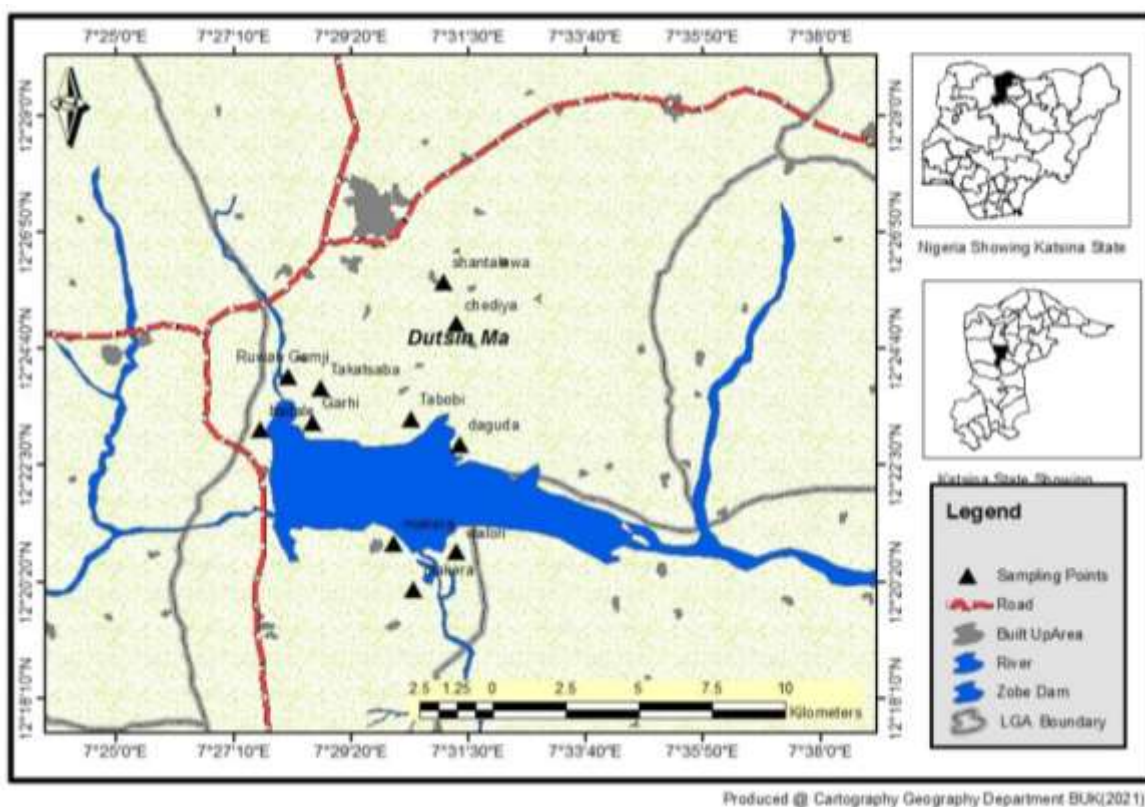
Figure 1: Map of sampling locations

Digestion of soil samples for metal determination
Accurately measured 0.25 g of pre-treated soil samples were separately weighed into platinum crucibles. The digestions were conducted with a mixture of 3 cm^3 of conc. HNO_3, 2 cm^3 of concentrated HF and 1 cm^3 of 40 % H_2O_2 solution on a sand bath at a temperature of 200 – 230ºC, After the acid mixture was evaporated to dryness, 20 cm^3 of 0.25M HNO_3 was added and warmed for 10 mins. The solution is then filtered into 50 cm^3 labeled plastic containers and filled to volume with the 0.25 M HNO_3 solution (Uduma and Jimoh, 2013). Reagent blanks were similarly conducted using every step but without sample. The solutions were analysed using flame atomic absorption spectroscopy (FAAS) (Chem Tech Analytical Alpha Star Model 4) at the Centre for Dry land agriculture (CCDA) of the Bayero University, Kano, Nigeria.

Determination of Contamination Factor (CF)
Contamination factor (CF) is the result of dividing the metal concentration in the soil by the concentration of background value of the respective metal
CF = Cm (sample) / Cm (Background)   (1)
Where, Cm is heavy metal concentration in the soil.

Determination of Pollution Load Index (PLI)
Equation (ii) was used To calculate Pollution Load Index (PLI) of the soil
PLI = (CF1 × CF2 × CF3 × . . . × CFn)$^{1/n}$ ………….   (2)
where CF = Contamination factor, and n is the considered number of metals [13,14].

Determination of Geoaccumulation Index (Igeo)
Geoaccumulation Index (Igeo) is used to determine the extent of metal accumulation in soil and anthropogenic contribution to pollution in soil [15].   It is calculated using the equation (3) below:
Igeo = Log 2 (Cn /1.5Bn). ………….   (3)
Cn = Measured concentration of metal.
Bn = Concentration of background and 1.5 accounts for possible variation in the background data due to lithogenic effects

Statistical analysis
Results were mean ± of three determinations of each soil from ten (10) irrigated farmland. The results were further subjected to Analysis of variance (ANOVA) and Pearson Product Moment Correlations using statistical package for social science (SPSS) 21.0 version software.

RESULTS AND DISCUSSION
Concentration of cadmium in soil samples
Results of the analysed soil samples from Dutsin - Ma irrigated farmlands during dry and wet seasons are presented in Figure 2 and 3 and Table 2 - 5. Level of cadmium in soil samples was found to be between 0.11 ± 0.02 mg/kg to and 0.386 ± 0.02 mg/kg in dry season and 0.06 ± 0.03 mg/kg to 0.23 ± 0.02 mg/kg in rainy season. In dry season, Daguda soil (DSL) had the highest mean level (0.386 ± 0.02 mg/kg) followed by 0.363 ± 0.030 mg/kg while Shantalawa soil (SSL) had the lowest (0.11 ± 0.02 mg/kg). In wet season, DDM also had the highest value of 0.23 ± 0.02 mg/kg and Chediya soil (CSL) had the lowest level of 0.06 ± 0.03 mg/kg (Figure 2).
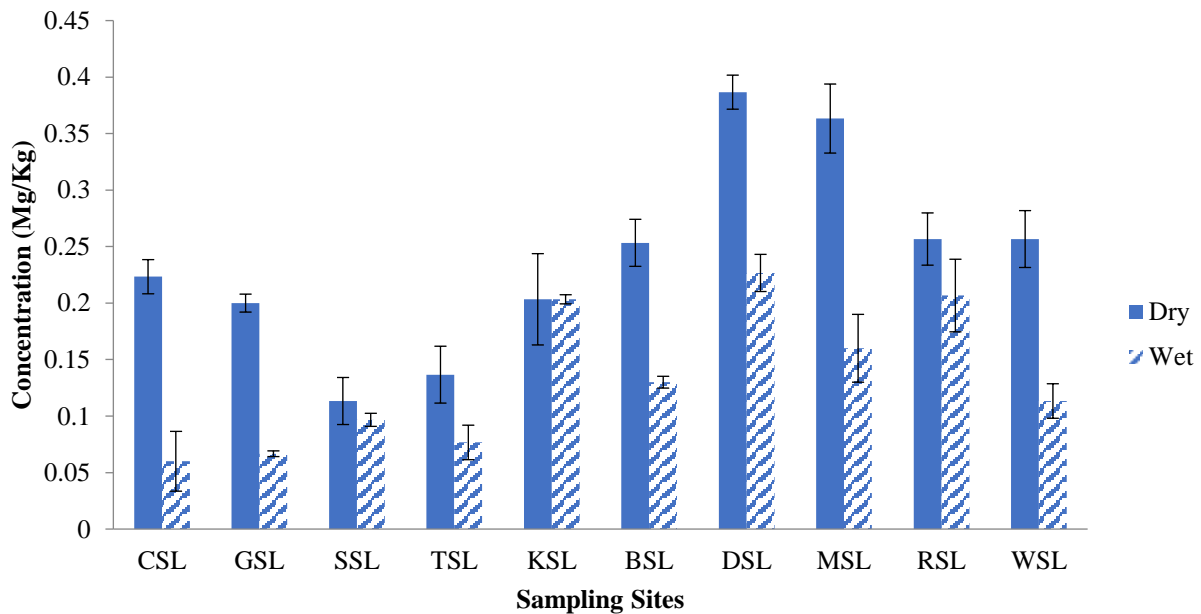
Figure 2: Mean variation of cadmium concentration in soil samples across the sampling sites

Concentration of lead in soil samples

Lead levels for dry seasons were 0.16 ± 0.01 mg/kg to 0.27 ± 0.03 mg/kg and 0.17 ± 0.01 mg/kg to 0.4 ± 0.017 mg/kg in wet season. Highest mean level of 0.27 ± 0.03 mg/kg was obtained in MSL while the least level of 0.16 ± 0.01 mg/kg were recorded at GSL. In rainy season, WSL had the high level of 0.4 ± 0.017 mg/kg while GSL had the low value of 0.17 ± 0.01 mg/kg (Figure 3).
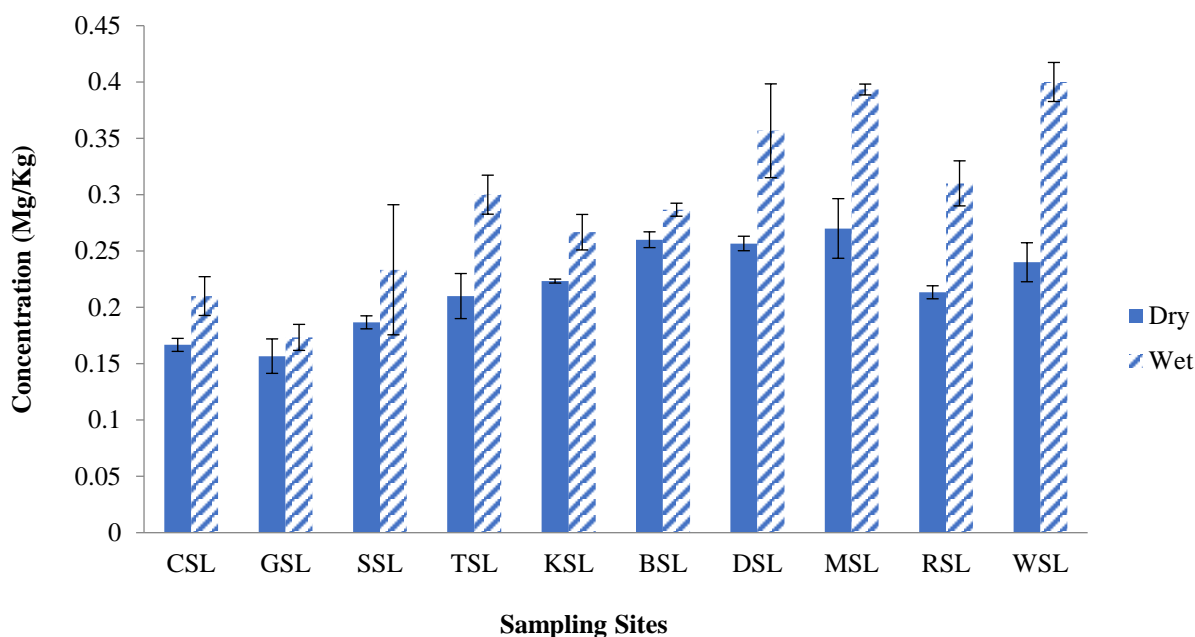
Figure 3: Mean variation of lead concentration in soil samples across the sampling sites.

Table 2: Concentration of metals in soil samples during dry season (mg/Kg)

	Cd		Pb	
S/Sites	Mean	Stdev	Mean	Stdev
Chediya (CSL)	0.223	0.01513 [a]	0.16667	0.00577 [a]
Garhi (GSL)	0.2	0.00794 [a]	0.15667	0.01528 [a]
Shantalwa (SSL)	0.1133	0.02082 [a]	0.18667	0.00577 [a]
Tabobi (TSL)	0.13667	0.02517 [a]	0.21	0.02 [a]
Katsaba (KSL)	0.2033	0.04042 [a]	0.22333	0.001 [a] 77
Badole (BSL)	0.25333	0.02082 [b]	0.26	0.007 [b]
Daguda (DSL)	0.38667	0.01506 [b]	0.25667	0.00643 [b]
Makera (MSL)	0.36333	0.03055 [b]	0.27	0.02646 [b]
Ruwangamji (RSL)	0.25667	0.02309 [b]	0.21333	0.00577 [b]
Walari (WSL)	0.25667	0.02517 [b]	0.24	0.01732 [b]
Mean	0.23933	0.02242	0.21833	0.01116
WHO (2011)	3		100	
NESREA(2011)	3		30	

Values are means ± of 3 determinations. Same superscripts along the same column indicates non-significant difference (P>0.05) while different superscripts along the same column indicates significant difference (P<0.05).

Table 3: Concentration of metals in soil samples during wet season (mg/kg)

	Cd		Pb	
S/Sites	Mean	Stdev	Mean	Stdev
Chediya (CSL)	0.06	0.0264 [a]	0.21	0.0172 [a]
Garhi (GSL)	0.06667	0.0025 [a]	0.17333	0.0115 [a]
Shantalwa (SSL)	0.09667	0.0057 [a]	0.23333	0.0577 [a]
Tabobi (TSL)	0.07667	0.0152 [a]	0.3	0.0173 [a]

Katsaba (KSL)	0.20333	0.0040 [a]	0.26667	0.0157 [a]
Badole (BSL)	0.13	0.0052 [b]	0.28667	0.0057 [b]
Daguda (DSL)	0.22667	0.0164 [b]	0.35667	0.0416 [b]
Makera (MSL)	0.16	0.03 [b]	0.39333	0.0048 [b]
Ruwangamji(RSL)	0.20667	0.032 [b]	0.31	0.02 [b]
Walari (WSL)	0.11333	0.0152 [b]	0.4	0.0172 [b]
Mean	0.134	0.01531	0.293	0.02092
WHO (2011)	3		100	
NESREA(2011)	3		30	

Values are means ± of 3 determinations. Same superscripts along the same column indicates non-significant difference (P>0.05) while different superscripts along the same column indicates significant difference (P<0.05).

Table 4: Correlation matrix of Cd and Pb in soil samples during dry season

	Cd	Pb
Cd	+ 1	
Pb	+ 0.680	+ 1

Table 5: Correlation matrix of Cd and Pb in soil samples during wet season

	Cd	Pb
Cd	+ 1	
Pb	+ 0.517	+1

Contamination factor of soil
The mean contamination factor recorded for cadmium in all the farm sites is 0.290 in dry season and 0.166 in wet season while Lead showed CF mean in dry and wet season of 0.0025 and 0.0034 respectively.

Pollution load index (PLi) of soil
The results of this study showed that the calculated PLI of soils from the ten irrigated farmlands varied from 0.082 in dry season and 0.047 in rainy season which were generally far below 1 i.e (PLI < 1)

Geoaccumulation index (Igeo) of soil
Igeo of Cadmium in dry season was 0.059 and 0.034 in wet season while Lead had Igeo of 0.00059 and 0.00061 for dry and wet season respectively.

Discussion
Soil and sediments are the major sinks for heavy metals, therefore landfills and waste dumpsites which characterize urban settlements are among the major contributors in polluting river and stream around them (Adeniyi and Yusuf, 2007) The specific problem associated with heavy metals in the environment is their accumulation through food chain and persistence in nature (Dimari *et al.,* 2008). Bioavailability of metal concentration in soil also depends on the physicochemical characteristics of the soil such as pH, clay content, salinity, cation exchange capacity, mineral, and organic matter (Jiao *et al.,*2012; Roberts, 2014). Metal solubility and bioavailability in soils is strongly dependent on pH (Roberts, 2014; Kabata-Pendias and Szteke 2015). Lower mobility is observed when the pH is above 7.5, and a higher availability under lower pH conditions. The critical pH range is between 4.0 and 4.5 where a decrease of 0.2 pH units can cause up to five times higher mobilization and bioavailability (Kabata and Pendias, 2001). Organic matter plays an important role in metal binding, complexation by organic ligands, control of metal solubility, and mobility. High level of metals in polluted soil could change the mineralization rate of organic matter in soil and affect its accumulation and distribution Zhao *et al.,* 2010).
From the results of the analysis, there was a significant difference in the levels of all the metals across the sampling locations and seasons. All soil samples across the sampling locations had mean value of Cd below World Health Organization, and National Environmental Standards and Regulations Enforcement Agency threshold limit of 3.0 mg/kg, except Daguda soil (DSL) and Makera soil (MSL) with mean levels of 0.386 ± 0.02 mg/kg and 0.363 ± 0.030 mg/kg respectively). Higher levels of cadmium in Daguda soil (DSL) and Makera soil (MSL) could be due to the proximity of the sampling site to place where a lot of farming, fishing and other laundry activities take place. Cadmium may be detrimental to soil microbial populations. The cumulative addition of Cadmium via phosphatic fertilizers may have a detrimental effect on soil microorganisms (Andrea Giovanna, 2019). Due to its high mobility, cadmium can be transferred from soil to plants thereby increasing the risk of bioaccumulation along the food chain (Khan *et al.,* 2007).

The lowest values of cadmium in soil obtained from this research were in agreement with results reported by Linton *et al.,* (2016); Emurotu and Onianwa, (2017).

Soil samples across the sampling sites were found to have Lead mean level below the WHO maximum limit of 100 mg/kg and NESREA 30 mg/kg limit. This is a welcome development because high lead levels in soil can transfer to humans via plant. Because lead is a highly toxic metal that can pose a number of health implications such as kidney and liver damage and so on. These values support the levels reported by Mahdi *et al.,* (2020) but disagree with levels reported by Adeel and Riffat, (2014). Pearson Product Moment Correlation statistics was conducted to determine the relationship between metals level in soil during dry and wet seasons. Results (Table 4 and 5) revealed a strong positive correlation coefficient (r) of Cd and Pb in soils during dry and wet seasons. Strong positive correlation suggest that such metals may come from the same pollution source (Natural or anthropogenic). The concentration of heavy metals in soil depended mainly on the physicochemical properties of the soil sample and the distance from the source of contamination. Analysis of variance of Cd and Pb in the soil samples across the sampling sites revealed ($p < 0.05$) a significant difference in the level the metals across the locations. Cd showed high level in soil in dry season compare to the wet season while lead showed high level in wet season than dry season. High level of Cd obtained in this soil during dry season was similar to the findings of Amadi *et al.,* (2010) who reported higher mean level of this metal in dry season than wet season. This could be due to adsorption of metals by soil particles because of the reduction in moisture content of the soil associated with increased evaporation rate in dry season. The results obtained showed that all the soil from Dutsin- Ma irrigated farmlands (Chediya - Walari) fall within the values of 1 < for both seasons which indicated low contamination of these soils. Geoaccumulation index (Igeo) rating indicated that all topsoil (0–15 cm) analysed belong to unpolluted class (<0). Hence the present experimental data indicates low level of pollution of soils from Dutsin- Ma irrigated farmland and therefore of acceptable quality for agricultural and pastoral farming.

The level of cadmium contamination factor obtained from this current study is consistent with results reported by Yaradua *et al.,* (2018); Okereke *et al.,* (2019); Sharhabil *et al.,* (2021) but contradict with the levels reported of Mathias *et al.,* (2016). Also, result of contamination factor for lead reported in this current study align with Yaradua *et al.,* (2018) but lower than the values reported by Sharhabil *et al.,* (2021); Mathias *et al.,* (2016). The difference in Contamination factor of metals reported in this study compared to other related studies could be as a result of differences in geographical location of the soils and anthropogenic activities around the study area.

Applying the pollution load index classification category to interpret the result indicated low contamination of the soils from chediya, Garhi, Shantalawa, Tabobi, Takatsaba, Badole, Daguda, Makera, Ruwan gamji, and Walari farm soils see Appendix IV.

Geoacumulation index (Igeo) of Cadmium obtained in this study support the findings of Mathias *et al.,* (2016). but contradict the value reported by Sharhabil *et al.,* (2021) Contrary to the result obtained in this present study, higher Igeo of lead was obtained from the findings of Mathias *et al.,* (2016); Eze *et al.,* (2018). From the results of this present study, Igeo values calculated for various metals in all the farm sites were in the zero categories for both seasons indicating that the soils from all the various farm sites were unpolluted by these metals.

CONCLUSION

Based on the results obtained, the results shows that all the soil across the sampling location had Cd and Pb below WHO, and NESREA threshold limit except Daguda soil (DSL) and Makera soil (MSL) with Cd mean levels of 0.386 ± 0.02 mg/kg and 0.363 ± 0.030 mg/kg respectively during dry season. The contamination factor (CF), pollution load index (PLI), and geoaccumulation index (Igeo) of the soils were low across the sampling sites and therefore of acceptable quality for agricultural and pastoral farming as at the time of this study. Further study should include other other irrigated farmlands within Katsina states.

AVAILABILITY OF DATA AND MATERIALS

The datasets used and/or analysed during the current study are available from the corresponding author on reasonable request.

REFERENCES

Adeel M and Riffat NM. (2014). Human Health Risk Assessment of Heavy Metals Via Consumption of Contaminated Vegetables Collected from Different Irrigation Sources in Lahore, Pakistan. *Arabian Journal of Chemistry*, 7, 91-99.

Adeniyi, A. A. and Yusuf K. A. (2007*): Assessment of the Exposure of two Fish Speciesto Pollution in the Ogun River Catchments, Ketu, Lagos, Nigeria Environmental Monitoring Assessment 37(5) pp.451 - 458.

Amadi, A.N., Olasehinde, P.I., Okosun, E.A. and Yisa, J. (2010). Assessment of the water quality index of Otamiri and Oramiriukwa Rivers.*Physics International Journal*,1(2):116 – 123.

Andrea Giovanna NS, Zhong Z, Xin MA, Andreas F, Huafen L Aohan T, Xuejun L I U (2019) Cadmium pollution from phosphate fertilizers in arable soils and crop. *Front. Agr. Sci. Eng*., 6(4): 419–430

Bempah, CK., Kwofie, AB., Tutu,A.O., Denutsui, D., and Bentil, N. (2011). Assessing Potential Dietary Intake of Heavy Metals in Some Selected Fruits and Vegetables From Ghanaian Markets. *Elixir Pollut.* 39:4921-4926.

Cui, Y.J., Zhu, Y.G., Zhai, R.H., Chen, D.Y., Huang, Y.Z., Qui, Y. and Liang, J.Z. (2004). Transfer of Metals from Soil to Vegetables in an Area Near Smelter in Nanning, China *Environmental International*, 30 **:** 785-791.

Dimari, G.A, Abdulrahman, F.F.I, Akan, J.C. Garba, S.T (2008):Metals Concentrations in tissues of Tilapia gallier, CrrariasLazera and Osteaglossidae caught from Alau Dam, Maiduguri, Borno State, *Nigeria American Journal of Environmental Sciences*, Vol.3(1);pp3 2

Edem, C.A., Iniama, G., Osabor, V., Etuima, R.., and Ochelebe, M. (2009). A comparative evaluation of heavy metals in commercial wheat flours sold in Calabar, Nigeria. *Pak. J. Nut*. 85): 585-587

Emurotu and Onianwa (2017). Bioaccumulation of heavy metals in soil and selected food crops cultivated in Kogi State, north central Nigeria.. *Environ Syst Res (2017) 6:21*

Eze O C, Tukura B W., Atolaiye B O., and Opaluwa O D (2018) Index Model Assessment of Heavy Metal Pollution in Soils Selected from Three Irrigated Farm Sites in Fct Abuja, Nigeria. *International Journal of Advances in Scientific Research and Engineering* (ijasre) Volume 4, Issue 6*J*: 2454-7352

Jiao W, Chen W, Chang A C, Page A L (2012). Environmental risks of trace elements associated with long-term phosphate fertilizers applications: a review. *Environmental Pollution*, 168: 44–53

Jibrin, N. N. and Adewuyi, G. O. (2008): Radioprotection 43(2): 203-212.

Kabata-Pendias A, and Szteke B (2015). Chapter 5: trace elements in abiotic and biotic environments. Boca Raton: CRC Press, 3-9

Kabata-Pendias A, Pendias H (2001). Trace elements in soils and plants. 3rd ed. Boca Raton: CRC Press, 2001

Khan M A, Khan S, Khan A, Alam M (2017). Soil contamination with cadmium, consequences and remediation using organic amendments. Science of the Total Environment, 2017, 601–602: 1591– 1605

Linton H, Ranjan K.B, Smriti S. Phukana, K G (2016). Assessment of vegetables and soils for some heavy metals from irrigated farmlands irrigated with industrial effluents of hpc, nagaon, assam (india). *Oct. Jour. Env. Res.* Vol. 4(1): 033-040

Mahadi G. D 1, NuraTasiu 1, Isaac Aloba 1, ShamsuIshaqAbdullahi 2 and DattiYau (2020) Comparative analysis of potentially toxic elements in the soils and some vegetable collected from wastewater and river water irrigated areas in Kano city and Bichi town, Kano state, Nigeria. *World Journal of Advanced Research and Reviews*, 07(02), 063–074

Mathias O. Nweke and Stephen N. Ukpai (2016). Use of Enrichment, Ecological Risk and Contamination Factors with Geoaccumulation Indexes to Evaluate Heavy Metal Contents in the Soils around Ameka Mining Area, South of Abakaliki, Nigeria. *Journal of Geography, Environment and Earth Science International* 5(4): 1-13

Ndabula, C and Jidauna, G. G. (2010). Domestic water use in Selected Settlements in the Sudano-Sahelian Region of Nigeria. *International Journal of Water and Soil Resources Research*, 1(1-3):1-11.

Okereke J. N., Nduka, J. N., Ukaoma, A.A., Ogidi I. O (2019) Level of Heavy Metals in Soil Samples from Farmlands along Highways in Parts of Owerri, Nigeria. *World Journal of Innovative Research (WJIR) Volume-7, Issue-1,* 01-07

Rabee, A.M., Al-Fatlawy, Y.F., Najim, A.A. and Nameer, M. (2011) Using Pollution Load Index (PLI) and Geoaccumulation Index (I-geo) for the Assessment of Heavy Metals Pollution in Tigris River Sediment in Baghdad Region. *Journal of Al-Nahrain University*, 14, 108-114

Roberts T L. (2014) Cadmium and phosphorous fertilizers: the issues and the science. Procedia Engineering, , 83: 52 –59 21.

Sharhabil M Y, Abubakar F, Nafu A (2021). Ecological risk assessment of heavy metal contaminated soils of selected villages in Zamfara State, Nigeria. https://doi.org/10.1007/s42452-021-04175-6www.ijasre.net Page 93

Sharma, RK., Agrawal, M., and Marshall, FM. (2008). Heavy metal (Cu, Zn, Cd and Pb) contamination of vegetables in urban India: a case study in Varanasi. *Environmental Pollution*. 154(2): 254-63.

Türkdoğan, MK., Kilicel, F., Kara, K., Tuncer, I., and Uygan, I (2003). Heavy metals in soil,vegetables and fruits in the endemic upper gastrointestinal cancer region of Turkey. *Environmental toxicology and pharmacology* 13(3):175-9.

Uduma, A and Jimoh, L. (2013), Sequential extraction procedure for partitioning of lead, copper, cadmium, chromium and zinc in contaminated arable soils of Nigeria. AJEEPR. 1, 186–208.

Uwah, I .E., Dan, S.F., Etiuma, R.A. and Umoh, U.U. (2013). Evaluation of status of heavy metals pollution of sediments in Qua Iboe River Estuary and associated creeks, South-Eastern Nigeria. *Journal of Environmental Pollution*,2(4):110-112.

Vousta, D., Grimanis, A., and Samara, C. (1996). Environmental pollution, 94: 325-335.

Yaradua AI, Alhassan AJ, Nasir A, Matazu KI, Muhammad I, Idi A, Muhammad IU and Aliyu SM. (2018). Evaluation Of Heavy Metals In Sediment Of Some Selected Dams From Katsina State Nigeria. *international Journal of Scientific and Technical Research in Engineering (IJSTRE)* Volume 3 Issue 2 ‖ Page 13

Zhao, K. – Liu, X. – Xu, J. – Selim, H.M. (2010). Heavy metal contaminations in a soil-rice system: Identification of spatial dependence in relation to soil properties of paddy fields. In *Journal Hazardous Material*, vol. *181*, pp. 778–787.

APPENDIX I: Soil Sample Codes

S/N	Soil Sample	Sample Code
1	Chediya Soil	CSL
2	Garhi Soil	GSL
3	Shantalawa Soil	SSL
4	Tabobi Soil	TSL
5	Katsaba Soil	KSL
6	Badole Soil	BSL
7	Daguda Soil	DSL
8	Makera Soil	MSL
9	Ruwangamji Soil	RSL
10	Walari Soil	WSL

Appendix II: Contamination factor (CF)   Classification Categories

Contamination factor (CF)	Class
<1 indicate	low contamination
3 < CF < 6	indicate moderate contamination while

CF > 6	indicate high contamination factor

Manoj *et al.,* (2012)

Appendix III: **Geo-accumulation Index Factor Classification Categories (Igeo)**

Igeo- classes	Igeo – Values	Soil Quality
Class 0	Igeo ≤ 0	Practically Unpolluted
Class 1	0 <Igeo< 1	Unpolluted to Moderately Polluted
Class 2	1 <Igeo< 2	Moderately Polluted
Class 3	2 <Igeo< 3	Moderately Polluted to Highly Polluted
Class 4	3 <Igeo< 4	Highly Polluted
Class 5	4 <Igeo< 5	Highly to Very Highly Polluted
Class 6	5 <Igeo> 6	Extremely Polluted

Source: (Charkaravarty & Patgiri, 2009).

Appendix IV: Pollution Load Index (PLI) Classification Categories

Pollution Class	PLI-Values	Soil Quality
Class 1	PLI=0	Perfection
Class 2	PLI<1	Low Contamination
Class 3	1<PLI<3	Moderate Contamination
Class 4	3<PLI<6	ConsiderableContamination
Class 5	6<PLI<6	Very High contamination

Source : (Hari- Kumar *et al.,* 2009)

Implementation of New Iterative Method for Solving Nonlinear Partial Differential Problems

*Khadeejah James Audu and Stephen Ameh

Department of Mathematics, Federal University of Technology, Minna, Niger State, Nigeria
*Corresponding Author's e-mail: k.james@futminna.edu.ng

ABSTRACT
Nonlinear partial differential equations (PDEs) are prevalent in various scientific and engineering fields, demanding efficient solution methods. This study focuses on the practical application and evaluation of a well-established iterative method; New Iterative Method (NIM) for solving nonlinear PDEs. The primary aim is to assess the method's performance and applicability in solving nonlinear PDEs. We present the chosen iterative method, discuss its mathematical basis, and analyze its convergence properties, accuracy, and computational efficiency. We also provide insights into practical implementations and conduct numerical experiments on diverse nonlinear PDEs. Numerical experiments across various nonlinear PDEs confirm the method's accuracy and computational efficiency, positioning it favorably compared to existing approaches. The NIM's versatility and computational efficiency makes it a valuable tool for tackling complex problems. This innovation has the potential to greatly benefit scientific and engineering communities dealing with nonlinear PDEs, offering a promising solution for challenging real-world problems.
Keywords: Nonlinear Partial Differential Problems, Iterative Method, Computational Efficiency, Practical Implementation, Numerical Experiments

INTRODUCTION

Nonlinear partial differential equations (PDEs) are ubiquitous in various scientific and engineering disciplines, yet their efficient and accurate solutions remain a challenging endeavor. This study is focused on applying the New Iterative Method (NIM) to numerically solve nonlinear Partial Differential Equations that models physical complex processes. The NIM scheme have proven to be an effective mathematical tool in dealing with various scenarios and addressing linear and nonlinear differential equations. The method offers promise as numerical techniques that amalgamate analytical and iterative strategies to approximate solutions for differential equations. The NIM, initially introduced by Daftardar and Jafari in 2006 and subsequently referred to as the Daftardar-Jafari method by Batiha and Ghanim (2022), is a well-established technique. It is a straightforward and effective semi-analytical approach utilized for solving differential equations with applications spanning various fields. The NIM employs an iterative framework to linearize the problem and enhance the solution. Its successful applications encompass differential equations featuring variable coefficients (as shown by Falade *et al*., 2020), fractional differential equations (as demonstrated by Batiha *et al*., 2023), and cancer model (as illustrated by Falade and Tiamiyu, 2021).

Many natural phenomena, encompassing chemical, physical, and biological processes, often find representation through nonlinear differential equations. In addition to seeking exact solutions, there's a practical necessity for approximating these solutions to make them applicable. Consequently, a multitude of both numerical and analytical approximate methods have been devised and put into practice for addressing nonlinear models. As an illustration of this, the authors in Zada *et al.,* (2021) employed a numerical approach to solve fractional order inhomogeneous PDE. The numerical solutions for system of coupled Fractional-order drinfeld–sokolov–wilson and Fractional shallow water equations using NIM was studied by Ali *et al*., (2023). Zeleke and Regassa (2017) applied the reduced differential transform method to provide solutions concerning some PDEs such as beam and airy equations. Recently, Shihab *et al*., (2023) conducted an analysis and application of a Variational Iteration based scheme for approximating solutions of some PDEs such as Korteweg-De-Vries, Benjamin, and Airy equations. Their study indicates that the approach allows for rapid implementation without the need to deconstruct the nonlinear variables.

The implementation of the New Iterative Method (NIM) for tackling nonlinear partial differential problems presents a novel and highly motivated approach in the realm of computational mathematics. The novelty lies in NIM's ability to efficiently address complex nonlinear PDEs, offering a unique perspective on solving these intricate equations. The motivation for this topic stems from the growing importance of accurately simulating real-world phenomena in fields such as physics, engineering, and biology, where nonlinear PDEs play a pivotal role. The justification for this research lies in the demand for improved numerical methods that can provide more accurate and stable solutions to nonlinear PDEs, ultimately advancing our understanding and problem-solving capabilities in various scientific and engineering applications.

Description of New Iterative Method (NIM)

To elucidate the concept of the New Iterative Method, contemplate the subsequent generic functional equation;

$$Z = F + L(z) + N(z) \tag{1}$$

where L, N are linear and nonlinear operators respectively, and f is a given function. The solution of equation (1) has the form

$$z = \sum_{p=0}^{\infty} z_p \tag{2}$$

Now, suppose we have the relation in (3)

$$Z_0 = N(z_0) = f$$

$$Z_p = N\left(\sum_{p=0}^{n} z_p\right) - N\left(\sum_{p=0}^{n-1} z_p\right) \tag{3}$$

Then we can easily get

$$R_0 = N(z_0)$$
$$R_1 = N(z_0 + z_1) - N(z_0)$$
$$R_2 = N(z_0 + z_1 + z_2) - N(z_0 + z_1) \tag{4}$$
$$R_3 = N(z_0 + z_1 + z_2 + z_3) - N(z_0 + z_1 + z_2) + \cdots.$$

Such that $N(z)$ can be splitted as:

$$N\left(\sum_{p=0}^{m} z_p\right) = N(z_0 + z_1) - N(z_0) + N(z_0 + z_1 + z_2) - N(z_0 + z_1) \tag{5}$$

$$+ N(z_0 + z_1 + z_2 + z_3) - N(z_0 + z_1 + z_2) + \cdots.$$

To obtain a recurrence relation of the form:

$$z_0 = f$$
$$z_1 = L(z_0) + R_0 \tag{6}$$
$$z_{p+1} = L(z_p) + R_p \quad p = 1, 2, 3 \cdots.$$

Since L is linear, then

$$\sum_{p=0}^{n} L(z_p) = L\left(\sum_{p=0}^{n} z_p\right) \tag{7}$$

So

$$\sum_{p=0}^{n+1} z_p = \sum_{p=0}^{n} L(z_p) + N\left(\sum_{i=0}^{n} z_p\right) \tag{8}$$

$$= L\left(\sum_{p=0}^{n} z_p\right) + N\left(\sum_{p=0}^{n} z_p\right), \quad p = 1, 2, \cdots.$$

Thus,

$$\sum_{p=0}^{\infty} z_p = f + L\left(\sum_{p=0}^{\infty} z_p\right) + N\left(\sum_{p=0}^{\infty} z_p\right) \tag{9}$$

The k-term solution is given by the following form: $z = \sum_{i=0}^{k-1} z_i$

Convergence Analysis

We examine the convergence of NIM for resolving any functional equation. Suppose $E = Z^* - Z$, where Z^* denotes the exact solution, Z is the approximate solution, and E is the error in the solution. Then we have

$$E(x) = f(x) + N(E(x)) \tag{10}$$

Applying the above equation to the NIM scheme, the recurrence relation becomes

$$E_0 = f$$
$$E_1 = N(E_0)$$
$$E_{p+1} = N(E_0 + E_1 + \cdots + E_n) - N(E_0 + E_1 + \cdots + E_{n-}), \quad p = 1, 2, \cdots.$$
(11)

If $\| N(\mathrm{x}) - N(t) \| \le n \| \mathrm{x} - t \|, 0 < n < 1,$ then we obtain

$$E_0 = f$$
$$\| E_1 \| = \| N(E_0) \| \le n \| E_0 \|,$$
$$\| E_2 \| = \| N(E_0 + E_1) - N(E_0) \| \le n \| E_1 \| \le n^2 \| E_0 \|,$$
$$\vdots$$
$$\| E_{p+1} \| = N(E_0 + \cdots + E_n) - N(E_0 + \cdots + E_{p-1}) \| \le n \| E_p \| \le n^{p+1} \| E_0 \|,$$
$$p = 0, 1, 2, \ldots$$
(12)

Thus $E_{p+1} \to 0$ as $p \to \infty$, which proves the convergence of the NIM for solving general functional equation.

Implementations and Results
We implemented the NIM method on some PDEs, by applying it to a set of benchmark problems with known solutions. This is to assess its performance in terms of accuracy, convergence behavior, and computational efficiency. Furthermore, the results obtained through Maple 2021 software were compared with other established methods to determine its advantages and limitations. The computed results are tabulated in Tables 1-3.

Problem 1: We compute the nonlinear PDE (Shihab *et al.*, 2023);
$$z_t + a(z_x)^2 + b z_{xxx} = 0, \quad \text{with initial condition: } z(x,0) = A \tanh(Bx),$$
where $A = \dfrac{6bB}{a}$, $B = \dfrac{1}{2}\sqrt{\dfrac{v}{b}}$ True solution: $z(x,t) = A \tanh[B(x - vt)]$

As a result, the PDE problem described above can be expressed as the subsequent set of integral equations:
$$Z(x,t) = -I_t(aZ_x^2 + b Z_{xxx})$$
Taking
$$N(Z) = -I_t(aZ_x^2 + b Z_{xxx})$$
Hence, by examining equations (3), (4), (5)and (6), we can readily deduce the initial components of the New iterative solution for problem 1 as

$$z_0 := A \tanh(Bx)$$
$$z_1 := \left(2AB^3 \left(1 - \tanh(Bx)^2\right)^2 - 4AB^3 \tanh(Bx)^2 \left(1 - \tanh(Bx)^2\right) - A^2 B^2 \left(1 - \tanh(Bx)^2\right)^2 \right) t$$

The remaining components of the iterative formula (9) are derived using Maple software 2023 version and the computed solutions are tabulated in Table 1.

Problem 2: Considering the nonlinear PDE (Shihab *et al.*, 2023)
$$z_{tt} + a(zz_x)_x + \beta z_{xxxx} = 0, \quad \text{with initial conditions } z(x,0) = A \sec h^2(Bx)$$
$$z_t(x,0) = 2ABv \operatorname{sech}^2(Bx)\tanh(Bx)$$
where $A = \dfrac{12\beta B^2}{a}$, $B = \dfrac{1}{2}\dfrac{v}{\sqrt{-\beta}}$ True solution: $z(x,t) = A \operatorname{sech}^2[B(x - vt)]$

Consequently, the previously described PDE problem can be reformulated as the following collection of integral equations:

$$Z(x,t) = -I_t^2 \left(a(ZZ_x)_x + \beta Z_{xxxx} \right)$$

taking

$$N(Z) = -I_t^2 \left(a(ZZ_x)_x + \beta Z_{xxxx} \right)$$

Therefore, by analyzing equations (3), (4), (5), and (6), we can easily infer the initial components of the New Iterative solution for problem 2, such as:

$z_0 := 3tAB\,\mathrm{sech}(Bx)^2\,\tanh(Bx)^2 + A\,\mathrm{sech}(Bx)^2$

$z_1 := 48\,t^2\,A\,B^5\,\mathrm{sech}(Bx)^2\,\tanh(Bx)^5 - 624\,t^2\,A\,B^5\,\mathrm{sech}(Bx)^2\,\tanh(Bx)^3\left(1 - \tanh(Bx)^2\right)$

$\quad + 408\,t^2\,A\,B^5\,\mathrm{sech}(Bx)^2\,\tanh(Bx)\left(1 - \tanh(Bx)^2\right)^2 + 48\,t\,A\,B^4\,\mathrm{sech}(Bx)^2\,\tanh(Bx)^4$

$\quad - 264\,t\,A\,B^4\,\mathrm{sech}(Bx)^2\,\tanh(Bx)^2\left(1 - \tanh(Bx)^2\right) + 48\,t\,A\,B^4\,\mathrm{sech}(Bx)^2\,(1$

$\quad - \tanh(Bx)^2)^2 + \frac{1}{3}\left(\left(-4\,A\,B^2\,\mathrm{sech}(Bx)^2\,\tanh(Bx)^2 + 2\,A\,B^2\,\mathrm{sech}(Bx)^2\,(1\right.\right.$

$\quad - \tanh(Bx)^2))\left(8\,A\,B^3\,\mathrm{sech}(Bx)^2\,\tanh(Bx)^3 - 16\,A\,B^3\,\mathrm{sech}(Bx)^2\,\tanh(Bx)\,(1\right.$

$\quad - \tanh(Bx)^2))\,t^3\big) + \frac{1}{2}\left(\left(-2\,A\,B\,\mathrm{sech}(Bx)^2\,\tanh(Bx)\left(8\,A\,B^3\,\mathrm{sech}(Bx)^2\,\tanh(Bx)^3\right.\right.\right.$

$\quad - 16\,A\,B^3\,\mathrm{sech}(Bx)^2\,\tanh(Bx)\left(1 - \tanh(Bx)^2\right)\big) + \left(-4\,A\,B^2\,\mathrm{sech}(Bx)^2\,\tanh(Bx)^2\right.$

$\quad + 2\,A\,B^2\,\mathrm{sech}(Bx)^2\left(1 - \tanh(Bx)^2\right)\big)\left(4\,A\,B^2\,\mathrm{sech}(Bx)^2\,\tanh(Bx)^2\right.$

$\quad - 2\,A\,B^2\,\mathrm{sech}(Bx)^2\left(1 - \tanh(Bx)^2\right)\big)\big)\,t^2\big)$

$\quad - 2\,A\,B\,\mathrm{sech}(Bx)^2\,\tanh(Bx)\left(4\,A\,B^2\,\mathrm{sech}(Bx)^2\,\tanh(Bx)^2 - 2\,A\,B^2\,\mathrm{sech}(Bx)^2\,(1\right.$

$\quad - \tanh(Bx)^2))\,t$

The remaining elements of the iterative formula (9) are computed through the utilization of Maple software, version 2023, and the resulting solutions are presented in Table 2.

Problem 3: We apply the NIM to solve the following nonlinear PDE;

$$Z_{tt} + Z_{xx} + Z_{x^2} = 2x + t^4$$

$$Z(x,0) = 0;\, Z(0,t) = at;\, Z_t(x,0) = a;\, Z_x(0,t) = t^2$$

Exact solution: $Z(x,t) = at + xt^2$

The problem mentioned above is analogous to the subsequent integral equation.

$$Z = at + \frac{t^6}{30} + xt^2 - I_t^2\left(Z_{xx} + Z_x^2\right)$$

Let $N(Z) = -I_t^2\left(Z_{xx} + Z_x^2\right)$, in view of the procedure in equations (3-6), we obtain the following relations

$$Z_0 = at + \frac{t^6}{30} + xt^2,$$

$$Z_1 = N(Z_0) = -\frac{t^6}{30}$$

$$Z_2 = 0,\, Z_3 = 0, \cdots.$$

The remaining components of the iterative formula (9) are calculated using Maple software, and the outcomes are showcased in Table 3. And consequently, further iterations leads to $Z(x,t) = at + xt^2$, which is the exact solution.

Table 1: Analysis of NIM Result for Problem One

x/t	NIM Solutions	VIM Solutions	True Solutions	Error of NIM $\lvert Z_{NIM} - Z\rvert$	Error of VIM $\lvert Z_{VIM} - Z\rvert$
0.10	0.03749609425	0.03749606573	0.03749609425	5.0×10^{-11}	2.852×10^{-10}
0.25	0.09369151252	0.09368693050	0.09368901252	2.0×10^{-11}	2.082035141×10^{-8}
0.50	0.1866728295	0.1870085540	0.1870132399	0.00000	4.685844×10^{-6}
0.75	0.2702871420	0.2800088572	0.2796135561	2.40×10^{-8}	3.953011×10^{-6}
1.00	0.3711410670	0.3734682012	0.3711419684	9.014×10^{-7}	2.3262328×10^{-6}
2.00	0.7202371522	0.6889158600	0.7202372565	2.40×10^{-8}	3.13213965×10^{-4}

x/t					
3.00	1.030174037	1.0547476570	1.030183947	9.910×10^{-6}	2.456277×10^{-4}
4.00	1.29157557	1.4121069	1.291585757	1.1087×10^{-5}	1.205169×10^{-3}
5.00	1.502646418	1.37114764	1.502657418	1.1×10^{-4}	1.316×10^{-2}

Table 1 displays the results calculated using the New Iterative Method, providing approximate solutions in comparison to the exact solutions for problem 1. The selection of parameters $V = 0.5$ & $a = b = 1$ is made to address the PDE in problem 1. After the fourth iteration, it is evident that the computed errors of the NIM approximate solutions are lower than those of the Variational Iterative method (VIM). This observation indicates that the NIM technique is more efficient in computing the solutions of the PDE compared to the VIM technique.

Table 2: Analysis of NIM Result for Problem Two

x/t	NIM Solutions	VIM Solutions	True Solutions	ror of NIM $\|Z_{NIM} - Z\|$	Error of VIM $\|Z_{VIM} - Z\|$
0.10	0.1874945069	0.1874945069	0.1874945069	0.000000	1.10×10^{-10}
0.25	0.1874656719	0.1874656719	0.1874656719	0.000000	$5.645801890 \times 10^{-11}$
0.50	0.1873627379	0.1873627380	0.1873627379	0.000000	$8.318579018 \times 10^{-11}$
0.75	0.1871913487	0.1871913486	0.1871913487	0.000000	2.72945×10^{-11}
1.00	0.1869517547	0.1869517548	0.1869517547	0.000000	4.62×10^{-11}
2.00	0.1853197872	0.1853197871	0.1853197872	0.000000	$4.036710999 \times 10^{-11}$
3.00	0.1826417751	0.1826417747	0.1826417751	0.000000	$3.194813670 \times 10^{-10}$
4.00	0.1789784742	0.1789784710	0.1789784742	0.000000	3.2×10^{-9}
5.00	0.1744108363	0.1744108342	0.1744108363	0.000000	$2.000290866 \times 10^{-9}$

Table 2 exhibits the numerical solutions obtained through the New Iterative Method, the Variational Iterative Method, as well as the exact solutions for problem 2. We have configured the parameters $v = 0.25$, $\beta = -3$, and $a = -1$ for problem 2, to assess the accuracy and reliability of the NIM's approximate solution for the considered PDE. A comparison of the results after the fourth iteration of the NIM with the exact solution and the VIM reveals a notable trend. It is evident that the NIM's solution converges more effectively to the exact solution in comparison to the VIM. This demonstrates the NIM's superior efficiency in handling nonlinear PDEs.

Table 3: Analysis of NIM Result for Problem three

x/t	NIM Solutions	VIM Solutions	True Solutions	Error of NIM $\|Z_{NIM} - Z\|$	Error of VIM $\|Z_{VIM} - Z\|$
0.10	0.1010000000	0.1010000000	0.10100000000	0.00000	0.0000
0.25	0.2080000000	0.2080000000	0.20800000000	0.00000	0.00000
0.50	0.3270000000	0.3270000000	0.32700000000	0.00000	0.00000
0.75	0.4640000000	0.4640000000	0.46400000000	0.00000	0.00000
1.00	0.625000000	0.6250000000	0.62500000000	0.00000	0.00000
2.00	0.8160000000	0.8160000000	0.8160000000	0.00000	0.00000
3.00	1.0430000000	1.0430000000	1.04300000000	0.00000	0.00000
4.00	1.3120000000	1.3120000000	1.31200000000	0.00000	0.00000
5.00	1.6290000000	1.6290000000	1.62900000000	0.00000	0.00000
0.10	2.0000000000	2.0000000000	2.0000000000	0.00000	0.00000

Within the table provided, you can find the approximate solutions derived using the NIM, the Variational Iterative Method (VIM), and the exact solutions for problem 3. Notably, what's interesting is that, by the 10th iteration, both the NIM and VIM approximate solutions converge remarkably close to the exact solutions. An intriguing observation in the results is that the errors for both methods have reached zero. This outcome strongly indicates the high efficiency and effectiveness of these two methods when it comes to solving problems involving partial differential equations (PDEs).

CONCLUSION

In this study, we introduced and implemented a numerical approach for tackling nonlinear partial differential equations. We carried out an extensive analysis and practical application of the New Iterative method to approximate solutions for a set of chosen PDEs. This method consistently generates a sequence of solutions that progressively approaches the exact solution. The New Iterative technique marks a substantial leap forward in the domain of solving nonlinear PDEs, and its potential impact extends across a wide range of scientific and engineering domains. Its adaptability, precision, and computational efficiency position it as a promising option for addressing intricate nonlinear issues in the future. The outcomes of this study hold the potential to guide scientists and engineers, enhancing their comprehension of complex physical problems. This, in turn, may pave the way for the formulation of strategies and plans aimed at addressing such issues more effectively. We propose that future research should explore the application of the New Iterative Method to address various other categories of differential equations.

REFERENCES

Ali, F., Yassen, M. F., Asiri, S. A., Nawaz, R., Zada, L., Alam, M. M. & Sene. N. (2022). New Iterative Method for Solving a Coupled System of Fractional-Order Drinfeld–Sokolov–Wilson (FDSW) and Fractional Shallow Water (FSW) Equations. *Hindawi Journal of Nanomaterials*, 1-13.

Batiha B., Ghanim G., Batiha, K. (2023a). Application of the New Iterative Method (NIM) to the Generalized Burgers–Huxley Equation, Symmetry, 15, 21-45.

Batiha, B., Heilat, A. S. & Ghanim, F. (2023b). Closed-Form Solutions for Cauchy-Euler Differential Equations through the New Iterative Method (NIM). *Applied Mathematics & Information Sciences, 17*(3), 459-467.

Batiha B., & Ghanim, F. (2022). Numerical Implementation of Daftardar-Gejji and Jafari Method to the Quadratic Riccati Equation. *Buletinul Academiei De S̨Tiint̨E A Republicii Moldova. Matematica*, *3*(97), 21–29.

Daftardar, G. V. & Jafari, H. (2006). An iterative method for solving nonlinear functional equations, Journal of Mathematical Analysis and Applications, 16(2), 753-763.

Falade, K. I., Tiamiyu A. T. & Isa U. (2021). Numerical Comparison of Runge-Kutta (Rk5) and New Iterative Method (Nim) for solving Metastatic Cancer Model. *Malaysian Journal of Computing, 6*, 758-771.

Falade KI, Tiamiyu AT. (2020) Numerical solution of partial differential equations with fractional variable coefficients using new iterative method (NIM). *Mathematical Sciences and Computing*, 3, 12-21.

Shihab, M. A., Taha, W. M., Hameed, R. A., Jameel, A. & Ibrahim, S. M. (2023). Implementation of variational iteration method for various types of linear and nonlinear partial differential equations. *International Journal of Electrical and Computer Engineering*, *13*(2), 2131-2141.

Zada, L., Nawaz, R., Ahsan, S., Nisar, K.S. & Baleanu, D. (2021). "New iterative approach for the solutions of fractional order inhomogeneous partial differential equations," *AIMS Mathematics*, *6*(2), 1348–1365.

Zeleke, B. & Regassa, A. (2017). The reduced differential transform method for solving beam and airy equations. *Editorial Board*, *6*(12), 1-20.

Ensuring Privacy in IoT Applications: An in-Depth Examination through Literature Review

*Abdulwasiu, A. A. and Olanrewaju, O. M.

Department of Computer Science, Faculty of Computing, Federal University Dutsin-Ma, Katsina State, Nigeria.
*Corresponding Author's E-mail: ibnwasar@gmail.com

ABSTRACT
The Internet of Things (IoT) has revolutionized how smart devices collaborate with each other and interact with both physical and virtual objects over the Internet to accomplish complex tasks. These smart devices find application in various fields such as smart grids, healthcare, and smart environments, where multiple stakeholders share data for specific purposes. In these domains, data often contain sensitive information and are closely tied to the habits of their owners. Consequently, the IoT has given rise to significant concerns regarding data privacy and protection. This paper presents the findings of a comprehensive literature review that delves into privacy-preserving solutions employed within Cooperative Information Systems (CIS) in the IoT domain. The research work conducted an exhaustive search for scholarly works on this topic. This paper focused on a subset of these aspects, which include: definition of IoT, techniques used for safeguarding privacy, and adherence to ISO privacy principles. Ultimately, the research work offered recommendations to enhance the integration of privacy principles and fulfill security requirements in IoT applications by combining Blockchain and machine learning method.
Keywords: Internet of Things, Privacy, Blockchain, IoT Architecture.

INTRODUCTION
The rapid expansion of Internet of Things (IoT) technology has given rise to various advancements in the IoT sector, impacting both businesses and individuals alike. In general, IoT applications, such as smart grids and smart cities, necessitate the collaboration of multiple stakeholders to accomplish their objectives. These stakeholders can encompass data owners or requesters, ranging from individuals and groups of individuals to organizations. For example, these parties may share their energy consumption data to assist energy providers in predicting energy production. Nevertheless, despite the promising aspects of IoT, several concerns persist, hindering its widespread adoption. Collecting data in IoT applications has raised concerns among data owners regarding the potential uses of their data. Some of the data collected can be sensitive, and data owners may be reluctant to share them with competing organizations without maintaining a degree of control. Therefore, this study zeroes in on a non-functional requirement of IoT applications, namely, safeguarding the privacy of collaborating parties (Liu et al., 2021).

As part of research initiative made on privacy in the IoT era, it is imperative to conduct a thorough analysis of this issue. To this end, this research work presents an overview of existing privacy-preserving solutions in the IoT domain with the aim of identifying gaps and formulating solutions and recommendations.

The primary objective is to pinpoint areas of concern and emerging trends related to privacy preservation in IoT applications. As a result, this research work classification scheme comprises some dimensions that emphasize application domains, IoT architectures, security attributes and prerequisites, and techniques for privacy preservation and also provided a recommendation.

Literature Review
In this section, the research work illuminates the definitions of IoT, security, and privacy by exploring their conceptual aspects. It also delve into the various IoT application domains and architectures, as well as security attributes and requirements, as defined by the ISO standard. Additionally, it provides insights into existing privacy regulations and privacy-preserving techniques and related works.

Definitions of IoT
There is no universally accepted set of definitions for IoT, security, and privacy. Therefore, this research work provides an overview of the definitions that are pertinent to this study. The Internet of Things (IoT) is a network of physical objects embedded with technology for communication with the external environment Engelhardt-Nowitzki et al., (2020). As described by Mkrttchian et al., (2021) IoT facilitates the connection of people and things at any time, in any place, with anything and anyone, ideally using any available pathway or network and any service.

Security involves the implementation and management of suitable measures that encompass a wide spectrum of threats. In this context, the ISO standard. Liu et al., (2021) outlines a set of security properties and requirements, as detailed in Section 2.4.

Privacy is the right of individuals, groups, or institutions to determine when, how, and to what extent information about them is disclosed to others (Monea, 2020). In the context of IoT applications, it is essential to consider the contextual aspects when addressing privacy issues. Data privacy encompasses data security while taking into account legal regulations and individual preferences (Liang et al., 2019).

Application Domains of IoT
Various application domains within the realm of IoT exist. These applications can be categorized into two domains:
- **i. Personal and Home**: This category includes aspects like location sharing, with the aim of offering services based on the collected location data of IoT devices (i.e., geographical location), healthcare services aimed at remote patient monitoring without the need for hospital visits, and smart home automation for controlling connected devices within a household (Mkrttchian et al., 2021)
- **ii. Government and Industry**: This domain encompasses applications such as the smart city, which monitors critical infrastructures, and the smart grid, designed for monitoring and reducing energy consumption. These IoT applications require collaboration among multiple parties to achieve their objectives. For instance, consumers in households, offices, and industries should be aware of the benefits of collaborating within a smart grid to reduce energy consumption. Moreover, the smart grid must ensure adequate privacy protection for the participating parties to gain their trust (Rai et al., 2023).

Architectures of IoT
There are various evolving architectures of IoT, some of these are highlighted below.
- i. **Centralized Architecture**: This architecture involves passive entities in the network whose sole responsibility is to provide data. Collected data is stored and processed by a central server, which serves as the sole provider of IoT services to other entities. The primary challenge with this architecture is its susceptibility to resilience issues, as all computational tasks are managed by a single server. Consequently, a server failure can render IoT services unavailable (Sethi and Sarangi, 2017)
- ii. **Decentralized Architecture**: In this architecture, each entity can process data and provide IoT services to other entities in the network. This architecture overcomes the single point of failure issue associated with the centralized architecture. However, it introduces the potential for intrusion by malicious entities, as any entity can connect with any other entity at any time (Alhusayni et al., 2023)
- iii. **Third-Party Architecture**: This architecture involves a public institution or private corporation responsible for data collection, transfer, storage, and/or processing. An example of a ready-to-use platform is the Smart-Meter-Analytics (SAP) (Rai et al., 2023). The main challenge with such an architecture is that it places complete trust in the third party for data management.
- iv. **Hybrid Architecture**: This architecture combines various architecture structures to leverage their advantages and mitigate their disadvantages. For example, Birman et al., (2015) addressed privacy issues in the data collection phase of a smart grid by combining peer-to-peer communications with elements of centralized control, effectively utilizing collected data while preserving consumers' privacy.

Security Properties and Requirements
According to the ISO standard (Alhusayni et al., 2023), the aim of information security is to safeguard three fundamental properties:
- i. **Confidentiality**: This pertains to protecting data from unauthorized access, disclosure, and processing.
- ii. **Integrity**: This involves safeguarding the accuracy and completeness of data from unauthorized modifications.
- iii. **Availability**: Ensuring data remains accessible and usable upon demand by authorized entities.

Furthermore, information security may encompass protecting authenticity, authorization, and ensuring entities can be held accountable. This includes:
- i. **Authentication**: Ensuring that an entity's claimed characteristic is accurate.
- ii. **Authorization**: Providing permissions regarding information.
- iii. **Accountability:** Holding entities responsible for their actions.

Privacy Legislation
In 1980, the Organization for Economic Co-operation and Development (OECD) issued Guidelines on the Protection of Privacy and Transborder Flows of Personal Data. These guidelines consist of eight principles known as Fair

Information Practices (FIP), which allow individuals to express their privacy preferences and impose obligations on organizations to adhere to those preferences.

Privacy Preservation Techniques in IoT

Privacy preservation techniques in IoT are methods and strategies designed to safeguard the privacy of individuals and their data within the IoT ecosystem. These techniques are essential because IoT devices collect vast amounts of data, often including personal and sensitive information. Common privacy preservation techniques in IoT include:

Data Perturbation Techniques: These techniques encompass a set of operations that either modify or conceal sensitive elements within the original data to uphold privacy (Talebkhah et al., 2021). Two primary categories of techniques are employed for this purpose: noise addition and anonymization.

i. **Noise Addition Techniques**: These approaches involve the transformation of confidential attributes by introducing noise into the original data to prevent the identification of specific individuals . They can be further divided into four groups:

  a. **Data Sampling Techniques**: These methods aim to release a new dataset that includes only a sample of the entire population's data.

  b. **Random-Noise Techniques**: These involve adding or multiplying the value of the sensitive attribute with a randomized number (Hameed, 2022).

  c. **Data Swapping Techniques**: In this category, a subset of the data is modified to introduce uncertainty about the true data value.

  d. **Differential Privacy Techniques:** This approach entails adding Laplace noise to the result of a database query (Huang and Nazir, 2021).

ii. **Anonymization Protection Techniques:** These techniques conceal the identity of a data owner by eliminating explicit identifiers and making the data less specific. Three well-known privacy preservation methods are k-anonymity, l-diversity and t-closeness (Lova Raju et al., 2020). K-anonymity is a formal method designed to mitigate the re-identification risk associated with quasi-identifier attributes. However, it may still be vulnerable to background knowledge attacks, leading to the development of other versions like l-diversity, which ensures there are at least l distinct values for the sensitive attribute in each quasi-identifier group. T-closeness requires the distribution of a sensitive attribute in any quasi-identifier group to closely match the attribute's distribution in the overall dataset.

iii. **Data Restriction Techniques**: These methods focus on limiting data usage by either blocking access or encrypting inputs. Data restriction techniques encompass access control and cryptography-based methods.

  a. **Access Control**: These techniques are effective for managing data sharing (Liu et al., 2021). Data owners can express their individual preferences regarding who can access their data and how others can manipulate the shared data. Control mechanisms include Role-Based Access Control (RBAC) and Attribute-Based Access Control (ABAC). RBAC assigns access permissions based on roles, while ABAC defines permissions based on attributes like subject, resource, and environment attributes.

  b. **Cryptographic Protection**: These techniques are widely employed for privacy preservation. They fall into three major categories, which are Secure Multiparty Computation: This approach aggregates inputs from distributed entities to generate outputs while preserving the privacy of inputs (Huang and Nazir, 2021). Secondly, Asymmetric/Symmetric Encryption: These methods use keys to safeguard data. And the third is Public Key Infrastructure: This system provides entities with certificates to ensure that a public key belongs to the identified entity.

Related works

Shankar, (2017) proposed AndroTaint: An Efficient Android Malware Detection Framework Using Dynamic Taint Analysis. This employs four distinct approaches to identify malware, categorizing applications into four groups: malicious, benign, aggressive, and risky. However, there is a need to enhance the speed of this technique to reduce the time required for malware analysis

Yang et al., (2017) explored lightweight computing, which encompassed a detailed discussion of mechanisms and architectures related to authentication and access control. This study conducted an extensive survey to analyze the constraints of IoT devices and the various types of attacks to which they are susceptible. The primary focus of this research revolved around four distinct layers: perception, network, transport, and application layers. The article primarily addresses the authentication of IoT devices and the implementation of access control mechanisms, although it underscores the necessity for further improvements in data security

In an effort to alleviate the processing burden associated with user authentication and key generation at physical layer devices, a research endeavor was undertaken. This study centers around the utilization of mobile edge computing within the physical layer for heterogeneous cloud-based IoT (Internet of Things) systems, particularly in the context of multiple access mobile edge computing for smart cities and smart homes (Wang et al., 2019). The proposed approach, which seeks to enhance the overall security of IoT, is expected to have a substantial impact, provided it is implemented comprehensively across the entirety of IoT infrastructure, rather than concentrating solely on the physical layer encompassing components such as sensors and actuators.

Ramamoorthi et al., (2021) wrote that blockchain technology was recognized as the most effective solution for enhancing the security of IoT systems. The primary objective of this research is to provide an in-depth explanation of blockchain technology while exploring various techniques such as double blockchain and the time stamp method, aimed at reducing transaction processing times. However, It is important to note that blockchain technology requires further refinement to adapt to dynamic architectures that encompass a diverse range of sensors, devices, and actuators, necessitating a departure from the conventional chain-type structure which this work did not put into consideration.

Research Gap

Blockchain technology has emerged as a solution that addresses the issue of trust in centralized authorities. The original system, Bitcoin enables secure currency (bitcoins) transfers without the need for a central regulator Alam et al., (2023). Specific nodes, known as miners, are responsible for collecting transactions, solving computational puzzles (proof-of-work) to reach consensus, and adding transactions to a distributed public ledger called the blockchain. Since then, blockchain technology has extended to other domains, including projects like Storj, a decentralized peer-to-peer cloud storage network, and Onename a distributed and secure identity platform (Alkhazaali and Kurnaz, 2023). Blockchain technology is also being utilized to tackle privacy concerns in the IoT domain. However, current blockchain-based solutions primarily focus on addressing access control issues in IoT applications Ahamad, (2022) and there is a need to enhance the speed of some of the technique to reduce the time required for malware analysis.

CONCLUSION

The Internet of Things (IoT) is viewed as a promising technology that can potentially enhance collaborative work, allowing individuals to connect at any time, in any place, with any device, and with anyone. However, IoT's adoption exposes users to potential privacy risks. Consequently, both privacy and security must be meticulously considered within this technology. This paper is dedicated to providing an in-depth examination of privacy preservation solutions in IoT applications. In the ongoing efforts, it is intended to propose a blockchain-based solution that incorporates the recommendations outlined in this study to safeguard privacy within IoT applications. The blockchain technology together with machine learning, recognized for its success in addressing issues related to trust in centralized entities across various domains, can be adapted by IoT application designers to advance collaborative work in Cooperative Information Systems (CIS) and mitigate privacy concerns within IoT applications.

RECOMMENDATION

In comparison to lightweight security solutions and blockchain solutions, the integration of blockchain and machine learning methods will offer a more secured and adaptive approach to enhancing security in IoT environments. The strengths and benefits of this advanced approach are worth considering for organizations and individuals seeking comprehensive IoT security solutions.

REFERENCES

Ahamad, S., Gupta, P., Acharjee, P. B., Kiran, K. P., Khan, Z., and Hasan, M. F. (2022). The role of blockchain technology and Internet of Things (IoT) to protect financial transactions in the cryptocurrency market. Materials Today: Proceedings, 56(4), 2070-2074. https://doi.org/10.1016/j.matpr.2021.11.405

Alam, T. (2023). Blockchain-Based Internet of Things: Review, Current Trends, Applications, and Future Challenges. Computers, 12(1), 6. https://doi.org/10.3390/computers12010006

Alhusayni, A., Thayananthan, V., Albeshri, A., and Alghamdi, S. (2023). Decentralized Multi-Layered Architecture to Strengthen the Security in the Internet of Things Environment Using Blockchain Technology. Electronics, 12(20), 4314. https://doi.org/10.3390/electronics12204314

Al-Khazaali, A. A. T., and Kurnaz, S. (2023). Study of integration of blockchain and Internet of Things (IoT): an opportunity, challenges, and applications in the medical sector and healthcare. Applied Nanoscience, 13, 1531-1537. https://doi.org/10.1007/s13204-021-01834-5

Birman, K., Jelasity, M., Kleinberg, R., and Tremel, E. (2015). Building a Secure and Privacy-Preserving Smart Grid. ACM SIGOPS Operating Systems Review, 49(1), 131-136. https://doi.org/10.1145/2723872.2723891

Engelhardt-Nowitzki, C., Aburaia, M., Otrebski, R., Rauer, J., and Orsolits, H. (2020). Research-based teaching in digital manufacturing and robotics - the digital factory at the UAS technikum wien as a case example. Procedia Manufacturing, 45, 164–170.

Hameed, A., Violos, J., and Leivadeas, A. (2022). A deep learning approach for IoT traffic multi-classification in a smart-city scenario. IEEE Access. https://doi.org/10.1109/ACCESS.2022.3153331.

Huang, C., and Nazir, S. (2021). Analyzing and evaluating smart cities for IoT based on use cases using the analytic network process. Mobile Information Systems. https://doi.org/10.1155/2021/6674479.

Liang, J.M., Su, W.C., Chen, Y.L., Wu, S.L., and Chen, J.J. (2019). Smart interactive education system based on wearable devices. Sensors, 19(15), 3260.

Liu, J., Wang, C., and Xiao, X. (2021). Internet of Things (IoT) Technology for the Development of Intelligent Decision Support Education Platform. Scientific Programming, 2021, 6482088. https://doi.org/10.1155/2021/6482088

Lova Raju, K., Md Khasim, S., Pavankalyan, K. Y., Naveen, A., and Vikas, P. (2020). The State of Art of Internet of Things for Smart City Research Issues. In Proceedings—International Conference on Vision Towards Emerging Trends in Communication and Networking, ViTECoN 2019. https://doi.org/10.1109/ViTECoN.2019.8899388.

Mkrttchian, V., Gamidullaeva, L., Finogeev, A., and Chernyshenko, S. (2021). Big data and internet of things (IoT) technologies' influence on higher education: current state and future prospects. International Journal of Web-Based Learning and Teaching Technologies, 16.

Monea, B. (2020). Looking at screens: examining human-computer interaction and communicative breakdown in an educational online writing community. Computers and Composition, 58(2), Article ID 102605.

Rai, H. M., Rehman, A.U., Pal, A., Mishra, S., and Shukla, K. K. (2023). Use of Internet of Things in the context of execution of smart city applications: a review. Discover Internet of Things, 3(8). https://doi.org/10.1007/s43926-023-00037-2

Ramamoorthi, S., Kumar, B. M., Sithik, M. M., Kumar, T. T., Ragaventheran, J., and Islabudeen, M. (2021). Enhanced Security in IoT Environment Using Blockchain: A Survey. Materials Today Proc., Elsevier, 1–4. https://doi.org/10.1016/j.matpr.2021.03.346.

Sethi, P., and Sarangi, S. R. (2017). Internet of Things: Architectures, Protocols, and Applications. Volume 2017, Article ID 9324035. https://doi.org/10.1155/2017/9324035.

Shankar, V. G., Somani, G., Gaur, M. S., Laxmi, V., and Conti, M. (2017). AndroTaint: An Efficient Android Malware Detection Framework Using Dynamic Taint Analysis. In 2017 ISEA Asia Security and Privacy (ISEASP), 1–13.

Talebkhah, M., Sali, A., Marjani, M., Gordan, M., Hashim, S. J., and Rokhani, F. Z. (2021). IoT and big data applications in smart cities: recent advances, challenges, and critical issues. IEEE Access, 9, 55465–84. https://doi.org/10.1109/ACCESS.2021.3070905.

Wang, D., Bai, B., Lei, K., Zhao, W., Yang, Y., and Han, Z. (2019). Enhancing Information Security via Physical Layer Approaches in Heterogeneous IoT With Multiple Access Mobile Edge Computing in Smart City. IEEE Access, 7, 54508–54521

Yang, Y., Wu, L., Yin, G., Li, L., and Zhao, H. (2017). A Survey on Security and Privacy Issues in Internet-of-Things. IEEE Internet of Things Journal, 4(5), 1250–1258.

Network Topology Analysis and Structures

Bakare, K. A., Olanrewaju, O. M., Abubakar, S. and *Abdulwasiu, A. A.

Department of Computer Science, Faculty of Computing, Federal University Dutsin-Ma, Katsina State, Nigeria.
*Corresponding Author's E-mail: ibnwasar@gmail.com

ABSTRACT
Distributed computer systems have gained significant importance and popularity in modern computing. They offer high-performance capabilities at a cost-effective price point. These autonomous computers are interconnected through communication networks within a distributed computing environment, organized into geometric structures known as network topologies. This paper offers a comprehensive examination and analysis of network topologies, including definitions of both physical and logical network topologies. This paper explores the evolution of network topologies and logical communication structures within computer networks. For the physical topology, the types and the weaknesses were provided more so, it analyzes the shortcomings of traditional shared media and token-based topologies and proposes an advanced approach, Mesh-hybrid for physical topology the Switched Ethernet Topology for logical based, which eliminates collisions, optimizes bandwidth, ensures low latency, and offers scalability. This innovative method addresses the complexities of modern network communication, providing enhanced reliability and efficiency for a wide range of applications.
Keywords: Internet of Things (IoT), Thread-Level Parallelism (TLP), Scalability

INTRODUCTION
Distributed computing systems have become an indispensable part of the ever-expanding field of information technology. The performance of any distributed system is undeniably affected by the technology used to establish network connections. Network topologies serve as the underlying structure for organizing various computer components, including links and nodes. Essentially, network topology refers to the configuration of a computer network. In the realm of mathematics, topology deals with the connectedness of objects, which is a fundamental property of space. In simpler terms, network topology describes how computers in a network are interconnected. Each topology is tailored to specific tasks and comes with its own set of advantages and drawbacks. A prime example of network topology includes Star, Linear, Mesh, Ring topology etc. (Guo et al., 2023)

In recent times, there are primarily two main categories of network topologies: Physical and Logical. Physical Network Topology places emphasis on the hardware components of the system, encompassing workstations, remote terminals, servers, and the associated wiring between them. Conversely, Logical Network Topology focuses on representing the flow of data between nodes. This paper provides a concise overview of these topologies and is structured as follows:

Literature Review
Network Classification
Classification of Network can be seen in two ways, either by physical topology or by logical topology.

Physical Topology
Physical Network Topology focuses on the hardware components within the system, which encompass workstations, remote terminals, servers, and the interconnecting wiring. It defines how the systems are physically linked, essentially referring to the arrangement of devices in a computer network through the tangible cables responsible for data transmission. There are eight fundamental topologies, and each of them is elaborated below.

A. Point to Point
A point-to-point topology establishes a direct connection between two devices or nodes. The primary advantage of a permanent point-to-point network is the unobstructed communication between the two endpoints. An illustrative example is a personal computer connected directly to a printer. A more common scenario is a mainframe terminal linked to a mainframe front-end processor (Jalil, 2022). Figure 1 depicts Point to point topology.
Loophole: While the direct connection offers unobstructed communication, it can be limiting when multiple devices need to communicate with each other as it necessitates a dedicated connection for each pair of devices. Scalability can be an issue as adding more devices requires more physical connections, which can become unwieldy
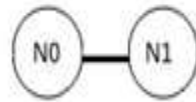
Figure 1: Point-to-point

B. Bus

In the bus topology, messages are carried along the cable. When a message reaches a device or node, the node examines the destination address contained in the message to determine if it matches its own. If the address doesn't match, the node takes no further action. However, a significant drawback of this network topology is that if the node's address matches the one in the message, the node processes the message. Consequently, the message is transmitted along the cable and becomes visible to all devices connected to that same cable (Selvi and Velupillai, 2022).

Loophole: One significant loophole is the lack of security and privacy. Since data is transmitted along a shared cable, all devices on the network can potentially view the data. Additionally, if the cable is damaged or severed at any point, the entire network can become non-functional. Figure 2 depicts Bus topology.
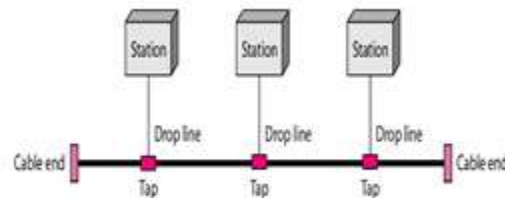

Figure 2: Bus topology

C. Star

The star topology represents one of the most prevalent network configurations, where every device or node within a network links to a central hub. A significant drawback of this network setup is that in the event of the central hub failing, all computers connected to it would lose their connection. It's essential to note that this topology exhibits a high reliance on the proper functioning of the central hub, as the failure of this hub results in the network becoming non-operational (Deepak, 2022) Figure 3 depicts Star topology.

Loophole: The central hub is a single point of failure. If the hub fails, all connected devices lose their connection, which can result in network downtime. This topology is heavily dependent on the proper functioning of the central hub.

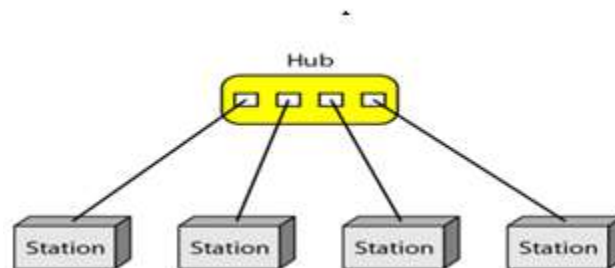Figure 3: Star Topology

D. Ring

Within a ring topology, all nodes or devices form a circular connection, with data circulating from one device to the next, continually traversing the ring until it reaches the intended destination node. One notable disadvantage is that if even a single device is powered off, the entire network ceases to function (Wang et al., 2022). The figure 4 shows Ring topology.

Loophole: Similar to the star topology, a single point of failure can disrupt the entire network. If even one device is powered off or a cable connection is broken, data transmission is halted. Troubleshooting and finding the location of a failure can be challenging.
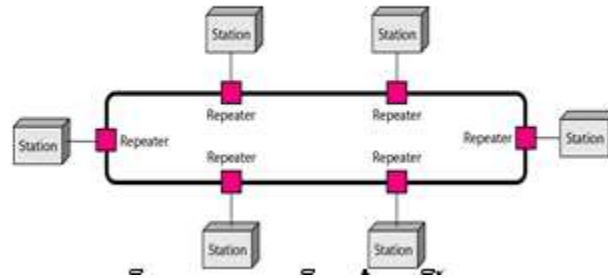

Figure 4: Ring Topology

E. Mesh

In this type of topology, every device is interconnected with one another, enabling the distribution of most transmissions even if one of the connections experiences an issue. However, a notable downside is the increased likelihood of redundancy in many network connections, leading to elevated overall costs in comparison to other network topologies (Guo et al., 2023). Figure 5 is Mesh topology.

Loophole: While it offers high reliability due to redundancy, this topology can be expensive to implement as it requires a large number of connections. Managing and maintaining such a complex network can also be challenging and costly.
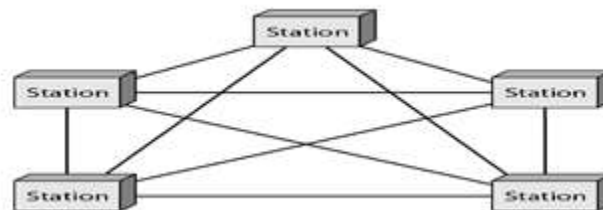
Figure 5: Mesh topology

F. Tree

The tree structure is most suitable for expansive and highly segmented networks. It combines elements of both the bus and star topologies. In a tree topology, each star network functions as a local area network (LAN) with a central computer or server to which all connected nodes are directly linked. These central computers of the star networks are connected to a main cable known as the bus. However, a significant drawback is that the network's length depends on the type of cable in use, and the entire tree topology network relies heavily on the trunk, which serves as the central backbone. If the trunk were to experience a failure, the entire network would also fail (Lowe and Pinskier, 2023). This is shown in figure 6.

Loophole: Like the star and ring topologies, the tree structure is vulnerable to the failure of the central trunk cable. If the trunk fails, the entire network becomes non-operational. The length of the network is limited by the type of cable in use.

Figure 6: Tree

G. Hybrid

A hybrid topology encompasses a network structure that consists of one or more connections between two or more networks using different physical topologies, or it may involve the interconnection of two or more networks based on the same physical topology. However, the resulting network from such interconnecti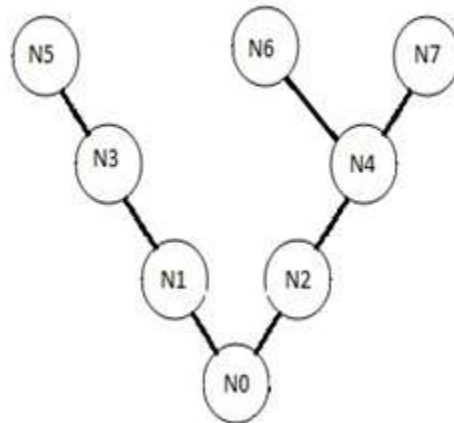ons may not strictly adhere to the definition of the original physical topology of the interconnected networks. Notably, a drawback of this topology is its generally higher cost compared to other networks, as it leverages the characteristics of its constituent topologies. It necessitates more cabling between hardware devices than other types of network topologies, making hybrid networks more challenging to set up and troubleshoot (Wei, 2022). Figure 7 shows Hybrid topology.

Loophole: The main drawback is the increased cost and complexity. Hybrid topologies combine different physical topologies or networks, which can lead to more cabling and equipment requirements. Troubleshooting and maintaining such a network can be challenging due to its heterogeneous nature.
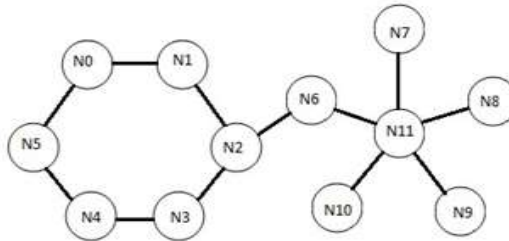
Figure 7: Hybrid topology

H. Daisy Chain

In a daisy chain network topology, your devices are interconnected in a linear or ring-like manner. The master controller links to a slave device, which then links to another slave device, and the chain continues in this manner. If a break occurs in the ring at a specific link, data transmission can be rerouted in the reverse direction, ensuring that all nodes remain connected in the event of a single failure. However, a significant drawback is that a component or cable failure at any point in the chain will render the entire network inoperative. Additionally, if you wish to add a device in the middle of the chain or ring, the network experiences downtime during the process. These networks often feature cabling placed in open spaces, making them more susceptible to accidental disconnections and physical damage (Liu, 2020), figure 8 shows Daisy Chain topology.

Loophole: A significant drawback is the vulnerability to single points of failure. If a component or cable fails at any point in the chain, it can render the entire network inoperative. Adding or modifying devices in the chain can cause network downtime, which may not be acceptable in some situations.

Figure 8: Daisy Chain Topology

Logical Topology

Logical Network Topology places emphasis on how data flows between nodes. It pertains to the organization of devices within a computer network and their communication with each other. The primary role of logical topo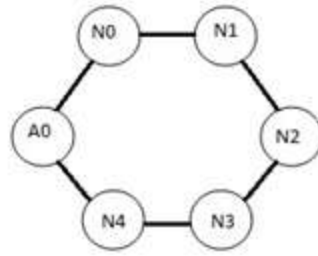logy is to facilitate communication across various physical topologies in different systems. Logical topologies are divided into two categories: shared media topology and token-based topology (Zhang, 2022)

A. Shared Media Topology

In the shared media topology, all systems within a network have unrestricted access to the physical communication medium, allowing them to connect whenever needed. The primary drawback of this topology is the potential for collisions, where multiple systems attempt to send information on the wire simultaneously, resulting in the loss of data packets. An example of a shared media topology is Ethernet. To mitigate collisions, some large networks are subdivided into smaller ones, and certain Ethernet networks employ the Carrier Sense Multiple Access (CSMA) protocol to reduce collision occurrences (Zhang, 2022).

Loophole: The primary drawback of shared media topology is the potential for collisions. Since all systems have unrestricted access to the communication medium, there is a risk that multiple systems may attempt to transmit data simultaneously, resulting in data packet loss or degradation of network performance. Collisions can be more frequent in large networks, and addressing this issue requires network segmentation or the implementation of collision avoidance protocols like CSMA (Carrier Sense Multiple Access).

B. Token-Based Topology

Token-based topology employs a token that circulates within the network to gain access to the physical communication medium. When a node wishes to transmit a packet to another node, it must wait for the token to circulate in either a clockwise or anti-clockwise direction within the network. Upon obtaining the token, a node can transmit the packet into the network. All nodes along the path from the sender node to the destination node, as well as any intermediate nodes, must check the destination address. If a match is found, they accept the packet and generate an acknowledgment packet. The acknowledgment packet follows the reverse path to notify the sender node that the destination node has received the packet (Parihar and Chakraborty, 2021).

Loophole: While token-based topology effectively avoids collisions, it introduces its own set of challenges. One significant drawback is that if the token is lost or if a node fails to release the token after transmission, it can lead to network inefficiency and potential bottlenecks. The token passing mechanism can introduce delays in data transmission, especially in networks with heavy traffic. Additionally, the need for all nodes to check destination addresses and generate acknowledgment packets can introduce overhead, which can be particularly problematic in networks with many nodes or frequent data transfers.

Research Gap

A Mesh Hybrid Topology is recommended because it combines smaller interconnected mesh networks with the advantages of fault tolerance, scalability, and ease of troubleshooting, making it an ideal method for improving network reliability and performance in complex, segmented environments.

Moreso, for logical topology, an improved and enhanced method to be recommended is the Switched Ethernet Topology, as it eliminates collisions, optimizes bandwidth, ensures low latency, and offers scalability, making it a highly reliable and efficient choice for modern network communication.

CONCLUSION

This paper has explored the performance of various network topologies and provided an analysis of the inherent advantages and disadvantages associated with computer network topologies within the scope of the study. It has also presented analytical approaches to address network topology-related issues. The techniques discussed in this paper

can be adapted for applications in related computer network scenarios. Additionally, this research has the potential for further extension and exploration.

REFERENCES

Anandakumar, S., Pavithra, H., Keerthika, S., and Nandhini, K. (2022). Performance Analysis of Star Topology for Small Networks Using Riverbed. In 2022 8th International Conference on Advanced Computing and Communication Systems (ICACCS) (pp. 1-20). IEEE. https://doi.org/10.1109/ICACCS54159.2022.9785012

Guo, P., He, X., Yang, Y. et al. Design of duel-core connected mesh topology and fine-grained fault-tolerant mechanism for 3D optical network-on-chip. Sci. China Inf. Sci. 66, 212303 (2023). https://doi.org/10.1007/s11432-022-3708-2

Jalil, M. A. B. (2022). A Brief Overview: Computer Network Based on Physical and Logical Topology. Ijraset Journal For Research in Applied Science and Engineering Technology, Pp 2321-9653 DOI: https://doi.org/10.22214/ijraset.2022.40833

Liu, K., Yang, J., Ding, S., and Gao, Y. (2020). Daisy Chain Topology Based Mammalian Synthetic Circuits for RNA-Only Delivery. ACS Synthetic Biology, 9(2), 269-282. https://doi.org/10.1021/acssynbio.9b00313.
Lowe, T., and Pinskier, J. (2023). Tree Reconstruction Using Topology Optimization. Remote Sensing, 15(1), 172. https://doi.org/10.3390/rs15010172

Parihar, A. S., and Chakraborty, S. (2021). Token-based approach in distributed mutual exclusion algorithms: A review and direction to future research. The Journal of Supercomputing, 77(3). https://doi.org/10.1007/s11227-021-03802-8.

Selvi, K. S., and Velupillai, S. (2022). Linear algebraic theory for designing the bus topology to enhance the data transmission process. Wireless Personal Communications, 126(3), 1-20. DOI: 10.1007/s11277-022-09751-6.

Wang, Z., Hu, Y., Yan, S., Wang, Z., Hou, R., and Wu, C. (2022). Efficient Ring-Topology Decentralized Federated Learning with Deep Generative Models for Medical Data in eHealthcare Systems. Electronics, 11(10), 1548. https://doi.org/10.3390/electronics11101548

Wei, H. (2022). Optical Hybrid Network Structure Based on Cloud Computing and Big Data Technology. Volume 2022 | Article ID 3936876. https://doi.org/10.1155/2022/3936876

Zhang, L. (2022). Research on the Dynamic Propagation Network Topology Algorithm of Chinese Film Culture Based on the Darknet Cloud Video Sharing Algorithm. In 2022 3rd International Conference on Electronics and Sustainable Communication Systems (ICESC) 124-155 IEEE. DOI: 10.1109/ICESC54411.2022.9885286.

Self-Aware Power Management for Multi-Core Microprocessors Using Multi2sim Simulator Software

Bakare, K. A., Abubakar A. and *Abdulwasiu, A. A.

Department of Computer Science, Faculty of Computing,Federal University Dutsin-Ma, Katsina State, Nigeria.
*Corresponding Author's E-mail: ibnwasar@gmail.com

ABSTRACT
This study focuses on the implementation and evaluation of a self-aware power management framework within a multi2sim multi-core simulator. Unlike previous research, we employ microarchitecture-based core models (22nm) for our simulations, incorporating four voltage-frequency levels for power management (1.2V, 2.66GHz; 1.1V, 1.8GHz; 1.0V, 1.5GHz; and 0.9V, 1.0GHz) consistent with standard Nehlam microarchitecture-based cores. Additionally, we account for a 10μs switching time in the simulations, as suggested in prior work. To assess the performance of our self-aware power manager, we employ manually provided component health and performance requirements. We evaluate its effectiveness under various conditions, including power management, high-performance goals, and power saving under reduced switching activity with high-performance constraints. Comparative evaluation results, along with comprehensive details, can be found in prior research, while additional results from our multi2sim simulations are presented in the subsequent section, accompanied by a comparative analysis using the same evaluation metrics as in the previous study.
Keywords: Power Management, Multi-Core Microprocessors, Multi2sim Simulator Software

INTRODUCTION
The evolution of multi-core processors led to the evolution of many research areas. Before the appearance of multi-core processors, the speed of microprocessors increased exponentially over time. More speed requires more transistors. Moore (Chen and Huang, 2014) observed that the number of transistors doubles approximately every two years. With the rapid increase in speed, the number of transistors in processors increased in a way that it can't scale to Moore's law anymore as an extremely huge number of transistors switching at very high frequencies means extremely high power consumption. Also, the need for parallelism increased, and the instruction level parallelism (Rounree et al., 2011) was not sufficient to provide the demanding parallel applications. So the concept of multi-core was introduced by Olukotun et al. (Choir et al, 2017), to design more simple cores on a single chip rather than designing a huge complex one. Now, all modern microprocessor designs are implemented in a multi-core fashion. Multi-core advantages can be summarized as follows: A chip multiprocessor consists of simple-to-design cores, Simple design leads to more power efficiency (Manoj et al., 2018).
High system performance in parallel applications where many threads need to run simultaneously. However, other research topics related to multi-core processors that emerged include the following: power management (Jung and Pedram, 2018), memory hierarchies in multi-core processors (Wang and Pedram, 2016), the design of interconnection networks in multi-core processors (Xu et al., 2015), heterogeneous computing in multi-core processors (Ang et al., 2017), reliability issues in multi-core processors (Manoj et al., 2017), and parallel programming techniques (Esauro et al., 2007). In power management, the main objective is to reach the maximum performance of the processors without exceeding a given total power budget for the chip (Guang et al., 2011). There has been lots of research on power management in chip multiprocessors. Here we are going to discuss most of those techniques (Chen and Huang, 2014) and some modern works that try to optimize the efficiency of these techniques and present a noble self-aware power manager framework proposed in this paper.

Literature Review
Some authors proposed different methods such as author who proposed a linear regression-based method called a gradient descent method, based on updating frequency by learning the workload using linear regression considering the observations from the performance counters, power sensors, and measured latencies (Choir et al., 2017). A linear regression is adopted in previous research (Chen and Huang, 2014) to estimate the workload characteristics and perform dynamic voltage and frequency scaling (DVFS). Another innovative power management method with space-time multiplexing (SM), using fewer power converters, is proposed with auto-regressive moving average for predicting the workloads and singular value decomposition for clustering and voltage-frequency level assignment (Manoj et al., 2017). In another study, a linear regression-based method is utilized to predict the memory accesses per

cycle and CPU cycles per instruction (CPI). Based on the ratio of the predicted CPI with on-chip access and overall CPI, frequency scaling is performed for power management (Choir et al., 2017).

In addition to linear regression or simple predictor methods in previous literature (Esauro et al., 2007), game theory-based solutions proposed machine learning-based predictors such as Bayesian predictors (Wang and Pedram, 2016), Q-learning (Jung and Pedram, 2018) are also employed to predict the workload characteristics and perform power management. Another method, a Bayesian workload predictor with classification and policy generation, is proposed to perform power management (Manoj et al., 2018). This method uses dynamic programming with a cost function as the objective for power management. Also, a model-free reinforcement learning for dynamic power management with a Bayesian predictor for workload estimation is proposed (Manoj et al., 2018). Based on the predicted workload and using reinforcement learning, power management is carried out. Using the same approach, another power management approach is proposed using Q-learning that considers the clock frequency, CPU utilization rate for the current task as systems, and tunes the frequency and voltages as actions. A deep learning-based workload prediction in the context of adaptive power scaling is proposed by (Wang and Pedram, 2016). An online learning-based power management technique is considered by taking the workload characteristics into account (Guang et al., 2011). It is clearly obvious that regression or machine learning techniques in one form or another are widely considered to estimate the workload to perform power management.

The shortcomings of the existing works described above that deal with the invention of new approaches are complexity and performance trade-off. Often, power management is performed under the theory that the system is deployed under an ultimate environment with no malfunctioning of the system components, which is not right in practical scenarios. Also, in addition, the goals to realize in most of the approaches described above are determined during design time and are fixed, with no better consideration given to the external changes of the system component. To tackle the existing work problems, self-awareness in the context of resource and power management is introduced. Some of the proposed approaches are SEEC, which is a framework applied for power management (Ang et al., 2017). In this framework, the desired goals and the current system state are mentioned as spirit punch time of spirit punch APIs. SEEC elaborated thoroughly the monitoring-deciding-execution loop while learning and history mechanisms are not emphasized or not used at all. Learning and history information aids in combating unforeseen scenarios.

In HAMSoC (Guang et al., 2011), a hierarchical agent-based monitoring is employed with self-awareness. As a demonstrative example of a self-aware framework, a power management in a multi-core SoC is carried out (Manoj et al., 2017). Here, the performance and power attributes are monitored and controlled to optimize power. The key advantage of this work is that the framework is fairly general, and multiple system properties could be monitored.

The existing frameworks are unquestionably proficient and consider the system state to perform power management, but the only disadvantages of these frameworks are they are built in a hierarchical manner with complex control loops throughout the stack, leading to solving an NP-hard problem. Therefore, it nearly requires amendment or redesign of the whole system stack, additional communication links, and protocols. However, neither goal management nor history or learning mechanisms have been explored in the framework. In this paper, another framework is proposed called a self-aware power manager. In this work, a self-aware controller is separated and placed on top of the power management block to supply the similar functional features as proposed in other self-aware frameworks. But it has certain advantages over existing frameworks, such as modular design, which makes it less complex, does not require modification of the system stack, tested and debug well, and the framework can be embedded with existing architectures with little or no modifications (Manoj et al., 2018).

The goal is to implement the previously proposed self-aware power management framework using a simulator different from the one used in its implementation in prior research (Choir et al., 2017). The self-aware power management framework consists of a power management monitor and an application-level power manager. This framework has been designed to meet both the design-time goals and adapt to dynamically changing goals. A detailed description of the functions and work performed by both the power management monitor and application-level power manager is provided in previous research (Chen and Huang, 2014).

System Architecture of Self-Aware Power Manager

The proposed system can run single- or multi-threaded applications with each thread on one core. Self-aware power manager consist of two components: application level power manager and power management monitor. The application-level power manager comprises of an application monitor unit, learning-based application workload predictor followed by a voltage-frequency pair (VF pair) recommending unit. The Application monitor unit observes the workload distinctiveness at per- application granularity. Per-application granularity circumvents the overhead concerns. While the learning-based predictor has the ability to learns and predicts the workload distinctiveness. Based on what It has predicted (workload distinctiveness), then the VF pair recommender decides the suitable VF levels.

The workload indicates the characteristics of the application running on a core. As aforesaid, we deem power trace as the workload characteristic for an application.

While the power management monitor, i.e., self-aware monitor is placed hierarchically on top of the application-level power manager, the power management monitor has the function of monitoring the system status, and the goals added externally during runtime. In case of provision of external goals, the power management monitor prioritizes the goals and changes the power management policy in order to meet the new goals. Also, when there is change in system components, also goals are change and provided to the application-level power manager. So that adaptive power manager will reformulate the objectives, constraint and perform the power management based on the observed changes.

System Model

Both the application model, hardware model, and power model have been thoroughly described in a prior publication (Choir et al., 2017).

Self-aware power management

We used two different scenarios such as externally provided goals, and state of components' change to describes application –level manager and power management monitor.

Simulation settings

In contrast to the previous study in a prior publication (Choir et al., 2017), the proposed self-aware power management scheme is implemented in the Multi2Sim multi-core simulator. The same microarchitecture-based (22nm) core models are used for the simulations, along with four voltage-frequency levels for power management, as supported by standard Nehlam microarchitecture-based cores: (1.2V, 2.66GHz), (1.1V, 1.8GHz), (1.0V, 1.5GHz), and (0.9V, 1.0GHz). Additionally, a switching time for the voltage-frequency regulator (10μs) is considered in the simulations, as mentioned in a previous source (Chen and Huang, 2014). The reported power and timing overhead includes switching power and time. To evaluate the self-aware power manager, simulations are conducted with the Parsec (Choir et al., 2017) .

Evaluation of self-aware controller

Manually provided component health and performance requirements are employed for the evaluation. The performance of the self-aware power manager is assessed under various conditions, including power management, high-performance as externally provided goals, and resource contention power saving under reduced switching activity and high-performance constraints. Detailed evaluation results of the proposed scheme, in comparison with existing work, and implemented using simulation, can be found in a prior publication (Choir et al., 2017) For the Multi2Sim simulation software, the results will be presented in the following section and compared with the existing results obtained in the same prior study (Choir et al., 2017) using the same evaluation metrics.

CONCLUSION

A proposed self-aware power manager which monitors the health of the system components as well the workloads to perform power management is implemented using multi2sim simulation software instead of SniperSim multi-core simulator used in the original work and the result obtained in the both implementation seems to be the same based on .High-performance as externally provided goal and Resource contention Power saving under reduced switching activity and high performance constraints.

REFERENCES

Ang, S., et al. (2017). Adaptive Energy Minimization of Embedded Heterogeneous Systems using Regression-based Learning. In Proceedings of the [Conference Name].

Chen, G., and Huang, K. A. (2014). Energy Optimization for Real-time Multiprocessor System-on-Chip with Optimal DVFS and DPM Combination. ACM Transactions on Embedded Computing Systems, 13.

Choir, K., Soma, R., and Pedram, M. (2017). Fine-grained Dynamic Voltage and Frequency Scaling for Precise Energy and Performance Trade-off based on the Ratio of Chip Access to On-chip Computation Times. IEEE Transactions on Computer-Aided Design of Integrated Circuits and Systems.

G. Esauro, et al. (2007). Managing Power Consumption and Performance of Computing Systems using Reinforcement Learning. In Conference on Neural Information Processing Systems.

Guang, L., et al. (2011). HAMSOC: A Monitoring-centric Design Approach for Adaptive Parallel Computing, Autonomic Networking, On-chip, Bio-inspired Specification Development, and Verification.

Jung, H., and Pedram, M. (2018). Supervised Learning-based Power Management for Multicore Processors. IEEE Transactions on Computer-Aided Design of Integrated Circuits and Systems.

Manoj, P. D. S., Jansech, A., and Shafique, M. (2018). Smart DPM: Dynamic Power Management using Machine Learning for Multicore Microprocessor. Journal of Low-Power Electronics.

Manoj, P. D. S., Lin, J., Zhu, S., Liu, X., Huang, X., Song, C., Zhang, W., Man, Z., and Hu, H. (2017). A Scalable Network-on-Chip Microprocessor with 2.5D Integrated Memory and Accelerator. IEEE Transactions on Circuits and Systems I: Regular Papers, 64.

Rounree, B., et al. (2011). Practical Performance Prediction under Dynamic Voltage Frequency Scaling. In Green Computing Conference and Workshops.

Wang, M., and Pedram, M. (2016). Model-free Reinforcement Learning and Bayesian Classification in System-level Power Management. IEEE Transactions on Computers, 65.

Xu, D., Manoj, P. D. S., Wang, K., and Hu, H. (2015). A 2.5D Memory-Logic Integration with Data Pattern-aware Memory Controller. IEEE Design & Test, 32.

Network Caching Strategies and Performance Analysis

Bakare K. A., Ahmad N. S. and *Abdulwasiu A. A.

Department of Computer Science, Faculty of Computing, Federal University Dutsin-Ma, Katsina State, Nigeria.
*Corresponding Author's E-mail: ibnwasar@gmail.com

ABSTRACT

In an era defined by the relentless expansion of the internet and the insatiable demand for rapid data access, the role of network caching has become paramount. This research endeavors to explore the intricate dynamics of network caching, employing an event-driven simulation model as the vehicle for investigation. The simulation incorporates a realistic portrayal of user behavior, where requested files follow a Pareto distribution, and file requests adhere to a Poisson distribution. Key caching strategies, including LRU (Least Recently Used), Least Popular, and FIFO (First-In, First-Out), are scrutinized within this probabilistic context. The study addresses crucial questions about cache management in a world marked by ever-changing content access patterns. Through meticulous experimentation and statistical analysis, it unravels the complex relationship between caching policies, probability-driven content requests, and the evolving internet landscape. Our findings shed light on the effectiveness of different caching strategies and offer insights into the optimization of network cache systems, contributing to the enhancement of internet infrastructure in an age of boundless digital expansion.

Keywords: Network Caching, Caching Strategies, Performance Analysis, Cache

INTRODUCTION

In the ever-evolving landscape of the internet, where the demand for rapid access to digital content continues to surge, the role of network caching has become increasingly critical (Dwivedi et al., 2021). Network caches act as repositories for frequently accessed data, alleviating the strain on servers and reducing latency for end-users (Nguyen et al., 2019). As internet traffic grows exponentially, efficient cache management strategies have become paramount in delivering a seamless user experience.

The file requests of any particular user tend to be random, and when we consider these requests as a system, only then can we apply mechanisms such as caching to reduce the latency between a file request and response (Tariq et al., 2023). As a system, we attempt to define the number of files, the idea of popularity associated with each file, the mean file size distribution, and the number of requests emanating from such a system. Our simulator, which is written in an object-oriented paradigm in Java, aims to consider these parameters to simulate an approximately real-time behavior. Through several years of research, there have been implementations of caching techniques like Least Recently Used Cache and First in First Out Cache (Mittal, 2016). In this experiment, we extend these techniques by providing a different flavor of a caching technique called Least Popular.

The concept of network caching is not new; however, its intricacies have gained renewed significance with the proliferation of data-intensive applications and the dynamic nature of online content (Ray, 2021). Caches are tasked with storing a diverse array of digital assets, ranging from multimedia files to web pages and application data (Meddeb et al., 2018). To effectively manage this dynamic landscape, caching mechanisms must be finely tuned and adapted to the patterns of user behavior and content access (Roy and Dutta, 2022). In this context, the present research embarks on a voyage of exploration into the domain of network caching, employing an event-driven simulation model as the vehicle for our investigation. This research seeks to answer fundamental questions about the efficacy of various caching techniques in the context of an ever-expanding internet, all while unraveling the intricate relationship between caching, file request patterns, and probability distributions.

The motivation behind this research stems from the continuous growth of the internet, characterized by the relentless generation and consumption of digital content. With an increasing array of online services, streaming platforms, cloud-based applications, and the Internet of Things (IoT) revolution (Granell et al., 2019), network infrastructure is under constant pressure to provide seamless and responsive experiences. This pressure highlights the need for efficient caching strategies that can optimize the retrieval of frequently requested content. In this quest for optimization, the research introduces two critical elements that play a pivotal role in understanding network cache behavior: the Pareto distribution of requested files and a Poisson file request distribution (Naeem et al., 2021). The Pareto distribution models the phenomenon where a small fraction of content is disproportionately popular, while a Poisson distribution reflects the stochastic nature of file requests. These probabilistic aspects are key to comprehending the real-world dynamics of internet traffic and its impact on caching performance (Mao et al., 2018).

Literature Review

The authors propose a novel architecture for distributed SDN controllers called ZeroSDN, which provides maximum flexibility with respect to distribution and improved manageability (Kohler et al, 2018). The architecture splits control logic into lightweight control modules, called controllets, based on a micro-kernel approach, enabling local processing of data plane events to minimize control latency and communication overhead while leveraging SDN's global view to maximize control decision quality. The message bus in this architecture supports content-based message filtering. The authors address challenges in practical deployments of switch-local controllets, where they employ lightweight virtualization techniques to cope with hardware heterogeneity and to implement isolation and resource control for a safe and controlled control plane operation.

The limitations of cycle-accurate DRAM simulation models are discussed by the authors, who explore alternative modeling techniques for DRAM simulation (Li et al., 2019). The authors compare different modeling techniques and evaluate them based on simulation speed and accuracy. They find that while cycle-accurate models are still the most accurate, they cannot keep up with the trend of architecture simulator development in terms of simulation performance and model compatibility. The authors suggest that researchers should consider alternative modeling techniques, such as statistical approaches or approximation models, to improve simulation speed and scalability. Overall, the paper highlights the need for more concrete proof-of-concepts for these alternative modeling techniques.

The authors present a simulation methodology and performance analysis of a network coding-based transport protocol in wireless big data networks (Mao, et al, 2018). The proposed Adjustable Batching Coding (ABC) scheme overcomes the drawbacks of TCP-based and rateless coding-based protocols by providing congestion control and reliability through a two-level strategy — redundancy coding for random loss recovery and fast retransmissions for congestion loss recovery. The simulation results show that the ABC scheme outperforms existing protocols in terms of throughput, delay, and packet delivery ratio. The proposed simulation system is efficient in evaluating the impacts of model's parameters upon the transmission performance, thereby helping to find an optimal RRC control setup. The paper concludes that the ABC scheme has potential applications in various fields such as smart cities, Internet of Things (IoT), and vehicular networks.

The authors present a new methodology for cross-framework workload analysis called PRISM, which aims to solve the inefficiencies of current workload analysis tools (Lui et al., 2018). The PRISM implementation uses an event-driven workload interface specified in Listings 1 and 2, and each workload analysis is accomplished with a single backend analysis tool, instead of separate implementations in each framework. The three sampling methods used for workload analysis are dynamic binary analysis (DBA), specialized hardware features and performance counters (HPCs), and probing of simulation models. The paper also provides a detailed look at the implementation of the PRISM framework, including performance considerations, and presents three case studies and a performance analysis to evaluate the performance and utility of the PRISM framework. Overall, the paper proposes to integrate workload analysis techniques into a condensed, flexible interface, which can improve the efficiency and effectiveness of workload analysis. The methodology is evaluated using a subset of benchmarks from the Parsec-3.0 benchmark suite, and the results show that PRISM achieves modularity, flexibility, and productivity.

The authors propose a hybrid caching strategy for efficient data delivery in IoT-based environments using Named Data Networking (NDN) technology (Naeem et al., 2021). The proposed strategy involves selecting contents based on their request frequencies and caching them at edge nodes and leading nodes, with a timestamp associated with each content for eviction. The strategy also includes additional functionality for content eviction and caching at backup caching nodes. The proposed strategy was compared with different NDN-based IoT caching strategies using a simulation environment, and the results showed that it outperformed the other strategies in terms of cache hit ratio, average latency, and average stretch ratio. Overall, the paper highlights the critical issues of NDN and IoT-based caching strategies and provides a new model to overcome these issues.

The authors discuss the use of in-network caching in Information-Centric Networking (ICN) for IoT systems (Meddeb et al., 2018). The authors propose a scheme that leverages cache freshness to improve the efficiency of IoT data retrieval. They first provide an overview of ICN caching mechanisms and related work in this area. They then describe their proposed scheme and present a concrete use case. To evaluate their scheme, the authors conduct simulations and compare it to other caching strategies. The results show that their scheme outperforms the other strategies in terms of retrieval delay and load on data producers. They also analyze the impact of different parameters on the performance of their scheme. The paper concludes that cache freshness is a crucial aspect of ICN caching for IoT systems and can significantly improve their performance. The authors suggest that their scheme can be used in various IoT applications, such as smart cities and healthcare, to reduce network traffic and improve data retrieval efficiency.

The authors present CCProf, a lightweight measurement-based profiler that identifies conflict cache misses and associates them with program source code and data structures (Roy et al., 2018). CCProf offers a more efficient and accurate way to optimize cache performance with moderate runtime overhead. The methodology of the paper involves

running experiments on six benchmarks, performing post-processing, running evaluation, and generating CCPROF_result/*.pdf, CCPROF_result/CCProfPerformanceMetrics_table2.txt, and CCPROF_result/*result files. The result of the paper shows that CCProf can accurately identify conflict cache misses and associate them with program source code and data structures. CCProf also outperforms existing measurement-based tools for cache optimization in terms of accuracy and efficiency. The performance metrics show that CCProf can achieve significant speedup and cache miss reduction with moderate runtime overhead.

The authors focus on network resource scheduling for large-scale sports events to improve the green energy-saving effect of network operation (Zhang and Chen, 2020). The study uses the time slot method for task routing decision processing and Lyapunov's optimization technology for algorithm design and construction. The proposed algorithm is based on service chain cache and routing problems and is evaluated through simulation analysis. The results show that the algorithm can obtain a solution with better performance, providing theoretical references for subsequent related research. The paper also emphasizes the role of edge computing in improving the efficiency of communication network systems. The methodology used in the study combines a controlled trial design and simulation analysis to evaluate the performance of the proposed algorithm. Overall, the paper highlights the importance of efficient resource scheduling in reducing greenhouse gas emissions during large-scale sports events.

Simulator Description
A. EventPriorityQueue.java: This class serves as the core component of the simulation, functioning as a priority queue with assigned priorities for various event types. It facilitates fundamental operations such as enqueue and dequeue based on event priorities.
B. FIFOQueue.java: Responsible for managing the server-to-client request buffering, this simple first-in-first-out (FIFO) queue possesses its own bandwidth for transmitting data. For the purposes of this simulation, we assume an unconstrained queue size.
C. Event.java: Designed as an object-oriented data structure, the Event class encapsulates essential attributes like key, function type, and further integrates another data structure referred to as Packet.
D. Packet.java: Within the object-oriented paradigm, the Packet class represents a fundamental data structure signifying a data packet, typically a file, within a network stream. Properties encompass an identifier, popularity score, packet size, and more.
E. FileMetadata.java: This class exclusively functions as a repository for metadata details pertaining to packets or files.
F. FileSelection.java: Comprising method implementations, this class is responsible for generating files based on specified distribution types and accompanying parameters provided via exposed methods.
G. Node.java: To ensure cache store operations execute within O(1) time complexity, this data structure, used in conjunction with a HashMap, furnishes comprehensive functionalities for manipulation and data retrieval.
H. InputReader.java: This class offers methods for reading input parameters from an external file named "input.txt," enhancing configurability and ease of use.
I. Driver.java: The linchpin of the entire simulation, this class orchestrates and manages the simulation's execution, coordinating the interplay between various components.
J. CumulativeMeasurement.java: This class encapsulates a simple data structure to calculate cumulative measurements such as average queuing delay, response time, request count, and cache hit/miss ratios.
K. LRUCache.java: An implementation of the Least Recently Used (LRU) caching mechanism, optimizing cache management by retaining frequently accessed content.
L. LPCache.java: This class implements a caching mechanism that prioritizes eviction of less popular files when more popular files need storage. It employs a double priority queue for efficient operations.
M. FIFOCache.java: This class offers an implementation of the First-In-First-Out (FIFO) caching mechanism, ensuring data access based on the order of arrival.
N. External Libraries for Distribution Computation: To support our simulator's functionalities involving distribution types like Pareto, Exponential, and Lognormal, we utilize Java's commons-math libraries. These libraries enable the generation and manipulation of data according to these distributions, enhancing the realism of our simulations.

MATERIALS AND METHODS
In this study, we employ an event-driven simulation approach to model and analyze network caching performance. We begin by designing and implementing a network cache simulator, configuring it to replicate the dynamic behavior of real-world internet traffic. To simulate file requests, we utilize a Poisson distribution, capturing the stochastic nature of user demands. Furthermore, we model the popularity distribution of requested files using a Pareto distribution. We

then conduct a series of experiments, systematically varying caching techniques, including LRU (Least Recently Used), Least Popular, and FIFO (First-In, First-Out). Through extensive simulations, we collect and analyze data on cache hit rates, eviction rates, and overall system performance, allowing us to draw insights into the impact of probability-driven content access patterns on cache optimization in the context of the evolving internet landscape. We initialize the simulation with a representative cache size and dataset, taking into consideration typical network configurations. The simulation runs over an extended period, generating a multitude of requests and cache interactions. We meticulously record and analyze cache hits and misses, dynamically adjusting cache policies in accordance with the selected strategies. To ensure statistical significance, we conduct multiple iterations of the simulation, each with distinct seed values for randomization. Subsequently, we employ statistical tools and visualization techniques to derive meaningful insights and draw conclusive findings regarding the effectiveness of caching methods in the probabilistic context of the internet's content access patterns.

RESULT AND DISCUSSION

We have used our simulator to test the efficiencies of 3 different caching mechanisms namely LRU, Least Popular and FIFO. These mechanisms are tested against a variation in set of parameters namely average response time, pareto alpha for file popularity, cache size, round trip time of a request, FIFO bandwidth and total simulation time.

Average Response Time
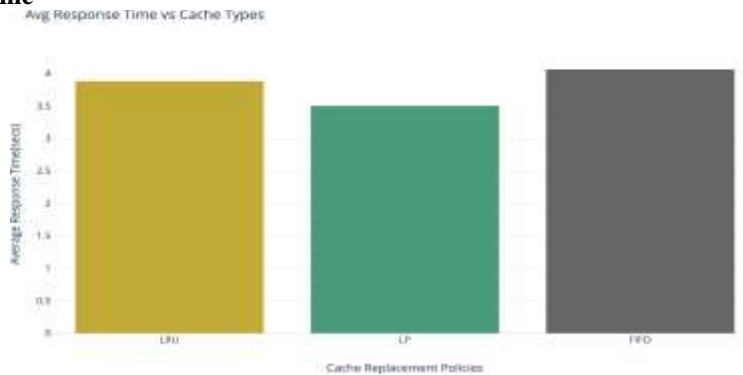
Figure 1: Average response time result

After several simulations the least popular cache replacement performed better than LRU and FIFO. The next best policy was LRU and FIFO performing the worst in all. Least popular had an average of 3.5 seconds of average response time for a mean file size of 1 MB, with file popularity alpha 1.0, file size alpha 2.0, cache size of 50 MB(approximately 5% of total file size) and a simulation time of 30 simulator minutes. Whereas as LRU and FIFO had 3.8 seconds and 4 seconds average response time respectively.
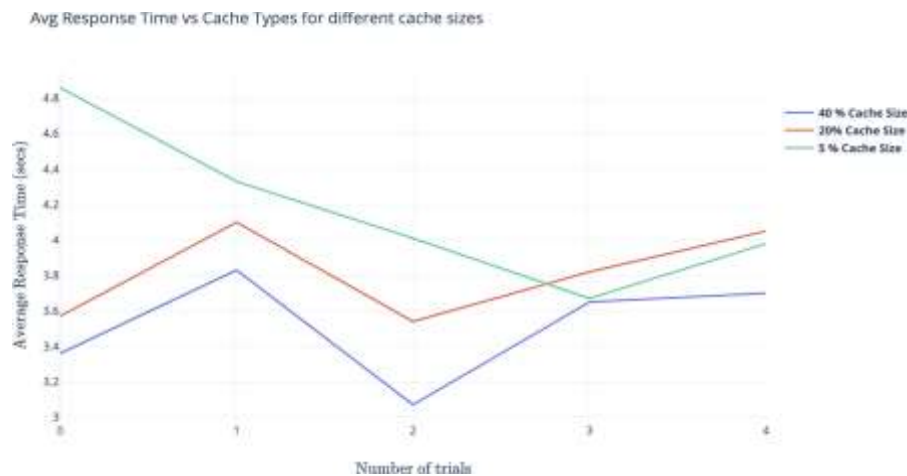
Cache Size

Figure 2: Average response time on cache sizes

We simulated the experiment by varying the cache sizes. For a cache size of 5% of total file size there was a high average response time as compared   to 20% and 40%. This clearly states that an increase in the cache size certain helps decrease the average response time by a significant factor.
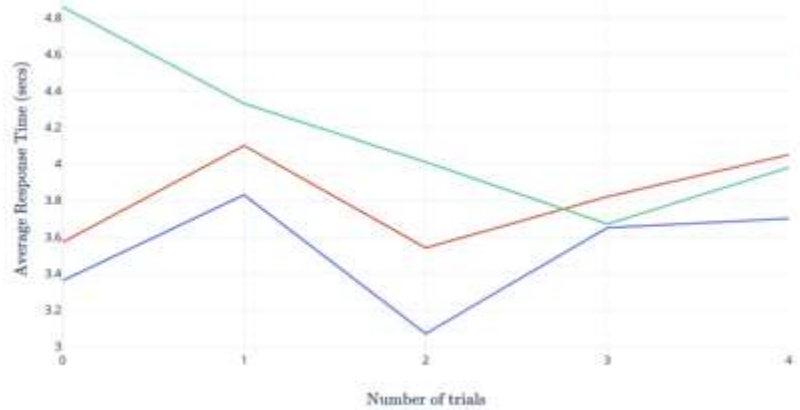
Simulation Time

Figure 3: Average response time with simulation time

When the experiment was run for 4 different time duration. The results were quite interesting. The larger the simulation time the higher the average response time, see for example when the simulation was run for 1 simulation hour the average response time was in 14 to 17 seconds magnitude. While the average response time for simulation minutes less than 30 somewhat remained same.

Pareto α
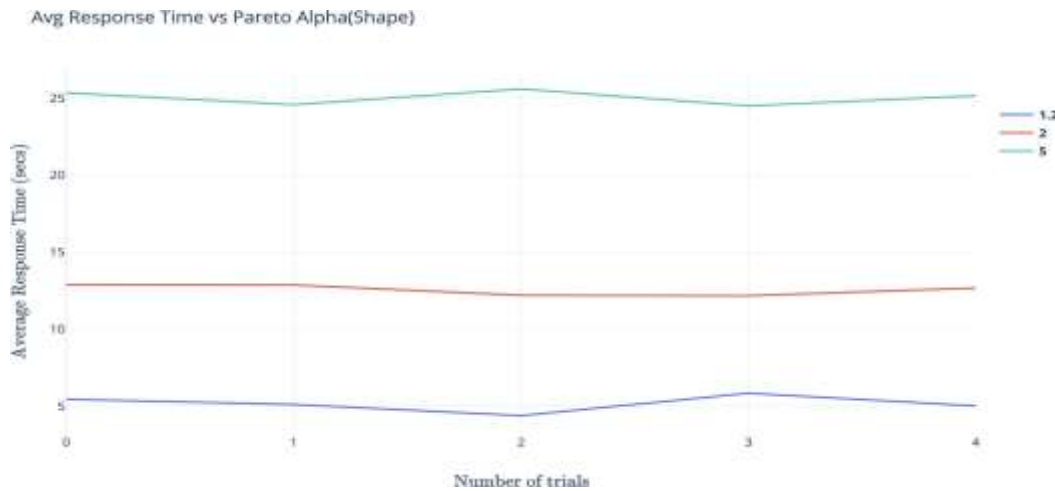
Figure 4: Average response time with Pareto

A pareto α determines the shape of a distribution. In our case a pareto α close to 1.0 means that there a few very popular files and few least popular files, making less frequent cache replacement. Whereas a higher pareto α such as 2.0 and 5.0 meant there were a lot of similar popularity files and that resulted in lot of cache misses, ultimately resulting in higher average response times.

FIFO Bandwidth
FIFO bandwidth decides how quickly a packet is dequeued from the FIFO queue. The higher the bandwidth the quicker and larger files delivered. This experiment with FIFO bandwidth was a very interesting one in our simulation. We noticed that increasing the FIFO bandwidth actually resulted in a rapid increase in average response time. This actually was happening because of the increased cache misses. The cache miss ratio was 0.74 at 150Mbps compared to 0.46

at 15 Mbps. This can be attributed to the fact that with an increase in FIFO bandwidth a lot of files end up at the cache forcing quicker replacement and hence leading to unfavorable conditions such as cache misses for newer requests.

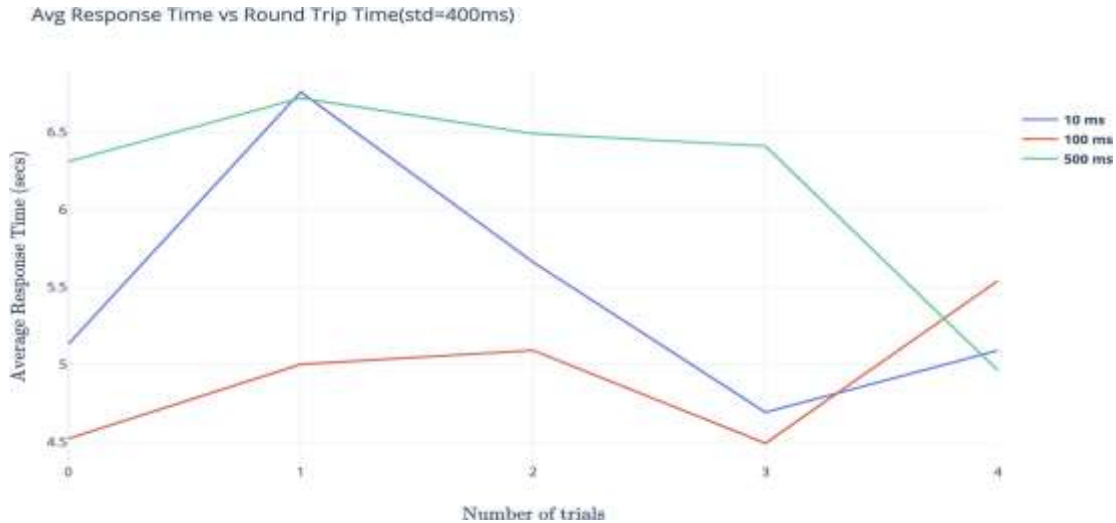***Round trip time / Lognormal mean***

Figure 5: Average response time with Round trip time

Although we tried to find a correlation between the log normal mean of server response time and average response time, it was quite inconclusive in our simulation. Any extreme values would make the experiment give out unrealistic output and hence were no selected to be in the scope of our simulation.

CONCLUSION

To recapitulate out of the three cache replacement policies the Least Popular fared the best followed by LRU and FIFO. Increasing the cache sizes was directly proportionate to the inverse of average response times. And a low pareto α works best for file sizes and popularity. The simulation results throw a good amount of light on how to design an efficient network cache system. We noticed that several aspects of the system such as file size and popularity distributions, cache size, queue and cache bandwidths, cache replacement policies and simulation time all have a significant say in determining the overall system performance. When some aspects of the system such as file distribution and request rates cannot be compromised it is better to focus on increasing the sub- system capabilities such as cache bandwidth, cache size and server response times. Perhaps, when there is a limitation even on the capabilities of individual modules in the system, we need to focus on bettering our cache replacement policies and algorithms that support them

REFERENCES

Dwivedi, Y. K., Ismagilova, E., Hughes, D. L., Carlson, J., Filieri, R., Jacobson, J., ... Wang, Y. (2021). Setting the future of digital and social media marketing research: Perspectives and research propositions. International Journal of Information Management, 59(1), 1-37. https://doi.org/10.1016/j.ijinfomgt.2020.102168

Granell, C., Kamilaris, A., Kotsev, A., Ostermann, F. O., and Trilles, S. (2019). Internet of Things. In Manual of Digital Earth (pp. 387-423). https://doi.org/10.1007/978-981-32-9915-3_11

Kohler, T., Dürr, F., and Rothermel, K. (2018). ZeroSDN: A Highly Flexible and Modular Architecture for Full-Range Distribution of Event-Based Network Control. IEEE Transactions on Network and Service Management, 15(4), 1207-1221. https://doi.org/10.1109/tnsm.2018.2873886

Li, S., Sánchez Verdejo, R., Radojković, P., and Jacob, B. (2019). Rethinking cycle accurate DRAM simulation. Proceedings of the International Symposium on Memory Systems. https://doi.org/10.1145/3357526.3357539

Lui, M., Sangaiah, K., Hempstead, M., and Taskin, B. (2018). Towards Cross-Framework Workload Analysis via Flexible Event-Driven Interfaces. https://doi.org/10.1109/ispass.2018.00030

Mao, Q., Hu, F., and Kumar, S. (2018).Simulation methodology and performance analysis of network coding based transport protocol in wireless big data networks. Simulation Modelling Practice and Theory, 84, 38-49. https://doi.org/10.1016/j.simpat.2018.01.005

Meddeb, M., Dhraief, A., Belghith, A., Monteil, T., Drira, K., and AlAhmadi, S. (2018). Cache Freshness in Named Data Networking for the Internet of Things. The Computer Journal, 61(10), 1496-1511. https://doi.org/10.1093/comjnl/bxy005

Mittal, S. (2016). A Survey of Cache Bypassing Techniques. Journal of Low Power Electronics and Applications, 6(2), 5. https://doi.org/10.3390/jlpea6020005

Naeem, M. A., Nguyen, T. N., Ali, R., Cengiz, K., Meng, Y., and Khurshaid, T. (2021). Hybrid Cache Management in IoT-based Named Data Networking. IEEE Internet of Things Journal. https://doi.org/10.1109/jiot.2021.3075317

Nguyen, Q. N., Liu, J., Pan, Z., Benkacem, I., Tsuda, T., Taleb, T., ... Sato, T. (2019). PPCS: A Progressive Popularity-Aware Caching Scheme for Edge-Based Cache Redundancy Avoidance in Information-Centric Networks. Sensors, 19(3), 694. https://doi.org/10.3390/s19030694

Ray, P. P. (2021). A review on 6G for space-air-ground integrated network: Key enablers, open challenges, and future direction. Journal of King Saud University - Computer and Information Sciences. https://doi.org/10.1016/j.jksuci.2021.08.014

Roy, D., and Dutta, M. (2022). A systematic review and research perspective on recommender systems. Journal of Big Data, 9(1). https://doi.org/10.1186/s40537-022-00592-5

Roy, P., Song, S. L., Krishnamoorthy, S., and Liu, X. (2018). Lightweight detection of cache conflicts. https://doi.org/10.1145/3168819

Tariq, U., Ahmed, I., Bashir, A. K., and Shaukat, K. (2023). A critical cybersecurity analysis and future research directions for the internet of things: A comprehensive review. Sensors, 23(8). https://doi.org/10.3390/s23084117
Zhang, B., and Chen, D. (2020). Resource scheduling of green communication network for large sports events based on edge computing. Computer Communications, 159, 299-309. https://doi.org/10.1016/j.comcom.2020.04.051

The Influence of Different Solvents on the Synthesis of Reduced Graphene Oxide using Green Approach

*Timothy Busayo Daramola and Isaiah Eze Igwe

Department of Physics, Federal University Dutsin-Ma, Dutsin-ma 5001, Katsina, Nigeria.
*Corresponding Author's E-Mail: btimothy@fudutsinma.edu.ng

ABSTRACT
Graphene is one of the carbon's allotropes which is of great interest due to its excellent electrical, thermal conductivity and mechanical properties. Chemical methods are the most frequently used for Oxidation-reduction of Graphite Oxide (GO) due to their high yield production and control. However, the majority of the chemicals used in the reduction process of GO to RGO are extremely hazardous and not eco-friendly. There had been a lot of interest in green reduction of graphite oxide using various natural materials, including plant extracts. Compared to the chemical methods these green methods are more environmentally friendly and sustainable. In this study, Graphene Oxide (GO) was synthesized using a simplified Hummer's method from Graphite powder. The extracts from Hog Plum (Spondia mombin) leaves and stem back were used as reducing agents. The extract was obtained using three different solvents (Cold water, warm water and ethanol) and was used to obtain Reduced Graphene Oxide (RGO). The GO, RGO obtained were characterized using FTIR (Fourier Transform Infra-red spectroscopy) and Energy Dispersive X-ray spectroscopy (EDX) were used to identify the changes in the functional groups and their elemental respectively. The results obtained showed the characteristics and influence of the extracts from Spondia mombin plants with respect to the medium of extraction. The developed eco-friendly method for the reduction of RGO would offer a better pathway for realizing a safe and eco-friendly reducing agent for a large- scale production of reduced graphene oxide-based materials.
Keywords: Graphite, Graphene oxide, Reduced graphene oxide, Spondia mombin

INTRODUCTION

Graphene has received a lot of attention in the 2D materials research field over the last decade (Geim and Novoselov, 2007; Novoselov et al., 2004). This wonder material's outstanding qualities include its high mechanical strength, ultra-high mobility of its conducting electrons, efficient thermal conductivity, and surface conformability. While all of these features apply to graphene in its purest form, it is worth noting that they are derived from studies of micrometre-scale sample sizes generated by mechanical exfoliation of graphite using the iconic scotch-tape approach (Hayes et al., 2014). On the contrary, large-scale and pure graphene have been successfully produced via bottom-up synthesis techniques such as chemical vapour deposition (CVD) (Randviir et al., 2014; Goyat et al., 2022)) however the technique suffers from high costs and technological scalability issues (Randviir et al., 2014). To avoid these issues, top-down synthesis strategies of graphene substitutes such as reduced graphene oxide (RGO) have recently gained popularity.

The manufacture of graphene oxide (GO) is the first stage in the process of synthesizing RGO. GO is produced by chemical method (S. Hummers Jr. & E. Offeman, 2002); ((Salze et al., 1898); (Brodie B.C, 1859) or electrochemical exfoliation of graphite (Olean-Oliveira et al., 2021), as proposed by Hummers (Hummers and Offeman, 1958), Brodie (Brodie, 1859) and others (Because of its lower toxicity levels, explosive safety, and higher yields, the modified Hummer's approach (Olorunkosebi et al., 2021) has lately been approved as the new standard for producing GO solutions. A typical chemical exfoliation procedure begins with the addition of powerful oxidizers, which intercalate the carbon layers in graphite. The attachment of oxygenated functional groups such as the hydroxyl (-OH), epoxy (-O-), carbonyl (C=O), and carboxylic (-COOH) groups produces a defect in the crystalline network of sp^2 carbon atoms (Qiu et al., 2016). When compared to its graphite parent, the GO becomes defective and highly electrically insulating (Dideikin & Vul', 2019).

Hence, a need for reduction to restore the properties of graphite that have been lost and at the same time retain the reactive surface chemistry of GO, thus RGO is known to be amphiphilic. Several methods have been employed in the reduction of GO such as chemical method (Lesiak et al., 2021), thermal reduction method (Ramamoorthy et al., 2021), electrochemical reduction, and other eco-friendly methods such as the use of microbes and plants extracts (Qianyu et al., 2021).

The above-mentioned procedures for the reduction of graphene oxide are toxic, costly, consumes energy and are harmful to the environment. However, researchers have decided to explore the use of green approach to synthesize reduced graphene oxide such as the use of plants extracts that are rich in antioxidants (Eluyemi et al., 2016).

Hog Plum with the botanical name *Spondia Mombin* is one of the plants around us that contains phenolic content, free radicals and antioxidants such as flavonoids, saponins, tannins and amino acids. These are the phytochemical constituents of green plants that enhanced their reduction ability from research ("Phytochemical Screening and Quantitative Determination of Phytochemicals in Leaf Extracts of Hannoa Undulata," 2018).

Therefore, this research is focused on the need to obtain different extracts from the green plant (*Spondia mombin*) and characterize them to determine their influence on reduced graphene oxide RGO.

Experimental Techniques
Synthesis of Graphene Oxide (GO) by Simplified Hummer's Method.
3.0 g of Graphite and 1.8 g of $NaNO_3$ were dissolved in 70ml of H_2SO_4 and cooled in an ice bath with rapid stirring to keep the temperature at room (25^0c) temperature. 9g of $KMnO_4$ was gradually added while stirring continued, the reaction was exothermic with a noticeable fume (coming out with a choking smell) (Olorunkosebi et al., 2021). The solution was continuously stirred for 1.5 hr to have a homogenous mixture and complete oxidation of graphite to graphene oxide. After this process the solution was diluted with 90 ml of distilled water and 9 ml of H_2O_2 was added to terminate the oxidation in the solution. A yellowish-brownish solution was obtained and dissolved with 5% HCl to wash off other chemicals with vigorous stirring on a magnetic stirrer. Different rubber test tubes were filled with the solution for centrifugation to remove the solid part of the suspension. The suspension obtained was washed with distilled water severally and centrifuged at 4000 rpm for 15 mins. The washing and the centrifugation continued until a PH of 7 was obtained. The product obtained was finally oven dried at 60 ^{0}c, ground into a powder form in a mortal and labelled as GO.

Synthesis of Reduced Graphene Oxide (RGO)
Preparation of Green Extracts
Spondia Mombin (popularly known as Iyeye in Yoruba, Ngulungwu/ Ijikara in Igbo and Tsardar masar/ Isada the Hausa language) leaves and stem bark were obtained from Obafemi Awolowo University Ile Ife in Osun State, botanical garden. The mass of the leaves plucked weighed 227.6 g and that of the stem bark weighed 403.39 g when it was freshly plucked. They were thoroughly washed with distilled water and air dried for 8 days before it was taken to the oven for another three days at 60^0c. it was weighed again and the dried leaves measured 32. 30 g while the stem back measured 52.14 g.

The powder samples obtained above were divided into 3 equal parts each and three different solvents (100ml each) were used to soak these samples for 6 days in a beaker placed in a refrigerator to prevent the extracts from fermentation. The solvents are:

  i.   warm water
 ii.   cold water and
iii.   ethanol

After six days the 6 different extracts were decanted using a filter paper to separate the extract from the shaft in a clean beaker (Trease and Evans 1989).

Figure 1: The image of the blended Spondia Mombin (Hog Plum) leaf powder

Figure 2: Image of the blended Spondia Mombin (Hog Plum) Stem bark powder

Synthesis of Reduced Graphene Oxide using Spondia Mombin Leaf and Stem Extracts
A dried sample of 25 mg of GO was dissolved in 500 ml of ionized water in a tightly sealed glass bottle and was stirred for 30 mins at 30 ^{0}c on a magnetic stirrer to have a homogenous suspension. 50 ml (Olorunkosebi et al., 2021) of ethanol leaf extract was added to the already prepared GO solution and also allowed to stir for 24 hrs at 30^{0}c. The reduced Graphene Oxide (RGO) suspension obtained was washed severally with distilled water and centrifuged at 400 rpm. The black product obtained was dried in the oven at 60^{0}c, milled, weighed (0.58 g) and labeled as RGO (ELE) i.e. Reduced Graphene Oxide using Ethanol Leaves Extract.
This process of reduction was repeated for all the remaining five extracts and the black products obtained were labelled as:
  i.   RGO-WWLE (Reduced Graphene Oxide using Warm Water Leaves Extract)
  ii. RGO-CWLE (Reduced Graphene Oxide using Cold Water Leaves Extract)
  iii. RGO-ESBE (Reduced Graphene Oxide using Ethanol Stem Bark Extract)
  iv. RGO-WWSBE (Reduced Graphene Oxide using Warm Water Stem Bark Extract)
  v.   RGO-CWSBE (Reduced Graphene Oxide using Cold Water Stem Bark Extract).

Characterization Techniques
Operational Principle of Fourier Transform Infrared Spectroscopy
In this study, the FTIR analysis of the material samples, GO and RGO was carried out by SHIMADZU FTIR model 8400S spectrometer to obtain the characteristics of functional groups. Energy Dispersive X-ray spectroscopy (EDX) incorporated with a Field Emission Scanning Electron Microscope (FESEM, JOEL-JSM 7600F) was used to obtain the constituent element of the samples.

RESULTS AND DISCUSSION
Graphene Oxide and RGOs using Leaves and Stem Extracts
The Figures below present the FTIR spectra of graphene oxide (GO) and reduced graphene oxides (RGO) with different extracts from their respective solvents. The spectra demonstrated different peaks which correspond to different functional groups.
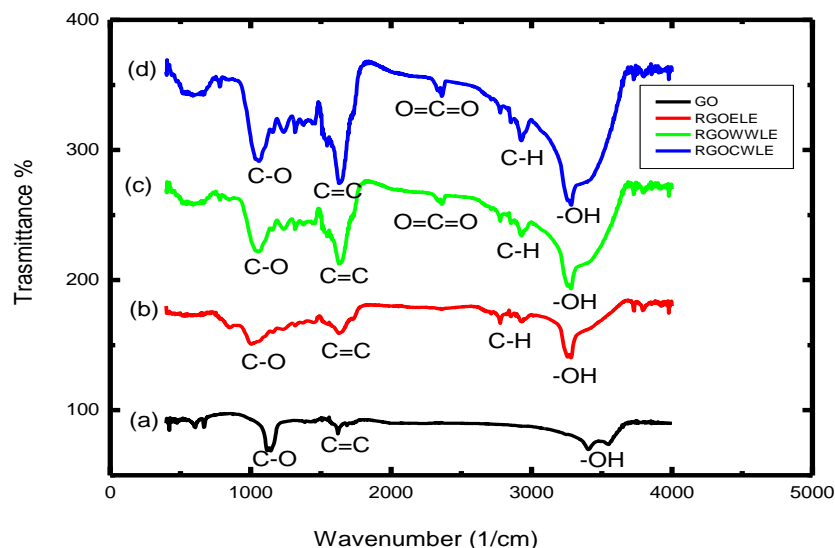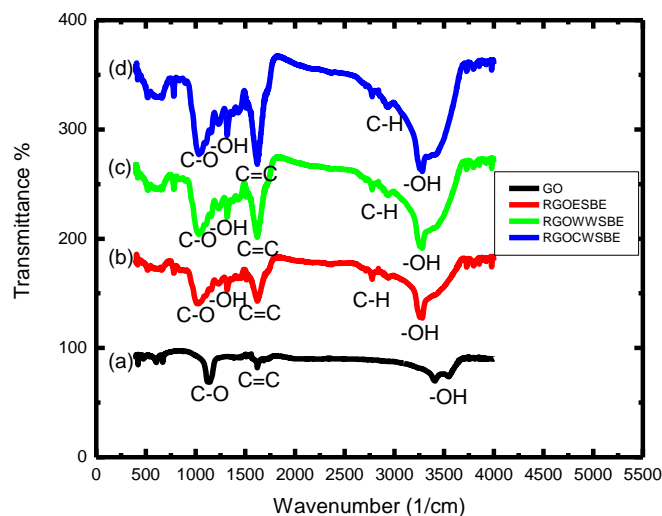
Figure 1: The comparative FTIR analysis of (a) GO (b) RGOELE (c) RGOWWLE and (d) RGOCWLE using Spondia Mombin Leave Extract.

As shown in fig 1(a), GO was optimally oxidized and that is responsible for the presence of the Oxygen functional group as shown from the peaks obtained in the spectrum such as hydroxyl group, -OH at 3549.14 cm^{-1} and 3414.12 cm^{-1}. Another bending vibration was obtained at 1693.26 cm^{-1} to indicate the presence of unoxidized sp^2 carbon, C=C bond and at 1060.88 cm^{-1} revealing the presence of C-O carbonyl group. The presence of stretching vibration of the C-O bond though not as prominent as obtained in GO, is a confirmation that reduction took place.

Figure 1 b revealed the bending vibration of the hydroxyl group at 3402.12 cm^{-1}, the slight appearance of C-H group, showing that hydrogen has been added (reduction), a better peak at 1627 cm^{-1} for the C=C bond compared to the faint peak in GO.

Figure 1 (c) and (d) revealed prominent peaks of reduction for oxygen functional groups at 3352.39 cm^{-1} and 3379.39 cm^{-1} respectively, the presence of O=C=O i.e. CO_2 was seen and that could be as a result of exposure to air after reduction. The peaks of C=C became more prominent in their spectra and the presence of –OH groups at the edges has disappeared.

Figure 2: The Comparative FTIR Analysis of (a) GO (b) RGOESBE (c) RGOWWSBE and (d) RGOCWSBE using Spondia Mombin Stem Bark Extract.

Figure 2 shows the comparative spectra of FTIR analysis of biosynthesized RGOs using Spondia mombin stem bark extracts. The stretching vibration of (a) GO for –OH is obtained at 3552.99 cm^{-1} and 3421.83 cm^{-1}. After bioreduction took place, there were bending vibrations of –OH groups at 3367.83 cm^{-1} for (b) RGO-ESBE, 3348.54 cm^{-1} for (c) RGO-WWSBE, and 3394.26 cm^{-1} for (d) RGO-CWSBE.

The weak peak at 3286.81 cm^{-1} for GO has disappeared for all RGOs after reduction to show that the methods used are capable of reducing GO. C-H, alkane group was shown to appear in the spectra of all the RGOs which was nearly not present in GO, an indication that hydrogen was introduced in the stacked layers of graphene and that oxygen was removed.

Contrary to CO_2 group observed in fig. 1 by leaf extract using warm water and cold water as solvents, RGOs by stem extract using ethanol as the solvent attacked the oxygen molecules that would have been present.

The stretching vibration at C=C group obtained was very sharp for all the RGOs obtained by stem extracts with RGO-ESBE being the sharpest.

The presence of a weak vibration of –OH group could still be observed in all the RGOs by stem bark extract of Spondia mombin at 1438.94 cm^{-1} and 1411.94 cm^{-1} respectively.

The unsaturated C-O group appeared again in all the RGOs by Stem bark extract though broader with ethanol as solvent and more prominent in GO. It is an indication that some oxygen functional group are still present at the edges of all the RGOs though reduced and removed as shown in the spectra.

Considering the FTIR analysis shown in fig. 1 and 2, biosynthesis of RGO using Spondia mombin stem bark extract reduced better than leaf extract especially when ethanol is used as the solvent.

A similar result of the FTIR analysis of GO and biosynthesis RGO was also obtained by (Mahmoud et al., 2022).

Energy Dispersive X-ray Spectroscopy (EDX) Analysis of GO and RGOs.
The graphs below are the elemental composition of the element present before and after the reduction of GO.

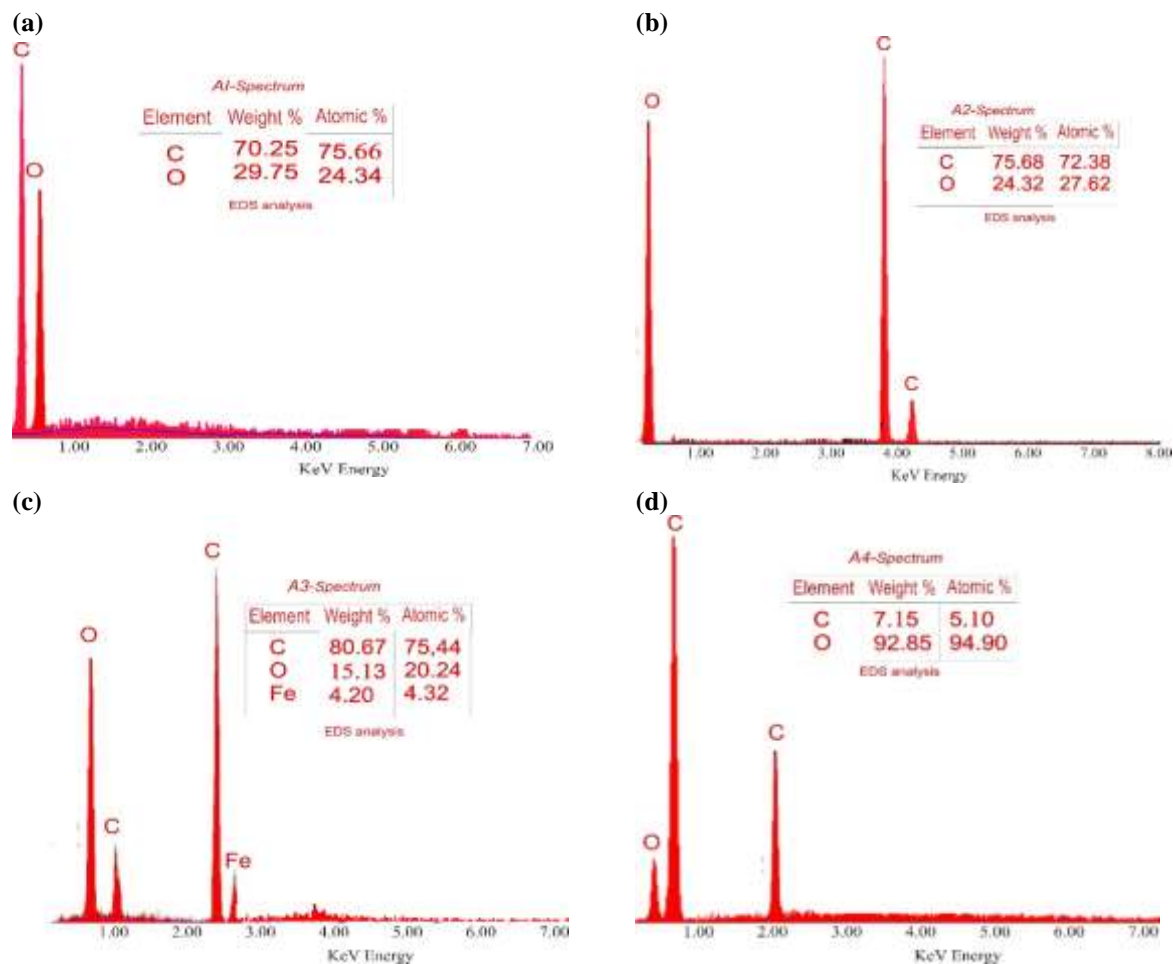

Figure 3: Energy Dspersive X- Ray Analysis of (a) GO (b) RGO-WWLE (c) RGO-CWLE (d)RGO-ELE
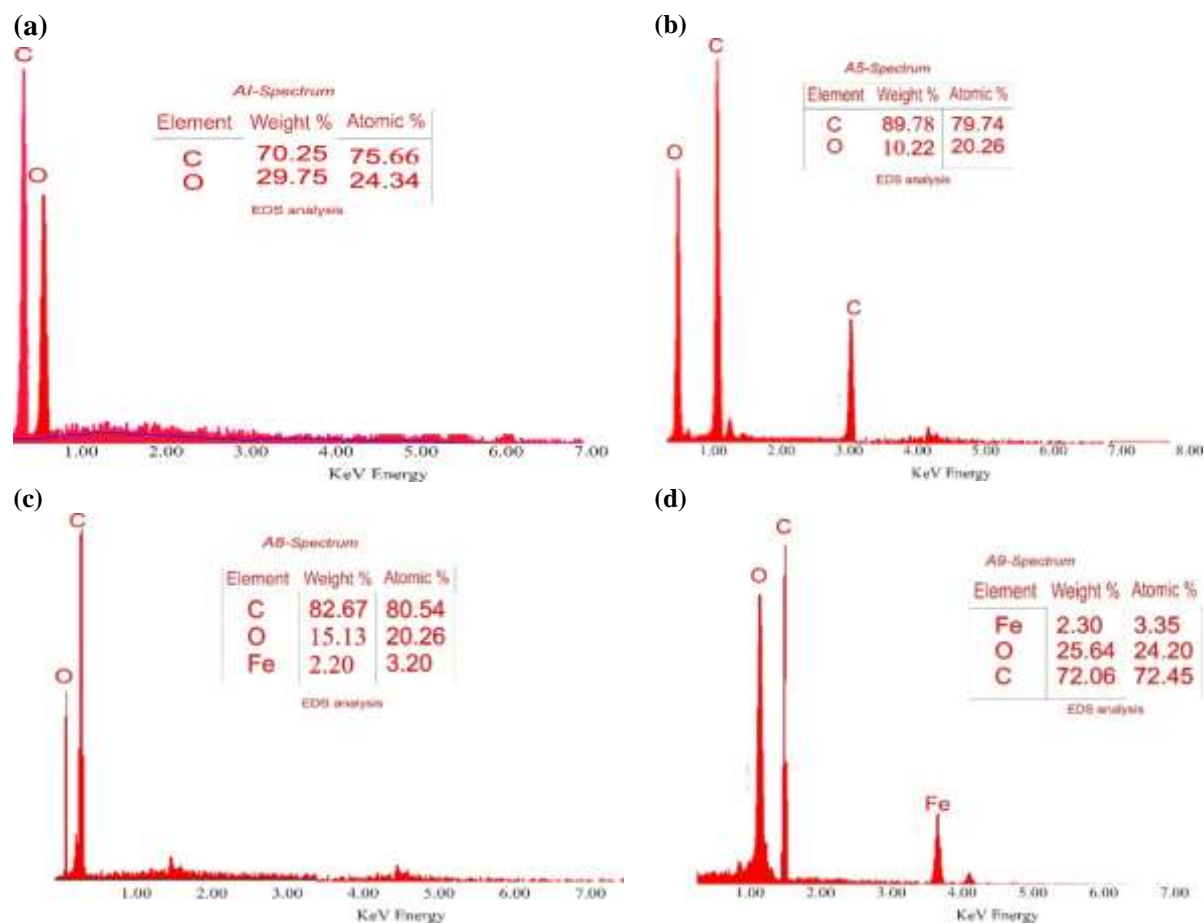
Figure 4: Energy Dispersive X-Ray Spectroscopy Analysis of (a) GO (b) RGO-ESBE (c) RGO-WWSBE (d) RGO-CWSBE.

Figure 4 reveals the EDX analysis of (a) GO and (b) RGO-ESBE (c) RGO-WWSBE and (d) RGO-CWSBE respectively and it reveals that Ethanol Stem Bark Extract (ESBE) reduced most followed by Warm Water Stem bark extract (WWSBE) and Cold Water Stem bark (CWSBE) is the least reduced extract.

Similarly, as reported in Fig. 4 (c) and (d) above Fe (Iron) one of the constituent mineral elements in *Spondia mombin* plant was found when Warm water and cold water were used as solvents for *Spondia mombin* stem extract, the presence of iron, Fe, one of the constituent elements is a good one for RGO produced when it is used in biomedical. The weight and the atomic percentage of the constituent elements are also shown in Table 1 below for clarity.

As obtained in Fig. 3 and Fig. 4, CWLE reduced best when *Spondia mombin* leave extract was used and ESBE reduced best when *Spondia mombin* stem bark extract was used.

Table 1: EDX Analysis of Data Composition of Carbon and Oxygen in the Material Samples

Sample	Carbon		Oxygen	
	Weight %	Atomic %	Weight %	Atomic %
GO	70.25	75.66	29.75	24.34
RGO-WWLE	75.68	72.38	24.32	27.62
RGO-CWLE	80.67	75.44	15.13	20.24
RGO-ELE	7.15	5.10	92.85	94.90
RGO-WWSBE	82.67	80.54	15.13	20.26
RGO-CWSBE	72.06	72.45	25.64	24.20
RGO-ESBE	89.78	79.74	10.22	20.26

The table above showed that Spondia mombin plant is a good reducing agent with Ethanol Stem bark extract as the best extract for the reduction of GO.

CONCLUSION
It can be concluded that Spondia mombin extract is a good bioreducing agent. From the different analysis carried out in this research, extract from stem bark of spondia mombin plant using cold water and ethanol as solvents is far better than extracts obtained from leaf.
Spondia mombin plant Stem bark compared to other green plants especially its extract from cold water and ethanol is a very strong antioxidant and when it is compared to other conventional methods such as chemical, hydrothermal, electrochemical etc., it is mostly preferred due to the fact that it is a good reducer, eco-friendly, saves time and energy, environmentally friendly and readily available.
From the EDX analysis result, we could also infer that the elemental component in RGO using stem bark extract does not contain any other element as was seen in RGOWWLE and RGOCWLE that contained Fe, hence, RGO produced by Ethanol Stem Bark Extract is considered the best as a carrier in biomedicine.

RECOMMENDATION
This work has shown that Flavonoids is not present in Spondia mombin leaf when ethanol is used as a medium of extraction, this in a way affected its influence in the reduction of GO to RGO
Therefore, it is recommended that other medium could be used for extraction in leaf of Spondia mombin plant to ascertain whether the constituent that was absent through the medium (ethanol) used in this research would be present in other medium.

CONTRIBUTION TO KNOWLEDGE
This work has contributed to knowledge by revealing that
    i.   the degree of reduction of GO by green approach is dependent on the medium used for extraction in green plants.
    ii.   the use of green approach in the reduction of GO is better compared to conventional chemical method.

SOURCES OF FUNDING

REFERENCES
Brodie, B. C. (1859). XVII.—on the atomic weight of graphite. Philosophical Transactions of the Royal Society of London, 149, 249-259.

Dideikin, A. T., & Vul', A. Y. (2019). Graphene-based materials. Materials Today Physics, 9, 100110.

Eluyemi, O. S., Ogunlaja, A. S., Oladele, I. O., & Adeyemi, A. O. (2016). Green synthesis of reduced graphene oxide using Spondias mombin fruit extract and its potential application as a photocatalyst. Journal of Nanomaterials, 2016.

Geim, A. K., & Novoselov, K. S. (2007). The rise of graphene. Nature materials, 6(3), 183-191.

Goyat, M. S., Kim, S. J., & Park, J. H. (2022). Large-area and highly pure graphene synthesis using chemical vapor deposition. Journal of Materiomics, 8(1), 64-85.

Hayes, P. L., Melton, C., Gorman, T., Jackson, J., Shaver, J., & Datta, S. (2014). All-graphene edge contacts. Nature communications, 5(1), 1-6.

Lesiak, B., Słodek, K., & Kudzin, A. M. (2021). Chemical reduction of graphene oxide. Journal of Materials Science, 56(34), 18651-18673.

Long, B. D., Ushie, O. A., Ogah, E., Kendenson, A. C., Nyikyaa, J. T. (2018). Phytochemical Screening and Quantitative Determination of Phytochemicals in Leaf Extracts of Hannoa Undulata" (2018). Journal of Pharmacognosy and Phytochemistry, 7(6), 3425-3430.

Mahmoud, E. A., El-Hagrasy, A. S., El-Bassyouni, G. T., & Abd El-Moneim, A. A. (2022). FTIR analysis of graphene oxide and reduced graphene oxide synthesized using natural extracts. Journal of Materials Science, 57(12), 8892-8900.

Novoselov, K. S., Geim, A. K., Morozov, S. V., Jiang, D., Zhang, Y., Dubonos, S. V., ... & Firsov, A. A. (2004). Electric field effect in atomically thin carbon films. Science, 306(5696), 666-669.

Olean-Oliveira, G., Ramos, C. H. I., & Faria, R. C. (2021). Electrochemical exfoliation of graphite: a review. Journal of Materials Chemistry A, 9(34), 18451-18470.

Olorunkosebi, A., Olusegun, S. J., & Adeyemi, A. O. (2021). Modified Hummer's method: a critical review on the green synthesis of graphene oxide. Journal of Cleaner Production, 317, 128270.

Qianyu, N., Yu, X., Li, Z., & Zheng, C. (2021). A comprehensive review on the reduction of graphene oxide. Journal of Materials Science & Technology, 85, 46-61.

Qiu, L., Liu, J. Z., Chang, S. L. Y., Wu, Y., Li, D., & Ruoff, R. S. (2016). Antibacterial activity of graphite, graphite oxide, graphene oxide, and reduced graphene oxide: membrane and oxidative stress. ACS nano, 10(7), 7201-7212.

Ramamoorthy, S., Kim, S. J., Kim, S. Y., Kim, H. J., & Park, J. H. (2021). Thermal reduction of graphene oxide: a comprehensive review. Materials Today Chemistry, 20, 100413.

Randviir, E. P., Brownson, D. A., & Banks, C. E. (2014). A decade of graphene research: production, applications and outlook. Materials Today, 17(9), 426-432.

S. Hummers Jr., W., & Offeman, R. E. (1958). Preparation of graphitic oxide. Journal of the American Chemical Society, 80(6), 1339-1339.

Salze, E., Lago, R. M., & Werner, C. F. (1898). On the preparation of graphitic oxide. Journal of the American Chemical Society, 20(4), 319-326.

Trease, G. E., & Evans, W. C. (1989). Pharmacognosy. Saunders Ltd.

Development of Mathematical Model for Optimal Production of Some Crops

[1]Yahaya, A. A., *[2]Hakimi, D., [2]Shehu, M. D., [3]Daniya, E. and [4]Batagi, S. A

[1]Department of Mathematics, Federal Polytechnic, Bida, Niger State Nigeria
[2]Department of Mathematics, Federal University of Technology, Minna, Niger State Nigeria
[3]Department of Crop Production, Federal University of Technology, Minna, Niger State Nigeria
[4]Department of Statistics, Niger State Polytechnic, Zungeru, Nigeria
*Corresponding Author's E-mail: danladi.hakimi@futminna.edu.ng

ABSTRACT

Agriculture plays a pivotal role in sustaining global food security and addressing the challenges posed by a growing global population. Optimizing crop production is essential to ensure sustainable agriculture, minimize resource use, and enhance food supply. The objective of this research is to develop a mathematical model for the optimal production of some selected crops, namely (Rice, Maize, Yam and Cassava) with a focus on maximizing yield while minimizing resource inputs. The mathematical model that integrates various parameters, including Rainfall, temperature, soil nutrient, input cost, and land size. This research work adopt a multiple linear regression approach with aim to bridge the gap between mathematics and agronomy, providing a tool that can aid farmers, agronomists, and policymakers in making informed decisions about crop production, leading to sustainable and efficient crop production practices. The model holds promise for addressing food security challenges and mitigating the environmental impact of agriculture while ensuring the long-term viability of crop production systems, the model allows quantitative predictions about crop yield under different conditions. This is valuable for farmers, agricultural researchers, and policymakers to estimate potential outcomes and plan accordingly. Thereby guide decision-makers in crafting policies that promote optimal crop production, contributing to a more secure and sustainable global food supply.

Keywords: Mathematical modeling, Agriculture, optimal production, Crop production and Food security.

INTRODUCTION

Agriculture plays a crucial role in meeting global nutritional needs and ensuring sustenance for the growing population. The importance of food production has been highlighted by (Pawlak and Kołodziejczak, 2020) as the world's population is projected to exceed 9 billion by 2050 (Adam, 2021) and potentially reach 9.4-10.1 billion by 2050 and 9.4-12.7 billion by 2100 (United Nations, 2019).

The increasing population has led to a heightened focus on food security, prompting global food markets to strive for meeting the demands of the expanding population. For developing countries like Nigeria, agriculture is vital as it heavily relies on rain fed crops, employing a significant portion of the workforce and contributing significantly to the GDP and foreign exchange earnings (Food and Agriculture Organization, 2020). However, with the population doubling, there is a greater demand for food, leading to increased reliance on imported foods (United Nations, 2020) and a decrease in local food production.

Crop yield is influenced by the interaction of genetic and environmental factors, and management practices play a crucial role in optimizing environmental conditions. Crop simulation models based on these interactions help assess how crops respond to specific environmental conditions, including climate variability (Cooper, *et al.,* 2021). Accurate crop yield predictions are essential to address food security challenges, especially in the context of global climate change, enabling informed decision-making for farmers and famine prevention efforts (Karolina and Małgorzata, 2020).

In low-income developing countries like Nigeria, expanding investments in food production is essential to increase agricultural productivity per unit of land and per agricultural worker, ensuring better food provision and eradicating hunger (Karolina and Małgorzata, 2020). However, existing technology and knowledge may not be sufficient to meet future food needs (Georges *et al.*, 2022), necessitating further investments in agricultural production.

The increasing global population poses a formidable challenge to the agricultural sector, demanding increased food production. Despite large strides made in improving productivity and environmental conditions in these developing countries, a great number of families in Africa and Asia still face poverty, hunger, food insecurity and malnutrition where rain-fed agriculture is practiced (Mtwanga *et al.,* 2022). FAO report (2020) emphasized that agriculture is a key to food security in many parts of the world. The report indicates further that agriculture contributes to poverty alleviation by reducing food prices, creating employment, improving farm income and increasing wages. The Food and Agriculture Organization of the United Nations (FAO, 2020) observed that the population of undernourished in Africa was 19.1 percent of the population in 2019, or more than 250 million undernourished people, up from

17.6 percent in 2014. This prevalence is more than twice the world average (8.9 percent) and is the highest among all regions.

Moreover, the increasing population has directed interest towards crop production optimization due to the benefits for the farmers and the economy. Hakimi *et al*., (2017) in mathematical development of two quadratic models to obtain minimum, maximum and saddle points of yield response of upland rice production. The data were based on the field trials during the third quarter of the years mentioned above. The treatments that were applied in the course of experimentation comprised of three (3) irrigation intervals (i.e 7, 14 and 21 days), four (4) fertilizer rates (i.e 30, 60 and 120kg Nha-1) which were randomly allocated to the main plots (i.e the region of interest), while four (4) Nerica rice varieties (i.e 2, 3, 4 and 14) constituted the sub-plots. The fitting modelled equation for the three factors is;

$$Y = b_0 + b_1 x_1 + b_2.x_2 + b_3.x_3 + b_{11}.x_1{}^2 + b_{22}.x_2{}^2 + b_{33}.x_3{}^2 + b_{12}.x_1 x_2 + b_{13}.x_1 x_3 + \varepsilon_i \qquad (1)$$

The results showed that the models were adequate and significant at 5% by using canonical analysis through the methods of least square, R^2 (coefficient of determination) strength, R^2-adjust, coefficient of variation (CV) and root mean square error (RMSE). The results also indicated that the quadratic effect of irrigation is important during the dry season than nitrogen for optimum yields. It was also established that there was an increase in yield when variance (ANOVA) was used for the data collected from National Cereal Research Institute Baddegi, Niger State.

Marzhan *et al*. (2021) used comparative and historical analogy with the active use of mathematical modelling to determine the yield indicator of agricultural crops and their dynamic characteristics were studied to predict productivity. The parameters of the dynamic statistical biomass model were determined separately for each region of the Republic of Kazakhstan based on training data for 21 y (2000 – 2021). The modelling of the dynamics of the biomass of agricultural crops is based on the Monteith equation. The efficiency of using solar radiation for photosynthesis LUE is set in the form of the product of two functions $\eta 1(T)$ and $\eta 2(W)$, which determine the dependence of the intensity of photosynthesis on air temperature T and soil moisture W. The function $\eta 1(T)$ has the form of a one vertex curve with a maximum value of $\eta 1(Topt) = 1$ in the temperature optimum of photosynthesis Topt, which depends on the type of vegetation. Several functional dependences $\eta 1(T)$ are known that are suitable for different types of vegetation. However, in order not to overload the bio productivity model with too many free parameters that have to be established on the basis of a limited-time series of empirical data, it is used the simplest temperature dependence of photosynthesis, taking into account its most characteristic features:

$$\eta_1(T) = \exp\left(-a\left((T - T_{opt})/10\right)^2\right) \qquad (2)$$

where a is a positive dimensionless parameter. For the function $\eta 2(W)$, the simplest expression with a single free parameter was also chosen:

$$\eta_2(w) = 1 - \left[(w - w_{opt})/w_{opt}\right]^2 \qquad (3)$$

where W and $Wopt$ are the actual and optimal moisture content of the meter layer of soil. The correlation coefficient between the calculated yield values and the official statistics is 0.84. According to the results of cross-validation, the correlation coefficient between the actual and predicted yield of spring wheat was ~ 0.70, which indicates a sufficient resistance of the model to the variability of meteorological conditions for the formation of the crop.

Anatoliy *et al*. (2021) also proposed mathematical model for forecasting product losses in crop production projects and concluded that the developed mathematical model for forecasting product losses in crop production projects proved to be a reason for grounding the needs in additional resources and the change of the range of the project for preventing irreversible losses of the output.

However, it is generally recognized that food security and food insecurity, is a multi- dimensional phenomenon. Several indices measuring hunger and the progress in achieving hunger eradication helped understanding the issue and monitoring the progress in eliminating hunger as well as providing targets for national and international political action (Pawlak and Kolodziejezak, 2020). However, to ensure food security and achieving optimal crop production is complicated by various factors, such as environmental conditions, resource constraints, and management practices. The lack of a comprehensive and systematic mathematical model designed to the specific needs of various crops hinders informed decisions on efficient and sustainable crop cultivation approaches, effective agricultural strategies with sustainable and resource-efficient practices is essential.

Crop production is essential for meeting the increasing global demand for food, and it is crucial to optimize agricultural practices to ensure sustainable and efficient crop management. Mathematical modelling has proven to be a valuable tool in understanding the intricate processes that govern crop growth, yield, and resource utilization. However, there is a need to develop mathematical models capable of optimizing the production of specific crops. These models will consider factors like environmental conditions, crop characteristics, resource availability, and management practices, to identify the most effective strategies for maximizing crop yields and productivity.

MATERIALS AND METHOD

The development of mathematical model for optimal production of some crops will be an extension of the work of (Rania, 2020), following the model equation that takes the forms:

$$Y_i = a_0 + a_1.x_{1i} + a_2.x_{2i} + a_3.x_{3i} + a_4.x_{4i} + a_5.x_{5i} + a_6.x_{6i} + a_7.x_{7i} + \varepsilon_i \qquad (3)$$

Where:

a_0 = Constant

a_1 - a_7 = Model parameters (coefficients)

y_i (kg ha^{-1}) = The crop yield

x_{ji}, j = 1, ..., 7 = The predictors

ε_i = A random error.

The modify model will integrate key variables as inputs, the variables may include; crop types; such as (rice, yam, maize and cassava), rainfall, soil fertility, land size, input cost, and temperature. The mathematical model will be formulated using the method of multiple linear regression. The model will incorporate linear combination of this variables.

Development of Mathematical Model

In this research work, we derive from the existing literatures a Mathematical Model that represents the relationship between Crop production and the variables (rainfall, soil nutrient levels, land size, temperature and input cost) and incorporate the selected variables into the model. However, the following assumptions will be considered in the development of the model;

   i.   Crop production is determined by a combination of rainfall, soil nutrient level, land size, and temperature.
   ii. Each crop is grown on a separate plot of land with uniform soil fertility.
   iii. The relationship between these variables and crop yield is assumed to be linear.

Model formulation

In formulation of the mathematical model, the following variables are denoted as follows:

Variables:-

$R : Rain\ fall\ (in\ mil\lim eter)$

$N : Soil\ Nuttrient\ Level\ (normalized value)$

$A : Land\ size\ (in\ hectares)$

$T : Temprature\ (in\ \deg ree\ celsius)$

$I : Input\ \cos t$

Let the Crop yields (output) be represented as follows

$Y_{rice} : Rice\ yield\ (in\ tons\ per\ hectare)$

$Y_{maize} : Maize\ yield\ (in\ tons\ per\ hectare)$

$Y_{yam} : Yam\ yield\ (in\ tons\ per\ hectare)$

$Y_{cassava} : Cassava\ yield\ (in\ tons\ per\ hectare)$

Then by assuming a linear relationship between the variables and Crop yields gives a model:

$$Y_{crop} = \alpha + \beta_R.R + \beta_N.N + \beta_A.A + \beta_T..T + \beta_I..I + \varepsilon \qquad (4)$$

Where:

Y_{crop} is the yield of the specific crop (rice, maize, yam, cassava).

α is the $\operatorname{int}ercept$, representing the base yield without any inputs.

$\beta_R, \beta_N, \beta_I, \beta_A, \beta_I$ are the coefficients of the effects of each variable on crop yield.

ε is the errorr term accounting for factors not included in the $\mod el$.

These crops are selected due to high demand for the crops and the selected variables are critical parameters for crop yield.

Expected Result

The following results are expected from the research:

i. New mathematical model was developed for optimal crops production using identified variables.

ii. The model would be able to predict crop production based on the given data. By plugging in specific values for the predictor variables, you can calculate an estimated response variable (predicted value), helping to anticipate outcomes under different conditions

iii. The model can optimize crop production, by manipulating input variables, such as adjusting land size, input costs, and find combinations that lead to highest prediction of crop yields.

iv. The magnitude of coefficients indicates the relative importance of predictor variables. Larger coefficients imply a stronger influence on the response variable, while smaller coefficients suggest a less pronounced impact.

CONCLUSION

In conclusion, the development of this mathematical model is a significant step towards a more sustainable and efficient agricultural sector. It not only contributes to the global efforts to ensure food security but also bridging the gap between scientific research and practical applications, this study will contribute to a more sustainable food-secure future for the world's population. The implementation of this model in agricultural practices has the potential to transform the way we produce crops, fostering a more harmonious coexistence between agriculture and Mathematics. The research serve as a foundation for future studies, paving the way for further refinement and expansion of mathematical models for crop production, with the ultimate goal of achieving a more resilient and sustainable global agricultural system.

RECOMMENDATION

The researchers makes the following recommendations:

i. The model coefficients should be determined. These coefficients can indicate the variable that has the most significant impact on crop yield.

ii. Stability and sensitivity analysis would be obtained. The result from the sensitivity analysis can interpret trends, patterns, and relationships among the variables also identify the variables that have most significant impact on crop production and those that have minimal influence.

iii. The graphical simulations would be determined by using R and MATLAB software.

iv. The model can be used as an educational tool to raise awareness about the complex interactions between different factors affecting crop yield. It can be used in training programs for farmers, agricultural students, and extension workers.

REFERENCES

Adam, D. (2021). How far will Global Population Rise? Researchers can't agree. *Nature*, 597, 462-465.

Anatoliy, T., Roman, P., Vasyl, T. & Pavlo, L. (2021). Mathematical model for forecasting product losses in crop production projects. *ITEA-2021: 1st Workshop of the 10th International scientific and practical conference Information technologies in energy and agroindustrial* (pp. 25-31). Lviv: ITEA.

Cooper, M., Voss-Fels, K. P., Messina, C. D. (2021).Tackling G × E × M interactions to Close On-Farm Yield-Gaps Creating Novel Pathways for Crop Improvement by Predicting Contributions of Genetics and Management to Crop Productivity. *Journal of Theoretical and Applied Genetics*, 134, 1625-1644.

Food and Agriculture Organization (2020). United Nations (FAO) Rome.

Georges, G., Heba S., Tara-Maria S., Nour J., Fayez D., Jennifer A. (2022). The Future of Food Security Implantation of Technologies. *Journal of A*dvances in Food Security and Sustainability 7, 83-111.

Hakimi, D., Batagi, S. A., & Shehu, M. D. (2017). Development of a mathematical model for upland rice production (a case study of national cereal research institute Baddegi, Nigeria). *Journal of Science, Technology, Mathematics and Education (JOSTMED)*, 13(1), 112-120.

Karolina P. & Małgorzata K. (2020). The role of Agriculture in Ensuring Food Security in Developing Countries Considerations in the Context of the Problem of Sustainable Food Production. *Journal of sustainability and rural agriculture* 28, 60-637.

Marzhan, A., Sadenovaa,N. A. B., Marzhan, R., Petar, S. V. & Jiří, J. K. (2021). Mathematical Modelling in Crop Production to Predict Crop Yields. *Chemical Engineering Transactions*, 88, 1225-1230.

Mtwanga, J., Haule, T. R., & Fundisha, E. (2022).Sustainability of Adaptation Strategies in Rainfed Agriculture to Climate Change and Variability in Nyang'oro Ward in Iringa District, Tanzania. *Journal of the Geographical Association of Tanzania*, *42*(1).

Pawlak, K., & Kołodziejczak, M. (2020). The Role of Agriculture in Ensuring Food Security in Developing Countries: Considerations in the Context of the Problem of Sustainable Food Production. *Sustainability*, 12(13), 5488.

Rania, B. M. (2020). The Different Mathematical Modeling for Conducting Yields Growth. *Journal of Engineering and Applied Sciences*, 15(8), 1977-1984.

United Nations (2019).*World population prospects: The 2019 revision*. Department of Economic and Social Affairs, Population Division, United Nations

United Nations. (2020) Department of Economic and Social Affairs, Population Division. *In World Population Prospects: Highlights (ST/ESA/SER.A/423)*; UN: New York, NY, USA, 5, 12.

A Note on Generalized Multiset Theory ($\mathcal{T}$)

Balogun, F., *Wahab, O. A., and Sule, B.

Department of Mathematics, Federal University Dutsin-Ma
*Corresponding Author's E-mail: ojowahab@gmail.com

ABSTRACT
This work studies the generalized multiset theory $\mathcal{T}$. We present an analysis of axioms proposed in $\mathcal{T}$ and the two-sorted multiset theory **MST**, which appears to be a widely used multiset theory. Multisets in $\mathcal{T}$ contain objects whose multiplicities are from the set $\mathbb{R}$ (this could be a negative number), making it an extension of the theory **MST**; which deals with multisets that are modeled by positive integer-valued functions. Relative to the classical set theory, multiset theory is in a primal stage of development and has no unanimous approach to its axiomatization. This study presents axioms of the theory $\mathcal{T}$ in contrast with **MST**. The strengths and possible limitations of the two multiset theories are discussed and recommendations are outlined.
Keywords: Multisets, Axiomatic systems, Multiset theory, Generalized Multiset theory

INTRODUCTION
The Zermelo-Fraenkel set theory **ZF** is regarded as a basic pre-requisite in extending set theory to multiset theory (Balogun & Wahab, 2022; Kunen, 2011). A multiset can be viewed as an extension of the classical set where the repetition of an element is taken into consideration. A multiset consists of elements, but the notion of a multiset is distinguished from that of a set by carrying information of how many times each element occurs in a given collection. Multisets have been applied in diverse fields (Singh et al., 2007). In this study, an analysis of axioms in the multiset theory **MST** (Blizard, 1988) and the generalized multiset theory $\mathcal{T}$ (Felisiak et al., 2020) is presented. The similarities and peculiarities of these multiset theories are discussed. A comparative analysis of the theory **MST** and the single sorted multiset theory **MS** (Dang, 2014) is presented in Balogun & Wahab (2023).

Axioms of the Generalized Multiset Theory ($\mathcal{T}$)
Peculiar and common axioms of the multiset theory $\mathcal{T}$, relative to the theory **MST** are presented in this section.
Axiom of multiplicity of $\mathcal{T}$
$$\forall x, y \,\exists g (x \in^g y)$$
This extends the axiom of multiplicity of **MST**:
$$\forall x \forall y \forall n \forall m \,((x \in^n y \land x \in^m y) \to n = m)$$
In the case of the generalized multiset theory, the value of g can be an arbitrary real number.

Extensionality Axiom of $\mathcal{T}$
$$\forall x, y(x = y \leftrightarrow \forall y, z[z \in^g x \leftrightarrow z \in^g y])$$
The axiom above guarantees the equality of two multisets. If two multisets $x \ and \ y$ have the same objects occurring with exactly the same multiplicities, then they are equal. This generalizes extensionality in **MST** - $\forall x \forall y(\forall z \forall n(z \in^n x \leftrightarrow z \in^n y) \to x = y)$, the value of g in $\mathcal{T}$ is an arbitrary real number.

Power set Axiom of $\mathcal{T}$
$$\forall x, \exists y(set(y) \land \forall z[z \in y \leftrightarrow z \subseteq x])$$
For every multiset x there is a set whose elements are exactly the submultisets of x. The set y is the power set of x. The representations for power set axiom are basically the same in both theories and differing only in the range of the characteristic function. The axiom guarantees all possible subsets of a multiset.

Axiom of Infinite Generalized Multiset of $\mathcal{T}$
Similar to the axiom of infinity in **MST**, the axiom of infinite generalized multiset is as follows:
$$\exists x[\emptyset \in x \land \forall y(y \in x \to \cup \{y, [y]_1 \in x)]$$

Axiom of Empty Generalized Multiset (Empty gm)
The existence of the empty gm, which generalizes the *empty multiset axiom* in **MST**, is established by the following result in $\mathcal{T}$:
$$\exists w(w = \emptyset)$$

Axiom of Foundation of $\mathcal{T}$

$\forall x[x \neq \emptyset \rightarrow \exists y(y \in x \land \forall z[z \in y \rightarrow z \notin x])]$

Remark

Axioms and axiom schema introduced in the multiset theory $\mathcal{T}$ include; Axiom of Herd, Axiom Schema of Substitutivity of Identicals, and Multiplicity Axiom.

Axiom of Herd of $\mathcal{T}$

$\forall g, x \exists y \ (x \in^g y \ \land \forall z[z \in y \leftrightarrow z = x])$.

The axiom of herd guarantees the uniqueness of different multisets. The theory $\mathcal{T}$ establishes that the relation that associates a generalized multiset x and a nonzero number g to the herd of x with multiplicity g is an injective function.

Axiom Schema of Substitutivity of Identicals of $\mathcal{T}$

For all $L-$formulas $\varphi[x]$, the axiom schema of substitutivity of identicals is given by the universal closure of

$\forall x, y[x = y \rightarrow (\varphi[x] \rightarrow \varphi[y])]$

Axiom Schema of Replacement of $\mathcal{T}$

For all $L-$formulas $\varphi[g]$, if w is not free in $\varphi[g]$, the axiom schema of replacement is the universal closure of

$\forall v[\forall x(x \in v \rightarrow \exists! y \varphi[x,y]) \rightarrow \exists w(Set\langle w \rangle \land \forall y[y \in w \leftrightarrow \exists x(x \in v \land \varphi[x,y])])]$

In **MST**, the least multiplicity is considered whenever we have more than one x in multiset z mapped by the function $\varphi(x,y)$ where $x \ and \ y$ are free variables. The $L-$formula $\varphi[g]$ is functional if w is not free in $\varphi[g]$.

Axiom of Pairing of $\mathcal{T}$

$\forall x, y[x \neq y \rightarrow \forall g, h \exists s(x \in^g s \land y \in^h s \land \forall z[z \in s \leftrightarrow z = x \lor z = y])]$

The theory **MST** considers singleton and non-singleton sets.

Discussions

The generalized multiset theory $\mathcal{T}$ describes multisets with elements whose multiplicities can be arbitrary real numbers. The theory makes a clear distinction between true multisets (which exist by axiomatic theories), and artificial multisets (which are set-based multisets). The multiset theory $\mathcal{T}$ is a unification of existing multiset theories. It generalizes the multiset theory **MST** since multiplicities are drawn from the set $\mathbb{R}$. It is hybrid and a more suitable theory to adopt when dealing with vagueness or modeling uncertainties. The analogous distinction can be made in the case of multisets generalized by extending the range of multiplicities. The multiset theory **MST** appears to be the most sustained in the literature, however, the generalized multiset theory offers a more flexible framework for modeling real-world situations where repetition or multiple occurrences of elements are relevant and vagueness is to be captured. It has a unique feature in queries and search engines, also in areas that deal with large databases, real-time stock, computation in mega stores, and data duplication science (Singh et al 2007; Clement, 1988; William-West *et al.*, 2020; Pagh *et al.,* 2004).

CONCLUSION

The multiset theory **MST** contains a copy of the Zermelo-Fraenkel set theory and it is a suitable theory to adopt or study when dealing with foundational works in multiset context. The generalized multiset theory $\mathcal{T}$ extends existing multiset and fuzzy set theories (Zadeh, 1965; Blizard, 1988; Dang, 2014) and can be employed in studies that involve a combination of multiset and fuzzy set theories. The theory $\mathcal{T}$ can serve as a basis for solving application problems that involve uncertainties.

REFERENCES

Balogun, F. and Wahab, O.A. (2022). A study on axioms and models of Zermelo-Fraenkel Set Theory, *Anchor University Journal of Science and Technology*2(2):63-69

Balogun, F. and Wahab, O.A. (2022). Axiomatization of multisets: A Comparative Analysis, , *Dutse Journal of Pure and Applied Science,* 9(3):155-163

Blizard, W. (1988). Multiset theory. *Notre Dame Journal of formal logic,* 30:36–66

Clements, G. F. (1988). On multisets k–families. *Discrete Mathematics,* 69:153 – 164.

Dang, H. (2014).A single-sorted theory of multisets. *Notre Dame Journal of Formal Logic,* 55(3)299-332

Felisiak, P. A., Qin, K., and Li, G. (2020). Generalized multiset theory. *Fuzzy Sets and Systems,* 380:104-130

Kunen, K. (2011). *Set Theory*. Studies in Logic: Mathematical Logic and Foundations. Vol. 34. College Publications, London.

Pagh A., Pagh R., and Rao, S. (2004). An optimal bloom filter replacement. Seminar on Data Structures, 1-7

Singh, D., Ibrahim, A. M., Yohanna, T. and Singh, J. N. (2007). An overview of the applications of multisets. *Novi Sad Journal of Mathematics*, *2(*37): 73–92

William-West, T.O., Ejegwa, A. P., and Amaonyeiro, A. U. (2021). On dynamic multisets and their operations. *Annals of Communications in Mathematics,* 4(3): 284-292

Zadeh, L. A. (1965). Fuzzy sets. *Information and contro*l, 8; 338-353

Results on Generalized Reverse Derivations and Jordan Triple Reverse Derivations on Semiprime Rings

*1Hafsat Mohammed Rumah, 1Funmilola Balogun, 2Tasiu Abdullahi Yusuf, and 1Muhammad Sani

1Department of Mathematics, Federal University Dutsin-Ma, Katsina
2Department of Mathematics and Statistics, Umaru Musa Yar'adua University, Katsina
*Corresponding Author's E-mail: hafsatmohd1980@gmail.com

ABSTRACT
In this paper, R represents a semiprime ring. By introducing some new definitions, we prove that a generalized reverse derivation $d: R \to R$ coincides with a generalized derivation. We also show that a generalized Jordan triple reverse derivation d on R is a generalized triple reverse derivation.
Keywords: Semiprime ring, derivation, generalized reverse derivation, generalized Jordan triple derivation, left centralizer.

INTRODUCTION
The concept of derivation on algebraic structures is well established in the literature (Aboubakr and Gonzalez, 2015; Balogun, 2014; Chaudhry and Ulah, 2011; Bresar and Vukman, 1989, Posner, 1957). This work is motivated by the paper Tasiu and Audu (2018). A ring R is prime if for all $x, y \in R$, $x R y = 0$ implies that either $x = 0$ or $y = 0$, and is semiprime if $x R x = 0$ implies $x = 0$. An additive mapping $d: R \to R$ is called a derivation if $d(xy) = d(x)y + xd(y)d$, holds for all pairs $x, y \in R$ and is called a Jordan derivation if $d(x^2) = d(x)x + xd(x)$ for all $x, y \in R$. Herstein, (1957) proved that every derivation is a Jordan derivation but the converse is in general not true. Cusack (1975) generalized the results of Herstein to 2-torsion free semiprime rings (see also Bresar, 1988 for an alternative proof). An additive mapping $d: R \to R$ is called Jordan triple derivation if $d(xyx) = d(x)yx + xd(y)x + xyd(x)$ for all $x, y \in R$. Bresar (1989) proved that in 2-torsion free semiprime ring, any Jordan triple derivation is a derivation and asserts that any Jordan derivation of an arbitrary ring is a Jordan triple derivation. Bresar & Vukman (1988) generalized the result of Cusack (1975). An additive mapping $T: R \to R$ is called a left centralizer if $T(xy) = T(x)y$, for all $x, y \in R$. An additive mapping $d: R \to R$ is called left Jordan centralizer if $T(x^2) = T(x)x$ holds for all $x \in R$. Zalar (1991) proved that any left Jordan centralizer on a 2− torsion free semiprime ring is a left centralizer. Molnar (1995) proved the following result: Let R be a 2-torsion free prime ring and let $T: R \to R$ be an additive mapping. If $T(xyx) = T(x)yx$, $x, y \in R$, *then T is a left triple centralizer of R.* The concept of generalized derivation was introduced in Bresar (1991). In Mohammed *et al*., (2023), the authors proved that prime rings with multiplicative generalized reverse derivations are commutative. It is easy to see that $T: R \to R$ is a generalized derivation if and only if F is of the form $F = T + d$, where d is a derivation and T a left centralizer. In addition, Jing & Lu (2003) defined the concept of generalized Jordan derivation and generalized triple derivation. An additive mapping $F: R \to R$ is a generalized Jordan derivation if $F(x^2) = F(x)x + xd(x)$, holds for all $x \in R$ where $d: R \to R$ is a Jordan derivation An additive mapping $F: R \to R$ is a generalized Jordan triple derivation if $F(xyx) = F(x)yx + xd(y)x + xyd(x)$ holds for all $x, y \in R$, where $d: R \to R$ is a Jordan triple derivation. In this work, our aim is to prove both conjectures. Recently, Tasiu & Audu (2018) proved that every generalized Jordan derivation is a generalized derivation and every generalized Jordan triple derivation is a generalized derivation.
We extend the work of Tasiu and Audu (2018) to reverse derivations.
Below are the definitions that will be extended in section 2
Definition 1.1
According to Cusack (1975) An additive mapping $T: R \to R$ is called a left centralizer of R, if $T(xy) = T(x)y$, for all $x, y \in R$.
Definition 1.2
Molnar (1995) proved the following result: Let R be a 2-torsion free prime ring and let $T: R \to R$ be an additive mapping. If $T(xyx) = T(x)yx$, for all $x, y \in R$, *then T is a left triple centralizer of R.*
Definition 1.3
An additive mapping $d: R \to R$ is called Jordan triple derivation if $d(xyx) = d(x)yx + xd(y)x + xyd(x)$ for all $x, y \in R$.
Definition 1.4
An additive mapping $F: R \to R$ is a generalized Jordan triple derivation if $F(xyx) = F(x)yx + xd(y)x + xyd(x)$ holds for all $x, y \in R$, where $d: R \to R$ is a Jordan triple derivation.

Below are the results of Tasiu & Madugu that will be extended in section 2

Theorem 1.5

Let R be a 2−torsion free semiprime ring and let $F: R \to R$ be a generalized Jordan derivation, then F is a generalized derivation.

Theorem 1.6

Let R be a 2−torsion free semiprime ring and let $F: R \to R$ be a generalized Jordan triple derivation, then F is a generalized derivation.

Main Results

We extend definitions from section 1, and establish new results as follows:

Definition 2.1: An additive mapping $T: R \to R$ is called left reverse centralizer of R, if $T(xy) = T(y)x$, for all $x, y \in R$.

Definition 2.2: An additive mapping $T: R \to R$ is said to be left triple reverse centralizer of R, if $T(xyx) = T(x)xy$, for all $x, y \in R$.

Definition 2.3: Let R be a prime ring. A mapping $d: R \to R$ is called Jordan triple reverse derivation, if $d(xyx) = d(x)xy + xd(y)x + yxd(x)$ for all $x, y \in R$.

Definition 2.4: Let R be a prime ring. A mapping $F: R \to R$ is called generalized Jordan triple reverse derivation associated with Jordan triple reverse derivation d, if $F(xyx) = F(x)xy + xd(y)x + yxd(x)$ for all $x, y \in R$.

Theorem 2.5

Let R be a semiprime ring and $F: R \to R$ be a generalized reverse derivation associated with reverse derivation d and $T: R \to R$ be a left centralizer of R, if $T(xy) = F(xy) - D(xy)$ for all $x, y \in R$ then F is a generalized derivation.

Proof:

Given that F is a generalized reverse derivation associated with reverse derivation d,

that is;

$$F(xy) = F(y)x + yd(x), \text{ for all } x, y \in R \tag{1}$$

by definition of generalized reverse-derivation.

Now let,

$\quad T = F - d$ (that is, $F = T + d$)

then,

$$T(xy) = F(xy) - d(xy), \text{for all } x, y \in R \tag{2}$$

From the definition of generalized reverse-derivation and reverse-derivation, we have

$$T(xy) = F(xy) - d(xy) \tag{3}$$

$$\quad = F(y)x - yd(x) - (d(y)x + yd(x)) \text{ for all } x, y \in R$$

$$= F(y)x - yd(x) - d(y)x - yd(x), \tag{4}$$

$$= F(y)x - d(y)x \tag{5}$$

$$= (F(y) - d(y))x$$

$$= T(y)x, \text{ for all } x, y \in R. \tag{6}$$

Therefore $T(xy) = T(y)x$, for all $x, y \in R$. By definition 2.1, T is a left reverse centralizer of R.

Hence proved.

Theorem 2.6

Let R be a semiprime ring and $F: R \to R$ be a generalized Jordan triple reverse derivation associated with Jordan triple reverse derivation d. Let $T: R \to R$ be a left Jordan triple reverse centralizer of R, if $T(xyx) = F(xyx) - d(xyx)$, for all $x, y \in R$, then F is a generalized triple reverse derivation.

Proof:

Given that F is a generalized Jordan triple reverse derivation associated with Jordan triple reverse derivation d, that is;

$$F(xyx) = F(x)xy - xd(y)x + yxd(x), \text{ for all } x, y \in R. \tag{7}$$

Now suppose,

$T = F - d$,

then,

$$T(xyx) = F(xyx) - d(xyx), \text{ for all } x, y \in R \tag{8}$$

by definition

$$= F(x)xy + xd(y)x + xyd(x) - (d(x)xy + xd(y)x + yxd(x)), \tag{9}$$

for all $x, y \in R$

$$= F(x)xy + xd(y)x + yxd(x) - (d(x)xy + xd(y)x + yx(d(x)) \tag{10}$$
$$= F(x)xy + xd(y)x + yxd(x) - d(x)xy - xd(y)x - yxd(x)$$
$$= F(x)xy - d(x)xy \text{ , for all } x, y \in R$$
$$= F(x)xy - d(x)xy$$
$$= (F(x) - d(x))xy \tag{11}$$
$$= T(x)xy, \text{ for all } x, y \in R.$$

That is,
$$T(xyx) = T(x)xy \text{ for all } x, y \in R. \tag{12}$$
By definition 2.2, T is left triple reverse centralizer of R. Hence, we have the require result.

CONCLUSION

In this work, we introduced some definitions and established new results on semiprime rings with a centralizer R. It is shown that generalized reverse derivations $d: R \to R$ coincide with generalized derivations. We also proved that a generalized Jordan triple reverse derivation d is a generalized triple reverse derivation.

REFERENCES

Aboubakr, A. and Gonzalez, S. (2015) Generalized reverse derivations on semiprime rings. *Seberian Mathematical Journal 56(2): 199-205*.

Balogun, F. (2014). A study on derivations on lattices. *Mathematical Theory and Modeling, 4(11): 14-19*.

Bresar, M. (1988). Jordan derivations on semiprime rings. Proc. Amer. Math. Soc., 1003-1006.

Bresar, M. (1989). Jordan mapping of semiprime rings. J. Algebra, 218-228.

Bresar, M. (1991). On the distance of the composition of two derivations to the generalized derivation. Glasgow Math. J., 89-93.

Bresar, M., & Vukman, J. (1988). Jordan derivations on prime rings. Bull. Austral. Math. Soc., 321-322.

Cusack, J. (1975). Jordan derivations on rings. Proc. Amer. Math. Soc., 321-324.

Chaudary, M. A., and Ullah, Z. (2011).On generalized α, β -derivations on lattices. *Uaestiones Mathematicae,34. 417-424*.

Herstein, I. N. (1957). Jordan derivations of prime rings. Proc. Amer. Math. Soc., 1104- 1119.

Jing, W., & Lu, S. (2003). Generalized Jordan derivations on prime rings and standard operator algebras. Taiwanese J. Math. , 605-613.

Mohammed, H. R., Balogun, F., and Yusuf T. A. (2023). Commutativity of prime rings with multiplicative (generalized-reverse) derivation. *Science World Journal* 18(3); 386-388.

Molnar L. (1995). On centralizers of an H - algebra. Publ. Math. Debrecen, 89-95.

Posner, E. C. (1957). Derivations in prime rings. *Proceedings of the American Mathematical Society*, *8*(6), 1093-1100.

Tasiu A.Y & Audu M. (2018). On generalized derivation on semiprime rings. International   Journal of Trend in Research and Development, 5(2): 2394-9333.

Zalar, B. (1991). On centralizers of semiprime rings. Comment. Math. Univ. Carol, 609- 614.

An Assessment of Rainfall Variability and Trends in Wukari, Nigeria from 1981 to 2021

*Abel Jacob and Moses O. Omopekunola

Department of Pure and Applied Physics, Federal University Wukari. Taraba State
*Corresponding Author's E-mail: j.abel@fuwukari.edu.ng Phone: +2348035379860

ABSTRACT
This study assessed the trends and variability of rainfall in Wukari, Nigeria, from 1981 to 2021, using the ECMWF ERA5 reanalysis data sets. Rainfall trends and variations over the study period were analyzed using the Mann Kendal trend test and the Theil Sen slope estimator. The assessment of monthly rainfall variation for the rainy months (May-October) showed an increasing trend for August, September, and October, with August having the highest increasing trend of magnitude 0.051mm/month. The result also showed an encroachment of the dry spell towards the rainy season and vice versa. This will create a variation in the onset of rainfall and cessation in the coming decades, which will affect the farming season in Wukari in terms of the planting and harvesting time of crops. A decline in annual rainfall of magnitude -0.005mm/ year was observed from1981 to 2021. The rainfall pattern revealed a periodic trend on a decadal basis, with an increasing trend followed by a decreasing trend in the next decade. The highest increasing trend of magnitude 0.945mm/decade was observed in the third decade and the lowest in the fourth decade, with a magnitude -0.014mm/decade. Based on the trend pattern, an increasing trend in rainfall amount is expected in the next decade (2021-2030), with a higher increasing trend magnitude greater than that of the third decade. Therefore, it is recommended that Government Agencies and stakeholders in the agriculture sector be proactive in educating/enlightening farmers on the likelihood of a change in the farming season and make adequate preparations to mitigate the effect of flooding in the area.
Keywords: Rainfall trend; rainfall variation; climate change; climate change impact; rainfall variability

INTRODUCTION
Weather and climate are described majorly by some atmospheric parameters, such as rainfall, atmospheric pressure, temperature, humidity, wind, and albedo. An area's weather over a given period is referred to as the climate (IPCC, 2013). It is a statistical analysis of relevant quantities and their variation over timescales ranging from months to thousands or even millions of years. Temperature and precipitation can be used as indicators to understand the climate change of any region in terms of its yearly or seasonal variations (El Mallah, 2011).This variation can differ significantly from region to region, and there may be major spatiotemporal differences across places with various climates (Yue and Hashino, 2003). Evidence of climate system warming has been provided locally and globally by the changes seen during the decades since the 1950s (Bates et al., 2008). Sea levels are rising, the ocean and atmosphere are warming, the amount of ice and snow is declining, and the concentration of greenhouse gases is rising (IPCC, 2013).Global warming has lately altered the climate of the Earth, and it will likely continue to do so in the future (Sen and Balling, 2004). Even a simple glance at the current weather shows how much this transformation has occurred (Kevin et al., 2000).Scientists have identified climate variations, trends, and changes in many parts of the world using climatic indicators such as air temperature, precipitation, evapotranspiration, and surface relative humidity (Bates et al.,2008). According to NAS and RAS (2014), the patterns that scientists anticipated are occurring because of increasing carbon dioxide levels and other changes brought on by anthropogenic activities that are consistent with the evidence of climate change. The impacts of climate change on the environment and humans are severe (El–Tantawi, 2005).

Despite technological advances, the weather and climate continue to determine possible farming practices (Ayoade, 2004). Rainfall variation under global warming is a major problem that could greatly influence society and the environment regarding the availability of water supplies for domestic, industrial, and agricultural needs (Granados, 2017). This variability of climatic factors, such as rainfall, impacts farmers' ability to plan the phases of crop growth, which impacts overall crop yield. Farmers decide when to plant crops and apply agricultural inputs during the growing season based on variations in the timing of seasonal rainfall (Bannaya, 2011). In recent years, it has also enhanced natural environmental hazards like drought and flood occurrences in Nigeria's climate, especially in the north's drier parts (López, 2015). Recent decades have seen rainfall variability events and recurring extreme weather events in Taraba State, which have impacted infrastructures, people, and agricultural output. With irrigation agriculture making up a smaller portion of the cultivated land, the state primarily depends on natural rainfall. As a result, the state's crop yields and food production depend greatly on the quantity, timing, and distribution of rainfall and other climatic elements during the growing season (Oruonye, 2012; Oruonye and Adebayo, 2013). The rainfall regime in this area of the country is distinguished by high concentrations in a few months, with August/September serving as the peak

month. These high concentrations are not only intermittent but occasionally at the extreme. As a result, the area is particularly susceptible to severe and dangerous weather, such as flooding, particularly in the southern parts like Wukari and Ibi. The current level of climatic variability will likely rise and amplify in the coming years; storms, floods, and droughts are expected to become more frequent and severe (Oruonye, 2012). Therefore, this study aims to comprehensively assess rainfall variability and trends in Wukari, Taraba state, from 1981 to 2021to assist farmers with necessary information. The specific objectives include:

1. To assess the monthly distribution of rainfall variation in Wukari
2. To analyze annual and decadal trends of rainfall in Wukari

MATERIALS AND METHODS
Study Area
Wukari is the Headquarters of Wukari Local Government Area of Taraba State; Taraba State is located in Nigeria at latitude 7°51′N and longitude 9°47′E with capital in Jalingo. Wukari is located in the southern region of Taraba State. Its borders are Gassol Local Government Area to the east, Donga to the south,Ukum (in Benue State) to the west, and Ibi Local Government Area to the north. It covers an area of 4,308 square kilometers (1,663 square miles). There are sixteen LGAs (Local Government Areas) in Taraba State. The 2006 National Population Census estimates that 241,546 people are living in Wukari (NPC, 2006).
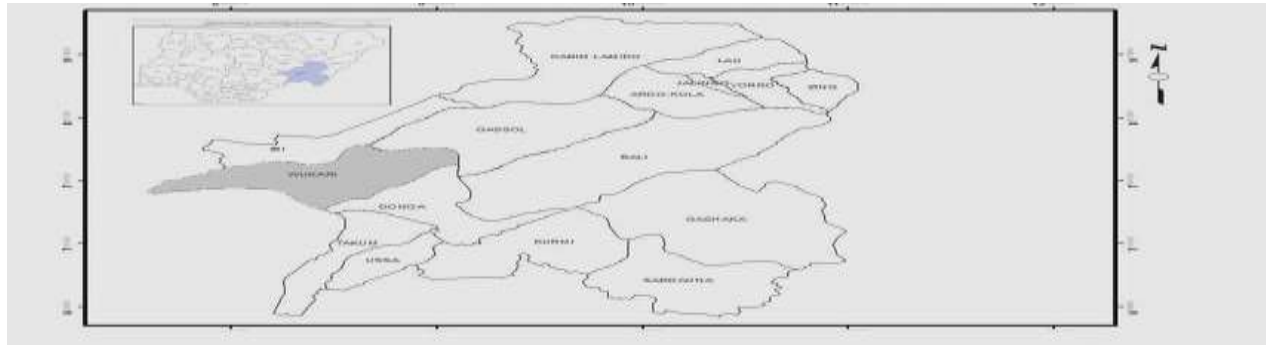
Figure 1: Map of the study area

Sources of Data
The observed surface data from rain gauges over Africa have inadequate spatial coverage, missing data, and even dropping recently. Due to the issues with point observations with an uneven spatial distribution or missing data, gridded-rainfall data from the European Centre for Medium-Range Weather Forecasts (ECMWF) fifth Generation (ERA5) model was used for this study. It has been proven suitable for climate monitoring (Sen and Habib 2000; Boers et al. 2014a, 2015b and Dai et al. 1997).

We employed monthly mean rainfall data from 1981 to 2021 from the ERA-5 reanalysis. The yearly mean rainfall statistics were obtained by averaging the daily record of precipitation data with the monthly mean rainfall data. The seasonal means for the wet (April, May, June, July, August, September, and October) and the dry/harmattan (November, December, January, February, and March) seasons were also produced by averaging the monthly averages for each season.

Rainy Days
There are differing opinions on what conditions qualify as rainy days. Some contend that any day with precipitation that drops to the ground and can be measured by a rain gauge qualifies as a wet day. In contrast, others claim that the amount of precipitation must surpass a specific threshold. For a day to be deemed a rainy day in West Africa, according to Odekunle (2004), the precipitation must be greater than or equal to 0.85mm, not just what the rain gauge could detect. As a result, in this study, we defined a rainy day as one with a rainfall total of 0.85 mm or more.

Data Analysis
i.   The mean rainfall for each month, year, and decade was computed from the daily measurements.
ii. Theil Sen's estimator and the Mann-Kendall trend test were used to analyze the monthly, annual, and decadal rainfall trends from 1981 and 2021.

RESULTS AND DISCUSSION
Table 1: The monthly rainfall trend in Wukari from 1981 to 2021

Months Parameters	Kendall's tau	P - Value	Sen's slope	Regre Slope
Jan	-0.088	0.380	0.000	-0.022
Feb	-0.086	0.574	0,000	0.120
Mar	-0.212	0.053	-0.010	0.028
Apr	-0.105	0.339	-0.013	-9.150
May	-0.148	0.117	-0.028	-0.009
Jun	-0.148	0.138	-0.029	-0.012
Jul	-0.0248	0.023	-0.042	0.002
Aug	0.160	0.144	0.051	0.025
Sep	0.122	0.266	0.024	0.020
Oct	0.025	0.822	0.005	-0.021
Nov	-0.047	0.686	0	0.010
Dec	-0.241	0.052	0	0.022
Annual	-0.091	0.405	-0.005	-0.004

Table 2: Long/ short (decadal) terms rainfall trend in Wukari from 1981-2021

Period	Kendall tau	P-value	Sen's slope	Trend description
1981-1990	0.289	0.283	0.038	Increasing trend
1991-2000	-0.156	0.591	-0.031	Decreasing trend
2001-2010	0.467	0.073	0.945	Increasing trend
2011-2020	-0.066	0.858	-0.014	Decreasing trend
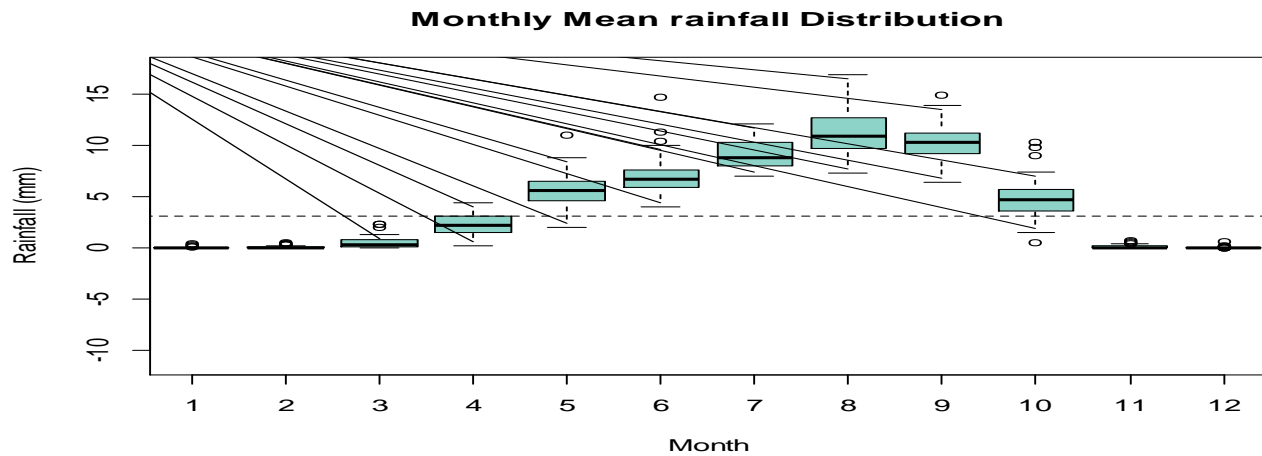
Figure 1: Monthly mean rainfall distribution in Wukari from 1981 to 2021

In order to further analyze the rainfall trend, an annual average rainfall time series for the study area from 1981 to 2021 was derived from ERA5 as illustrated in Figure 2.

Wukari Annual mean Rainfall Trend
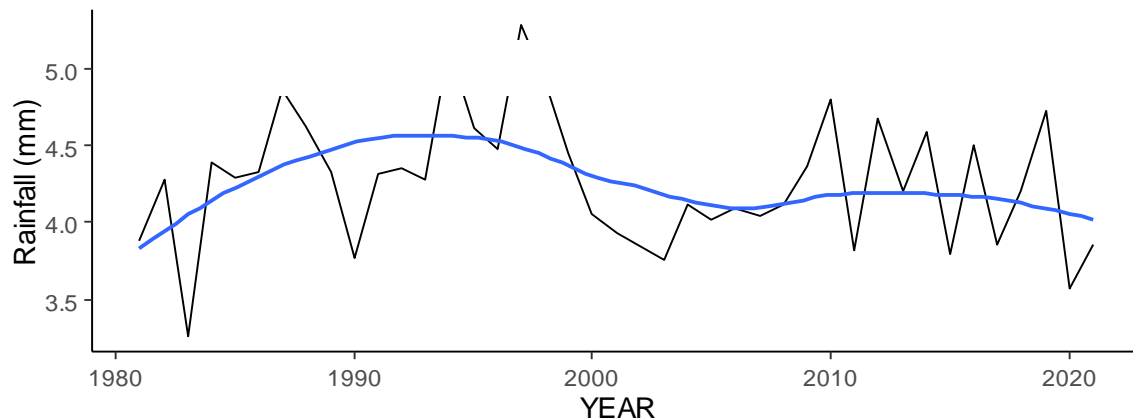
Figure 2: Annual averaged rainfall time series derived from ERA5 for Wukari from 1981 to 2021

Discussion

Monthly rainfall Variation

The mean monthly rainfall pattern/ distribution in Wukari for the forty-one year period under study, showing the degree of variation of rainfall in the study area showed that January, February, November, and December did not receive rainfall except in trace amounts, while March and April experienced light rainfall. Rainfall rises gradually from April to peak in August, and then declines till October. June, July, August, and September are the study area's months of heavy rainfall. This indicates that rainfall in Wukari is a single mode that has one season of peak rainfall. The analysis showed a high degree of variability within the period under study. The magnitude of the variation is from -0.01mm/month in March to 0.051mm/month in August followed by July with a magnitude of 0.042mm/month with June and September having the same magnitude of 0.029. However, the rainfall variation significance in July at a 5% level (p-value) is less than 0.05 as seen in Table 1 compared to other months indicating a serious decline in rainfall in July.

Decadal monthly rainfall variation

The decadal-scale monthly rainfall distribution in Wukari is shown in Table 2, there is a minimal variation in the rainfall pattern in January, February, March, November, and December. From the first to the third decade, there is a noticeable decrease in rainfall in April, May, June, and July and a slight increase in the fourth decade. In the fourth decade, there was a slight decrease in August and a light increase in October.

Trend Analysis

The trend analysis shows in Table 1 that there is no change in the rainfall trend in January, February, November, and December and a decreasing trend in March, April, May, June, and July. July has the highest rainfall decline trend, with a magnitude of -0.042mm/month. This shows an encroachment of the dry season towards the rainy season following the IPCC report on climate change. An increasing trend in rainfall was observed in August, September, and October, with August having the highest increase trend of magnitude 0.051mm/month. This scenario will impact farming activities in the study area. The decreasing trend of rainfall will affect the onset of farming activities as farmers will have to wait for the normalization of rainfalls before commencing planting of crops, while the increasing trend around October, the transition month between the wet and dry seasons, will also affect the harvest of some early maturing crops

In Table 2, the rainfall pattern reveals a periodic pattern in trend on a decadal basis. An increasing rainfall decadal trend is followed by a decreasing trend in the next decade. The first decade (1981-1990) showed an increasing trend of magnitude 0.038mm/decade, followed by a decreasing trend of magnitude -0.031mm/decade in the second decade (1991-2000). An increasing trend of magnitude 0.945 mm/decade was seen in the third decade (2001-2010), followed by a decreasing trend of magnitude -0.014 mm/decade in the fourth decade (2011-2020). Projecting from this trend analysis, Wukari is expected to experience an increase in rainfall over the next decade (2021-2030). This result agrees with the study conducted by Garba and Iliyasu (2021) in the same location using a dataset from the Nigerian Meteorological Agency (NiMet) from 1999-2018.

CONCLUSION

The assessment of rainfall variability and trend in Wukari, Nigeria, between 1981 and 2021 showed high variability of rainfall in the area with a trend indicating a gradual decrease in rainfall amount April, May, June, and July and an increasing trend in August, September, and October which indicate encroachment of dry season towards the raining season and likely extension of rains towards the dry season around October and November. This scenario is observed to have a likely impact on the activities of farmers in the area regarding the onset of farming activities and harvesting of farm produce. Another likely implication of the increase in rainfall around August, September, and October is the issue of flooding in the area. The area is likely to experience flooding in the next decade. The study also revealed that the decadal rainfall trend in the area is periodic. An increasing trend in one decade is followed by a decreasing trend in the next decade. It is therefore projected that the fifth decade, 2021 to 2030, will experience a higher amount of rainfall than the preceding decade, 2011 to 2020. It is therefore recommended that the stakeholders and Government Agencies in the agriculture sector should be proactive in educating/enlightening farmers on the likelihood of a change in the farming season and make adequate arrangements to mitigate the effect of flooding in the area.

ACKNOWLEDGMENTS

REFERENCES

Ayoade, J.O. (2004). *Climate Change: A Synopsis of Its Nature, Causes, Effects and Management.* Ibadan: Vantage Publishers Ltd.

Bannayan, M., Lotfabadi, S. S., Sanjani, S., Mohamadian, A. and Aghaalikhani, M. (2011). Effects of precipitation and temperature on crop production variability in northeast Iran. *International Journal of Biometeorology*, 55(3): 387–401.

Bates, B.C., Kundzewicz, Z.W., Wu, S. and Palutikof, J.P. (2008). *Climate Change and Water*. Technical paper of the Intergovernmental Panel on Climate Change, IPCC Secretariat. Intergovernmental Panel on Climate Change, Geneva.

Boers, N, Bookhagen, B and Barbosa, H. (2014a). Prediction of extreme floods in the Central Andes by means of Complex Networks. *Nature Communication*, 5(1). 158- 174.

Boers. N; Donner, R.V; Bookhagen, B. and Kurths, J. (2014b). Complex network analysis helps to identify impacts of the El Niño Southern oscillation on moisture divergence in South America. *Climatology Dynamism*, 8-9.

Dai, A; Fung, I.Y. and Del, A.D. (1997). Surface observed global land precipitation variations during 1900-88. *Journal of Climatology*, 10(1): 2943–2962

El Mallah, E. S. and Elsharkawy, S.G. (2011). Influence of circulation indices upon winter temperature variability in Egypt. *Journal of Atmospheric and Solar-Terrestrial Physics*, 73(4), 439- 448.

El-Tantawi, A. M. M., (2005): *Climate Change in Libya and Desertification of Jifara Plain Using Geographical Information System and Remote Sensing Techniques*. Unpublished PhD thesis Johannes Gutenberg-Universität in Mainz, Germany.

Garba Umar, G. A., and Anzaku, I. M. (2021). Effects of Climate Variability on Maize Yield in Wukari Local Government Area of Taraba State, Nigeria. *Global Journal of Science Frontier Research: H Environment and Earth Science*, 21(3): 1-16

Granados, R., Soria, J. and Cortina, M.(2017). Rainfall variability, rainfed agriculture and degree of human marginality in North Guanajuato, Mexico. *Singapore J. Tropical Geography*, 38(1): 153–166.

Intergovernmental Panel on Climate Change (IPCC) (2013). *Climate change: the physical science basis. Working Group 1 contribution to the IPCC Fifth Assessment Report*. Cambridge, United Kingdom: Cambridge University Press.

Kevin, E., Trenberth, K.M., Linda, M. and Steven, R. (2000). *Effects of changing climate on weather and human activities. Global change Instruction Programme* (pp 25-32). Sausalito, California: University Science Books, ,.

López, R. E., Thomas, V. and Troncoso, P. (2015). *Climate Change and Natural Disasters*. London: Transaction Publishers.

National Academic of Science (NAS) and Royal Society (RS) (2014). *Climate change evidence and causes:* An overview from the Royal Society and the US National Academic of Sciences. 5 – 7.

Odekunle, T.O. (2004). Rainfall and The Length of the Growing Season in Nigeria. *International Journal of Climatology,* 24(1): 467 – 479.

Oruonye, E. D. and Adebayo, A. (2013). *An Assessment of the effects of the 2012 Floods in Taraba State*. Proceedings of the fifth annual conference of the Nigerian Association of Hydrological Sciences, Nsukka Pp 13-20.

Oruonye, E.D. (2012) An Assessment of Food Risk Perception and Response in Jalingo Metropolis. Jaingo Taraba State. *International Journal of Forest, Soil and Erosion*, 3(1): 4-12.

Sen, R.S. and Balling, R.C. (2004). Trends in extreme daily precipitation indices in India. *International Journal of Climatology*, 24(1):457–466.

Sen, Z. and Habib, Z. (2000). Spatial analysis of monthly precipitation in Turkey. *Journal of Theoretical Applied Climatology*, 67(1):81–96.

Yue, S. and Hashino, M., (2003). Long term trends of annual and monthly precipitation in Japan. *Journal of American Water Resources Association*, 39(3): 587 – 596

Proximate Analysis and Assessment of Minerals Composition of Four Different Varieties of Chicken Legs Sold in Yankaji Site Katsina Metropolis, Katsina State, Nigeria

*[1]Muhammad M. Rumah, [2]Kamal S. K, [3]Abdulkarim D. K. and [4]Sani Ibrahim

[1]Department of Chemistry, Al-Qalam University Katsina, Katsina State, Nigeria
[2]Department of Chemistry, Federal University Dutsin-ma, Katsina State, Nigeria
[3]Department of Chemistry, Umaru Musa Yar adua University Katsina, Nigeria
[4]Department of Chemistry, College of Education Maru, Zamfara State, Nigeria
*Corresponding Author's E-mail: muntasirmuhammadrumah@gmail.com Phone: +2348033370462

ABSTRACT

Proximate analysis and mineral compositions were carried out on four different poultry chickens purchased from yankaji poultry site behind central market in Katsina Local government area of Katsina State. Mineral and proximate compositions were determined using their standard methods of analyses. Results of proximate analyses in percentage showed the following ranges in ascending order as; moisture content for sample B= 0.71%, sample A= 0.76%, sample C= 1.3% and sample D= 1.98%. Ash content for sample A= 2.88%, sample B= 2.94%, sample C= 1% and sample D= 3.70%. Fibre content for the samples are in the ranges as; sample B= 0.4%, sample A= 0.5% and sample C= 1.5%. Protein content with 74.4% for sample B, 69.73% for sample A, 68.1% for sample C and 59.6% for sample D. Fat content were as follows; sample B 23%, sample A 19%, sample C 16% and 2% for sample D being the least in the ranges. Carbohydrate reads as; sample D= 8.72%, sample A= 7.13%, sample C= 12.1% and sample B -1.55%. For mineral content, calcium values ranges from 0.68% sample A, 0.53% for sample B, 0.47% for sample C and 0.45% for sample D. Potassium as; 4.61% for sample A, 4.54% for sample C, 4.43% for sample D and sample B with 3.66%. Sodium having the following; sample D= 4.68%, sample B= 4.56% followed by sample A with 3.69% and lastly sample C having 3.58% respectively. These results showed that all the samples analysed are of nutritional value except sample B with deficiency in carbohydrate and meanwhile the mineral value contents showed higher percentages in all the samples except sample B and A with deficiency in magnesium. Conclusively, the three poultry chicken legs used in the study are of good nutritional values and are within the set of different review and hence they are recommended for consumption

Keywords: Proximate Analysis, Minerals Composition, Poultry Chickens

INTRODUCTION

Poultry has now turned into one of the most important division of agriculture throughout the world. Poultry industry is one of the fastest growing segments in agricultural sector and undoubtly, it plays an important role in Nigeria economy (Bukar and Saeed, 2014). Poultry is basically a source of economical, palatable and healthy food protein (Mahasar *et al.,*2010). Broilers are chicken (Gallus domesticus) bred and raised specifically for meat production (Kruchten, 2019). The behaviour of broiler chickens are similar to those of other gallinaceous birds since they are the same species as egg laying hens. Broiler chicks today are the most widely grown birds throughout the world as the fastest source of animal's protein (FAO 2018). In the light of the above, Oluyemi and Robert (2017) reported that broiler keeping has been recognized to provide a method by which rapid transformation of animal protein can be achieved. Broilers are best meat producers because of their ability to put on much weight in the shortest possible time. The short production cycle of boiler chicks is one of the special characteristics of poultry production that provides animal protein for human feeding (Edney *et al.,*2014). Broiler chickens are also easy and convenient to distribute over a wide territory. With the increasing human population, the consumption of meat is increasing in the world and intensive animal production has many more challenges to solve including environmental pollution and animal welfare (Ishibashi and Yonemochi, 2019).

Nowadays, most meat processing enterprises face an acute problem of the maximum and rational use of secondary products of processing farm animals and poultry. When processing initial raw materials, valuable kinds of secondary raw material resources are obtained, such as blood, bone, by-products of the 2nd category, crude fat, non edible by-products and others. They can be used for manufacturing additional food, feed and technical products. Wider introduction of complex processing of secondary raw materials will enable its rational use as themain components in the meat product technology increasing product output and assortment (Ziołecki *et al.*, 2019).

Minerals are inorganic substances, present in all body tissues and fluids and their presence is necessary for the maintenance of certain physicochemical processes which are essential to life. Minerals are chemical constituents used by the body in many ways. Although they yield no energy, they have important roles to play in many activities in the

body (Eruvbetine, 2021). Every form of living matter requires these inorganic elements or minerals for their normal life processes (Ozcan, 2021). Minerals may be broadly classified as macro (major) or micro (trace) elements. The third category is the ultra trace elements. The macro-minerals include calcium, phosphorus, sodium and chloride, while the micro-elements include iron, copper, cobalt, potassium, magnesium, iodine, zinc, manganese, molybdenum, fluoride, chromium, selenium and sulfur (Eruvbetine, 2021).

The mineral elements are separate entities from the other essential nutrients like proteins, fats, carbohydrates, and vitamins. Animal husbandry had demonstrated the need for minerals in the diet (Hegsted *et al.,* 2016). In this century, biological assay methods clarified the significance and importance of mineral elements for human and animal nutrition and modern analytical techniques led to the detection of trace elements as essential nutrients and this is still an active area of current research.

Aim and Objectives of the Study
The aim of this study is to compare the proximate analysis and mineral element composition of four varieties of chicken legs sold in Yan Kaji Market, behind central market Katsina, and the objectives of the study are as follows:-
  i. To purchased the different varieties of chickens leg
  ii. To determine the proximate and mineral elements compositions of chicken legs
  iii. To determine the mineral content present in chicken legs around Katsina metropolis
  iv. To assess and compare the proximate composition, dietary presence in chicken legs.

MATERIALS AND METHODS
Sample and Sampling Collection
Four poultry chicken was purchase from Yan Kaji poultry site behind central market in Katsina Local government area of Katsina State. A total of four (4) chickens legs were obtained and will be determined using a flame atomic absorption spectrophotometer (Shamspur et al., 2015).

Figure 1: Map of the Study area

Sample Preparation
The samples were cut into pieces with a stainless steel knife and oven-dried at a specific temperature for 1 day and pulverized to coarse fine powder, using metal mortar and pestle. The determination of proximate composition and mineral composition was carried out using AOAC, 2003 procedure.

Determination of Mineral Content
0.5g of each sample of different poultry was introduced into a digestion flask. 18ml of nitric acid HNO_3 (concentrated) and 6ml of perchloric acid ($HClO_4$) was carefully added. The mixture was digested at moderate heat until a cleared solution was obtained which indicate a complete digestion of the sample and the flask was left to cool. The sample was filtered into a $100cm^3$ volumetric flask and was filled to the mark using deionize water. It was then stored in

$100cm^3$ polyethylene bottle for flame test to determine calcium, potassium, sodium and magnesium. The solution on each crucible was filtered into 100ml volumetric flask and the volume made up to 100ml with demonized water

Determination of Proximate Composition
Moisture Content
The method described by Schütz et al., 2019 was adopted. A clean crucible was dried to constant weight in an air oven at 105 °C for 3 hrs, cooled in desiccators and weighed (W_1). 2g of sample was accurately weighed into the previously labelled crucible and reweighed (W_2). The crucible was dried in oven to a constant weighed (W_3). The percentage of moisture content was calculated thus:

$$\% \, moisture = \frac{W1 - W2}{W1} x \, 100$$

Where
W_1 = weight of empty crucible
W_2 = weight of the sample + crucible
W_3 = weight of the crucible after drying

Ash Content
The Schütz et al., 2019, method was used. The porcelain crucible was dried in an oven at 100ºC for 10 minutes, cooled in desiccators and weighed (W_1). 2g of the sample was placed into the previously weighed porcelain crucible and weighed (W_2). The sample was first ignited and transferred into a furnace, which was then set at 550 °C for 3hr 30minutes. The sample was left in the furnace for eight hours to ensure proper ashing. The crucible containing the ash was then removed cooled in the desiccator and weighed W_3. The percentage ash Content was calculated as:

$$\% \, Ash = \frac{W_1 - W_2}{W_1 - W_3} x \, 100$$

Determination of Crude Fibre Content
The method described by Schütz et al., 2019, was adopted. 2g of sample was weighed out into a round bottom flask. 100ml of 0.25M Sulphuric acid Solution was added and the mixture boiled under reflux for 30mins. The hot solution was quickly filtered under sanction. The insoluble matter was washed several times with hot water until it was acid free. It was quantitatively transferred into the flask and 100ml of hot 0.31M Sodium hydroxide solution was added and the mixture boiled again under reflux for 30mins and quickly filtered under sanction. The insoluble residue was washed with boiling water until it was based free. It was dried to constant weight in the oven at 100°C cooled in a desiccator and weighed (W_1) was then incinerated in a muffle furnace at 550ºC for 2 hours, cooled in the desiccator and reweighed (W_2).
Calculation
% Crude Lipid Content

$$\% \, Crude \, Lipid \, fiber \ = \frac{W_1 - W_2}{W_0} x \, 100$$

Determination of Crude Lipid Content
The lipid content was determined as provided in the Schütz et al.,2019, method. A clean, dried 500ml round bottom flask, containing few anti-bumping granules was weighed (W_1) and 300ml of Petroleum ether (40-60°C) for extraction was poured into the flask fitted with soxhlet extraction unit. The extractor thimble containing eight grams of the sample was fixed into the soxhlet extraction unit. The round bottom flask and a condenser were connected to the soxhlet extractor and cold water circulation was put on. The heating mantle was switched on and the heating rate was adjusted until the solvent was refluxing at a steady rate. Extraction was carried out for six hours. The solvent was recovered and the oil was dried in the oven at 70°C for one hour. The round bottom flask containing the oil was cooled in the desiccator and then weighed W_2.
The lipid content was calculated thus

$$\%\% \, Crude \, Lipid \, Content \ = \frac{W_2 - W_1}{Waight of sample} x \, 100$$

Determination of Protein
The dried and powdered samples were extracted by stirring with 50ml of methanol (1:5 w/v) at 25°C for 24hrs and centrifuged at 7,000rpm for 10min. 0.2ml of extract was pipette out and the volume was made to 1.0ml with distilled water. 5.0ml of alkaline copper reagent was added to all tubes and allowed to stand for 10min. 0.5ml of Folin's

Ciocalteau reagent was added and incubated in dark for 30min. The intensity of the colour developed was read at 660nm. To calculate the amount of crude protein Schütz *et al.,* 2019 method was used.

Calculation:

% Crude protein = % Nitrogen (N_2) x 6.25

Determination of Carbohydrate (by difference)

The total carbohydrate content was determined by difference. The sum of the

Percentage moisture, ash, crude lipid, crude protein and crude fibre were subtracted from 100 (Schütz *et al.,* 2019).

Calculation

% Total Carbohydrate= 100 – (% Moisture + % Ash + % Fat + % Protein + % Fibre)

RESULTS AND DISCUSSION

Results

Table 1: Result of Proximate analysis for four varieties of chicken legs

	Moisture (%)	Ash (%)	Crude Lipid (%)	Crude Fibre (%)	Crude Protein (%)	Carbohydrate (%)
A	0.76	2.88	19	0.5	69.73	7.13
B	0.71	2.94	23	0.5	74.4	-1.55
C	1.3	1	16	1.5	68.1	12.1
D	1.98	3.70	25	1	59.6	8.72

Fat values obtained from table 1 indicate that, the percentage of fat present in the sample C, were far higher than those of the sample A and B. Lipids are the major components of food as they offer a good source of energy. Fats being made up of hydrogen carbon and oxygen supply essential fatty acids that are not made by the body. Fat makes up about 99% of the lipids fraction of food (Craig *et al.,* 2017).

The Crude protein content in sample B, were more than 40% higher than in sample D, as shown in table 1, indicating a higher value in leaves than sample A and C. Protein is essential in all animal life. Protein makes up a large part of the muscle, skin beak feathers cartilage and internal organ of animal. The dietary function of protein is to supply amino acids for maintenance, muscle growth and synthesis of egg protein (Ravindran and Bryden, 2015).
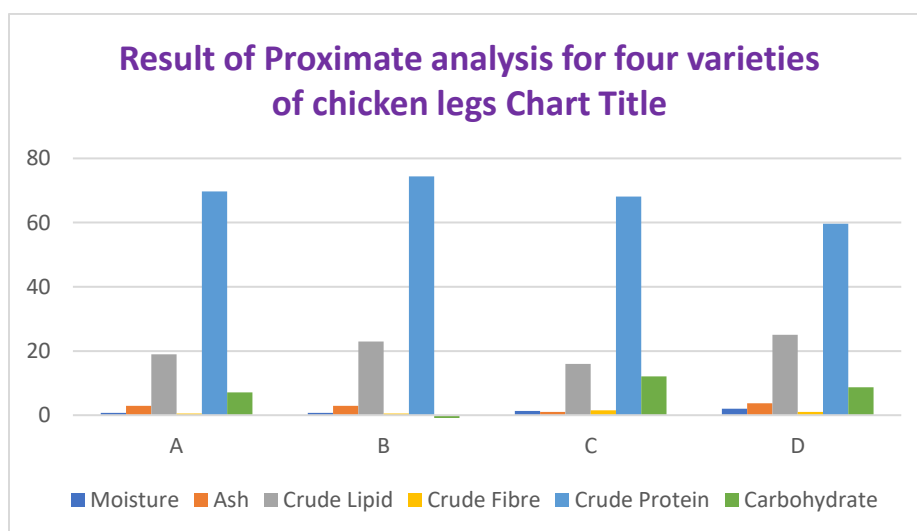
Figure1: Result of Proximate analysis for four varieties of chicken legs

Table 2: Result of Mineral composition of for four varieties of chicken legs

Samples	Calcium (%)	Magnesium (%)	Potassium (%)	Sodium (%)
A	0.68	0.16	4.61	3.69
B	0.53	0.11	3.66	4.56
C	0.47	0.90	4.54	3.58
D	0.45	0.25	4.43	4.68

Table 2 shows the result of mineral composition of calcium value of sample A 0.68% recorded with highest concentration. It also shows that is a good source of calcium in the body. Calcium is required in the formation of strong bones and teeth. The value of magnesium showed in table 2. Also indicating higher value in sample A. Magnesium is required for retention of calcium in teeth and constituents of bones. It also serves as the energy storage unit of the body's cells and as enzyme cofactors. The trends in the concentration of calcium and magnesium in the local chicken are the same with their highest values occurring in the namaja followed by the boilers and lastly the layers, While for Potassium values, recorded sample A as showed in table 2 with highest in potassium. Potassium is essential for the regulation of osmotic pressure and pH equilibrium and control of acid alkaline reaction of the blood. Sodium is also essential for osmotic equilibrium and body fluid volume as well as in the transmission of nerve impulses. Which from the result above in table 2, sample D have the highest sodium value when compared with the other samples.
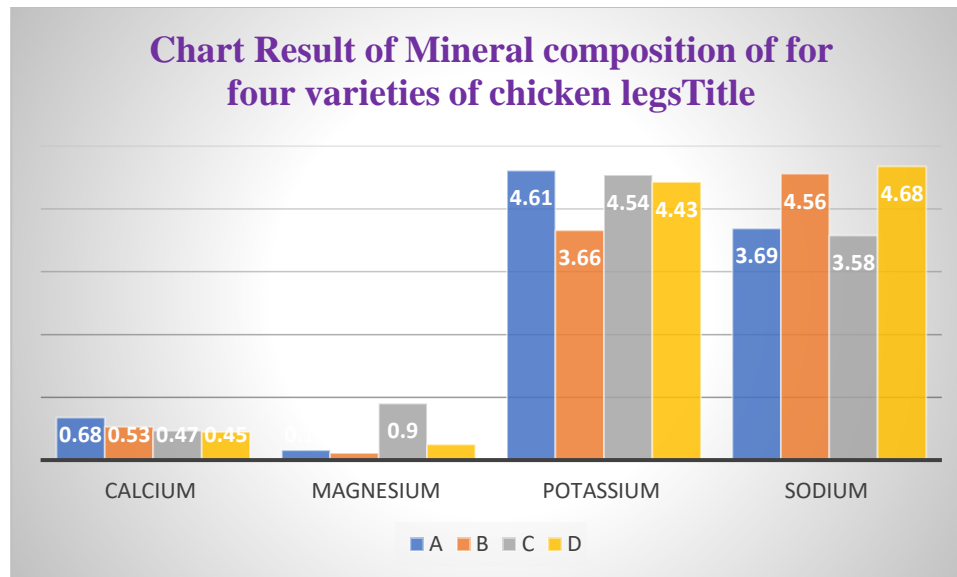
Figure 2; Result of Mineral composition of for four varieties of chicken legs
Key: Sample A: Local Chicken, Sample B: Na maja, Sample C: Broilers, Sample D: Layers

Discussion

Ash content is a measure of the total amount of minerals, present within the food substance. Ash content in Sample D 3.70% is the highest followed by the 2.94% Sample B then and lastly by the Sample C 1% indicating a significantly high value of the minerals in the chicken leg sample.

Moisture content indicates the amount of water present in the material and is very crucial as it serves as benchmark to evaluate the quality and stability (Shell-life) of food. A lot of biochemical reactions and physiological changes that occur in food are dependent on the moisture content. High moisture content increases the biochemical reactions. A variety of factors affect the moisture, content of food and usually the period and methods of harvesting contributes enormously to the moisture content (Mgbemena and Obodo, 2016). The result also showed that, dry matter content, indicating higher values in Sample D, followed by sample C then sample A and lastly sample B. Dry matter is very crucial since it ensures adequate nutrients balance. The nutrients required for the maintenance of animal's growth, pregnancy and lactation are part of the dry matter portion of the food (Noblet *et al.,* 2019).

The carbohydrate values obtained showed that values in the sample C were recorded high. Carbohydrate is an imprtant source of energy for poultry. It represents a considerable percentage of the body's energy supply as such sample C is highly energetic and nutrition.

Crude fibre content values showed in the table is that sample D, recorded with highest value while the sample C is the lowest value. Crude fibres are materials that are indigestible in human and animal organisms. Fibre consumption is regarded as essential because it absorbs water and provides roughage for the bowels, assisting intestinal transit and well normalizes blood lipids thereby reducing cardiovascular disease. It also helps to prevent constipation and decreases blood cholesterol levels (Palomeras *et al.,* 2010).

CONCLUSION

From the result obtained in table 1, it is clearly seen that all sample are highly proteinous which show a range of variation in carbohydrate with exception of sample B. Meanwhile sample A deficiency of either calcium or phosphorus results, is lack of normal skeletal calcification. Rickets is seen mainly in growing birds, whereas calcium deficiency in laying chickens, results in reduced shell quality and subsequently osteoporosis. This depletion of bone structure causes a disorder commonly referred to as "cage layer fatigue." When calcium is mobilized from bone to overcome a dietary deficiency, the cortical bone erodes and is unable to support the weight of the chickens. The entire samples have good feeding source and highly nutrition as feed to humans except Sample B which have low deficiency in magnesium and will suffer the effect.

RECOMMENDATIONS
  i.   That the feeding of sample B should be improving and be put into consideration
  ii.   Subsequent work on heavy metal can be carried out to know the dosage of toxic heavy metal present.

REFERENCES

Bukar, H, and Saeed M.O. (2014). Proximate analysis and consecration of some heavy metals in selected poultry feeds in Kano metropolis, Nigeria. Bayero J. Pure and Appl. Sci. 7(1):75 - 79

Craig, S. R., Helfrich, L. A., Kuhn, D., & Schwarz, M. H. (2017). Understanding fish nutrition, feeds, and feeding.

Edney,P., Carlos, B.R, Michele,B.L, Jorge, V.L,Emmanuel, M.F.A And Luiz F.T.A (2014) Poultry Offal Meal In Boiler Chicken Feed. Anim Sci and Pasture. 71(3): 188 - 194

Eruvbetine, H.L.(2021). The effect of β – glucanase supplementation on nutrient digestibility and growth in broilers given diets containing barley, oat, groats or wheat. Anim. Feed Sci. Technol. 25:193 -201

FAO (2018). Feed resources information system, animal health and production division.

Hegsted, H., svihus, B. and Choct, M. (2016). Role of insoluble fiber on gizzard activity in layers. Brit. poult. Sci. 42:354-361.

Ishibashi I, Yonemochi U. (2019). Effects of reducing crude protein in broilers diet. Anim. Sci. J. 73:155-165.

Kruchten S. (2019). Effect of decreasing dietary protein levels with optimum amino acids profile on the performance of broilers. Pak. Vet. J., 24:165 – 168

Mahasar, S.A., SheraziAbudul, S. T. H., Abuldul. N., Bhangar, Sijuddin, and Abdul R. (2010). Simultaneous assessment of zinc, cadmium, lead and cooper in poultry feed by different pulse anodic striping voltammetry. Food chem. Toxicol. 10(1016):111-119

Oluyemi, J.A. and Robert, F.A. (2017). Poultry production in warm wet climate. Mac press limited. Pp.14-20.

Mgbemena, N. M., &Obodo, G. A. (2016). Comparative Analysis of Proximate and mineral composition of Moringa oleifera root, leave and seed obtained in Okigwe Imo State, Nigeria. *J Mol Stud Med Res*, *1*(2), 57-62.

Noblet, J., Dourmad, J. Y., & Etienne, M. (2019). Energy utilization in pregnant and lactating sows: modeling of energy requirements. *Journal of animal science*, *68*(2), 562-572.

Ozcan, G.O (2021). Improving poultry feed and supply in Nigeria. In: In improving poultry feed and supply in Nigeria in management. Proceedings of a one day workshop organized by word's poultry science association, Nigeria branch in conjunction with the department of animal science faculty of agriculture, Obafemi Awolowo university, Ile - Ife, Nigeria. Pennsylvania, USA, Saunders.

Palomeras Soler, E., & Casado Ruiz, V. (2010). Epidemiology and risk factors of cerebral ischemia and ischemic heart diseases: similarities and differences. *Current cardiology reviews*, *6*(3), 138-149.

Ravindran, V. & Blair, R. (2015). Feed resources for poultry production in Asia and the Pacific. III. Animal protein sources. World's Poult Sci. J, 49: 219–235.

Shamspur, T., Sheikhshoaie, I., &Mashhadizadeh, M. H. (2015). Flame atomic absorption spectroscopy (FAAS) determination of iron (III) after preconcentration on to modified analcime zeolite with 5-((4-nitrophenylazo)-N-(2′, 4′-dimethoxyphenyl)) salicylaldimine by column method. *Journal of Analytical Atomic Spectrometry*, *20*(5), 476-478.

Schütz, H., Seiler, W., & Conrad, R. (2019). Processes involved in formation and emission of methane in rice paddies. *Biogeochemistry*, *7*, 33-53.

Ziołecki, J.M., Eliezer, N. and Simha, R. (2019). The characterization of amino acid sequences in proteins by statistical methods. J. Theo. Bio. 21:170-201.

Effect of 3-Chloroacetophenone Derivative on Corrosion Inhibition of Mild Steel in Acidic Medium

*[1,2]Sani Ibrahim, [2]Siaka, A. A., [2]Kabo, K. S., [1]Garba, A., [1]Lawali Hashimu, [3]Ibrahim Garba, [4]J. Arockia Selvi and [5]Muhammad M Rumah

[1]Department of Chemistry, Zamfara State College of Education Maru, P.M.B 1002, Maru, Zamfara, Nigeria
[2]Department of Chemistry, Federal University Dustinma, Katsina, Nigeria.
[3]Department of Physics, Zamfara State College of Education Maru, P.M.B 1002, Maru, Zamfara, Nigeria.
[4]Department of Chemistry, SRM Institute of Science &Technology, Kattankulathur-603203, Tamil Nadu, India.
[5]Department of Chemistry, Al-Qalam University Katsina, Katsina State, Nigeria
*Corresponding Author's E-mail: ibrahimsaniwadata@gmail.com

ABSTRACT

Acetophenone derivatives are environmentally friendly corrosion inhibitors having an excellent trammel efficiency upon corrosion of Mild Steel (MS). This study investigated the inhibition behaviour of 3-Chloroacetophenone (3-CA) on mild steel in 1N hydrochloric acid Solution. Five different concentrations of the inhibitor ranging from 50-250ppm were used at four temperatures (303, 313, 323 and 333k) to determine the optimum corrosion inhibition behaviour. The inhibition effect of 3-CA was examined employing weight loss measurement, potentiodynamic polarization techniques and electrochemical impedance spectroscopy, scanning electron microscopy and Density Functional Theory (DFT) measurement was also used. The results showed that the adsorption of 3-CA on mid steel sample obeys Langmuir adsorption isotherm and that polarization studies revealed that the 3-CA behave as a mixed type of inhibitor mostly controlling anodic reaction. The result of the surface morphology study supported the adsorption of 3-CA on MS. The effect of 3-CA on corrosion IEs and certain molecular parameters were further studied by quantum chemical calculations based on density functional theory (DFT). The wettability and hydrophobicity nature of the mild steel surface was also observed through contact angle measurement. Finally, the results obtained revealed that 3-Chloroacetophenone performs fairly as a corrosion inhibitor for mild steel due to less percentage inhibition efficiency.

Keywords: Mild Steel, Corrosion inhibition, Weight loss measurement, EIS, SEM, DFT.

INTRODUCTION

Corrosion of mild steel is an issue that considerably affects the industrial and natural environment. It is substantially applied in different industries for different purposes which comprises of production of pipelines, metal tanks, gas cylinders, heat exchangers and so on, because of its superb machine-like strength and relatively low cost, it extends to to lifespan of appliances, the Mild Steel corrosion control became necessary. Application of inhibitors is the finest approach to be used to shield Mild Steel from corrosion, specifically in acidic conditions. Acetophenone derivatives are notable categories of organic compounds that serve as a substance for the synthesis of different kinds of heterocyclic compounds of physiological importance and they also behave as corrosion inhibitors in belligerence media (Mamedov, I. et al, 2019), (Nowakowska Z., et al, 2008) and (Patil S.G., et al, 2012)**.** Due to the presence of dissimilar functionality, 3-Nitroacetophenone compound confers biological activity like anticancer, antimicrobial, antibacterial, antiviral, and antitubercular (Sharma V. and Sharma K.V. 2010), (Bouklah M., et al, 2016) and (Fouda A.S. et al, 2014)**.** To control the corrosion of the metal, its surface needs to be masked significantly with an organic or an inorganic interdict material to be segregated from corrosive territory or domain (Fouda A.S. et al, 2014)**.** Application of molecules as an interdict species is the finest and most reliable practical technique used to shield the metal from dissipation in acidic means (Y. Meng, M.A. Deyb et al, 2017). This study aimed to determine the behaviour of 3-Cloroactophenone (3-CA) on mild steel in 1NHCl. The corrosion-forbidding ability of 3-CA on mild steel was examined via theoretical and experimental techniques. The Obstruction property was scrutinized via the authentic method of weight loss measurement, polarization techniques and electrochemical impedance spectroscopy, SEM analysis, Contact angle measurement and Computational study. Previous research in a paper titled Synthesis characterization, and Corrosion Inhibition Screening on 2-chloroacetophenone 4-ethyle-3-thiosemicarbazone (2ClAcTSC) in 1M HCl and H_2SO_4 using weight loss, SEM and DFT studies.

It was reported that the 2-chloroacetophenone 4-ethyle-3-thiosemicarbazone has better effectiveness in 1M HCl than in H_2SO_4 solution (Nur Zalin Khaleda Razali et.al, 2022)[13]**.** It was also reported that 3-Nitroacetophenone inhibits the corrosion of mild steel in 1N HCl solution and the maximum inhibition efficiency reaches 64 % at an inhibitor concentration of 250 ppm at 30 ºC (S. Ibrahim, R. et al, 2022)[14]**.** In this research study, the inhibition behaviour of 3-Chloroacetophenone as an organic inhibitor on mild steel (MS) in 1M hydrochloric acid solution was studied using

weight loss measurement, open circuit potentials, potentiodynamic polarization studies and electrochemical impedance spectroscopy (EIS). The hydrophobicity of the MS specimen was determined through contact angle measurement and molecular parameters were studied by quantum chemical calculations based on density functional theory (DFT). Surface morphologies and elemental composition of MS sample was investigated by scanning electron microscopy (SEM) and energy-dispersive X-ray spectroscopy (EDX).

MATERIALS AND METHODS
Materials
The experiments were performed with mild steel sample specimen which was purchased from Agaram Industries in Chennai. The elemental composition of the mild steel sample was Carbon (0.160%) Manganese (0.845%) Sulphur (0.007%) Silicon (0.050%) Phosphorus (0.024%) and Iron (balance; 98.7%). The 3-Chloroacetophenone and hydrochloric acids were also purchased and supplied by Agaram Industries laboratory equipment supplier. Various concentrations of the 3-CA comprised of 50 ppm, 100 ppm, 150 ppm, 200ppm, 250 ppm were prepared in purified water and acid solution (1M HCl) as corroding electrolyte was used.

Preparation of mild steel specimen
In this research, the 1x1 cm^2 size of the samples (MS) were polished successfully with an emery sheet of dissimilar grades (600-1200) until the metal surface was mirror polished and later degreased with Trichloroethylene (TCE), dried with drier and placed in a desiccator. In the end, the mirror polished sample and the clean specimen was immersed in the solution.

Weight loss measurements
The inhibition behaviour of 3-Chloroacetophenone (3-CA) on mild steel was examined via weight loss measurement. After the immersion process in 1M HCl and in 1M HCl plus various concentrations of the 3-CA (before and after), the weight of the abraded mild steel specimen was recorded using analytical balance. The effect of temperature on corrosion inhibition was also studied using 250 ppm concentrations of 3-CA at 303 K, 313 K, 323 K and 333 K, respectively. The mild steel samples were washed with water, rinsed with acetone, dried with the drier and weighed after each measurement. Corrosion rate (CR), Surface coverage (SC) and Inhibition efficiency (IE %) were calculated using the following formula. The experiments were performed in triplicate and average values are reported.

$$CR = \frac{87.6\ W.}{A.d.t} \tag{1}$$

Where, W, A, d and t represent weight loss in mg, surface area in cm^2 and density in g cm^{-3} of the MS sample, respectively. The geometric surface coverage (θ) is given by.

$$\theta = \frac{W_1 - W_2}{W_1} \tag{2}$$

Where, W$_1$ and W$_2$ weight loss of MS sample in 1M HCl and 1 M HCl + 3-CA, respectively. Finally, inhibition efficiency is calculated as

$$IE(\%) = \frac{W_1 - W_2}{W_1} \times 100 \tag{3}$$

Electrochemical measurements
The electrochemical measurements were carried out in Ivium Vertex potentiostat/galvanostat/ZRA with IviumSoft Electrochemistry Software, using an electrochemical cell assembled with three electrode cells. The saturated calomel electrode (SCE) was used as the reference electrode, mild steel with the surface area of 1 cm^2 was used as working electrode, platinum electrode as counter electrode and 3-Chloroacetophenone inhibitor in 1M HCl was used as electrolyte mixture. The electrochemical measurements were performed after 15 mins at room temperature (303 K) to attain a stable open circuit potential (OCP) of the system. The Potentiodynamic Polarization (PDP) tests were recorded by sweeping the potential of ± 250 mV vs OCP with a scan rate of 1 mV s^{-1}. The potential (E_{corr}) and corrosion current (i_{corr}) obtained would be examined via log current (i) versus potentials (E) plots. Consequently, the inhibition efficiency of the inhibitor was computed via the formula.

$$IE(\%) = \frac{i^\circ_{corr} - i_{corr}}{i^\circ_{corr}}\ X\ 100 \tag{4}$$

Where i°_{corr} and i_{corr} are the corrosion current densities without and with inhibitor.
EIS technique was carried out with a similar electrochemical setup as that was used for polarization technique using the same Ivium Vertex potentiostat. The impedance technique measurements were accomplished between 100 KHz to 0.01 Hz frequency by utilization of a 10-mV amplitude with respect to open circuit potential at room temperature.

To compute the inhibition efficiency, the charge transfer resistance (R_t) and double layer capacitance (C_{dl}) values would be employed via the following formula.

$$I.E(\%) = \frac{R_t - R_t^{\circ}}{R_t} \times 100 \tag{5}$$

Where R_t° and R_t are charge transfer resistance for mild steel in the absence and presence of inhibitors, respectively.

SEM - EDX analysis
In this study, the mild steel specimen was exposed to 1N HCl in the absence and presence of 3-Chloroacetophenone inhibitor to analyze the surface morphology of the mild steel surface for 1 hour. The mild steel samples were eroded, degreased with Trichloroethylene (TCE), dried with drying machine, and was examined using Scanning Electron Microscope. Similar procedure was employed for EDX to examine the elemental composition of the analyte (mild steel).

Contact angle measurements.
In contact angle measurement, the water contact angles (WCA) of the mild steel surface were measured by contact angle meter KYOWA DMs-40, following sessile drop method using half-angle method fitting and FAMAS (interFAce Measurement and Analysis System) software. The volume of water droplet of 2 μL was placed on mild steel surfaces. The measurements for each metal sample were repeated 10 times.

Computational studies
In corrosion studies, the efficiency of inhibition (%) is highly correlated with the molecular structure of the corrosion inhibitors. Consequently, the molecular structure of the 3-Chloroacetophenone was optimized by quantum chemical calculations using the Density Functional Theory (DFT) with B3LYP correlation functional (A. D. Becke, C. T. Lee, et al, 1988)[15, 16] and the 6-31 G (d, p) basis set. Quantum chemical calculations were carried out using Gaussian 16 software (M. J. Frisch, et al, 2016)[17]. The ionization potential (I) and electron affinity (A) are defined by $I = -E_{HOMO}$ and $A = -E_{LUMO}$, respectively. The electronegativity, $\chi = I + A/2$ and global hardness, $\gamma = I - A/2$ are calculated. Then the ΔN value can be calculated according to equation (T. K. Bhuvaneswari, et al, 2020) [18].

$$\Delta N = \frac{\chi_{Fe} - \chi_{inh}}{2(\gamma_{Fe} + \gamma_{inh})} \tag{6}$$

Where, $\chi_{Fe=7.0\,eV}$ and $\gamma_{Fe \approx 0}$ for iron is quoted from literature.

RESULTS AND DISCURSIONS
Weight loss measurement
The mild steel specimens were abraded with an emery sheet and immersed in the solution (1N hydrochloric acid with different concentrations of the 3-chloroacetophenone inhibitor) for an hour. The corrosion rate (CR in mm/y) and inhibition efficiency (IE in %) were calculated and the results obtained are shown in Table 1and Figure 1 table 1 and respectively. It is apparent that the corrosion rate decreases with an increase in the concentration of the inhibitor (3-chloroacetophenone) but the inhibition efficiency increases with an increase in the concentration of the inhibitor which is indicated that there is considerable surface coverage by the inhibit and strong bonding to surface of the Mild steel.

Table 1: Corrosion rate (mm/y) and inhibition efficiency obtained from weight loss measurement for mild steel specimen in the absence and presence of 0-250ppm concentrations of 3-Chloroacetophenone inhibitor acidic medium (1N HCl)

Conc. (ppm)	Blank	50	100	150	200	250
Weight loss(g)	0.0073	0.0039	0.0033	0.0029	0.0025	0.0021
Corrosion rate (mm/y)	8.1259	4.3466	3.6779	3.2321	2.7863	2.3405
Surface coverage (θ)	-	0.4658	0.5479	0.6027	0.6575	0.7123
Inhibition efficiency (%)	-	46.58	54.79	60.27	65.75	71.23

In the table above it is apparent that the corrosion rate decreases with an increase in the concentration of the 3-Chloroacetophenone and that the inhibition efficiency increases with an increase in the concentration of the inhibitor (3-CA) which indicates that there is a considerable surface coverage by the inhibit and strong bonding to the surface of the mild steel.
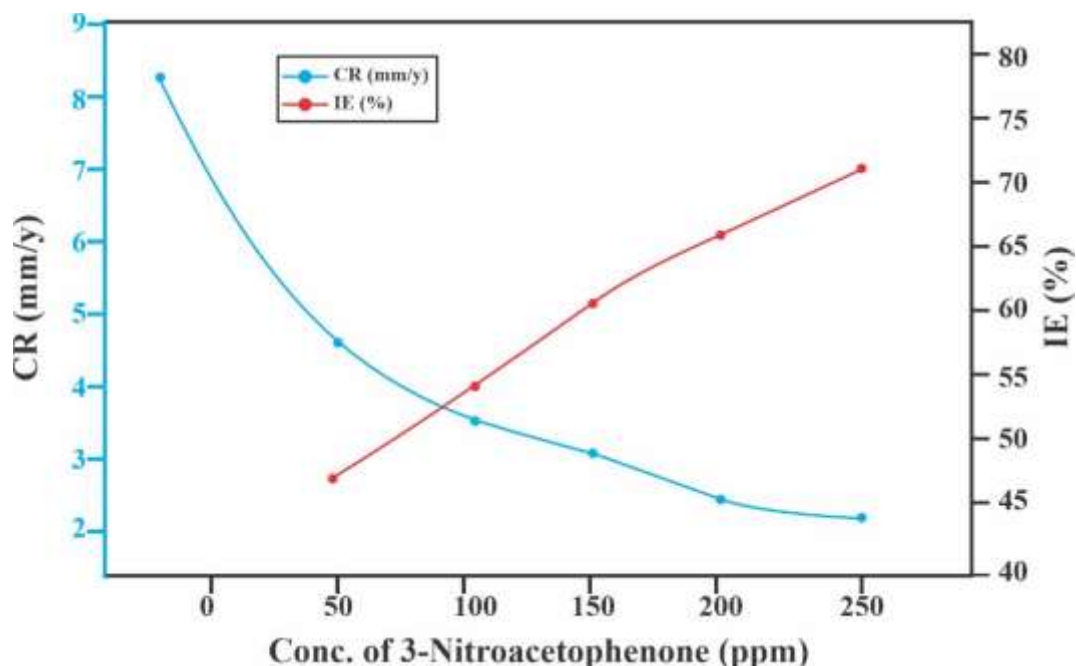
Figure 1: Corrosion rates and inhibition efficiency of 3-Chloroacetophenone (3-CA) from weight loss measurements

Effect of temperature
It is reported that the rate of chemical reaction increases with an increase in temperature, then the faster adsorption of 3-Chloroacetophenone on mild steel occurs due to the increase in temperature, so this temperature increase leads to faster desorption of the inhibitor on the metal surface.[15]. It is also revealed that the propensity of an organic corrosion inhibitor to shield mild steel is via the formation of an adherent common monomolecular layer of the metal surface[15]. Table 2 revealed the corrosion rate and inhibition efficiency of 3-Chloroacetophenone concerning temperature ranges from 30-60°C, after obtaining results at room temperature from the weight loss method, it showed that there is a gradual decrease in inhibition efficiency with an increase in temperature at 250ppm concentration which is due to desorption processes occurred between the 3-Chloroacetophenone and the mild steel.

Table 2: Corrosion rate and inhibition efficiency obtained from weight loss measurement for mild steel specimen with respect to different temperature in the absence and presence of 250ppm concentration of 3-Chloracetophenone inhibitor in acidic medium (1N HCl

Temperature (K)		303	313	323	333
Blank (1M HCl)	CR (mm/y)	8.1260	14.1545	16.1695	22.1221
3-Chloroacetophenone	CR(mm/y)	2.2406	4.3466	5.2382	6.7985
(250 ppm)	IE (%)	71.23	58.95	55.24	46.49
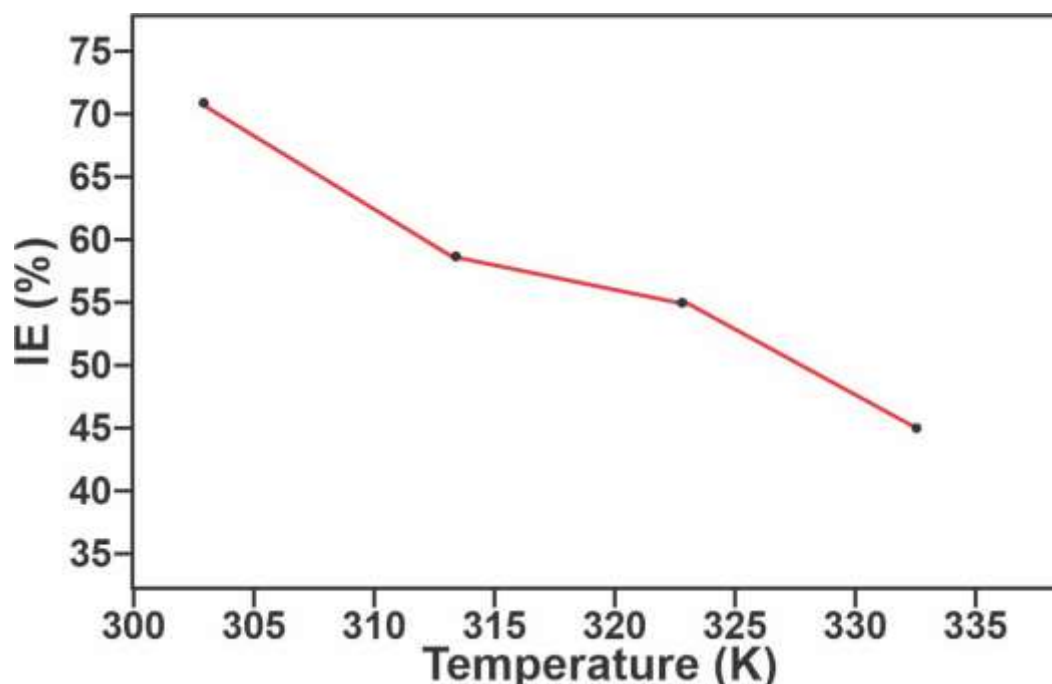
Figure 2: Inhibition efficiency for mild steel in 1N HCl in the presence of 250 ppm of 3-Chloroacetophenone with different temperature ranging from 303-323 K.

Electrochemical Impedance Spectroscopy (EIS)

The electrochemical impedance spectroscopy technique was used to find the inhibition efficiency of acetophenone derivatives and was accomplished in the frequency span of 100 KHz to 0.01Hz. Nyquist plots and Bode plots for the MS in the absence and presence of 3-CA inhibitor at 50-250 ppm concentration in 1N HCl are shown in Figure 3 and Figure 4 respectively. Table 3 shows the impedance parameters comprised of charge transfer resistance (R_{ct}), double layer capacitance (C_{dl}) and inhibition efficiency, respectively. The increase in charge transfer resistance (R_{ct}) from 43.85 ohm.cm^2 (blank)-to 69.26 ohm.cm^2 (250 ppm) revealed the formation of a defensive film of 3-CA on the surface of MS by adsorption. The maximum inhibition efficiency reaches to 36.69% in 3-CA concentration of 250 ppm. The adsorption of 3-CA inhibitor on the metal surface leads to the formation of a double-layer, which could form a barrier between the metal surface and the corrosive medium. This is further confirmed by the decrease in the double-layer capacitance (C_{dl}) from 1.082 X 10^{-4} F cm^{-2} (blank) to 4.244 X 10^{-5} F cm^{-2} (250 ppm of 3-CA). The impedance increases with increase in the concentration of 3-CA. Nyquist and Bode plots confirmed the single charge transfer process in the corrosion inhibition mechanism. The EIS spectra obtained for mild steel were best fitted with the equivalent circuit as shown in Figure 3, where R1 is the solution resistance, R2 is the polarization resistance and C1 is the double-layer capacitance. R(CR) model is used for the protective isolated layer formed at the metal surface and that provides a protective performance by 3-CA.
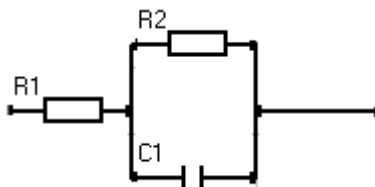
Figure 3: Equivalent circuit for EIS spectra of the studied system

Table 3: The EIS parameter for MS in 1 N HCl in the presence and absence of 3-Chroacetophenone A

Conc. of inhibitor (ppm)	R_{ct} (ohm.cm^2)	C_{dl} (F cm^{-2})	IE (%)
Blank 1N HCl	43.85	1.082 X 10^{-4}	-
250 ppm	69.26	4.244 X 10^{-5}	36.69
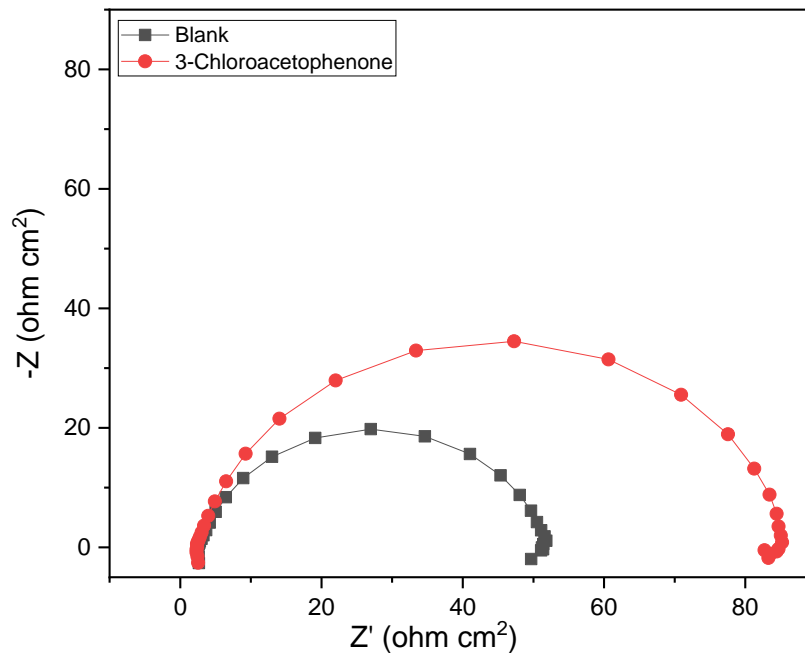
Figure 4: Nyquist plot for mild steel obtained with absence and with presence 250 ppm of 3-Chloroacetophenone in 1N HCl.
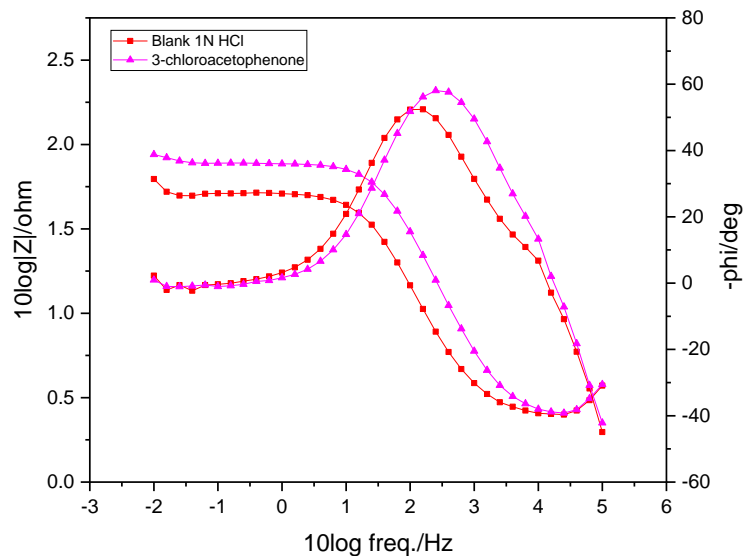
Figure 5: Bode plot for mild steel obtained with absence and with presence OF 250 ppm of 3-Chloroacetophenone in 1N HCl.

Potentiodynamic polarization study

The Potentiodynamic polarization measurements were studied to investigate the effect of 3-CA on the anodic and cathodic reactions on corrosion phenomenon. The saturated calomel electrode (SCE) was used as the reference electrode, mild steel with the surface area of 1 cm^2 was used as the working electrode, platinum electrode as counter electrode and 3-Chloroacetophenone inhibitor in 1N HCl was used as electrolyte mixture. The polarization curves for MS in 1N HCl solution containing a concentration 250ppm of 3-CA are shown in Figure 6. The different parameter obtained from polarization measurements such corrosion potentials (E$_{corr}$), as well as kinetic values like corrosion current density (i$_{corr}$), cathodic and anodic Tafel slopes (βc and βa) and polarization resistance (Rp) ware presented in table 4. There are little changes in parameters for βa and βc upon the addition of the inhibitors as compared to the

blank value which indicates that the inhibitor gets adsorbed on mild steel surface controlling both anodic and cathodic reactions. The inhibitor 3-CA is a mixed type of inhibitor as the difference in corrosion potential, E_{corr}, between the inhibitor and that of blank is less than 80 mV. The decrease in corrosion current, i_{corr}, from 5.871×10^{-4} (blank) to 5.484×10^{-4} (250 ppm of 3-Chloroacetophenone) is observed and exhibits 38.51% IE.

Table 4: The polarization parameters for mild steel in 1 N HCl in the presence and absence of 250 ppm of 3-Chloroacetophenone.

Conc. of inhibitor (ppm)	E_{corr} (V vs SCE)	I_{corr} (A/cm²)	R_p (ohm)	β_a (V dec⁻¹)	β_c (V dec⁻¹)	CR (mm/y)	IE (%)
Blank 1N HCl	-0. 527	5.871×10^{-4}	61.9	0.100	0.068	3.1168	-
3-Chloroacetophenone	- 0.5226	5.484×10^{-4}	66.84	0.136	0.221	6.45	38.51
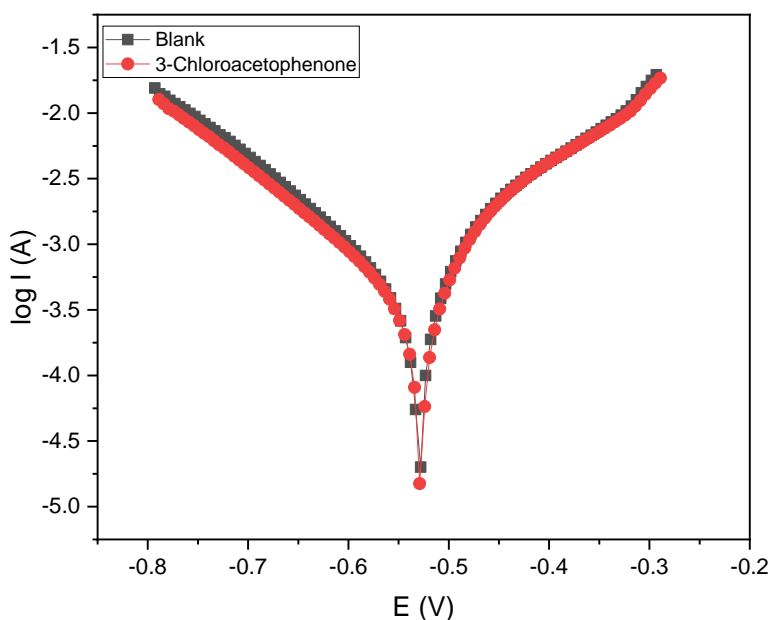
Figure 6: Tafel plot for MS obtained with absence and with presence of 50-250 ppm of 3-Chloroacetophenone in 1N HCl.

Adsorption isotherms

The adsorption isotherms are numerical utterances which give clear information on the mutual effect of the surface of the metal and adsorbing species at a constant temperature. there are many adsorption isotherms that give the correlation between metal surface coverage and concentration of the adsorbed species[19]. The prominent adsorption isotherm is Langmuir adsorption isotherm and can be expressed via the following (Vandana Saraswat, et al, 2014)[19] **and** (M.M. El-Naggar, 2007) [20].

$$\frac{C}{\theta} = \frac{1}{K_{ads}} + C \tag{7}$$

Where C is the concentration of the inhibitor, Θ is the standard degree of the surface coverage on the mild steel (from electrochemical impedance and polarization studies) and K_{ads} is the equilibrium constant for the adsorption. The Langmuir adsorption isotherm of the 3-Chloroacetophenone gave the most shaped curve for the adsorption on a mild steel surface in 1 N HCl solution. The values plotted (C/Θ as a function of C) in figure 7 gave a straight line with a big correlation coefficient of nearest unity and an intercept of 0.04451. It should be noted that the adsorbed 3-Chloroacetophenone lined up on the surface of mild steel as seen in (vii). The K_{ads} of the inhibitor were calculated using an intercept of the equation of the C/Θ by C plots as in (vii) (viii) and was used to calculate the free energy of adsorption(ΔG^0_{ads}) via the following:

$$\Delta G^0_{ads} = -RT ln(55.5 K_{ads}) \tag{8}$$

Where R was the gas constant (8.3142 J K^{-1}Mol^{-1}), T is the absolute temperature (K) and 55.5 was the molar concentration of water. The adsorption parameters, K_{ads} = 22.47 Lg^{-1} and ΔG^0_{ads}= −17.96 KJ mol^{-1} were calculated. In which the negative value of the standard free energy of adsorption indicated that the molecule adsorbed on the mild steel surface. The values of ΔG^0_{ads} obtained (−17.96) revealed the physical adsorption due to electrostatic communication between charged particles and charged metal.

SEM-EDX analysis

The Surface morphology of the mild steel specimen was assessed by a scanning Electron Microscope which accorded the nature of the film formed on the mild steel surface. It is proved that an increase in surface roughness makes the sites to attack metal surface in aggressive media (Vandana Saraswat, M. Yadav, 2014) [21] and (M.M. El-Naggar, 2007)[22]. The SEM images are shown in Figure 8. It is proved that the mild steel surface is uniform before the analysis while in Figure 8a, the surface is damaged in solution of 1N HCl after immersion process. However, in the presence of 3-Chloroacetophenone inhibitor at of 250ppm concentration, the mild steel surface is smooth and less damaged. It's observed that the surface of the mild steel is shielded and protected in the presence of the 3-Chloroacetophenone inhibitor as presented in figure 8b. Hence, the presence of an inhibitor indicates a good corrosion inhibition efficiency on the surface of the metal. The elemental analysis by EDAX, reveals the absence of chlorine in the inhibited metal surface, thereby shows the protective layer formed by the inhibitor prevents the attack of Cl$^-$ towards the metal surface. However, the surface of the metal is not fully covered by the inhibitor, as is evident from that of the higher mass % of Fe shown for the inhibited metal surface in Table 5.
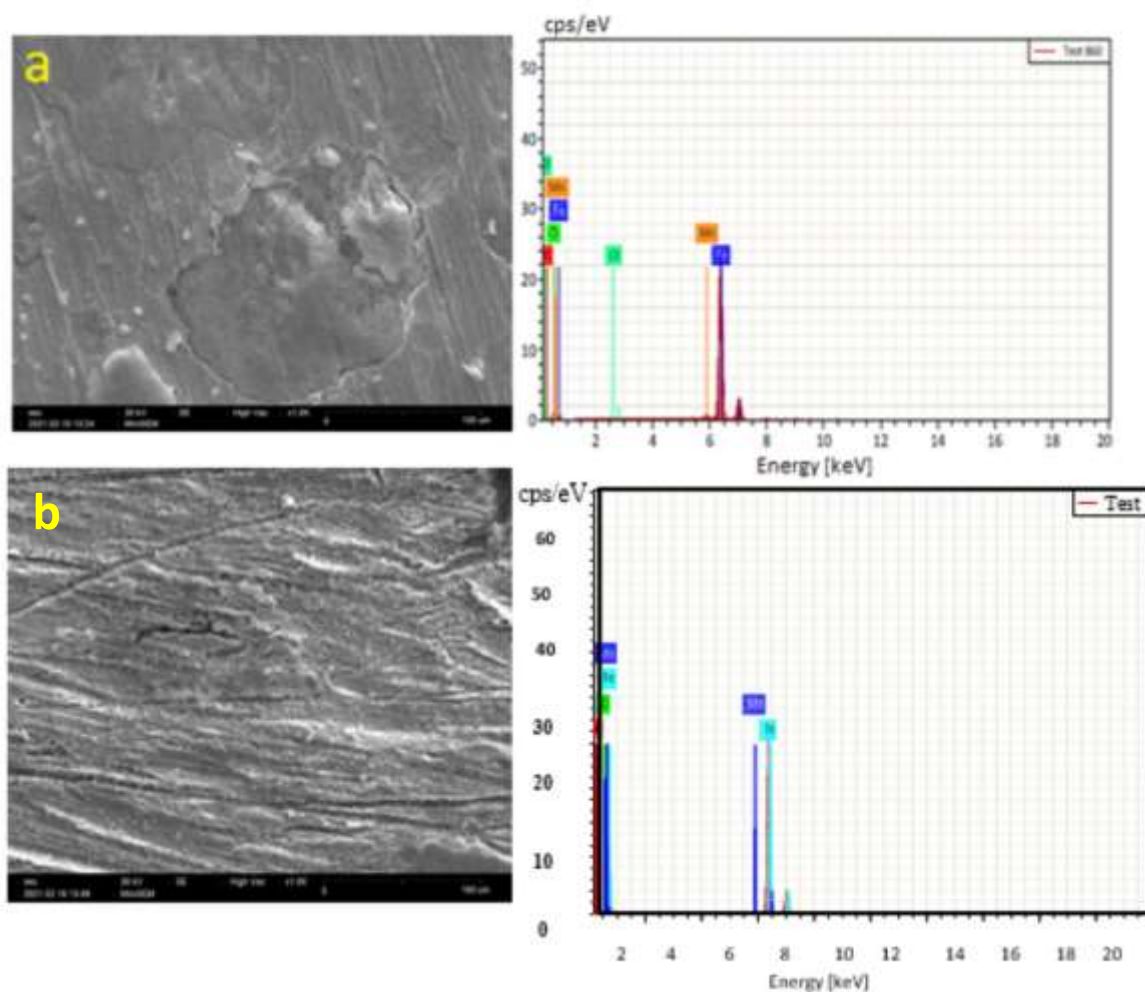
Figure 7: SEM-EDX micrographs of the mild steel surface:(a) in 1N HCl solution (b) in 1N HCl solution with 250 ppm of 3-Chloroacetophenone.

Table 5: Elemental composition from EDX analysis

Element	Mass %	
	Blank	3-Chloroacetophenone
Carbon	9.02	8.93
Oxygen	12.78	10.15
Chlorine	0.13	-
Manganese	0.46	-
Iron	142.57	155.33

Computational studies

The optimized molecular orbital structure, electronic structure, and molecular orbital energy of the 3-Chloroacetophenone are shown in Figure 9 and the resonance structure in Figure 10. The quantum chemical values such as the energy of the highest occupied molecular orbital molecular. The quantum chemical parameters, such as the energy of highest occupied molecular orbital (E_{HOMO}, -5.9476 eV), energy of lowest unoccupied molecular orbital (E_{LUMO}, -2.9328 eV), energy gap ($E_{LUMO} – E_{HOMO}$, -3.0148 eV), dipole moment (1.4476 D), and ionization potential (5.9476 eV) and electron affinity (2.9328 eV) are obtained for 3-Chloroacetophenone. Higher the values of E_{HOMO} denotes the electron-donating abilities of the molecule. Also, the molecule with a lower energy gap value in the range of 6.40 to 3.38 eV shows higher inhibition efficiency (Luna M Corrales, Chandrabhan Verma, et al, 2019), (Elshafie A.M et al, 2018) and (A. S. Fouda, M. M. Gouda, and S. I. Abd El-Rahman 2002) [23-26]. However, the energy gap calculated in 3-CA is 2.3996 eV, which is not in the range required for better IE %. The measure of electron transfer from inhibitor molecule to metal is favored, if $\Delta N > 0$ (Ziyi Cao, Yongming Tang, et al, 2014)[27]. Thereby, the calculated value of $\Delta N = 0.8014$ for 3-CA reveals the electron-donating ability of the inhibitor at the metal surface. The Mullikan charges on the atoms are used to analyze the adsorption center of the inhibitor, it is observed that, if the atom has a more negative charge, then the adsorption is more on the surface. The optimized structure of 3-CA with charges is shown in Figure 8(a). It is inferred that adsorption of inhibitors on metal surfaces is through the Oxygen atom rather than the carbon-atom as a greater negative charge is observed on O-atoms. π-electrons also interact with the vacant d-orbital of metal. However, the presence of electron-withdrawing nitro group attracts the π-electrons of the aromatic ring. Thereby, this leads to a decrease in the electron density of the aromatic ring and thus, shows lower inhibition efficiency of 3-Chloroacetophenone.

Table 6: Quantum chemical parameters of 3-Chloroacetophenone

Total Energy (KJ/mole)	E_{homo}(eV)	E_{lumo} (eV)	Energy gap (eV)	Ionization potential (eV)	Electron affinity (eV)	Dipole moment
-2215501.92	-5.9476	-2.9328	3.0148	5.9476	2.9328	1.4476

Ehomo   **Elumo**

Figure 8: Structure of E HOMO and E LUMO of 3-Chloroacetophenone.

Contact Angle Measurement

The sessile drop contact angle measurements were shown in Figure 11 for (a) a polished metal surface, (b) A surface of mild steel immersed in 1N HCl and (c) an inhibited metal surface with 250 ppm of 3-CA in 1N HCl. The water wetting nature of the metal surfaces was carried out on all three metal surfaces. Generally, if WCA is smaller than 90º, the metal surface is hydrophilic and if WCA is greater than 90º, then the metal surface is hydrophobic (Pooja Singh, Ashish K. Singh, Vinod P., H. Jafari, I. Danaee, et al, 2013)[28,29]. The WCA for polished metal sample is observed at 99.5º and since WCA is greater than 90º, it is hydrophobic. Furthermore, WCA of metal surface immersed in 1N HCl is found at 55.1º. This confirms the wettability of the uninhibited metal surface and, its hydrophilic nature. However, for inhibited metal surface using 250 ppm of 3-Chloroacetophenone, WCA is seen at 65.1º and a slight

increase in WCA relatively shows the protective layer formed on the metal surface by the inhibitor. The decrease in wettability and increase in hydrophobicity confirms the protective nature of the mild steel surface from wetting.
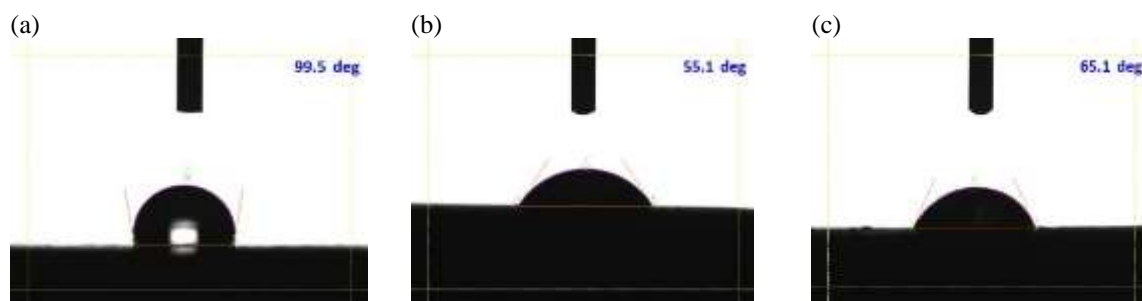
Figure 9: Sessile drop method - Contact Angle of a) Polished mild steel b) mild steel immersed in 1N HCl and c) mild steel immersed in 250 ppm of 3-Chloroacetophenone.

CONCLUSION

In conclusion, this research study was aimed in investigating and finding out the inhibition behaviour of 3-Chloroacetophenone as a corrosion inhibitor of mild steel sample in an acidic medium (1N HCl) via weight loss measurement, electrochemical studies, scanning electron microscopy, contact angle measurement and computational studies via density function theory as summarized below:

  i. The result revealed that the inhibition efficiency (IE %) increases with an increase in concentration of 3-Chloroacetophenone, giving maximum inhibition efficiency of 71.23% in 250ppm concentration of the 3-CA.
 ii. Electrochemical impedance analysis revealed that the explored inhibitor remarkably in charge transfer resistance parameters and double layer capacitance value low which revealed the adsorption of inhibitor on metal surface.
iii. Potentiodynamic polarisation studies reported that the 3-Chloroacetophenone act as a mixed category of inhibitor.
 iv. The adsorption of 3-CA on MS surface Obeys Langmuir adsorption isotherm and the ΔG^0 Value indicates spontaneous adsorption of 3-CA by physical interaction.
  v. SEM-EDX analysis showed that there are dissimilarities on the surface morphology of the sample metal which is due to the formation of coating by the inhibitors.
 vi. Computational studies explained that there is remarkable inhibition efficiency in 3-Chloroacetophenone due higher dipole moment value.
vii. EHUMO, ELUMO and µ are chemical quantum parameters used in DFT studies, were good in agreement with the results.

RESEARCH HIGLIGHTS:

  i. The 3-Chloroactophenone proved to be a fair inhibitor due to less inhibition efficiency value via weight loss measurement.
 ii. The Low inhibition efficiency of the 3-Chloroacetophenone is a result of electron withdrawing nature of the Chloro substituent.
iii. The adsorption behaviour of 3-Chloroactophenone inhibitor on mild steel Obeys the Langmuir adsorption isotherm.
 iv. The polarization studies confirmed that the 3-Chloroacetophenone inhibitor behave as an assorted type of inhibitors.
  v. The surface analysis and contact angle measurement also support the obtained results.
 vi. The values obtained in computational studies were correlated with the experimental results.

REFERENCES:

Mamedov, I., Shikhaliyeva, I., Mamedova, Y., Gasimova, S., & Maharramov, A. M. (2019) "Some Acetophenone Derivatives as Corrosion Inhibitors", *Chemical Problems,* 17(2), 302-309. doi:10.32737/2221-8688-2019-2-302-309.

Nowakowska Z., Kedzia B., Schroeder G. (2008) "Synthesis, physicochemical properties and antimicrobial evaluation of new (E)- chalcones", *Eur. J. Med. Chem.,* vol. 43, pp. 707-713.

Patil S.G., Utale P.S., Gholse S.B., Thakur S.D., Pande S.V.J. (2012) "Synthesis, characteriza-tion and antimicrobial activity of 6-bromo- 4-methoxy4-(substituted phenyl) iminofla- vone", *Chem. and Pharm. Research*. , vol. 4, pp. 501-507.

Sharma V., Sharma K.V. (2010) "Synthesis and bio- logical activity of some 3,5- diarylisoxazoline derivatives: reaction of substituted chalcones with hydroxylamine hydrochloride", *E-Jour. Chem*. vol. 7, pp. 203-209.

Bouklah M., Hammouti B., Aouniti A., Benkaddour M., Bouyanzer A. (2016) "Synergistic effect of iodide ions on the corrosion inhibition of steel in 0.5 M H2SO4 by new chalcone derivatives", *Appl. Surf. Sci.*, vol. 252, pp. 6236-6242.

Fouda A.S., Hassan A.F., Elmorsi M.A. Fayed T.A, Abdelhakim A. (2014) "Chalcones as Environmentally Friendly Corrosion Inhibitors for Stainless Steel Type 304 in 1M HCl Solutions", *Int. J. Electrochem. Sci*.2014, vol. 9, pp. 1298-1320.

Fouda A.S., Shalabi K., Elewady G.Y., Merayyed H.F. (2014) "Chalcone Derivatives as Corrosion Inhibitors for Carbon Steel in 1M HCl Solutions"*, Int. J. Electrochem. Sci*., vol. 9, pp. 7038-7058.

Singh P., Quraishi M.A., Ebenso E.E. Verma C.B. (2014) "Ultrasound Assisted Synthesis of Chalcones as Green Corrosion Inhibitors for Mild Steel in 1M Hydrochloric Solution", *Int. J. Electrochem. Sci*., vol. 9, pp. 7446-7459.

H. El Attari, S. Mengouch, M. Siniti, E. Zahidi, L. Khamliche and A. Kheribech, (2018) *Journal of Materials and Environmental Science*, 9, 2 DOI:10.26872/jmes.2018.9.2.76.

S. Cao, D. Liu, P. Zhang, L. Yang, P. Yang, H. Lu and J. Gui, (2017) *Scientific Reports*, 7, 1, DOI: 10.1038/s41598-017-07925-y.

Y. Meng, W. Ning, B. Xu, W. Yang, K. Zhang, Y. Chen, L. Li, X. Liu, J. Zheng and Y. Zhang (2017). "Inhibition of mild steel corrosion in hydrochloric acid using two novel pyridine Schiff base derivatives": a comparative study of experimental and theoretical results. RSC Advances, vol. 7, 68, DOI: 10.1039/C7RA08170G

M. A. Deyab, A. S. Fouda, M. M. Osman and S. Abdel-Fattah. (2017) "Mitigation of acid corrosion on carbon steel by novel pyrazolone derivatives". *RSC Advances*, vol. 7, pp. 71, DOI: 10.1039/C7RA08761F.

Nur Zalin Khaleda Razali et.al (2022) "Synthesis, characterization, and corrosion inhibition screening on 2-chloroacetophenone 4-ethyle-3-thiosemicarbazone (2ClAcTSC) in 1M HCl and H$_2$SO$_4$", *Chemical papers- Slovak Academy of Sciences*, DOI: 10.1007/s11696-022-02297-8.

S. Ibrahim, R. Sanmugapriya, J. Arockia Selvi, T. Pushpa Malini, P. Kamaraj, P. A. Vivekanad, Govindasami Periyasami, Ali Aldalbani, Karthikeyan Perumal, J. Madhavan Santosh Khanal (2022) "Effect of 3-Nitroacetophenone on corrosion inhibition of mild steel in Acidic medium", *International of photo energy,* DOI: 10.115/2022/7276670.

A. D. Becke, "Density-functional thermochemistry. III. The role of exact exchange", *J. Chem. Phys.*, 98, 5648-56521993.

C. T. Lee, W. T. Yang and R. G. Parr, (1988) "Development of the Colle-Salvetti correlation-energy formula into a functional of the electron density", *Phys. Rev. B*. 37, 785-789–789.

M. J. Frisch, G. W. Trucks, H. B. Schlegel, G. E. Scuseria, M. A. Robb, J. R. Cheeseman, G. Scalmani, V. Barone, G. A. Petersson and H. Nakatsuji, (2016) "*Gaussian 16, Revision B.01*; Gaussian", *Inc.: Wallingford CT, UK*.

T. K. Bhuvaneswari, C. Jeyaprabha and P. Arulmathi, (2020) "Corrosion inhibition of mild Steel in hydrochloric acid by leaves extract of Tephrosiapurpurea", *Journal of Adhesion Science and Technology*, vol. 34, pp. 2424-2427 DOI: 10.1080/01694243.2020.1766395.

Vandana Saraswat, M. Yadav (2014) "adsorption behavior of o-hydroxy acetophenone benzoyl hydrazone on mild

steel /hydrochloric acid interface". *Journal of industrial and Engineering chemistry*, vol. 21 pp 03-018.

M.M. El-Naggar, (2007) "Corrosion inhibition of mild steel in acidic medium by some sulfa drugs compounds", *Corrosion Science* vol. 49*,* pp. 2226–2236. Doi: 10.1016/j.corsci.2006.10.03.

Vandana Saraswat, M. Yadav (2014) "adsorption behavior of o-hydroxy acetophenone benzoyl hydrazone on mild steel /hydrochloric acid interface". *Journal of industrial and Engineering chemistry*, vol. 21 pp 03-018.

M.M. El-Naggar, (2007) "Corrosion inhibition of mild steel in acidic medium by some sulfa drugs compounds", *Corrosion Science* vol. 49*,* pp. 2226–2236. Doi: 10.1016/j.corsci.2006.10.03.

Luna M Corrales, Tu Le Manh, R Cabrera Sierra, JV Medina Flores, L Lartundo Rojas, EM Arce Estrada. Study of corrosion behavior of API 5L X52 steel in sulfuric acid in the presence of ionic liquid 1-ethyl 3-methylimidazolium thiocyanate as corrosion inhibitor. *Journal of Molecular Liquids,* 111106, 2019.

Chandrabhan Verma, Lukman O. Olasunkanmi, Indra Bahadur, H. Lgaz, M.A. Quraishi, J. Haque, El-Sayed M. Sherif, Eno E. Ebenso (2019) "Experimental, density functional theory and molecular dynamics supported adsorption behaviour of environmental benign imidazolium based ionic liquids on mild steel surface in acidic medium", *Journal of Molecular Liquids* vol. 273 pp. 1-15.

Elshafie A.M et al, (2018) "Theoretical approach for the performance of 4-mercapto-1-alkylpyridine-1-ium bromide as corrosion inhibitors using DFT", *Egyptian journal of petroleum*, vol. 27, pp. 695-699.

A. S. Fouda, M. M. Gouda, and S. I. Abd El-Rahman. (2000) "1,2,4-triazole on carbon steel corrosion in hydrochloric acid". *Bull. Korean Chem. Soc.* Vol. 21, No. 11 1085.

Ziyi Cao, Yongming Tang, Hui Cang, Jinqiu Xu, Gang Lu, Wenheng Jing, Novel benzimidazole derivatives as corrosion inhibitors of mild steel in the acidic media. Part II: Theoretical studies, *Corrosion Science* 83 (2014) 292–298

Pooja Singh, Ashish K. Singh and Vinod P. Singh (2013): "Synthesis, structural and corrosion inhibition properties of some transition metal (II) complexes with o-hydroxyacetophenone2-thiophenoyl hydrazone Polyhedron" vol. 65, pp. 73–81.

H. Jafari, I. Danaee, H. Eskandari and M. RashvandAvei, (2013) "Electrochemical and Theoretical studies of adsorption and corrosion inhibition of N, N-Bis (2-hydroxy ethoxy acetophenone) 2-dimethyl-1,2-propanediimine on low carbon steel (API 5L Geade B) in acidc medium" *Industrial & Engineering Chemistry Research*, vol. 52, 20, pp. 6617-663220, DOI:10.1021/ie400066x.

Insilico Design of Novel Drug Candidates against *Staphylococcus aureus* from Some Hydrazide Derivatives: QSAR, Molecular Docking, Drug-likeness and ADMET Investigation

*[1]Mary Ikhaote Ohiole and [2]Siaka Abdulfatai

[1]Department of Chemistry, Federal University Lokoja, P.M.B. 1154, Lokoja Kogi State
[2]Department of Applied Chemistry, Federal University Dutsinma, P.M.B 5004, Katsina State.
*Corresponding Author's E-mail: mary.ohiole@fulokoja.edu.ng

ABSTRACT
It is urgently necessary to look for fresh drug candidates in the pipeline of antibacterial drug development since *S. aureus* cases are becoming more resistant to current antibiotics. The purpose of this study was to use QSAR modeling to connect the biological activities of a series of bioactive hydrazide derivatives against S. aureus that had been shown to have bioactivities. Using the Spartan 14 software's DFT approach at the B3LYP level of theory and the 6-31G** basis set, the compounds were geometry optimized to determine their minimal energy conformations before the model was built. Based on the measured minimum inhibitory concentration (MIC) of the compounds, the validated QSAR model (R^2 = 0.73, R^2Adj = 0.70, Q^2LOO = 0.62, R^2Pred = 0.76) suggested that TDB10u, MDEC-12, and Dm descriptions dominated. Two newly developed hydrazide analogues, C-1 and C-2, were predicted by the validated model to have MICs of 11.27 and 7.17 µg/mL, respectively. The novel ligands' projected minimum inhibitory concentration (MIC) values indicate that their potencies surpass those of the most potent compounds in the dataset. C-1 and C-2 binding energies of -8.2 and -8.1 kcal/mol were found in molecular docking simulations conducted against the bacterium's DNA gyrase active sites, respectively. Additionally, the superior pharmacokinetic and toxicological characteristics of the proposed ligands were disclosed by their ADMET profiles. The abundance of knowledge gained from this research is expected to aid in the identification and creation of new antibiotics that are effective against *S. aureus.*
Keywords: *Staphylococcus aureus*, Hydrazide, QSAR, descriptors, molecular docking

INTRODUCTION
One of the main pathogenic microorganisms that cause infections in hospitals and the community is the Gram-positive bacterium Staphylococcus aureus (*S. aureus*). Numerous diseases, including bacteremia, pneumonia that can be deadly, moderate infections of the skin and soft tissues, infective endocarditis, and osteomyelitis, are caused by this microorganism (Guo *et al.,* 2020; Humphreys, 2012). Antibiotic therapy is typically used to treat S. aureus infections; but, due to the microbe's increasing resistance to current antibiotics, drug developers must constantly look for novel medications. (Klemm *et al.,* 2018; Obanda *et al.,* 2022).
A novel drug's discovery and development are difficult tasks since they need a significant investment of time and money. Nonetheless, the bottlenecks associated with the conventional trial-and-error methods have been considerably reduced by the use of computer-aided approaches in contemporary medication research (Ameji *et al.,* 2023; Kore *et al.,* 2012). Quantitative Structure-Activity Relationship (QSAR) modeling is a crucial in silico method used in drug discovery and development. Using a regression model similar to the one in equation 1, QSAR connects the characteristics of chemicals to their biological functions.

$$Y = \beta x_1 + \gamma x_2 + \omega x_3 + c \tag{1}$$

where the biological feature of interest is denoted by Y, the molecular descriptors by x1, x2, and x3, the numerical coefficients by β, γ, and ω, and the regression model constant by c. The QSAR approach is important for ligand-based drug discovery because it maximizes lead compound potency and drug-like qualities (Ameji *et al.,* 2023; Sprous *et al.,* 2006). Modern drug design also heavily relies on the application of molecular docking studies, which simulate the binding interaction between ligands, or small molecules, and the active sites of macromolecular targets. The standard expression for the strength of the interaction between a ligand and a target macromolecule is the change in Gibb's free energy (ΔG). The strength of the binding interaction increases with decreasing binding magnitude (ΔG) and vice versa (Behl *et al.,* 2021; Hussain *et al.,* 2021). Furthermore, the absorption, distribution, metabolism, excretion, and toxicity (ADMET) of a biologically active ligand determine its safety as well as its capacity to perform the necessary pharmacological functions in the biological system. Because it helps reduce the attrition rates of drug-like candidates during the preclinical and clinical stages of drug development, in silico ADMET profiling is a crucial part of contemporary drug research (Ameji *et al.,* 2022; Daoud *et al.,* 2021).

Heterocyclic molecules known as hydrazides are produced by acylating hydrazine. Their atoms of nitrogen and carbon are the active centers of their pharmacological activity. Hydrazides are special because they have a covalent link between nitrogen and four substituents, at least one of which is an acyl group. Hydrazine does not have an acyl group, in contrast to hydrazides. Largely beneficial, hydrazides are therefore fundamental to medications like iproniazide (anti-tuberculosis), nifuroxazide (antibiotic), nifurtimox (antiameboic), 2-azetidiones (an inhibitor of β-lactamase), thiazolidinediones (an inhibitor of peptidoglycan synthesis), etc (Kumari and Narang, 2016).

This study aims to develop powerful and non-toxic hydrazide-based new therapeutic candidates against *S. aureus* by utilizing in-silico approaches as QSAR modeling, molecular docking simulation, and ADMET profiling. Recent in-silico research on anti-*S. aureus* thienopyrimidine derivatives includes the work of Ouassaf *et al.,* (2021), in which the authors conducted combined 3D-QSAR, molecular docking simulation, and ADMET studies. The goal of this research was to develop novel therapeutic ligands against *S. aureus.* Their CoMFA and CoMSIA models, which have been validated, were utilized in the formulation of several new medications.

QSAR modeling was done by Khatkar *et al.,* (2014) on a number of synthetic compounds of p-coumaric acid. The first order molecular connectivity index, Wiener index, topological characteristics, and electronic energy of the molecules all had an impact on the compounds' antibacterial activity, the authors discovered.

Additionally, Cortes *et al.,* (2020) used molecular docking and QSAR modeling to examine the bioactivity of twenty-four cannabinoids against Methicillin-Resistant S. aureus. Three novel ligands with notable activity against the pathogenic microorganisms were designed by the scientists using the validated model. Additionally, they discovered that the chemicals under investigation exhibit a notable binding affinity for the bacterium's DNA gyrase and penicillin binding protein.

MATERIALS AND METHODS
Acquisition of Data, Geometry Optimization and Descriptor Calculation
From the literature, a set of thirty-nine (39) hydrazide derivatives with known minimum inhibitory concentrations (MICs) of their inhibitory activity against S. aureus were retrieved (Bhole and Bhusari, 2010; Ozdemir *et al.,* 2009). During the model-building process, the MIC values of the substances under investigation were converted into logarithm form (jMIC = log MIC) to obtain a more linear response and decrease data dispersion (Ameji *et al.,* 2023). A molecule's minimal energy conformation can be found by a technique called geometry optimization. The 2D structures of the compounds were drawn using ChemDraw Ultra 12.0. The Spartan 14 version 1.1.4 software from Wavefunction Inc. was used to export these structures one at a time into 3D geometry. Density functional theory (DFT/B3LYP) method and 6-31G* basis set were used to optimize the geometry of each molecule. The PaDEL descriptor tool set (Ameji *et al.,* 2023; Ameji *et al.,* 2022b; Yap *et al.,* 2011) was utilized to calculate the descriptors of the optimized structures. These bioactive compounds' pMIC and chemical structures are shown in Table 1.

Building and Validation of QSAR Model
The QSAR model was constructed by dividing the studied hydrazide derivatives data set using the Data-set-Division GUI V2.1 tool of DTC laboratory into 70% training set and 30% test set. The test set served as an external validation source for the model, whereas the training set was used to develop it. In order to eliminate redundant descriptors from the generated pool of descriptors, the V-WSP data pretreatment tool 1.2v was utilized. Using Equation length of 4, Mutation probability of 0.3, variance cut off of 0.001, and inter-correlation cut off of 0.9, the Genetic Algorithm v4.1 tool was utilized to construct the best QSAR model. Internal validation of the constructed QSAR model was performed using adjusted R-squared (R2Adj.), cross-validated R-squared (Q2LOO), and least squares fit (R2). R2Pred, the predicted R2 for the external test set, was used to determine the best model's external prediction ability." According to Ameji *et al.,* (2023) and Rajer-Kandu *et al.,* (2000), the validation metrics derived for the model were compared with typical validation metrics in QSAR modeling.
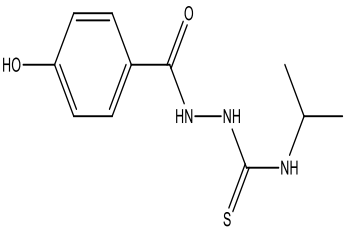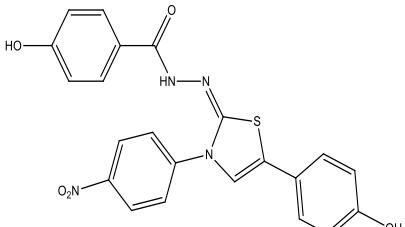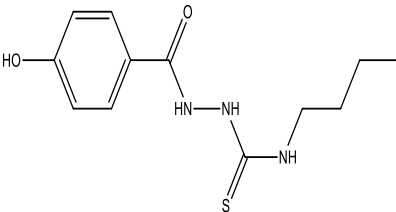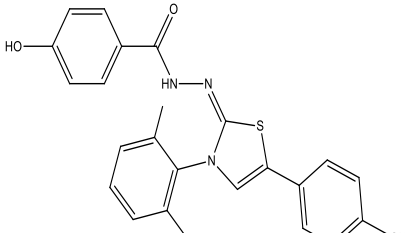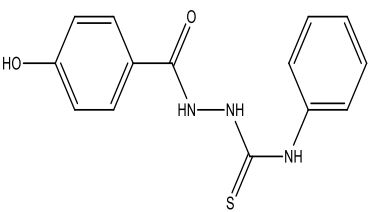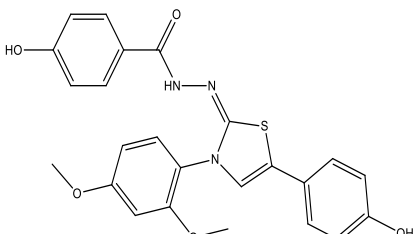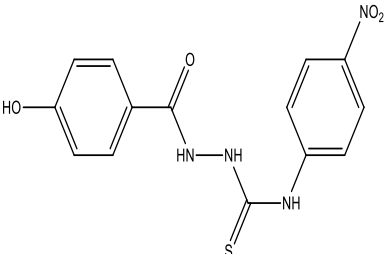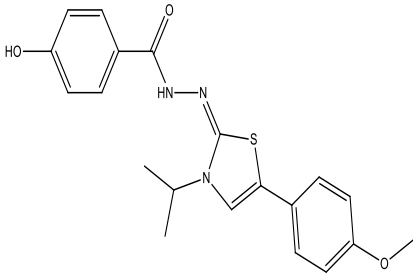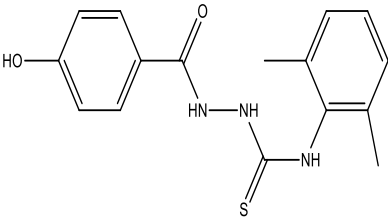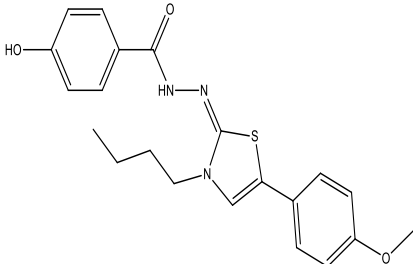
Applicability domain definition
The bioactivity of every molecule in the cosmos cannot be predicted by a single QSAR. It has thus become important to define its applicability domain (AD), which is the chemical space of molecules within its supervision. Kunal *et al.,* (2015) used the standardization strategy of the AD executable jar file in the DTC laboratory to define the AD of the optimal QSAR model.
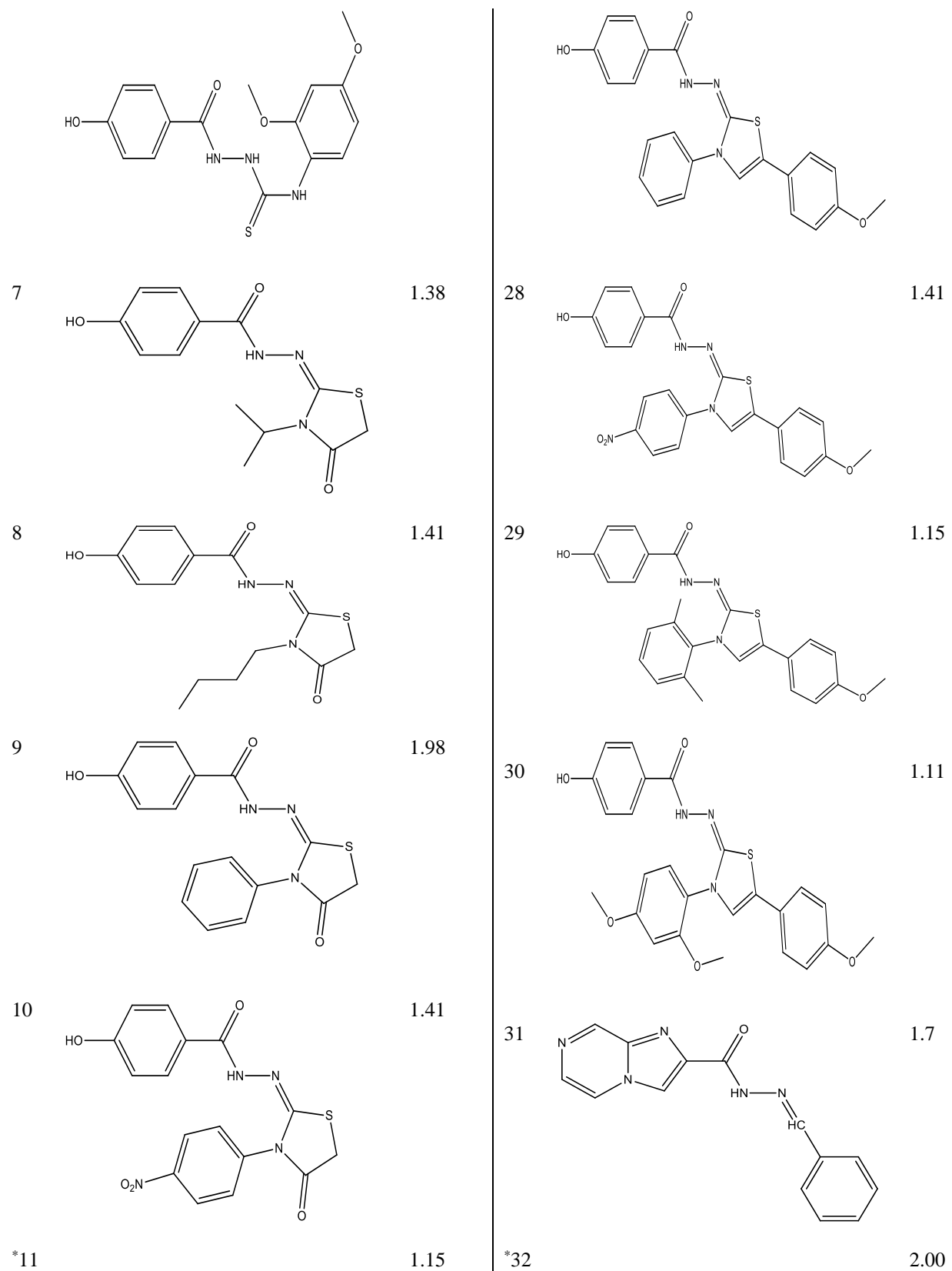
The Euclidean distance norms' distance scores serve as the foundation for the Euclidean Based Applicability Domain. Initially, the training set compounds' normalized mean distance score is computed; this number spans from 0 to 1 (0 being the least diverse training set compound, and 1 being the most diverse). After the test set's normalized mean distance score is determined, test compounds that have scores outside of the 0–1 range are deemed to be outside of the applicability domain. An additional way to verify this is to create a "Scatter plot" with the training and test sets,
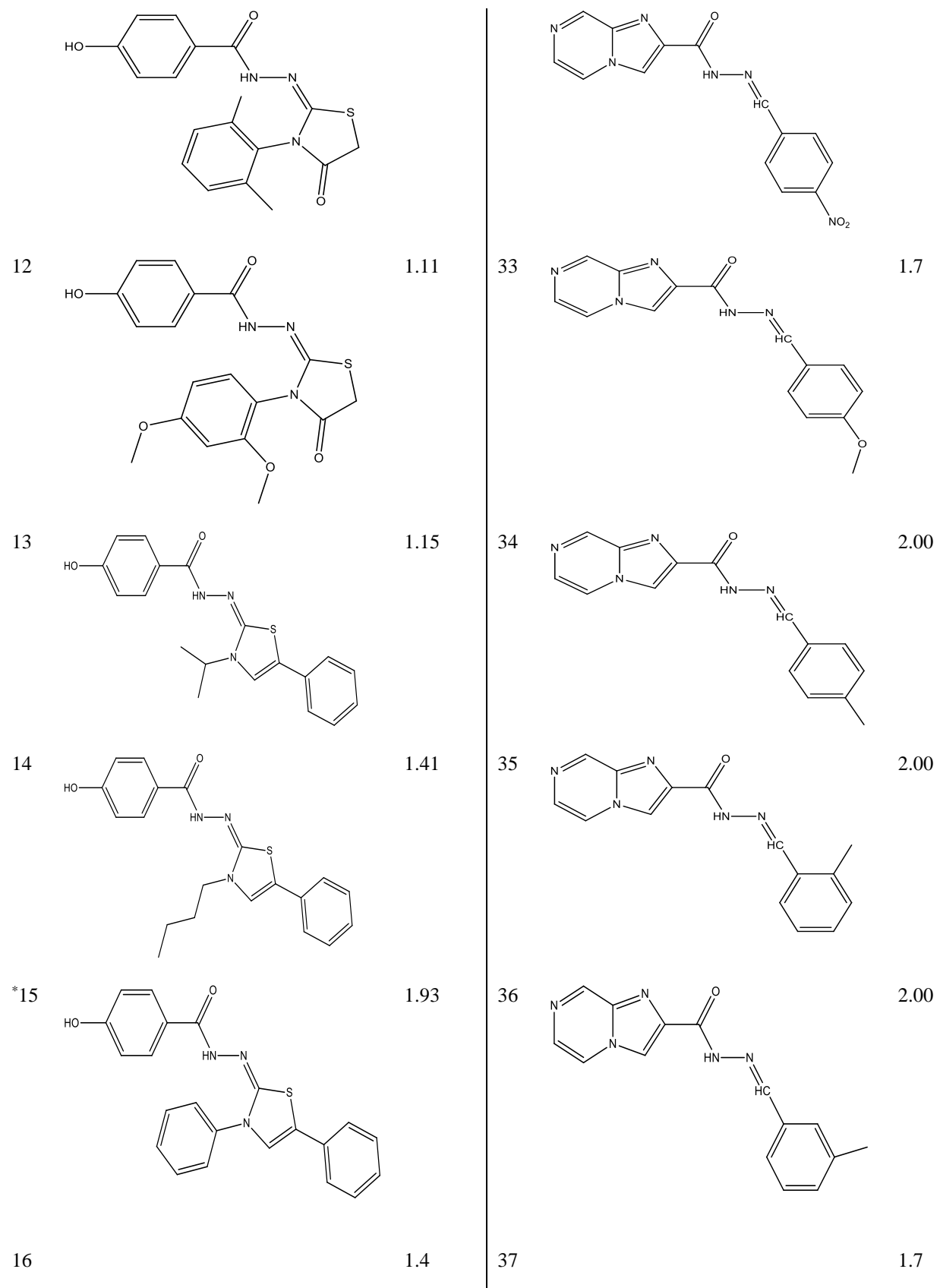
showing the normalized mean distance vs the appropriate activity/property. Compounds in the test set are inside the application domain if they are within the domain/area covered by the compounds in the training set; otherwise, they are not (Gramatica, 2013).
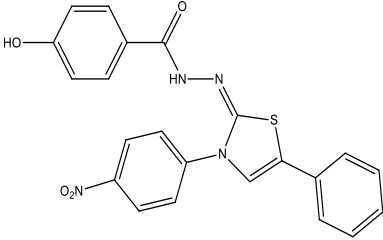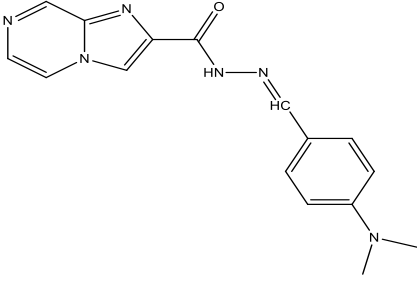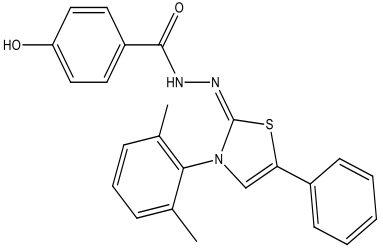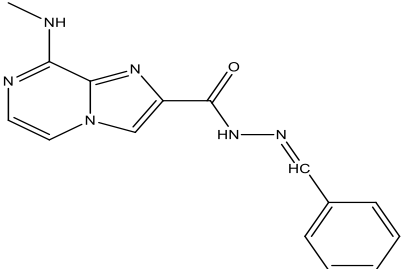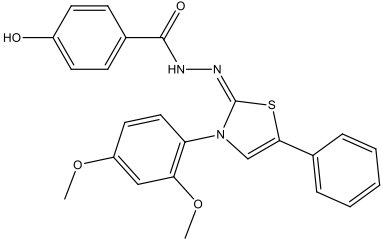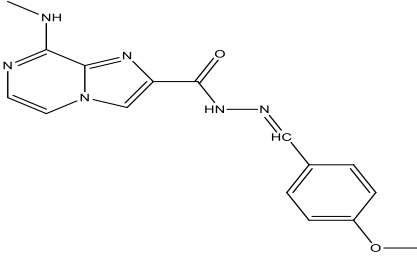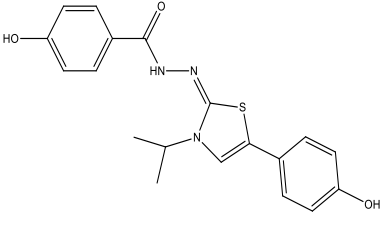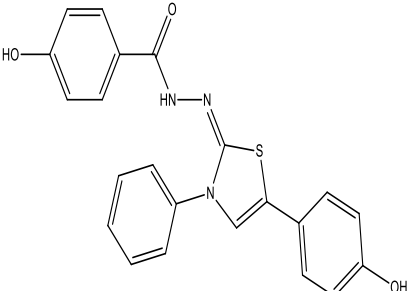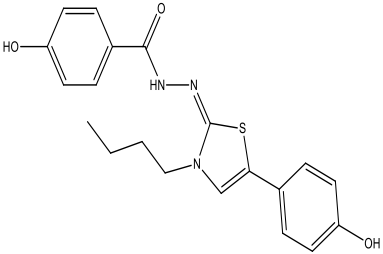
Table 1: Chemical structures and antibacterial activities of the hydrazide derivatives

S/n	Structure	jMIC (µg/mL)	S/n	Structure	jMIC (µg/mL)
*1		1.75	22		1.77
2		1.69	23		1.51
3		1.75	24		1.4
4		1.77	25		1.38
5		1.51	26		1.41
6		1.4	27		1.98

7		1.38
28		1.41
8		1.41
29		1.15
9		1.98
30		1.11
10		1.41
31		1.7
*11		1.15
*32		2.00

12		1.11	33		1.7
13		1.15	34		2.00
14		1.41	35		2.00
*15		1.93	36		2.00
16		1.4	37		1.7

17	1.28	38	2.00
18	1.4	39	2.00
*19	1.75	21	1.75
20	1.69		

*Outlier

Design of New Ligands

Creating new hydrazide-based medication options with good potencies and low toxicity is a main goal of this research. Here, the data set of the examined compounds was used to choose compounds 12 and 30, which had the best

antibacterial properties against *S. aureus*. These compounds were then exposed to pharmacophoric alterations by creating several derivatives of the selected compounds. The validated QSAR model was used to predict the MIC values of the proposed ligands. Furthermore, the new ligands were tested using molecular docking simulation against DNA gyrase, an essential bacterial enzyme that is important for the pathogenic germs' reproduction processes.

Molecular Docking Procedures
An important sign of a powerful bioactive ligand is its capacity to form a strong bond with a target macromolecule within the pathogenic microorganism. In this study, the interaction between the proposed ligands and the active sites of S. aureus DNA gyrase was investigated using the molecular docking technique. The hydrazide derivatives' (ligands') optimal structures were created using the AutoDock Vina interface and saved in pdbqt file formats. After downloading the DNA gyrase PDB file with PDB code 5ztj from the Protein Data Bank (www.rcsb. org/pdb), the associated ligands, water molecules, and heteroatoms were eliminated using the Discovery Studio 2016 interface. The target protein was then exported to the AutoDock Vina interface, where Kollman charges and polar hydrogens were added to further improve the protein. The protein's missing atoms were also examined and fixed. Docking calculations were carried out using the PyRx GUI of the AutoDock Vina program. With the help of Discovery Studio 2016, the protein-ligand interactions were visualized (Adeniji *et al.,* 2022; Ejeh *et al.,* 2022; Trott *et al.,* 2010).

Druglikeness and ADMET Profiling
Druglikeness, a measure of a bioactive ligand's oral bioavailability, was predicted for the new ligands using the Lipinski's and Veber's rule. The SwissADME (www.swissadme.ch/ accessed on May 12, 2023) and DataWarrior V5.5.0 Chemoinformatics program (Ameji *et al.,* 2023; Ameji *et al.,* 2022a; Ameji *et al.*, 2022b) were used to predict the ligands' pharmacokinetics and toxicity.

RESULTS AND DISCUSSION
Model and Statistical Substantiation
Equation 2 represents the best QSAR model for predicting the anti-*S. aureus* bioactivities of the drugs under study. Tables 2 and 3 include, respectively, the regression model's validation parameters and the model's descriptor definitions. Table 4: Orthogonality Descriptor Verify each and every descriptor in the model. Additionally, Figures 1 and 2 exhibit the experimental pMIC against the anticipated pMIC for the molecules in the training and test sets, respectively. The residual plot of the model and the importance of the model's descriptors are shown in Figures 3 and 4, respectively.

$$jMIC = 1.4888 + 0.0961 * TDB10u - 0.1422 * MDEC - 12 - 0.5831 * Dm \tag{1}$$

Table 2: Validation metrics of QSAR Model

S/n	Parameter	Threshold	Model value	Statement
1.	Square of Coefficient of determination (R^2)	≥ 0.6	0.73	Excellent
2	Adjusted R-squared ($R^2_{Adj.}$)	≥ 0.6	0.70	Stable
3	Cross validated R-squared (Q^2_{LOO})	≥ 0.5	0.62	Reliable
4	Predictive R-squared (R^2_{pred})	≥ 0.5	0.76	Robust
5	$R^2 - Q^2_{LOO}$	≤ 0.3	0.11	Stable

Table 3: Definition of the Descriptors in the QSAR Model

S/n	Descriptor	Definition	Class
1	TDB10u	3D topological distance based autocorrelation - lag 10 / unweighted	3D
2	MDEC-12	Molecular distance edge between all primary and secondary carbons	2D
3	Dm	D total accessibility index / weighted by relative mass	3D

Table 4: Descriptor Orthogonality Check

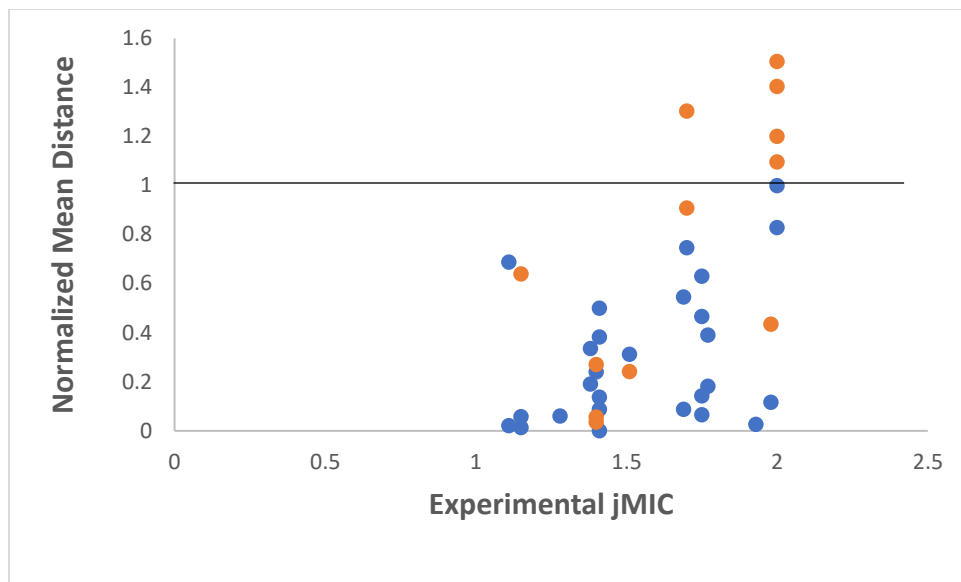|	jMIC	Dm	TDB10u	MDEC-12
jMIC	1			
Dm	-0.07679	1		
TDB10u	0.560056	-0.35103	1	
MDEC-12	-0.70279	-0.40502	-0.17988	1

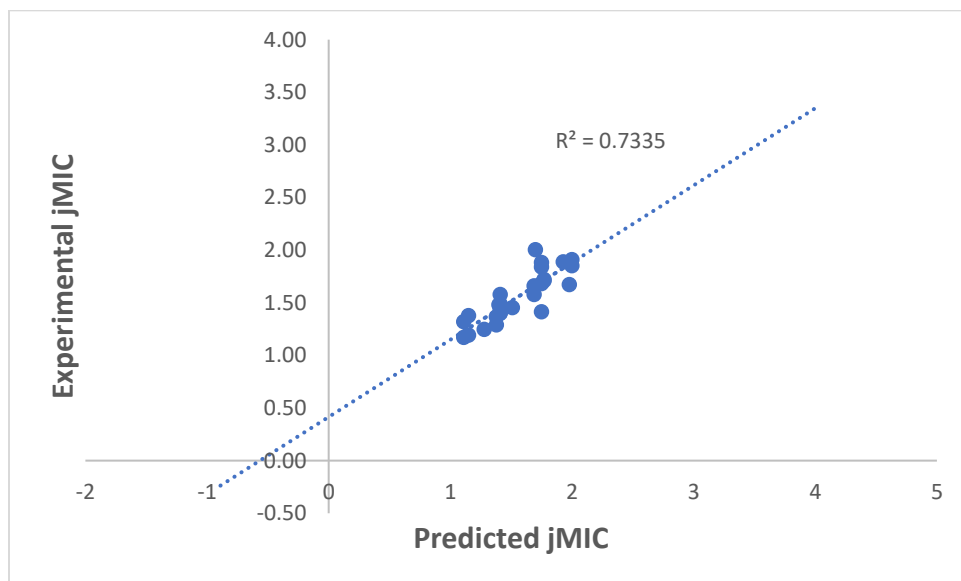Figure 1: Scatter plot of the Optimum QSAR Model

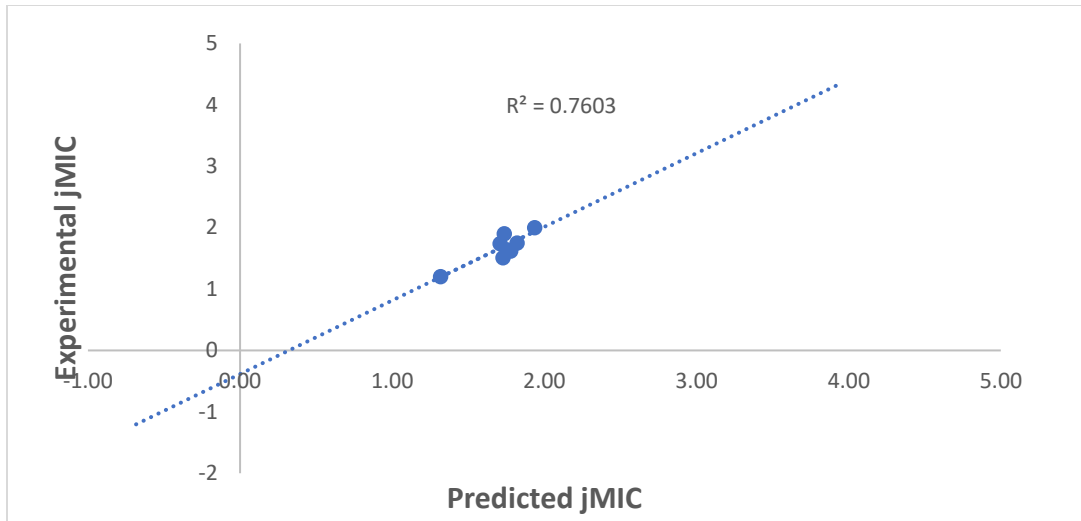Figure 2: Plot of experimental jMIC against predicted jMIC (training set)

Figure 3: Plot of experimental jMIC against predicted jMIC (test set)
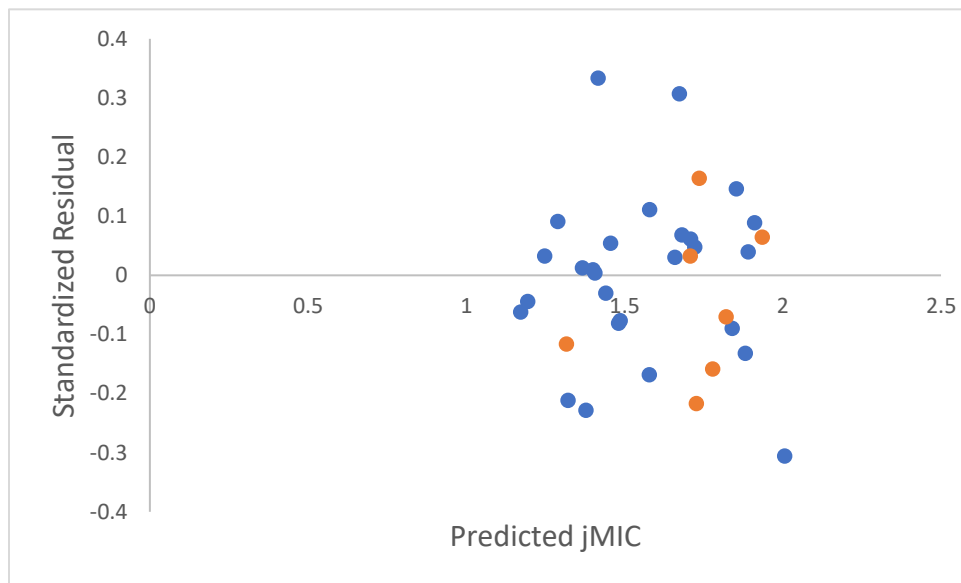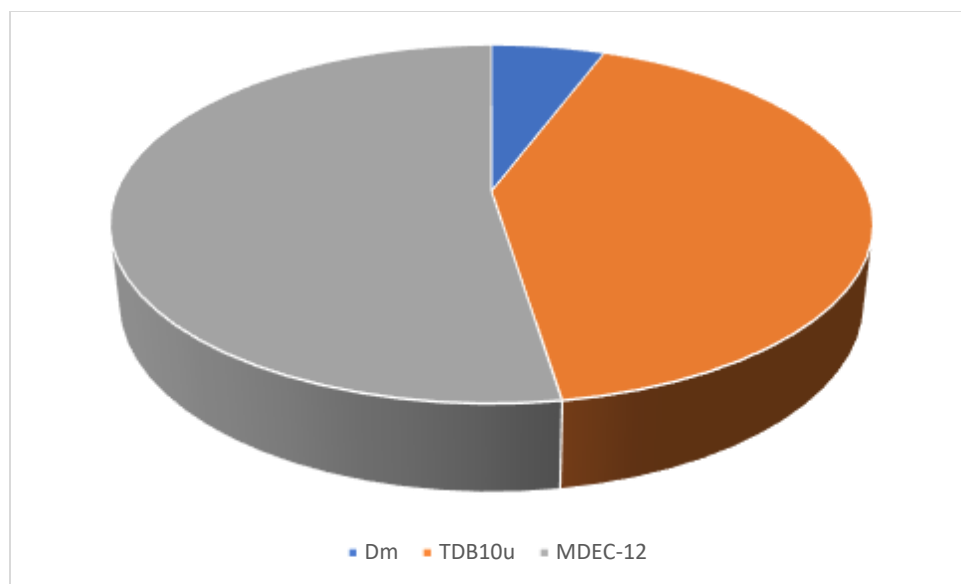

Figure 4: Residual Plot of the validated Model

Figure 5: Descriptors Contribution to the QSAR Model

Designed ligands and their predicted MIC

Figure 5 presents the chemical structures of the newly designed hydrazide derivatives and a standard inhibitor of DNA gyrase (Ciprofloxacin) of *S. aureus*. The descriptors of the two designed ligands and their predicted MIC values are presented in Table 5.

C-1

C-2
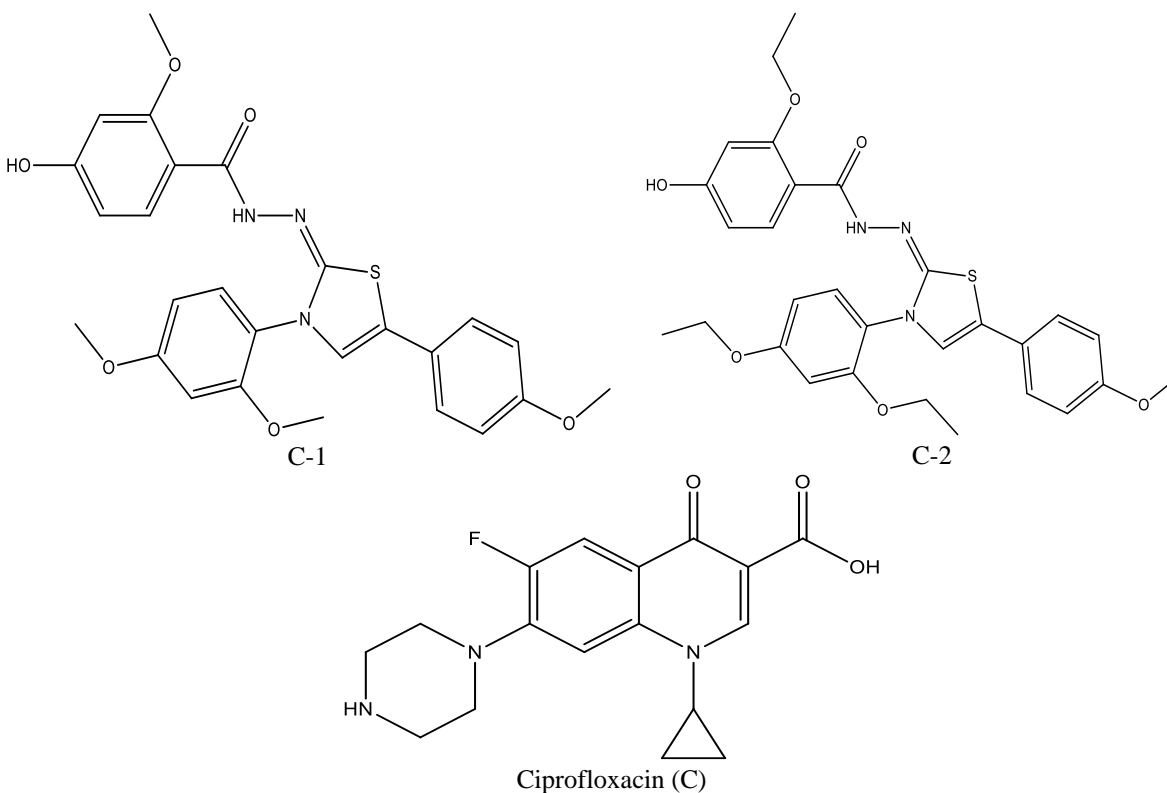
Ciprofloxacin (C)

Figure 5: 2D Chemical structures of the designed ligands and Ciprofloxacin

Table 5: Predicted MIC of the designed ligand

Ligand	TDB10u	MDEC-12	Dm	jMIC	MIC (µg/mL)
C-1	8.489297	5.832412	0.726064	1.051884	11.27
C-2	8.442955	7.094066	0.747697	0.855409	7.17

Applicability Domain Determination

Table 6a: Normalized Mean Distance Score for Training Set

Compound	Distance Score	Mean Distance	Normalized Mean Distance
1	545.614	20.208	0.621
2	545.088	20.188	0.619
3	526.99	19.518	0.569
4	480.891	17.811	0.442
5	395.438	14.646	0.207
6	380.858	14.106	0.167
7	372.305	13.789	0.143
8	351.944	13.035	0.087
9	415.13	15.375	0.261
10	346.937	12.85	0.073
11	407.446	15.091	0.24
12	429.843	15.92	0.302
13	320.302	11.863	0
14	327.048	12.113	0.019
15	336.545	12.465	0.045
17	363.581	13.466	0.119
19	332.007	12.297	0.032
20	351.761	13.028	0.087
21	357.641	13.246	0.103
22	395.554	14.65	0.207
25	410.417	15.201	0.248
26	448.384	16.607	0.353
28	442.115	16.375	0.336
30	683.246	25.305	1
31	547.554	20.28	0.626
32	579.566	21.465	0.714
34	601.426	22.275	0.775

Table 6b: Normalized Mean Distance Score for Test Set

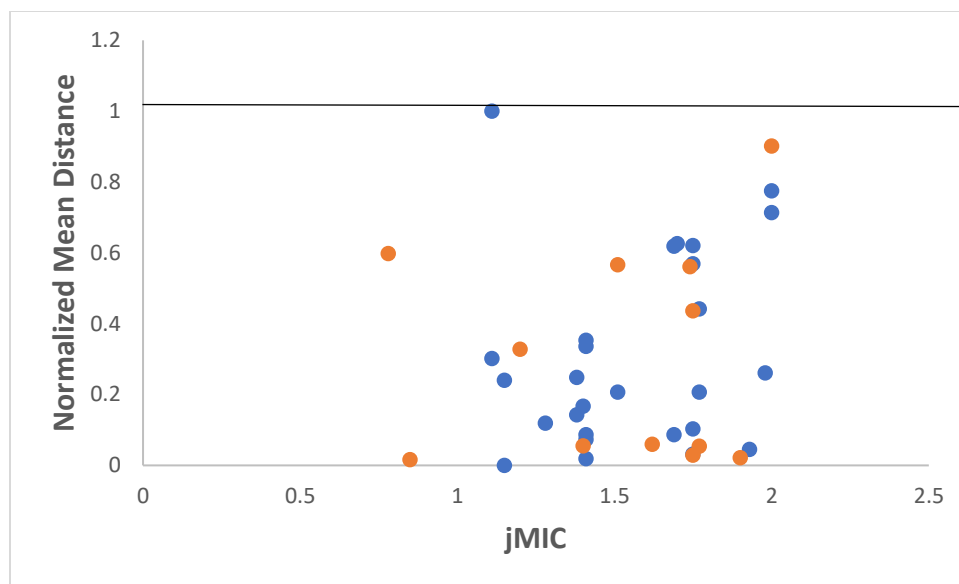| Compound	Distance Score	Mean Distance	Normalized Mean Distance
1	478.632	17.727	0.436
8	439.383	16.273	0.328
11	340.06	12.595	0.054
12	330.687	12.248	0.029
13	328.362	12.162	0.022
15	325.953	12.072	0.016
19	340.256	12.602	0.055
20	342.185	12.674	0.06
24	525.587	19.466	0.566
31	523.747	19.398	0.561
32	537.424	19.905	0.598
37	647.837	23.994	0.902

Figure 6: Scatter Plot of the model

Molecular Docking Simulation Studies on the designed compounds

The strength of the binding interaction between the ligands in Figure 5 and the active sites of DNA gyrase target expressed as change in Gibb's free energy of binding are presented in Table 6 while the visual forms of the interaction are presented in Figure 6.

Table 7: The Mechanism and strength of interaction of the designed ligands and Ciprofloxacin with active sites of DNA gyrase

| Ligands | Binding affinity(kcal/mol) | Amino acids | |
		Bond Length (Å)$^{bond\ type}$	Hydrophobic interaction $^{bond\ type}$
C-1	-8.2	ARG 580	two attractive charges interactions, one hdrogen bond
		ALA 786	one unfavourable acceptor-acceptor interaction
		PRO 636	one pi-alkyl interaction
		LEU 582	one pi-alkyl interaction
C-2	-8.1	ASP 686	one attractive charges and one pi-anion interaction
		GLN 837	one pi-anion interaction
		ARG 580	One pi-cation interaction, one convectional hydrogen bond
		LEU 735	one convectional hdrogen bond
C	-7.6	ARG 630	three alkyl and pi-alkyl
		GLN 546	an amide-pi-stacked
		GLU 626	one carbon-hydrogen
		HIS 545	one carbon-hydrogen
		ILE 631	one conventional hydrogen bond
		SER 544	one conventional hydrogen bond

C-1/Gyrase complex

C-2/Gyrase complex
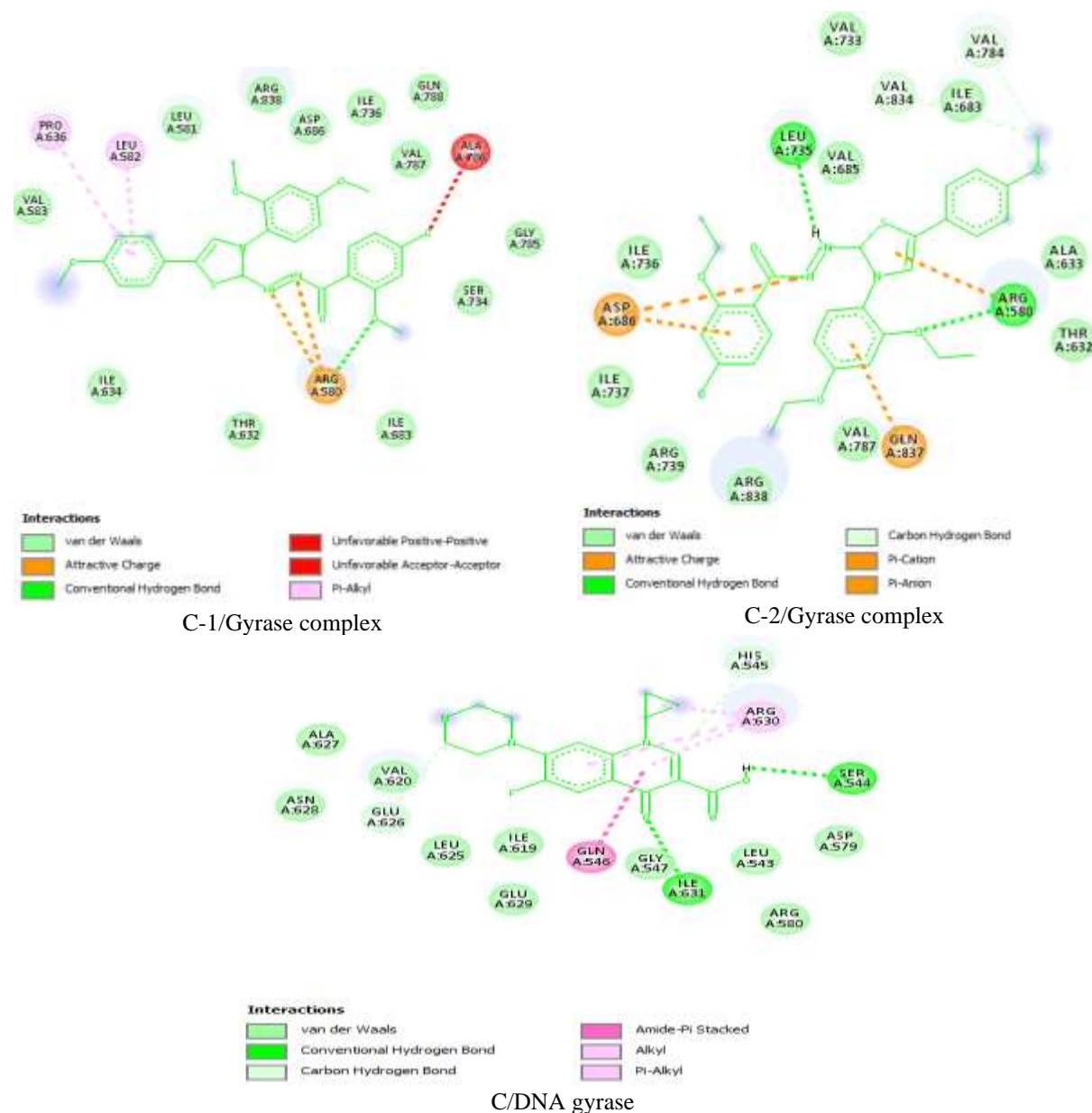
C/DNA gyrase

Figure 7: Mechanism of interaction of the Ligands with DNA gyrase

Table 8: Drug-likeness Profiles of the ligands

Ligand Rule	C-1	C-2	Ciprofloxacin (C)
Lipinski's	Yes	Yes	yes
HBA	7	7	5
HBD	2	2	2
MW (gmol^{-1})	507.6	549.6	331.34
cLogP$_{(o/w)}$	3.9	4.9	1.10
Veber's	Yes	No	Yes
NRB	9	12	3
TPSA (Å^2)	131.8	131.8	74.54

HBA; hydrogen bond acceptor, HBD; hydrogen bond donor, Mw; molecular weight, cLogP; consensus octanol water partition coefficient, NRB; number of rotatable bond, TPSA; topological polar surface area

Table 9: ADMET profiles of Ligands

Ligand	CYP450 Substrate	GIA	P-gp+	BBB	MUT	TUM	IR	RE	LogK$_p$ (cm/s)
C-1	Yes	Low	No	No	None	None	None	None	-6.52
C-2	Yes	Low	No	No	None	None	None	None	-5.60
C	Yes	High	Yes	No	None	None	None	None	-9.1

ESOL; estimated solubility, GIA; gastrointestinal absorption, BBB; blood brain barrier penetration, P-gp+; P-glycoprotein substrate, MU; mutagenicity, TUM; tumorigenic, IR; irritating effect, RE; reproductive effect

Discussion of Results

Validated QSAR Model and its Statistical Significance

In the twenty-first century, a serious hazard to public health is the increase in incidences of harmful bacteria developing resistance to drugs. One noteworthy harmful microorganism is S. aureus, a Gram-positive bacterial species that is rapidly developing new drug resistance mechanisms. A purposeful search for novel medication candidates with distinct mechanisms of action that are unknown to the organism can help to lessen this threat. QSAR modeling, which connects the biological activity descriptors of congeneric compounds to their biological activities, is an in silico method for finding new therapeutic candidates. The QSAR methodology for estimating the MIC of hydrazide derivatives is shown in Equation 2. The model's statistical parameters align with the suggested threshold in Table 2, indicating the model's stability, resilience, and high predictive quality (Adeniji *et al.,* 2018; Gramatica, 2013). Additionally, Figure 1 shows the plot of the experimental jMIC against the predicted jMIC for the molecules in the training set. The plot's strong linearity provides more evidence for the model's internal stability. A QSAR model's stability cannot be adequately described by its internal validation. It should be possible for the model to forecast the bioactivities of an external collection of molecules. Plotting the experimental jMIC against the predicted jMIC for the compounds in the test set is shown in Figure 2. Given that the predictive R2 (R2pred) value of 0.76 agrees with Table 2's suggested threshold for this parameter, it may be inferred that, within its applicability domain, the model is capable of accurately predicting the jMIC of novel hydrazide derivatives. Additionally, biases in the model-building process have a negative impact on the quality of the QSAR model. The plot of the standardized residuals against the anticipated jMIC values was used to verify this (Figure 3). The absence of systematic error in the model development is confirmed by the residuals propagating on both sides of the zero lines (Ameji *et al.,* 2023; Zakari *et al.,* 2021).

Multicollinearity in multiple linear regression is statistically defined as a high level of inter-correlation between the independent variables.

Descriptors' Significance

The current paradigm in medicinal chemistry holds that a molecule's molecular characteristics determine whatever property it exhibits. Molecular descriptors are used to encode these characteristics. The TDB10u, MDEC-12, and Dm descriptors were shown to have a substantially dependent effect on the anti-S. aureus properties of the hydrazide derivatives under investigation. Figure 4's analysis of the descriptor contributions showed that TDB10u and MDEC-12 descriptors were mostly responsible for the reported inhibitory effects of the hydrazide derivatives under investigation. The model indicates that the MIC of the compounds changes inversely with the values of both descriptors and vice versa, as indicated by the negative coefficients of both descriptors. A molecule's minimum inhibitory concentration (MIC) against S. aureus increases with decreasing values of these characteristics. Additionally, among all the model's descriptors, the Dm descriptor has the least amount of influence. The compounds' MIC is directly correlated with the values of these descriptors, as indicated by their positive coefficients. In summary, since potency correlates inversely with MIC, the values of TDB10u and MDEC-12 descriptors should be significantly greater than those of Dm descriptors for enhanced inhibitory activities of the examined drugs.

Applicability Domain Determination

From the Table 6a and 6b, all the compounds have Normalized Mean Distance Scores in the range of 0-1 except ligand 30. It implies they are all within the applicability domain of the model. This is also reflected in the scatter plot in Figure 6.

Predicted MIC of the Designed Ligands

The most potent analogues, C-1 and C-2, were designed using ligands 12 and 30, which had a minimum inhibitory concentration (MIC) of 13 µg/mL and were the most potent of the hydrazide derivatives under investigation. When the compounds' MIC values (Table 5) are calculated using the verified QSAR model, it is evident that their inhibitory actions are superior to those of their template molecules.

Molecular Docking Investigation

Antibiotics generally work by forming a tight bond with a disease-causing microbe's important protein target, which inhibits the macromolecule's enzymatic functions and causes the organism to become inactivated or die. After applying the conventional antibiotic (C) and its tailored ligands, C-1 and C-2, to the active sites of S. aureus DNA gyrase, the results of molecular docking (Table 7) indicate that C-1, C-2, and C bind to the target macromolecule with ΔG values of -82, -8.1, and -7.6 kcal/mol. Similar binding affinities were shown by the proposed ligands with the common antibiotic that was employed in this instance for quality control. According to an analysis of their modes of action, C-1 created two attractive charges with ARG 580, one conventional hydrogen bond and one unfavorable acceptor-acceptor contact with ALA 786, a pi-alkyl interaction with PRO 636, and an amino acid residue of DNA gyrase with LEU 582.

Additionally, C-2 creates one attractive charge, one conventional hydrogen bond with ARG 580, one conventional hydrogen bond with DNA gyrase's LEU 735 residue, and one pi-anion interaction with each of ASP 686, GLN 837, and pi-cation interactions. Ciprofloxacin, the standard ligand, interacted with the target protein's active sites by forming three alkyl and pi-alkyl bonds with ARG 630, GLN 546 (an amide-pi-stacked bond), one carbon-hydrogen bond with GLU 626, one carbon-hydrogen interaction with HIS 545, and one conventional hydrogen bond with DNA gyrase's amino acid residues ILE 631 and SER 544.

It is clear from evaluating the developed ligands' interaction with DNA gyrase that the bioactive ligands exhibit different mechanisms of action when it comes to Ciprofloxacin.

Druglikeness Data

In the initial stages of drug development and discovery, a crucial factor assessed is the drug-likeness of a bioactive ligand, which pertains to the compound's oral bioavailability capacities. Since the majority of medications intended for systemic effects are conveniently taken orally, this evaluation is inviolable (Azman *et al.,* 2022). Both the Veber rule and the Lipinski rule of five were used to assess the druglikeness of C-1, C-2, and C. A medication that is orally bioavailable could not have more than one infraction against the following rules: Mw < 500, nHBD ≤ 5, Log P ≤ 5, and nHBA ≤ 10. However, an orally accessible medication must have nNRB < 10 and TPSA < 140 Å2 according to the later rule (Ameji *et al.,* 2023; Ameji *et al.,* 2023b; Ameji *et al.,* 2023c ; Ameji *et al.,* 2022). According to Table 8's druglikeness profile, the ligands exhibit positive drug-likeness since they follow both guidelines just like the reference antibiotic.

Predicted Pharmacokinetic and Toxicity Profiles

Pharmacokinetics is mainly interested in how the body interacts with medicinal substances that are supplied during the course of the exposure, with a focus on the compounds' absorption, distribution, metabolism, and excretion. An essential aspect of pharmacokinetics research is a therapeutic compound's capacity to undergo intestinal absorption before being distributed to the suggested target region, where it can have its desired pharmacological effects (Cárdenas *et al.,* 2017). Unlike the reference antibiotic, C-1 and C-2 have minimal gastrointestinal absorption, according to the ADMET profile of the ligands shown in Table 9. Since non-polar alkyl groups in a molecule can reduce its overall polarity, the longer alkyl chains in C-1 and C-2 may be the source of their low GIA.

Another crucial pharmacokinetic characteristic for medicinal drugs to be assessed is penetration of the blood-brain barrier (BBB), a monolayer of endothelial cells separating the blood from the central nervous system (CNS). According to Abbott *et al.,* (2010), Erickson and Banks (2018), Lippmann *et al.,* (2013), Wilhelm and Krizbai (2014), the blood-brain barrier (BBB) regulates the flow of chemicals from the blood into the brain, promoting steady neuronal function and preventing acute central nervous system injury. The novel ligands may not be dangerous to the central nervous system (CNS) based on their anticipated BBB penetration potential (Table 9), which indicates that they are not endothelial cell permeant.

In the gastrointestinal tract, blood, kidney, liver, and placenta, permeability glycoprotein (P-gp+) is a membrane-embedded protein that, by its efflux activity, removes toxic substances from the body (Chen *et al.,* 2018). The proposed ligands are all shown to be non-substrate of P-gp+, in contrast to the conventional antibiotic (Table 9). The efflux action of P-gp+ may not have an impact on their pharmacokinetic profiles, it may be concluded.

Skin permeability (LogKp) is another crucial pharmacokinetic characteristic that should be taken into account, particularly for medicinal drugs that need to be administered transdermally. The LogKp statistics of the examined ligands, which are shown in Table 9, showed that all of the compounds have low skin penetration potentials because of their negative LogKp values, just like the standard reference antibiotic (Khan *et al.,* 2017). Furthermore, none of the chemicals are mutagenic, tumorigenic, inflammatory, or harmful to the reproductive system, according to Table 9's toxicity profiles of the compounds.

CONCLUSION

QSAR modelling was used to determine the mathematical relationship between the structures of a series of bioactive hydrazide derivatives that exhibited shown antibacterial activity against S. aureus. The MIC of the compounds was indicated by the validated QSAR model to be dominated by the Dm, MDEC-12, and TDB10u descriptors. Next, the model was utilized to forecast the minimum inhibitory concentration (MIC) of a few recently created analogs of the studied compounds. To further understand the mechanism of interactions between the developed chemicals and the target macromolecule, they were further put through molecular docking simulation against the organism's DNA gyrase. In this study, they were discovered to exhibit binding affinity values comparable to those of ciprofloxacin, a common inhibitor of DNA gyrase used for quality control. Furthermore, the new ligands exhibit positive drug-likeness and good pharmacokinetic and toxicological profiles, according to the ADMET evaluation. The engineered ligands may offer a great starting point for the development of new hydrazide-based antibiotics that are effective against S. aureus.

REFERENCES

Abbott, N. J., Patabendige, A. A. K., Dolman, D. E. M., Yusof, S. R., and Begley, D. J. (2010). Structure and function of the blood-brain barrier. Neurobiol. Dis.37, 13–25. doi: 10.1016/j.nbd.2009.07.030

Adeniji SE, Ajala A, Arthur DE, Abdullahi M, Areguamen OI (2022). Chemometric Study, Homology Modeling of G Protein-Coupled Bile Acids Receptor (GPBAR_HUMAN) of Type-2 Diabetes Mellitus, Virtual Screening Evaluation, Drug-Likeness and ADME Prediction for Newly Designed Compounds, Macromolecular research, 1-19, DOI 10.1007/s13233-022-0071-3

Adeniji ES, Uba S, Uzairu A. Theoretical modelling for predicting the activities of some active compounds as potent inhibitors against Mycobacterium tuberculosis using GFA-MLR approach. *J King Saud Univ Sci*, 32:575–586, 2018, doi.org/10.1016/j.jksus.2018.08.010

Ameji JP, Uzairu A, Shallangwa GA, Uba S (2023a). Obstructing Salmonella typhi's virulence in eukaryotic cells through design of its SipB protein antagonists. Journal of Taibah University Medical Sciences (2023) 18(4), 726e736

Ameji JP, Ebune OA, Aderemi WI, Moyosore A, Idah G (2023b). Theoretical Investigation and Design of Novel Anti-proliferative Agents against Hepatocellular Carcinoma from Benzimidazole-Chalcone derivatives. *Adv. J. Chem. A 2023, 6(2), 92-104.*

Ameji JP, Uzairu U, Shallangwa GA, Uba S (2023c) Design, pharmacokinetic profiling, and assessment of kinetic and thermodynamic stability of novel anti-Salmonella typhi imidazole analogues. Bulletin of the National Research Centre. 47:6 https://doi.org/10.1186/s42269-023-00983-5

Ameji, J.P., Uzairu, U., Shallangwa, G.A., Uba, S., (2022). Virtual screening of novel pyridine derivatives as effective inhibitors of DNA gyrase (GyrA) of salmonella typhi, Current Chemistry Letters. 12, 1–16. DOI: 10.5267/j.ccl.2022.10.002

Azman, M.; Sabri, A.H.; Anjani, Q.K.; Mustaffa, M.F.; Hamid, K.A. Intestinal Absorption Study: Challenges and Absorption Enhancement Strategies in Improving Oral Drug Delivery. Pharmaceuticals **2022**, 15, 975. https://doi.org/10.3390/ph15080975

Behl T, Kaur I, Sehgal A, Singh S, Bhatia S, Al-Harrasi A, et al (2021) Bioinformatics Accelerates the Major Tetrad: A Real Boost for the Pharmaceutical Industry. IJMS 22:1-28

Bhole PR, Bhusari PK (2010). Synthesis and 3D-QSAR of p-Hydroxybenzohydrazide Derivatives With Antimicrobial Activity Against Multidrug-Resistant Staphylococcus aureus Article. Journal of the Korean Chemical Society. 54 (1): 77-87. DOI: 10.5012/jkcs.2010.54.01.077

Cárdenas, P.A.; Kratz, J.M.; Hernández, A.; Costa, G.; Ospina, L.F.; Baena, Y.; Simões, C.M.O.; Jimenez-Kairuz, Á.; Aragon, M. In vitro intestinal permeability studies, pharmacokinetics and tissue distribution of 6-methylcoumarin after oral and intraperitoneal administration in Wistar rats. Braz. J. Pharm. Sci. **2017**, 53

Chen C, Lee M, Weng C; Leong MK (2018). Theoretical Prediction of the Complex P-Glycoprotein Substrate Efflux Based on the Novel Hierarchical Support Vector Regression Scheme. Molecules 2018, 23, 1820; doi:10.3390/molecules23071820

Cortes E, Mora J, Márquez E (2020). Modelling the Anti-Methicillin-Resistant Staphylococcus aureus (MRSA) Activity of Cannabinoids: A QSAR and Docking Study. *Crystals* 2020, *10*, 692; doi:10.3390/cryst10080692

Daoud, N.E.K., Deb, P.K., Alzweiri, M., Borah, P., Venugopala, K.N., Hourani, W., et al., 2021. ADMET profiling in drug discovery and development: perspectives of in silico, in vitro and integrated approaches. Curr Drug Metab. https:// doi. org/ 10. 2174/ 13892 00222 66621 07051 22913

Ejeh S, Uzairu A, Shallangwa GA, Abechi SE , Ibrahim MT (2022). In silico design and pharmacokinetics investigation of some novel hepatitis C virus NS5B inhibitors: pharmacoinformatics approach, Bulletin of the National Research Centre 46; 109 https://doi.org/10.1186/s42269-022-00796-y

Erickson, M. A., and Banks, W. A. (2018). Neuroimmune axes of the bloodbrain barriers and blood-brain interfaces: bases for physiological regulation, disease states, and pharmacological interventions. Pharmacol. Rev. 70, 278–314. doi: 10.1124/pr.117.014647

Gramatica, P. 2013. On the Development and Validation of QSAR Models. In: Computational Toxicology. Methods in Molecular Biology, B, Reisfeld, and A. Mayeno, eds., vol 930. Humana Press, Totowa, NJ. doi: 10.1007/978-1-62703-059-5-21.

Guo Y, Song G, Sun M, Wang J and Wang Y (2020) Prevalence and Therapies of Antibiotic-Resistance in Staphylococcus aureus. Front. Cell. Infect. Microbiol. 10:107. doi: 10.3389/fcimb.2020.00107

Hussain W, Rasool N, Khan YD (2021) Insights into Machine Learning-based approaches for Virtual Screening in Drug Discovery: Existing strategies and streamlining through FP-CADD. Current Drug Discovery Technologies 18: 463–72

Khan MF, Bari MA, Islam MK, Islam MS, Kayser MS, Nahar N, Al-Faruk M, Rashid MA. The   natural anti-tubercular agents: In silico study of physicochemical, pharmacokinetic and toxicological properties. J App Pharm Sci. 2017;7:034-8

Khatkar A, Nanda A, Kumar P, Narasimhan B (2014). Synthesis, antimicrobial evaluation and QSAR studies of p-coumaric acid derivatives. Arabian Journal of Chemistry, http://dx.doi.org/10.1016/j.arabjc.2014.05.018

Klemm EJ, Shakoor S, Page AJ, Qamar FN, Judge, et al. Emergence of an extensively drug-resistant Salmonella enterica serovar Typhi clone harboring a promiscuous plasmid encoding resistance to fluoroquinolones and third-generation cephalosporins. mBio 2018; 9: e00105ee00118.

Kore PP, Mutha MM, Antre VR, Oswal JR, Kshirsagar SS. Computer-aided drug design: an innovative tool for modeling. Open J Med Chem 2012; 2: 139e148.

Kumari M., Narang R. Structure activity relationship and mechanism of action of hydrazide derivatives as antimicrobial molecule. J Chem Pharmaceut Res, 2016, 8, 823-836.

Kunal R, Kar S, Ambure P. On a simple approach for determining applicability domain of QSAR models. Chemometr Intell Lab Syst 2015; 145: 22e29.

Lippmann, E. S., Al-Ahmad, A., Palecek, S. P., and Shusta, E. V. (2013). Modeling the blood-brain barrier using stem cell sources. Fluids Barriers CNS 10:2. doi: 10.1186/2045-8118-10-2

Obanda, B.A.; Gibbons, C.L.; Fèvre, E.M.; Bebora, L.; Gitao, G.; Ogara,W.;Wang, S.-H.; Gebreyes, W.; Ngetich, R.; Blane, B.; et al. Multi-Drug Resistant Staphylococcus aureus Carriage in AbattoirWorkers in Busia, Kenya. Antibiotics **2022**, 11, 1726. https://doi.org/10.3390/ antibiotics11121726

Ozdemir A, Turan-Zitouni G, Kaplancikli AZ, Tunali Y (2009). Synthesis and biological activities of new hydrazide derivatives. Journal of Enzyme Inhibition and Medicinal Chemistry, 24(3): 825–831. DOI: 10.1080/14756360802399712

Rajer-Kandu K, Zupan J, Majcen N. Separation of data on the training and test set for modelling: a case study for modelling of five colour properties of a white pigment. Chemometr Intell Lab Syst 2003; 65(2): 221e229.

Sprous DG, Zhang J, Zhang L, Wang Z, Tepper MA. Kinase inhibitor recognition by use of a multivariable QSAR model. J Mol Graph Model 2006; 24(4): 278e295. https://doi.org/ 10.1016/j.jmgm.2005.09.004.

Trott O, Olson AJ (2010). AutoDock Vina: improving the speed and accuracy of docking with a new scoring function, efficient optimization, and multithreading, Journal of Computational Chemistry, 31(2010) 455-61. doi: 10.1002/jcc.21334.

Wilhelm, I., and Krizbai, I. A. (2014). In vitro models of the blood-brain barrier for the study of drug delivery to the brain. Mol. Pharm. 11, 1949–1963. doi: 10.1021/mp500046f

Yap CW. PaDEL-descriptor: an open source software to calculate molecular descriptors and fingerprints. J Comput Chem 2011; 32(7): 1466e1474.

Zakari YI, Uzairu A, Shallangwa GA, Abechi SE. Molecular modelling and design of some β-amino alcohol grafted 1,4,5-trisubstituted 1,2,3-triazoles derivatives against chloroquine sensitive, 3D7 strain of Plasmodium falciparum, Heliyon 7:e05924, 2021

Diospyros mespiliformis Hochst. Ex A.DC: A Brief Review of its Phytochemistry and Pharmacological Activities

*Sani Suleiman, Shema Shehu Abdulsalam and Bello, Oluwasesan M.

Department of Chemistry, Federal University Dutsin-Ma, Dutsin-Ma, Katsina State
*Corresponding Author's E-mail: sanisuleiman660@gmail.com

ABSTRACT
Ficus glumosa (*F. glumosa*) is a medicinal plant with ethnomedicinal significance and is widely distributed throughout tropical Africa, especially in the Savannah zones. The red fruits of *F. glumosa* are responsible for attracting birds and numerous animals involved in seed dispersal; they are edible and eaten raw by humans. *F. glumosa* has varied traditional uses, as folk remedies by many tribes, for treating several human diseases such as diarrhea, anemia, hepatitis, malaria, abdominal pains, bronchitis, cough, and kidney diseases. Various extracts of *F. glumosa*, including the leaf, stem bark, and root, have been used to treat some health conditions. Several chemical constituents, such as flavonoids, phenolic acids, tannins, lignans, stilbenoids, and furanocoumarins, have also been reported in the leaf of *F. glumosa*. The plant has broad pharmacological activities, such as hepatoprotective, antidiabetic, *in vivo* and *in vitro* antimalarial, antidiarrheal, anti-Burkitt's lymphoma, antioxidant, antibacterial, antifungal, acetylcholinesterase inhibitory, antitrypanosomal, anthelmintic, vasorelaxant, antiplasmodial, and antironchitic properties, including antihypertensive, analgesic, anti-inflammatory, and bronchodilatory effects. By correlating traditional uses with pharmacological studies, the review validates the medicinal potential of *Ficus glumosa*, offering scientific backing for its use in traditional medicine
Keywords: *Ficus glumosa*, Ethnomedicine, terpenes, Red fruits

INTRODUCTION

Ficus glumosa Del. (1832) is an Indigenous tree widespread and significant in the vegetation folk culture of West and Central Africa. It is a typical Moraceae with some peculiarities such as a white, smooth, and horizontal layer on the bottom of its branches that earns it the commercial name "Gbanda" (Fulani language in Northern Nigeria) (Sofowora, 1993). The commercial name is derived from the unique traits in the international market and ranks among the top four commercial species exported and marketed by ethnic producers and traders in the northern savanna (East, Niger, Nigeria, and Chad) region of West and Central Africa, and the central African region, part of its ecological distribution in Senegal, Gambia, Guinea, the Democratic Republic of the Congo, and Angola (Sofowora, 1993; Abubakar *et al.,* 2011)

Ficus glumosa is a popular and valued fruit-producing tree species with potential for commercialization. It plays a pivotal role in coping with food, economic, health, and environmental issues in West and Central Africa (Adzu *et al.,* 2003; Kokwaro, 2009). Despite the high potential of the species in the increasing efforts to reduce hunger, and poverty, and maintain the non-carbon benefits from forest landscapes, the available literature on the species is very limited and scattered. This review report summarizes the fragmented knowledge collected from the existing research papers and related documents on the *F. glumosa* species and presents recommendations for further studies (Usman *et al.,* 2007; Tiwari *et al.,* 2011).

Ficus glumosa, locally known as gbafing (Jula, Bambara) or goumi ya (Minyanka), occurs across open woodlands of also and northern Sierra Leone, Guinea, both Ivory Coasts, Mali, Burkina Faso, Ghana, and Senegal. It is especially common in Mali, where the local dialects belong to the (incompletely) written-down Mande, a diverse language originating from empire-building farmers herding cattle across the Niger River valley (Ahmed *et al.,* 2008; Kamanyi *et al.,* 2009). This information could serve as a specific guideline for the exploitation of non-toxic, environmentally friendly, fast, and accessible remedies, and as a common framework for investigating the empirically stated therapeutic effects of unique *F. glumosa* leaf extracts in the management of diseases (Usman *et al.,* 2007; Ahmed *et al.,* 2008; Kamanyi *et al.,* 2009; Tiwari *et al.,* 2011). These findings emphasize the need for further research into the toxicity studies on *F. glumosa* to establish their safety and efficacy before their commercial production and use, to develop affordable plant-based remedies for improving the treatment efficacies of local communities. Species belonging to the same family are usually known to possess similar ethnomedicinal uses and represent promising sources for the discovery of new bioactive compounds with potential applications for the management of diseases affecting humans and animals. In this vein, the medicinal potential of the *Ficus glumosa* Delile (Moraceae) plant was reviewed.

Taxonomy and Botanical Description

The vernacular names of *Ficus glumosa* generally denote an inedible fruit. As with most figs of the Moraceae family, *F. glumosa* is non-climacteric and matures from green to fully ripe when the cherries are at the dark brown and attraction phase. The seeds in the tree can reach 90% of the dry weight of this fruit. The odor, as well as the sweetness of the fruit, is attractive to the birds during the period when the fruit is mature and depicts several apparent phenological stages. The robustness and medicinal properties have led to various uses for fruits and other parts of the plant. It is traditionally used to manage many health conditions such as malaria, tapeworm, and the roots to treat heart pain. The boiled root of *F. glumosa* has been used to alleviate pain in the heart, stomach, uterus, or urinary.

Ficus glumosa Delile is a small evergreen plant of the family Moraceae. The taxon is cylindrical, 6-16 mm in diameter with a greyish dense pubescence. The syconium is sub-cylindrical, usually exserted, or sometimes sunken with a short 2-3 mm peduncle and showy cup-shaped scutella. Ficus glumosa is closely related to Ficus sur and can be distinguished by sturdy branches, thicker alternate leaves, and cup-shaped scutella of the syconium. The taxon has a wide ecological amplitude, from the Sahel known for its semi-aridity to the wet Guineo-Congolese forest, characterized by an abundant water regime (Usman *et al.,* 2007; Ahmed *et al.,* 2008). The second flora of the germs or seedlings in the syconium is universal as it is found at all the latitudes of the distribution of the species. It is commonly known as red-leaved rock fig, hairy-leaved fig, or "Mubau" in Wolof language, and is a West African native species belonging to the Moraceae family. *F. glumosa* is mostly grown as a multi-trunked, spreading shrub or small to medium-sized tree with thick, peeling, and grey-white bark on the main stems (Kamanyi *et al.,* 2009; Tiwari *et al.,* 2011).

Botanical Classification of *Ficus glumosa*

Botanical name	*Ficus glumosa*
Kingdom	Plantae
Order	Rosales
Division	Tracheophyta
Family	Moraceae
Genus	Ficus
Specie	*F.glumosa*
Common name	Mountain rock fig
Local name	Kawuri

Literature Search

A systematic literature review of data on *Ficus glumosa* was carried out by the use of four electronic databases - PubMed, Scopus, Web of Science, and Science Direct. Searches included all manuscripts from the first record to the end of October 2021 without any language restrictions. The literature search findings provided insight into the available ethnoveterinary and animal pharmacological properties of *F. glumosa* in local communities, as well as the phytochemical compounds demonstrated in *F. glumosa*.

Figure 1: Leaves and stem of *Ficus glumosa*

Morphology of *Ficus glumosa*

The medium-sized tree *Ficus glumosa* (Moraceae), often known as the "African rock fig," is native to portions of West Asia and semi-tropical and tropical African nations (Beentje, 1988). It can be found in woods, at different locations, and in different kinds of broken terrain, including kopjes, outcrops, escarpments, and lava flows. It is mostly absent from the tropical rainforest zone and the desert interior regions of Namibia, Botswana, and South Africa. The bark is cream in color, and the branchlets are heavily covered in yellow-brown hairs. Small veins are elevated on the underside of the elliptical, 20–100 mm-sized leaves. The fruit is highly preferred by bats, birds, monkeys, antelope, and baboons (Burkill, 1985; Arbonnier, 2000).

Traditional uses of *Ficus glumosa*

Ficus glumosa has many health conditions, including diarrhea, edema, hypertension, headaches, stomach ailments, menstrual pains, skin diseases, rheumatism, diabetes mellitus, and female infertility, which are known to be treated and managed by African traditional medicine (Burkill, 1985; Arbonnier, 2000; Orwa *et al*., 2009; Madubunyi *et al*., 2012). Toothaches can be treated with latex and bark mouthwash, and ulcers can be treated by swallowing crushed bark soaked in water or by using it to clean wounds until they heal (Burkill, 1985). Fruits are eaten when they are ripe.

Pharmacological Properties of *Ficus Glumosa*

The reported pharmacological activities exhibited by *F. glumosa*, as well as the potentially responsible compounds, illustrate the therapeutic importance of this species in many ethnoveterinary uses or traditional practices by local communities.

Antidiabetic properties of *Ficus glumosa*

Diabetes, the most common metabolic disease, is typified by hyperglycemia during the postprandial or fasting phases due to reduced insulin sensitivity or production. The various subtypes of diabetes are type 1, type 2, and gestational diabetes. The two primary etiopathogenetic groups that account for the majority of cases of diabetes are type 1 and type 2 diabetes (Wang *et al*., 2016). Due to pancreatic beta-cell degeneration, the main cause of type 1 diabetes is an absolute lack of insulin secretion. Furthermore, the underlying etiology of type 2 diabetes is a combination of peripheral and hepatic tissue resistance to insulin action and inadequate insulin synthesis (Adams *et al*., 2011; Inzucchi and Sherwin, 2005). Pharmacological therapy has been employed to treat diabetes in recent years. Common synthetic drugs used to treat diabetes include glinides, a-glucosidase inhibitors, biguanides, sulfonylureas, etc. Negative side effects of these drugs often include headaches, low blood sugar, dark urine, fluid retention, nausea, vomiting, diarrhea, cramping in the stomach or intestines, and edema. In addition, according to Anbu *et al.* (2013), they are unsafe to use when breastfeeding. Using traditionally used medicinal plants, a new anti-diabetic treatment has been intensively studied as a potential substitute for current synthetic drugs. Furthermore, the World Health Organization's guidance on investigating medicinal plants with potential as antidiabetic agents is essential and naturally draws the interest of several researchers to this endeavor (WHO, 2002).

For a very long time, indigenous people have employed different organs from different Ficus species to treat ailments, including diabetes. Many studies have been carried out in the past few years on the isolated compounds and crude extracts from many Ficus species, especially those *from F. benghalensis, F. religiosa, F. glumosa, F. deltoidea, F. racemosa,* and *F. carica*. These Ficus species not only shielded diabetic animals from the harmful effects of *streptozotocin* and alloxan, but they also significantly decreased all diabetes-related issues by increasing insulin secretion, decreasing pancreatic cell levels, promoting glucose uptake, and enhancing glucose absorption (Farsi *et al*., 2014; Irudayaraj *et al*., 2016).

An ideal anti-diabetic drug decreases blood sugar, improves glucose use by the body, and delays the development and advancement of diseases associated with diabetes. It must be inexpensive, harmless, and effective when given orally. According to World Health Organization guidelines, the search is still ongoing because none of the current anti-diabetic drugs satisfy these requirements (WHO 1980). Numerous medicinal plants have been shown to have antidiabetic properties by science (Nadkarni, 1989). On the other hand, not much is known about plants that can also regulate blood sugar levels and act as antioxidants. Such a plant would be a great way to manage diabetes.

F. glumosa is an important medicinal plant that is widely used to treat inflammation, bleeding disorders, heart disease, high blood pressure, skin diseases, and diabetes in Cameroon, Senegal, and East Africa (Madubunyi *et al*., 2012). *F. glumosa* contains flavonoids, saponins, polysaccharides, tannins, and triterpenes (Ntchapda *et al*., 2014). The stem, leaves, and bark of this plant are used to cure diabetes in African countries (Madubunyi *et al*., 2012; Ogbonnaya *et al*., 2013). Madubunyi et al. (2012) examined the in vitro antioxidant and in vivo anti-diabetic. Effects of the methanol extract of *F. glumosa* stem bark in mice with alloxan-induced diabetes. The methanol extract of *F. glumosa* stem bark showed good anti-diabetic action in rats with diabetes caused by the chemical (Onoja *et al*., 2014). Umar et al. (2013)

investigated the effects of an ethanol extract of *F. glumosa* leaves on the serum lipid profiles and fasting blood sugar levels of diabetic rats. In a different investigation, an ethanol extract of *F. glumosa* leaves was given to alloxan-induced diabetic mice. This resulted in a significant decrease in fasting blood glucose levels and an increase in the liver enzymes alkaline phosphatase (ALP), alanine aminotransferase (ALT), and aspartate aminotransferase (AST) (Usman and Mohamed, 2015). In acute toxicity research, the methanol extract of *F. glumosa* leaves was found to be safe at doses ranging from 200 to 2,500 mg/kg (Madubunyi *et al.,* 2012).

Research by Michael et al. (2022) on the antioxidant efficacy of the n-butanol fraction of *Ficus glumosa* leaves against oxidative stress produced by the presence of carbon tetrachloride (CCL4) in rat kidneys revealed that the rats were grouped into 7 groups of 5. Groups 1 and 2 were employed as normal and vehicle controls, respectively. Group 3 did not get an extract or a traditional treatment; instead, they were given an induction. However, Groups 3, 4, and 5 were initiated with CCl4, and they were given varying dosages of the n-butanol fraction. Group 6 received regular antioxidant drug treatment in addition to CC14-induced induction. Results showed that *F. glumosa* leaf n-butanol fraction and silymarin treatments significantly ($p < 0.05$) restored SOD, GPx, and CAT activity to levels comparable to normal values, i.e 2.100.07 U/L and 34.22.59 U/L, respectively.

Furthermore, the EA fraction exhibited notable cytotoxicity towards human A549 and HT-29 cells that are used to treat lung and colon cancer. Additionally, liquid chromatography, in conjunction with electrospray ionization tandem mass spectrometry (LC-ESI-MS/MS), was used to characterize the chemical components of the EA fraction of *Ficus glumosa* stem bark. Sixteen compounds from the EA fraction have been found to have strong antioxidant and anti-proliferative activities.

Using alloxan-induced diabetic rats, Madubunyi et al. (2012) determined the methanol extract of *Ficus glumosa* Del stem bark's potential as an in vitro antioxidant and an in vivo antidiabetic. The extract showed a significant time-dependent reduction in blood glucose levels at doses of 62.5, 125, and 250 mg/kg. The groups treated with extract and the groups treated with glibenclamide at a dose of 2 mg/kg and distilled water at a dose of 10 mg/kg did not show any appreciable differences. Six hours after treatment, the blood glucose levels of the groups given 62.5 mg/kg of *F. glumosa* and 2 mg/kg of glibenclamide, respectively, were lower than the equivalent levels for the groups not receiving diabetes induction. In an experiment using DPPH spectrophotometry, *F. glumosa* displayed its best antioxidant activity at a concentration of 100 g/ml. Abubakar et al. (2020) investigated the anti-kindling and antioxidant characteristics of *T. globiferus* aqueous extract in a different investigation. Forty rats in all were divided into four groups of 10. The extract was given orally to Groups 1 through 3 at doses of 100, 200, and 400 mg/kg. They also received intravenous pentylenetetrazole (PTZ) at a dose of 35 mg/kg after an hour. In addition to receiving 35 mg/kg of PTZ and saline, Group 4 (the control) was observed for 30 minutes. This was carried out every 48 hours until 2.100.07 U/L, 43.82.49 U/L, and 34.22.59 U/L, respectively, were reached by all of the rats in the control group or until they were fully kindled. Furthermore, the treatments result in kidney MDA levels in rats treated with the n-butanol fraction that are similar to 0.34–0.05 mmol/L in normal rats. Urea dropped dramatically ($p < 0.05$) in the treated groups, from 5.24 mg/dL to 3.5 mg/dL (standard value). There was a substantial (p 0.05) drop in creatinine from 71.2 mg/dL in the treated groups to 43.3 mg/dL in the normal group. The electrolyte, Na+, K+, and Cl-levels in the CC14-induced rats dropped dramatically (p 0.05) to 137.82.59 mole/L, 3.980.54 mole/L, and 92.81.92 mmol/L, respectively, when the n-butanol fraction of *F. glumosa* leaves was administered.

Antioxidant properties of *Ficus glumosa*

Several investigations have demonstrated a robust correlation between oxidative stress and diabetes mellitus (Mahboob *et al*., 2005). The breakdown of glucose, non-enzymatic protein glycation, and the ensuing oxidative damage can all lead to an excess of free radical generation (Mahboob *et al*., 2005). Diabetes is tightly correlated with levels of lipid peroxidation and antioxidant enzymes, including glutathione peroxidase, catalase, and superoxide dismutase (SOD) (Latha and Pari, 2003). Raising antioxidant enzyme levels while reducing lipid peroxidation is a crucial strategy for reducing the risk of diabetic complications (Kamalakannan and Prince, 2006). The concentrations of flavonoids and phenolic in the ethanol extracts and the four extracted fractions of the *Ficus glumosa* stem bark (petroleum ether (PE), n-butanol, ethyl acetate (EA), and water) were determined in a study conducted by Mutungi *et al*. (2021). It further determined whether they have anti-proliferative and antioxidant properties. The results of the quantitative analysis indicated that the fractions containing n-butanol and EA had the highest total flavonoid/phenolic content, with respective values of 78.87 0.97 mg GAE/g and 274.05 0.68 mg RE/g. In the 2, 2 - azino-bis-(3-ethylbenzothiazoline-6-sulfonic acid) (ABTS), 2, 2-diphenyl-1-picrylhydrazyl (DPPH), and ferric-reducing antioxidant power (FRAP) assays, the EA fraction likewise showed outstanding efficacy, routinely achieving a Racine score of 4 or 5. The brain tissues of every rat were removed at the. The data obtained from this study may validate the traditional use of *T. globiferus* in the treatment of epilepsy by indicating the presence of bioactive compounds with antikindling and antioxidant activities in the aqueous extract obtained from the plant growing on *F. glumosa*.

Ficus asperifolia is a species in the Ficus family. Its aqueous extract was tested for its reductive ability and its capacity to scavenge free radicals, including 2, 2-diphenyl-1-picrylhydrazyl (DPPH), hydroxyl (OH), nitric oxide (NO), and iron chelation. Spectrophotometric methods were employed to determine the total concentrations of flavonoids and phenolic compounds. The *Ficus asperifolia* aqueous extract exhibited a reductive potential of 44.05 ± 0.05 mm.AAE/g and a DPPH scavenging activity of $78.65 \pm 1.15\%$ at 5 mg/ml. The plant extract had a phenolic content of 69.20 0.00 mg equivalent to garlic acid and a flavonoid content of 39.90 0.00 mg equivalent to rutin. FRE showed that DPPH and ABTS were concentration-dependent. Lipid peroxidation is avoided, along with the scavenging of hydroxyl and superoxide radicals.

The in vitro radioprotective ability of FRE was examined in radioirradiated Chinese hamster lung fibroblast cells (V79) using the micronucleus assay. An hour before 2 Gy y-radiation, the proportion of micro-nucleated binuclear V79 cells dramatically ($P<0.001$) dropped following pretreatment with different dosages of FRE. The maximum amount of radioprotection was 20 g/ml of FRE. Within an hour before being exposed to 0.5, 1, 2, 3, and 4 Gy y-radiation, cells treated with the optimal dose of FRE (20 g/ml) exhibited considerably higher radioprotection ($P < 0.01$) compared to the corresponding radiation controls. The cytokinesis-block proliferation index demonstrated that FRE did not affect the radiation-induced cell cycle delay. Based on all of these data, we infer that the ethanol extract of *F. racemosa* acts as a potent antioxidant and perhaps as a radioprotector.

Antibacterial activity of *Ficus glumosa*

The antibacterial activity and phytochemical screening of a crude water extract of *Ficus glumosa* stem bark were reported by Kwazo *et al*. (2015). The results of the antimicrobial test showed that the extract is effective against both species of Salmonella; in fact, it was significantly more effective against illnesses caused by *S. typhi* than *S. paratyphi* pathogens. Kitzberger *et al*. (2006) state that when the inhibitory zone diameter surrounding the paper disc is 9 mm or more, antibacterial activity can be taken into consideration. *Clerodendrum capitatum* (verbenaceae) and *Ficus glumosa* (moraceae) leaf extracts were compared for phytochemistry and in vitro antimicrobial effectiveness by Hamidu *et al*. (2017). The results showed that *Clerodendrum capitatum* was most effective against Candida albicans, with a susceptibility value of 20.330.58 mm, but least effective against the bacteria *Staphylococcus aureus* (7.330.58). Moreover, *Ficus glumosa* exhibited the least amount of activity (7.670.58) against E. coli but the same inhibitory zone (20.330.58 mm) against *Streptococcus pyogenes*. Both preparations' ethanolic leaf extracts contained tannins, cardiac glycosides, flavonoid saponins, and cardenolides. The only source of terpenoids was *F. glumosa*. Alkaloids and anthraquinones, however, were absent from both extracts. Therefore, increased amounts of these secondary metabolites in *C. capitatum* may explain its enhanced action against most examined species compared to *F. glumosa*, making it a good choice for treating the above-mentioned infections.

Antiulcer activity of *Ficus glumosa* species

At 200 mg kg1, the methanol-soluble extract of *Ficus glumosa* leaves showed signs of protecting the gastrointestinal system. With significant protection in experimental ulcer models caused by pylorus, indomethacin, and ethanol. The extract was determined to be non-toxic at 2 g/kg. (Awolola *et al*., 2019).

The laxative effect of *Ficus glumosa*

Ficus glumosa has a reputation for treating and managing a variety of health issues, including diarrhea, dysentery, edema, headache, stomach illnesses, and ulcers. The aerial portions of *F. glumosa* were used to isolate three phenolic acids (1-3), two coumarins (4 and 5), three flavonoid glycosides (6, 7a, 7b), and five triterpenoids (8-12). The methanol-soluble extract of the leaves demonstrated gastrointestinal protection at 200 mg kg 1 with considerable protection in ethanol, indomethacin, and pylorus-induced experimental ulcer models. At 2 g kg 1, the extract was found to be non-toxic. Isolated from the leaf extract, quercetin-3-O-D-glucopyranoside (isoquercitrin) 7a, quercetin-3-O-D-galactopyranoside 7b, and p-hydroxybenzoic acid 1 are thought to have a role in the observed gastro-protective effect (Awolola *et al.,* 2019).

Antiproliferative properties of *Ficus glumosa*

Research was carried out on the antiproliferative and antioxidant qualities. The quantitative analysis revealed that the EA and n-butanol fractions had the highest total flavonoid and phenolic levels, at 274.05 0.68 mg RE/g and 78.87 0.97 mg GAE/g, respectively. Similar to this, the EA fraction showed excellent potency in both DPPH and ABTS+ scavenging activities in the 2,2diphenyl-1-picrylhydrazyl (DPPH), 2,2'-casino-bis-(3-ethylbenzothiazoline-6-sulfonic acid) (ABTS), and ferric-reducing antioxidant power (FRAP) experiments, with IC50 values of 0.23 mg/mL, 0. Furthermore, human lung (A549) and colon (HT-29) cancer cells were highly vulnerable to the EA fraction (Mutungi *et al*., 2021). The study discovered that *F. glumosa* leaf extract decreased serum electrolytes (Na and C1), aspartate

aminotransferase, and HDL-c levels in Wister rats with testosterone-induced benign prostatic hyperplasia. Serum electrolytes (Na and Cl) significantly decreased in the *F. glumosa* extract-treated groups compared to the control groups (p<0.05). Serum urea, uric acid, and creatinine levels considerably decreased in the groups treated with 200 mg/kg and 400 mg/kg of *F. glumosa* leaf extract when compared to the BPHC standard and normal control groups. Similar trends were also observed in the serum level of aspartate aminotransferase (Obi Abang *et al*., 2021).

Phytochemistry of *Ficus glumosa*
The Ficus genus is highly significant because it includes a wide range of chemical classes, including triterpenes, steroids, alkaloids, megastigmanes, ligands, ceramides, tannins, and, in certain situations, stilbenes, and volatile compounds. Polyphenolic compounds include flavonoids, coumarins, phenolic acids, phenylpropanoids, and anthocyanins (Gbonjubola, 2015).

Terpenoids and sterols
Ficus glumosa contained the following compounds: lupeol (**1**), lupeol acetate (**2**), lupenone (**3**), lupeol hexanoate (**4**), and betulinic acid (**5**), each with a distinct substituent at positions 3 and 28. Three? -Hydroxy-20-oxo29 (20->19) abeolupane (**6**), which differs from compounds 1–5 and 29 in that it has an extra methyl group at C-19. Thirty-dinor-3? *F. microcarpa* was also the source of acetoxy-18, 19-dioxo-18, and 19-secularupane (**7**), which had an open cyclopentane ring. ? -amyrin (**8**) and its derivative in acetate. *Ficus benghalensis, F. carica, F. cordata, F. glumosa, F. lutea, F. microcarpa, F. nervosa, F. ovata,* and *F. Religiosa* were among the nineteen Ficus species that contained -amyrin acetate (**9**), and oleanolic acid (**10**), of the oleanane triterpenoids with a double bond at A12 and differing in their substituents at positions 3 and 28 (Ragasa *et al*., 2013). *Ficus religiosa and F. glumosa* were found to include campesterol (**11**), 28-isofucosterol (**12**), ergosterol peroxide (**13**), and dongnoside E (**14**) according to Ceramides and Cytotoxic Constituents from *Ficus glumosa* Del. (Moraceae) (Magdalene *et al*., 2021).

Originally, it was established that the stem bark of *Ficus glumosa* included antioxidant and antiproliferative properties in ethanol extracts and four extracted fractions: petroleum ether, ethyl acetate, n-butanol, and water. According to the quantitative study, the fractions containing n-butanol and ethyl acetate exhibited the highest amounts of total flavonoid and phenolics, with 78.87 + 0.97 mg GAE/g and 274.05 + 0.68 mg RE/g, respectively. The ethyl acetate fraction also demonstrated notable efficacy in the ferric-reducing antioxidant power (FRAP) assay, with IC50 values of 0.23 + 0.03 mg/mL, 0.22 + 0.03 mg/mL, and 2,2-diphenyl-1-picrylhydrazyl (DPPH), 2,2-azino-bis-(3-ethylbenzothiazoline-6-sulfonic acid) (ABTS), and DPPH testing. In addition, human lung (A549) and colon (HT-29) cancer cells were strongly exposed to the ethyl acetate fraction. Furthermore, *Ficus glumosa* stem bark ethyl acetate fraction's chemical composition was identified through the use of liquid chromatography coupled with electrospray ionization tandem mass spectrometry (LC-ESI-MS/MS). In the ethyl acetate fraction, the researchers found 16 compounds that may be in charge of the antiproliferative and antioxidant properties.
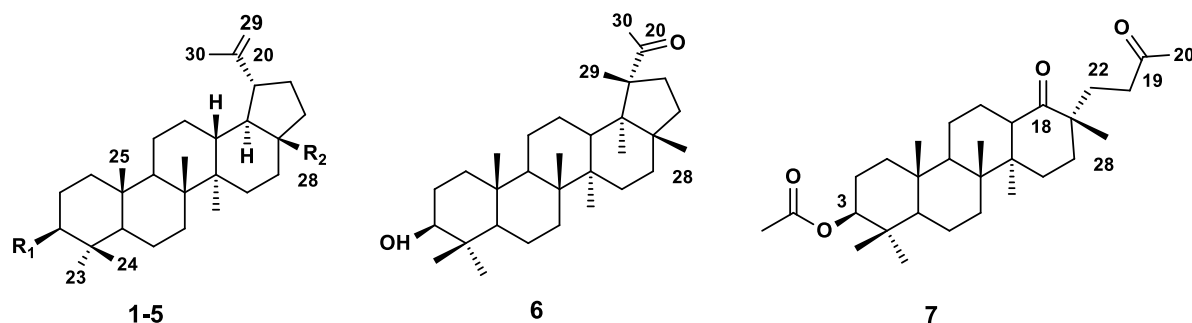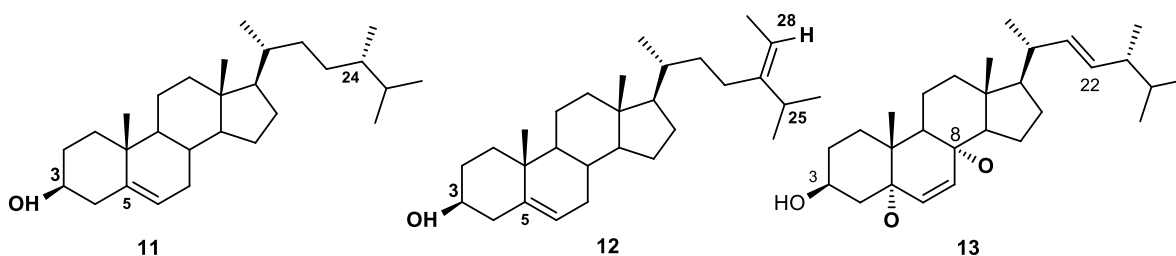

	R1	R2
1. Lupeol	OH	CH3
2.Lupeol acetate	OAc	CH3
3. Lupenone	O	CH3
4. Lupeol hexanoate	OCO(CH2)4-CH3	CH3
5. Betulinic acid	OH	COOH

Figure 2 (a): Terpenoid and Sterols
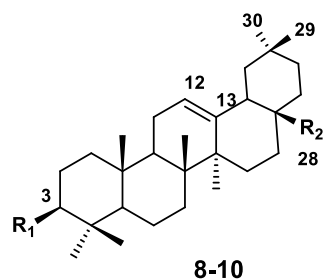
	R1	**R2**
8. Beta-amyrin	OH	CH3
9. Beta-amyrin acetate	OA	CH3
10.Oleonolic acid	OH	COOH

Figure 2 (b): Amyrin and its derivatives

Figure 2 (c): Other compounds from *Ficus glumosa*

The identification and structural characterization of secondary metabolites have received minimal attention up to this point. The following compounds were isolated and their structures were clarified based on the chemicals found in the butanol and n-hexane fractions. The n-hexane fraction was used to isolate and structurally describe 29-nor-cycloartanol (**15**), lanost-8-en-3-ol (**16**), cycloartanol (**17**), and kampferol-3,4'-dimethyl ether (**18**), in addition to 24 compounds that were tentatively identified by GC-MS (Aljubiri *et al*., 2020). The polar n-butanol fraction contained the following compounds: 4-O-D-glucopyranosyl-2-hydroxy-6-methoxyacetophenone (**19**), 4-O-L-rhamnosyl-(1 6)-D-glucopyranosyl-2-hydroxy-6-methoxy26 acetophenone (**20**), quercetin-3-O-glucopyranoside (**21**), and isoorientin (**22**).

CONCLUSION

By correlating traditional uses with pharmacological studies, the review validates the medicinal potential of *Ficus glumosa*, offering scientific backing for its use in traditional medicine. The review highlights areas needing further research, particularly in isolating specific bioactive compounds and understanding their mechanisms of action, paving the way for drug development and more targeted therapeutic applications. Furthermore**,** this review, therefore, endeavors to provide a comprehensive and up-to-date compilation of documented ethnopharmacological information about the ethnomedicinal, phytochemistry, and biological activities of *Ficus glumosa*, which can subsequently open new perspectives for further pharmacological research.

REFERENCES

Abubakar, K., Yunus, A. T., Abubakar, M. R., Ugwah-Oguejiofor, J. C. and Muhammad, A. A (2017). Antioxidant and anti-kindling effect of Tapinanthus globiferus growing on Ficus glumosa in pentylenetetrazole induced kindled rats, Afr. J. Biotechnol. 17(4). 73-80, 24

Ahmed, S., Yousaf, M., Mothana, R.A., Al-Rehaily, A.J., (2016). Studies on wound healing activity of some 01,

Aljubiri, S. M., Mahgoub, S. A., Almansour, A. I., Shaaban, M., & Shaker, K. H. (2020). Isolation of Diverse Bioactive Compounds from Euphorbia balsamifera: Cytotoxicity and Antibacterial Activity Studies. Saudi Journal of Biological Sciences. 12, 18-23.

Arbonnier, M., (2000). Arbres, arbustes et lianes des zones, ches d'Afrique de l'Ouest(Trees, shrubs, and vines in dry areas of West Africa). Cirad, Montpellier. 27-33.

Awolola, G. V., Sofidiya, M. O., Baijnath, H., Noren, S. S., & Koorbanally, N. A. (2019). The phytochemistry and gastroprotective activities of the leaves of Ficus glumosa. South African Journal of Botany. 1, 173-180

Beentje, H.J., (1988). Fig trees (Ficus, Moraceae) of Kenya. J. East Afr. Nat. Hist. Soc. Natl. Mus, 76, 53-76

Benedict C, Jacobsson JA, Rönnemaa E, Sällman-Almén M, Brooks S, Schultes B, Fredriksson R, Lannfelt L, Kilander L, Schiöth HB (2011). "The fat mass and obesity gene is linked to reduced verbal fluency in overweight and obese elderly men". *Neurobiology ofAging*. **32** (6):1159.e15. Doi:10.1016/j.neurobiolaging.2011.02.006. PMID 21458110. S2CID 20051507.

Ben-Jannet, S ., Hymery, N ., Bourgou, S ., J dey, A ., Lachaal, M ., Magn?, C ., Ksouri, R ., (2017). Antioxidant and selective anticancer activities of two Euphorbia species in human acute myeloid leukemia. Biomed. Pharmacother. 90, 375-385.

Boveris, AD; Galatro, A; Sambrotta, L; Ricco, R; Gurni, AA; Puntarulo, S (December 2001). "Antioxidant capacity of a 3-deoxyanthocyanidin from soybean". *Phytochemistry*. **58** (7): 1097–105. doi:10.1016/s0031-9422(01)00378-8. PMID 11730874.

Burkill H. M. (1985): The Useful Plants of West Tropical Africa. 2 The Royal Botanic Garden. New York. pp336

Conversion of procyanidin B-type (catechin dimer) to A-type: evidence for abstraction of C-2 hydrogen in catechin during radical oxidation. Kazunari Kondo, Masaaki Kurihara, Kiyoshi Fukuhara, Takashi Tanaka, Takashi Suzuki, Naoki Miyata and Masatake Toyoda, Tetrahedron Letters, 22 January 2000, Volume 41, Issue 4, Pages 485–488, doi:10.1016/S0040-4039(99)02097-

Gbonjubola V.A., (2015). Phytochemical Analyses and Biological Activities of Four South African Ficus Species (Moraceae). A Research Thesis. Pharmacognosy. 49. 210-216.

Hamidu, U ., Vivian, I ., Helen, E ., Suyi, H ., and Umar, A. (2017). Comparative Phytochemistry and In Vitro Antimicrobial Effectiveness of the Leaf Extracts of Clerodendrum capitatum (Verbenaceae) and Ficus glumosa (Moraceae). Food Chemistry. 39, 83-95

Kamba, A.S., and Hassan, L.G. (2010). Phytochemical Screening and Antimicrobial Activities of Euphorbia balsamifera Leaves Stems and Root against Some Pathogenic Microorganisms. African Journal of Pharmacy and Pharmacology, 1, 645-652.

Kwazo, Hadiza & Faruq, U. & Dangoggo, Sani M. & B, S & Moronkola, Dorcas. (2015). Antimicrobial activity and phytochemical screening of crude water extract of the stem bark of Ficus glumosa. Scientific Research and Essays. 10. 177-183.

Madubunyi, I.I., Onoja, S.O., Asuzu, I.U., (2012). In vitro antioxidant and in vivo antidiabetic   potential of the methanol extract of Ficus glumosa Del (Moraceae) stems bark in alloxan-induced diabetic mice. Comparative Clinical Pathology 21, 389-394

Magdalene O ., Ironya O ., Jonathan O, E ., Margaret A. E ., Godwin E. E ., (2021). Ficus glumosa edible leaf extract attenuates some biochemical markers in testosterone-induced benign prostatic hyperplasia in Wistar rats. World J. Agric. Sci. 28, 30-33.

Mahboob, B., Satish, S., (2005). Antimicrobial Activity of Some Important Medicinal Plants against Plant and Human Pathogens. World J. Agric. Sci. 4, 839-843.

Ogbonnaya, E. C., and Chinedum, E. K. (2013). Health-promoting compounds and in vitro antioxidant activity of raw and decoctions of Gnetum aficanuAfrican Welw. Asian Pacific Journal of Tropical Disease, 3(6), 472-479.

Semwal, R. B., Semwal, D. K., Combrinck, S., & Viljoen, A. (2015). Butein: From ancient traditional remedy to modern nutraceutical. Phytochemistry Letters, 11, 188-201. doi:10.1016/j.phytol.2014.12.014

Usman Akiyama, T., Ishida, J., Nakagawa, S., Ogawara, H., Watanabe, S., Itoh, N., Shibuya, M., & Fukami, Y. (1987). Genistein, a specific inhibitor of tyrosine-specific protein kinases. The Journal of Biological Chemistry, 262(12), 5592-5595

Usman Akiyama, T., Ishida, J., Nakagawa, S., Ogawara, H., Watanabe, S., Itoh, N., Shibuya, M., & Fukami, Y. (1987). Genistein, a specific inhibitor of tyrosine-specific protein kinases. The Journal of Biological Chemistry, 262(12), 5592-5595

Wang, X.; Ouyang, Y.Y.; Liu, J.; Zhao, G. (2016). Flavonoid intake and risk of CVD: A systematic review and meta-analysis of prospective cohort studies. Br. J. Nutr. 111, 1-11.

Bioautography Studies of *Crinum ornatum* (Aiton) Bulb Extracts against Salmonella Typhi

*[1]Aminu Bello Riji, [1]Tijjani Ali and [2]Adikwu Gowon Jacob

[1]Department of Chemistry, Federal University Dutsin-Ma, Katsina, Nigeria
[2]Department of Industrial Chemistry, Federal University Dutsin-Ma, Katsina, Nigeria
*Corresponding Author's E-mail: abriji@fudutsinma.edu.ng

ABSTRACT

Crinum Ornatum (Aiton), is a recognized traditional plant with medicinal properties. It is also known to contain bioactive compounds with potential for antibacterial activity. *Salmonella Typhi*, the causative agent of typhoid fever continues to pose a significant global health threat due to its increasing antibiotic resistance. In search of alternative and complementary therapies, this study investigated the antibacterial potential of *Crinum Ornatum* bulb extract against *Salmonella Typhi* using the bioautography method. Two crude extracts of *Crinum Ornatum* bulbs were obtained by maceration with ethyl acetate and methanol as solvents. The extract was subjected to thin-layer chromatography (TLC), and a bioautography assay was performed to assess its antibacterial activity against *Salmonella Typhi*. This method allowed for the visualization of zones of inhibition on TLC plates with ultraviolet light at 254 nm and 366 nm. Results from the bioautography studies revealed distinct inhibitory zones on the TLC plates, suggesting the presence of antibacterial compounds within the *Crinum Ornatum* bulb extracts. These inhibitory zones were particularly evident when exposed to *Salmonella Typhi* cultures indicating the specificity of the antibacterial activity against the target pathogen. In a nutshell, the findings of this study proved that *Crinum Ornatum* bulb is a source of effective antibacterial compounds against *Salmonella Typhi*. Furthermore, the antibacterial activity demonstrated in this study could be attributed to some of the major phytocompounds in the bulb including saponins, carbohydrates, tannins, steroids, terpenoids, alkaloids, flavonoids and anthraquinones. This study therefore had scientifically confirmed the traditional uses of *Crinum Ornatum* to cure certain diseases

Keywords: *Crinum Ornatum*, Phytocompounds, Bioautography, *Salmonella Typhi,* Antibacterial

INTRODUCTION

Planar chromatographic analysis hyphenated with the biological detection method which is called bioautography, is a specific method within the field of Natural Products Chemistry and Microbiology. It allows for the identification and characterization of bioactive compounds present in complex mixtures, particularly plant extracts. It has emerged as a valuable approach for screening and assessing the antibacterial, antifungal, and antioxidant properties of Natural Products, and plays a pivotal role in the search for novel drug leads and the development of herbal medicines (Cowan, 1999). This method combines the principles of chromatography with microbial assays, enabling to location of the bioactive compounds within a complex mixture, which could show as zones of inhibition in microbial cultures. Bioautography, thus, provides an efficient and cost-effective approach for isolating and identifying bioactive compounds, reducing the labor-intensive and time-consuming nature of traditional bioassay-guided fractionation processes (Atanasov, 2015). It is also a versatile method that is extensively applied to assess various bioactivities. It can be used to identify compounds with antibacterial properties against a range of pathogenic bacteria, including Gram-positive and Gram-negative bacteria. Correspondingly, antifungal bioautography screens for compounds' effectiveness against fungal pathogens. Moreover, antioxidant bioautography identifies compounds with free radical scavenging capabilities, offering insights into potential natural antioxidants for various applications (Saikat *et al.,* 2014).

Typhoid fever is a life-threatening infection caused by the bacterium *Salmonella Typhi*. A person with typhoid fever carries the bacteria in the bloodstream and intestinal tract (Claire *et al.,* 2002). In parts of the world with poor sanitation, infected human wastes can pollute the water supply. Symptoms of typhoid fever include prolonged high fever, fatigue, headache, nausea, abdominal pain, and constipation or diarrhea (Claire *et al.,* 2002). Some infected persons may have a rash, and severe cases may result in grave complications including death. This fever can be confirmed only by a blood test. *Salmonella Typhi* is a gram-negative bacterium that has been a burden on developing nations for generations wherein it rapidly multiplies and causes a high temperature, stomach pain, and constipation or diarrhea. Typhoid fever continues to be a public health issue in several developing parts of the world (WHO, 2023). According to WHO, about 9 million cases of typhoid fever causing roughly 110,000 deaths annually were reported in 2019 (WHO, 2023).

MATERIALS AND METHODS

Materials and Chemicals

All chemicals and reagents used in the study were of analytical grade and obtained from the Department of Chemistry, Federal University Dutsin-Ma, Katsina State. Dichloromethane, n-hexane, ethyl acetate, methanol, Maeyer's reagent, concentrated sulfuric acid, chloroform, 5% acetone, acetic anhydride, distilled water, disinfectant, nutrients agar, tetrazolium salt amongst others were used in the work. Rotary evaporator, glass bottles, TLC kits, Whatman filter paper, measuring cylinders, hand gloves, masking tape, beakers, spatula, test tubes, washing bottles, cotton wool, petri dishes, syringes and needles, sample bottle, pipettes, autoclave, nutrients broth, capillary tubes, chromatographic tank, ultraviolet lamp, burette, micro beakers, conical flasks and weighing balance were also used

Sample Collection and Preparation

Fresh bulbs of *Crinum Ornatum* were collected at Dutsin-Ma Local Government Area, Katsina State, Nigeria. The plant was authenticated at the Department of Biological Sciences, Federal University Dutsin-Ma, Katsina state, Nigeria. The bulbs samples were air-dried and ground into fine powder using a mortar and pestle in the laboratory. Extractions were carried out through conventional method as described by (Mann *et al.,* 2008). Exactly, 100.0 g of powdered sample was soaked with ethyl acetate solvent in a Bama bottle at room temperature for 72 h. The resulting ethyl acetate solution was filtered and the residue was re-extracted with methanol for another 72 h and filtered. Yields of the crude extracts were determined.

Preliminary Phytochemical Screening

A few milligrams of the four different dried extracts were obtained from ethyl acetate and methanol was first dissolved and the various solutions obtained were all subjected to phytochemical screening employing the standard screening test (Trease & Evan, 1996).

Test for Flavonoids

A few drops of concentrated hydrochloric acid were added to a small amount of the extracts of the plant material. The immediate development of a red color indicates the presence of

Test for Alkaloids

A Few drops of Maeyer's reagent were added to 1 mL of extract. A yellowish or white precipitate was formed, indicating the present of alkaloids (Trease & Evan, 1996).

Test for Terpenoids

To 5 mL of the extract add 2 ml of chloroform and 3 mL of H_2SO_4, conc.,The formation of a reddish brown ring confirms the presence of terpenoids (Evan, & Trease 1996).

Test for Tannins

To a portion of the extract, 3-5 drops of ferric chloride was added. A greenish-black precipitate indicates the presence of tannins (Evan, & Trease, 1996).

Test for Carbohydrate

Molish reagent (4 drops) was added to 2 mL of extract later drops of concentrated H_2SO_4 were added along the walls of the test tube, the junction of two liquids, a violet colour ring appeared, indicating that carbohydrates were present

Test for Anthraquinones

5 mL of conc. H_2SO_4 was added to 5 ml of extract, followed by 1 mL of diluted ammonia. The existence of anthraquinones is confirmed by the appearance of rose pink.

Test for Steroids

The presence of steroids is shown by the emergence of red color and yellowish-green fluorescence after mixing 2 ml of the extract with 2 ml of chloroform and 2 ml of concentrated H_2SO_4, the appearance of red color and yellowish green fluorescence confirms the presence of steroids.

Test for Saponins

With a few ml of distilled water, 0.5 mg of extract was quickly shaken. For saponins, the production of foaming is a favorable sign

Thin Layer Chromatography (TLC)

The two extracts were subjected to thin layer chromatography (TLC) using several solvent-system (Hexane per ethyl acetate (4:1), Hexane per ethyl acetate (5:3) and Hexane per ethyl acetate (3:2)) to obtain the best solvent system that would give good separation for the compounds suitable for bioautography. The extracts were then spotted on TLC plates and allowed to dry. After drying, the plates were developed in an air-tight chromatographic tank using the perceived solvent system. The developed chromatograms were air dried and visualized; under normal day light using ultra violetlight (254 nm & 366 nm).

Direct TLC Bioautography

For the bioautography study, the developed TLC plate containing crude extract spots with good separation was sprayed with fungal or bacterial suspension. The salmonella typhi bacteria were chosen for the study. The bioautogram was then incubated at 25 °C for 48 h under humid conditions for visualization of microbial growth, tetrazolium salts were used. These salts were converted by the dehydrogenases of living microorganisms to intensely colored formazen. These salts are sprayed onto the bioautogram and are reincubated at 25 °C for 24 h (Silva, *et al.,* 2005). A clear white zone against a purple background on the TLC plate indicated an antimicrobial activity of the sample. Afterwards, the bioautogram was re-view with ultraviolet light (254 nm & 366 nm).

RESULTS AND DISCUSSION

Table 1: Phytochemical screening of the crude extracts

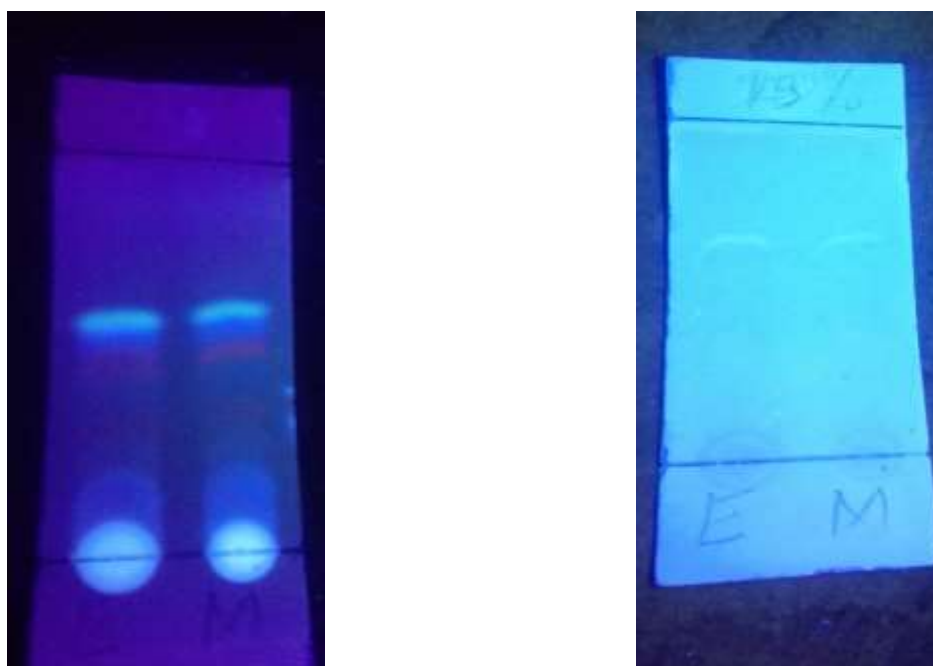| Phytochemicals	Ethyl acetate	Methanol
Tannins	-	+
Flavonoids	+	+
Saponins	+	+
Steroids	+	-
Alkaloids	+	+
Terpenoids	+	-
Anthraquinones	+	+
Carbohydrate	+	+

Key: + = Present,   - = Absent

Figure 1: TLC showing plates a) before bioautography, and b) after bioautography

Discussions

Phytochemical screening of ethyl acetate and methanol crude extracts of *Crinum ornatum* are presented in Table 1. Results revealed that for all the phytocompounds screened including tannins, flavonoids, saponins, steroids, alkaloids, terpenoids, anthraquinones, and carbohydrates, only tannins were not detected in ethyl acetate extract. Conversely, the results showed the methanolic extract contained tannins, flavonoids, alkaloids, anthraquinones, saponins and carbohydarates while steroids and terpenoids were absent. The presence of these phytocompounds as revealed in the two extracts could be ascribed to the high polarity of the solvents used. Alkaloids tested positive in both ethyl acetate and methanol extracts (Table 1). Alkaloids have been reported to have a wide range of pharmacological properties. According to according Russo *et al.* 2013 and Kittakoop 2014, certain alkaloids have antimalarial activity (e.g. quinine), and anti-asthma activity (e.g. ephedrine), as well as anticancer properties (e.g. homoharringtonine). Alkaloids also possess vasodilatory properties (e.g. vincamine), antiarrhythmic activities (e.g. quinidine), and analgesic properties (e.g. morphine) antibacterial alkaloids (e.g. chelerythrine) as reported by Cushnie *et al.,* (2005). Furthermore, antihyperglycemic activities of alkaloids (e.g. pyridine) were equally reported by Qiu *et al.,* (2014). The presence of these compounds in plant extracts could be linked to the ethnomedicinal uses of *Crinum ornatum bulb* in traditional medicine practices. These secondary metabolites have been known scientifically to act as antioxidants, anti-inflammatory, anticancer and antimicrobial, anti-malarial agents (Song *et al.,* 2019; Yang *et al.,* 2018; Wang *et al.,* 2020 and Mao *et al.,* 2019). Therefore, the presence of these phytochemicals in *Crinum ornatum bulb* could be scientific evidence for the traditional and biological uses of the plants.

CONCLUSION

The bioautography experiments conducted in this study revealed that the tested sample had antibacterial activity against *salmonella typhi*. The presence of active compounds was observed as clear zones of inhibition on the TLC plates indicating that the sample contains compounds that are capable of inhibiting bacterial growth. The size of the inhibition zones varied depending on the concentration of the sample applied to the TLC plate, with higher concentrations resulting in larger zones. Findings from this study suggest that the antibacterial activity of the samples is concentration-dependent and that increasing the sample concentration could enhance its bioactivity. The studies were evaluated using, ethyl acetate and methanol extracts (Figure 1a & b). Ethyl acetate extract showed broad-spectrum antibacterial activity with clear zones observed on the TLC plate (Figure 1a). The size of the clear zones suggested that the extract has a higher concentration of active compounds. The methanol extract showed the broadest antibacterial activity with the largest clear zones observed on the TLC plate. The results suggested that the methanol extract contains the highest concentration of active compounds with the broadest range of antibacterial properties. Finally, the bioautography results imply that the methanol extract is the most promising extract for further investigation due to its broad-spectrum antimicrobial activity. However, further studies are required to isolate and identify the bioactive compounds responsible for the observed antimicrobial activity.

REFERENCES

Atanasov, A. G., Waltenberger, B., Pferschy-Wenzig, E. M., (2015). Discovery and resupply of pharmacologically active plant-derived natural products: a review. Biotechnology Advances, 33(8), 1582-1614.

Claire Kidgell, Ulrike Reichard, John Wain, Bodo Linz, Mia Torpdahl, Gordon Dougan, Mark Achtman (2002).*Salmonella typhi*, the causative agent of typhoid fever, is approximately 50,000 *years old, Infection, Genetics and Evolution* Volume 2, Issue 1, October, 39-45.

Cowan, M. M. (1999). Plant products as antimicrobial agents. Clinical Microbiology Reviews, 12(4), 564-582.
Cushnie, T.P., Lamb, A.J. (2005). Antimicrobial activity of flavonoids. *Int J Antimicrob Agents.*26: 343–56.
Evans WC and Trease (1996). Pharmacognosy 14th Edition. Saunders W.B Company Ltd. London

Kittakoop Prasat, Chulabhorn Mahidol and Somsak Ruchirawat (2014). Alkaloids as Important Scaffolds in Therapeutic Drugs for the Treatments of Cancer, Tuberculosis, and Smoking Cessation.*Bentham Science is a science, technology, and medical publisher*.Volume 14, Issue 2, 2014

Mann, A. Y. Yahaya, A. Banso and F. John (2008).Phytochemical and antimicrobial activity of *Terminalia avicennioides* extracts against some bacteria pathogens associated with patients suffering from complicated respiratory tract diseases. *Journal of Medicinal Plants Research* Vol. 2(5), pp. 094-097.

Qiu, Z.Y., Tang, M.L., Deng, G.J. (2014) Antioxidant and Antigenotoxic Activities of Ethanol Extracts from Rhus chinensis Mill Leaves. Food Science and Biotechnology, 23, 1213-1221.

Russo, P, A Frustaci, A Del Bufalo, M Fini, & A Cesario (2013).From traditional European medicine to discovery of new drug candidates for the treatment of dementia and Alzheimer's disease: acetylcholinesterase inhibitors. *Curr Med Chem* ;20(8):976-83

Silva, M.T.G. S.M.Simas,T. and Batista. (2005). Studies on antimicrobialactivity, invitro of Physalis angulata L. (Solanaceae) fraction and physalinB bringing ou the importance of assay determination,Mem.Instit.Oswaldo Cruz 100-779–782..

Saikat Dewanjeea , Moumita Gangopadhyayb , Niloy Bhattacharyaa , Ritu Khanraa , Tarun K. Duaa,(2014). Bioautography and its scope in the field of natural product chemistry In Advanced Pharmacognosy. *Journal of Pharmaceutical Analysis; 5(2):75-84*

World Health Organization (WHO) 2023. World health organization on Salmonella Typhi report

Information on Corrosion Inhibition Potential for *Caralluma Dalzielii* N.E Brown

*[1]Siaka A. A., [1]Hussaini A., and [2]Gafar M. K.

[1]Department of Chemistry, Federal University Dutsin-Ma, Katsina State Nigeria
[2]Department of Chemistry, Federal University Gusau, Zamafara State Nigeria
*Corresponding Author's E-mail: ahussaini@fudutsinma.edu.ng Phone: +2348166790510

ABSTRACT
The corrosion study of Caralluma Dalzielii (N.E Brown) was carried out and the Gas Chromatography and Mass spectrum (GC-MS) done, revealed the presence of twelve (12) compounds in the extracts of the plant stems. The functional groups in the compounds of the stem extracts were also examined and identified by Fourier Transformed Infra-Red Spectroscopy (FTIR) which revealed the presence of ten (10) functional group. The FTIR study investigate the various functional groups among the extract, the blank and the inhibited corrosion product, while the GC-MS investigation reveals the organic molecules in the stem extracts.
Keywords: Corrosion, *Caralluma Dalzielii*, FTIR

INTRODUCTION
Corrosion inhibitor is defined as a substance which when added to a small amount in an environment can effectively reduce the rate of corrosion of an exposed metal by controlling the dissolution of the metal as well as the acid consumption (Chigondo and Chigondo, 2016). The corrosion inhibition process first started with the adsorption of the inhibitors on to the surface of the metal, then forming the protective barrier and then interacting with anodic and cathodic reaction sites, thus decreasing the oxidation or reduction reactions. Over the years, several inhibitors have been synthesized or chosen from the existing compounds where it has been found that the best inhibitors are those that possess the center for π electron donations that is usually enhanced by the presence of hetero atoms in the aromatic compounds while others may be gotten from the extracts of naturally occurring compounds (Eddy *et al.,* 2008). Coming to the last class of the inhibitors which are green corrosion inhibitors, are very significant because of their non-toxicity and do not contains heavy metals hence they are environmentally friendly and of course has great effect on the chosen metal like Mild steel in this case. *Caralluma Dalzielii* (N.E Brown) Mosque Stalk/Reed which is also known as Karan Masallaci in Hausa are important medicinal green plants which are widely used by most of the people. *Caralluma* is one of the prominent genera and it grows well in dry regions such as India, Africa, and the Middle East (Zakaria *et al.,* 2001). In folkloric medicine, as well as in Unani and Ayurvedic systems of medicine, the plants of *Caralluma* are being used for the treatment of diabetic patients and rheumatism. Some of them are valued by tribes as food during famines and as components of their traditional medical practices. According to research by Ugwah-Oguejiofor *et al*. (2019), the aqueous extract of *Caralluma Dalzielii* contains saponins, flavonoids, steroids, alkaloids, volatile oils, steroids, glycosides, terpenoids, and saponin glycosides and a number of compounds have been isolated from the plant extract (Oyama *et al*., 2007). *Caralluma* species are predicted to exhibit a range of biological activities (Abdel-satta *et al*., 2014) which contain stigmasterol and other phytochemicals (Bader *et al*., 2003). *Caralluma* is currently receiving a lot of attention from researchers since it has a variety of immune-stimulating properties because of the presence of numerous phytochemicals (Sireesha and others 2014). In Nigeria, according to Ugwah *et al*. (2019) it has historically been used to treat rheumatoid arthritis, leprosy, diabetes, infertility, and severe discomfort in the epigastrium. Also, as an aphrodisiac by Oyama *et al*. (2007). *Caralluma* species have been used as emergency foods in India and Pakistan for many years. Due to the presence of pregnane glycosides, *Caralluma* species are predicted to exhibit a range of biological activities which contain stigmasterol and other phytochemicals (Bader *et al*., 2003). The aim of the study is to identify the phytochemical constituents in the extracts of *Caralluma Dalzielii* for corrosion study which were characterized via Fourier transform infra-red spectroscopy (FT-IR) and Gas Chromatography and mass spectrum (GC-MS) in the process.

Plate 1: Image of *Caralumma Dalzeilii N.E Brown`s stem*

MATERIALS AND METHODS
Sample Preparation
The stems of *Caralluma Deilzelii* (N.E Brown) was collected, washed, and dried in the shade away from sun light for up to three (3) months, purposely to prevent the loss of active components in the plant, some of the stems were preserved in the refrigerator while others were grounded well into a fine powder using local motor and pestle, transferred into an air tight container with proper labeling for immediate used (Hojatollah *et al*., 2013) .

Maceration Procedure
300g of powdered stem of *Caralluma Dallzeilii* (NE Brown) were soaked in 1.25L of ethanol which serves as an extraction solvent for 48 hours. The extracts collected were concentrated using a rotary evaporator (RE-52A) to obtain the crude extracts (Mann *et al*., 2011). The ethanol was also recovered completely and the crude extracts were further air dried and packed in a glass bottle with proper labeling and kept under refrigerator at 40 ºC away from sun light by wrapping it with aluminum foil until required for use.

RESULT AND DISCUSSION
Characterization
FTIR Analysis
The vibrational frequencies, functional groups and the frequency of the stem extract of the *Caralluma Dalzeilii* (N.E Brown) are presented in Table 1, while the FT-IR spectrum is presented as Fig. 1.
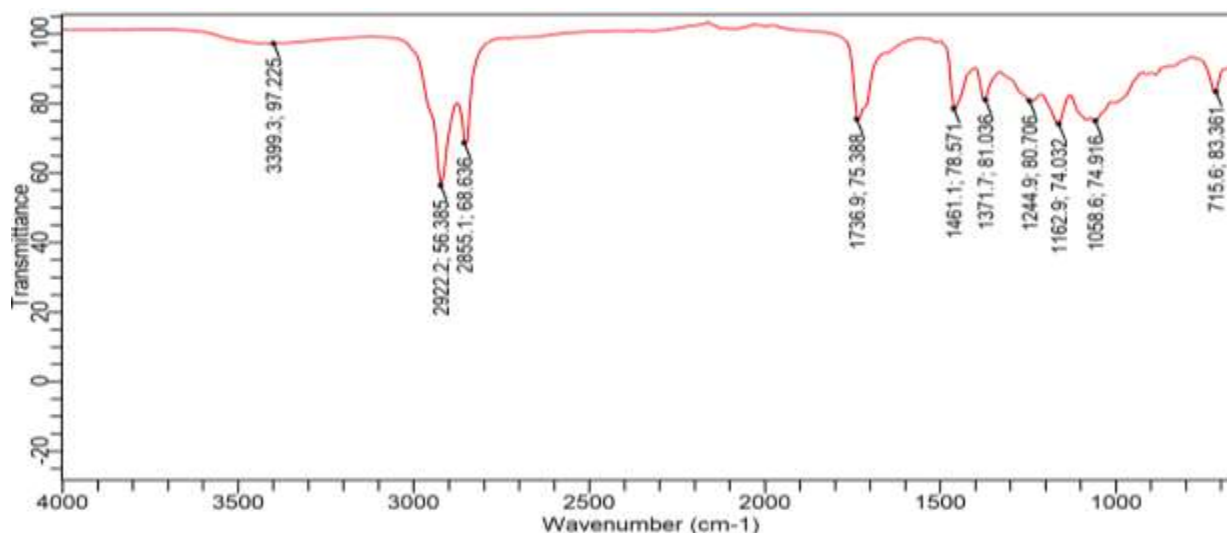
Figure 1. FT-IR spectrum characteristics for *Caralluma Dalzeilii N.E Brown* stem extracts

Table 1. FT-IR peaks and assignment for *Caralluma Dalzeilii N.E Brown* stem extract

S/NO	Functional Groups	Observed Vibrational Frequency (cm^{-1})	Frequency of Extract	Assignment
1	C=C bending	730-665	715.64886 83.36128	Alkene
2	C-O stretching	1085-1050	1058.56395 74.91577	Primary alcohol
3	O-H bending	1400-1000	1162.9294,74.03164	Carboxylic acid
4	C-O stretching	1275-1200	1244.93084,80.7055	alkyl aryl ester
5	O-H bending	1576- 1300	1371.66032,81.0356	Phenol
6	C-H bending	1465-1648	1461.11643 78.57130	Methyl group
7	C=O stretching	1740-1720	1736.93943,75.3884	Aldehyde
8	C-H stretching	3000-2840	2855.14078,68.6364	Alkane
9	N-H stretching	3000-2800	2922.23286,56.3845	Amine salt
10	O-H stretching	3550-3200	3399.33211,97.2253	Alcohol

Discussion on the FT-IR spectrum of Caralluma Dalzeilii (N.E Brown) stem extracts
The FT-IR Spectrum for the *Caralluma Dalzeilii* (N.E Brown) stem extract is presented in Figure 1 and the vibrational frequency, functional group, frequency of leaves and assignment are presented in Table 1. It is evident from the results that the *Caralluma Dalzeilii* (N.E Brown) stem extract contains compounds such as Alkene, Primary alcohol, carboxylic acid, alkyl aryl ester, Phenol, methyl group, Aldehyde, Alkene, Amine salt and alcohol. which contain heteroatom, a corrosion inhibiting substance. The presence of C=C at 715cm^{-1}, C-O at 1058 cm^{-1}, O-H at 1162 cm^{-1}, C-O at 1244 cm^{-1}, O-H at 1371 cm^{-1}, C-H at 1461 cm^{-1} , C=O at 1736 cm^{-1} , C-H 2855 cm^{-1} , N-H at 2922cm^{-1} and O-H at 3399cm^{-1} were suggests to play a major role in the inhibiting efficiency of the *Caralluma Dalzeilii* (N.E Brown) stem extracts.
The GC-MS Study for *Caralluma Dalzeilii* (N.E Brown) Stem Extracts
The GC-MS chromatogram of *Caralluma Dalzeilii* (N.E Brown) extract is presented in Figure 2 and the major phytochemical compounds contained in the alcoholic extract of the extracts (with higher concentration percentage) are presented in Table 2 which the representative structures of this major components is given in Figure 3
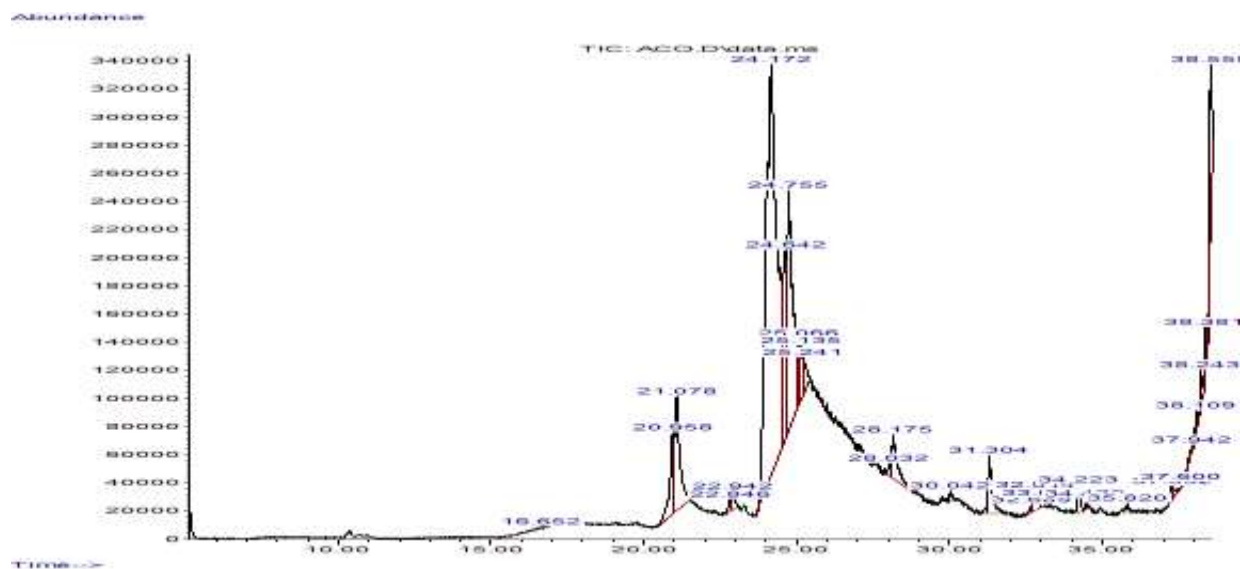
Figure 2: GC-MS chromatogram of ethanolic extract of *Caralluma Dalzeilii N.E Brown's stem*

The retention time, molecular formula, mass peaks, and the concentrations of major From the result that was abstained, it's evident that the separated compounds can be classified into hydrocarbons (2(1H)-Napthaleneone,octahydro-4a-methyl-7-(1-methylethyl)-,(4a.alpha.,7.beta.,8a.beta.), Cyclopropaneoctanal 2-octyl- etc. Aromatic hydrocarbons such as Campesterol. The spectra pointed out the attendance of carboxylic acid such as Octadecanoic acid, Octadecanoic acid, 9-Oxabicyclo[6.1.0]nonane, Octadecanoic acid ethyl ester, 5-Ecosene (E)- , 9-Octadecanoic acid (Z)-,2,3,-dihydroxypropyl ester, Eicosanoic acid ethyl ester and Docosanoic acid, ethyl ester alkanoate and alkanol (Arthur & Abechi, 2019). etc. and these compounds possess π-electrons and heteroatoms like N, S and O which acted as adsorption center's (Eddy & Ebenso, 2010).

Table 2: presents the main phytochemical compounds in the crude extract of *Caralluma Dalzeilii N.E Brown's stem*

| Line	Concentrations (%)	Chemical Formula	Rentation Time	Molecular Weight(g/mol)	Name of the compounds
1	3.576807154	$C_{18}H_{36}O_2$	20.958	284.478	Octadecanoic acid
2	6.322812646	$C_{18}H_{36}O_2$	21.0785	284.478	Octadecanoic acid
3	47.70269541	$C_8H_{14}O$	24.1719	126.2	9-Oxabicyclo [6.1.0] nonane, cis-
4	7.282314565	$C_{19}H_{36}O$	24.6418	280.5	Cyclopropaneoctanal,2octyl-
5	15.37803076	$C_{20}H_{40}O_2$	24.7551	312.5	Octadecanoic acid, ethyl ester
6	1.220502441	$C_{20}H_{40}$	25.0655	280.5	5-Eicosene, (E)-
7	1.346702693	$C_{21}H_{40}O_4$	25.1354	356.5399	9-Octadecenoic acid (Z)-, 2,3-dihydroxypropyl ester
8	1.051102102	$C_{20}H_{40}$	25.2413	280.5	3-Eicosene, (E)-
9	2.691805384	$C_{22}H_{44}O_2$	28.1752	340.5836	Eicosanoic acid, ethyl ester
10	2.566005132	$C_{24}H_{48}O_2$	31.3036	368.6	Docosanoic acid, ethyl ester
11	0.31020062	$C_{15}H_{24}$	37.942	204.35	(E)-.beta.-Famesene
12	3.62500725	$C_{28}H_{48}O$	38.5578	400.7	Campesterol
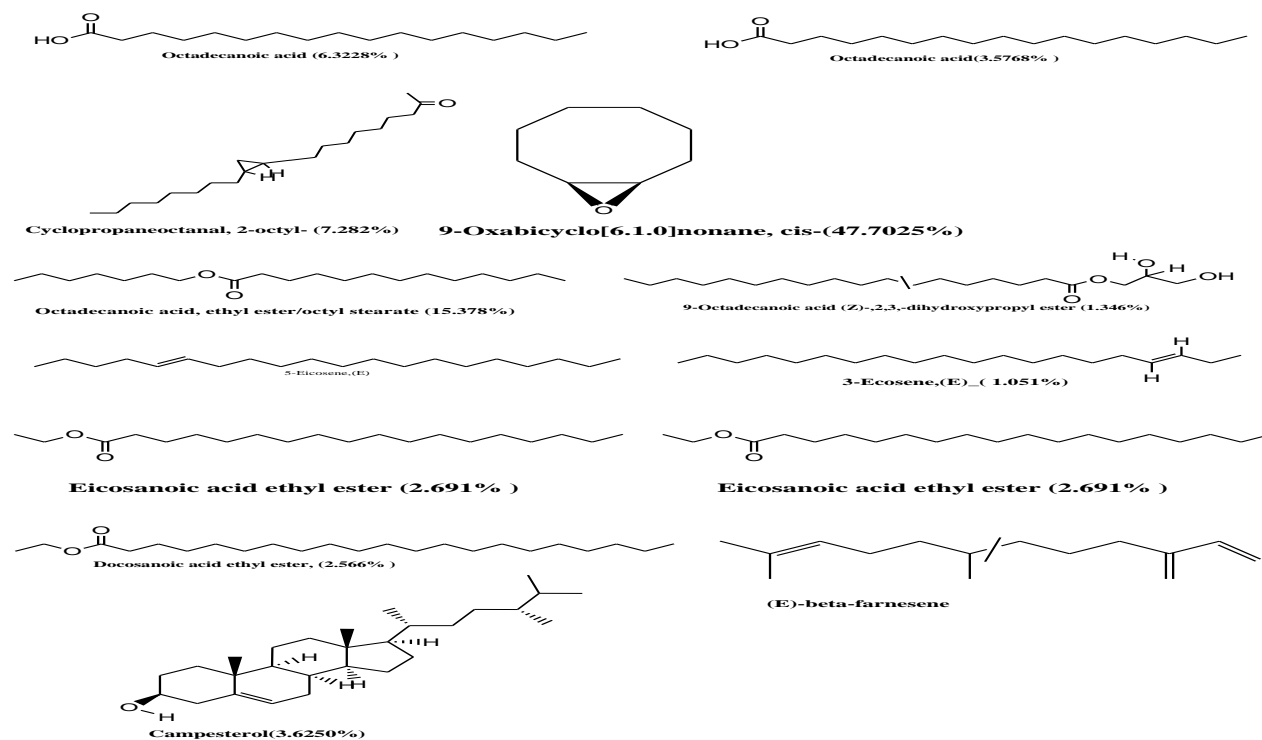
Figure 3: Phytochemical compounds in the crude extract of *Caralluma Dalzeilii N.E Brown's stem*

The GC-MS analysis of *Caralluma Dalzeilli N.E Brown* stem extracts revealed the presence of many compounds containing nitrogen, sulphur and oxygen in their hydrocarbon chain (phytochemical constituents) in fractions. The peaks in the chromatogram were integrated and compared with the database of spectrum of known components stored in the GC-MS library. In the stems of *Caralluma Deilzeilii N.E Brown*, the GC-MS analysis identifies the presence of twelve (12) chemical constituents in fractions with their concentrations, the compound with the highest concentration in *Caralluma Dalzeilli N.E Brown* stem inhibitor was 9-Oxabicyclo [6.1.0] nonane **(47.704%).**

(1)**3.5768%** Octadecanoic acid (2) **6.3228%** Octadecanoic acid (3) **47.702%** 9-Oxabicyclo[6.1.0]nonane with a highest concentration (4) **7.282%** Cyclopropaneoctanal 2-octyl- (5)**15.378%** Octadecanoic acid ethyl ester, the second most highest (6) **1.220%** 5-Ecosene (E)- (7) **1.346%** 9-Octadecanoic acid (Z)-,2,3,-dihydroxypropyl ester (8) **1.051%** 3-Ecosene (E)- (9) **2.691%** Eicosanoic acid ethyl ester   (10) **2.566%** Docosanoic acid, ethyl ester (12) **3.6250%** Campesterol.

3.4 Conclusion

In the present study the corrosion of extract of *Caralluma Dalzeilii N.E Brown* were analyzed and the FTIR that reveals that the ethanolic extract of *Caralluma Dalzeilii N.E Brown* was contained phenolic groups and compounds with hetero atoms such as, -OH, nitro compounds N-H, carbonyl groups C=O, and unsaturated groups C=C, C=H, etc. The presence of C=C at 715cm^{-1}, C-O at 1058 cm^{-1}, O-H at 1162 cm^{-1}, C-O at 1244 cm^{-1}, O-H at 1371 cm^{-1}, C-H at 1461 cm^{-1} , C=O at 1736 cm^{-1} , C-H 2855 cm^{-1}, N-H at 2922cm^{-1} and O-H at 3399cm^{-1} were suggests to play a major role in the inhibiting efficiency of the *Caralluma Dalzeilii N.E Brown* stem extract. Figure 1 shows the FT-IR Spectrum Characteristics of *Caralluma Dalzeilii N.E Brown* stem extract, these functional groups serve as an active location for the adsorption process, on the metal substrates (Mild Steel).The Gas chromatography and Mass spectrum (GC-MS) for the two plant inhibitors revealed the presence of twelve (12) compounds in the inhibitor of *Caralluma Dalzeilii N.E Brown* stem among which possessed hetero atoms (S.N.O) responsible for the corrosion inhibition effect.

REFERENCES

Abdel-Sattar E., Ahmed A. A., Hegazy M. E., Farag M. A., Al-Yahya M., A. (2007). Acylated pregnane glycosides from *Caralluma russeliana*. *Phytochemistry*. 68:1459-6z3.

Arthur, D. E., Abechi, S.E. (2019). Corrosion inhibition studies of Mild Steel using *Acalypha chamaedrifolia* leaves extract in hydrochloric acid medium. *SN Appl. Sci*. 1, 1–11.

Bader, A., Braca, A. De, Tommasi, N. Morelli, by I. Further constituents from *Caralluma negevensis. Phytochemistry*, 2003. 62:1277-81.

Chigondo, M., Chigondo, F. (2016). Recent Natural Corrosion inhibitors for Mild Steel: An Overview. 895 *J. Chem*. https://doi.org/10.1155/2016/6208937.

Eddy, N. O. (2008). Inhibition of the corrosion of Mild Mteel in H_2SO_4 by some antibiotics. Ph.D Thesis, University of Calabar, Calabar, Enenebeaku, C. K.

Eddy, N.O., Ebenso, E.E., and Ibok, U.J. (2010). Adsorption, synergistic inhibitive effect and quantum chemical studies of ampicillin (AMP) and halides for the corrosion of Mild Steel in H_2SO_4. *Journal of Applied Electrochemistry*, *40*: 445-456.

Hojatollah, J. Iman, D. Hadi, E. Mehdi, R. A., (2013). Electrochemical and Theoretical Studies of Adsorption and Corrosion Inhibition of N,N′-Bis (2hydroxyethoxyacetophenone)-2,2-dimethyl1,2-propanediimine on Low Carbon Steel (API 5L Grade B) in Acidic media. *Ind.Eng.Chem.Res*;52: 6617-6632.

Mann, A. Ibrahim, K. Oyewale, A.O., Amupitan, J.O., Fatope, M.O., and Okogun, J.I. (2011).

Oyama, M. (2007) Five new steroidal glycosides from *Caralluma Dalzielii. Helv Chim Acta*; *90*: 63–71.

Sireesha, M. Nadh, R.V., Babu KS. Phytochemical library of *Caralluma genus*, communicated article. *J Pharm Phytochemistry* 2014 ;3:155-9

Ugwah-Oguejiofor, C.J., Okoli, C.O., Ugwah, M.O., M.L., Ogbulie, C.S Mshelia, H.E., Umar, M., Njan, A.A., (2019).

Zakaria, M.N., Islam M.W., Radhakrishnan, R., Chen HB, Kamil M, Al-Gifri AN, *et al*. (2001). Antinociceptive and anti-inflammatory properties of *Caralluma arabica*. *J Ethnopharmacol,* 76:155-8

Extraction And Production of Biodiesel from Baobab Seed Oil using CaO/Al-MCM-41 as a Solid Based Catalyst

*Abdullahi H., Abdullahi Aminu G. and Alisi I. O.

Department of Applied Chemistry Federal University Dutsin-Ma katsina, Katsina State, Nigeria
*Corresponding Author's E-mail: aagarba1@fudutsinma.edu.ng

ABSTRACT
Production of biodiesel as a renewable, biodegradable and environmentally friendly fuel for use in diesel engines. It can overwhelmed the problem related with fossil fuels such as its non-renewability, poisoning nature and its global policy which is a matter of distress to many nations. The biodiesel was produced from the baobab (*Adansonia digitata*tata) seed oil removed using Soxhlet setup with methanol to oil ratio of 6:1 (v/v), using CaO/Al-MCM-41 mesoporous structure as a synthesized solid based catalyst which was confirmed by X-Ray Flourescence spectroscopy and N_2 adsorption-desorption analysis were the basicity of the catalyst was found to be increasing due to addition of CaO nano-particles, the reaction was optimized at 1 g catalyst amount at 90 min and 55 ℃ reaction condition, the results obtained shows high biodiesel yield of 74 %. It was clear that the produced biodiesel formed was confirmed by the GC-MS analysis. In this research, the transesterification reaction, the acid value was found to drops less than 1% and the oil conversion using solid base-catalyzed reaction reveals that, CaO/Al-MCM-41 such a catalyst shows a catalytic performance. Abundantly underutilized available seed oils has been explored to produce biodiesel. The baobab seed examined in this work have been shown to contain oil in reasonable amount, from the work conducted, the produced biodiesel can be used for many required purposes
Keywords: Optimization, Fatty acid, Catalyst, Soxhlet-apparatus

INTRODUCTION
Biodiesel is a renewable, biodegradable, and non-toxic fuel that can be produced from various feedstocks. The fuel known as biodiesel is made up of long-chain fatty acid mono-alkyl esters that are derived from renewable sources like vegetable oils and animal fats which can overcome problem associated with fossil fuels such as its non-renewability, polluting nature and global politics dependence on petrol.
Biodiesel is a renewable, biodegradable, and non-toxic fuel that can be produced from various feedstocks. The fuel known as biodiesel is made up of long-chain fatty acid mono-alkyl esters that are derived from renewable sources like vegetable oils and animal fats (Math *et al.,* 2010)..
It is well suited for biodiesel production due to its oil content (30-40%), low moisture content, and relatively low free fatty acid (FFA) content. The oil can be extracted using various methods, including mechanical pressing, solvent extraction, and supercritical fluid extraction. Furthermore, energy from fossil fuels has significantly increased because of the world's population rise and rapid industrial development (Betiku *et al.,* 2017 and Nath, *et al.,* 2019). Due to its bio-renewable nature, biodegradability, lower harmful emission, and good transport and storage capabilities, biodiesel is a viable alternative to fossil fuels. Because biodiesel contains more oxygen and has a lower carbon to hydrogen ratio than diesel, it can be utilized in place of diesel engines without any changes (Bhatti *et al.,* 2008). Reduced particle emissions, lower sulfur content, and a smaller amount of hydrogen and carbon monoxide are some of the main benefits of biodiesel (Due *et al.,* 2011).
The combustion emission profile of biodiesel is favorable, with little emissions of carbon monoxide, particulate matter, and unburned hydrocarbons (Mishra and Goswami 2018, Olivier *et al.,* 2010). Photosynthesis can recycle the carbon dioxide created during the combustion of biodiesel, reducing the harm that too much carbon dioxide can do to the ozone layer (Das, 2008). It has a greater flash point (150°C or above) than petroleum diesel, biodiesel is less flammable and safer to transport or handle (Akhihiero and Odu 2012).
It has lubricating qualities that can lengthen engine life and lessen engine wear. The exploration and utilization of an efficient catalyst are two key components for the cost-effective production of biodiesel (Andrade, *et al.,* 2011). Liquid catalysts such as sodium methoxide ($NaOCH_3$), potassium hydroxide (KOH), potassium methoxide ($KOCH_3$), sodium hydroxide (NaOH), and sodium ethoxide ($NaOCH_2CH_3$) have been employed frequently in the trans-esterification of vegetable oil or animal fat with methanol (Talha and Sulaiman, 2016).
Despite the widespread use of these liquid catalysts, producing biodiesel with liquid catalysts has remained difficult due to the high cost of the manufacturing process, the high cost of separation and purification, the hazardous state, the non-regeneration of catalysts, and the excess waste water produced during the purification processes. Because of the ease of separation and purification, using solid catalysts like calcium oxide lowers manufacturing costs. Higher

glycerin quality, reduced catalyst prices, and little to no waste streams are further advantages of using solid catalysts (Michel, 2006). Shorter reaction times than using enzyme catalyst are another advantage of using solid catalyst. For the direct trans-esterification of oils with high free fatty acid content, solid and enzyme catalysts are both often utilized. When a solid catalyst is utilized, there is no inhibition of the process, although glycerol formation does reduce the activity of the enzyme (Marchetti *et al.*, 2008). Although alkaline earth oxides with high alkalinity have been reported to be able to produce FAME, solid catalysts with high alkalinity, such as animal bones and aluminium or zinc doped calcium oxide catalyst, have been used recently for the production of biodiesel (Cherian, *et al.*, 2019; Jatinder, *et al.*, 2016), (Sudsakorn *et al.*, 2017). Calcium oxide is the most popular heterogeneous base catalyst (CaO). CaO is inexpensive, durable, resistant to moisture, and has a low solubility in a liquid mixture. Additionally, it yields a lot of FAME.

Formation of FAME (biodiesel) …………………………………………………………….   (1)
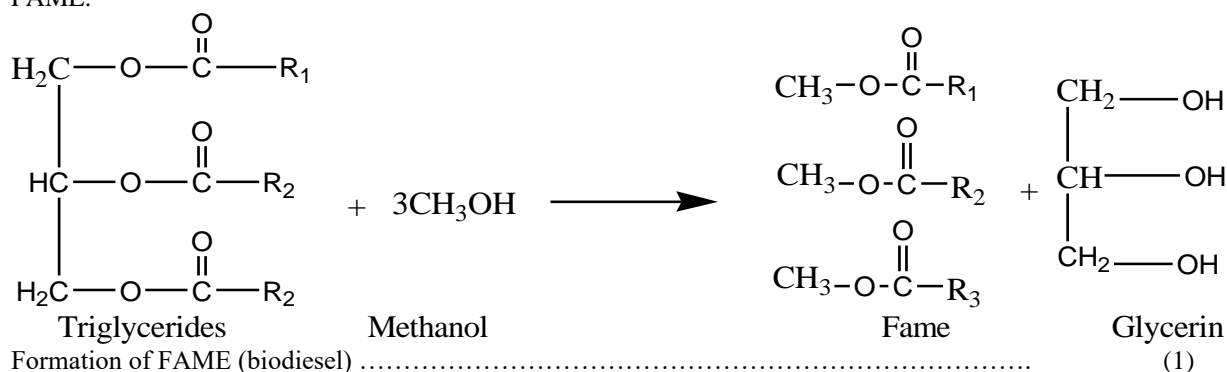
Biodiesel production from baobab seed oil can be achieved using solid-based catalysts. Several studies have explored the use of different solid catalysts for biodiesel production. Lotero *et al.* (2005) reviewed the synthesis of biodiesel using acid catalysis, including the use of solid acids as catalysts. Khodary *et al.* (2021) investigated the utilization of electric arc furnace dust as a solid catalyst for biodiesel production. Faruque *et al.* (2020) discussed the application of heterogeneous catalysts for biodiesel production from microalgal oil. Buchori *et al.* (2020) studied the effect of zeolite catalysts from geothermal solid waste on biodiesel production. Colombo *et al.* (2017) focused on the use of calcium oxide as a solid base catalyst for transesterification reactions in biodiesel production. Oloyede *et al.* (2022) explored the use of agricultural residue ash as a solid base catalyst for biodiesel production. CaO/Al-MCM-41 is a solid-based catalyst to be used in the production of biodiesel from *Adansonia digitatatata* oil extract.

MATERIALS AND METHODS
Materials
Materials used in this work include *Adansonia digitatatata* seed oil which was extracted from fresh *Adansonia digitatatata* seeds using soxlet apparatus, hot plate with a magnetic stirrer and mercury in glass thermometer, cotton wool, n-Hexane, and methanol, furnace, dry-oven and separating funnel.

Seed preparation
The seeds of the *Adansonia digitatatata* (baobab) were gathered, steeped in water with detergent, and carefully cleaned. The clean seeds were dried for 48 hours at a room-temperature. To make the extraction of the oils easier, the dried seeds were crushed into tiny pieces.

Extraction of oil
For the experiment carried out, the oil extraction, 100 g of ground baobab seed was wrapped in a filter paper and placed inside the thimble chamber of the 250 ml Soxhlet extractor. A round bottom flask containing n-hexane as well as a condenser was fixed to the extractor. 150 ml of n-hexane was measured and poured into each of the tied baobab seed samples with a foil used to cover the flasks to avoid evaporation of the solvent (n-hexane).

Figure 1: Soxhlet apparatus setup used for the oil extraction

Cool water flowing through the condenser was used to condense the evaporating solvent back into the Soxhlet extractor where the sample was packed to ensure sufficient extraction of the oil from the seeds. After a specified time of 4 hrs at 60 °C, the mixture of the n-hexane and the extracted oil was separated from the solid chaff and the n-hexane was removed from the extracted oil by gently heating off the mixture to evaporate the solvent. At the end of the experiment, the yield of the oil was obtained as the percentage of the extract from the seed using Equation.
The cake obtained after the extraction can be seen to be different from the initial material used.

$$\% \text{ of oil yield} = \frac{weight\ of\ oil\ extract\ (g)}{weight\ of\ seed\ sample\ used} \times 100 \ldots \tag{2}$$

Figure 2. Ground *Jatropha* seed sample

Determination of acid value
The procedure for determining the acid number is as follows. Weight 5 g of oil and put in a 250 ml Erlenmeyer. Then add 20ml of Isopropyl alcohol stirred with a magnetic stirrer at a temperature of 50 °C for 30 min. After cooling, add 3-4 drops of Phenolphthalein indicator, shaken to mix. Then titrate with KOH until the colour changes to pink. Record how many ml of KOH are used.

$$\text{Acid value} = \frac{volume\ of\ KOH\ \times N \times BM}{wieght\ of\ oil} \tag{3}$$

Where, the volume of KOH is the number of ml used for the titration.
N is Molar KOH (0.1).
BM is the molecular weight of KOH (56.1), Oil weight is the weighted amount of oil. (Cooks *et al*, 1997).

Trans-esterification of the crude oil extract
Preparation of methoxide
Measured amount of methanol was put into a stopped flask. 1 g of CaO/Al-MCM-41 was weighed and added to the methanol. The flask was stirred until all the CaO/Al-MCM-41 dissolved in the methanol (Cheng *et al.*, 2004).

The methoxide is not a chemical compound but a mixture because there are no bonds between the methanol and the catalyst.

Trans-esterification Process

Measured amount of the oil sample was put into a beaker; the methoxide was added to it. The temperature was raised on a hot plate and the mixture was stirred with magnetic stirrer. The mixture was allowed to stand overnight in a separating funnel. A thick brown liquid layer settled at the bottom, this was the glycerin and the lighter liquid above was the biodiesel. The glycerin which is the byproduct was drawn off through the bottom tap. The biodiesel was then washed with warm water to remove the soaps and methanol in the biodiesel. The water is better at dissolving the impurities than the biodiesel. A straw-yellow and a cloudy liquid layer were formed, the cloudy liquid was drained out and pH test was conducted to confirm the neutrality of the washed water. The Biodiesel was heated to 55 °C on a hot plate to allow the remaining water to evaporate and was finally filtered (Mondala *et al.,* 2009). The volume of the biodiesel obtained were recorded.

RESULTS AND DISCUSSION

XRF Analysis of the samples

Table 1 shows the XRF formation of Al-MCM-41 and different samples loaded with CaO at different percentages i.e 5% and 15%. The Si/Al ratio decreasing due to incorporation of CaO into the frame work. The basicity of the samples was checked using back titration method. The 15% CaO/Al-MCM-41 sample showed highest basicity (250 µmol g^{-1}), due to the high number of basic site contained. In contrast, the Al-MCM-41 which is made up of pure siliceous framework recorded the lowest basicity (20 µmol g^{-1}). It is because the number of CaO responsible for the formation of active basic site is absent.

Table 1: XRF Formation

Samples	XRF spectroscopy analysis				Si/Al molar ratio	Basicity (µmol/g)
	SiO$_2$ (%)	Al$_2$O$_3$ (%)	CaO (%)	Others (%)		
Al-α	94.43	1.83	N/A	0.25	91.68	20
Al-5%	92.82	2.02	0.13	0.33	80.96	180
Al-15%	91.90	2.47	0.75	0.36	65.94	250

N$_2$ Adsorption-Desorption Isotherm

The AlMCM-41 synthesized showed typical type IV isotherm (Figure 3a) of Al-MCM-41 mesoporous materials with two-dimensional hexagonal structures, Due to multilayer adsorption, the amount adsorbed at the adsorption branch gradually rises as the relative pressure rises. It is possible that the instability of the liquid nitrogen meniscus inside the small channels was what caused the small hysteresis loop that was detected at relative pressures of 0.25 to 0.4 P/P$_0$. No noticeable hysteresis loop was seen at a relative pressure of 0.9, but a rapid step rise in the isotherm of the calcined sample at P/P$_0$ 0.25 to 0.40 shows both the sample's uniform pore size distribution and its well-ordered mesoporous structure.
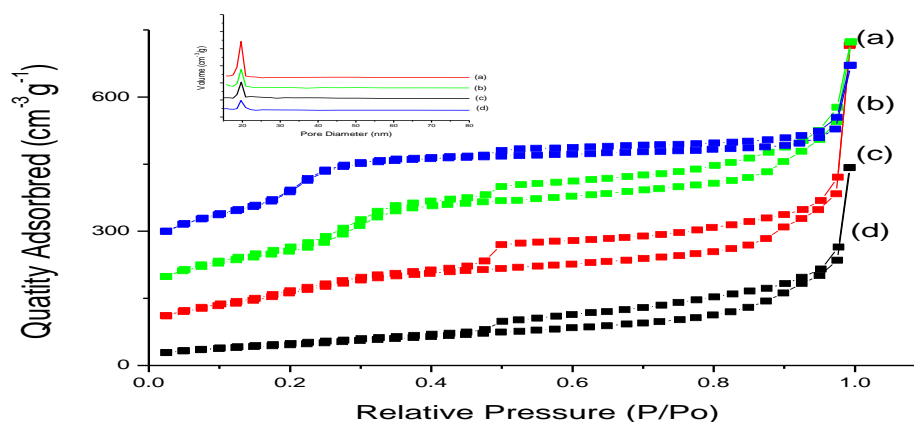

Figure 3: N$_2$ adsorption (close symbol) and desorption (open symbol) isotherms, and pore size distribution (inset) of calcined (a) Al-MCM-41, (b) Al-M-5%, (c) Al-M-15% and (d) Al-M-20% nanoparticles.

The CaO-Al-MCM-41 sample (Figure 3b) keeps the same isotherm shape, but there was a reduction in the amount of nitrogen that was adsorbed, and the beginning of the capillary condensation step occurs at a lower relative pressure. The decreased pore size, which was linked to the pore-filling action due to the integration of the CaO nanoparticles into the mesopores of the solid materials was what causes the shift of the inflection point of the step to lower relative pressure P/P_0 and the decrease in absorption quantity. The presence of comparatively homogenous mesopores in the samples is shown by the pore size distribution (Figure 3a, b) computed from the adsorption branches of the isotherms using the BJH model. While the pore volume and pore diameter reduce the BET surface area also decreases, comparatively, the Al-MCM-41 sample (Figure 3d) nearly loses the isotherm shape and uniform pore distribution, indicating that the CaO nanoparticles blocked the matrix's mesopores.

Biodiesel

From the result obtained, the oils form acid value was found to be 11 mg-KOH which drops to 0.32 mg-KOH/g-oil in *Adansonia digitatatata* using titration method. It can observed that a maximum conversion of *Adansonia digitatatata* is 74 % at a temperature of 55 °C and in a time period of 90 min from transesterification reaction. However, the percentage increase is in line with increases in temperature at different level. The percentage conversion can be raised by manipulating such variables as time and temperature. For example, at a temperature of 120 °C for a time period of 2 h. These values can be considered high when compared with other catalysts as presented by (Mbaraka *et al.,* 2003).

Effect of catalyst amount

The effect of the catalyst amount on the production of biodiesel yield was investigated within the range of 1 to 3 g of catalyst. The biodiesel production conducted at 333 k as reaction temperature and methanol to oil molar ratio 6:1.
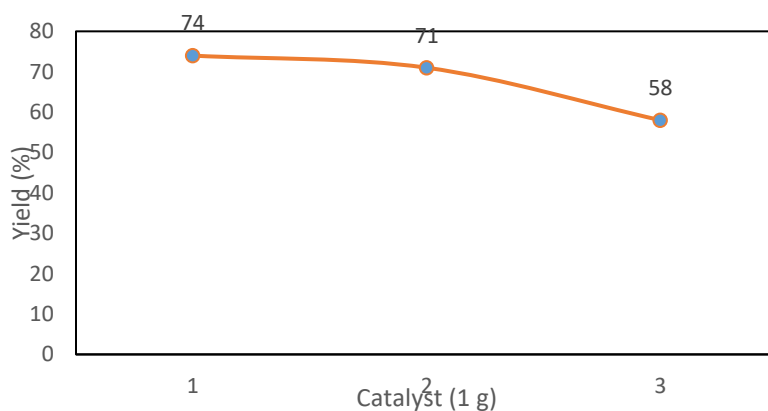

Figure 4: Biodiesel produced using differnt catalyst amount at 55 °C

According to previous studies, the catalytic activity was extremely influenced by alkalinity and the number of basic and the degree of dispersion of the active sites on the surface of the catalyst. Continuous using more catalyst amount, more basic sites will be available for transesterification. But in a catalyst amount more than 1 g the higher amount of alkaline catalyst prevails side reaction (saponification reaction and emulsification), thus decreases the methyl ester yield (Keera *et al.,* 2018). Moreover, too much catalyst (3 g) with a little bit less yield compared to 1g catalyst could only make the mixture of reactants viscous and lead to the problem of separation that decreases the yield and quality of the product as reported by (Yang *et al.,* 2009).

Effect of reaction time

Figure 5, shows the effect of reaction time on biodiesel yield, as the reaction time increases from 40 to 120 min, the biodiesel yield rapidly increases until the reaction has reached equilibrium, the reaction reversibility of transesterification reaction as reported by (Samart, *et al.,* 2009).
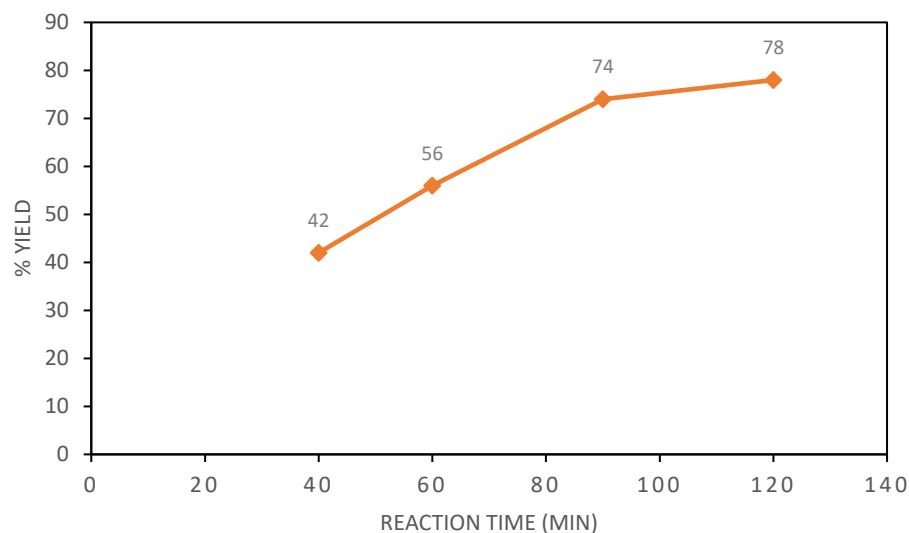
Figure 5: Biodiesel produced at 1 g catalyst amount and different reaction time at 55 ℃

Effect of reaction temperature

From figure 6, as the temperature increases from 30 to 55 °C, the biodiesel yield significantly increases. Initially, some thermal energy was needed for transesterification as the reaction was endothermic (Samart *et al.,* 2009). Since reaction mixture constitutes a three-phase system (methanol-oil-catalyst), the thermal energy was sufficiently needed to overcome the diffusion resistance between different phases. However, the high temperature is not preferred, as the temperature increase and reached the boiling point of methanol (64.70 °C), the methanol immediately vaporize and form many bubbles, which inhibits the reaction on the two-phase interface and thus decreases the biodiesel yield (Long, *et al.,* 2010).
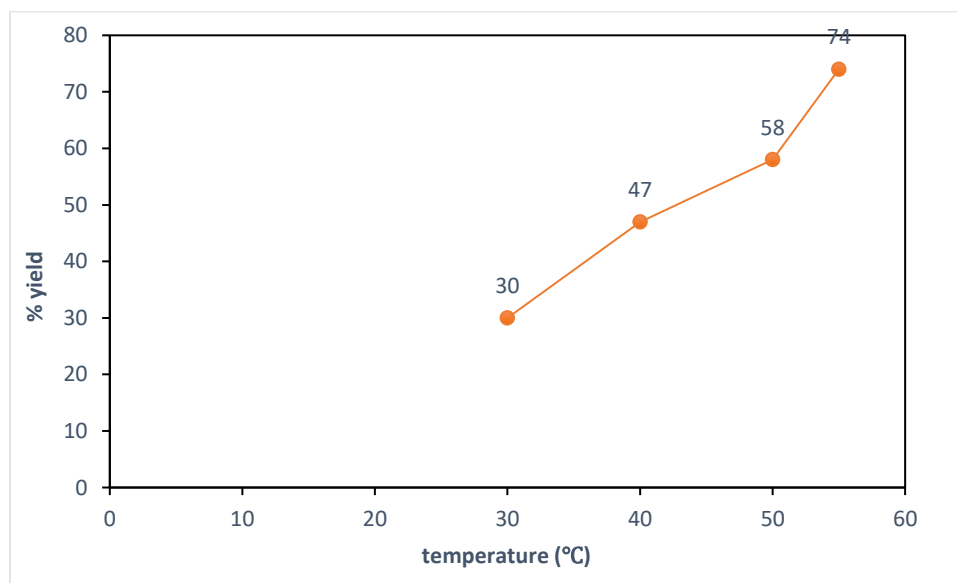

Figure 6: Biodiesel at different temperature and fixed reaction time 90 min

Characterization of biodiesel from baobab seed oil

The percentage oil yield of *Adansonia digitata*tata seeds is in the range of 30 - 45% which may be considered to be reasonable yield levels. The acid value is 2.083g oleic acid in the case of the oil investigated and therefore it suggests low level of fatty acid in the oil which was confirmed through GC-MS analysis.

Table 2: GC-MS analysis of *Adansonia digitatatata* oil showing the major fatty acids derived from hexane extract of *Adansonia digitatatata* seed oil

S/NO	Fatty acid	MF	MW	TC%
1	Hexadecanoic acid	$C_{17}H_{34}O_2$	270	92
2	Stearic acid	$C_{18}H_{36}O_2$	284	89
3	Myristic acid	$C_{14}H_{24}O_2$	228	88
4	Behemic acid	$C_{23}H_{46}O_2$	354	90
5	Linoleic acid	$C_{18}H_{32}O_2$	280	92
6	Oleic acid	$C_{18}H_{34}O_2$	284	91
7	Veleric acid	$C_{16}H_{30}O_2$	254	90

The biodiesel from baobab seed oil were characterized by GC- MS analysis which shows the presences of fatty acid from table 2 which are Oleic acid, Stearic acid, behemic acid, linoleic acid, veleric acid, myristic acid, hexadecanoic acid were the major fatty acids found, which shows the plant contain low acid value, the formation of fatty acid methyl ester (FAME) was presented in table 3.

Table 3: GC-MS Analysis of biodiesel from *Adansonia digitatatata*

S/NO	FAME	MF	MW	TC%
1	Hexadecanoic acid, methyl ester	$C_{17}H_{34}O_2$	270.45	98
2	Methyl stearate	$C_{19}H_{38}O$	298.5	99
3	9,12-Octadecadienoic acid, methyl ester	$C_{19}H_{34}O$	294.47	99
4	Methyl 18-methylnonadecanoate	$C_{21}H_{42}O$	326.56	98
5	Isobutyric acid, tetradecyl ester	$C_{18}H_{36}O$	284.47	86
6	Octaethylene glycol monododecyl ether	$C_{28}H_{58}O_9$	538.8	41
7	Methyl 13-eicosenoate	$C_{21}H_{40}O_2$	324.5	72
8	11-Octadecenoic acid, methyl ester	$C_{19}H_{36}O_2$	296.5	99

CONCLUSION

In this research, molecular sieve Al-MCM-41 supported with CaO exhibits characteristic mesoporous structures and acidic–basic properties which was confirmed by X-Ray Fluorescence spectroscopy and N_2 adsorption-desorption analysis. The addition of a measured amount of CaO on Al-MCM-41 enhances the basicity of the catalyst but with a concomitant decrease of surface area, this is due to blockage of pore spaces of the molecular sieve frame. In the transesterification reaction, the oil conversion using solid base-catalyzed reveals that, CaO/Al-MCM-41 such a catalyst shows a catalytic performance. Abundantly available high oil content underutilized seed has been investigated to produce biodiesel. The seed of *Adansonia digitata*tata examined in this work have been shown to contain oil amount in the range of 38 - 43% which may be considered to be reasonable yield while the acid value was found to be 2.083g oleic acid and was dropped to 0.32 mg NaOH/g after esterification- transesterification reaction in the case of the oil investigated and therefore it suggests low level fatty acid in the oil. From the work conducted, the produced biodiesel produced the highest value of 74 % using CaO/Al-MCM-41 at optimized reaction condition and therefore, it can be used for any required purpose.

REFERENCES

Akhihiero, E. T. and Odu, G. O. (2012). Environmental Impact of Climate Change and Renewable Energy Options for Sustainable Development. *International Journal of Advancement in Chemistry, 4*(1), 29-31.

Andrade J.E, A. Perez, P.J. Sebastian, D. Eapen,(2011) Biomass Bioenergy 35. 1008–1020.

Betiku E, A.O. Etim, O. Pereao, T.V. Ojumu, 2017. Two-step conversion of neem (Azadirachta indica) seed oil into fatty methyl esters using heterogeneous biomass based catalyst: an example of cocoa pod husk, Energy Fuels 31. 6182–6193.

Bhatti, H. N., Hanif, M. A., and Qasim, M. Rehman, A. (2008). Biodiesel production from waste tallow. Fuel, 87, 2961 – 2966.

Buchori, L., Widayat, W., Muraza, O., Amali, M., Maulida, R., & Prameswari, J. (2020). Effect of temperature and concentration of zeolite catalysts from geothermal solid waste in biodiesel production from used cooking oil by esterification–transesterification process. Processes, 8(12), 1629. https://doi.org/10.3390/pr8121629

Cheng, S.F., Choo, Y.M., Ma, A.N., Chuah, C.H. (2004). Kinetics Study on Transesterification of palm oil, J. of Palm oil Res., 16(2), p. 19-29.

Cherian, E., Yazhini, D., Merlin, V. and Baskar, G. (2019). Production of biodiesel from pork using alumina-doped calcium oxide nanocomposite as heterogeneous catalyst. *Energy Sources, Part A: Recovery, Utilization, and Environmental Effects*. https://doi.org/10.1080/15567036.2019.1637971

Colombo, K., Ender, L., & Barros, A. (2017). The study of biodiesel production using cao as a heterogeneous catalytic reaction. Egyptian Journal of Petroleum, 26(2), 341-349. https://doi.org/10.1016/j.ejpe.2016.05.006

Cooks L. V. and C. Van Rede (eds) (1997). Laboratory Handbook, for oil and fat analysis (Eds L.V Cooks and C. Van Rede).

Due, J., Grift, T.E., and Hansen, A.C. (2011). Effect to biodiesel on engine performances and emissions. Renew. Sustain. Energy, 15, 1098 – 1116.

Faruque, M., Razzak, S., & Hossain, M. (2020). Application of heterogeneous catalysts for biodiesel production from microalgal oil—a review. Catalysts, 10(9), 1025. https://doi.org/10.3390/catal10091025

Jatinder, K., Mohapatra, S. K. and Kundu, K. (2016). Biodiesel production from frying oil using zinc-doped calcium oxide as heterogeneous catalysts. *Energy Sources, Part A: Recovery, Utilization, and Environmental Effects*. https://doi.org/10.1080/15567036.2016.1270376

Keera, S. T., El Sabagh, S. M., & Taman, A. R. (2018). Castor oil biodiesel production and optimization. Egyptian Journal of Petroleum. doi:10.1016/j.ejpe.2018.02.007

Khodary, K., Naeem, M., & Roushdy, M. (2021). Utilization of electric arc furnace dust as a solid catalyst in biodiesel production. Clean Technologies and Environmental Policy, 25(1), 299-309. https://doi.org/10.1007/s10098-021-02174-0

Long T, Deng Y, Gan S, Chen J (2010) Application of Choline Chloride·xZnCl2 ionic Liquids for Preparation of Biodiesel. Chinese Journal of Chemical Engineering 18: 322-327.

Lotero, E., Liu, Y., López, D., Suwannakarn, K., Bruce, D., & Goodwin, J. (2005). Synthesis of biodiesel via acid catalysis. Industrial & Engineering Chemistry Research, 44(14), 5353-5363. https://doi.org/10.1021/ie049157g

Marchetti, J. M., Miguel, V. U. and Errazu, A. F. (2008). Techno-economic study of different alternatives for biodiesel production. *Fuel Process Technology, 89*, 740-748. https://doi.org/10.1016/j.fuproc.2008.01.007

Math, M. e., Kumar, S. P., and Chetty, S.V. (2010). Technologies for biodiesel production from used cooking oil- a review. Energy for Sustainable Development, 14, 339 - 34S.

Mbaraka IK, Radu DR, Lin VS-Y, Shanks BH. (2003). Organosulfonic acid-functionalized mesoporous silicas for the esterification of fatty acid. J Catal. 219:329–36.

Michel, B. (2006). Improved Glycerin Quality through Solid Catalyst. Bio-Oil International Conference, Vigo, Feb. 2006. Retrieved from http://www.axens.net

Mishra, V. K. and Goswami, R. (2018). A review of production, properties and advantages of biodiesel. *Biofuels, 9*(2), 273-289. https://doi.org/10.1080/17597269.2017.1336350

Mondala, A., Liang, K., Toghiani, H. and Hernandez, R. (2009). Biodiesel production by in situ Transesterification of municipal primary and secondary sludges. Bioresource Technology 100, 1203–1210.

Msalilwa, U., Makule, E., & Ndakidemi, P. (2020). Physicochemical properties, fatty acid composition, and the effect of heating on the reduction of cyclopropenoid fatty acids on baobab (*adansonia digitata*tata l.) crude seed oil. Journal of Lipids, 2020, 1-13. https://doi.org/10.1155/2020/6691298

Nath B, B. Das, P. Kalita, S. Basumatary, (2019). Waste to value addition: utilization of waste Brassica nigra plant derived novel green heterogeneous base catalyst for effective synthesis of biodiesel, J. Clean. Prod. 239. 118112.

Olivier, H., William, J. P. and Charles, K. W. (2010). Detailed Chemical kinetic mechanism for the oxidation of biodiesel fuels blend surrogate. *Combustion and Flame, 157*(5), 893-908. https://doi.org/10.1016/j.combustflame.2009.10.013

Oloyede, C., Jekayinfa, S., Alade, A., Ogunkunle, O., Otung, N., & Laseinde, O. (2022). Exploration of agricultural residue ash as a solid green heterogeneous base catalyst for biodiesel production. Engineering Reports, 5(1). https://doi.org/10.1002/eng2.12585

Samart C, Sreetongkittikul P, Sookman C (2009) Heterogeneous Catalysis of Transesterification of Soybean Oil using KI/mesoporous Silica. Fuel Processing Technology 90: 922-925.

Sudsakorn K, Saiwuttikul S, Palitsakun S, Seubsai A. Limtrakul J. (2017) Biodiesel production from *Jatropha* Curcas oil using strontium-doped CaO/MgO catalyst. Journal of Environmental Chemical Engineering;5(3),2845–2852. DOI:10.1016/j.jece.2017.05.033.

Talha, N. S. and Sulaiman, S. (2016). Overview of catalyst in biodiesel production. *ARPN. J. Eng Applied Science, 11*, 439-442

Yang FX, Su YQ, Li XH, Zhang Q, Sun RC (2009) Preparation of Biodiesel from Idesia Polycarpa var. Vestita Fruit Oil. Industrial Crops and Products 29: 622-628.